



THE UNIVERSITY OF
WAIKATO
Te Whare Wānanga o Waikato

Research Commons

<http://researchcommons.waikato.ac.nz/>

Research Commons at the University of Waikato

Copyright Statement:

The digital copy of this thesis is protected by the Copyright Act 1994 (New Zealand).

The thesis may be consulted by you, provided you comply with the provisions of the Act and the following conditions of use:

- Any use you make of these documents or images must be for research or private study purposes only, and you may not make them available to any other person.
- Authors control the copyright of their thesis. You will recognise the author's right to be identified as the author of the thesis, and due acknowledgement will be made to the author where appropriate.
- You will obtain the author's permission before publishing any material from the thesis.

Title of Thesis:
**The Impact of Dredging on the Stability
of the Matakana Banks Ebb-Tidal Delta**

A thesis
submitted in fulfilment
of the requirements for the degree
of
Doctor of Philosophy
at
The University of Waikato
by
ANDI YULIANTI RAMLI



THE UNIVERSITY OF
WAIKATO
Te Whare Wānanga o Waikato

2016

Abstract

The Matakana Banks ebb-tidal delta is located offshore from the Tauranga Entrance to Tauranga Harbour, Bay of Plenty New Zealand. In order to access the Port of Tauranga, Matakana Banks has been dredged to provide a shipping channel with sufficient depth for navigational purposes. In 1968 the first capital-dredging programme included an Entrance Channel through the delta, which was further enlarged in 1992. A biennial maintenance dredging programme has been required to deal with subsequent infilling of the Channel.

Recently, the Port has obtained resource consent to further widen and deepen the Entrance Channel. However, while granting the consent, the Environment Court accepted that dredging could result in adverse impacts to the stability of Matakana Banks and the adjacent Panepane Point on the western side of the tidal inlet. Therefore, this study was undertaken to assess the response of the ebb tidal delta to dredging, and determine possible mitigation measures if dredging has adverse effects.

The study analysed bathymetric data from single beam echo sounder (SBES) surveys obtained from 1998 to 2011. These data indicate that the main body of the ebb tidal delta is stable and undergoes little change. However, the swash bars located on the swash platform are very mobile, and probably account for the changes reported by the earlier assessments of changes between bathymetric surveys. In order to better track swash bars and assess variations in ebb-tidal delta morphology, multibeam echo sounder (MBES) surveys have been instituted.

Comparison of morphological changes with the dredging volume and the wave climate during 1998 to 2011 indicated that the storm events may trigger erosion of the ebb-tidal delta, particularly after a maintenance dredging campaign. However, the ebb-tidal delta volume recovered quickly between dredging campaigns, suggesting that the sediment was redistributed within the system and not permanently removed.

To provide insights into the processes affecting the ebb-tidal delta, and provide the necessary data for the calibration and verification of numerical models, and a major 27-day field programme was undertaken. Sediment traps were used to assess sedimentation rates, and provide sediment samples for characterising the

sediment grain size and bed roughness distribution for numerical modelling. Concentric arcs of wave and current recorders were used to measure hydrodynamic processes within and around the ebb-tidal delta and tidal inlet, and along the Matakana Island shoreface.

The field and historical bathymetric data showed that the ebb-tidal delta can be divided into 3 sub-regions according to the dominant hydrodynamic regime; (1) close to the Entrance Channel and ebb-jet where tidal currents dominate; (2) the central area of the swash platform, where the influence of tidal currents is still present but waves also play important role; and (3) the margins of the swash platform where waves are dominant and tidal influence is minimal. Overall the wave influence becomes more dominant as the distance from the Entrance Channel (main ebb jet) increases, and vice versa for tidal processes.

The short- and long-term impacts of dredging on the Matakana Banks ebb-tidal delta were investigated by numerical modelling using Delft3D. The model covered dredging locations inside Tauranga Harbour and the offshore areas around the Matakana Banks ebb-tidal delta, and was calibrated by the field measurement data. A month-long time series of wave conditions were used to force a wave model coupled with a hydrodynamic model for the 2013 bathymetry to simulate the present day situation. The modelling results showed that the sediment volume of the ebb-tidal delta fluctuates with tidal range; accretion occurred during neap tides; and erosion during spring tides.

To assess the long term impact, the *morphological factor (morfac)* tool in Delft3D was used. A *morfac* of 60 was applied to 12-days simulations to predict 2-year morphological changes, corresponding to the approximate time interval between maintenance dredging campaigns. The impacts of dredging were then investigated by modelling three different conditions: (1) before dredging started in 1968, using 1967 bathymetry; (2) the present situation using 2013 bathymetry with existing dredging and dumping activities; and (3) future scenarios using the 2013 bathymetry with alternative offshore disposal locations. Conditions of average waves (no storm) and with storm waves were also simulated.

Before dredging commenced, the ebb-tidal delta had a continuous terminal lobe from the north to southeast with a minimum depth of 5 m. Sediment transport

modelling indicated that bar by-passing transported sediment past the inlet via mobile bedforms on the terminal lobe, and suggested that the ebb-tidal delta was getting shallower and broader.

Simulations incorporating dredging revealed that the tidal currents in the channels of the ebb-tidal delta became more asymmetric (stronger ebb-current), and the ebb-tidal delta became bifurcated and more complex in its morphology. The system changed to inlet bypassing, although only small quantities of sediment appear to be transported past the tidal inlet (most sediment recirculates within the tidal inlet system). Overall dredging does not appear to have affected the stability of the Matakana Banks ebb-tidal delta, but there may have been an increase in the morphologic variability as bedforms circulate over the swash platform, and additional bands of sand bars have formed on the seaward margin of the swash platform.

Modelling of alternative spoil disposal sites indicated that shallow nearshore spoil disposal sites were more rapidly dispersed than the offshore spoil disposal site in 20 m depth, particularly during storm events. However, the volumetric differences between the models were small (less than 0.2%). The smallest volumetric changes compared to an initial ebb-tidal delta volume are associated with spoil disposal located northeast of the ebb-tidal delta (DaD New), and the most effective site for contributing sediment to mitigate erosion of Matakana Island is on the shoreface to the west of the ebb-tidal delta.

Acknowledgement

This thesis is the fruit of 4 years of up and down being a PhD student and I would not have been possible without the help, assistance, support, encouragement and guidance of many people in my life. I am very blessed and grateful for the opportunity to study and finish my PhD education at Waikato University. It has been a valuable academic and life-enriching experience.

First and foremost, I'd like to express my highest appreciation to my superb Chief Supervisor, Dr Willem de Lange. Willem has always been very helpful and patient in answering my questions and in guiding my research. As my academic advisor, Willem was very generous in his support and encouragements. I would also like to thank Karin Bryan and Julia Mullerney for their support, encouragements, hard questions and insightful comments as members of the supervisory panels.

I am grateful to receive the scholarship provided by the local government of South Sulawesi Province at the beginning years of my PhD program. I am also thankful to Port of Tauranga Ltd. on the funding of my research and field campaign. My appreciation also to Waikato University for the Doctoral Scholarship with Special Condition completion funds.

This thesis would not be completed without help from fellow graduate students (who are already PhDs) during the field work; Ehsan Jorat, Alex Port, Shawn Harrison, Steve Hunt, and the field technician Dirk Immenga, and the laboratory technician Dean Sandwell.

My life as a graduate student has become more enjoyable and enriching because of the friendships of so many people especially the Indonesian Society in Hamilton, Waikato.

I will be forever grateful to have Varvara Vetrova as my best friend, for all the talks and laughter that we had especially in going through the rough days as a graduate student.

Last but not least, I would like to thank my family, my wonderful sons, Farrel, Mikhail, and Omar for the patience and understanding of my hectic schedule. My highest gratitude and appreciation to my husband, Arief, for his relentless support and unconditional love that has been instrumental in my finishing the PhD program.

Table of Contents

Abstract	I
Acknowledgement	IV
List of Figures	XI
List of Tables	XIX
Chapter 1: Introduction	1
1.1 Background	1
1.2 Aims and Objectives	5
1.3 Thesis Outline	6
1.4 References	7
Chapter 2: Tauranga Harbour: History and Previous Dredging Studies	9
2.1 Introduction	9
2.2 Physical Setting and Hydrodynamics.....	9
2.3 Morphological Variability of the Matakana Banks Ebb-Tidal Delta..	15
2.3.1 Century Time Scale Evolution	15
2.4 Dredging and Dumping Activities	20
2.4.1 Dredging Types and Techniques.....	20
2.4.2 New Zealand Marine Dumping Legislation.....	21
2.4.3 Brief history of Port of Tauranga	27
2.4.4 Dredging and Dumping Programme in Port of Tauranga.....	28
2.5 Previous Studies of Hydrodynamic and Morphodynamic Changes due to Dredging and Dumping	33
2.6 Summary	37
2.7References	38
Chapter 3: Morphodynamics of Ebb-Tidal Delta Systems	47
3.1 Introduction	47
3.2 Sand Transport in Estuaries and Coastal Waters	48
3.3 Inlet Circulation.....	49
3.4 Ebb Tidal Delta System.....	50
3.4.1 Definition	50
3.4.2 Tidal Inlet and Ebb Delta – Tidal Prism Relationships.....	53

3.4.3 Sediment Transport Patterns on the Ebb-Tidal Delta.....	54
3.4.4 General Sediment Dispersal from Tidal Inlets	55
3.4.5 Inlet Sediment Bypassing	56
3.5 Modelling Sediment Transport and Morphological Evolution.....	58
3.5.1 General.....	58
3.5.2 Definition of Model Boundaries	59
3.5.3 Hydrodynamic Model	60
3.5.4 Suspended Transport	61
3.5.5 Bed Load and Total Transport Formulation	62
3.5.6 Morphological Up-dating	65
3.5.7 Representation of Dredging	67
3.6 Summary.....	67
3.7 References.....	68

Chapter 4: Morphological Evolution of Matakana Banks Ebb-Tidal Delta.. 75

4.1 Introduction.....	75
4.1.1 Acknowledgements.....	76
4.2 Material and Methods	76
4.2.1 Bathymetric Maps.....	76
4.2.2 Ebb-Tidal Delta Volume Calculation	79
4.2.3 Cross-Section Profiles	80
4.2.4 Net Morphological Change.....	81
4.2.5 Hydrodynamic Conditions during the Observation Period	81
4.3 Results and Discussion	83
4.3.1 Bathymetric Changes (SBES) from April 1998 to November 2011 ..	83
4.3.2 Sand Volume Variability from April 1998 to November 2011	89
4.3.3 Short-Term (MBES) Ebb-Tidal Delta Bathymetry Changes.....	124
4.4 Discussion.....	128
4.4.1 Group Areas of the Ebb-Tidal Delta.....	130
4.4.2 Sediment Transport Patterns.....	132
4.4.3 Dredging and ebb-tidal delta volumetric changes	136
4.4.4 Single- vs Multibeam Echosounder Surveys	138
4.4.5 Conceptual Model.....	138
4.5 Summary.....	140
4.6 References.....	144

Chapter 5. Field Measurement Campaign	149
5.1 Introduction	149
5.1.1 Acknowledgement.....	150
5.1.2 Aim.....	150
5.2 Instruments and Methods	151
5.2.1 Observational Techniques and Analysis Methods	152
5.2.1.1 Acoustic Doppler Velocimeter	152
5.2.1.2 S4.....	152
5.2.1.3 FSI Acoustic Current Meter.....	153
5.2.1.4 SCUFA Fluorometer.....	153
5.2.1.5 Acoustic Doppler Current Profiler (ADCP)	154
5.2.1.6 RBR Submersible Tide Gauge	154
5.2.1.7 Acoustic Doppler Profiler.....	155
5.2.1.8 Sediment and Water Sampling	155
5.3 Data Analysis	157
5.3.1 Acoustic and Backscatter Data.....	157
5.3.2 Sediment Grain Size Analysis.....	159
5.3.3 Total Suspended Solid Analysis.....	159
5.4 Results	161
5.4.1 Sea Level and Wave Data	161
5.4.2 Storm Events and Wave Power.....	172
5.4.3 Water Turbidity and Total Suspended Solid.....	173
5.4.4 Spatial Distribution of Sediment Grain Size and Sedimentation Rate	175
5.5 Summary	180
5.6 References	182
Chapter 6: Morphodynamic Modelling: Model Set-Up and Validation.....	185
6.1 Introduction	185
6.1.1 Acknowledgements	187
6.2 Model Overview.....	187
6.3 Delft3D FLOW Model Setup.....	189
6.3.1 Computational Grid and Bathymetry	189
6.3.2 Boundary Conditions.....	190
6.3.3 Model Parameter Settings	193

6.3.4 Delft3D-WAVE (SWAN) Setup	199
6.4 Model Results	199
6.4.1 Comparison and Calibration	199
6.4.2 Modelled Hydrodynamic Conditions	202
6.4.3 Modelled Wave Conditions	207
6.4.4 Coupled Flow (Morph) – Wave Model	212
6.5 Summary/Discussion	214
6.6 References.....	216

Chapter 7. Simulation of Dredging and Spoil Disposal Impacts..... 221

7.1 Introduction.....	221
7.2 Model Set-Up.....	221
7.2.1 Model Input	221
7.2.2 Morphological model setup	224
7.2.3 Alternative spoil disposal sites	225
7.3 Results and Discussion	227
7.3.1 Hydrodynamic and sediment transport under interaction of tides and waves.....	227
7.3.2 Influence of tidal currents and waves on the sediment transport rate	239
7.3.2 Influence of tides and waves on ebb-tidal delta daily volume changes.....	241
7.3.3 General sand dispersal trends: influence of dredging and storm events.....	243
7.3.4 Alternative spoil disposal sites for mitigation	252
7.3.7 Entrance channel infilling rate.....	260
7.3.5 Ebb-tidal delta volumetric comparisons for alternative disposal sites	261
7.4 Summary.....	263
7.5 References.....	266

Chapter 8: Conclusions and Recommendations 271

8.1 Responses to Research Questions.....	271
8.1.1 What changes in ebb-tidal morphology were evident following capital dredging?.....	271

8.1.2 How did the ebb-tidal delta respond to biannual maintenance dredging? What changes in ebb-tidal delta size (volume and area) and shape were noticeable? Are there separate sub-regions based on morphology and hydrodynamic regime that respond differently to forcing?	274
8.1.3 How well did the process-based morphological model simulate the hydrodynamic processes in the tidal inlet and over the ebb-tidal delta? To what extent this approach can be utilized by this study to predict dredging impacts?	277
8.1.4 What was the pattern of sand movement? What was the rate of change of the ebb-tidal delta, and what was the main hydrodynamic regime controlling the ebb-tidal delta sediment budget/volume?.....	278
8.1.5 What are the impacts of maintenance dredging and spoil disposal on the ebb-tidal delta?.....	280
8.2 Recommendations for further research	281
8.2.1 Two dimensional versus three dimensional processes	281
8.2.2 Morphological changes	282
8.2.3 Changes in dredge spoil characteristics	283
8.3 References	283
Appendices	285
Appendix 1 Wave and Wind Roses	286
Appendix 2 Computational Grid and Monitoring Stations	291
Appendix 3 Calculated Bed Roughness	309
Appendix 4 Wind Data Set for FLOW-MOR model	318
Appendix 5 Dredging and Dumping Files	319
Appendix 6 Comparison between Measured and Predicted Water Levels, and Current Speed and Direction	327
Appendix 7 Frequency Distributions of Measured and Modelled Wave.....	332
Appendix 8 Tidal Boundary for 1967 model	336

List of Figures

Figure 1-1. Location map of the study area at Tauranga, Bay of Plenty... ..	1
Figure 1-2. The position of the Matakana Banks, Matakana Island, Panepane Point and Entrance Channel of Tauranga Harbour.....	2
Figure 1-3. The Matakana Island’s shoreline positions from 1968 to 2004	4
Figure 2-1. Tauranga Harbour comprises of Katikati Entrance in the northwest and Tauranga Entrance in the southeast.....	10
Figure 2-2. The major geomorphologic units of Matakana and Rangiwaea Islands, and the locations of former tidal inlets.....	13
Figure 2-3. Conceptual model for nearshore and inner shelf dynamics off Tauranga Harbour.....	14
Figure 2-4. Inferred growth of the southeastern end of Matakana Island since 600 cal BP	19
Figure 2-5. Issuing authority jurisdiction.....	22
Figure 2-6. Permits for dumping: application and assessment under the MTA.....	24
Figure 2-7. Existing spoil disposal sites.....	26
Figure 3-1. Diagram of an ebb-tidal delta showing each of the sub- environments	51
Figure 3-2. Models of sediment bypassing tidal inlets	57
Figure 3-3. Example of Delft3D-FLOW horizontal model area showing the grid staggering, the grid enclosure and the position of open and closed boundaries	60
Figure 3-4. General structure of coastal morphodynamic models and the Morfac concept	66
Figure 4-1. 20 m resolution contour and shaded relief bathymetry maps of Matakana Banks ebb-tidal delta.....	78

Figure 4-2. High resolution bathymetric map obtained from MBES system of surveys March 2013. 5 m resolution contour and shaded relief maps of Matakana Banks ebb-tidal delta.....	79
Figure 4-3. Locations of the southeast to northwest aligned cross-sections for the Matakana Banks ebb-tidal delta.....	80
Figure 4-4. Significant wave heights (H_s) conditions of each survey period from 1998 to 2011.	82
Figure 4-5. The positions between 1998 and 2011 of the 1 m, 5 m, 10 m and 15 m depth contours reflect the bathymetric variability	84
Figure 4-6. Cross-section profiles 1 to 7 distributed evenly from the southeast to northwest Matakana Banks ebb-tidal delta for SBES surveys between 1998 and 2011	85
Figure 4-7. Comparison of the 1998 and 2011 cross-shore profiles to illustrate the net decadal differences in bed elevation (after 13 years)	86
Figure 4-8. Shaded relief surface maps of Matakana Banks ebb-tidal delta	88
Figure 4-9. Maps of slope gradients	89
Figure 4-10 Morphology of the Matakana Banks ETD from SBES surveys in 1998 and 1999. The upper images are colour-shaded 3D surfaces interpolated from the SBES data	91
Figure 4-11 Comparisons of cross-shore profiles obtained in 1998 and 1999, which show a general seaward movement of the sandbars	92
Figure 4-12 Morphology of the Matakana Banks ETD from SBES surveys in 1999 and 2000. The upper images are colour-shaded 3D surfaces interpolated from the SBES data	94
Figure 4-13 Comparisons of cross-shore profiles obtained in 1999 and 2000, which show a general seaward movement of the sandbars	95
Figure 4–14. Morphology of the Matakana Banks ETD from SBES surveys in 2000 and 2001. The upper images are colour-shaded 3D surfaces interpolated from the SBES data	97

Figure 4-15. Comparisons of cross-shore profiles obtained in 2000 and 2001, which show little change for most profiles and a seaward movement of the sandbars for profiles P5-P6	98
Figure 4-16. Morphology of the Matakana Banks ETD from SBES surveys in 2001 and 2002. The upper images are colour-shaded 3D surfaces interpolated from the SBES data	101
Figure 4-17. Comparisons of the cross-shore profiles for 2001 and 2002, showing erosion and seaward migration of sandbars	102
Figure 4-18. Morphology of the Matakana Banks ETD from SBES surveys in 2002 and 2006. The upper images are colour-shaded 3D surfaces interpolated from the SBES data	105
Figure 4-19. Comparison of the cross-shore profiles for 2002 and 2006 indicating that erosion was the dominant process	106
Figure 4-20. Morphology of the Matakana Banks ETD from SBES surveys in 2006 and 2008. The upper images are colour-shaded 3D surfaces interpolated from the SBES data	109
Figure 4-21. Comparisons of cross-shore profiles between 2006 and 2008. This period coincides with the largest volumetric gain observed, particularly along profile P5	111
Figure 4-22. Morphology of the Matakana Banks ETD from SBES surveys in 2008 and 2009. The upper images are colour-shaded 3D surfaces interpolated from the SBES data	113
Figure 4-23. Comparison of cross-sectional profiles for 2008 and 2009. Overall, the profiles accreted between these surveys, and the seabed remained stable offshore of the terminal lobe.....	114
Figure 4-24. Morphology of the Matakana Banks ETD from SBES surveys in 2009 and 2010. The upper images are colour-shaded 3D surfaces interpolated from the SBES data	117
Figure 4-25. Comparison of cross-sectional profiles for 2009 and 2010. Overall, the profiles eroded between these surveys	118

Figure 4-26. Morphology of the Matakana Banks ETD from SBES surveys in 2010 and 2011. The upper images are colour-shaded 3D surfaces interpolated from the SBES data	121
Figure 4-27. Comparison of cross-sectional profiles of surveys conducted in 2010 and 2011.....	123
Figure 4-28. Morphology of the Matakana Banks ETD from MBES surveys in March and July 2013	124
Figure 4-29. Comparisons of cross-sectional profiles from the November 2011 SBES survey and MBES surveys conducted in March and July 2013	127
Figure 4-30 Plots of the relationship among the ENSO condition where LN is La Niña and EN is El Niño, wave and wind roses, clockwise and anticlockwise direction of bedform migration, statistics of hydrodynamic regimes, and dredging volume and monthly volumetric changes for Matakana Banks ebb-tidal delta between surveys	133
Figure 4-31. Generalized sketch map illustrating the topographic features at tidal inlets along the Georgia coast. Refracted wave crests generally interfere along the axis of seaward extending shoals.....	134
Figure 4-32. The conceptual model of Matakana Banks ebb-tidal delta morphology. The OBC and IBC are abbreviation for outer blind channel and inner blind channel.....	139
Figure 5–1 Instruments and equipment used for hydrodynamic and turbidity measurements during this project	149
Figure 5-2. Instrumented seabed frame locations within the Entrance Channel and over Matakana Banks ebb-tidal delta during the field programme ..	151
Figure 5-3. Equipment for TSS analysis used in this study.	160
Figure 5-4. Tidal current roses for field measurements.....	163
Figure 5–5. Time-series of hydrodynamic condition on the terminal lobe of the Matakana Banks.....	165

Figure 5-6. Time series of hydrodynamic conditions at the most northern part of Matakana Banks	166
Figure 5-7. Time-series of hydrodynamic condition on the most eastern part of the Matakana Banks	167
Figure 5-8. Backscatter time-series recorded by ADCP	167
Figure 5-9. Time-series of hydrodynamic condition inside the Tauranga Harbour at the Entrance Channel	168
Figure 5-10. Time-series of the significant wave heights along the Matakana Banks from the north to inside the harbour.....	169
Figure 5-11. Wave roses indicating wave directions recorded by the S4s during the deployment period.....	170
Figure 5-12. Histograms of the time series observed wave peak periods	172
Figure 5-13. Variation of wave power P ($W.m^{-1}$) with significant wave height and peak period during field measurements	173
Figure 5-14. Time series of turbidity recorded by SCUFA (third panel) during field measurement, along with the corresponding water level and tidal current speed	174
Figure 5-15. Plot of the C3 fluorometer reading (RFU) against the total suspended solid	175
Figure 5-16. Median sediment grain size D_{50} (millimetres) sampled at the measurement stations	176
Figure 5-17. Plots of sediment influxes ($mg/cm^2/day$) obtained from the sediment traps against the current speed (m/s), wave heights (m), water depth (m)	179
Figure 6-1. Schematic of the computations and exchange of key parameters for a morphodynamic simulation.....	189
Figure 6-2. Delft3D computational grids for the 1967 bathymetry 1967 (left), before the first capital dredging was conducted, and for the 2013 bathymetry obtained by a MBES survey in March 2013	190

Figure 6-3. The locations where tidal forcing was applied to the 4 open boundaries in the initial hydrodynamic model.....	192
Figure 6-4. Map of the Manning bottom roughness estimated from the median grain size diameter (D_{50}) for the nested numerical model	195
Figure 6-5. The correlation values (r^2) of the observed and modelled water level at each stations in the study area	203
Figure 6-6. Time series of the observed and modelled water level, current magnitude and current direction at Station 390 inside the Harbour Entrance	204
Figure 6-7. The locations of S4 deployments for measured wave data.....	207
Figure 6-8. Predicted wave height results and comparison with measured wave	208
Figure 6-9. The R squared and RMAE values for predicted and measured wave height	208
Figure 6-10. Wave roses of the observed and predicted wave directions and heights for the S4 stations in the nearshore area, northwest of the Entrance Channel.....	209
Figure 6-11. Wave roses of the observed and predicted wave directions and heights for the S4 stations in the offshore area and inside the harbour.....	210
Figure 6-12. The observed and predicted wave periods.....	211
Figure 6-13. Observed and modelled sedimentation and erosion for Matakana Banks ebb-tidal delta over a 5 month period	212
Figure 6-14. Comparison of the coupled Wave-Flow Morph model results with the measured bathymetry for 5 months morphological updating	214
Figure 7-1. Matakana Banks ebb-tidal delta model bathymetries: before the first capital dredging in 1967 and in 2013 after two capital dredging programmes	223
Figure 7-2. Spoil disposal sites for materials dredged from around the Tauranga Harbour	224
Figure 7-3. Existing and alternative spoil disposal sites	226

Figure 7-4. Peak current speed during the tidal cycle of spring and neap tides...	228
Figure 7-5. Computed residual current during spring and neap tides	230
Figure 7-6. The maximum sediment transport rate ($m^3/s/m$) during consecutive ebb and flood half tidal cycles for a spring tide modelled by tidal forcing only.....	232
Figure 7-7. The maximum sediment transport rate ($m^3/s/m$) during consecutive ebb and flood half tidal cycles for a neap tide modelled by tidal forcing only	233
Figure 7-8. The computed significant wave height (H_s) during consecutive ebb and flood half tidal cycles for a spring tide predicted by the coupled FLOW-WAVE model.....	235
Figure 7-9. The computed significant wave height (H_s) during consecutive ebb and flood half tidal cycles for a neap tide predicted by the coupled FLOW-WAVE model.....	237
Figure 7-10. The maximum sediment transport rate ($m^3/s/m$) during consecutive ebb and flood half tidal cycles for a spring tide predicted by combined wave and tidal forcing	238
Figure 7-11. The maximum sediment transport rate ($m^3/s/m$) during consecutive ebb and flood half tidal cycles for a neap tide predicted by combined wave and tidal forcing	239
Figure 7-12. Mean total transport ($m^3/s/m$) for 12 days simulation time that covers spring and neap tidal cycle	240
Figure 7-13. Comparison between the computed cumulative total (net) transport over 12 days (m^3) model with only tidal forcing and combined wave and tidal forcing	241
Figure 7-14. Flow-Wave coupled model predictions of daily volumetric changes for the Matakana Banks ebb-tidal delta, and the corresponding observations of tide, current speed, and significant wave height.....	242
Figure 7-15. Comparison of the computed current speed and direction before and after DaD in the Lower Western Channel inside the harbour	243

Figure 7-16. Comparison of the computed current speed and direction before and after DaD in the middle of the Entrance Channel.....	245
Figure 7-17. Comparison of the computed current speed and direction before and after DaD at the distal end of the Entrance Channel	245
Figure 7-18. Computed mean total sediment transport before the first capital dredging in 1968 and spatial extension of cumulative erosion/sedimentation	247
Figure 7-19. Mean total sediment transport and cumulative erosion/sedimentation after dredging and spoil disposal programme.....	249
Figure 7-20. Comparison of the mean total transport of sediment sand and the spatial extent of erosion and accretion after 2 years simulation period with storm events	251
Figure 7-21. Computed patterns of cumulative erosion and sedimentation of the 2013 bathymetry, including different spoil disposal site options.....	253
Figure 7-22. Comparison of 2-year ebb-tidal delta morphological changes resulting from different spoil disposal site alternatives, compared with the baseline morphology of no dredging	255
Figure 7-23. Comparison of bed level changes resulting from alternative spoil disposal sites with respect to no dredging after 2 years.....	257
Figure 7-24. Mean and maximum total sediment transport flux magnitude and directions predicted by a 2-years simulation of actual maintenance dredging and disposal	259
Figure 7-25. Sub-sections of Matakana Banks ebb-tidal delta which were used to obtain volumetric comparison for the alternative spoil disposal sites	261
Figure 8-1. Comparisons of the patterns of sediment transport and erosion/accretion before and after capital dredging to create the Entrance Channel through the Matakana Banks ebb –tidal delta	273
Figure 8-2. 3D and shaded relief surface maps of Matakana Banks ebb-tidal delta.....	275

Figure 8-3. The sub-regions of Matakana Banks ebb-tidal delta based on the dominant hydrodynamic regime.....276

List of Tables

Table 2-1. Summary of the proposed dredging parameters	27
Table 2-2. Past dredging and dumping activities commenced in Tauranga Harbour during the late 60s to late 70s	31
Table 2-3. Dredging areas, materials and volumes during 90's to recently in 2014	32
Table 4-1. Months during which SBES surveys were carried out between 1998 and 2011.	77
Table 4-2. Grid information for bathymetry map from single beam echo sounder surveys	77
Table 4-3. Grid information for the bathymetry map derived from multibeam echosounder surveys	79
Table 4-4. Summary of mean tidal range, wave, energy and wind conditions of between surveys from 1998 to 2011	83
Table 4-5. Summary of volumetric changes extent of erosion and accretion, and average sand thickness changes for the Matakana Banks ebb-tidal delta over the period 1998 to 2011	90
Table 4-6. Summary of the observed ENSO extreme effects on the northeast coast of New Zealand (taken from de Lange, 2000).....	130
Table 5-1. Summary of the deployed instruments, and their locations and settings during 11 April – 8 May 2013	152
Table 5-2. Deployment period of sediment traps	156
Table 5-3. Amplitude (m) and phase lag (°) for the dominant tidal constituents measured during the deployment period	162
Table 5-4. Mean, maximum and minimum values of the tidal current speeds and directions during the field measurements	162
Table 5-5. Ranges of tidal current speeds (m/s) for spring and neap tides during field measurements	164

Table 5-6. Statistics of the measured waves in the study area	171
Table 5-7. The percentage of occurrence for H_s less than 1m, between 1 to 1.99m and higher than 2 m.....	171
Table 5-8. The highest significant wave height H_s (m) and period T_p (s) during storm events corresponding to the wave power P (kgms^{-3})	173
Table 5-9. Summary of sediment grain characteristics at each measurement station based on the Udden-Wentworth and Folk classifications (Folk, 1968)	177
Table 5-10. Dry weight of sediment captured by the sediment traps and the sedimentation rate (influx) at each station	178
Table 6-1. Tidal amplitudes (amp) and phase for the 7 major constituents used to generate the tidal forcing on the boundaries of the initial model.....	191
Table 6-2. Physical parameters used for the Delft3D FLOW and MOR	196
Table 6-3. Numerical parameter.....	198
Table 6-4. Statistical parameters used for model calibration and validation.....	200
Table 6-5. Statistical parameters used to assess the quality of the performance of modelled wave, velocity and morphology	201
Table 6-6. Performance rating according to RMAE and BSS values	206
Table 6-7. Statistical parameters for measured and modelled water level for S4 stations on and near the ebb-tidal delta.....	206
Table 6-8. Statistical parameters for measured and modelled water level and current speed at Station 390 inside the harbour. RMAE and r are dimensionless	205
Table 6-9. Volumetric comparison between the observed and modelled of Matakana Banks ebb-tidal delta over a 5 month period	213
Table 6-10. Brier Skill Score	213
Table 7-1. Summary of sediment types and volumes for different locations for the 2013 maintenance dredging by the Port of Tauranga	223

Table 7-2. Calculated ebb tidal delta final volumes and volume changes for different simulation durations and wave conditions	250
Table 7-3. The computed cumulative sediment transport along transects across the ebb-tidal delta between the tidal inlet and the northwestern margin of the ebb-tidal delta	258
Table 7-4. Summary of sediment volume changes along the Entrance Channel predicted by 2-year modelling assuming no DaD, actual DaD, and DaD combined with alternative sites	260
Table 7-5. Volume changes of ebb-tidal delta after 2 years simulation.....	262

Chapter 1: Introduction

1.1 Background

A problem common to almost every harbour in the world is adapting to and mitigating the effects of coastal processes that dynamically change over time due to the interactions between the atmosphere, ocean, land surface and human activities. One of the crucial problems is the interaction of sedimentation and dredging on coastal geomorphology and processes.

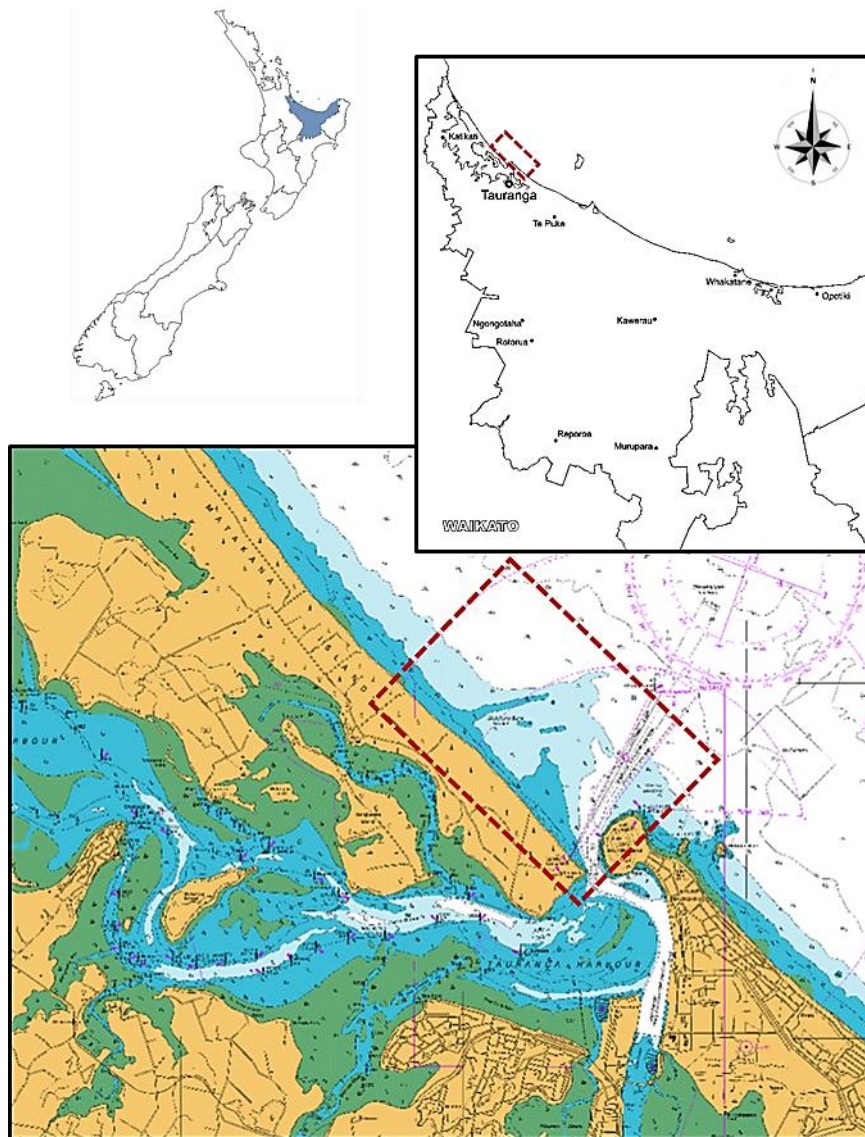


Figure 1-1. Location map of the study area at Tauranga, Bay of Plenty. The shallows of the ebb tidal delta, also known as Matakana Banks, are highlighted by the dashed box.

Tauranga Harbour is located within the Bay of Plenty, North Island, New Zealand (Figure 1). The harbour is sheltered by a long, narrow, barrier island known as Matakana Island, and two tombolos at Mt Maunganui and Bowentown, which protect the harbour from the open sea. There are two entrances to the harbour, with the Port of Tauranga being accessed by the southeastern inlet (Tauranga Entrance). The ebb tidal delta (Matakana Banks) of the south eastern channel (Tauranga Entrance) has been dredged to improve navigation for shipping since 1968 (Healy et al., 1996).



Figure 1-2. The position of the Matakana Banks, Matakana Island, Panepane Point and Entrance Channel of Tauranga Harbour. Photo is taken from (Figure is taken from Brannigan, 2009. Air photo source: Environment Bay of Plenty).

In 2010, the Port of Tauranga applied for and received resource consent to dredge about 15 million cubic metres of material from the harbour channels to enable access by larger capacity cargo vessels. This consent was then subject to an appeal to the Environment Court. During the appeal, it was suggested that the ebb tidal delta may be in a sensitive equilibrium between the supply of sediment by littoral drift, and the flushing associated with tidal circulation. Since dredging could alter the tidal circulation over the ebb tidal delta, it was suggested that the delta could suddenly undergo erosion. Any erosion of the delta could result in severe erosion of Matakana Island to replace the sediment lost from the delta.

Since the delta morphology controls wave refraction patterns, sediment transport and adjacent shoreline dynamics, minor changes in delta configuration have been shown to have pronounced effects on the erosion and accretion of adjacent shorelines (Oertel, 1977). The geomorphic stability of these sand bodies are important to adjacent shoreline morphodynamics, as a reduction in size, a change in position or loss of sediment volume have the potential to alter physical processes and promote coastal change. Preliminary analysis of bathymetric survey data indicated that Matakana Island shoreline from 1968 to 2004 was very dynamic and unstable, with the southeastern end of Matakana Island (Panepane Point) changing its position by up to 165 m since 1968 (Figure 1-3). Panepane Point is recognised as containing sites of significant cultural importance to local *iwi*, and these require protection from erosion. A review of the previous studies indicated that insufficient data were available to evaluate the likelihood of this scenario occurring.

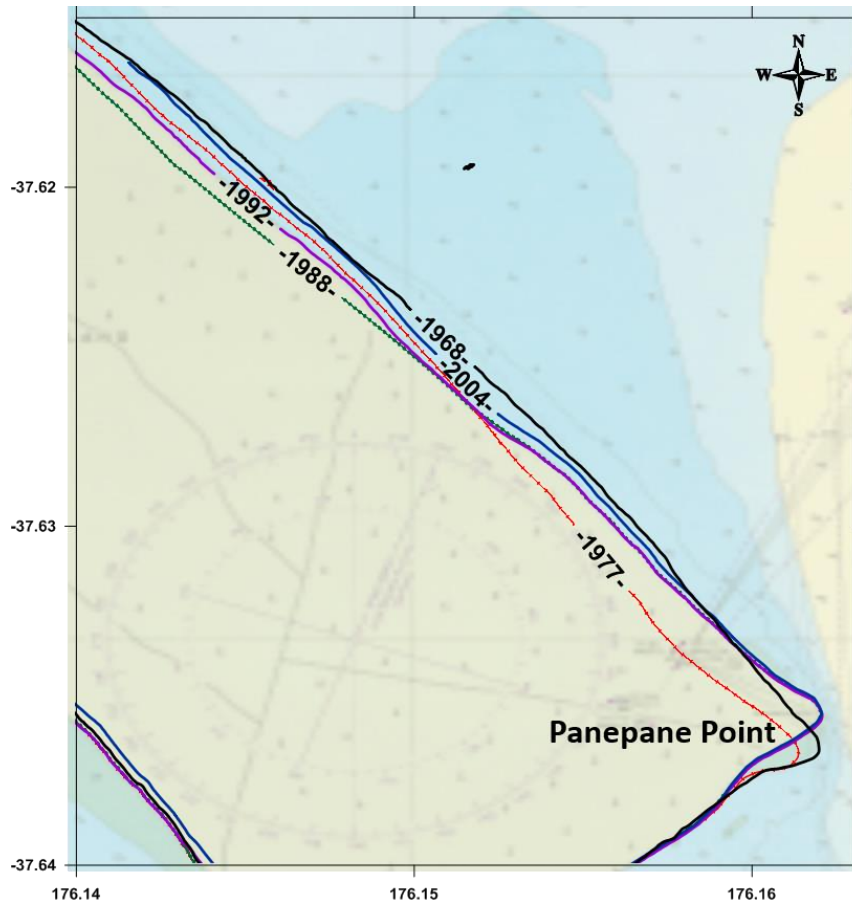


Figure 1-3. The Matakana Island's shoreline positions from 1968 to 2004 digitized from historical NZ541 hydrographic charts. The underlying image is the 1992 chart

Further, it was proposed in the Environment Court that a possible mitigation measure would be to renourish the ebb tidal delta to replace any sediment lost as a consequence of the dredging. Such renourishment would need to be undertaken in a manner that minimises the sedimentation within the Entrance Channel, and hence the frequency and volume of maintenance dredging. Therefore, the Environment Court decision indicated that it is necessary to ascertain the following:

- Is littoral drift is occurring along Matakana Island and feeding sediment to the ebb tidal delta, and if so, at what rate?
- If littoral drift is significant, would supplying extra sediment to the littoral drift renourish the ebb tidal delta?

- If dredge spoil is to be used to renourish the ebb tidal delta, where is the most suitable location for the disposal site to mitigate erosion while minimising maintenance dredging of the Entrance Channel.

1.2 Aims and Objectives

The rate of littoral drift along the Matakana shoreline is very uncertain, and previous studies have estimated the rate from the volume of maintenance dredging within the Entrance Channel cut through the ebb tidal delta (Healy et al., 1996). These estimates assumed that all of the excess sediment was derived by littoral drift, which may not be a valid approach. Therefore, it was considered important to examine the sediment transport patterns over the ebb tidal delta first in order to assess the sources and sinks of sediment, and determine the impacts of dredging.

Hence, the aims of this research are to identify and characterise the processes that control the stability of the Matakana Banks ebb tidal delta and to assess the impacts of dredging and potential mitigation measures. There are 5 basic questions which are addressed in this study;

- [1] What changes in ebb-tidal delta morphology were evident following capital dredging?
- [2] How did the ebb-tidal delta respond to biannual maintenance dredging? What changes in ebb-tidal delta size (volume and area) and shape were noticeable? Are there separate sub-region based on morphology and hydrodynamic regime that respond differently to forcing?
- [3] How well does process-based morphological modelling simulate the hydrodynamic processes in the tidal inlet and over the ebb-tidal delta? To what extent can this approach be utilized to predict dredging impacts?
- [4] What is the pattern of sand movement? What is the rate of change of the ebb-tidal delta, and what is the main hydrodynamic regime controlling the ebb-tidal delta sediment budget/volume?
- [5] What are the impacts of maintenance dredging and spoil disposal on the ebb-tidal delta?

Specific objectives include:

- 1) Collate relevant data from previous studies and topographic maps to characterise the historic morphodynamic changes of the Matakana Banks ebb tidal delta and environs.
- 2) Identify the main hydrodynamic and sedimentological controls on the stability of the ebb tidal delta at Tauranga. This includes:
 - a. Observations and mapping of surficial sediment characteristics and hydrodynamic processes.
 - b. Quantifying the temporal and spatial morphological changes of the ebb shoals on Matakana Bank using bathymetric mapping, in order to characterise the pre-dredging stability of the ebb tidal delta.
 - c. Laboratory analysis of surficial sediment samples to assess textural and strength characteristics.
- 3) Assessing the availability of sediment for transport.
- 4) Calibration and verification of numerical models to simulate hydrodynamic and morphological processes along Matakana Island and over Matakana Banks.
- 5) Simulation of different dredging and spoil disposal scenarios to assess the optimal management strategy.

1.3 Thesis Outline

In order to achieve the specific objectives the thesis is structured as follows:

Chapter 1 provides a rationale for the study and sets out the aim, research questions and specific objectives.

Chapter 2 provides an outline of the physical setting of Tauranga Harbour based on previous studies investigating hydrodynamics, sediment dynamics and climate variations. The dredging history for Tauranga Harbour, particularly the locations and dredged volumes from 1998 to 2014, are presented in this chapter.

Chapter 3 describes the general morphodynamics of tidal inlet and ebb-tidal delta systems, including the definition of an ebb tidal delta and the characteristics of processes that influence an ebb tidal delta. A mathematical model to simulate tidal flow, wave effects, sediment transport, and morphological changes due to, dredging and dumping activities in the coastal environment is presented.

Chapter 4 summarises the morphological evolution of the Matakana Banks ebb tidal delta based on previous studies, an analysis of single beam echo sounder (SBES) bathymetric data from 1998 to 2011, and from multi-beam echo sounder (MBES) bathymetric surveys in 2013 and 2014.

Chapter 5 presents the results of hydrodynamic measurements and sediment sampling conducted for 27 days on between April and May 2013.

Chapter 6 summarised the numerical model calibration and validation for the stand-alone Delft3D FLOW model and coupled Delft3D FLOW/WAVE models.

Chapter 7 presents the results of simulations of alternative spoil disposal sites, and different wave scenarios. Morphological model results based on the different forcing scenarios are also presented in this chapter.

Chapter 8 contains the conclusions of the study and makes recommendations for further study.

1.4 References

Brannigan, A. (2009). *Change in Geomorphology, Hydrodynamics and Surficial Sediment of Tauranga Entrance Tidal Delta System (MSc Thesis)*.

Hamilton, New Zealand: University of Waikato.

Healy, T., Mathew, J., de Lange, W.P., and Black, K.P. (1996). Adjustment toward equilibrium of a large flood-tidal delta after a major dredging program, Tauranga Harbour, New Zealand. *Coastal Engineering*, 3284-3294.

Oertel, G. (1977). Geomorphic cycles in ebb tidal flats and related patterns of shore erosion and accretion. *Journal of Sedimentary Petrology* Vol. 47, Issue 3., 1121-1131.

Chapter 2: Tauranga Harbour: History and Previous Dredging Studies

2.1 Introduction

This chapter presents the physical setting and the hydrodynamic condition in the vicinity of Tauranga Harbour, the brief geological history of Matakana Island in regards to the morphological variability of its ebb-tidal delta, and the dredge and dumping activities within the Tauranga Harbour vicinity. A review of studies on the impact of dredging and dumping will be also presented.

2.2 Physical Setting and Hydrodynamics

Tauranga Harbour is a mesotidal estuary located on the northeastern coast of the north island of New Zealand, and formed behind two tombolos and a barrier island (Davies-Colley and Healy, 1978). The harbour is characterised as a drowned valley complex with numerous marsh and tidal flat bounded reentrants along its margin (Davis Jr and Healy, 1993). The low gradient and wide shallow region that fronted the Tauranga Harbour's coast caused the area to be prone to coastal flooding and exacerbate coastal erosion by the storm surges and the wind stress effect (de Lange and Gibb, 2000).

The harbour is enclosed by two Holocene barrier tombolos linking rhyolite domes (Mauao and Bowentown) to the mainland, and the Pleistocene/Holocene barrier island of Matakana Island. At present, there are two tidal inlets located adjacent to the rhyolite domes: Katikati Entrance to the northwest, and Tauranga Entrance in the southeast. There is limited exchange of water between the two entrances due to shallow intertidal flats in the middle of the harbour, effectively creating two basins; the Katikati basin in the northwest and Tauranga basin in the

southeast (Spiers *et al.*, 2009). Hence, the Tauranga basin may be considered independent from the northern Katikati basin (Barnett, 1985).

An ebb-tidal delta is a complex of shoals and channels on the seaward side of an inlet. The delta is formed from a combination of sand eroded from the gorge of the inlet and sand supplied by longshore currents. FitzGerald (2012) stated that the ebb-tidal delta consists of sand that is intercepted from the longshore transport system and is carried seaward and deposited by ebb-tidal currents, where it is subsequently modified by incident waves and ambient tidal currents. This suggests that the long-term stability of the ebb-tidal delta is dependent on the longshore transport system. However, the Tauranga Harbour Sediment Study (Hume, 2009) found that most of the sediment transport over the Matakana Banks involved the recirculation of sediment, with relatively little net transport occurring over time.

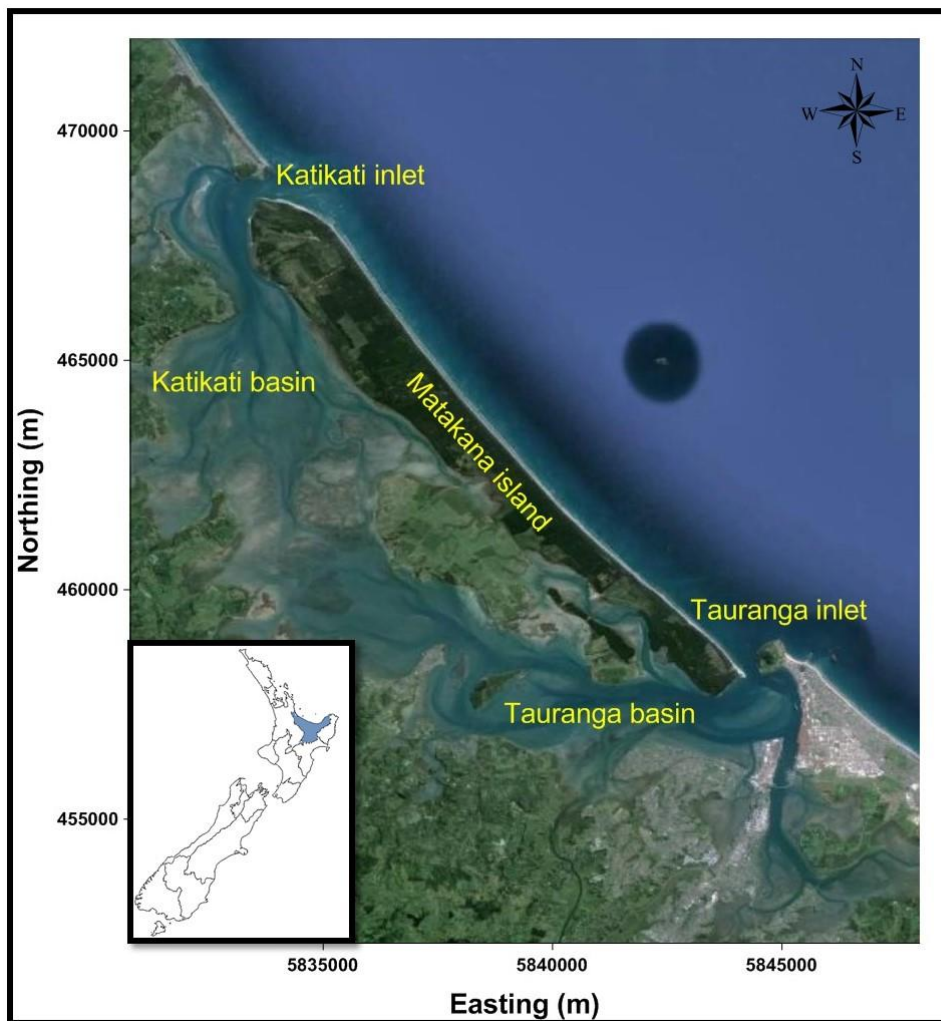


Figure 2-1. Tauranga Harbour comprises of Katikati Entrance in the northwest and Tauranga Entrance in the southeast. The index figure shows the location of Bay of Plenty in the north island of New Zealand. (Aerial photo is modified from Google Earth in 2015).

The most important factors that control the sediment transport on ebb-tidal deltas are waves and tide-induced currents (Komar, 1996). Studies have shown that the ebb-tidal delta volume depends upon the tidal prism, inlet geometry, shoreline configuration, offshore bathymetry, wave climate, littoral drift, sediment characteristics and freshwater runoff (Liria *et al.*, 2009). Based on the ebb-tidal delta “residual topography” interpretation by Hicks and Hume (1996), they stated that volume of the Tauranga ebb-tidal delta is about $47.3 \times 10^6 \text{ m}^3$.

Matakana Banks extends over 3.5 km offshore from the Tauranga inlet throat (Mathew, 1997); (Ramli and de Lange, 2013a) and about 3.5 km to the northwest along Matakana Island (Ramli and de Lange, 2013a). This shallow shoal is always submerged and formed of fine to coarse sand derived from source rocks in the Taupo and Coromandel volcanic zones (Badesab *et al.*, 2012). Previous studies have indicated that the ebb-tidal delta has been largely stable in terms of its gross morphology between 1989 and 1995 (Healy *et al.*, 1996). These studies show that there has been no sudden or substantial change to the ebb-tidal delta that can obviously be linked to the entrance shipping channel deepening in 1992. Brannigan (2009) expanded the time period of ebb-tidal delta bathymetric evolution back to 1852, and considering the period from 1954 to 2006 that was associated with dredging, he found that although the ebb-tidal delta showed variations in depth of about 2 m, the overall morphology was stable.

The inlet throat, which acts as the harbour entrance, is approximately 500 m wide with a maximum water depth of 34 m and a mean depth 15 m (Kruöger and Healy, 2006). This inlet is a tide-dominated inlet, with a mean tidal range of 1.4 m and a mean annual significant wave height of 0.5 m (de Lange, 1993). Based on the comparison of shoreline positions between 1954 and 2006 (Brannigan, 2009), this tidal inlet has narrowed over 100 m (shoreline near Panepane Point). This is consistent with the results of previous studies by the (Wallingford Hydraulic Research Station, 1963) and (Barnett, 1985) which showed over 300 m decrease in tidal inlet width between 1852 and 1954. Further, based on the inferred age of the earliest relict foredune and shorelines defined by tephra or sea rafted pumice,

Shepherd *et al.* (1997 estimate about 2-3 km progradation of southeastern end of the Matakana Island over the last 600 years (Figure 2-2).

The sandy littoral system of Bay of Plenty extends from Waihi Beach in the northwest to Opape in the southeast (Krüeger and Healy, 2006). The Matakana Banks ebb-tidal delta is included in a littoral cell that extends from Waihi Beach to Okurei Point. Based on mostly geomorphic indicators, it is suggested that the predominant littoral drift direction is southeasterly (Healy and de Lange, 2014) with an estimated net drift magnitude of about 80,000 m³/y (Healy, 1980). Earlier, Ewart (1961); Gibb (1977); Harray and Healy (1978); and Macky *et al.* (1995) indicated that the long-term net littoral drift on the Bay of Plenty coast appears to generally towards the southeast but, at least in the western part of the Bay (around Tauranga Harbour), is small compared to the gross drift.

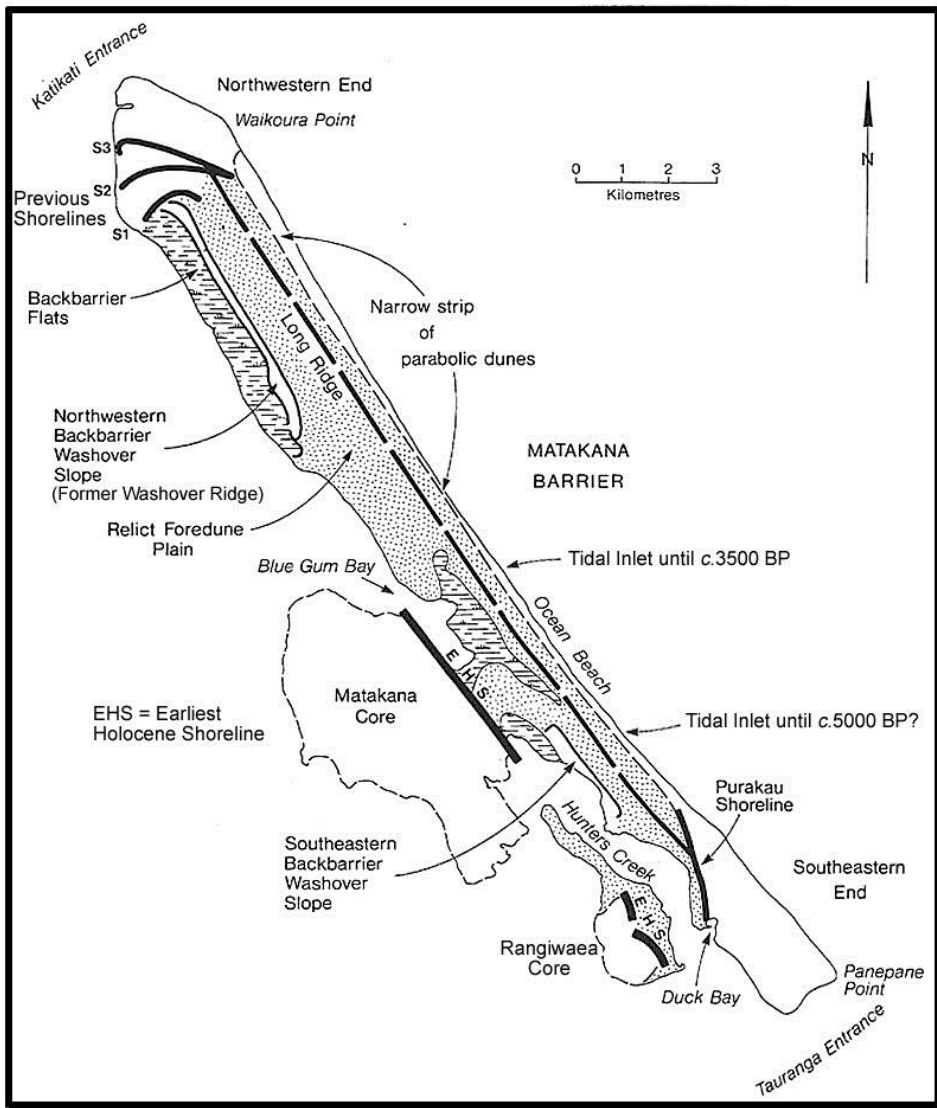


Figure 2-2. The major geomorphologic units of Matakana and Rangiwaea Islands, and the locations of former tidal inlets. EHS = Earliest Holocene Shoreline; S1 and S2 = Eroded shorelines; S3 = Kaharoa shoreline. (After Shepherd et al, 1997)

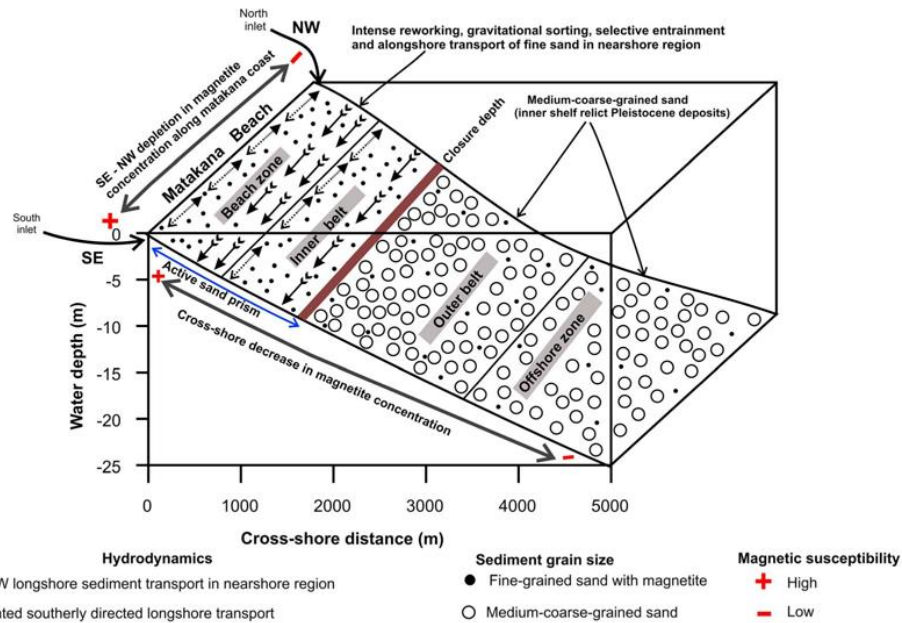


Figure 2-3. Conceptual model for nearshore and inner shelf dynamics off Tauranga Harbour (modified from Bradshaw *et al.*, 1994). Figure taken from Badesab *et al.*, 2012.

The most recent study of longshore transport along Matakana Island and the vicinity of Matakana Banks was done by Badesab *et al.* (2012) who used the spatial distribution of magnetite minerals as a tracer to track sediment transport within Tauranga Harbour and along the inner shelf between Waihi Beach and Omanu Beach east of Tauranga Harbour. Using a seven year wave data simulation, they indicated that longshore transport along the Matakana Island is bidirectional, but overall is southeasterly directed. The conceptual model for inner-shelf dynamics and sediment dispersal on the east Coromandel shelf of Bradshaw *et al.* (1991) and Bradshaw *et al.* (1994), demonstrates that the northerly-directed transport of coarse grained sand occurs during stormy condition and became the basis for hypothesis of Badesab *et al.* (2012), which states that alongshore transport only occur within the 10 m depth boundary along Matakana Island shoreline. Within this boundary, they suggest that the wave induced transport (< 6 m depth) along Matakana Island is towards southeast, and the innershelf transport occurring at a depth of 6 – 10 m is towards the southwest (Figure 2-3). However, Healy and de Lange (2014), stated that the rates and magnitude of the longshore sediment transport along Matakana Island and in the vicinity of Matakana Banks is still very uncertain.

2.3 Morphological Variability of the Matakana Banks Ebb-Tidal Delta

2.3.1 Century Time Scale Evolution

Variations in ebb-tidal delta morphology have also been linked to cyclical patterns of erosion and deposition of adjacent shorelines (Oertel, 1977); (Hume and Herdendorf, 1992); (FitzGerald *et al.*, 2002); (Robin *et al.*, 2009); and (Hansen *et al.*, 2013). The evolution of the Matakana Banks ebb-tidal delta is linked to the evolution of the adjacent Matakana Island barrier system. Their interaction is demonstrated by bulges in the beaches at the both ends of Matakana Island, which form the Bowentown Bar at the northwestern end and Matakana Bank at the southeastern end (Healy *et al.*, 1997). The Matakana Barrier is an accumulation of coastal sediments that contains extensive Quaternary alluvial valley-fill deposits (Davis Jr. and Healy, 1993), predominantly sand (Shepherd *et al.*, 1997). The barrier island appears to be developed by northward and southward longshore spit extension from an initial Holocene beach formed against Pleistocene outcrops (Dahm, 1983). Shepherd *et al.* (2000) classified the island into two distinct parts (Figure 2-4):

- (1) the larger, seaward unit, comprises of a 24 km length of Holocene sand barrier that stretches parallel to the oceanic shoreline, and
- (2) the landward unit, which adjoins the centre of the Holocene barriers, consists of Pleistocene terraces overlain by a mantle of tephra and other cover deposits.

The initial development of the Holocene barrier involved at least three parts: a northwestern; a central; and a southeastern part. These were separated by tidal entrances at Blue Gum Bay and between Matakana and Rangawea Island (Figure 2-5). The southeastern part, which is adjacent the Pleistocene core of the island, and the northwestern part enclosed the Katikati basin of Tauranga Harbour to the northwest. Unlike the steady progradation of relict foredune that forms the main part of the barrier, the landforms at each end of the barrier indicate more complex progradational histories. Both ends are lower than the rest of barrier, are characterized by wetlands, and have many ridges which often converge and diverge reflecting past changes in the shape of the harbour entrances. The southern end

(Panepane Pt) is characterized by hummocky dunes and few indistinct broad shoreline ridges (Shepherd *et al.*, 1997).

Further, Shepherd *et al.* (1997); (Shepherd *et al.* (2000) recognized the key landforms of the Matakana barrier as shown in Figure 2-5, which are briefly described as follows:

- Remnant *Pleistocene terraces*, which form the cores of Matakana Island and Rangiwaea Island. These are the landward components of the barrier system and they merge with the *Holocene barrier* at their seaward margins. Gibb (1986), determined that the Earliest Holocene Shoreline (EHS) consists of small sea cliffs that were formed at the end of the Postglacial Marine Transgression, which ended c. 7200 year BP when present sea level was reached around New Zealand.
- *Backbarrier washover slope*. Washover contributes to the sediment budget of barrier islands. Washover deposits are formed by the sand being washed over a barrier island, particularly during severe storm waves and/or by storm surges, and deposited on the landward side of the barrier. These deposits may range from a few centimetres to a few metres in thickness (SEPM STRATA., 2012), and may extend inland 100 m or more (Dean and Dalrymple, 2002). Overwash is also believed to be a major process in the retreat mechanism of some coastal barriers in response to sea level rise (Dillon, 1970); (Kraft *et al.*, 1973). At Matakana Island, these deposits are found on the harbour margins of both the north-eastern and south-western ends of the barrier, and vary between 180 m and 360 m wide. Dating of the Matakana innermost backbarrier washover deposits show ages between about 7600 to 5700 yr BP, and the soil at north-western end of the island has an age of about 1500 yr BP (Shepherd *et al.*, 1997).
- *Relict foredune plain*. This landform extends from the Pukarau Shoreline at the southeastern end of the barrier (Figure 2-2) to Shorelines S1, S2 and S3 at the Katikati Entrance, and from the EHS to the present shoreline. The landform consists of a series of linear features aligned parallel to the Holocene marine cliff, which represent relict foredunes of the Holocene barrier. These features are revealed in oblique aerial photographs by the presence of subdued ridges trending parallel to the present coastline (Shepherd *et al.*, 2000). Shepherd *et al.* (2000) argue that this feature is a buried Pleistocene surface

overlain by a thin veneer of Holocene sediment, and that the maximum age of this landform is c. 780,000 years.

- *Barrier ends.* At the northwestern end of Matakana Island, the older dune ridges are truncated by various periods of coastal erosion that were then followed by the formation of younger ridges. In Figure 2-2, it is shown that these younger ridges progressively moved further offshore. At the southeastern end, accretion has moved the shoreline c. 120 m seaward of the former Pukarau shoreline since c. 600 cal BP, indicating a seaward progradation rate of 0.2 m.y⁻¹. Middens, containing shell material that represent anthropogenic activities, found within this region have an ¹⁴C age of 751 ± 37 yr BP (Shepherd *et al.*, 1997). The southeastern end has also prograded 2-3 km towards the present tidal inlet in this time.
- *Contemporary foredune and beach.* The foredune height varies between approximately 1.7 m near the central part of the barrier to approximately 4 m near the harbour entrance (Shepherd *et al.*, 1997). Near to Panepane Point, the foredunes have been affected by shoreline erosion of more than 100 m since reaching the maximum seaward position in 1954 (Healy, 1977).

From the geomorphic features that reflect the development stages of the barrier island, it is evident that there were up to 4 tidal inlets prior to 5000 BP, the present day inlets, the Blue Gum Bay entrance, and entrance between Matakana and Rangiwaea Island (Figure 2-2). Spit extension of both ends of Matakana Island and the formation of successive foredune as the shoreline prograded seawards were probably the cause of the closure of the central entrances. The migration and eventual closure of the tidal inlets would influence the position and stability of any attached ebb-tidal delta. With the eventual closure of the entrances, it is likely that the sediment forming the ebb-tidal delta would have been redistributed along the barrier (Shepherd *et al.*, 1997). However, the channel lag deposits are likely to be preserved and can be detected by sub-bottom profiling.

It is not certain that the existing tidal inlets co-existed with the 2 central tidal inlets that have now closed. In particular, the existence of shallow Pleistocene ridges across the present day Tauranga Entrance (de Lange *et al.*, 2014) indicate that the tidal inlet could only have formed late in the Flandrian Marine Transgression. At least one ridge is exposed within the Entrance Channel, where it

has been excavated to a depth of 14.1 m below Chart Datum. The data of Gibb (1986) indicates that this depth corresponds to sea level between 7800-8500 BP. Seismic data indicate that before dredging the top of the ridge was located closer to 10 m below Chart Datum, which corresponds to younger ages between 7200-7800 BP. Most of the deepening and development of the tidal inlet has been observed since 1852 (de Lange *et al.*, 2015), possibly due to scouring resulting from increasing confinement of the tidal flows, and increased flows during major tsunami events.

Several important events that occurred around 600 BP, which may have influenced the evolution of Matakana Banks ebb-tidal delta, are also recorded as stratigraphic units found at the Matakana Island;

- Loiseles Pumice was deposited along the Pukarau Shoreline. This is a distinctive pumice type that derives from multiple eruptions and/or volcanoes in the oceanic Tonga-Kermadec arc north of New Zealand (Shane *et al.*, 1998). This deposit has an age of approximately 650 years BP (McFadgen, 1985) and its presence at Matakana Island is thought to link to a large regional tsunami around AD 1400, which is likely responsible for the erosion of both ends of Matakana Island (McFadgen, 2007). Since the deposition of the Loiseles Pumice, the southeastern end of Matakana Island has prograded by 2-3 km (Figure 2-4).
- Tephra of the Kaharoa Eruption from Mt. Tarawera was deposited at AD 1305 \pm 12 (Hogg *et al.*, 2003). A large amount of Kaharoa tephra was deposited on the harbour side of Matakana Island, but it is absent from the ocean side of the shoreline, suggesting the shoreline has accreted since the eruption. This accretion led to width of the northwestern opening reducing by 3 km (Law, 2008).
- Deforestation and gardening associated with human settlement on Matakana Island led to widespread destabilisation of coastal dunes (McFadgen, 2003); (Hawke and McConchie, 2006).

Panepane Point has prograded 2-3 km eastward since 600 BP (Figure 2-4), which resulted in a narrowing of the Tauranga Harbour Entrance. Within the period from the first complete bathymetric survey of the harbour entrance in 1852 to 1954, Panepane Point accreted 300 m eastward, and the harbour entrance had deepened

in response. Over this period the ebb jet orientation became increasingly oblique to the shoreline, and the width of the jet decreased with an increase in velocity and offshore extent (de Lange *et al.*, 2015). Velocity increments that lead to deepening the entrance and modification of ebb jet and associated eddies, which are important factors influencing sedimentation on the ebb tidal delta, was also identified in the study of (Spiers *et al.*, 2009).

In conclusion, the evolution of Matakana Island, particularly its southeastern end (Panepane Point) provide important information in assessing the natural variability and stability of the adjacent ebb-tidal delta system against the potential effects of dredging the Entrance Channel.

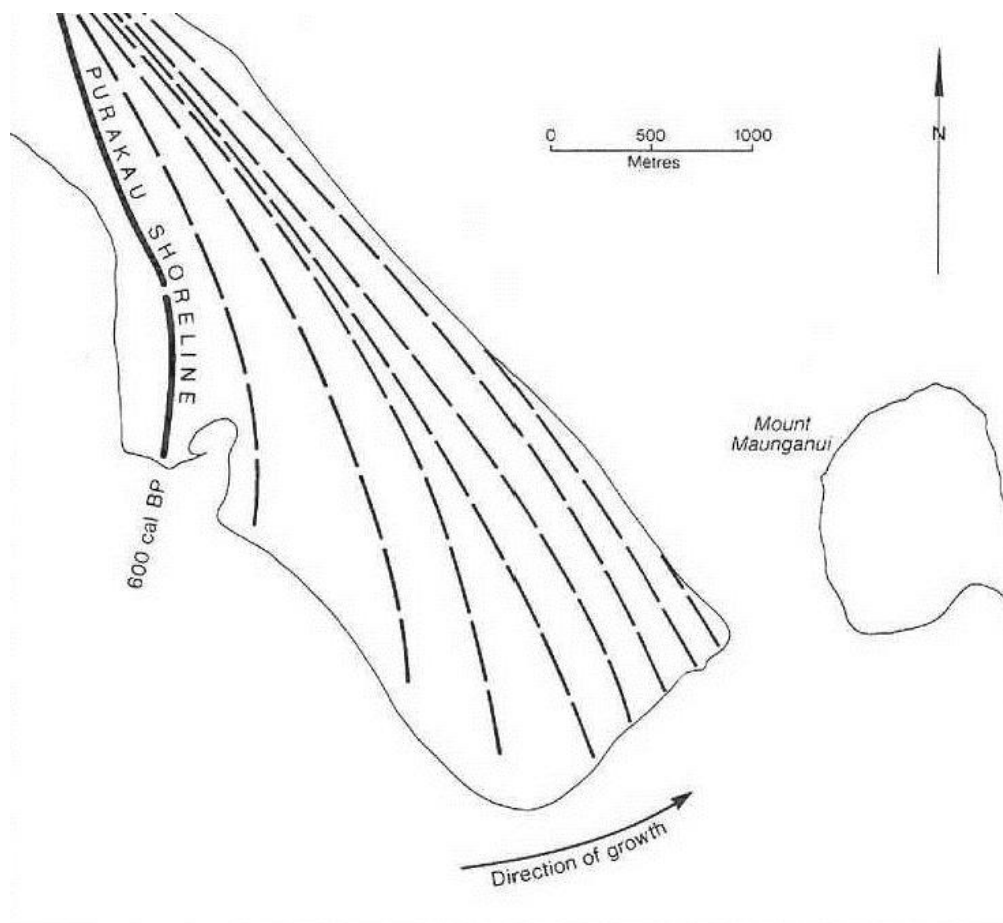


Figure 2-4. Inferred growth of the southeastern end of Matakana Island since 600 cal BP is estimated to be at about 0.20 m.y^{-1} seaward (c. 120 m), and 2-3 km towards the tidal inlet (Shepherd *et al.*, 1997).

2.4 Dredging and Dumping Activities

2.4.1 Dredging Types and Techniques

Dredging can be described as the process of removing part of the seabed or its overlying sediments with the aim of deepening the area commonly for the purposes of navigation or associated with construction projects. There are two types of dredging program that have been undertaken by the Port of Tauranga Ltd and its' predecessors; capital and maintenance works. Van Raalte (2006) describes these two types as follows:

a. Capital dredging works

Capital dredging involves the creation of new or improved facilities such as a harbour basin, a deeper navigation channel, a lake, or an area of reclaimed land for industrial or residential purposes. Such projects are generally characterised by the following parameters:

- relocation of large quantities of material,
- compact sediment,
- undisturbed sediment layers,
- low contaminant content (if any),
- significant layer thickness, and
- non-repetitive dredging action.

b. Maintenance dredging works

Maintenance dredging concerns the removal of siltation from channel beds, which generally occurs naturally, in order to maintain the design depth of navigation channels and ports. The main characteristics of maintenance dredging projects are:

- variable quantities of material,
- soft sediment,
- contamination possible,
- thin layers of material,
- occurring within navigation channels and harbours, and
- repetitive activity.

Appropriate dredging technique could optimise the benefits from projects as well as minimise environmental impacts. Selection of dredging equipment is

sediment specific, site specific, and operation specific. Further, Tamuno *et al.*(2009) listed factors that are usually considered for the selection of appropriate options in the UK including: task definition; access; vegetation cover, season, quantities and sediment characteristics, disposal, security of machinery during dredging, and environmental issues. However, no dredging technique is appropriate for all situations, and the duration of the proposed dredging is a determinant of the most appropriate technique that should be used (CIRIA, 1997).

Different types of dredging equipment and techniques are employed to achieve the required project outcomes in the most efficient way. Detailed of dredging equipment and techniques can be found in (USACE, 1983).

2.4.2 New Zealand Marine Dumping Legislation

Two legislative schemes give effect to New Zealand requirements for marine dumping of waste (MSANZ, 1999):

- the Resource Management Act 1991 (RMA) and the Resource Management (Marine Pollution) Regulations 1998.
- the Maritime Transport Act 1994 (MTA) and the marine protection rules in Part 80 – Dumping of Waste or Other Matter.

The former scheme applies to areas within the outer limits of the territorial sea of New Zealand (the coastal marine area or CMA); the latter applies to dumping beyond 12 nautical miles.

The application for resource consents/dumping permits must be directed to the appropriate issuing authority, as summarised in the Figure 2-5. In addition, both sets of legislation prohibit the dumping and storage of radioactive waste or other radioactive matter in the waters and seabed under New Zealand jurisdiction. The MTA also gives effect to a number of other New Zealand obligations under the 1996 Protocol, including prohibiting the export of waste or other matter to countries outside New Zealand for dumping or incineration at sea, and prohibiting the loading of waste on ships in New Zealand ports for the purpose of dumping, except where the appropriate permit/consent is held.

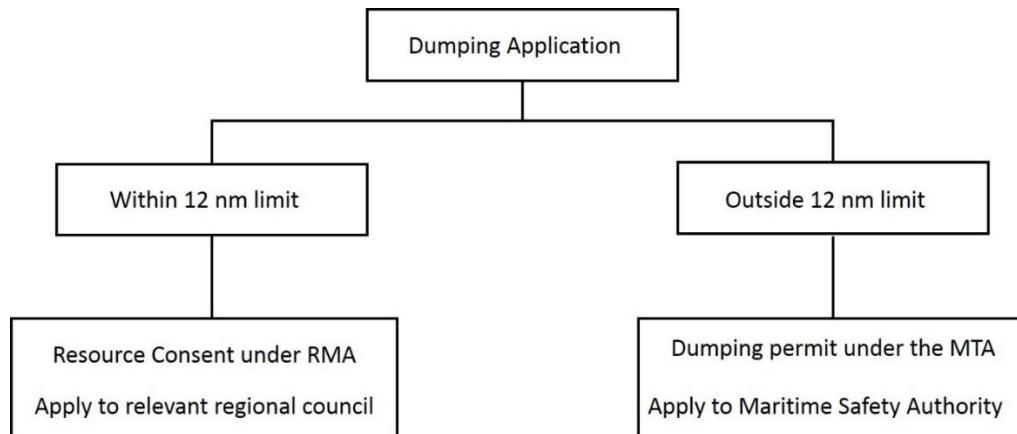


Figure 2-5. Issuing authority jurisdiction (MSANZ, 1999).

2.4.2.1 Within the Coastal Marine Area

Section 15A of the RMA establishes the primary requirement: no dumping may take place unless expressly allowed by a resource consent. The Resource Management (Marine Pollution) Regulations 1998, made under s360 of the RMA, deem the dumping of the wastes listed in the 1996 Protocol a discretionary activity in any regional coastal plan or proposed regional coastal plan. The dumping of any other waste is deemed to be a prohibited activity.

The regulations also require holders of coastal permits to dump to keep records describing:

- the types and sources of waste or other matter dumped
- the location of disposal sites
- the method of dumping
- the quantity of the waste or other matter dumped.

These records must be supplied annually to the Director of Maritime Safety. The Director of Maritime Safety provides this information to the International Maritime Organisation as part of New Zealand's obligations under the 1996 Protocol. For information on whether a particular proposal to dump waste in the CMA is a discretionary or prohibited activity, or whether it is required to be notified, applicants need to consult the Resource Management (Marine Pollution) Regulations 1998, the regional council exercising control over that part of the CMA and the relevant regional coastal plan. The regional council plan is prepared and administered by the regional council. The regional council is the consent authority

for coastal permits. The Minister of Conservation is the consent authority for “restricted coastal activities” including certain types of dumping.

Schedule 1 of the New Zealand Coastal Policy Statement (NZCPS) states that any proposal to dump in excess of 50,000 cubic meters of waste in any 12 month period is a restricted coastal activity, except if such dumping is designated in a regional coastal plan as a discretionary activity and for which the plan:

- defines or provides the criteria for determining the location where and the time during the dumping could be carried out
- requires consideration of the likely adverse effects of the dumping, and defines or provides the criteria for determining such effects.

The plan will also specify what information is required to be submitted with an application. For example, the plan will indicate what matters should be included in any application in addition to the requirements of the Fourth Schedule (which sets out the matters for assessment of a resource consent application under the RMA) and the requirements of Part 1 of Schedule 3 of the Regulations.

2.4.2.2 Beyond the Coastal Marine Area

Part XXI of the MTA establishes the framework for the application and enforcement of the standards and processes set out in the 1996 Protocol for dumping beyond the CMA. The specifics of the permitting regime and assessment are in the marine protection rules entitled *Part 180 – Dumping of Waste or Other Matter*. These rules require the Director of Maritime Safety to assess every application for a permit in accordance with the criteria, measures and requirements for the granting of dumping permits set out in the 1996 Protocols. The Director is also to have regard to these guidelines.

Permits for dumping beyond the coastal marine area are marine protection documents issued by the Director of Maritime Safety under s270 of the MTA. The process is summarised in Figure 2-6.

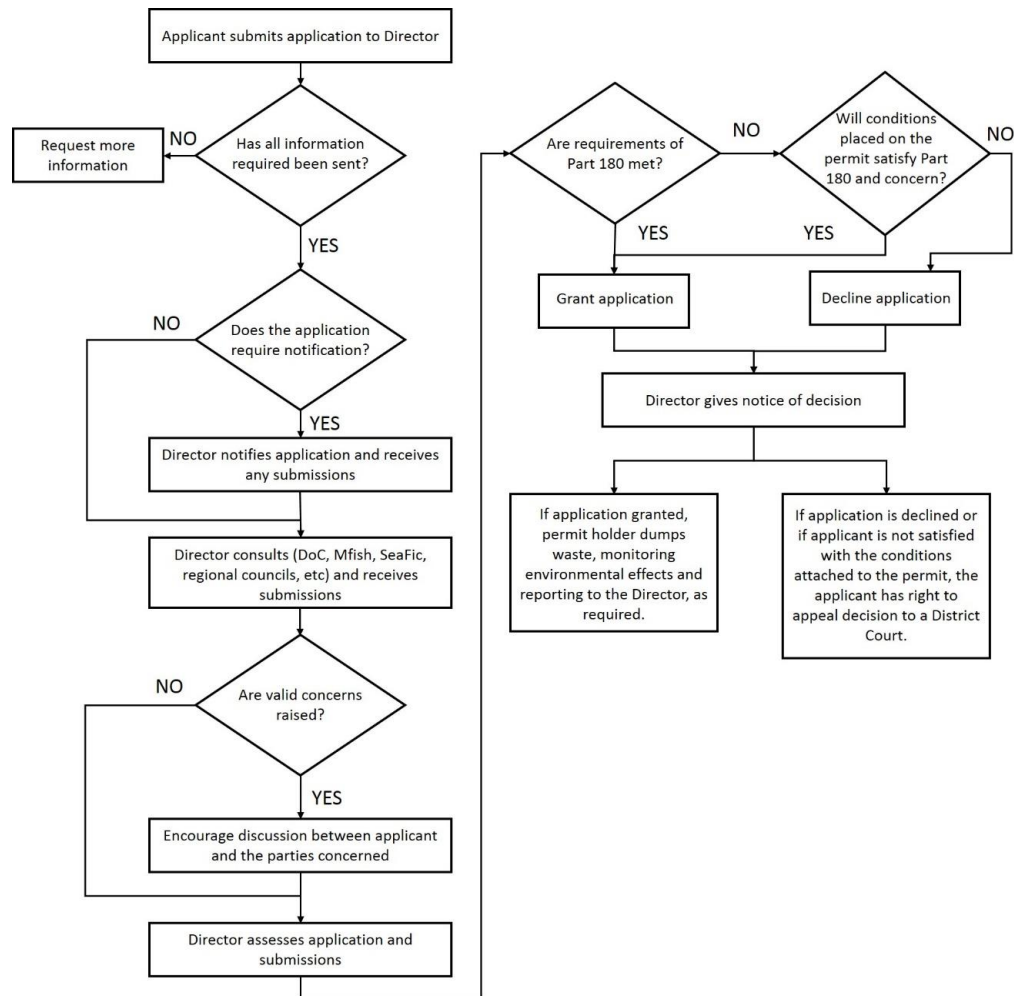


Figure 2-6. *Permits for dumping: application and assessment under the MTA (MSANZ, 1999).*

2.4.2.3 Resource Consents for Application Number 65806 and 65807

Port of Tauranga Limited (the Applicant) applied for a variety of linked resource consents to undertake the deepening of the main shipping channels and the entrance of Tauranga Harbour by dredging and the deposition and/or removal of the material from the coastal marine area.

The resource consents sought related to the dredging operation, disposal of the dredged material (request for an enlarged offshore disposal site (3,000 x 3,000 m) seaward of the main Mount Maunganui beach that had been granted previously), the right to remove some of the material so that it could be used for “beneficial use” such as for beach re-nourishment or use on land, and the diffuse discharge of sediment (turbidity) during dredging and disposal operations.

The Port Company proposed to deepen the channels from 12.9 m to 16.m below chart datum inside the Harbour entrance, and from 14.1 m to 17.4 m in the Entrance Channel. The objective of the proposal is to enable Port of Tauranga Limited to accept larger vessels of up to 7,000 TEU (Twenty-foot Equivalent Unit containers) with a maximum draught of 14.5 m and maximum length of 347 m, requiring a channel depth of up to 17.4 m depending on vessel speed.

The total volume material estimated to be dredged, over time, is up to 15 million m³ which is primarily marine sand (with some shell), some boulders and silt from the Tanea Shelf, and about 1.5 – 2.1 million m³ of fine sediment (i.e. more than 5% silt and clay).

The principal dredging method proposed was trailer-suction dredging for sand deposits in the Entrance Channel, Cutter Channel and northern Maunganui Roads (Figure 2-7). For the Stella Passage and turning basin, or when substantially finer sediments are encountered, a bucket excavator or back-hoe digger dredge was proposed. The dredging company undertaking the dredging has decided to also use a cutter suction dredge in the harder materials (Pleistocene silty sediments).

Disposal of the dredged material is based upon the existing consented disposal sites D (comprising an area 1,750 x 1,500 m) and G (comprising an area 2,300 x 1,300 m), which lie generally in water depths of 20 – 33 m chart datum. The outer site G is the existing muddy material disposal site (Figure 2-7). Both disposal sites have been extended eastward (H1 and H2) to accommodate the volume of sediment to be extracted by capital dredging.

In summary, Coastal Permit 65806 obtained by the Port of Tauranga is to (Table 2-1):

- Remove up to 15 million m³ of material from the foreshore and seabed by dredging (Disturb the Seabed of Tauranga by Dredging);
- Deposit (up to 15 million m³) of the dredged material in the Coastal Marine Area; and
- Remove the balance (up to 10 million m³) of the dredged material from the Coastal Marine Area.

Coastal Permit 65807 (in summary) allows the Port to undertake the following activities associated with the dredging and disposal:

- Diffusely discharge sediment and water to Tauranga Harbour during dredging;
- Take coastal water from within the Harbour during dredging; and
- Disturb the Seabed of Tauranga Harbour by Maintenance Dredging.

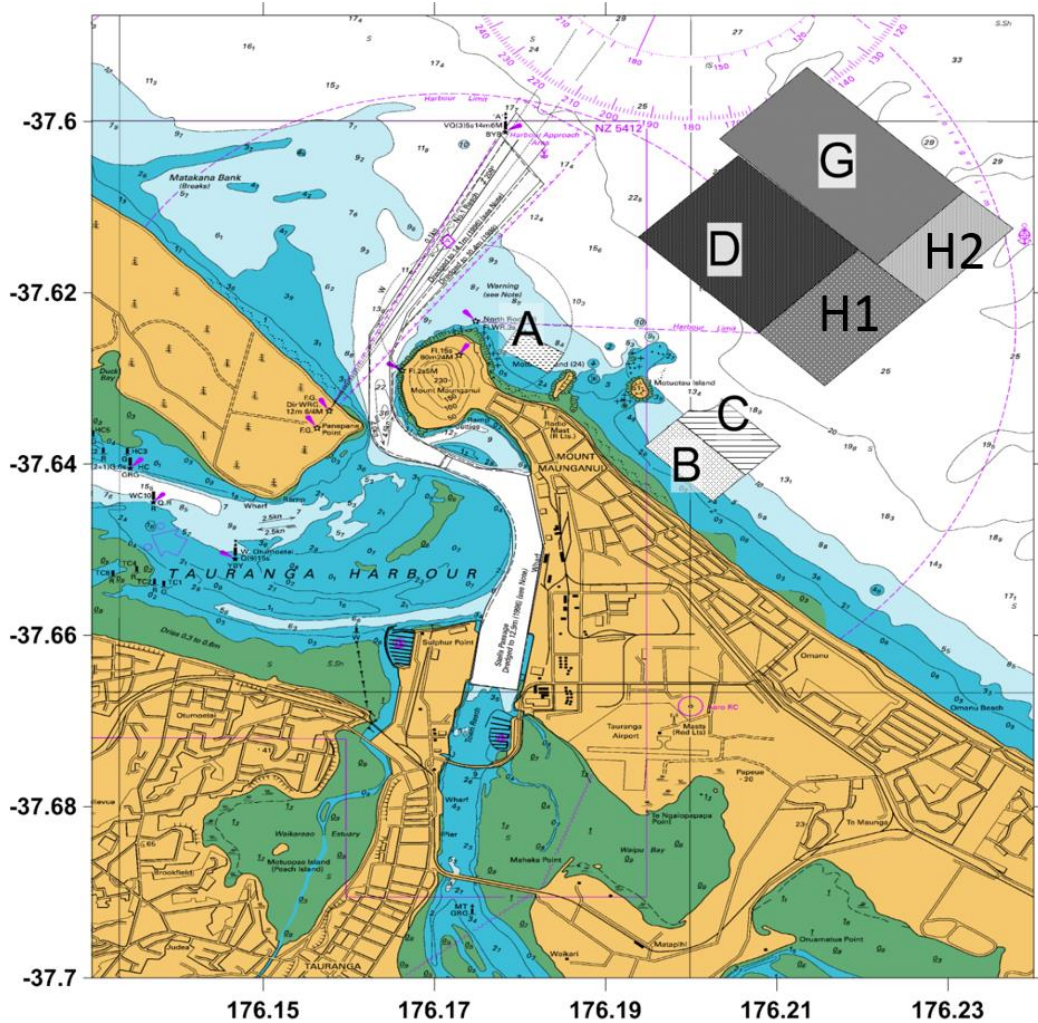


Figure 2-7. Existing spoil disposal (dump) sites, including the extensions granted as part of the consents for the 2015/16 Capital Dredging Programme (H1 and H2).

Table 2-1. Summary of the proposed dredging parameters (Source: Resource Management Act 1991, resource consents application number 65806 and 65807).

<i>Volumes, depths and materials to be dredged</i>			
<i>Locality</i>	<i>Description</i>	<i>Material description</i>	<i>Quantity m³ x 10⁶</i>
<i>Entrance Channel</i>	Depth 17.4 m	All sand	5.9
<i>Tanea Shelf</i>	Depth 17.4 m, widen 32 m	Silt and rocks	0.4
<i>Harbour</i>			
<i>Cutter Channel</i>	Depth 16.0 m, widen 50 m to 115 m	Sand	7.0
<i>Maunganui Roads</i>	Depth 16.0 m, widen 10 to 50 m	Silt	0.4
<i>Turning Basin</i>	Depth 16.0 m, widen 200 x 200 m		
<i>Stella Passage</i>	Depth 16.0 m, no widening	All silt	1.3
<i>Total</i>			15.0

2.4.3 Brief history of Port of Tauranga

The southern Tauranga Harbour is the location of the country’s largest export port, the Port of Tauranga (Foster, 1992). The early history of Tauranga Harbour was recorded in “Sketches of Ancient Maori Life and History” by Judge Wilson, who reported that the immigrants from Hawaiiiki arrived in approximately 1290 AD and found Te Awanui (as Tauranga was then named) in the possession of a tribe of aborigines (Port of Tauranga, 2013). Later following the arrival of Europeans, the coast and harbour area were surveyed and charted by Captain Drury in HMS Pandora in 1853, and the navigation channel for a Port was first defined in 1864 by the Marine Board Act of 1863. However, until the 1860s the Port did not possess a wharf, and it was common practice to load and unload cargo at low tide by ox carts operating between the beach at Tauranga and wooden sailing vessels (Port of Tauranga Ltd, 2011). At this time the entrance was wide and shallow (de Lange *et al.*, 2015).

The modern history of the Port began with early construction and growth in the 1950s based on the requirement to provide the best site in Bay of Plenty for a port to service the production forests and mills. The Government agreed to allow the authorities in the Bay of Plenty to built a deep sea wharf at Mt. Maunganui that was completed by November 1950, and operated by the Bay of Plenty Harbour Board. In the 1960s, Wallingford Hydraulics Laboratory of the UK was commissioned by the Board to undertake a study investigating improvements for

navigation approaches to the port. In order to keep pace with progress and demand, an almost continuous berth building programme had been undertaken, accompanied by channel and harbour deepening, reclamation works, construction of Port facilities, and the acquisition of floating and shore plant. In between 1961 to 1978, the maximum allowable draught for the Port was increased from 7.31 m to 10.7 m within the shipping channels. This development increased shipping activity and the Port's net register tonnage by 68% and 269% respectively (Port of Tauranga Ltd, 2011). During this period, the main wharf was lengthened from the original 372 m to 1,843 m (since lengthened to 2,060m).

Sulphur Point Wharf is a container terminal built on a reclaimed land, resulting from dredging of adjacent channels that commenced in 1965, and amounted to 90 hectares by 1990. The major Port extensions and adjacent Port facilities were completed in 1992 with a Capital Dredging Programme to deepen the main channels into the harbour. The wharf construction resulted in 600 m of wharf at Sulphur Point ready for use in April 1992, which has since been extended to a maximum of 1,155 m along Stella Passage, and a further 400 m on the northern face along the Otumoetai Channel. Wharf construction is a reinforced concrete deck poured on concrete piles with continuous fender piling. The deck loading withstands 60 tonne wheel or 120 tonne axle load, and has been extended to all wharves and paved areas. There is scope for specialised covered cargo handling and storage to be built by Port users to suit their requirements. Twenty seven hectares of paved open storage and handling areas, floodlit for 24 hour (seven days a week) operations has been developed.

2.4.4 Dredging and Dumping Programme in Port of Tauranga

Maintenance dredging of the navigational pathways at the entrance has been carried out since 1968 (Healy *et al.*, 1998). Prior to dredging in 1968, the natural channel depth reached 7-8 m through the ebb-tidal delta system, with the narrow inlet gorge attaining 30 m (Healy *et al.*, 1996). The first dredging and subsequent spoil disposal affecting the Tauranga Harbour entrance channel occurred in 1968. Subsequently, a biennial maintenance programme has become established to maintain the 7 km Entrance Channel at its' design depth.

Further capital dredging for port expansion in 1992 included deepening from 10 m to 13 m and widening the channels within the harbour, and deepening to 14.1 m within the Entrance Channel. Hence, the Port was able to handle vessels up to Length Overall (LOA) of 290 m (Port of Tauranga Ltd, 2011). The capital dredging in 1992 involved trailer-suction dredging of 5 Million m³ of sediment within the harbour and Entrance Channel (Healy *et al.*, (1991a); Mathew *et al.*, (1995); and Healy *et al.*, (1996)) consisted predominantly of sandy material with some shelly gravel (Healy *et al.*, 1991b), which was mostly disposed of in a large mound in Water Right Area 2192 (Michels and Healy, 1999) (Figure 2-7 – Site D).

Some sediment was also disposed of within the nearshore zone near Mt. Maunganui Beach (Site A) at water depths of 4-7 m below Chart Datum (Foster *et al.*, 1994) in order to renourish the ebb-tidal delta adjacent beach (Mt. Maunganui Beach). This effort was undertaken in the expectation that by dumping material dredged from the ebb-tidal delta close to the downdrift shore in a similar morphodynamic environment, it would act as a form of artificial bypassing (Foster *et al.*, 1996).

For dredged materials with significant silt and clay content, Michels and Healy (1999) suggested a disposal ground 17 km offshore at water depths of 28-33 m (Site G). This was based on the analysis of their data that dredged material of medium to coarse sand will only move during periods of large swells ($T_s = 11$ s, $H_s = 1.6$ m), and mud clasts (defined as cohesive sediment with <5% silt and clay) larger than ≈ 2 cm would be stable. Thus it was expected that this disposal ground would restrict dispersal of fine sediment.

Extra spoil disposal sites were developed under the Resource Management Act 1991 (the Act) and in the matter of applications for two Coastal Permits by Port of Tauranga Limited (Application Number 65806 and 65807) to dredge the main shipping channels in the Tauranga Harbour (up to 15 million cubic metres); depositing that material at identified sites within the coastal marine area; and also removing dredged material from the coastal marine area (up to 10 million cubic metres). The nearshore disposal site is located approximately 2 km offshore from Mt. Maunganui main beach and is described as Area D (Main Ocean) under consent 40157, which has a maximum deposition allowance of 720,000 m³ per year. The

largest annual volume of deposited within Area D within the 10 years from 2004 – 2014 was approximately 67,000 m³ (Ivamy and Reinen-Hamill, 2014). Port of Tauranga Ltd. (2013) describes that for the 2013 maintenance dredging and dumping campaign, sand-sized sediment from the Entrance Channel and No. 2 Reach went to sites B, C, and H1, while siltier sediment from Cutter Channel, Mt. Maunganui Roads and Stella Passage went to sites D, G, and H2 (Figure 2-7).

Tables 2-2 and 2-3 summarize the total volumes of dredging material from the Tauranga Harbour during the late 60s to late 70s and from the 90s to 2014 respectively. Between 1996 to 2014, the total dredged volume taken from the Entrance Channel was about 1.6 million m³ compared to about 2.8 million m³ in volume for the whole harbour (Table 2-3).

Table 2-2. Past dredging and dumping activities commenced in Tauranga Harbour during the late 60s to late 70s. Source: (Port of Tauranga Ltd, 2011).

Duration		Location	Quantity (m ³)	Depth (m)	Remarks	Capital / Maintenance
Start	Finish					
12 Jan 1969	15 Feb 1969	Entrance Trial	191,139	28.5ft	600ft wide, 1 & 2	Capital
26 April 1969	18 May 1969	Entrance Widening	120,799	28.5ft	Widening of West side. 3	Capital
8 April 1971	21 Sept 1971	Entrance Deepening	634,850	32ft	1 to 5	Capital
7 Jan 1974	5 March 1974	Entrance Deepening	389,923	33ft	1 to 7	Capital
5 May 1977	Sept 1977	Entrance Deepening	455,675	11	1 to 9	Capital
4 Nov 1977	22 Jan 1978	Entrance Deepening	108,567	11.3	1, 2 & 3	Capital
14 March 1978	9 July 1978	Entrance Deepening	304,293	11.6	Main Channel 2 to 4, 6, 8 & 10	Capital
			52,2995	10.7	East side Channel 1, 5, 7 & 9	Capital
1986		Entrance	197,248	11.2	Main Channel	Maintenance
			71,865	10.4	East side	Maintenance
1988		Entrance	24,083	11,3	Main Channel	Maintenance
1989		Entrance	57,492	11,3	Main Channel	Maintenance
				10.4	Side Channel	Maintenance
11 March 1968	31 Dec 1968	Cutter Channel	1,452,599	30ft	300ft. Bottom Width. 1	Capital
8 April 1971	21 Sept 1971	Cutter Channel	54,281	30ft	Widening to 400ft. 1 & 2	Capital
		Maunganui Roads	220,183	30ft	Widening on Western edge. 3 & 4	Capital
7 Jan 1974	5 March 1974	Cutter Channel	133,792	31ft	Widened to 450ft. 1, 2 & 5	Capital
5 May 1977	Sept 1977	Cutter Channel	128,695	10.4	Deepening. 1, 2 & 5	Capital
4 Nov 1977	22 Jan 1978	Cutter Channel	267,584	10.4	1, 2 & 5	Maintenance
27.02.78	28.04.78	Maunganui Roads	160,550	10.4	1,2 & 5	Maintenance
14.03.78	09.07.78	Cutter Channel	62,691	10.4	6	Maintenance
29.04.80	01.05.80	Cutter Channel	12,997	10.4	Sides and middle. 1, 2 & 5	Maintenance
27.02.78	28.04.78	Maunganui Roads	160,550	10.4	South side and middle. 7	Maintenance

Table 2-3. Dredging areas, materials and volumes during 90's to recently in 2014. Source: personal communication with Johnstone, 2014.

Dredge Areas	Material	Year and Volumes m ³												
		2014	Sept 2013	Sept 2012	July 2011	July 2010	Dec 2008	June 2006	July 2004	Aug 2002	Aug 2000	Nov 1998	Dec 1996	Total (m ³)
Entrance Channel	Coarse sand & shell	87,000	120,211	101,800	191,191	9,209	259,193	122,724	171,674	176,662	110,758	113,466	211,148	1,675,036
No 2 Reach	Shell and sand	10,000	17,890		29,323		12,254		825	11,541	27,834	12,033	6,260	127,960
Cutter Channel	Sand and shell			1,262	32,359		54,067	2,124	18,964	20,356	15,800		17,655	162,587
Maunganui Roads	Sand and shell	30,000	27,978	41,738	9,295	36,318	21,039	12,127	83,030	73,380	64,525	46,925	21,585	467,940
Stella Passage	Silt and sand	30,000	27,678	38,600	55,077		60,408	139,423	75,393	45,332	43,241	61,621	28,761	605,534
TOTAL		157,000	193,757	183,400	317,245	45,527	406,961	276,398	350,432	327,271	262,158	234,045	285,409	2,805,792

2.5 Previous Studies of Hydrodynamic and Morphodynamic Changes due to Dredging and Dumping

The effects of dredging and dumping in the environment are variable and depend on the estuarine area and other factors such as: magnitude and frequency of dredging and dumping, the sediment grain sizes, the density and composition of dredged material, the intertidal area dredged, the quality of water and sediment, the tidal range, the direction and intensity of tidal currents, the water mixing, the seasonal variability, the proximity to coastline, and the presence of biological communities (IADC/CEDA, 1998).

The impacts of dredging operations, particularly for ebb-tidal delta environments have been extensively studied, such as the study by Liria *et al.* (2009) where they investigated the effects of dredging operations on the hydrodynamics of an ebb-tidal delta combined with beach nourishment. The dredging and disposal affected the estuarine sediment dynamics and morphology by way of; (1) a permanent reduction in the tidal prism, due to the reclamation of the intertidal zones, and (2) changes in the natural shape of the main channel. Erosional trends for an ebb-tidal delta due to a reduction in the tidal prism of the estuary, and/or a decrease in sediment supply has been demonstrated by Dallas and Barnard (2009).

Changes to the morphology of ebb-tidal deltas have likely caused changes to wave refraction and focusing patterns and altered sediment transport pathways. Dredging activities may influence sediment transport pathways, which affect the morphodynamic conditions of the surrounding areas. The incorrect selection for dredged spoil sites can lead to the dumped material being transported by local water currents back into where it was originally dredged (Joyce, 1979). An unbalanced sedimentary regime, with increasingly accelerating changes, was linked to dredging and dumping activities by Monge-Ganuzas *et al.* (2012) through photo interpretation and identification of different sedimentary environments through temporal series of bathymetric surveys using GIS software. The dumping activities contributed to the short-term restoration of the supratidal area, but the mass of dumped sand was eroded rapidly by waves and tidal currents and re-introduced into the estuary through the tidal inlet. The sediment also accumulated on the ebb-tidal

delta, provoking an alteration in the pattern of the breaking waves (Monge-Ganuzas *et al.*, 2008).

Utilising numerical models in the studies of dredging and dumping impacts have enabled researchers to predict the short- and long-term responses of the morphodynamic of the surrounding areas. One example of this type of numerical model study was performed by (Beck and Wang, 2009). In their study, the hydrodynamics, sediment transport, and morphological changes were modelled using the Coastal Modeling System (Buttolph *et al.*, 2006) to assess the influence of channel dredging on flow and sedimentation patterns for microtidal inlets. They concentrated on three interactive aspects of short and long-term trends in morphological change: (1) the sediment bypass patterns, (2) natural patterns, and (3) combined natural and anthropogenically modified patterns.

Spiers *et al.* (2009) simulated the influence of a dredged sediment mound on local wave focusing patterns. Their study used the 3DD model suite (Black, 2006) and the results indicated that inshore wave heights were likely to be altered by the addition of a disposal mound at water depths between 27-31 m offshore. Previously, it was shown that reducing the water depths by the addition of spoil mounds enhanced the focusing of wave energy to the beaches adjacent the tidal inlet, depending to a degree on the shape of the mounds (Spiers and Healy, 2007). Increasing wave height was also claimed by Dallas and Barnard (2011) as one of the factors influencing ebb-tidal delta morphologic evolution (resulting in a decrease in its volume). Other factors which they mentioned were a reduction in tidal current strength due to a decrease in tidal prism, and erosion due to a decrease in sediment supply. Earlier studies of ebb-tidal delta evolution also indicated that the loss of tidal delta volume is associated with increasing wave energy.

Assessment the best strategy for dealing with the impact of dredging and dumping on the multiple channels of a combined ebb- and flood-tidal system was demonstrated by Jeuken and Wang (2010), using a sediment transport model based on the DELFT3D software package. They stated that degeneration of the channel systems occurs at large timescales. Therefore, a lot of historic data and system knowledge is required to allow for a careful analysis of the impact of dredging and dumping on the morphologic evolution of the channel or system. The recent study

of Wang (2015) on the sustainability of the multi-channel system under influence of dredging and disposal aimed to develop a method to produce better strategies for the disposal of dredged sediments, supporting decision making concerning sand mining and further deepening of navigation channels, and for monitoring the effects of human activities on the morphological development in the estuary.

Numerical models have also been applied to predict the sediment dispersion due to dredging, and from the associated disposal site (Foyle and Ireland, 2008), and also the sedimentation in the tidal drainage channels (Wang *et al.*, 2011). These models will be considered further in Chapter 3.

Sediment grain size analysis and the geotechnical behaviour of the sediments are important for assessing the stability of the dredge spoil material when deposited, as it may behave differently to the original material due to changes in the water content during dredging and transportation spoil disposal site. A simple method for characterising dredged material soil was suggested by Lee (2001), based on the American Society for Testing and Materials (ASTM).

Moon *et al.* (1994) monitored the geotechnical properties of dredged material placed disposal site D off Mt Maunganui for over a six-month period immediately after the disposal. Their aim was to determine the consolidation behaviour of the spoil mound, and the impact of dredged material on sediment transport behaviour. They found a high potential of bedload transport occurred immediately after deposition, due to the reduction of static friction angle (shear strength) of the dredged material during disposal. Earlier, as part of study to reduce the turbidity associated with disposal of spoil, Joyce (1979) monitored the behaviour of two different phases of fine sediment within dredge spoil as they are dumped into the marine environment. The study indicates that the solid phase (mud clasts) falls directly to the bed, where it forms a persistent deposit with a localized effect. Meanwhile, the semi-fluid phase is carried by the predominant currents in the form of a turbid cloud. The same behaviour was reported for “mud clasts” (>1-2 cm) by Michels and Healy (1999), in their evaluation for disposal of muddy-sand sediments at an inner shelf site off Tauranga Harbour.

Identifying morphological changes from bathymetric maps can be done directly by comparing the bathymetric maps from different periods. To quantify the

bathymetric differences due to accretion or erosion, the sand volume can also be calculated from measured cross-shore profiles, as demonstrated by Foster *et al.* (1994) for Ocean Beach, Mt. Maunganui, during a trial renourishment project using a shallow water disposal site. This work calculated the profile volumetric change (m^3) from the differences in height (m) between repeated profile measurements assuming a unit width (1 m). These changes were interpolated between adjacent profiles, and hence the area (m^2) that either accreted or eroded was determined.

Commercial mapping software, such as Golden Software Surfer, can be used to quantify the morphological and volumetric changes. The volume is calculated by three different methods including the Cut and Fill calculations; positive volume (Cut) (Golden Software, 2011). This method has been adopted by Hicks and Hume (1996) and Taaouati *et al.* (2011) to determine sediment volumes for ebb tidal deltas and beaches respectively.

The general stability of the gross morphology, but with significant localised changes, of Matakana Banks ebb-tidal delta was identified by Mathew *et al.* (1997) by comparing the bathymetry prior- and post channel dredging. They found that the proximal blind ebb channel northwest of Mount Maunganui infilled about 3.5 m between 1985 and 1989; and the deposition peaked during the dredging period. As a result of the infilling, the proximal blind ebb channel width reduced by about 100 m and its seaward extent decreased by about 50 m between 1989 and 1995.

A quantitative study of the impact of dumping of dredged material and the recovery of the seafloor after cessation of dumping was undertaken by Du Four and Van Lancker (2008). In their study, the approaches used include the interpretation of chrono-sequential single-beam echosounding, and high-resolution multibeam bathymetric and backscatter data ground truthed with boxcores. Their results show different morphological settings responded differently to the dumped sediment. The tide- and wave-driven currents rework the sediments and gradually winnow out the fine fraction. Hence homogenous sandy sediment was found at the initial sandy shoal dump site, and heterogeneous sediments were found in a tidal channel, where waves had a limited effect.

2.6 Summary

Tauranga Harbour is located on the northeast coast of the North Island of New Zealand. The harbour is a natural tidal lagoon protected from the open ocean (Pacific Ocean) by the Pleistocene/Holocene sand barrier known as Matakana Island, and two tombolos (Bowentown and Mt Maunganui). The ebb-tidal delta offshore of the Tauranga Entrance inlet throat, is known as Matakana Banks due to shallow shoals that extend over 3.5 km both along- and cross shore. This shallow shoal is always submerged and formed of fine to coarse sand derived from Taupo and Coromandel volcanic rocks.

Analysis of the historical charts indicates that the ebb-tidal delta has been largely stable in terms of its gross morphology (Healy *et al.*, 1996). However, based on the position of the shoreline, the tidal inlet has narrowed over 100 m between 1954 and 2006 due to the progradation of Panepane Point (Brannigan, 2009) that can be linked to the evolution of the ebb-tidal delta (Hicks *et al.*, 1999). The narrowing of the Tauranga tidal inlet has been detected in longer term analysis that showed Panepane Point has prograded 2-3 km eastward since 600 BP (Shepherd *et al.*, 1997). Between 1852 and 1954 Panepape Point advanced 300 m eastward (de Lange *et al.*, 2015). The increased tidal velocities as the result of tidal inlet narrowing have led to deepening of the entrance and modification of ebb jet and associated eddies, which then influence the sedimentation pattern on the ebb-tidal delta (Spiers *et al.*, 2009).

Ongoing development of the Port of Tauranga and changes to the nature of shipping traffic has required the Port to improve and maintain the shipping and navigation channel by commencing capital dredging in 2015, while continuing a biannual maintenance dredging programme. This dredging is based on resource consents 65806 and 65807, which permit the Port of Tauranga Ltd. to remove material from the foreshore and seabed and deposit the material in the Coastal Marine Area. Maintenance dredging since 1991 aimed to maintain the average channel depth outside and inside the harbour at 14.1 m, and between 10 m to 13 m respectively. The disposal sites for the dredged material was determined by the sediment size. Medium to coarse sand-sized sediment from the Entrance Channel and No. 2 Reach went to sites B, C, and H1 at depths less than 10 m, while siltier

finer sediment from Cutter Channel, Mt. Maunganui Roads and Stella Passage went to sites D, G, and H2 at depths greater than 20 m.

Extensive studies on the impacts of dredging and dumping activities on ebb-tidal delta have been published by coastal researchers. These identify that mostly the adverse impact is a reduction or imbalance in sediment budget for the system due to changes in sediment transport patterns and supply. Changes in the morphology that lead to changes in the hydrodynamic regime were also evident as an impact of dredging and dumping. Approaches used in these studies include the comparison of historical charts, photo interpretation and identification, repetitive bathymetric surveys, geotechnical tests in order to identify the behaviour of dredged material, and the application of numerical modelling for prediction of morpho-hydrodynamic changes. Overall, these studies aimed to develop better strategies for the disposal of dredged sediments, supporting decision making concerning sand mining and further deepening of navigation channels, and for monitoring the effects of human activities on the morphological development of estuaries (Wang, 2015).

2.7 References

- Badesab, F., von Dobeneck, T., Bryan, K.R., Mueller, H., Briggs, R.M., Frederichs, T., and Kwoil, E. (2012). Formation of magnetic-enriched zones in and offshore of a mesotidal estuarine lagoon: An environmental magnetic study of Tauranga Harbour and Bay of Plenty, New Zealand. *Geochemistry, Geophysics, Geosystems* Vol. 13. 1-20.
- Barnett, A. (1985). Overview and hydrodynamics. Tauranga Harbour Study, Parts 1 & III. Tauranga, New Zealand: Bay of Plenty Harbour Board.
- Barnett, A. (1985). Tauranga Harbour Study, Part I Overview, Part III Hydrodynamics. . Ministry of Works and Development.
- Beck, T.M., and Wang, P. (2009). Influences of channel dredging on flow and sedimentation patterns at microtidal inlets, West Central Florida, USA. *Coastal Dynamics*.
- Black, K. (2006). The 3DD computational marine and freshwater laboratory, Model WBEND. Version W5.3. Hamilton, New Zealand. : ASR Ltd.
- Bradshaw, B.E., Healy, T.R., Dell, P.M., and Bolstad, W.M. (1991). Inner-shelf dynamics on a storm-dominated coast, East Coromandel, New Zealand. *Journal of Coastal Research*, 11-30.

- Bradshaw, B.E., Healy, T.R., Nelson, C.S., Dell, P.M., and de Lange, W.P. (1994). Holocene sediment lithofacies and dispersal system on a storm-dominated, back-arc shelf margin: the east Coromandel Coast, New Zealand. *Marine Geology* Vol. 119, 75-98.
- Brannigan, A. (2009). Change in Geomorphology, Hydrodynamics and Surficial Sediment of Tauranga Entrance Tidal Delta System (MSc Thesis). Hamilton, New Zealand: University of Waikato.
- Buttolph, A.M., Reed, C.W., Kraus, N.C., Ono, N., Larson, M., Camenen, B., Hanson, H., Wamsley, T., and Zundel, A.K. (2006). Two-dimensional depth-averaged circulation model CMS-M2D: Version 3.0, Report 2: Sediment transport and morphology change. . Vicksburg, MS. USA.: US Army Engineer Research and Development Centre. .
- CIRIA. (1997). Inland dredging-Guidance on good practise. Construction Industry Research and Information Association (CIRIA). Westminster.
- Dahm, J. (1983). The geomorphic development bathymetric stability and sediment dynamics of Tauranga Harbour. MSc thesis in Earth Sciences. Hamilton, New Zealand: University of Waikato.
- Dallas, K.L., and Barnard, P.L. (2009). Linking human impacts within an estuary to ebb-tidal delta evolution. *Journal of Coastal Research*, 713-716.
- Dallas, K.L., and Barnard, P.L. (2011). Anthropogenic influences on shoreline and nearshore evolution in the San Francisco Bay coastal system. *Estuarine, Coastal and Shelf Science* Vol. 92. 195-204.
- Davies-Colley, R.J. and Healy, T.R. (1978). Sediment transport near the Tauranga Entrance to Tauranga Harbour. *New Zealand Journal of Marine and Freshwater Research* 12, 237-243.
- Davis Jr, R.A., and Healy, T.R. (1993). Holocene coastal depositional sequences on a tectonically active setting: southeastern Tauranga Harbour, New Zealand. *Sedimentary Geology*, 57-69.
- de Lange, W. P. (1993). Wave Climate for No. 1 Reach, Port of Tauranga Ltd. Hamilton, New Zealand: Department of Earth Sciences.
- de Lange, W.P. and Gibb, J.G. (2000). Seasonal, interannual, and decadal variability of storm surges at Tauranga, New Zealand. *New Zealand Journal of Marine and Freshwater Research* Vol. 34. , 419-434.
- de Lange, W.P., Moon, V., and Fox, B. (2014). Distribution of silty sediments in the shallow subsurface of the shipping channels of Tauranga Harbour. ERI report number 43 prepared for the Port of Tauranga Ltd. Hamilton, New Zealand: Environmental Research Institute, Waikato University.
- de Lange, W.P., Moon, V., and Johnstone, R. (2015). Evolution of the Tauranga Harbour Entrance: Influences of tsunami, geology and dredging.

Australasian Coasts & Ports Conference 2015 (pp. 1-6). Auckland, New Zealand. Australasian Coasts & Ports Conference 2015.

- Dean, R.G., and Dalrymple, R.A. (2002). Coastal Processes with Engineering Applications. Cambridge, UK. Cambridge University Press.
- Dillon, W. (1970). Submergence effects on a Rhode Island barrier lagoon and inferences on migration of barriers. . *Journal of Geology* Vol. 78, 94-106.
- Du Four, I., and Van Lancker, V. (2008). Changes of sedimentological patterns and morphological features due to the disposal of dredge spoil and the regeneration after cessation of the disposal activities. *Marine Geology*, 15-29.
- Ewart, A. (1961). Review of mineralogy and chemistry of acidic volcanic rocks of the Taupo volcanic zone New Zealand. *Bulletin of Volcanology* Vol. 29. pp. 147-171.
- FitzGerald, D. (2012). Morphodynamics and Facies Architecture of Tidal Inlets and Tidal Deltas. In R. Davies Jr., *Principles of Tidal Sedimentology* (pp. 301-333). New York: Springer Science+Business Media B.V.
- FitzGerald, D.M., Buynevich, I.V., Davies Jr., R.A., and Fenster, M.S. (2002). New England tidal inlets with special reference to riverine-associated inlet systems,. *Geomorphology* Vol. 48, 179-208.
- Foster, D. (1992). Environmental impacts of recent dredging and inner shelf spoil disposal at Tauranga. MSc Theses. Hamilton, New Zealand: Earth Science, University of Waikato. .
- Foster, G.A., Healy, T.R., and de Lange, W.P. (1994). Sediment budget and equilibrium beach profiles applied to renourishment of an ebb-tidal delta adjacent beach, Mt. Maunganui, New Zealand. . *Journal of Coastal Research*, 564-575.
- Foster, G.A., Healy, T.R., and de Lange, W.P. (1996). Presaging beach renourishment from a nearshore dredged dump mound, Mt. Maunganui Beach, New Zealand. . *Journal of Coastal Research*, 395-405.
- Foyle, L., and Ireland, N. (2008). Modelling of sediment dispersion due to maintenance dredging. Delft, The Netherlands: Deltares.
- Gibb, J. (1977). Late Quaternary sedimentary processes at Ohiwa Harbour, Eastern Bay of Plenty with special reference to property loss on Ohiwa Spit. Water and Soil Technical Publication No. 5. Wellington: Water & Soil Division, Ministry of Works and Development.
- Gibb, J. (1986). A New Zealand regional Holocene eustatic sea level curve and its application to determination of vertical tectonic movements. A Contribution to IGCP-project 200. International Symposium on Recent Crustal Movements from the Pacific Region. *Journal of the Royal Society of New Zealand Bulletin* 24, 377-395.

- Golden Software. (2011). Surfer Self-Paced Training Guide. Golden, CO. USA: Golden Software Inc.
- Hansen, J.E., Elias, E., Barnard, P.L. (2013). Changes in surfzone morphodynamics driven by multi-decadal contraction of a large ebb-tidal delta. *Marine Geology* Vol. 345, 221-234.
- Harray, K.G., and Healy, T.R. (1978). Beach erosion at Waihi Beach. *New Zealand Journal of Marine and Freshwater Research* Vol. 12, 99-107.
- Hawke, R.M., and McConchie, J.A. (2006). Dune phases in the Otaki-Te Horo area (New Zealand): a geomorphic history. *Earth Surface Process and Landforms* Vol. 31, 633-645.
- Healy, T. (1977). Progradation at the entrance, Tauranga Harbour Bay of Plenty, New Zealand. 90-92.
- Healy, T. (1980). Erosion and sediment drift on the Bay of Plenty coast. *Soil and Water*, 12-15.
- Healy, T., Mathew, J., de Lange, W.P., and Black, K. (1996). Adjustment toward equilibrium of a large flood-tidal delta after a major dredging program, Tauranga Harbour, New Zealand. *Coastal Engineering*, 3284-3294.
- Healy, T.R., and de Lange, W.P. (2014). Reliability of geomorphic indicators of littoral drift: examples from the Bay of Plenty, New Zealand. *Journal of Coastal Research*, 301-318.
- Healy, T.R., Harms, C., and de Lange, W.P. (1991a). Dredge spoil and inner shelf investigations off Tauranga Harbour, Bay of Plenty, New Zealand. *Coastal Sediment Conference (American Society of Civil Engineers)*, (pp. 2037-2051). Seattle, Washington.
- Healy, T.R., Harray, K.G., and Richmond, B. (1997). Bay of Plenty coastal erosion survey. Hamilton, New Zealand: Department of Earth Sciences, University of Waikato.
- Healy, T.R., Mathew, J., de Lange, W.P., and Black, K. (1996). Adjustment toward equilibrium of a large flood-tidal delta after a major dredging program, Tauranga Harbour, New Zealand. *Proceedings of the 10th International Conference on Coastal Engineering (ASCE)*, (pp. 3284-3294).
- Healy, T.R., McCabe, B., and Thompson, G. (1991b). Port of Tauranga Ltd. Channel Deepening and Widening Dredging Programme 1991-92 Environmental Impact Assessment. Hamilton, New Zealand: Waikato University.
- Healy, T.R., Thompson, G., Mathew, J., Pilditch, C., & Tian, F. (1998). Assessment of environmental effects for Port of Tauranga Ltd. Maintenance dredging and disposal. Hamilton, New Zealand: University of Waikato.

- Hicks, D.M., and Hume, T.M. (1996). Morphology and size of ebb tidal deltas at natural inlets on open-sea and Pocket-bay coast, North Island, New Zealand. *Journal of Coastal Research*, 12 (1), 47-63.
- Hicks, D.M., Hume, T.M., Swales, A., and Green, M.O. (1999). Magnitudes, spatial extent, time scales and causes of shoreline change adjacent to an ebb-tidal delta, Katikati Inlet, New Zealand. *Journal of Coastal Research* Vol. 15, Issue 1. 220-240.
- Hogg, A.G., Higham, T.G.F., Lowe, D.J., Palmer, J.G., Reimer, P.J., Newman, R.M. (2003). A wiggle-match date for Polynesian settlement of New Zealand. *Antiquity*, 116-125.
- Hume, T. (2009). *Tauranga Harbour Sediment Study: Hydrodynamic and Sediment Transport Modelling*. Hamilton, New Zealand: National Institute of Water & Atmosphere Research Ltd.
- Hume, T.M., and Herdendorf, C.E. (1992). Factors controlling tidal inlet characteristic on low drift coast. *Journal of Coastal Research* Vol. 8. Issue 2, 14-33.
- IADC/CEDA. (1998). *Environmental Aspect of Dredging: Investigation, Interpretation and Impact*. The Hague: International Association of Dredging Companies and Central Dredging Association.
- Ivamy, M., and Reinen-Hamill, R. (2014). *Opureora Dredging Spoil Disposal Assessment*. New Zealand: Tonkin & Taylor Ltd.
- Jeuken, M.C.J.L., and Wang, Z.B. (2010). Impact of dredging and dumping on the stability of ebb-flood channel systems. *Coastal Engineering* Vol. 57. 553-566.
- Joyce, J. (1979). On the behaviour of dumped dredged spoil. *Marine Pollution Bulletin*, Vol. 10. 158-160.
- Komar, P. (1996). Tidal-inlet processes and morphology related to the transport of sediments. *Journal of Coastal Research*, Special Issue No. 23, 23-45.
- Kraft, J.C., Biggs, R.B., and Halsey, S.D. (1973). Morphology and vertical sedimentary sequence models in holocene transgressive barrier systems. In *Publications in Geomorphology: Coastal Geomorphology*. (pp. 321-354). Albany, NY. : State University of New York.
- Krüger, J.C., and Healy, T.R. (2006). Mapping the morphology of a dredged ebb-tidal delta, Tauranga Harbour, New Zealand. *Journal of Coastal Research*, 22(3), 720-727.
- Law, G. (2008). *Archaeology of the Bay of Plenty*. Wellington, New Zealand: Science & Technical Publishing, Department of Conservation.
- Lee, L. (2001). *In Situ Expedient Test Methods to Determine Geotechnical Properties of Dredged Material*. DOER Technical Notes Collection (ERDC

TN DOER-N13). Vicksburg, Mississippi USA. : US Army Engineer Research and Development Centre. .

Liria, P., Garel, E., and Uriarte, A. (2009). The effects of dredging operations on the hydrodynamics of an ebb-tidal delta: Oka Estuary, northern Spain. *Continental Shelf Research* 29, 1983-1994.

Macky, G.H., Latimer, G.J., Smith, R.K. (1995). Wave observations in the western Bay of Plenty, New Zealand, 1991-94. *New Zealand Journal of Marine and Freshwater Research*, Vol. 29, 311-328.

Mathew, J. (1997). Morphologic changes of tidal deltas and an inner shelf dump ground from large scale dredging and dumping, Tauranga, New Zealand. PhD Thesis. Hamilton, New Zealand: University of Waikato.

Mathew, J., Healy, T.R., and de Lange, W.P. (1995). Changes to a large flood tidal delta system following major channel dredging, Tauranga Harbour, New Zealand. *International Conference on Coastal and Port Engineering in Developing Countries (COPEDEC)*, (pp. 1465-1478).

Mathew, J., Healy, T.R., de Lange, and Immenga, D. (1997). Ebb-tidal delta response to shipping channel dredging, Tauranga, New Zealand. *Combined Australasian Coastal Engineering and Ports Conference*, (pp. 823-828). Christchurch, New Zealand.

McFadgen, B. (1985). Late Holocene stratigraphy of coastal deposits between Auckland and Dunedin, New Zealand. *Journal of the Royal Society of New Zealand* Vol. 15, 27-65.

McFadgen, B. (2003). Pre-European archaeology of the coast. In J. N. Goff, *The New Zealand Coast* (pp. 265-296). Dunmore Press.

McFadgen, B. (2007). *Hostile shores: Catastrophic events in prehistoric New Zealand and their impact on Maori coastal communities*. Auckland, New Zealand: Auckland University Press.

Michels, K.H., and Healy, T.R. (1999). Evaluation of an inner shelf site off Tauranga Harbour, New Zealand, for disposal of muddy-sandy dredged sediments. *Journal of Coastal Research*, 830-838.

Michels, K.H., and Healy, T.R. (1999). Evaluation of an inner shelf site off Tauranga Harbour, New Zealand, for disposal of muddy-sandy dredged sediments. *Journal of Coastal Research*, 830-838.

Monge-Ganuzas, M., Cearreta, A., and Evans, G. (2012). Morphodynamic consequences of dredging and dumping activities along the lower Oka Estuary (Urdabai Biosphere Reserve, southeastern Bay of Biscay, Spain). *Ocean and Coastal Management* XXX. 1-10.

Monge-Ganuzas, M., Cearreta, A., Iriarte, E. (2008). Consequences of estuarine sand dredging and dumping on the Urdabai Reserve of the Biosphere (Bay

- of Biscay): the case of the "Mundaka left wave". *Journal of Iberian Geology* 34, 215-234.
- Moon, V., de Lange, W., Warren, S., and Healy, T. (1994). Post-disposal behaviour of sandy dredged material at an open-water, inner shelf disposal site. *Journal of Coastal Research*, 651-662.
- MSANZ. (1999). *New Zealand Guidelines for Sea Disposal of Waste*. Wellington, New Zealand: Maritime Safety Authority of New Zealand.
- Oertel, G. (1977). Geomorphic cycles in ebb-tidal delta and related patterns of shore erosion and accretion. *Journal of sedimentary Petrology* Vol. 47, Issue 3. 1121-1131.
- Port of Tauranga Ltd. (2011). *Port History to Modern Day*. Tauranga, New Zealand. Port of Tauranga Limited.
- Port of Tauranga Ltd. (2013). *Maintenance Dredging-Spoil Disposal Sites*. Tauranga, New Zealand. Port of Tauranga Ltd.
- Ramli, A. Y., and de Lange, W.P. (2013a). Dredging impacts on the stability of an ebb tidal delta system. *Coasts and Ports 2013*. Sydney, Australia.
- Ramli, A.Y., de Lange, W.P., Bryan, K., and Mullarney, J. (2015). Coupled flow-wave numerical model in assessing the impact of dredging on the morphology of Matakana Banks. *Australasian Coast and Port Conference 2015*, (pp. 1-6). Auckland, New Zealand.
- Robin, N., Levoy, F., Monfort, O., and Anthony, E. (2009). Short-term to decadal-scale onshore bar migration and shoreline changes in the vicinity of a megatidal ebb delta. *Journal of Geophysical Research* Vol. 113. 1-13.
- SEPM STRATA. (2012, May 26). *Barrier Island Introduction*. Retrieved from SEPM Stratigraphy Web: <http://www.sepmstrata.org/page.aspx?pageid=299>
- Shane, P., Froggatt, P., Smith, I., and Gregory, M. (1998). Multiple sources for sea-rafted Loiseles pumice, New Zealand. *Quaternary Research* Vol. 49 Issue 3. Article No. QR981968, pp. 271-279.
- Shepherd, M.J., Betts, H.D., McFadgen, B.G., and Sutton, D.G. (2000). Geomorphological evidence for Pleistocene barrier at Matakana Island, Bay of Plenty, New Zealand. *Journal of Geology and Geophysics* Vol. 43. 579-586.
- Shepherd, M.J., McFadgen, B.G., Betts, H.D., and Sutton, D.G. (1997). Formation, landforms and palaeoenvironment of Matakana Island implications for archaeology. *Science and Research Series No. 102*. . Wellington: Department of Conservation.
- Spiers, K.C., and Healy, T.R. (2007). Investigation of sorted bedforms, Tauranga Harbour, New Zealand. *Journal of Coastal Research Special Edition* 50, 353-357.

- Spiers, K.C., Healy, T.R., and Winter, C. (2009). Ebb-Jet Dynamics and Transient Eddy Formation at Tauranga Harbour: Implications for Entrance Channel Shoaling. *Journal of Coastal Research*, 234-247.
- Taaouati, M., El Mrini, A., and Nachite, D. (2011). Beach morphology and sediment budget variability based on high quality elevation models derived from field data sets. *International Journal of Geosciences*, 111-119.
- Tamuno, P.B.I., Smith, M.D., and Howard, G. (2009). "Good Dredging Practices": The knowledge of traditional eco-livelihood knowledge. *Water Resource Manage Vol. 23*, 1367-1385.
- USACE. (1983). *Dredging equipment and techniques EM 1110-2-5025*. USA: US Army Corps of Engineer.
- Van Raalte, G. (2006). Dredging techniques: adaptations to reduce enviromental impact. In D. Eisma, *Dredging in coastal waters. Proceeding and Monographs in Engineering, Water and Earth Sciences* (pp. 1-40). Leiden, The Netherlands: Balkema/Taylor & Francis.
- Wallingford Hydraulic Research Station. (1963). *Tauranga Harbour Investigation, Report on First Stage. Report No. 21*. England: Wallingford Hydraulic Research Station.
- Wang, Z. (2015). Sustainability of the multi-channel system in the Westerschelde under influence of dredging and disposal. 36th IAHR World Congress, (pp. 65-70). The Hague, the Netherlands.
- Wang, Z.B., Tse, M.L., and Lau, S.C. (2011). A study on sedimentation of tidal rivers and channel flowing into deep bay with a Delft3D model. *The Sixth International Conference on Asian and Pacific Coasts (APAC 2011)* (pp. 1444-1451). Hong Kong, China: APAC 2011

Chapter 3: Morphodynamics of Ebb-Tidal Delta Systems

3.1 Introduction

Tidal inlets represent a natural system of reversing currents due to tides, variable quantities of fresh-water flow contributed by land drainage, and different levels of wave activity acting along the ocean margin of the inlet. Due to these interacting processes, inlets are undoubtedly the most complex environment within the coastal zone (Komar, 1996). This complexity makes it difficult to quantify the sediment transport (FitzGerald *et al.*, 2000). The morphology and behaviour of associated sediment shoals in a tidal inlet system are dependent on the nature and magnitude of sediment supply (FitzGerald *et al.*, 2002): particularly for an ebb-tidal delta on the seaward side and a flood-tidal delta within the estuary.

An ebb tidal delta is a body of sediment that is folded around a main ebb-channel, in which the ebb current dominates over the flood current (Hayes, 1975) and it is shaped by both waves and tides. Based on the dominant flow regime that shaped it, an ebb-tidal delta can be classified as: wave-dominated, tide dominated, or mixed energy (Hayes, 1975; Hayes, 1980; FitzGerald *et al.*, 2012). Ebb-tidal deltas are important agents in the complex sediment budget of the coastal zone as they contain significant volume of sediment that is continuously exchanged with the adjacent coast and the tidal inlet (De Swart and Zimmerman, 2009). They also act as an important contributors to littoral sediment budgets (Hicks and Hume, 1996), and significantly influence the morphodynamics of adjacent shorelines (FitzGerald, 1988; Hicks *et al.*, 1999; and Carr-Betts *et al.*, 2012).

One approach to understand the tidal inlet and adjacent ebb-tidal delta dynamics is to simulate the system by mathematical modelling. Process-based models based on physical laws describing the water motion, sediment transport and morphological changes by a series of mathematical formulations have been used previously and are still applied for modelling of short- and long-term coastal processes. Studies of the tidal inlets and adjacent ebb-tidal delta in regards to

dredging activities using mathematical modelling have been presented by i.e. Hibma *et al.* (2008), Beck and Wang (2009); and Wang (2015). The results of this mathematical modelling then can provide valuable information on the governing flow, sediment transport patterns and how the tidal inlet systems respond to the dredging activities in various time frames. By utilizing mathematical modelling, the complexity of tidal inlet systems combined with the influence of anthropogenic activities (in this case dredging) can be replicated and observed, which enables coastal scientists/managers to predict the morphological changes, erosion/deposition locations, and evaluate mitigation measures.

This chapter reviews the general morphodynamics and hydrodynamics of tidal inlets, with a focus on ebb-tidal deltas and how they respond to different hydrodynamic regimes. Coastal process-based numerical models for tidal flow, wave processes, sediment transport, morphological evolution, and dredging and dumping (anthropogenic activities) will be briefly discussed, with a focus on modelling approaches using DELFT3D models.

3.2 Sand Transport in Estuaries and Coastal Waters

Sand transport is defined as the transport of particles with sizes in the range of 0.05 to 2 mm as found in the bed of rivers, estuaries and coastal waters (Van Rijn, 2015). Sand can be transported by gravity-, wind-, wave-, tide- and density-driven currents (current-related transport), by oscillatory water motions (wave-related transport) as caused by the deformation of short waves under the influence of decreasing water depth (wave asymmetry), or by a combination of currents and short waves.

In the lower reaches of a river (estuary or tidal river) the influence of the tidal motion may become noticeable, introducing non-steady effects with varying current velocities and water levels on a diurnal or semi-diurnal time scale. Furthermore, density-induced flow may be generated due to the interaction of fresh river water and saline sea water (for example, due to the formation of a salt wedge (Van Rijn, 2015)).

In coastal waters, the sediment transport processes are strongly affected by high-frequency (short period) waves introducing oscillatory motions acting on the

particles. The waves generally act as sediment stirring agents; the sediments are then transported by the mean current.

Observations in the coastal zone over a long period of time has led to the notion that storm waves cause sediments to move offshore while fair-weather waves and swell return the sediments shorewards. During conditions with low non-breaking waves, onshore-directed transport process related to wave-asymmetry and wave-induced streaming are dominant, usually resulting in accretion processes in the beach zone. During high-energy conditions with breaking waves (storm cycles), the beach and dune zone of the coast are attacked severely by the incoming waves, usually resulting in erosion processes.

3.3 Inlet Circulation

Inlet circulation is governed by tidal range, estuary geometry, inlet geometry, presence and configuration of structures, bottom topography, and non-tidal forcing, such as wind and river inflow. The rise and fall of the ocean tide is the primary forcing. As water traverses the inlet and enters the estuary, the current is primarily aligned with the inlet and flows over the flood shoal where the velocity is reduced and material is deposited. This process forms a flood ramp, which is the sloped frontal face of the flood shoal. During ebb tide, the primary conduits of water are channels located between the flood shoal and the ebb barrier island. These ebb channels merge at the inlet forming a main ebb channel. Strong ebb currents exiting the inlet form a jet (Joshi, 1982; Joshi and Taylor, 1983; Mehta and Joshi, 1998). As the jet exits the inlet, it expands and loses velocity, depositing material onto the ebb shoal.

The described pattern of flood and ebb circulation is common, but every inlet has unique patterns owing to the local situation. For example, the main ebb channel may be in the centre of the inlet or along one side. Factors that control the local circulation include inlet geometry, tide range, bay-channel orientation, distribution of discharge through channels, wave climate, number and configuration of jetties (if present), and dredging activity (Militello and Hughes, 2000). Tidal inlets around the New Zealand coast also tend to be constrained by rock headlands that distort the geometry of the ebb-tidal delta (Hicks and Hume, 1996).

3.4 Ebb Tidal Delta System

3.4.1 Definition

Ebb-tidal deltas are complex, highly dynamic, morphologic structures situated at the seaward side of tidal inlets. An ebb-tidal delta represents an accumulation of sediment that results from the interaction of tidal currents, waves and wave generated longshore currents at the seaward end of the inlet (Davis Jr, 2012). The morphology of an ebb-tidal delta has some common elements (Figure 3-1), but shows much variability. Most ebb-tidal deltas contain the same general features including FitzGerald (1988a), Boothroyd (1985); and FitzGerald *et al.* (2012):

- *Main ebb channel*- This is a seaward shallowing channel that is scoured in the ebb-tidal delta and is dominated by ebb-tidal currents.
- *Terminal lobe*- Sediment transported out the main ebb channel is deposited in an arcuate bank known as the terminal lobe. The deposit slopes relatively steeply on its seaward side. The outline of the terminal lobe is well defined by breaking waves during storms or periods of large swell at low tide.
- *Swash platform*- This is a broad shallow platform located on both sides of the main ebb channel, defining the general extent of the ebb delta and dominated by wave action.
- *Channel margin linear bars*- These are bars that border the main ebb channel and sit atop the swash platform. These bars tend to confine the ebb flow and may be exposed at low tide.
- *Swash bars*- Wave breaking over the terminal lobe and across the swash platform form arcuate-shaped swash bars that migrate onshore. The bars are usually 5—150 m long, 50 m wide, and 0.5-2 m in height.
- *Marginal-flood channels*- These are shallow channels (up to 2 m deep at mean low water) located between the channel margin linear bars and the onshore adjacent beaches. These channels are dominated by flood-tidal currents.

The general shape of an ebb-tidal delta and the distribution of its sediment bodies reveal the relative magnitude of different sediment transport processes operating at a tidal inlet if the delta is free to respond to forcings. Ebb-tidal deltas that have an elongated main ebb channel and channel margin linear bars that extend far offshore are common for tide-dominated inlets, including those having a strong tidal-versus-wave energy distribution, and/or a large tidal prism. Wave-generated sediment transport plays a secondary role in modifying the delta shape at these inlets. Because most sediment movement is in the onshore-offshore direction, the ebb-tidal delta overlaps a relatively small segment of inlet shoreline. This affects the extent to which this part of coast undergoes erosional and depositional changes caused by inlet processes (FitzGerald *et al.*, 2012).

Tide-dominated inlets have large ebb-deltas extending far offshore relative to the inlet width (FitzGerald, Interactions between the ebb-tidal delta and landward shoreline: Price Inlet, South Carolina, 1984a), well-defined deep main channels and inlet throats, a general absence of inner shoals of a flood-tide delta (Komar, 1996).

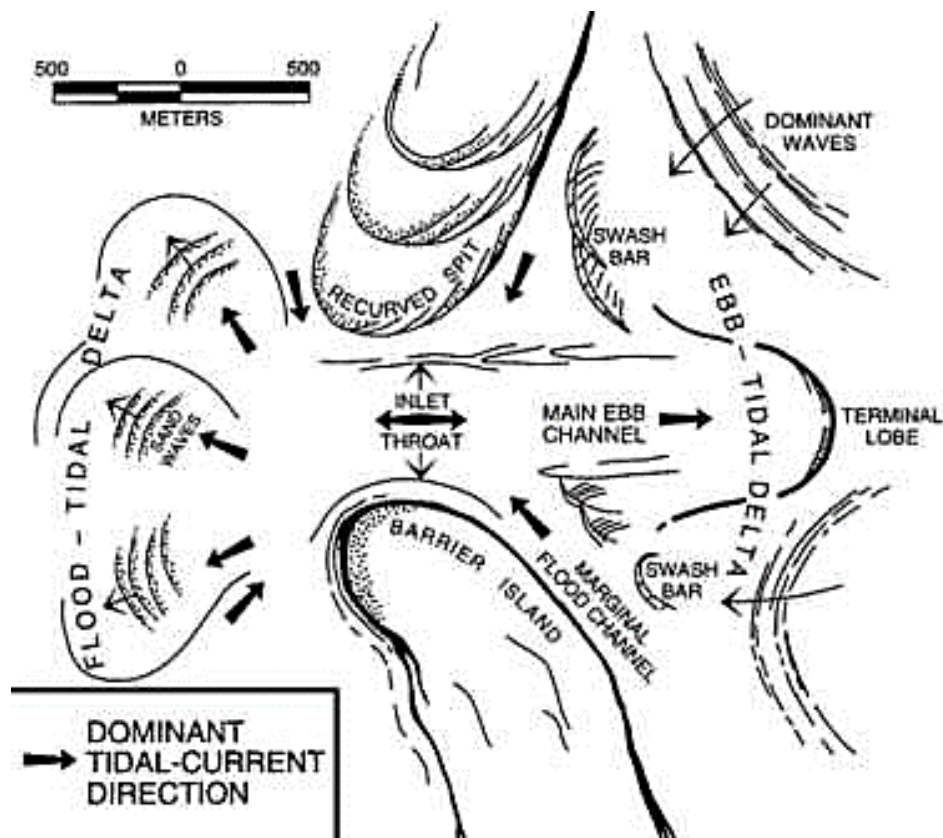


Figure 3-1. Diagram of an ebb-tidal delta showing each of the subenvironments (After Hayes, 1980)

Wave-dominated inlets tend to be small relative to tide-dominated systems. Their ebb-tidal deltas are driven onshore by the dominant wave processes, so their morphology are much flatter and located close to the inlet mouth. Commonly, the terminal lobe and/or swash bars form a small arc outlining the periphery of the delta. In many cases the ebb-tidal delta of these inlets is entirely subtidal. In other instances, sediment bodies clog the entrance to the inlet, leading to the formation of several major and minor tidal channels (FitzGerald *et al.*, 2012). Ebb-tidal deltas at wave-dominated tidal inlets typically have arcuate or horse-shaped bypassing bars and a shoal in front of the ebb jet (the “ebb delta proper” following the terminology of Kraus (2000) and Carr-Betts *et al.* (2012)).

At mixed-energy tidal inlets, the shape of the delta is the result of the interaction of tidal and wave processes. These deltas have a well-formed main ebb channel, which is a product of dominant ebb-tidal currents. Their swash platform and sediment bodies substantially overlap the inlet shoreline many times the width of the inlet throat due to wave processes and flood-tidal currents. Asymmetries in ebb delta configuration commonly result from the main ebb channel being deflected along the downdrift barrier shoreline due to the dominant longshore transport direction or the pattern of the dominant back-barrier channels (FitzGerald *et al.*, 2012). A similar effect results from bedrock constraining the orientation of the ebb channel (Hicks and Hume, 1996).

Because mixed-energy inlets tend to exhibit a wide range of energy forcing (both wave and tidal), their ebb-tidal deltas are not easily defined and may exhibit a variety of morphologies (FitzGerald, 1982). FitzGerald (1984a) reported that for this type of system, the patterns of erosion and deposition along the shoreline are strongly influenced by ebb-tidal delta processes. The shift on the shoreline alignment is controlled by the orientation of the main ebb channel and the resulting ebb-tidal delta morphology. Hicks and Hume (1996) suggested that the orientation of the ebb channel could be deliberately modified to manage adjacent shorelines, and as noted in Chapter 2, the Entrance Channel at Tauranga resulted in a change in ebb jet orientation.

Typical morphologic features associated with mixed-energy ebb deltas include an updrift channel margin-linear bar, a flood marginal channel along the updrift side of the delta, and a large and shallow bypassing platform along the downdrift side of the delta (Carr-Betts *et al.*, 2012). The longshore extent of the ebb-tidal delta ranges from a minimum of ~ 200 m i.e. inlets along the Florida coast (FitzGerald, 1996) to a maximum of ~ 5 km i.e. Texel delta, Dutch Wadden Sea (Oost and de Broer, 1994).

Changes in delta configuration have been shown to have pronounced effects on the erosion and accretion of adjacent shorelines (Oertel, 1977). The role of ebb-tidal deltas in influencing coastal processes in the vicinity of a tidal inlet through bypassing of littoral drift or by partially sheltering the adjacent shoreline from waves is evident in the study of FitzGerald (1988).

3.4.2 Tidal Inlet and Ebb Delta – Tidal Prism Relationships

Tidal inlets throughout the world exhibit several relatively consistent relationships that have allowed coastal engineers and scientists to formulate predictive models: (1) Inlet throat cross-sectional area is closely related to tidal prism, and (2) Ebb-tidal delta volume is function of the tidal prism (FitzGerald *et al.*, 2012; and, Roelvink and Reniers, 2012). If the ebb-tidal delta volume is defined as the volume of sediment relative to a hypothetical undisturbed sea bottom, (Walton, T.L., and Adams, W.D., 1976) found that it correlates with the tidal prism to the power of 1.23:

$$V = 1.89 * 10^{-5} P^{1.23} \quad (3.1)$$

Where V is the sediment volume of the ebb-tidal delta and P is the mean tidal prism. Hicks and Hume (1996) found a similar relationship for New Zealand ebb tidal deltas that also includes the angle between the ebb jet and the shoreline (θ), as given by:

$$V = 1.37 * 10^{-3} P^{1.32} (\sin \theta)^{1.33} \quad (3.2)$$

At equilibrium, the ebb-tidal delta volume decreases with increasing relative wave influence (Dean, 1988b). However, although the Walton and Adams relationship works well for inlets all over the world, field studies have shown that the volume of sediment comprising ebb-tidal deltas can change through time due to effects of storms or processes of inlet sediment bypassing, and these effects can change the shoal volume by more than 10% (FitzGerald *et al.*, 1984; and, Gaudio and Kana, 2001). Based on the distance to the downdrift attachment bar and the distance to the most seaward extent of the ebb tidal delta, Carr-Betts *et al.* (2012) found that the wave-energy exposure concept of Walton and Adams (1976) and tidal prism had the most predictive power.

3.4.3 Sediment Transport Patterns on the Ebb-Tidal Delta

It is generally accepted that the morphology of tidal inlets and tidal deltas and the associated sediment transport patterns are principally controlled by the interaction of waves and tidal currents (Sha, 1989a). The movement of sediment at a tidal inlet is complex due to reversing tidal currents, effects of storms, and interactions with the longshore transport system. During a storm, sediment is transported into the estuary when large waves increase the delivery of sediment to the inlet and the associated storm surge produces stronger flood currents (FitzGerald *et al.*, 2000).

The inlet contains short-term and long-term reservoirs of sediment, varying from relatively small sandwaves flooring the inlet channel that migrate metres each tidal cycle, to large flood-tidal and ebb-tidal delta shoals, where some sediment is recirculated, but the entire deposit may remain stable for hundreds of years. Sediment dispersal at tidal inlets is complicated because, in addition to the onshore-offshore movement of sediment produced by tidal and wave-generated currents, there is intermittent delivery of sediment to the inlet and removal by the longshore transport system (FitzGerald *et al.*, 2012). Biogenic sediment may also be generated *in situ*, such as occurs at Tauranga.

Waves influence sediment transport and deposition on the ebb-tidal delta in various ways, such as Roelvink, J.A. and Reniers (2012):

- They tend to increase the bed shear stress, leading to higher suspended sediment concentrations than for the case without waves. When combined with flood tidal flow, this may lead to more import of sediment into the estuary, but combined with ebb flow it can lead to deposition further out to sea and thus to a more extended, deeper ebb-tidal delta.
- When the ebb-tidal delta is shallow enough, the waves drive a circulation pattern, typically leading to onshore flows over the shoals that escape through the tidal channels, similar to observed with rip currents on an open coast beach.
- In case of obliquely incident waves, longshore transport feeds sediment towards the inlet, which may push the ebb channel into the down-wave direction; and oblique waves also lead to a longshore component in the circulation patterns that tends to shift the shoals in the down-wave direction.
- Finally, asymmetry and skewness of the wave orbital motion leads to generally onshore directed transport.

3.4.4 General Sediment Dispersal from Tidal Inlets

Ebb-tidal deltas consist of segregated areas of landward versus seaward sediment transport that are controlled primarily by the way water enters and discharges from the inlet, as well as the effects of wave-generated currents. The morphology of ebb-tidal deltas promotes feedback on the process regime of tidal inlets (Morgan *et al.*, 2011). During the ebbing cycle, the tidal flow leaving the estuary is constricted at the inlet throat, causing the currents to accelerate in a seaward direction. Once out of the confines of the inlet, the ebb flow (ebb jet) expands laterally and the velocity slows. Sediment in the main ebb channel is transported in a net seaward direction and is eventually deposited on the terminal lobe due to this decrease in current velocity.

At the beginning of the flood cycle, the ocean tide rises while water in the main ebb channel continues to flow seaward as a result of momentum. Due to this phenomenon, water initially enters the inlet through the marginal flood channels that are the pathways of least resistance. Generally the flood channels are dominated by landward sediment transport and are floored by flood-oriented bedforms. On both sides of the main ebb channel, the swash platform is most affected by landward

flow produced by the flood-tidal currents and breaking waves. As waves shoal and break, they generate a landward flow, which augments the flood-tidal currents but retards the ebb-tidal currents. The interaction of these forces acts to transport sediment in net landward direction across the swash platform.

In summary, at many inlets there is a general trend of seaward sediment transport in the main ebb channel, which is countered by landward sediment transport in the marginal flood channels and across the swash platform (FitzGerald *et al.*, 2012). However, when the development of a tidal inlet system is constrained by rock headlands, as occurs at Tauranga, the development of these flows and the distribution of wave energy across the delta can be modified (Hicks and Hume, 1996; Spiers *et al.*, 2009). This adds to the complexity of sediment transport patterns.

3.4.5 Inlet Sediment Bypassing

The mechanism whereby sediment moves past tidal inlets and is transferred to the downdrift shoreline is called inlet sediment bypassing. There are three modes of sediment bypassing (Bruun and Gerritsen, 1960; FitzGerald, 1982; Bruun, 2005):

- *Bar bypassing* - sediment predominantly moves due to wave-induced transport over the terminal lobe;
- *Tidal flow bypassing* – sediment predominantly moves due to tidal current transport within channels; and
- *Inlet bypassing* – sediment predominantly moves due to the migration of morphological elements such as the channels and shoals.

Sediment bypassing of natural mixed-energy inlets by the migration of shoals and tidal channels can result in three different patterns of evolving ebb-tidal delta morphology (FitzGerald *et al.*, 2001a) (Figure 3-2):

- *Stable inlet processes* - sediment bypassing occurs at inlets that do not migrate and have main ebb channels that remain approximately in the same position. Sediment entering the inlet via tidal and wave processes is transported to the terminal lobe due to the dominance of ebb-tidal currents in the main channel.
- *Ebb-tidal delta breaching* – sediment bypassing occurs at inlets with a stable throat position but with a main ebb channel that migrates through their ebb-tidal

deltas like the “wag of a dog’s tail”. Sediment delivered to the inlet is preferentially deposited on the updrift side of the ebb-tidal delta, which causes a deflection of the main ebb channel until it nearly parallels the downdrift inlet shoreline. Eventually the seaward bar is breached, and the ebb-channel is re-established offshore from the inlet, before migrating downdrift again.

- *Inlet migration and spit breaching* – sediment bypassing occurs at migrating inlets whereby an abundant sediment supply and a dominant longshore transport direction cause spit building and downdrift inlet migration. Along many coasts, as the inlet is displaced farther along the downdrift shoreline, the channel to the backbarrier lengthens, retarding the exchange of water between the ocean and backbarrier. This type of behaviour doesn’t occur when the inlet is constrained by bedrock.

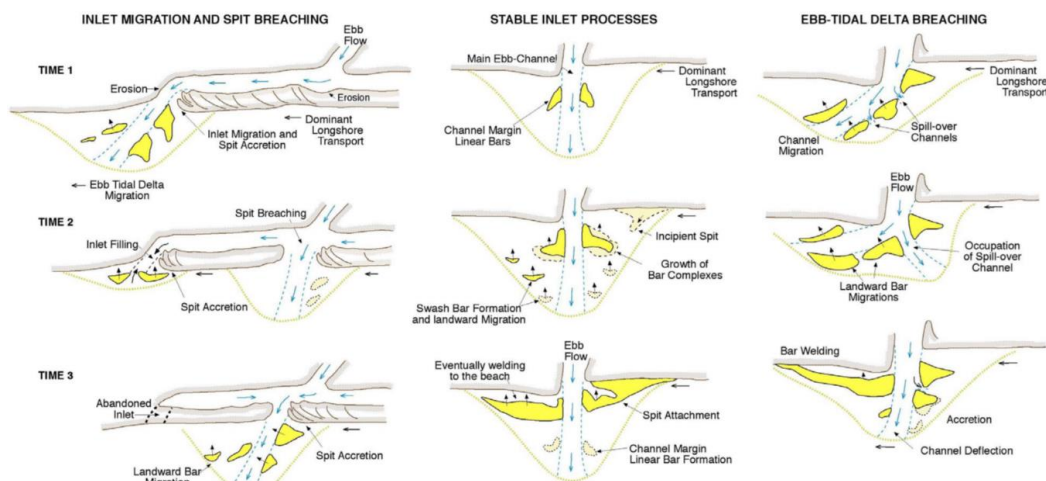


Figure 3-2. Models of sediment bypassing tidal inlets (From FitzGerald *et al.*, 2001a)

A general feature of unmodified tidal inlets is that the sediment bypassing ultimately results in the formation, landward migration, and attachment of large bars to the downdrift shoreline. The volume of sediment bypassing is dependent on inlet size, ebb-tidal delta morphology, rate at which sediment is delivered to the inlet, and the type of bypassing mechanism. Bar welding at these inlets is a repetitive process with a frequency of 4 to 10 years (FitzGerald *et al.*, 2000). FitzGerald (1988a) and Gaudio and Kana (2001) have documented episodic welding of bar complexes onto the downdrift beach at inlets in South Carolina. An exception to this trend are the wave-dominated inlets where bypassing occurs

continuously and sediment is moved primarily by wave action along the terminus of the delta to downdrift beach (FitzGerald *et al.*, 2000).

The study of Herrling and Winter (2014) using a process-based morphodynamic model indicated that during storm conditions for the tidal inlets of the Wadden Sea, bed load sediment transport is generally onshore directed over the shallower ebb-tidal delta shoals, whereas fine-grained suspended sediment bypasses the tidal inlet by wave-driven currents. During fair weather the sediment transport is concentrated within the inlet throat and the marginal flood channels.

3.5 Modelling Sediment Transport and Morphological Evolution

3.5.1 General

Sediment transport is the essential link between the waves and currents, and morphological changes in coastal systems. It is a strong and non-linear function of the current velocity and orbital motion, the sediment properties such as grain diameter and density and the small-scale bed features or “bed roughness” (Roelvink and Reniers, 2012). In the DELFT3D-FLOW model, the sediment transport and morphology module supports both bedload and suspended load transport of non-cohesive sediments and suspended load of cohesive sediments. However, due to the physical properties of the dredged sediment for the study site (predominantly sand), only non-cohesive sediment transport is considered.

The numerical algorithm of DELFT3D-FLOW is based on finite differences. To discretise the 3D shallow water equations in space, the model area is covered by a curvilinear grid, whose coordinates can be defined either in a Cartesian or in a spherical coordinate system. Variables on the grid are arranged in a staggered grid known as the Akarawa C-grid (Deltares, 2013). This grid arrangement means that water level points (pressure points) are defined in the centre of a (continuity) cell and the velocity components are perpendicular to the grid cell faces where they are situated. This means that strictly the velocities are not predicted at the same locations as water elevations, which makes it more difficult to calibrate the model against observations that are normally taken at one location within a grid cell. Although (Roelvink and Reniers (2012) stated that the complexities of sediment

transport make modelling difficult, staggered grids have several advantages such as:

- Boundary conditions can be implemented in a rather simple way.
- It is possible to use a smaller number of discrete state variables in comparison with discretizations on non-staggered grids, to obtain the same accuracy.
- Staggered grids for shallow water solvers prevent spatial oscillations in the water levels; see for example Stelling (1983).

The numerical aspects as well as the application and use of sediment transport and morphological modules of DELFT3D have been extensively described by Lesser *et al.* (2004); van Rijn and Walstra (2003); and Deltares (2013). Hence, the modules of DELFT3D will not be covered in detail here.

3.5.2 Definition of Model Boundaries

The horizontal model area is defined by specifying the computational grid enclosure consisting of one or more closed polygons that specify the boundaries of the model area (Figure 3-3). There are two types of boundaries: closed boundaries along “land-water” interfaces (coastlines, riverbanks) and open boundaries across the flow field. The open boundaries are artificial and chosen to limit the computational area. The polygons consist of line pieces connecting water level points on the numerical grid (Figure 3-3). The computational cells on the grid enclosure are land points (permanently dry) or open boundary points.

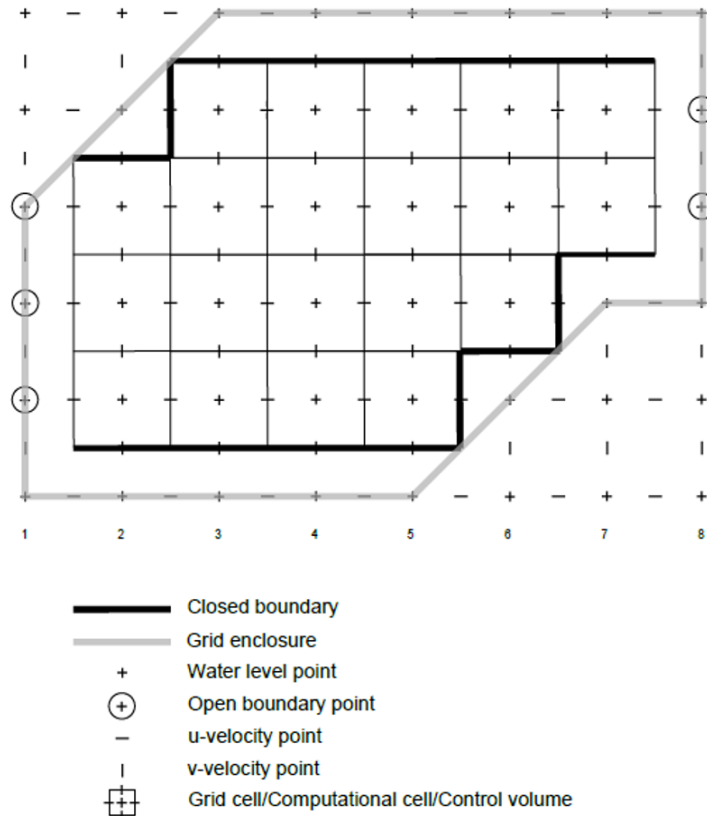


Figure 3-3. Example of Delft3D-FLOW horizontal model area showing the grid staggering, the grid enclosure and the position of open and closed boundaries (Deltares, 2013).

3.5.3 Hydrodynamic Model

The DELFT3D-FLOW module solves the unsteady shallow-water equations in two (depth-averaged) or three dimensions. The system of equations consists of the horizontal momentum equations, the continuity equation, the transport equation, and a turbulence closure model. The vertical momentum equation is reduced to the hydrostatic pressure relation as vertical accelerations are assumed to be small compared to gravitational acceleration and are not taken into account. This makes the DELFT3D-FLOW model suitable for predicting the flow in shallow seas, coastal areas, estuaries, lagoons, rivers, and lakes. It aims to model flow phenomena of which the horizontal length and time scales are significantly larger than the vertical scales.

The flow model, when run in 2DH mode, is based on the depth-averaged shallow water equations (Roelvink and Reniers, 2012). In most cases this means that the sediment transport direction is the same as the depth-averaged flow direction. When the mean return flow is taken into account, it is treated as the simplest quasi-3D concept rather than real 2DH. In such a model setup, the transport

generally follows the depth contours along the coast, unless there is a disturbance in the form of coastal structures, or dips in the bathymetry leading to rip currents.

The model can solve the hydrodynamic equations on a Cartesian rectangular, orthogonal curvilinear (boundary fitted), or spherical grid. In three-dimensional simulations, a boundary fitted (σ -coordinate) approach is used for the vertical grid direction. For the sake of clarity the equations are presented below in their Cartesian rectangular form only.

3.5.4 Suspended Transport

Three-dimensional transport of suspended sediment is calculated by solving the three-dimensional advection-diffusion (mass-balance) equation for the suspended sediment:

$$\begin{aligned} \frac{\partial c^{(\ell)}}{\partial t} + \frac{\partial uc^{(\ell)}}{\partial x} + \frac{\partial vc^{(\ell)}}{\partial y} + \frac{\partial (w - w_s^{(\ell)})c^{(\ell)}}{\partial z} + \\ - \frac{\partial}{\partial x} \left(\varepsilon_{s,x}^{(\ell)} \frac{\partial uc^{(\ell)}}{\partial x} \right) - \frac{\partial}{\partial y} \left(\varepsilon_{s,y}^{(\ell)} \frac{\partial vc^{(\ell)}}{\partial y} \right) - \frac{\partial}{\partial z} \left(\varepsilon_{s,z}^{(\ell)} \frac{\partial c^{(\ell)}}{\partial z} \right) = 0, \end{aligned} \quad (3.3)$$

where:

$c^{(\ell)}$ mass concentration of sediment fraction (ℓ) [kg/m^3]

u, v, w flow velocity components [m/s]

$\varepsilon_{s,x}^{(\ell)}, \varepsilon_{s,y}^{(\ell)}, \varepsilon_{s,z}^{(\ell)}$ eddy diffusivities of sediment fraction (ℓ) [m^2/s]

$w_s^{(\ell)}$ (hindered) sediment settling velocity of sediment fraction (ℓ) [m/s]

The local flow velocities and eddy diffusivities are determined from the results of the hydrodynamic computations. Computationally, the three-dimensional transport of sediment is computed in exactly the same way as the transport of any other conservative constituent, such as salinity, heat, and constituents. There are, however, a number of important differences between sediment and other constituents. For example, the exchange of sediment between the bed and the flow, and the settling velocity of sediment under the action of gravity. The formulation

of several of these processes (such as, settling velocity, sediment deposition and entrainment) are sediment-type specific, this especially applies for sand and mud.

3.5.5 Bed Load and Total Transport Formulation

3.5.5.1 Current-Only Situation

Bed load transport, which takes place in a thin layer above the bed, is assumed to react directly to local flow conditions. Most bed load transport formulations contain some or all of the following concepts:

- The bed shear stress exerted by the flow acting on the sediment grains. It is expressed in dimensionless form as the dimensionless shear stress or Shields parameter, given by Shields (1936):

$$\theta = \frac{\tau}{\rho g \Delta D_{50}} \quad (3.4)$$

Where τ is the bed shear stress, ρ the water density, g the acceleration due to gravity, $\Delta = (\rho_s - \rho)/\rho$ is the relative sediment density, and D_{50} is the median grain diameter. The dimensionless shear stress reflects the balance between lifting forces, which are proportional to shear stress and projected grain surface area, and gravity, which is proportional to the relative density, g and the grain volume.

- The critical shear stress or critical Shields parameter for initiation of motion;
- Bed load transport in the direction of near-bed flow, as a function of the Shields parameter (minus the critical Shields parameter) to some power.
- Bed slope effects in the direction of the flow and in the transverse direction.
- For rippled beds, the bed shear stress is often divided into form drag (because of the ripples) and skin friction (exerted directly on the sand grains), where the bed load transport is generally taken to be a function of the skin friction only.

A general form of bed load/total load transport formulation is given by Roelvink and Reniers (2012):

$$S_b \sim \sqrt{\Delta g D_{50}^3} \theta^{\frac{b}{2}} (m\theta - n\theta_{cr})^{c/2} \left(1 - \alpha \frac{\partial z_b}{\partial s}\right) \quad (3.5)$$

A number of bed load transport formulae are captured by this formulation, e.g. Meyer-Peter and Muller (1948) $c = 3, b = 0$, van Rijn (1984) $b = 0, c = 3-4$. The S_b denotes near-bed transport, coefficient m represents a ripple efficiency factor, which depends on the ratio of skin friction to form drag, and n may represent a factor for hiding and exposure in graded sediments. Roelvink and Reniers (2012) provide complete expressions of the physical processes and numerical implementation.

3.5.5.2 Waves plus Current

Waves interact with the current, and therefore modify the bed shear stress, the bed ripples, the sediment mobility and the near-bed current transporting the sediment (Roelvink and Reniers, 2012). After attempts to adapt bed-load transport formulae for current-only to combined current-wave situations by modifying the dimensionless shear stress (e.g. van de Graaff and van Overeem, 1979) most researchers have resorted to developing empirical formulations directly fitted against as many data points as could be obtained. In DELFT3D-FLOW, the default sediment formula is that of van Rijn (1993), which distinguishes between bedload sediment transport below a specified reference height and suspended sediment transport above the reference height. Sediment is entrained in the water column by imposing a reference concentration at the reference height.

Reference concentration

The reference concentration is calculated in accordance with van Rijn et al. (2000) as:

$$c_a^{(\ell)} = 0.015 \rho_s^{(\ell)} \frac{D_{50}^{(\ell)} (T_a^{(\ell)})^{1.5}}{a (D_*^{(\ell)})^{0.3}} \quad (3.6)$$

Where $c_a^{(\ell)}$ is the mass concentration at reference height a .

In order to evaluate this expression the following quantities must be calculated using the formulae specified by Deltares (2013): $D_*^{(\ell)}$ non-dimensional particle diameter; $T_a^{(\ell)}$ non-dimensional bed-shear stress; $\mu_c^{(\ell)}$ efficiency factor current; $f'_c^{(\ell)}$ gain related friction factor; $f_c^{(\ell)}$ total current-related friction factor; $\tau_{b,w}$ bed shear due to waves; and f_w total wave-related friction factor.

Bedload transport rate

For simulations including waves, the magnitude and direction of the bedload transport on a horizontal bed is calculated using an approximation method developed by van Rijn *et al.* (2003). The method computes the magnitude of the bedload transport as:

$$|S_b| = 0.006\rho_s w_s D_{50}^{(\ell)} M^{0.5} M_e^{0.7} \quad (3.7)$$

where:

S_b	bedload transport [$\text{kg m}^{-1} \text{s}^{-1}$]
M	sediment mobility number due to waves and currents [-]
M_e	excess sediment mobility number [-]

$$M = \frac{v_{eff}^2}{(s-1)gD_{50}} \quad (3.8)$$

$$M_e = \frac{(v_{eff} - v_{cr})^2}{(s-1)gD_{50}} \quad (3.9)$$

$$v_{eff} = \sqrt{v_R^2 + U_{on}^2} \quad (3.10)$$

in which

v_{cr}	critical depth averaged velocity for initiation of motion (based on a parameterisation of the Shields curve [m/s])
v_R	magnitude of an equivalent depth-averaged velocity computed from the velocity in the bottom computational layer, assuming a logarithmic velocity profile [m/s]
U_{on}	near-bed peak orbital velocity [m/s] in onshore direction (in the direction on wave propagation) based on the significant wave height.

U_{on} (and U_{off} used below) are the high frequency near-bed orbital velocities due to short period waves and are computed using a modification of the method of Isobe and Horikawa (1982). This method is a parameterisation of fifth-order Stokes wave theory and third-order cnoidal wave theory, which can be used over a wide

range of wave conditions and takes into account the non-linear effects that occur as waves propagate in shallow water (Grasmeijer and van Rijn, 1998).

The direction of the bedload transport vector is determined by assuming that it is composed of two parts: transport due to a current ($S_{b,c}$) which acts in the direction of the near-bed current; and transport due to waves ($S_{b,w}$) which acts in the direction of wave propagation. These components are determined as follows:

$$S_{b,c} = \frac{S_b}{\sqrt{1+r^2+2|r|\cos\varphi}} \quad (3.11)$$

$$|S_{b,w}| = r|S_{b,c}| \quad (3.12)$$

where

$$r = \frac{(|U_{on}| - v_{cr})^3}{(|v_R| - v_{cr})^3} \quad (3.13)$$

$S_{b,w} = 0$ if $r < 0.01$, $S_{b,c} = 0$ if $r = 100$, and φ = angle between current and wave direction for which van Rijn (2003) suggests a constant value of 90° .

3.5.6 Morphological Up-dating

In the Delft3D model, the elevation of the bed is dynamically updated at each computational time-step. This is one of the distinct advantages over an offline morphological computation as it means that the hydrodynamic flow calculations are always carried out using the correct bathymetry. At each time-step, the change in the mass of bed material that has occurred as a result of the sediment sink and source terms and transport gradients is calculated. This change in mass is then translated into a bed level change based on the dry bed densities of the various sediment fractions. Both the bed levels at the cell centres and cell interfaces are updated.

One of the complications inherent in carrying out morphological projections on the basis of hydrodynamic flows is that morphological developments often take place at time scales several times longer than typical flow changes (for example, tidal flows change significantly over periods of minutes to hours, whereas the morphology of a coastline will usually take weeks, months, or years to change

significantly). One technique for approaching this problem is to use a “morphological time scale factor” whereby the magnitude of morphological change at each time step is scaled up to effectively increase the rate of change, and the morphological changes begin to have a significant impact on the hydrodynamic flows (Figure 3-4). This can be achieved by specifying a non-unity value for the variable *Morfac* in the morphology input file for Delft3D.

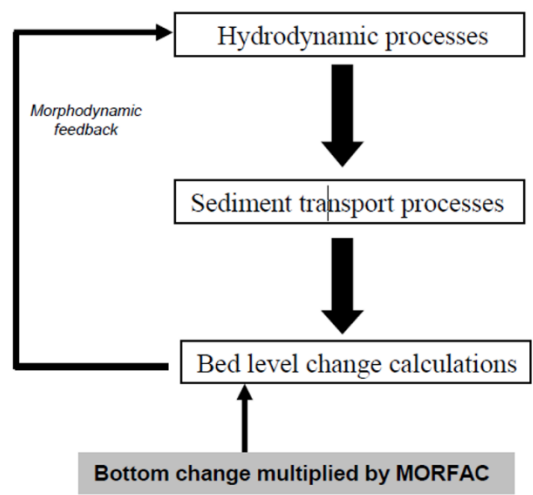


Figure 3-4. General structure of coastal morphodynamic models and the *Morfac* concept (Ranasinghe *et al.*, 2010)

The underlying assumption is that nothing irreversible happens within a single ebb or flood phase, even when all changes are multiplied by the factor of n , the net result can be scaled up. The implementation of the morphological time scale factor is achieved by simply multiplying the erosion and deposition fluxes from the bed to the flow and vice-versa by the *Morfac* factor, at each computational time-step. For example, if a n value of 60 is used, after completing 12 simulated tidal cycles, the model predicts approximately one year of morphological change. Hence, the morphological evolution must only be evaluated after a whole number of tidal cycles. This method has been extensively used in the morphological updating studies e.g. Lesser (2004); Ranasinghe *et al.* (2010); Knaapen and Joustra (2012); Vanzo *et al.* (2014), and Dewals *et al.* (2015).

3.5.7 Representation of Dredging

Dredging is an important aspect in many simulations of morphological change, and a necessary requirement for this study. Often the amount of dredging required to keep a navigation channel at its prescribed depth is an important output of a numerical simulation. Also, in longer-term morphological simulations dredging is essential to keep the simulation realistic; without it entrances may silt up and bypassing rates may become too large, affecting the large-scale behaviour (Roelvink and Reniers, 2012).

In DELFT3D, the user can specify a number of dredging areas where the bottom is kept at a specified minimum depth. If the depth becomes less than this minimum depth, the excess sediment is taken out of the cell and transferred to a specified dumping area. The model then provides output of the amounts of dredged and dumped material per area as a function of time. The impacts of dredging and dumping using the DELFT3D model has previously been investigated by e.g. Hibma et al. (2008); Silveira et al. (2012); Paarlberg et al. (2015); and van Maren et al. (2015).

3.6 Summary

The hydrodynamic and morphodynamic processes in tidal inlets (estuaries) and coastal areas involve the interaction of highly variable energy vectors i.e. fresh water flow from the river, tide, and wind-wave induced sediment transport. Sediment transport in tidal inlets is the consequence of continuously exchanging water into the estuary by the flood tide, and flushing out from the estuary as an ebb jet during ebb tide. Usually, the dominant sediment transport mode is as bedload. Strong ebb currents move sediment from the tidal inlet bed to towards the offshore, where it's eventually deposited as the current wanes to form an ebb-tidal delta. In coastal waters away from tidal inlets, wave action becomes more dominant than tidal currents for governing sediment transport. Hence, previous studies of ebb-tidal deltas have classified the deltas according to the dominant processes influencing sediment transport as tidal, wave, or mixed energy.

The volume of an ebb-tidal delta is correlated with the tidal prism of the connected estuary. However, this does not consider wave effects or the impacts of

human modifications, which can change the shoal volume by more than 10% (FitzGerald *et al.*, 1984). Studies of storm effects on ebb-tidal deltas utilizing process-based morphodynamic models indicate that during storm conditions, bed load sediment transport is generally onshore directed over the shallower parts of the ebb-tidal delta as shoal bars (Herrling and Winter, 2014).

The sediment transport model DELFT3D-FLOW can be used to replicate sediment transport for tidal inlets considering tidal flow only, or combining tidal currents and the influence of waves. In this model, the suspended and bed-load sediment transport modes are separately calculated. The morphological changes resulting from the forcing can be evaluated by integrating tidal currents, wind-wave action, sediment transport, and dredging activity. For long-term modelling, a morphological acceleration factor *Morfac* can be applied to amplify the response to changing forcing.

3.7 References

- Andrews, D.G., and McIntyre, M.E. (1978). An exact theory of non-linear waves on a Lagrangian-mean flow. *Journal of Fluid Mechanics*, Vol. 89., 609-646.
- Beck, T.M., and Wang, P. . (2009). Influences of channel dredging on flow and sedimentation patterns at microtidal inlets, West Central Florida, USA. *Coastal Dynamics*.
- Boothroyd, J. (1985). Tidal Inlets and Tidal Deltas. In R. Davis Jr., *Coastal Sedimentary Environments* (pp. 445-532). New York: Springer-Verlag.
- Bruun, P., and Gerritsen, F. (1960). *Stability of Coastal Inlets*. Amsterdam: North Holland Publishing Co.
- Carr-Betts, E., Beck, T.M., and Kraus, N.C. (2012). Tidal inlet morphology classification and empirical determination of seaward and down-drift extents of tidal inlets. *Journal of Coastal Research* 28(3)., 547-556.
- Davis Jr, R. (2012). *Geology of Holocene Barrier Island Systems*. Springer Science & Business Media.
- De Swart, H.E., and Zimmerman, J.T.F. (2009). Morphodynamics of tidal inlet systems. *Ann. Rev. Fluid Mechanic Vol. 41, No. 1*, 203-229.
- Dean, R. (1988b). Sediment interaction at modified coastal inlets: Processes and policies. In D. a. Aubrey, *Hydrodynamics and Sediment Dynamics of Tidal Inlets* (pp. 412-439). New York: Springer Verlag.

- Deltares. (2013). *Hydro-Morphodynamics User Manual*. Delft, The Netherlands: Deltares.
- Dewals, B., Sebastien, E., Pierre, A., and Michel, P. (2015). Application of the morphological acceleration factor in fluvial hydraulics. *36th IAHR World Congress, 28 June - 3 July 2015*. The Hague, The Netherlands: International Association for Hydro-Environment Engineering and Research (IAHR).
- FitzGerald, D. (1982). Sediment bypassing at mixed energy tidal inlets. . *Proceedings of the Eighteenth Coastal Engineering Conference* (pp. 1094-1118). Cape Town, South Africa: ASCEI.
- FitzGerald, D. (1984a). Interactions between the ebb-tidal delta and landward shoreline: Price Inlet, South Carolina. *Journal of Sedimentary Petrology, Vol. 54, No.4*, 1303-1318.
- FitzGerald, D. (1988a). Shoreline erosional-depositional processes associated with tidal inlets. In D. a. Aubrey, *Hydrodynamics and sediment dynamics of tidal inlets* (pp. 186-225). Berlin: Springer.
- FitzGerald, D. (1996). Geomorphic variability and morphologic and sedimentologic controls on tidal inlets. *Journal of Coastal Research* 23, 47-71.
- FitzGerald, D., Buynevich, I., and Hein, C. (2012). Morphodynamics and Facies Architecture of Tidal Inlets and Tidal Deltas. In R. a. Davis Jr., *Principles of Tidal Sedimentology* (pp. 301-333). New York: Springer Science & Business Media.
- FitzGerald, D.M., Buynevich I.V., and Rosen, P.S. (2001a). Geological evidence of former tidal inlets along a retrograding barrier: Duxbury Beach, Massachusetts, USA. . *Journal of Coastal Research*, 437-448.
- FitzGerald, D.M., Buynevich, I.V., Davies Jr., R.A., and Fenster, M.S. (2002). New England tidal inlets with special reference to riverine-associated inlet systems,. *Geomorphology Vol. 48*, 179-208.
- FitzGerald, D.M., Kraus, N.C., and Hands, E.B. (2000, December). Natural mechanisms of sediment bypassing at tidal inlets. *ERDC/CHL CHETN-IV-30 US Army Corps of Engineers*, pp. 1-10.
- FitzGerald, D.M., Penland, S., and Nummedal, D. (1984). Control of barrier island shape by inlet sediment bypassing: East Friesian Islands, West Germany. *Marine Geology* 60, 355-376.
- Gaudio, D.J., and Kana, T.W. (2001). Shoal bypassing in mixed energy inlets: geomorphic variables and empirical predictions for nine inlets. *Journal of Coastal Research* 17, 290-291.
- Grasmeijer, B., and van Rijn, L. (1998). Breaker bar formation and migration. *Coastal Engineering* , 2750-2758.

- Groeneweg, J. (1999). *Wave-current interactions in a generalised Lagrangian Mean formulation. PhD thesis.* . Delft, The Netherlands: Delft University of Technology.
- Groeneweg, J., and Klopman, G. (1998). Changes of the mean velocity profiles in the combined wave-current motion in a GLM formulation. *Journal of Fluid Mechanics, Vol. 370.*, 271-296.
- Hayes, M. (1975). Chap. Morphology of sand accumulation in estuaries: An introduction to the symposium. In *Estuarine Research Vol. II* (pp. 3-22). New York: Academic Press.
- Hayes, M. (1980). General Morphology and sediment patterns in tidal inlets. *Sedimentary Geology Vol. 26 Issue 1-3*, 139-156.
- Herrling, G., and Winter, C. (2014). Barrier island inlet dynamics and ebb-tidal delta sediment bypassing under high-energy storm and fair-weather conditions. *Earth Surface Dynamic 2*, 363-382.
- Hibma, A., Wang, Z.B., Stive, M.J.F., and de Vriend, H.J. (2008). Modelling impact of dredging and dumping in ebb-flood channel systems. *Transactions of Tianjin University, Vol. 14, Issue 4.*, 271-281.
- Hicks, D.M., and Hume, T.M. (1996). Morphology and size of ebb tidal deltas at natural inlets on open-sea and pocket-bay coasts, North Island, New Zealand. . *Journal of Coastal Research Vol 12 No. 1*, 47-63.
- Hicks, D.M., Hume, T.M., Swales, A., and Green, M.O. . (1999). Magnitudes, spatial extent, time scales and causes of shoreline change adjacent to an ebb-tidal delta, Katikati Inlet, New Zealand. *Journal of Coastal Research Vol. 15, Issue 1.*, 220-240.
- Isobe, M., and Horikawa, K. . (1982). Study on water particle velocities of shoaling and breaking waves. *Coastal Engineering in Japan Vol. 25.*, 109-123.
- Joshi, P. (1982). Hydrodynamic of tidal jets. *Journal of the Waterway, Port, Coastal and Ocean Division Vol. 108*, 239-253.
- Joshi, P.B., and Taylor, R.B. . (1983). Circulation induced by tidal jets. *Journal of Waterway, Port, Coastal and Ocean Division*, 445-464.
- Knaapen, M.A.F., and Joustra, R. (2012). Morphological acceleration factor: usability, accuracy and run time reductions. *Proceedings of XIXth TELEMAC-MASCARET User Conference, 18-19 October 2012.*, (pp. 1-10). Oxford, UK.
- Kolmogorov, A. (1942). *Equations of turbulent motion of an incompressible fluid. Ser. Phys., Vol. 6, pp.55-58. (translated into English by D.B. Spalding, as Imperial College, Mechanical Engineering Department Report ON/6, 1968, London, U.K).* London, U.K.: IZV Akad. Nauk. USSR.

- Komar, P. (1996). Tidal-inlet processes and morphology related to the transport of sediments. *Journal of Coastal Research, Special Issue No. 23*, 23-45.
- Kraus, N. (2000). Reservoir model of ebb-tidal delta evolution and sand bypassing. *Journal of Waterway, Port, Coastal, and Ocean Engineering* 126(3), 305-313.
- Leendertse, J. (1987). *A three-dimensional alternating direction implicit model with iterative fourth order dissipative non-linear advection terms. WD-333-NETH*. The Netherlands Rijkswaterstaat.
- Lesser, G. (2004). *An Approach to Medium-term Coastal Morphological Modelling. A PhD Dissertation*. Delft, The Netherlands: CRC Press/Balkema.
- Lesser, G.R., Roelvink, J.A., van Kester, J., and Stelling, G.S. (2004). Development and validation of a three-dimensional morphological model. *Coastal Engineering Vol. 51.*, 883-915.
- Mehta, A.J., and Joshi, P.B. (1998). Tidal inlet hydraulics. *Journal of Hydraulic Engineering Vol. 114, Issue 11.*, 1321-1338.
- Meyer-Peter, E., and Muller, R. (1948). Formulas for bed-load transport. *Proceedings of the 2nd Meeting of the International Association for Hydraulic Structures Research*, (pp. 39-64). Delft, The Netherlands.
- Militello, A., and Hughes, S.A. (2000, September). Circulation patterns at tidal inlets with jetties. *ERDC/CHL CETN-IV-29 US Army Corps of Engineers*, pp. 1-10.
- Morgan, K.M., Kench, P.S., and Ford, R.B. (2011). Geomorphic change of an ebb-tidal delta: Mair Bank, Whangarei Harbour, New Zealand. *New Zealand Journal of Marine and Freshwater Research* 45(1), 15-28.
- Oertel, G. (1977). Geomorphic cycles in ebb tidal deltas and related patterns of shore erosion and accretion. *Journal of Sedimentary Petrology Vol. 47, Issue 3.*, 1121-1131.
- Oost, A., and de Broer, P.D. (1994). Sedimentology and development of barrier islands, ebb-tidal deltas, inlets and backbarrier areas of the Dutch Wadden Sea. *Senckenbergiana Maritima* 24, 65-115.
- Paarlberg, A.J., Guerrero, M., Huthoff, F., and Re, M. (2015). Optimizing dredge-and-dump activities for river navigability using a hydro-morphodynamic model. *Water Vol. 7*, 3943-3962.
- Prandtl, L. (1945). *Über ein neues formelsystem für die ausgebildete turbulenz (On a new formation for fully developed turbulence)*. Gottingen, Germany. : Nachrichten der Akademie der Wissenschaften (Report of Academy of Sciences) .
- Ramli, A.Y., de Lange, W.P., Bryan, K., and Mullarney, J. (2015). Coupled flow-wave numerical model in assessing the impact of dredging on the

- morphology of Matakana Banks. *Australasian Coast and Port Conference 2015*, (pp. 1-6). Auckland, New Zealand.
- Ranasinghe, R., Swinkels, C., Luijendijk, A., Bosboom, J., Roelvink, R., Stive, M., and Walstra, D.J. (2010). Morphodynamic upscaling with the morfac approach. *Coastal Engineering*, 1-7.
- Rodi, W. (1984). Turbulence models and their application in Hydraulics, State-of-the-art paper sur l'etat de connaissance. *Paper presented by the IAHR-Section on Fundamentals of Division II: Experimental and Mathematical Fluid Dynamics*. The Netherlands.
- Roelvink, J.A., and Reniers, A.J.H.M. (2012). *Advances in Coastal and Ocean Engineering Vol. 12: A Guide to Modelling Coastal Morphology*. Singapore: World Scientific Publishing Co. Pte. Ltd.
- Sha, L. (1989a). Sand transport patterns in the ebb-tidal delta off Texel Inlet, Wadden Sea, The Netherlands. *Marine Geology* 86, 137-154.
- Shields, A. (1936). Application of similarity principles and turbulence research to bed-load movement. *Mitteilungen der Preussischen Versuchsanstalt für Wasserbau und Schiffbau*, (pp. 5-24). Berlin, Germany.
- Silveira, L., Benedet, L., Signorin, M., and Bonanata, R. (2012). Evaluation of the relationships between navigation channel dredging and erosion of adjacent beaches in southern Brazil. *Coastal Engineering*, 1-15.
- Simonin, O., Uittenbogaard, R.E., Baron, F., and Viollet, P.L. (1989). Possibilities and limitations to simulate turbulence fluxes of mass and momentum, measured in a steady stratified mixing layer. *Proceeding XXIII IAHR Congress, Ottawa, August 21-25*. (pp. A55-A62). Ottawa, Canada.: National Research Council Canada.
- Spiers, K.C., Healy, T.R., and Winter, C. . (2009). Ebb-Jet Dynamics and Transient Eddy Formation at Tauranga Harbour: Implications for Entrance Channel Shoaling. . *Journal of Coastal Research* 25, 234-247.
- Stelling, G. (1983). *On the construction of computational methods for shallow water flow problems. PhD Thesis*. Delft, The Netherlands: Delft University of Technology.
- Stelling, G.S., and van Kester, J.A.T.M. (1994). On the approximation of horizontal gradients in sigma coordinates for bathymetry with steep bottom slopes. *International Journal of Numerical Methods in Fluids*, Vol. 18., 915-955.
- Uittenbogaard, R. (1998). *Model for eddy diffusivity and viscosity related to subgrid velocity and bed topography (unpublished note)*.
- van de Graaff, J., and van Overeem, J. (1979). Evaluation of sediment transport formulae in coastal engineering practice. . *Coastal Engineering Vol. 3*, 1-32.

- van Maren, D.S., van Kessel, T., Cronin, K., and Sittoni, L. . (2015). The impact of channel deepening and dredging on estuarine sediment concentration. *Continental Shelf Research, Vol. 95.*, 1-14.
- van Rijn, L. (1984). Sediment pick-up functions. *Journal of Hydraulic Engineering Vol. 110*, 121-145.
- van Rijn, L. (1993). *Principles of Sediment Transport in Rivers, Estuaries and Coastal Seas*. Delft, The Netherlands: Aqua Publications.
- van Rijn, L. (2003). Sediment transport by currents and waves; general approximation formulae Coastal Sediments. *Corpus Christi, USA*.
- Van Rijn, L. (2015). *Simple general formulae for sand transport in rivers, estuaries and coastal waters*. Retrieved from LEOvanRIJN-Sediment: <http://www.leovanrijn-sediment.com/papers/Formulaesandtransport.pdf>
- van Rijn, L., Walstra, D., Grasmeyer, B., Sutherland, J., Pan, S., and Sierra, J. (2003). The predictability of cross-shore bed evolution of sandy beaches at the time scale of storms and seasons using process-based profile models. *Coastal Engineering Vol. 47*, 295-327.
- van Rijn, L.C., and Walstra, D.J.R. (2003). *Modelling of Sand Transport in DELFT3D*. Delft, The Netherlands: Delft Hydraulics.
- van Rijn, L.C., Roelvink, J.A., and Horst, W.T. (2000). *Approximation formulae for sand transport by currents and waves and implementation in DELFT-MOR. Technical Report Z3054*. Delft, The Netherlands: WL Delft Hydraulic.
- Vanzo, D., Siviglia, A., and Zolezzi, G. (2014). Long term 2D gravel-bed river morphodynamics simulations using morphological factor: are final configurations always reliable? *Advanced Water Research 52.*, 243-260.
- Verboom, G.K, and Slob, A. (1984). Weakly reflective boundary conditions for two-dimensional water flow problems. . *5th International Conference on Finite Elements in Water Resources, June 1984, Vermont, Advances in Water Resources, Vol. 7*. Vermont: Delft Hydraulics Publication No. 322.
- Vossen, v. B. (2000). *Horizontal Large Eddy Simulations: evaluation on computations with DELFT3D-FLOW. Report MEAH-197*. Delft, The Netherlands: Delft University of Technology.
- Walstra, D.J.R., Roelvink, J.A., and Groeneweg, J. (2000). Calculation of wave-driven currents in a 3D mean flow model. In B. E. (ed.), *Coastal Engineering 2000, Vol. 2*. (pp. 1050-1063). New York: ASCE.
- Walton, T.L., and Adams, W.D. (1976). Capacity of inlet outer bars to store sand. *Proceedings of the 15th International Conference on Coastal Engineering*. (pp. 1919-1938). Reston, Va USA.: Am. Soc. of Civil Engineer.

Wang, Z. (2015). Sustainability of the multi-channel system in the Westerschelde under influence of dredging and disposal. *36th IAHR World Congress*, (pp. 65-70). The Hague, the Netherlands.

Chapter 4: Morphological Evolution of Matakana Banks Ebb-Tidal Delta

4.1 Introduction

The morphodynamics of tidal inlets and associated sand shoals are governed by the tidal prism, interactions between tidal currents and waves, sediment supply, river discharge, and geological framework (Hayes, 1980; FitzGerald *et al.*, 2012). Assessment of the relative importance of these different factors can be undertaken by examining the morphological evolution of the tidal inlet (FitzGerald, 2005). This may indicate that the significance of different processes changes over time as the inlet evolves (FitzGerald, 2005).

Comparisons between successive bathymetric surveys can be used to quantify the morphological evolution of the tidal inlet, and has widely adopted by researchers; *viz.* the study of morphological evolution of a swash platform in Portugal by Balouin *et al.* (2001). The application of echo sounders to mapping the ebb-tidal delta and nearshore area has resulted in high-resolution and high-quality bathymetric maps as demonstrated by various studies such as; DeWitt *et al.* (2007), Beck and Kraus (2011), and Barnard *et al.* (2012).

Hence, this study also utilized the bathymetric data provided by the Port of Tauranga to assess the morphological evolution of the tidal inlet system, particularly the ebb-tidal delta (Matakana Banks). The Port of Tauranga routinely conducted bathymetric surveys every 1 to 2 years within the Tauranga Harbour areas and seaward of the tidal inlet. The main surveyed offshore area covered approximately 16 km² from just inside the tidal inlet and included the entire Matakana Banks area. The purpose of the surveys were to identify and evaluate the required and extracted dredging volumes before and after the Port of Tauranga biennial maintenance dredging programme. These data can also be used to assess the morphological changes between the surveys.

This chapter describes the methodologies used for analysing the bathymetric changes over the short- and long-term between the successive surveys, volumetric changes, and net erosion-deposition of sediment on the ebb-tidal delta. 3D maps were generated in order to visualize the bathymetric changes and to track the migration of the swash bars, sandbars and sand waves. For this analysis swash bars are considered to be discontinuous, low sand bodies within the interior of swash platform; sandbars are considered to be continuous, steeper ridges on the seaward margin of the swash platform and terminal lobe, which may consist of multiple linked swash bars; and sand waves are smaller-scale multiple subparallel ridges located in the area of maximum tidal velocities beneath the ebb jet as it exits the tidal inlet.

The results obtained from the bathymetric surveys are discussed in terms of the observed morphological changes and their potential drivers.

Parts of this chapter have been presented as papers at the Coast and Ports 2013 Conference in Sydney, Australia and the 7th Asian and Pacific Coasts Conference, Bali Indonesia (Ramli and de Lange, 2013a; 2013b).

4.1.1 Acknowledgements

All bathymetric data, both single- and multi-beam echo sounder surveys, were provided by Discovery Marine Ltd (DML), who obtained the data for the Port of Tauranga Ltd. Considering the individuals who contributed to the multi-beam echo sounder surveys requested as part of this project, I would particularly like to thank Dirk Immenga from The University of Waikato, and Greg Cox, Bruce Wallen and Declan Stubbing from DML.

4.2 Material and Methods

4.2.1 Bathymetric Maps

4.2.1.1 Single Beam Echo Sounder (SBES) Surveys

Repeated SBES bathymetric mapping was undertaken over 13 years, from 1998 to 2011 (Table 4-1), of the Matakana Banks ebb-tidal delta and Tauranga Entrance Channel employing a single-beam Knudsen 320M echosounder. This SBES system operated at a frequency of 210 kHz with a 9 degree beam width and range scale of 20 m. The bathymetric dataset obtained from these SBES surveys

were formatted as xyz ASCII text files, with the 3 columns representing the location as Easting and Northing coordinates, and elevation respectively.

Table 4-1. Months during which SBES surveys were carried out between 1998 and 2011.

Surveys	Months								
	Mar	Apr	May	June	July	Aug	Sept	Oct	Nov
1998									
1999									
2000									
2001									
2002									
2006									
2008									
2009									
2010									
2011									

The location and elevation xyz data were translated into a uniformly spaced terrain model, or grid (Caress *et al.*, 2008) using the mapping software SURFER™ version 10. Data were then interpolated by the krigging method to produce a grid with a 21 m x 25 m spacing. This study only focussed on the Matakana Banks area, so the gridded bathymetric maps were masked to display only the Matakana Banks area (Figure 4-1). The resulting mapped area spans about 3.7 km in both cross- and along-shore directions.

All bathymetry maps generated used the same grid size in order to be comparable (Table 4-2) for further analysis.

Table 4-2. Grid information for bathymetry map from single beam echo sounder surveys

Grid Size	153 rows x 176 columns
X Spacing	21.03 m
Y Spacing	24.75 m

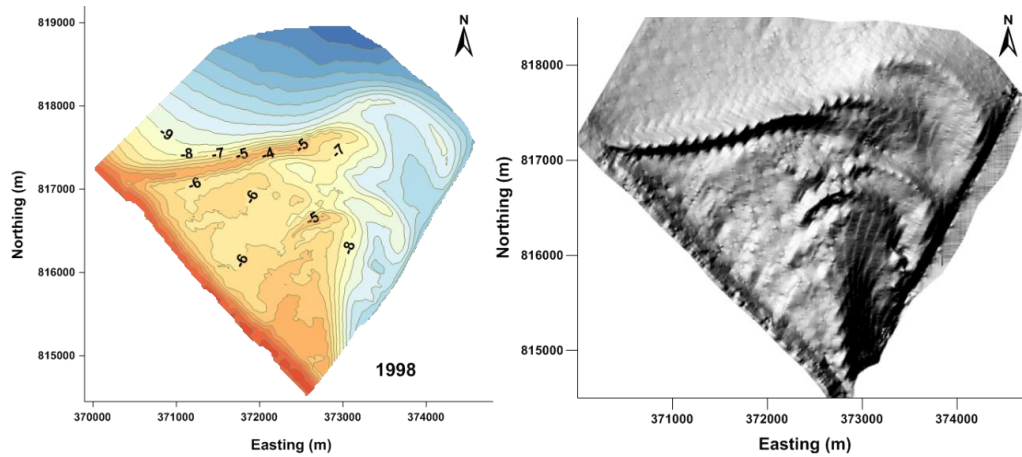


Figure 4-1. 20 m resolution contour and shaded relief bathymetry maps of Matakana Banks ebb-tidal delta. Bathymetry outside of the Matakana Banks ebb-tidal delta is blanked out to focus on study area only. Both maps are presented in the coordinate system of NZGD2000/Bay of Plenty Circuit.

4.2.1.2 Multi Beam Echo Sounder (MBES) Surveys

When plotted, the SBES survey data showed a relatively poor coverage of the Matakana Banks area, which is especially evident as artefacts in the shaded relief bathymetric maps (Figure 4-1, right hand image). Multi-beam echo sounder (MBES) surveys have a more complete coverage of the seafloor, which produces higher resolution thematic maps (Figure 4-2, right hand image) that can provide better information on seafloor characteristics. For example MBES systems in shallow-water have been used to derive the spatial distribution of seafloor relief, together with the bottom type and composition (Galparsoro et al., 2010); map the distribution of habitats in shallow coastal waters (Micallef et al., 2012); map detailed bed morphology (Bartholoma *et al.*, 2004); and measure bedform transport rate (Nittrouer *et al.*, 2008).

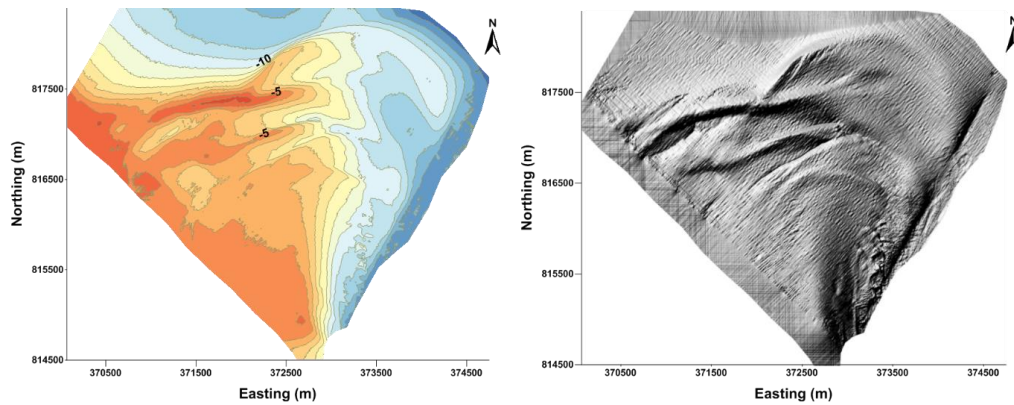


Figure 4-2. High resolution bathymetric map obtained from MBES system of surveys March 2013. 5 m resolution contour and shaded relief maps of Matakana Banks ebb-tidal delta. The raw xyz data were interpolated with krigging method. Contour interval is 1 m.

MBES surveys were carried out in March and July 2013, and October and November 2014. The surveys used a RESON 7125 system at 400 kHz with 512 beams, which measures the relative water depth across a 140° wide swath perpendicular to the track of the survey vessel (Ramli and de Lange., 2013). The resulting bathymetric dataset was interpolated using the krigging method, resulting in a 5 m resolution map (Table 4-32). The original survey coordinate system was the NZGD 2000/Bay of Plenty Circuit. For the purpose of numerical modeling with Delft3D, the coordinate system was converted to WGS84 UTM 60S.

Table 4-3. Grid information for the bathymetry map derived from multibeam echosounder surveys.

Grid Size	740 rows x 758 columns
X Spacing	5 m
Y Spacing	5 m

4.2.2 Ebb-Tidal Delta Volume Calculation

There are several methods used to quantify ebb-tidal delta area, total volume, and volume changes; such as by relating their volume to the tidal prism (Walton and Adams, 1976; Marino and Mehta, 1988; and Hicks and Hume, 1997). Hicks and Hume (1996) used a “no delta” method, which estimates the bathymetry without a delta, to determine the ebb-tidal delta sand volume calculation for Matakana Banks and obtained $47.3 \times 10^6 \text{ m}^3$. Subsequently, Hicks and Hume (1997) determined the ebb-tidal delta sand volume changes as volume differences between 2 successive surveys by subtracting corresponding grid points of two interpolated

bathymetric grids for the difference years. This later method is then adopted in this study.

The volume and sedimentation/erosion analyses were done using Surfer 10 from Golden Software (Golden Software, 2011). The grid points for the initial year of any comparison are treated as the *lower surface* and the final year as the *upper surface*, hence the difference is the volume difference between the two surfaces. In Surfer 10, the volume beneath a surface can be calculated by three different algorithms: Trapezoidal Rule; Simpson's Rule; and Simpson's 3/8 Rule, including the Cut and Fill calculations. The mean value of all three methods was taken as the total volume for a specific surface.

4.2.3 Cross-Section Profiles

Cross-section profiles were generated to help visualize the bathymetric changes and to track the migration of the swash bars. Each bathymetry map was subdivided by 7 standard cross-shore profiles defined by the distance from the southern-most corner of the gridded region (Figure 4-2).

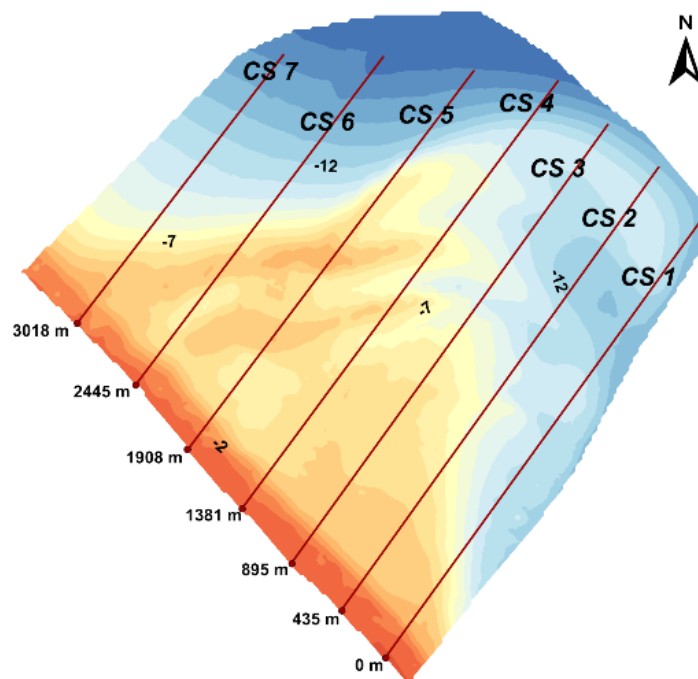


Figure 4-3. Locations of the southeast to northwest aligned cross-sections for the Matakana Banks ebb-tidal delta.

To simplify the analysis of cross-shore profiles, the 7 profiles (Figure 4-3) were classified into 3 groups: group A located nearest to the tidal inlet, which included profiles 1, 2 and 3, and tracked changes associated with the tidal inlet (particularly the ebb jet orientation and strength); group B for cross-sectional profiles that crossed the shallowest parts of Matakana Banks, including profiles 4 and 5, and focussed on tracking the morphological evolution of the swash bars; and group C for profiles 6 and 7 located on the northwest of Matakana Banks, which tracked any extension or retreat of the terminal lobe.

4.2.4 Net Morphological Change

Erosion and accretion result from the interactions between hydrodynamic forcing due to currents and waves, sediment transport and availability, and anthropogenic influences. Hence, characterising the spatial distribution of erosion and accretion is important for evaluating the morphological evolution after some period of time. In this study, the patterns of erosion and accretion were presented as maps of the net morphological change or residuals between two surfaces. In Surfer 10, erosion and accretion between two bathymetric surveys was calculated by using the Grid Math tool that subtracted one bathymetric surface from another to show net change.

4.2.5 Hydrodynamic Conditions during the Observation Period

Tauranga Harbour is known as a tide-dominated inlet, with a mean tidal range of 1.4 m and a mean annual significant wave height of 0.5 m (de Lange, 1991). Based on the field measurements at the Tauranga tidal inlet obtained during 11 April to 5 May 2013, the mean tidal range at station 390 (inside the harbour) is 1.3 m during neap tide and about 1.6 m in spring tide, with a mean tidal current speed of 0.74 m/s. Mean tidal ranges between 1.4 m to 1.6 m at the Tauranga Harbour Entrance were also obtained from the online tide forecaster (NIWA, 2013) for the same time period. Wave datasets were provided by MetOcean Solution Ltd, and wind datasets were downloaded from Cliflo (NIWA, 2014). Mean tidal range, wave

and wind conditions for each survey period are summarized in Table 4-4, and the significant wave height is displayed in Figure 4-4.

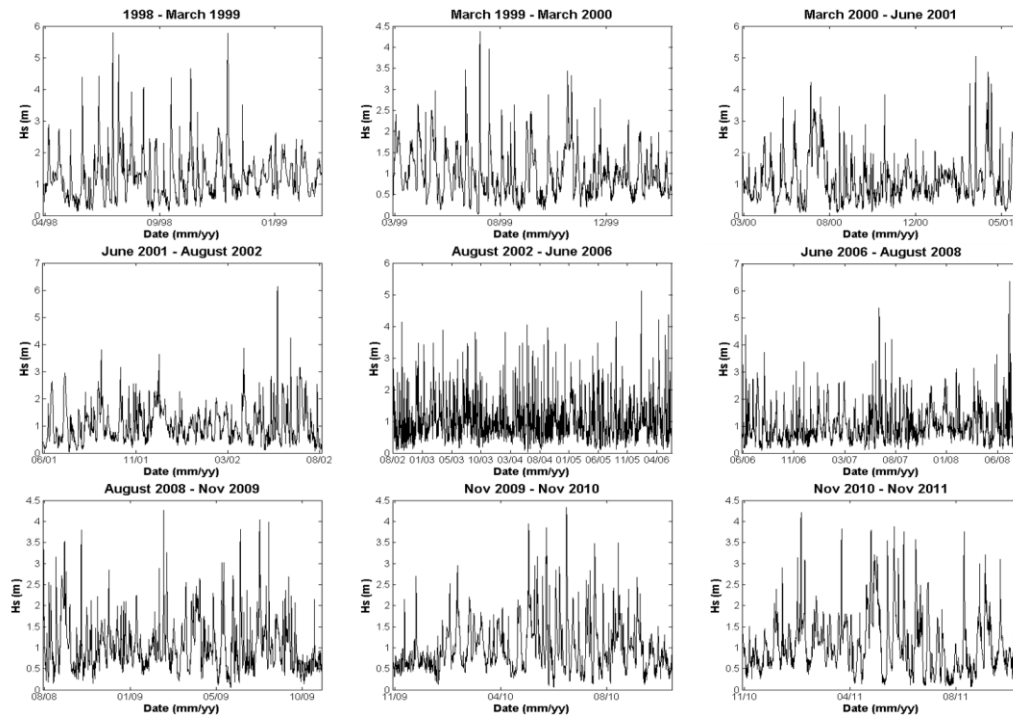


Figure 4-4. Significant wave heights (H_s) conditions of each survey period from 1998 to 2011. Note that the y axes are different scales.

The wave time series of significant wave heights indicate several storm events in between two successive surveys (Figure 4-4). Over the period from 1998 to 2011, there were four major storms with significant wave heights >5.5 m; between 1998-1999, 2001-2002, and 2006-2008. In the period of 1998-1999, there were two large storms recorded in July and November 1998, both with significant wave heights around 5.8 m. In June 2002, a storm event with significant wave height of 6.1 m occurred, while the highest significant wave height recorded was in July 2008 at about 6.3 m.

Table 4-4. Summary of mean tidal range, wave, energy and wind conditions of between surveys from 1998 to 2011.

Surveys	Mean Tidal Range (m)	H _s (m)	T _p (s)	Wave Dir (°)	Power (W.m ⁻¹)	Wind Speed (m/s)	Wind Dir (°)
1998 - 1999	1.6	1.2	9	68	1.11E+04	4.2	192
1999 - 2000	1.6	1	8	68	6.60E+03	3.8	197
2000 - 2001	1.5	1.1	8	82	8.02E+03	4.1	198
2001 - 2002	1.5	1	8	86	7.44E+03	4	203
2002 - 2006	1.5	1	9	94	7.58E+03	4.1	209
2006 - 2008	1.4	1	8	91	7.16E+03	3.9	205
2008 - 2009	1.5	1	8	89	7.16E+03	3.9	204
2009 - 2010	1.5	1	9	83	7.74E+03	3.9	203
2010 - 2011	1.5	1	8	81	7.58E+03	3.7	190

4.3 Results and Discussion

4.3.1 Bathymetric Changes (SBES) from April 1998 to November 2011

Generally, from 1998 to 2011 the main shape of Matakana Banks ebb-tidal delta (ETD) remained stable as determined by single beam echo-sounder surveys (Ramli and de Lange, 2013). This consistency was also observed by Brannigan (2009), based on annual surveys and volumetric calculations, and he concluded that the Matakana Banks ETD generally remained stable between 1989 and 1995 with minor localized changes.

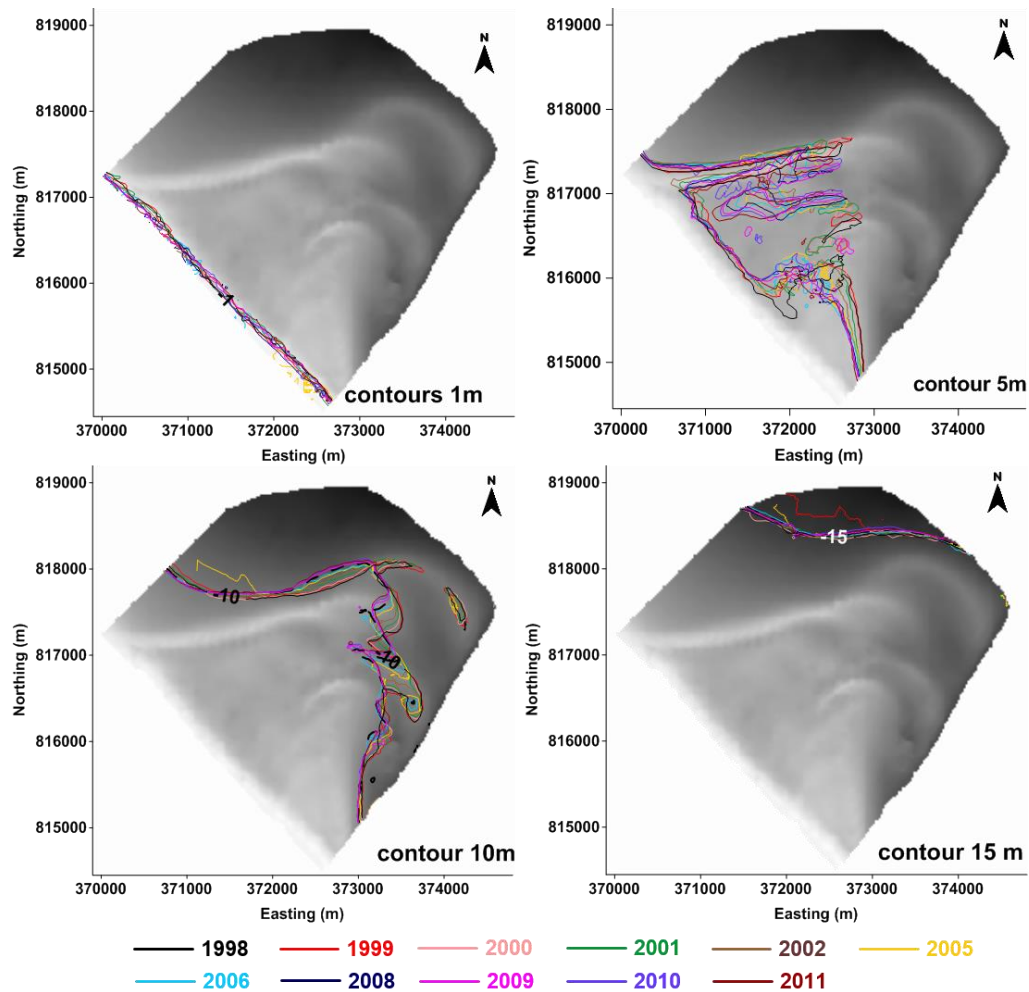


Figure 4-5. The positions between 1998 and 2011 of the 1 m, 5 m, 10 m and 15 m depth contours reflect the bathymetric variability associated with the location of the terminal lobe (particularly the 10 m contour) and the swash bar migrations over the ebb tidal delta (particularly the 5 m contour). The 1 m and 15 m contours indicate that the shoreward and seaward boundaries are relatively fixed.

The surface of the Matakana Banks ebb-tidal delta is always submerged and subject to tidal and wave-induced currents. The bedforms present are continually being modified by sediment transport, including the larger features such as swash bars and sand waves. Therefore, the positions of the swash bars and sandbars were not always precisely the same during the different surveys (Figure 4-5, 5 m contours). The terminal lobe in the northwest and spit shaped terminal lobe on the eastern part remain relatively consistent in its spatial extent and shape over the observation periods. The southeastern boundary of the Matakana Banks is the Tauranga Harbour Entrance Channel, where morphological changes are controlled by tidal currents due to the water depth within the channel.

Beyond the terminal lobe, which is represented by 15 m contour, the seabed seems to be stable (Figures 4-5 and 4-6) suggesting the 15 m contour is a good indicator of the outermost limit of the ebb-tidal delta. The spatial extent over which the morphology showed noticeable changes is mostly restricted toward the north-western part where the ebb-tidal delta welds into the shoreline (Figure 4-5).

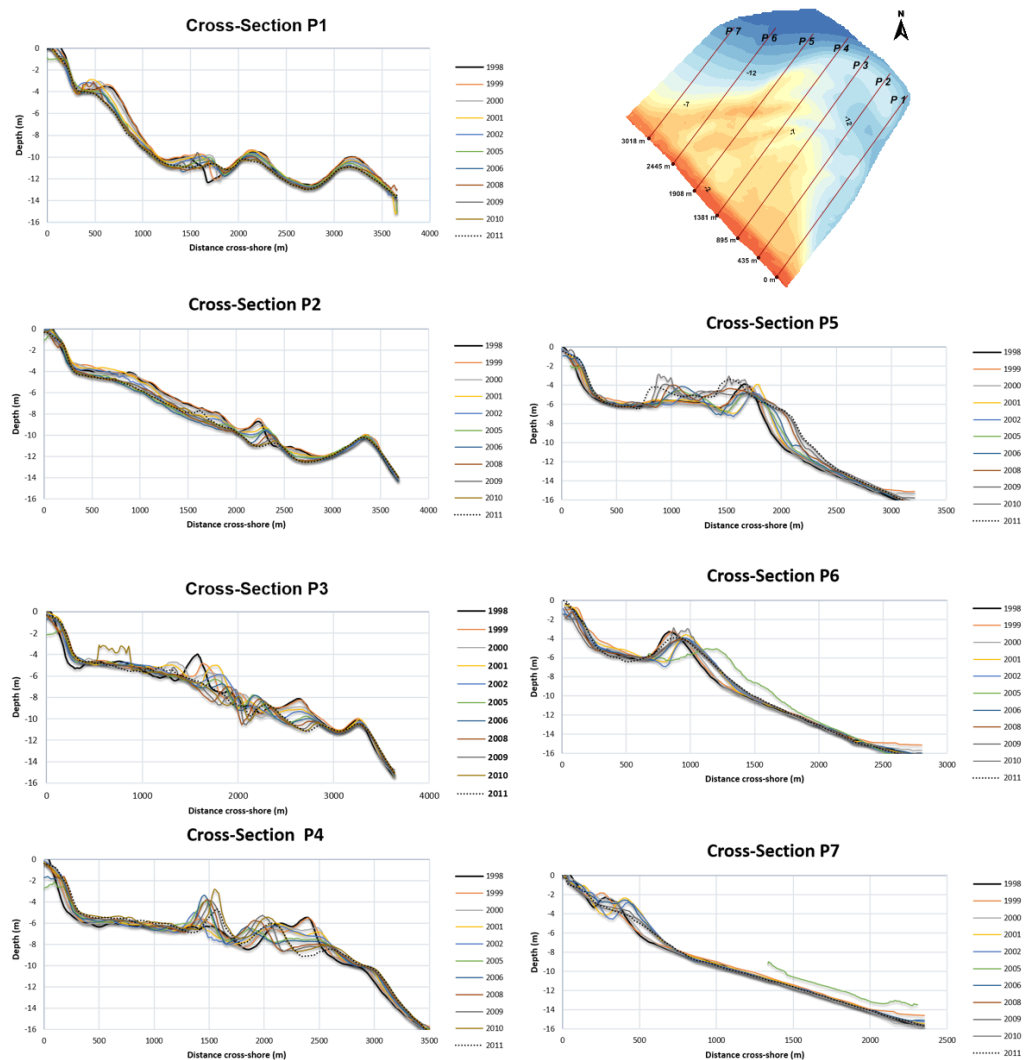


Figure 4-6. Cross-section profiles 1 to 7 distributed evenly from the southeast to northwest Matakana Banks ebb-tidal delta for SBES surveys between 1998 and 2011. These profiles show that the most dynamic area is on the swash platform (profile P3-P5) where the waves break. The least dynamic is the northwestern margin of the delta (terminal lobe).

Towards the middle part of Matakana Banks, over the ebb-delta shoals or the swash platform, waves become increasingly important. The swash platform with depths range between 5 m to 10 m where the distance from the reference April 1998 shoreline is less than 3000 m, more significant and more variable morphological changes took place (Figure 4-6). Sediment transport on the swash platform appears

to be bi-directional, with swash bars migrating onshore and offshore, consistent with the experimental findings of Yin *et al.* (2012).

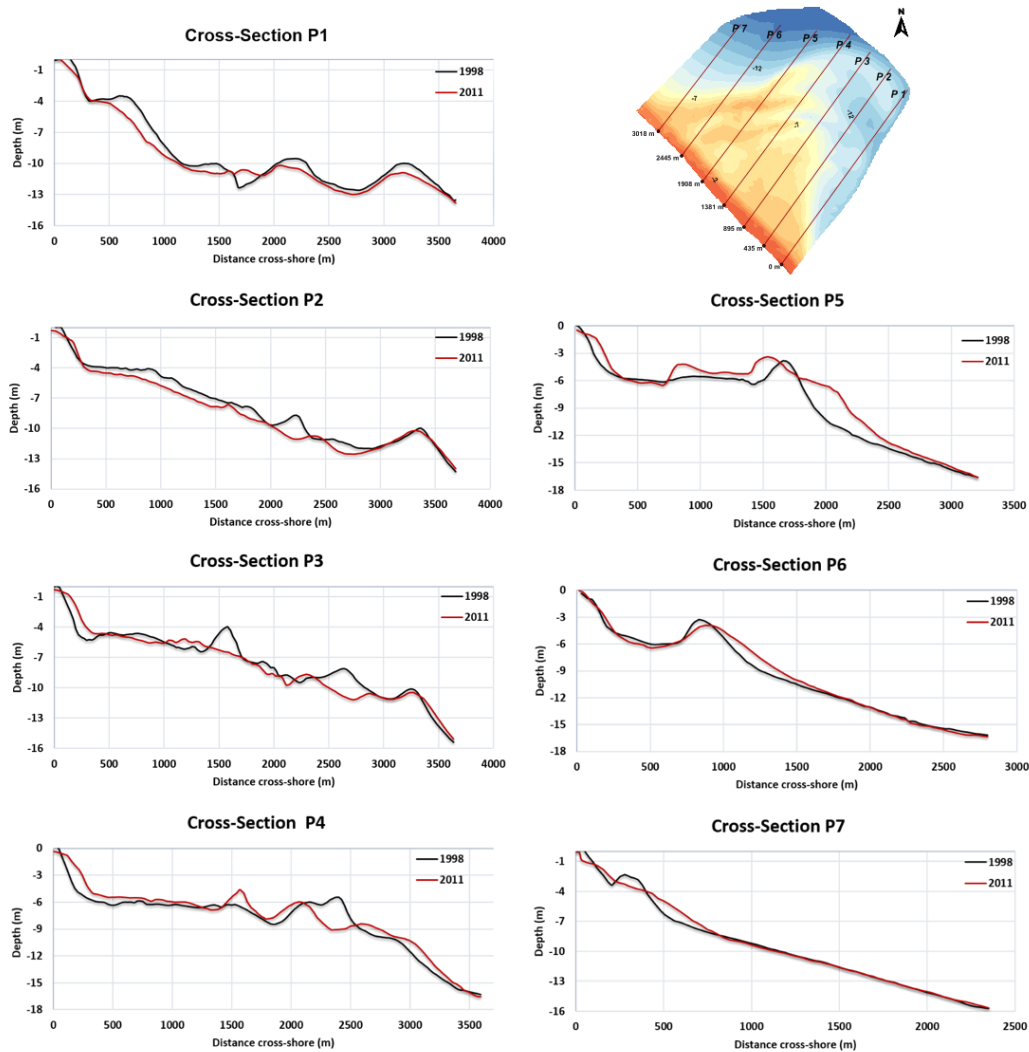


Figure 4-7. Comparison of the 1998 and 2011 cross-shore profiles to illustrate the net decadal differences in bed elevation (after 13 years).

Apart from wave-driven swash bars, the other main area of significant bathymetric changes are northwards migrating sand waves that appear in deeper water on the eastern margin of the Matakana Banks, as shown in the surface plots in Figure 4-5 and cross-sections P1-P3 or Figure 4-6. These sand waves contribute to the variability observed in the 10 m contour along the eastern margin of swash platform, and are attributed to sediment transport associated with the ebb jet (Ramli and de Lange, 2013). Unlike the generalised Hayes morphological model for an ebb-tidal delta (FitzGerald, 2005) discussed in Chapter 3, the Matakana Banks delta does not display well-developed channel margin linear bars. However, it does have

almost continuous bars formed from merged swash bars that are located on the seaward parts of the swash platform and on the terminal lobe (Figure 4-7).

Overall, the bathymetric changes are consistent with offshore sediment transport of sediment via migrating bed forms in the original pre-dredging ebb channel. The sand waves transport sediment up onto the swash platform and contribute sediment to the terminal lobe when the ebb current velocity weakens.

The annual SBES cross-section profiles from 1998 to 2011 of Matakana Banks ebb-tidal delta will be examined in more detail below. The profiles can be subdivided into three main groups based on their overall shape and behaviour (Figures 4-5 and 4-6): Group A – profiles P1-P3; Group B – profiles P4-P5; and Group C – profiles P6-P7.

Along profile P1 (group A), the morphologies of the swash bars are relatively stable, with bed elevation variations <2 m (Figures 4-5 and 4-6). However, over time the extent of the swash platform with swash bars expanded seaward (Figure 4-6). Profile P2 has a gentler seawards sloping surface and the first line of swash bars developed at about 2,200 m from the shoreline. During the period of observation, this line of swash bars migrated ~200 m further offshore, producing localised erosion of up to 4 m from the initial bed elevation at the original location. Beyond 2,800 m from the shoreline, where the depth is about 12 m, the bed elevations were more stable, and the outermost line of swash bars at 3,350 m offshore (on the terminal lobe) shows almost no variability. Profile P3 shows the bed elevation variability generally increases significantly beyond 1,400 m from the shoreline, although the 2010 survey indicates a temporary zone of accretion around 500-700 m that may be erroneous. Starting at about 1,400 m offshore, at a depth of about 6 m, the bed variations associated with offshore swash bar migration becomes more intense, until the bed elevation becomes more stable beyond 3,000 m offshore. Thus, this location was taken to indicate the northeastern boundary of the ebb-tidal delta.

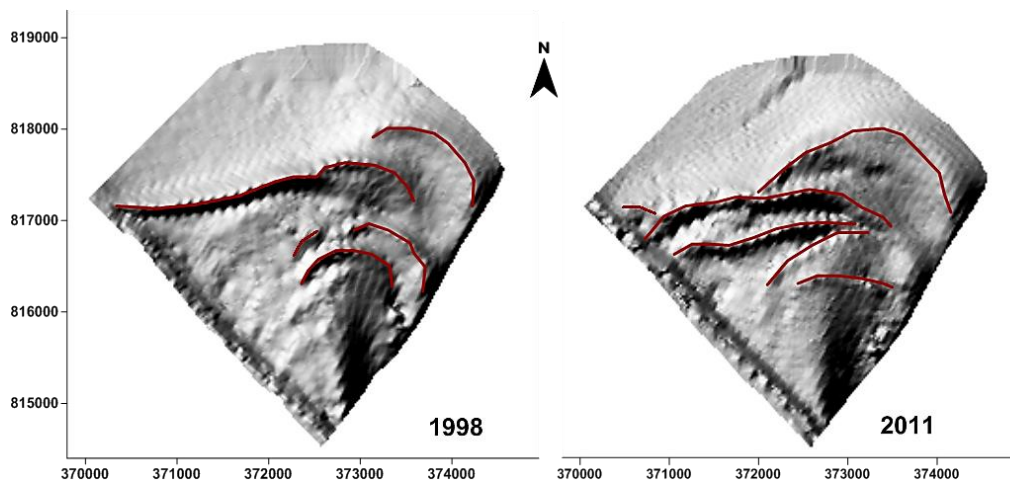


Figure 4-8. Shaded relief surface maps of Matakana Banks ebb-tidal delta. It is clearly seen that from 1998 to 2011, the swash bars changed shape, became more complex, and migrated offshore (modified from Ramli & de Lange, 2013).

The profiles in Group B (P4 and P5) correspond to the middle part of the ebb tidal delta (Figures 4-6 and 4-7). Along profile P4, the swash platform extended further offshore than any of the other profiles. In the beginning of the observation period (1998), the first (shoreward) line of swash bars, with a height up to 2 m, was located 1,875 m from the shoreline. This line of swash bars migrated up to 585 m landward by the end of observation period in 2011 (Figure 4-7), and additional lines of swash bars developed further offshore (Figure 4-8).

Cross-shore Profile P5 shows that the most dynamic swash bar migration occurs at a distance of between 700 m to 2,500 m from the shoreline (Figure 4-6). In this region, deposition dominated over the period analysed, as indicated by a 3.7 m increase in the bed elevation at of distance of 2,000 m by 2011. Beyond 2,500 m, the bed smoothly slopes down offshore. Double-ridge sandbars, which are captured in Profile P5 (Figure 4-7) are inferred as the result of the northward migration of sand towards the outermost sandbar on the terminal lobe. Once at the margin of the ebb tidal delta, sediment moves east and west, resulting in the eastward and westward extension of the seaward sandbar (Figure 4-8). Overall, the changing location of the seaward extent of the swash bars observed in profile P5 has resulted in a narrowing of the swash platform by 2011.

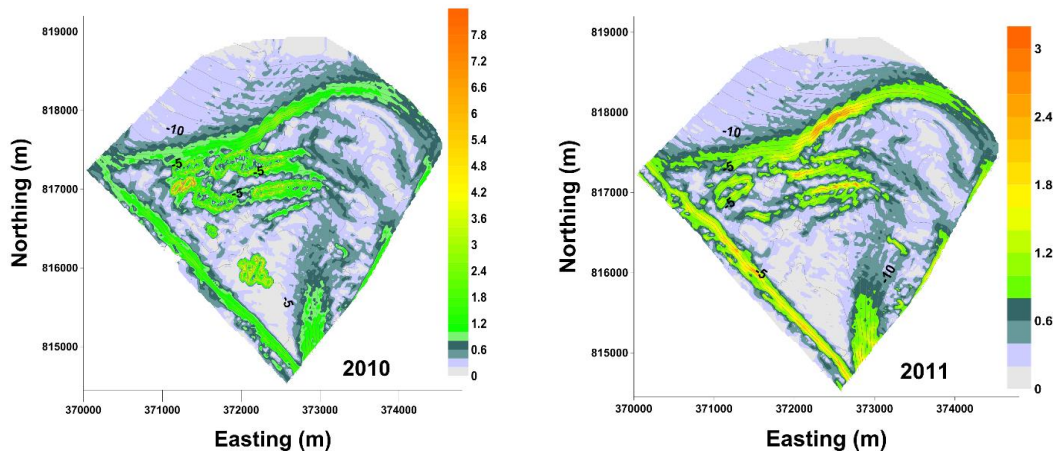


Figure 4-9. Maps of slope gradients. The steepest slope gradient up to 8.4° of Matakana Banks ebb-tidal delta was reached in 2010 and the gentlest slope was reached in the next year (2011) that less than 3.2° .

Group C represents the region on the northwest boundary of the ebb-tidal delta where the swash platform narrows and welds onto the surf-zone offshore bars of Matakana Island. During the observation period, the outer bar on profile P6 shifted ~ 200 m offshore. Meanwhile, profile P7 became flatter than the original profile in 1998.

Overall, the swash platform morphology was always consistent and characterised by a very gentle slope surface with a maximum angle 0.6° . The same slope gradient also found within the troughs between the sandbars and outside of the ebb tidal delta. However, the sandbars were steeper with slope angles of $1 - 8^\circ$ (Figure 4-9 and Appendix 4).

4.3.2 Sand Volume Variability from April 1998 to November

2011

Different volume calculation methods will give different total net volumes. For this study, the method demonstrated by Hicks and Hume (1996) is considered accurate enough to reflect the general volume trends of the ebb-tidal delta over a certain period. The ebb-tidal delta sand volume variability is summarized in Table 4-5 for the period April 1998 to November 2011. These data indicate that the sand volume variability increased as over time.

Over the 13 years analysed, the net sand volume increased, indicating that accretion was the dominant process. In November 2011, there was ~ 7 million m^3 sand added to the ebb tidal delta compared to 1998. Based on the total area of the

ebb-tidal delta in 2011, the volumetric changes correspond to an increment of about 0.68 m sand thickness. However, there were years where the volumetric changes were negative and erosion dominated, when the average sand thickness decreased by 0.32 - 1.35 m over the total ebb-tidal delta area. During other periods, accretion was indicated by sand addition of about 0.32 - 2.37 m. Hence, while there was overall accretion, it was smaller than the short-term variability that ranged over 3.72 m (-1.35 m to 2.37 m) averaged across the whole ebb tidal delta.

Table 4-5. Summary of volumetric changes extent of erosion and accretion, and average sand thickness changes for the Matakana Banks ebb-tidal delta over the period 1998 to 2011. Negative values denote erosion and positive values denote accretion.

Surveys	Volumetric changes		Affected Areas			Average sand thickness change (m)
	Between surveys (m ³)	Monthly (.10 ⁵ m ³)	Erosion (m ²)	Accretion (m ²)	Total Area (m ²)	
March 1999 - April 1998	- 5,853,244	-5.32	7,298,882	3,842,513	11,141,395	-0.52
March 2000 – March 1999	3,292,265	2.74	4,127,925	7,138,856	11,266,782	0.29
June 2001 – March 2000	3,683,616	2.46	4,195,099	7,160,759	11,355,858	0.32
Aug 2002 – June 2001	- 4,335,961	-3.10	8,502,050	3,170,386	11,672,436	-0.37
June 2006 – August 2002	- 7,603,186	-1.65	6,676,014	3,403,491	10,079,505	-0.75
August 2008 – June 2006	18,953,459	7.29	1,896,319	6,084,352	7,980,671	2.37
November 2009 – August 2008	11,463,426	7.64	2,263,364	8,122,995	10,386,359	1.1
November 2010 – November 2009	- 14,268,542	-1.19	7,144,001	3,350,828	10,494,829	-1.35
November 2011 – November 2010	-11,063,405	-9.22	9,547,381	1,318,820	10,866,201	-1.02
November 2011 - April 1998	7,078,462	-	3,645,769	6,746,417	10,392,187	0.68

The largest sand volume increment occurred between June 2006 and August 2008, which followed the dredging of 276,398 m³ from the Entrance Channel in 2006 (see Table 4-5 dredging volume). For the negative volumetric changes, the largest sand volume decrement occurred between November 2009 and November 2010 (Table 4-5).

4.3.2.1 Bathymetry April 1998 to March 1999

The morphological changes of the ebb-tidal delta over 11 months between 1998 and 1999 is shown in the Figure 4-10. This period corresponds to a strong La Niña event that followed the “super-El Niño” of 1997-98, and 113,466 m³ of sediment, corresponding to ~0.01 m over the area of the delta, was dredged from the Entrance Channel in November 1998 (Table 4-5). The 3D single-beam bathymetry maps of 1998 and 1999 show that the seaward margin of the ebb-tidal delta consisted of five curved bands of large sandbars separated by wide troughs. The alignment of the bands, particularly the inner ones, changed between the two surveys.

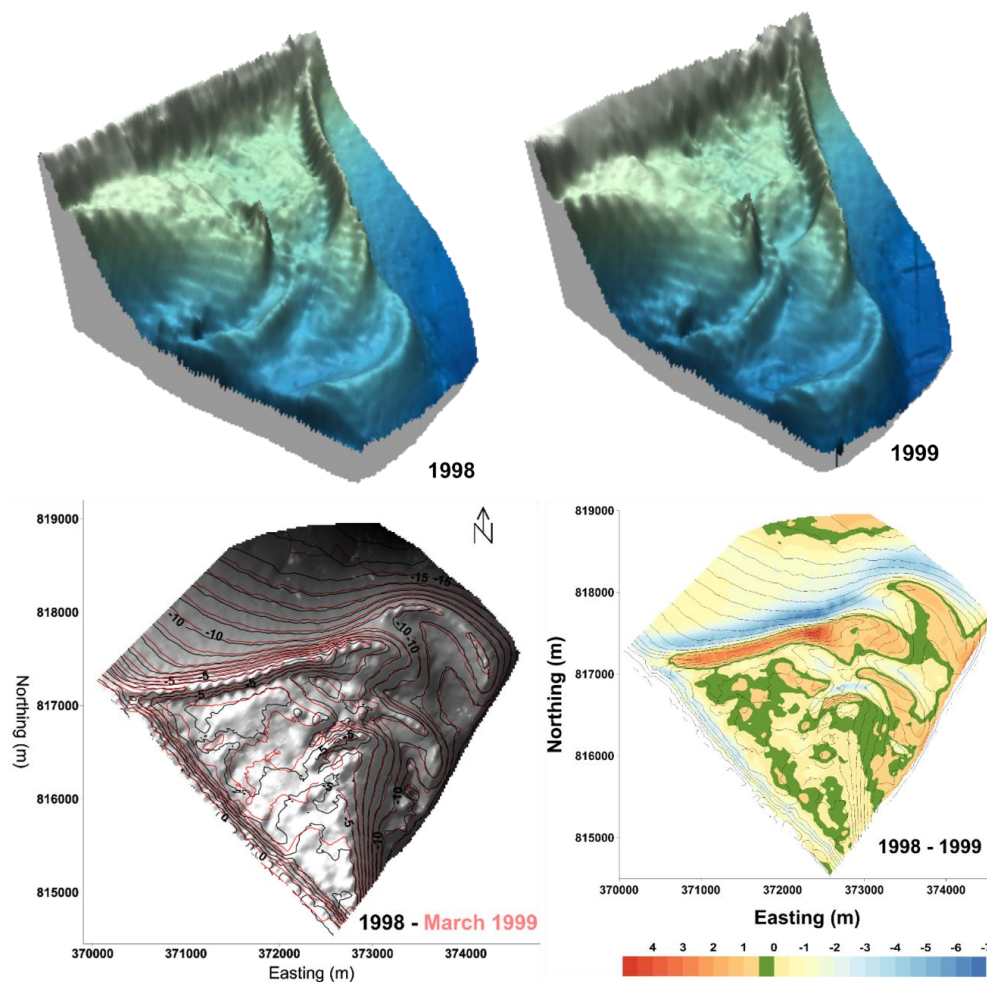


Figure 4-10 Morphology of the Matakana Banks ETD from SBES surveys in 1998 and 1999. The upper images are colour-shaded 3D surfaces interpolated from the SBES data. The lower images highlight the sandbars migration for Matakana Banks. The lower left image is a shaded relief map of the 1998 bathymetry overlaid with the contours for the 1998 (black) and 1999 (red) surveys. The lower right image is a residual map that shows the locations where accretion (positive) and erosion (negative) occurred after a year of hydrodynamic forcing.

Between 1998 and 1999 the sandbars migrated seaward, as shown in the superimposed contour map (Figure 4-10 lower left), and in the cross-section profiles (Figure 4-11). From the contour map, the general migration of the sandbars was seaward by up to about 145 m on the margins of the shoal platform, and up to 123 m at the northeastern-most sandbar on the terminal lobe.

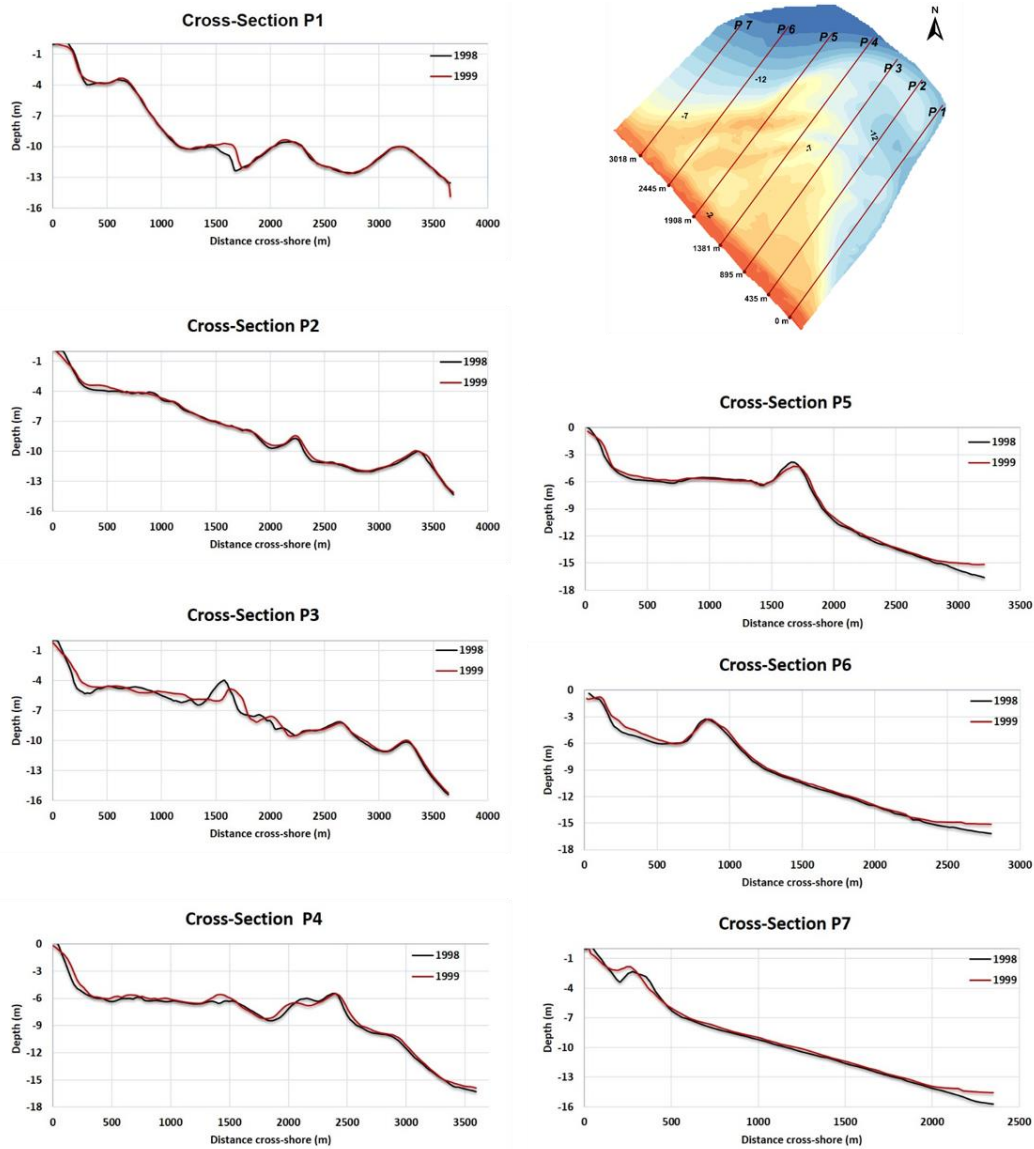


Figure 4-11 Comparisons of cross-shore profiles obtained in 1998 and 1999, which show a general seaward movement of the sandbars.

Cross-sectional profiles show that the steepest slopes and the narrowest swash platform of the ebb-tidal delta are developed closest to the tidal inlet and ebb jet (group A: P1-P3). The swash platform width increases with gentler slopes in the central area represented by group B (P4 and P5). Finally cross-sectional profiles P6

and P7 represent the northwestern boundary of the ebb-tidal delta, where the swash platform narrows and the seaward slopes are the flattest.

Net volumetric changes show that between 1998 and 1999 sediment erosion dominated over accretion. Erosion affected about 66% of the total ebb-tidal delta area, decreasing the ebb tidal delta volume by $\sim 5.85 \times 10^6 \text{ m}^3$ ($\sim 0.532 \times 10^6 \text{ m}^3 \cdot \text{month}^{-1}$) corresponding to -0.52 m sand thickness decrement by March 1999 (Table 4-5). Most of the erosion occurred on the seaward margin of the terminal lobe and localised spots along the shoreface of Matakana Island (Figure 4-10). There were no significant changes in the terminal lobe slope gradient; in 1999 the steepest slope of 4.8° was located on the NW terminal lobe and this was 0.6° steeper than in 1998. For both years, gentle slopes $< 0.6^\circ$ dominated the swash platform area.

4.3.2.2 Bathymetry March 1999 to March 2000

The morphological changes of the ebb-tidal delta for one year from March 1999 to March 2000 are presented in Figure 4-12. This period was associated with neutral to La Niña conditions, and no dredging occurred. A strong tidal influence is evident in cross-sectional profile P1 (Figure 4-13) located adjacent to the Entrance Channel, with no swash platform developed in this area and steepest slopes of the ebb-tidal delta. Sandbar migration is evident up to 1,900 m from the shore. However, further than that the bed surface became stable.

The widest swash platform is seen in profiles P3 to P5 (group B) between 895-1,900 m from the Entrance Channel. Here the swash platform is well developed at depths between 4-7 m.

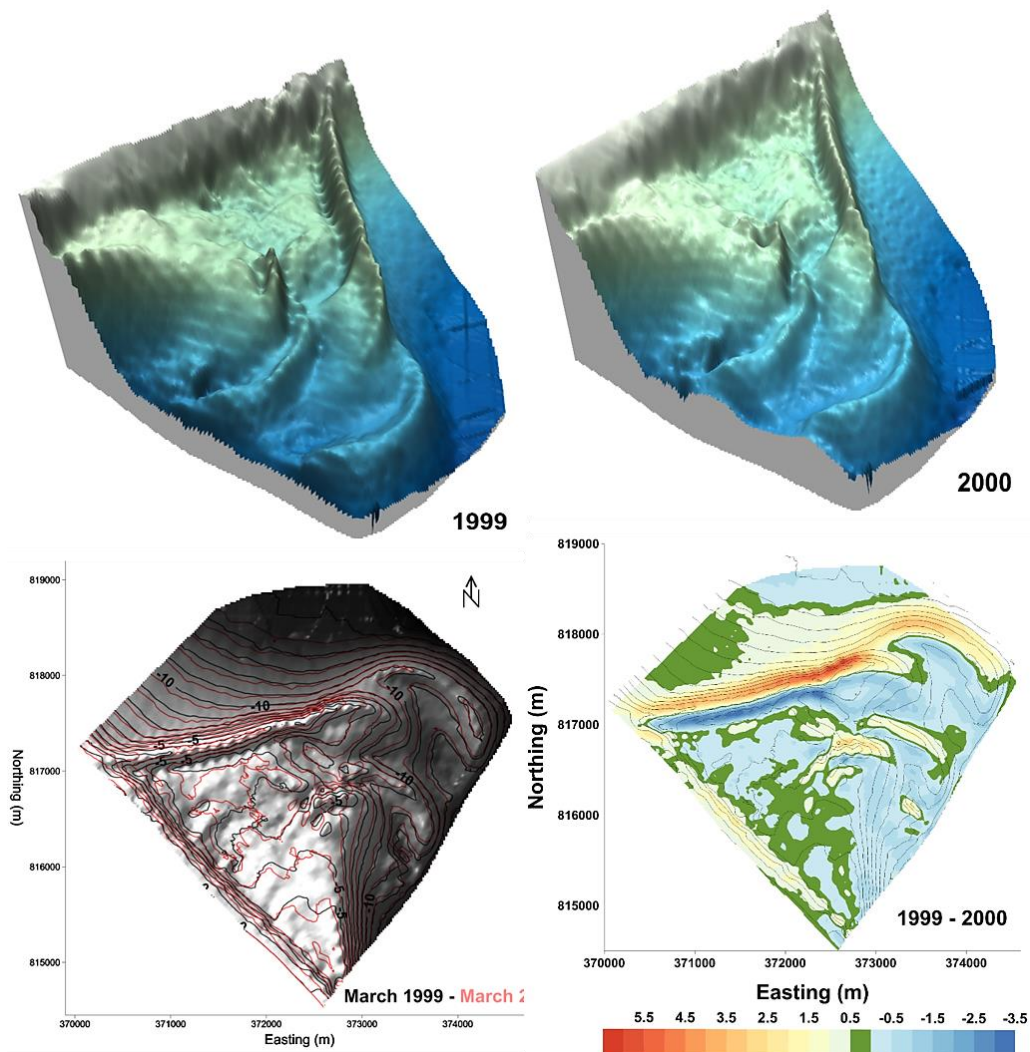


Figure 4-12 Morphology of the Matakana Banks ETD from SBES surveys in 1999 and 2000. The upper images are colour-shaded 3D surfaces interpolated from the SBES data. The lower images highlight the sandbars migration for Matakana Banks. The lower left image is a shaded relief map of the 1999 bathymetry overlaid with the contours for the 1999 (black) and 2000 (red) surveys. The lower right image is a residual map that shows the locations where accretion (positive) and erosion (negative) occurred after a year of hydrodynamic forcing.

Group C profiles are located more than 2,445 m to the NW of the Entrance Channel. In this zone, the swash platform narrows (P6) before disappearing complete at 3,018 m (P7). Hence, this region indicates the furthest alongshore extension of the ebb tidal delta, where the outermost sandbar or terminal lobe welds to the shore. The slope gradients of this NW terminal lobe were up to 4.8°.

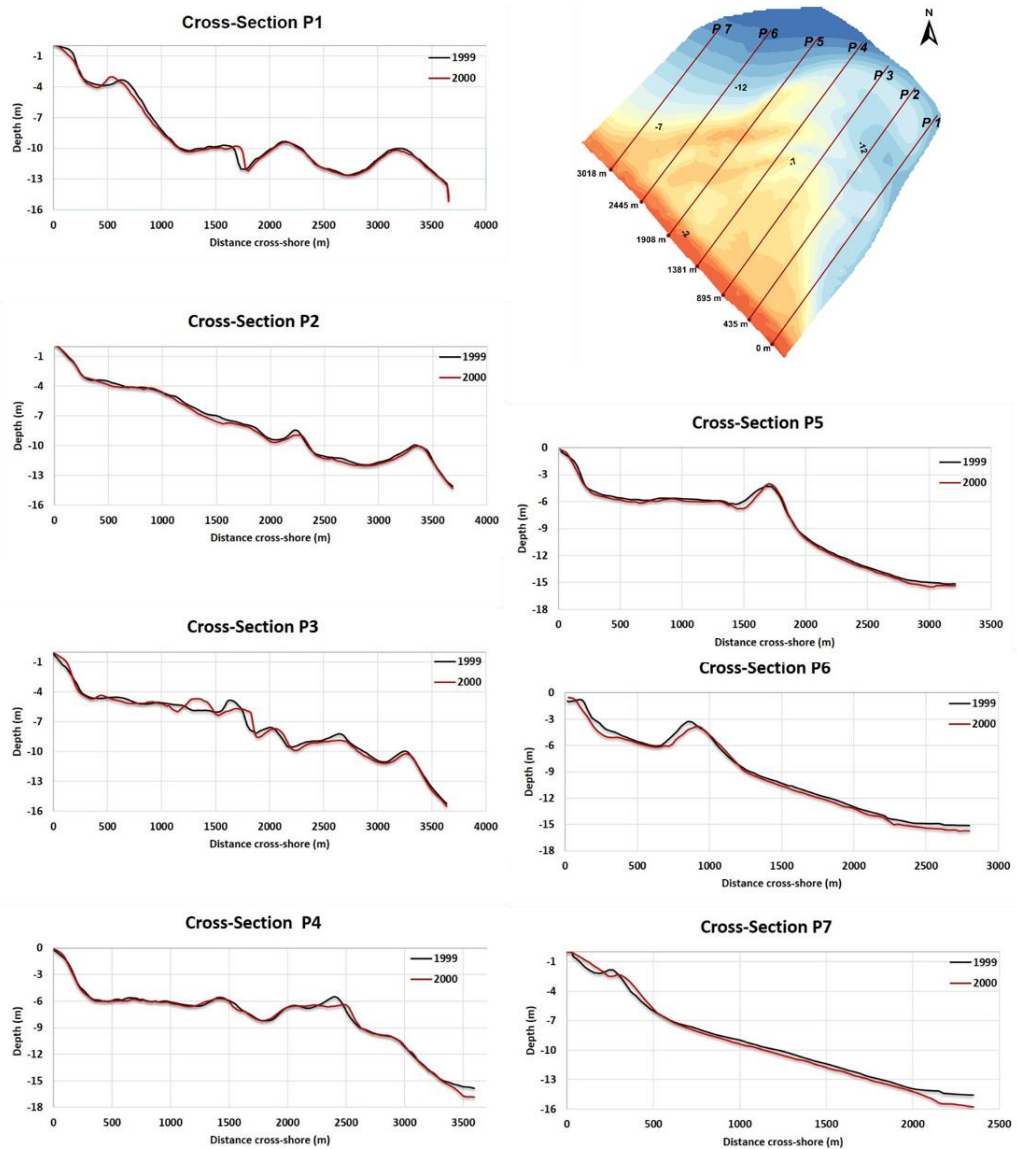


Figure 4-13 Comparisons of cross-shore profiles obtained in 1999 and 2000, which show a general seaward movement of the sandbars.

During this period, the sandbar migration on the area adjacent to the Entrance Channel reflects the influence of the ebb jet, which is indicated by the movement of depth contours towards the NW and N with an overall displacement of up to 202 $\text{m}\cdot\text{y}^{-1}$. Further away from the Entrance Channel on the swash platform, waves appear to be the dominant control on bedform migration. At depths <8 m, the bedforms moved irregularly, but mostly migrated shorewards.

On the terminal lobe, where the ebb jet influence is minimal, the sandbars and bedforms migrated onshore (Figure 4-12, lower left panel). This phenomenon is clearly shown by the outermost spit shaped sandbar on the terminal lobe, which shortened and migrated up to 346 m towards the west (shorewards).

Based on the volumetric change between 1999 and 2000, accretion was the dominant process, with $\sim 3.29 \times 10^6 \text{ m}^3$ of sediment added on the ETD area. The accretion mostly occurred on the NW-NE sections of the terminal lobe, along the Matakana shoreline and at some spots on the offshore of the swash platform. These areas sum up to about 63% of the total ETD area (Figure 4-12 - lower right panel). On average, the sediment accumulation was about 0.26 m above the initial level in 1999.

4.3.2.3 Bathymetry March 2000 to June 2001

This period coincided with weak La Niña to neutral ENSO conditions, and 110,758 m^3 of sediment was dredged from the Entrance Channel in August 2000 (Table 4-5), which corresponds to $\sim 0.01 \text{ m}$ sediment thickness change over the delta. The ebb-tidal delta morphologies for 2000 and 2001 were very similar, with minor changes in the bed surface morphology associated with sandbar migration evident in the 3D images (Figure 4-14, upper panel). The trough landward of the inner sandbar lengthened (A in Figure 4-14), as it scoured towards the east. A deeper trough also formed landward of the outer sandbar on the north terminal lobe (B). However, overall the positions of the main sandbars remained stable, with no significant changes in their morphology.

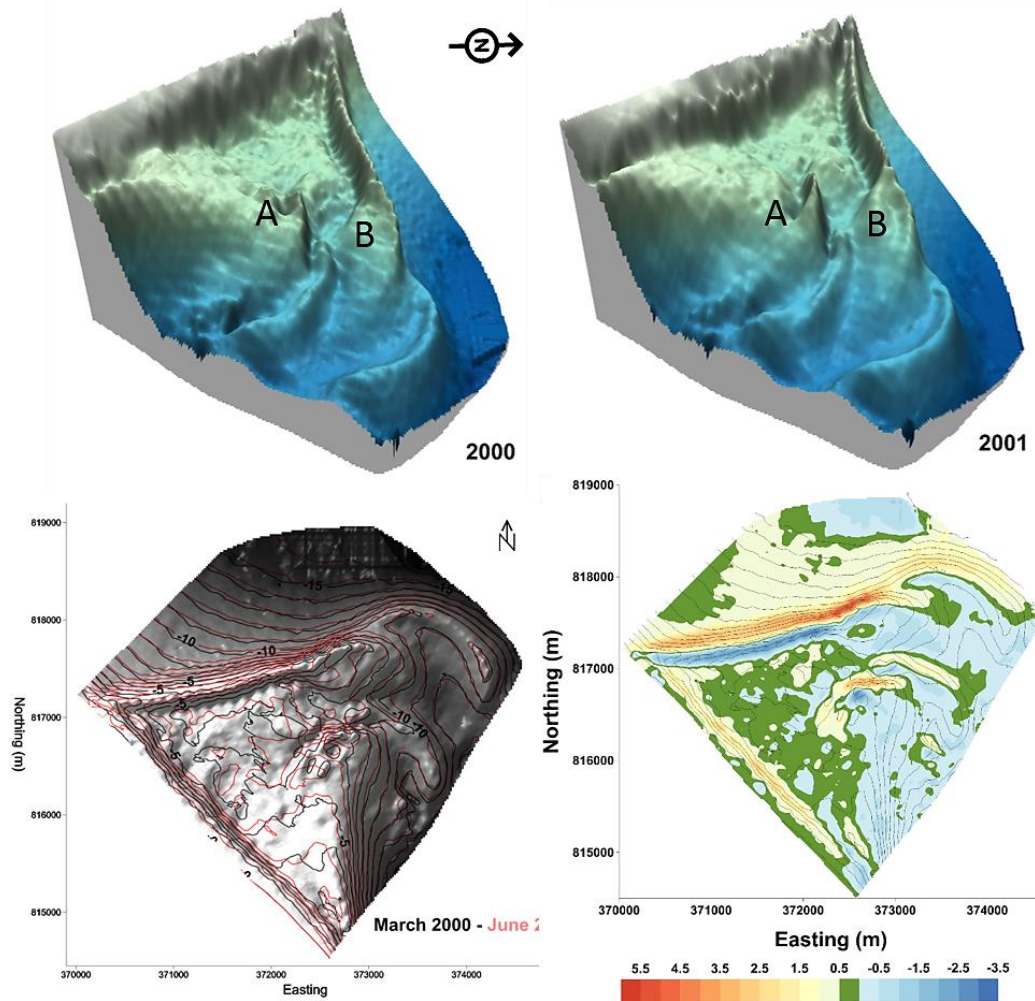


Figure 4–14. Morphology of the Matakana Banks ETD from SBES surveys in 2000 and 2001. The upper images are colour-shaded 3D surfaces interpolated from the SBES data. The lower images highlight the migration of sandbars for Matakana Banks. Two areas of erosion (A & B) associated with the deepening and extension of troughs landward of sandbars are highlighted. The lower left image is a shaded relief map of the 2000 bathymetry overlaid with the contours for the 2000 (black) and 2001 (red) surveys. The lower right image is a residual map that shows the locations where accretion (positive) and erosion (negative) occurred after 16 months of hydrodynamic forcing.

In the superimposed contour map (Figure 4-14 lower left), even though the changes are small, it is seen that the bedforms migrated in a clockwise direction; the NW terminal lobe shortened as the sandbar migrated toward the shore; and offshore of the NW terminal lobe, the contours migrated offshore. Adjacent to the Entrance Channel SE the ebb-tidal delta migrated slightly toward the NNW by $\sim 2.1 \text{ m.y}^{-1}$. Beyond the terminal lobe, bedforms migrated slightly offshore at a rate of $< 0.6 \text{ m.y}^{-1}$.

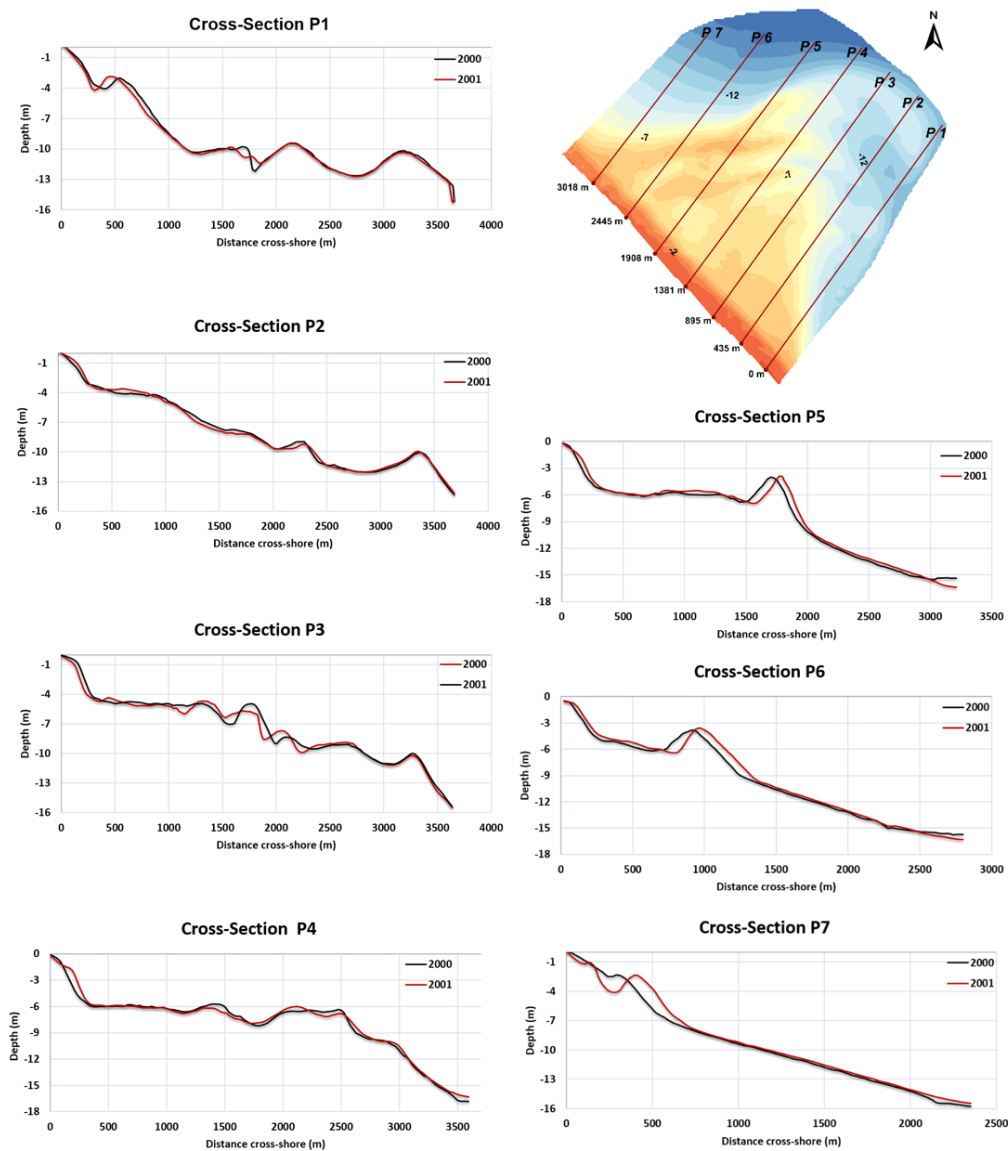


Figure 4-15. Comparisons of cross-shore profiles obtained in 2000 and 2001, which show little change for most profiles and a seaward movement of the sandbars for profiles P5-P6.

The areas coloured in green in Figure 4-14 (lower right) highlight the overall stability between 2000 and 2001. Despite the relatively small changes in morphology, the total volumetric changes for the 16 months of observation was around $3.68 \times 10^6 \text{ m}^3$, which is equal to about 0.32 m sediment thickness increment of the total area. Of this, nearly 63% of the total ETD area was accreted, mostly on the NW terminal lobe and along the shoreface. Erosion mostly occurred in the areas adjacent to the Entrance Channel.

Shoreward sandbar migration is seen in cross-shore profile P1 adjacent to the Entrance Channel (Figure 4-15). In 2000, the first sandbar occurred in 3.3 m depth at 548 m from the shoreline. By 2001, the sandbar crest migrated about 68 m

shoreward, to 480 m from the shoreline, producing a narrower trough than in 2000. Cross-shore profile P2 had a gentler slope than profile P1. During 2000 to 2001, the sandbar closest to the shoreline (at 146 m) migrated ~24 m seaward. Further offshore, the first swash bar was developed in 9 m depth at 2238 m from the shoreline, and it migrated ~48 m seaward by 2001. Beyond 2700 m, the depth was around 12 m below the sea level and only slight changes in elevation were observed. The crest of the most outer sandbar (terminal lobe) was located at 3371 m in 2000. By 2001, the terminal lobe's crest migrated slightly shoreward to 3341 m from the reference shoreline.

Group B profiles (P3, P4, and P5) showed a variable change between 2000 and 2001. Profile P3 recorded the most extensive offshore swash bar migration at depths between 5 m to 10 m between 1100 m to 2500 m from shoreline. In 2000, the first swashbar trough was at 1150 m with the crest at 1340 m. By 2001, the first trough was located at 1580 m and the crest at 1760 m, resulting in a wider swash platform than before. Beyond 2750 m no more migration was visible on the terminal lobe, although the crest slightly accreted by 0.2 m. Profile P4 showed less seabed variability than profile P3. There was some seaward movement for the first 79 m of the profile. The rest of the profile was relatively stable, with up to 0.8 m of sediment accretion during the 16 months observation period. Along profile P5 the bedform features migrated seaward, and the shoreface accreted. The swash platform, migrated seaward from 289 m to 311 m, and became wider from 1188 m to 1265 m. Slight accretion occurred on the swash platform and the terminal lobe migrated up to 56 m seaward.

Within Group C accretion dominated. The swash platform along profile P6 had a gentle sloping surface ($<0.6^\circ$) that extended from 280-740 m at depths of 5-6 m in 2000 and it moved to 252-813 m in 2001. The crest of the terminal lobe also migrated 50 m offshore and accreted 0.5 m. Beyond the terminal lobe, the bed morphology became relatively stable with slight accretion. At profile P7 the swash platform became very narrow, being almost totally replaced by the 4 m deep trough shoreward of the 1.7 m sandbar (surf zone offshore bar) that developed on the terminal lobe. The terminal lobe migrated 110 m seaward, and up to 2.1 m of accretion occurred further offshore out to 750 m where the seabed became stable.

4.3.2.4 Bathymetry June 2001 to August 2002

This period was dominated by erosion as shown by the residual map (Figure 4-16, lower right panel), with about 73% of the total ebb-tidal delta area experiencing erosion. This coincided with the transition from La Niña to El Niño conditions at the end of 2002, and the dredging of 176,662 m³ of sediment from the Entrance Channel in August 2002 (Table 4-5). The main sandbars remained stable in terms of their shapes and positions (Figure 4-16, upper panel). However, the superimposed contours map (Figure 4-16 lower left panel) shows that the bedforms on the swash platform migrated shorewards. Further, the middle part of swash platform became 1 m deeper than in 2001. Erosion of the ebb-tidal delta mostly occurred at depths below 1.5 m, and the most severe erosion occurred on the outer part of NW terminal lobe. Overall the net volumetric change between these two surveys was $-4.335 \times 10^6 \text{ m}^3$ (Table 4-5).

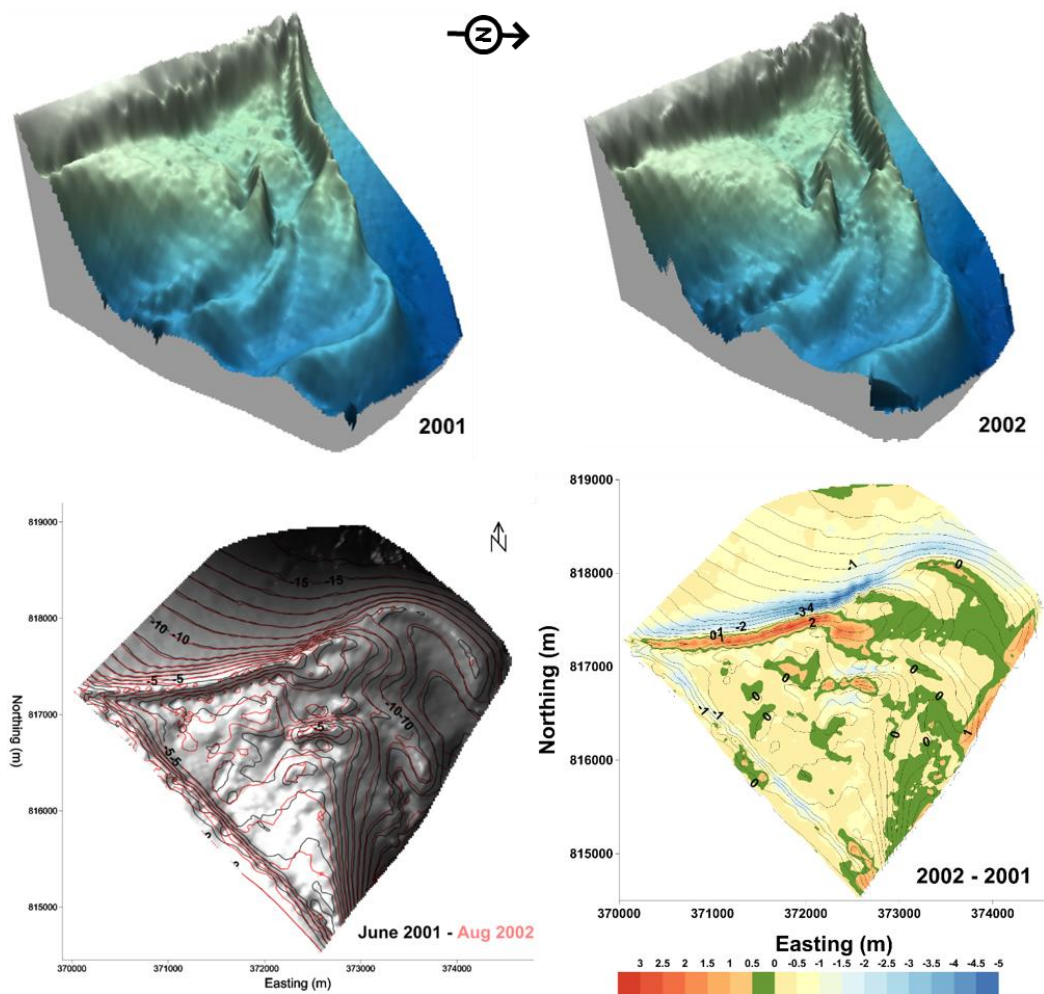


Figure 4-16. Morphology of the Matakana Banks ETD from SBES surveys in 2001 and 2002. The upper images are colour-shaded 3D surfaces interpolated from the SBES data. The lower images highlight the migration of sandbars for Matakana Banks. The lower left image is a shaded relief map of the 2001 bathymetry overlaid with the contours for the 2001 (black) and 2002 (red) surveys. The lower right image is a residual map that shows the locations where accretion (positive) and erosion (negative) occurred after 14 months of hydrodynamic forcing.

In 2002, the offshore slope of the NW sector of the terminal lobe (P1, Figure 4-17) became slightly steeper, changing from $\sim 4.6^\circ$ to 5.6° after 14 months. Elsewhere there were no significant changes to the seabed slope (Figure 4-17).

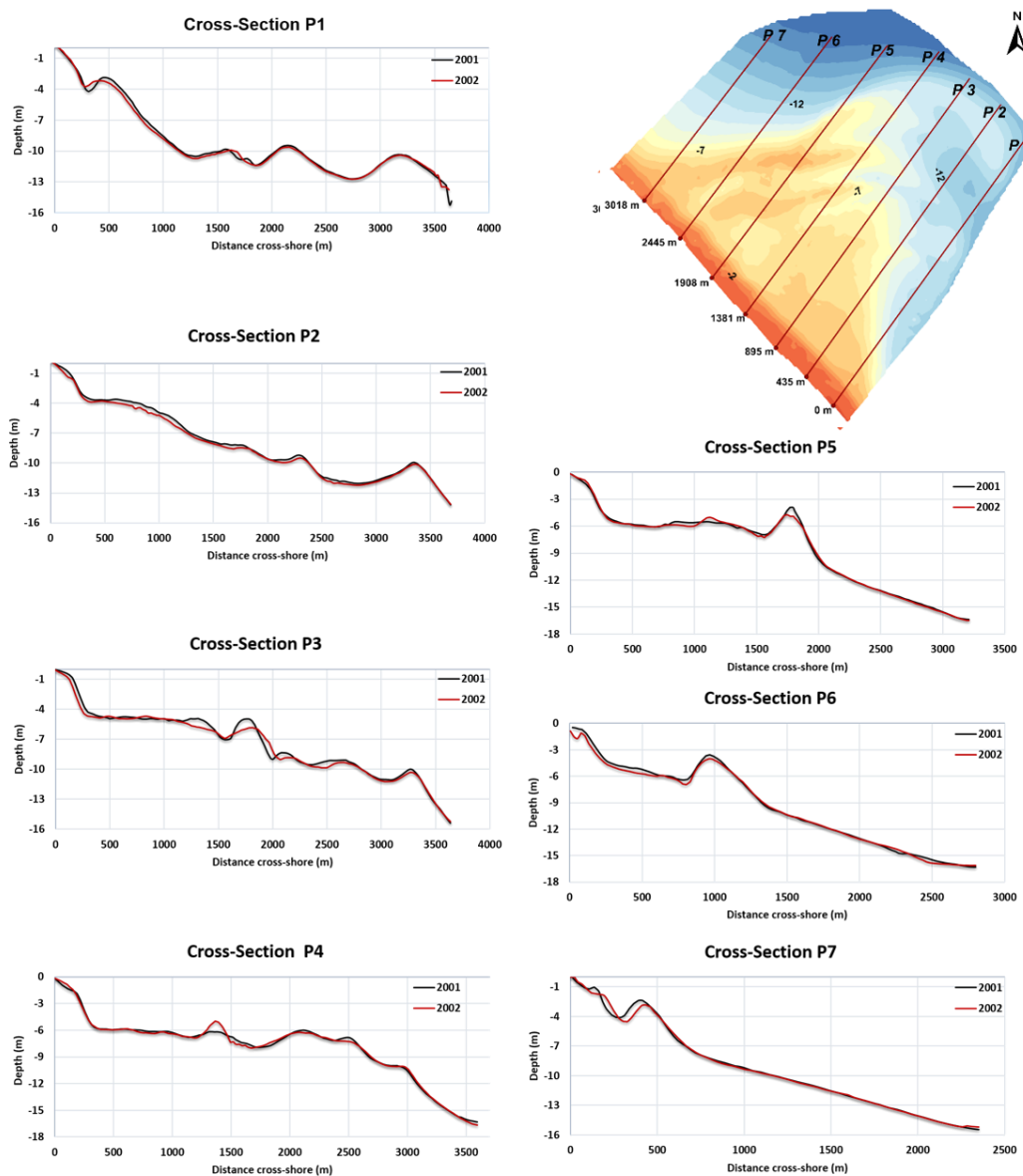


Figure 4-17. Comparisons of the cross-shore profiles for 2001 and 2002, showing erosion and seaward migration of sandbars.

Consistent with the 3D images for 2001 and 2002 (Figure 4-16, upper panel), the cross-shore profiles also show no significant changes occurred to the morphology across the swash platform. However, some erosion associated with a lowered bed elevation occurred in all cross-shore profiles. Within group A, the first sandbar at distance 450 m along profile P1 migrated 30 m landward and sediment infilled the first trough by ~ 0.6 m. Beyond the sandbar to 1830 m offshore, slight erosion up to 0.6 m took place. Further offshore, the seabed was stable. Minor lowering of seabed elevation also dominated profile P2. With a gentle slope of less than 0.6° , the swash platform laterally extended to around 485 m in 2001, and became ~ 100 m narrower in 2002, extending to around 380 m offshore. This

was primarily due to erosion steepening the slope seaward of ~400 m until ~1800 m where the first of the sandbars occurred. The terminal lobe remained stable at 3340 m from the shoreline. Overall, the average decrease in elevation along P2 between 2001 and 2002 was ~0.2 m.

Wider swash platforms and more dynamic bedforms were displayed within group B (P3, P4 and P5). The lateral extent of the swash platform along profile P3 ranged between 995-1375 m. Between surveys the first sandbar trough at 1580 m became narrower and the first sandbar crest migrated 70 m offshore from 1760 m to 1830 m while the crest depth from 5 m to 5.9 m depth. Erosion along profile P3 lowered the sandbar crests, producing gentler slope than in 2000. Slope gradients decreased seaward with a maximum grade around 1.2° . For both years, the seabed stabilized beyond 2700 m from the shoreline.

About 1 m thickness of sediment accumulated and formed a swash bar by 2002 at 1360 m from the shoreline in profile P4. Following this first swash bar, the sandbar crests were truncated by erosion, resulting in a gentler overall slope than in 2001. No bathymetric variability was seen beyond 2600 m from the shoreline. Slight bathymetric variability was evident along profile P5. About 0.4 m to 1 m sediment thickness eroded from the seabed, mostly from the crest of terminal lobe sandbar, and associated with development of a trough landward of the inner sandbar. The lateral extent of the swash platform relatively unchanged, with the swash platform truncated by the terminal lobe at 1575 m from the shoreline. Beyond 2040 m at depths >10 m, the seabed remained stable during the observation period.

Morphological changes around the NW boundary of the ebb-tidal delta are displayed in profiles P6 and P7 (group C). Along profile P6, the swash platform extended between 252 m and 813 m. The seabed gently sloped seaward at depths between ~4.2 m and 6.4 m. The terminal lobe also remained at the same distance from the shoreline. Minor changes were deepening of the trough landward of the terminal lobe and ~0.4 m of erosion from the crest of the sandbar on the lobe, and accretion to form a mound on the swash platform. No bathymetric variability occurred beyond 1090 m.

The seaward slope of the shoreface along profile P7 shifted from 1.1 m depth in 2001 to 1.8 m in 2002, and the associated swash bar crest migrated toward offshore up to 51 m. On the terminal lobe, the sandbar trough and crest deepened by 0.5 m and the sandbar crest migrated offshore by about 30 m.

4.3.2.5 Bathymetry August 2002 to June 2006

There were no bathymetric surveys during 2003, 2004 and 2005 (Table 4-5). Maintenance dredging removed 294,398 m³ of sediment from the Entrance Channel during two dredging campaigns (Table 4-5), and ENSO conditions ranged from weak El Niño to neutral. During this period, bedforms on the swash platform generally migrated towards the north-northwest and shoreward.

By 2006, pronounced morphological changes are evident, including a steeper and more variable swash platform surface (area labelled **A** on Figure 4-15, upper panel) and sandbar growth on the lee side of the terminal lobe (area labelled **B** on Figure 4-18, upper panel). Further, while the location of the terminal lobe of the ebb-tidal delta remained the same, the landward slopes flattened, particularly in the western area close to Matakana Island. The superimposed contours map (Figure 4-15, lower left panel) displays the NW up to 320 m (80 m.y⁻¹) migration of sand waves adjacent to the Entrance Channel and swash and bars towards the W-NW. These progressively widened the swash platform (**A**) and extended the inner sandbar (**B**) towards the Entrance Channel. Less variability is evident on the seaward margin of the terminal lobe, and the shoreface.

The residual map (Figure 4-18 lower right panel) also shows the accretion associated with extension of the swash platform and inner sandbar. However, this map also indicates that erosion affected about 66% of the total area of the ebb tidal delta. On the seaward slope of northwestern terminal lobe, up to 5 m of sediment was eroded. While at the shoreface, the sediment loss was up to 3 m by 2006. (Figure 4-18, lower right panel). The net volumetric changes over the observation period indicates about 7.6 x 10⁶ m³ of sediment loss, which is equivalent to 0.19 m.y⁻¹ average seabed elevation decrease and more than an order of magnitude larger than the dredging volumes.

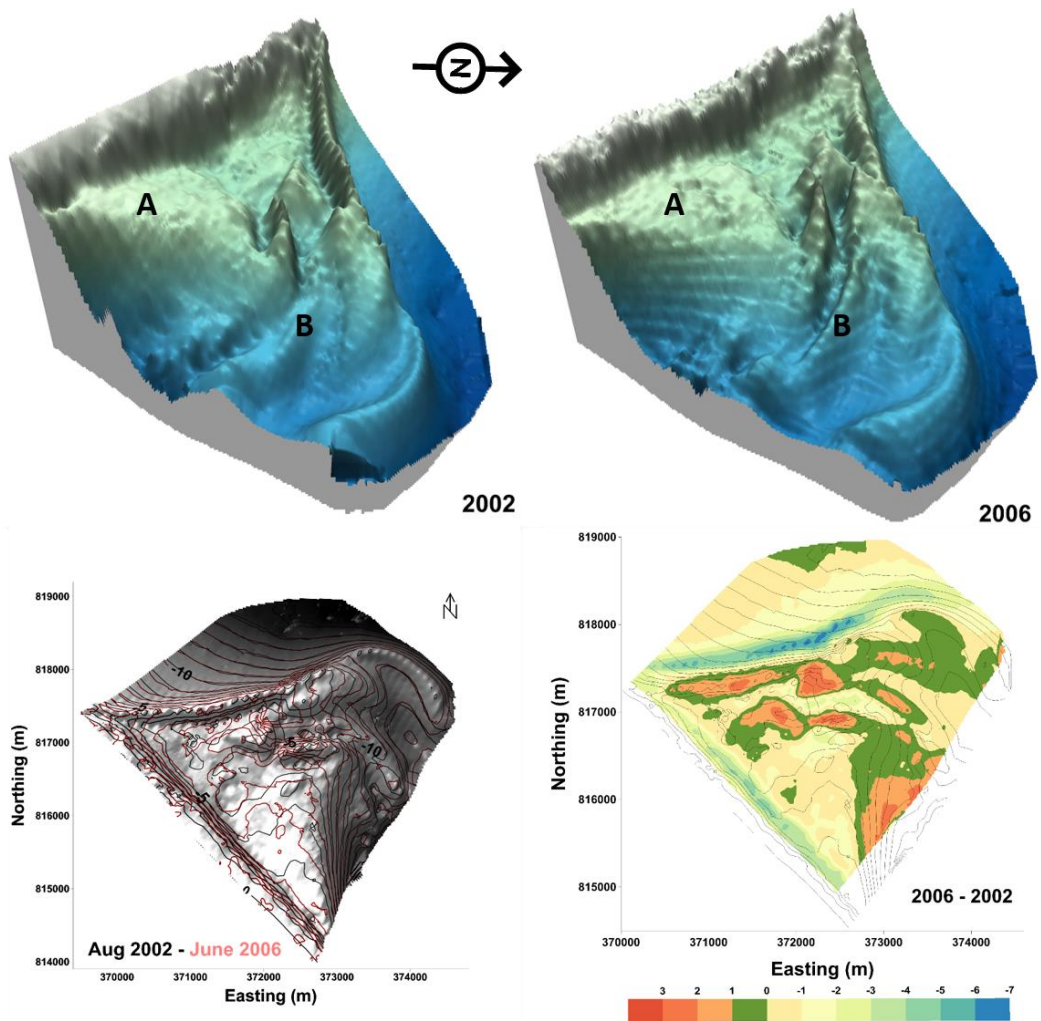


Figure 4-18. Morphology of the Matakana Banks ETD from SBES surveys in 2002 and 2006. The upper images are colour-shaded 3D surfaces interpolated from the SBES data. Letters A and B denote the locations where significant morphological changes occurred as discussed in the text. The lower images highlight the migration of sandbars for Matakana Banks. The lower left image is a shaded relief map of the 2002 bathymetry overlaid with the contours for the 2002 (black) and 2006 (red) surveys. The lower right image is a residual map that shows the locations where accretion (positive) and erosion (negative) occurred after almost 4 years of hydrodynamic forcing.

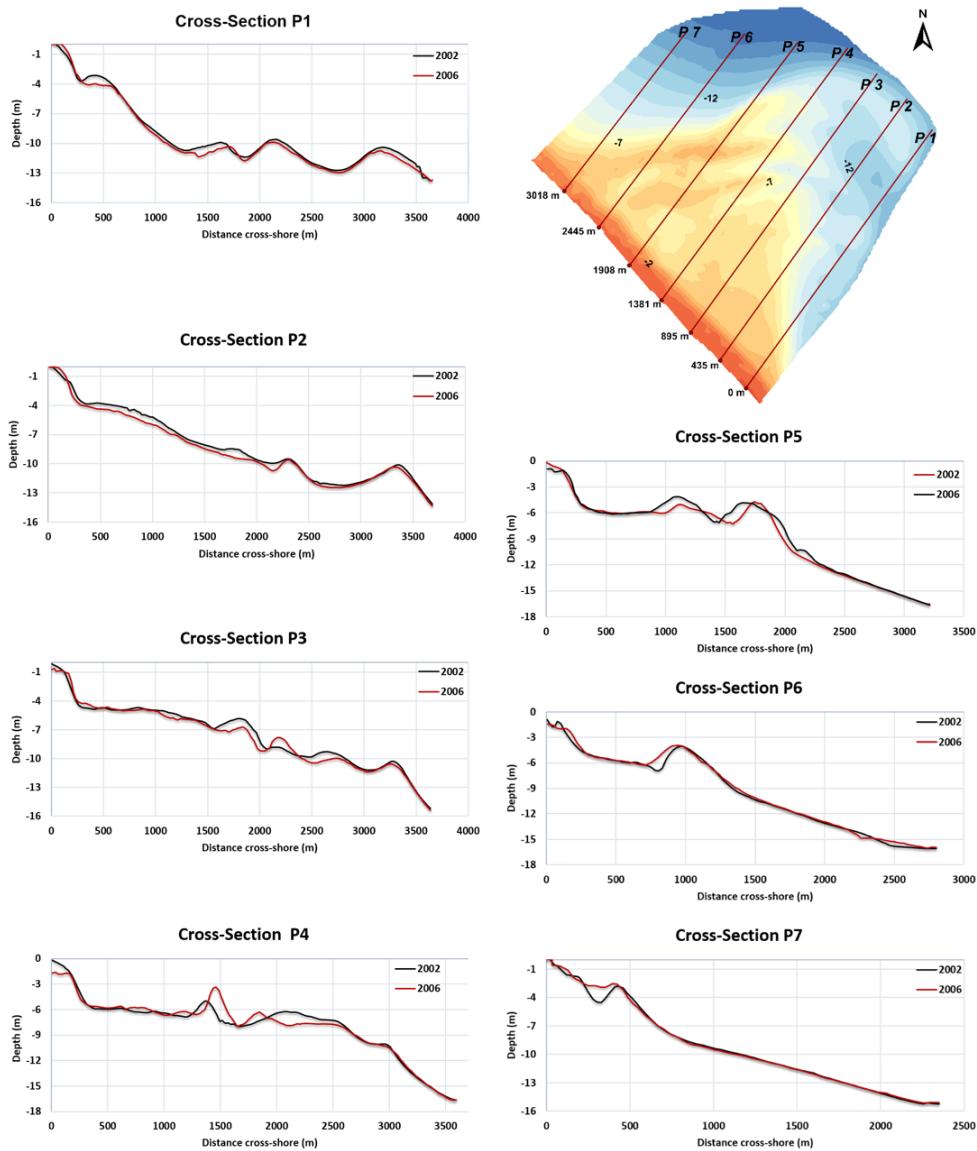


Figure 4-19. Comparison of the cross-shore profiles for 2002 and 2006 indicating that erosion was the dominant process.

Group A cross-shore profiles (P1 and P2) show a general flattening due to erosion (Figure 4-19). Along profile P1, the swash bar adjoining the shoreface underwent significant erosion (around 300 m) losing about 1.1 m of height and resulting a flat seabed surface with a lateral extent of 270 m. Further significant erosion occurred at >11 m depth between 1414 m to 1750 m offshore. The crest of sandbar in this region migrated 100 m offshore and lowered by 0.6 m. Beyond 1850 m, there was slight erosion and terminal lobe crest migrated shoreward by about 0.28 m. No bedform variability was observed more than 3500 m from the shoreline.

Along profile P2, the swash platform consistently underwent erosion that lowered the platform. The maximum erosion occurred at 2140 m, with up to 0.8 m

removed resulting in a deeper trough landward of the first sandbar. Beyond 2300 m, the seabed was relatively stable and the terminal lobe crest only slightly shifted at around 3350 m.

Group B profiles (P3, P4 and P5) were characterized by more complex morphology and an expanding swash platform. Profile P3 shows that the swash platform increased in width from 1251 m to 1450 m, continuing the trend observed during the previous observation period. Initially in 2002, the first sandbar's crest was located at 1830 m. By 2006 the crest had lowered by up to 0.9 m and it had migrated seaward at a rate of 0.875 m per year. This was associated with the formation of a more pronounced sandbar at 2170 m, where the seabed was elevated up to 1 m from the initial level in 2002. Beyond this new sandbar, erosion occurred as far as the crest of the terminal lobe. Further offshore the seabed was stable.

Profile P4 shows that the shoreface eroded by up to 1.5 m, while the seabed fluctuated on the swash platform. The first sandbar at the seaward margin of the swash platform shifted ~95 m offshore and its' crest shallowed by up to 1.6 m. The broad second sandbar present at 2082 m in 2002 migrated landward and formed a narrower sandbar 1.5 m in height at 1852 m. Further offshore (>2700 m) at depths >10 m, the seabed was stable.

Along profile P5, the swash platform occurs at a depth of ~6 m, and displayed almost no variation of elevation between the two surveys with an average erosion of ~0.2 m. However, the lateral extent increased from 558 m to 690 m, while the first sandbar migrated 34 m offshore. The terminal lobe migrated offshore and by 2006 the crest was at 1740 m, which was about 93 m further offshore than the initial position in 2002. Seaward of the terminal lobe, slight erosion occurred up to 2500 m from the shoreline at a depth of 12 m. Further offshore the seabed was stable.

Group C profiles (P6 and P7) correspond with narrowest extent of the swash platform. Along profile P6, the shoreface eroded and a flat shoreface developed at depth of ~2 m by 2006. Between surveys the swash platform's surface seems to be stable. However, by 2006, its' lateral extent decreased as the terminal lobe migrated shorewards. Initially, swash platform was 560 m wide, and this reduced by 127 m. The shoreward migration of the terminal lobe also resulted in a shallower trough on the shoreward side of the lobe. Offshore from the terminal lobe, starting at <1000 m from the shoreline, the seabed was relatively stable with minor zones of accretion and erosion.

Sediment deposition is evident in profile P7. The trough landward of the terminal lobe infilled, directly connecting the shoreface to the terminal lobe and resulting in a very gentle shoreface slope. The terminal lobe's crest also slightly shifted towards the shore by ~32 m.

4.3.2.6 Bathymetry June 2006 to August 2008

No dredging occurred during this period and ENSO conditions were neutral. Overall, the main shape of the ebb-tidal delta did not change significantly. Morphological changes predominantly occurred along the Entrance Channel margin of the ebb tidal delta, with some minor changes along the terminal lobe. The seabed features that significantly changed can be visually identified from Figure 4-20; (A) the morphology of the swash platform became less variable than 2006, and a cluster of swash bars formed on the SE margin, (B) the first sandbar gradually moved toward the north; and (C) the troughs flanking the second sandbar became more pronounced, less irregular, and extended towards the shore.

The superimposed contours map (Figure 4-20, lower left panel) shows clockwise sandbar migration and it indicates that close to the inlet throat, where the slope gradients were up to 3.6° , the bedforms moved toward the Entrance Channel by up to 77 m (or about 36 m.y^{-1}). On the deeper areas of the swash platform the bedforms moved shorewards, whilst on the shallower parts the bedforms moved towards the northwest. On the landward side of the terminal lobe, bedforms migrated towards the shoreline, and on the offshore side they migrated towards the northwest to north sector. The bedforms migrated up to 133 m during observation period (61 m.y^{-1}).

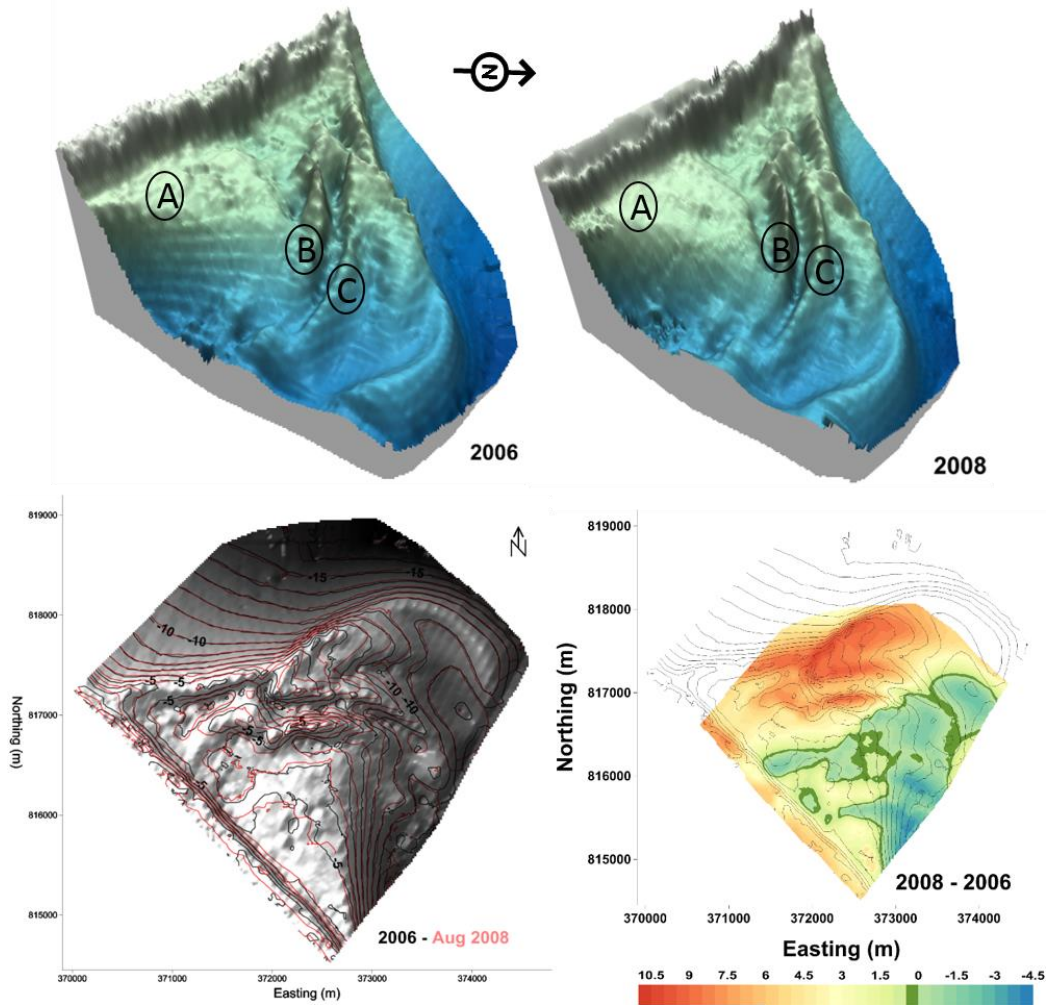


Figure 4-20. Morphology of the Matakana Banks ETD from SBES surveys in 2006 and 2008. The upper images are colour-shaded 3D surfaces interpolated from the SBES data. Letters A, B and C denote the locations where significant morphological changes occurred as discussed in the text. The lower images highlight the migration of sandbars for Matakana Banks. The lower left image is a shaded relief map of the 2006 bathymetry overlaid with the contours for the 2006 (black) and 2008 (red) surveys. The lower right images is a residual map that shows the locations where accretion (positive) and erosion (negative) occurred after 26 months of hydrodynamic forcing

The residual map (Figure 4-20, lower right panel) indicates that deposition was the dominant process between these two consecutive surveys. About 76% of the total ebb-tidal delta area accreted, which represents the deposition of about $18.95 \times 10^6 \text{ m}^3$ (Table 4-5) and corresponds to an average sediment thickness of about 2.4 m. However, the area surveyed was significantly smaller than for most surveys (Table 4-5), which may exaggerate the calculated average sediment thickness.

Within Group A cross sections, profile P1 shows little bathymetric change between 2006 and 2008. However, on the narrow swash platform, sediment

accretion formed small swash bars with a maximum height of about 1 m (Figure 4-21, and areas labelled (A) in Figure 4-20 upper panel). The first sandbar at 1717 m migrated 20 m offshore and its' crest became 0.25 m lower. The trough between the first sandbars accreted, which elevated the seabed from a depth of 11.8 m to 11.4 m. Beyond 1960 m, the seabed appeared stable and the terminal lobe was unchanged at 3140 m with a crest at 10.8 m depth.

Although the maximum accretion rate was low, $\sim 0.3 \text{ m.y}^{-1}$, accretion dominated along profile P2. The shoreface area eroded and the swash platform accreted, producing a relatively flat surface that gently sloped offshore. Bedform migration was seen at the first sandbar at 2197 m, where its' crest shifted 98 m seaward ($\sim 45 \text{ m.y}^{-1}$). Beyond 2396 m, the outer part of the ebb-tidal delta was stable with hardly any bathymetric changes observed.

Within group B, profile P3 mostly showed erosion patterns associated with sandbar migration, which included deepening of flanking troughs. Minor erosion of the shoreface occurred with the development of a swash bar, and the lateral extent of the swash platform slightly decreased from 1450 m in 2006 to 1370 m in 2008. Both large sandbars seawards of the swash platform migrated offshore by $\sim 90 \text{ m}$ and $\sim 70 \text{ m}$ (42 m.y^{-1} and 32 m.y^{-1}). Beyond 2780 m only slight erosion and bedform migration occurred, and the location of the terminal lobe's crest remained fixed at 3270 m.

There were no significant changes observed in profile P4, although slight accretion was visible along the swash platform section of the profile. The first sandbar slightly migrated offshore from 1455 m to 1477 m ($\sim 10 \text{ m.y}^{-1}$). Further offshore, the crest of the second large sandbar accreted 0.7 m and shifted about 56 m (26 m.y^{-1}) offshore, and significant erosion of up to 0.9 m was associated with development of a flanking trough at 2169 m. Beyond 2600 m at depths $> 8 \text{ m}$ depth the seabed was stable.

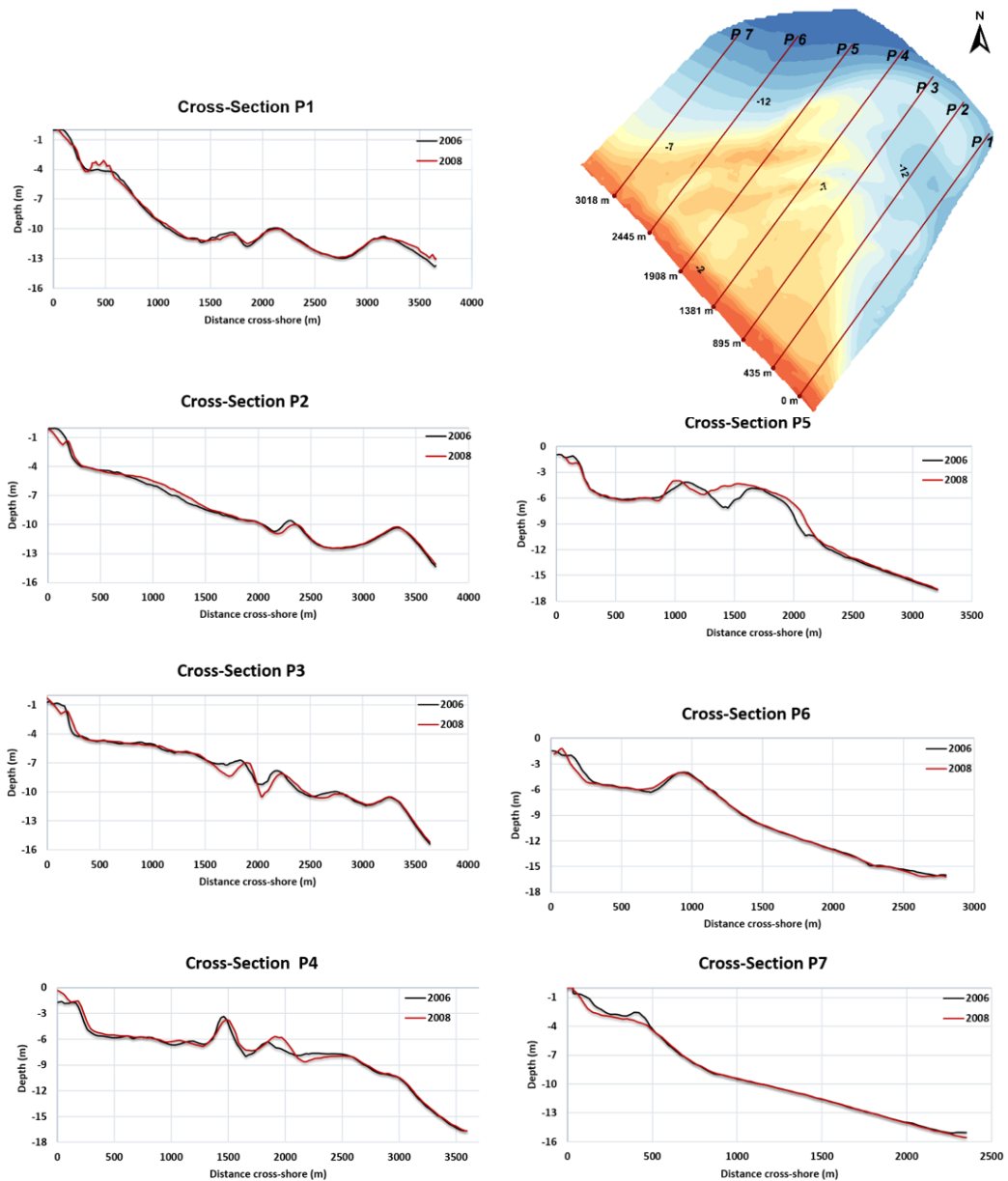


Figure 4-21. Comparisons of cross-shore profiles between 2006 and 2008. This period coincides with the largest volumetric gain observed, particularly along profile P5.

Morphological changes along profile P5 shows that accretion dominated between 2006 and 2008,. Even though the landward sandbar bordering the swash platform migrated shorewards, the lateral extent of the swash platform remained relatively unchanged. The sandbar migration mainly involved steepening of the landward slope resulting in the crest moving shoreward from 1061 m to 980 m ($\sim 37 \text{ m.y}^{-1}$). Further offshore, pronounced accretion took place, as the trough between the first and second sandbars moved $\sim 197 \text{ m}$ (91 m.y^{-1}) toward the shoreward and infilled by about 1.2 m. The seaward sandbar broadened, shallowed and the crest

migrated shoreward in response to accretion that extended to 2190 m and a depth of 11 m. Beyond this point, the seabed was stable.

Group C profiles showed shoreward migration (P6) and minor erosion (P7). Along profile P6, the swash platform moved ~45 m shoreward and narrowed by ~34 m. The position of the crest of the terminal lobe remained the same, and the seabed was stable further offshore. Along profile P7, the sandbar on the terminal lobe at 398 m was eroded, lowered by up to 0.9 m, leaving no obvious sandbar (Figure 4-20) and an unclear terminal boundary of ebb-tidal delta. The seabed was stable at distances > 495 m, corresponding to depths >4.3 m.

4.3.2.7 Bathymetry August 2008 to November 2009

This period included the removal of the largest dredged volume of 259,193 m³ from the Entrance Channel between 1998 and 2014 (Table 4-5), and occurred during a developing La Niña event. There were no significant morphological changes to the ebb-tidal delta evident in the 3D images (Figure 4-22, upper panel), although there were changes to the number and location of swash bars.

However, the superimposed contours map shows an anti-clockwise migration of bedforms (Figure 4-22, lower left). Bedforms located close to the Entrance Channel migrated offshore, while towards the western margin of the delta the bedforms migrated shorewards. The rates of bedform migration varied between different regions of the ebb-tidal delta; on the swash platform bedforms migrated further and faster than on the terminal lobe. The swash bars and sandbars on the swash platform migrated up to 177 m (~ 142 m.y⁻¹) from initial position, while the sandbars at the margin of the swash platform migrated up to 133 m (~106 m.y⁻¹). On and seaward of the terminal lobe, the bedforms were more stable and no migrations were identified. About 78% of the ebb-tidal delta area accreted (Table 4-5), with the greatest accretion occurring along the shoreface of Matakana Island and on NW to N face of the terminal lobe (Figure 4-22, bottom right panel).

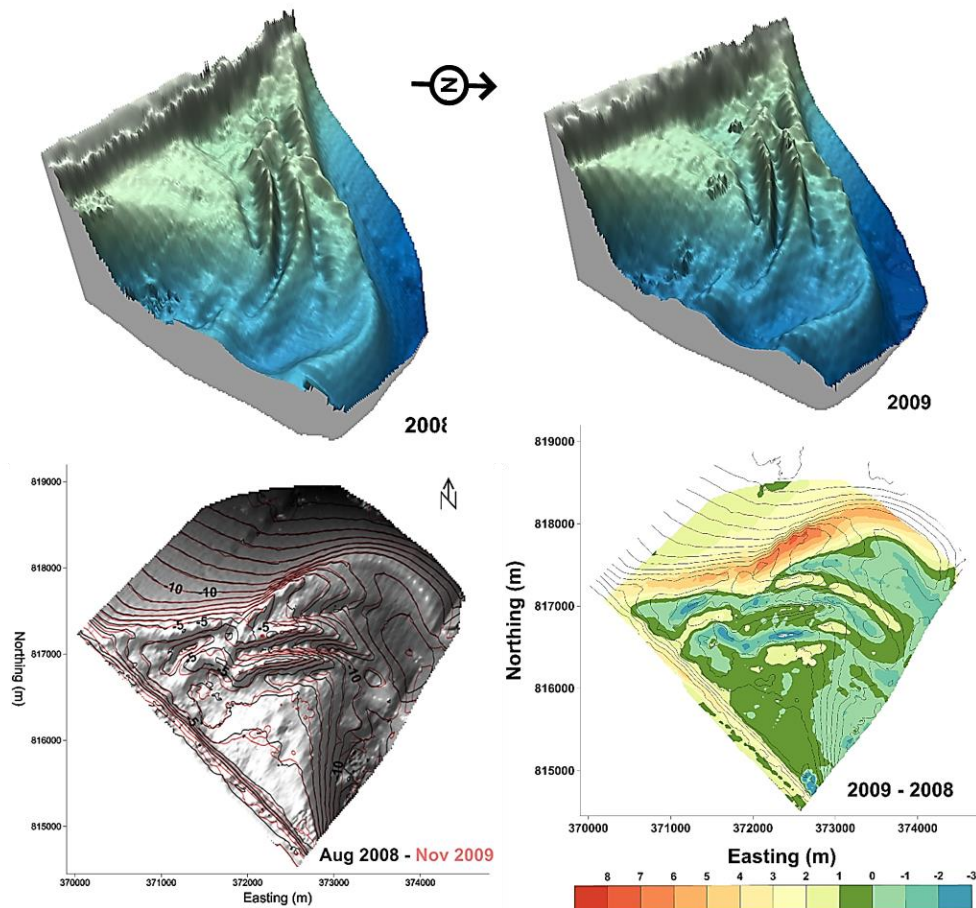


Figure 4-22. Morphology of the Matakana Banks ETD from SBES surveys in 2008 and 2009. The upper images are colour-shaded 3D surfaces interpolated from the SBES data, which show the changing distribution of swash bars on the shoreface and swash platform. The lower left image is a shaded relief map of the 2008 bathymetry overlaid with the contours for the 2008 (black) and 2009 (red) surveys, and indicates the anti-clockwise movement of bedforms. The lower right image is a residual map that shows the locations where accretion (positive) and erosion (negative) occurred after 15 months of hydrodynamic forcing

The net volumetric change from August 2008 to November 2009 was $\sim 11.45 \times 10^6 \text{ m}^3$, which is equivalent to an average of 1.1 m sediment accumulation on the ebb-tidal delta. It is also 2 orders of magnitude larger than the volume removed by dredging in December 2008 (Table 4-5).

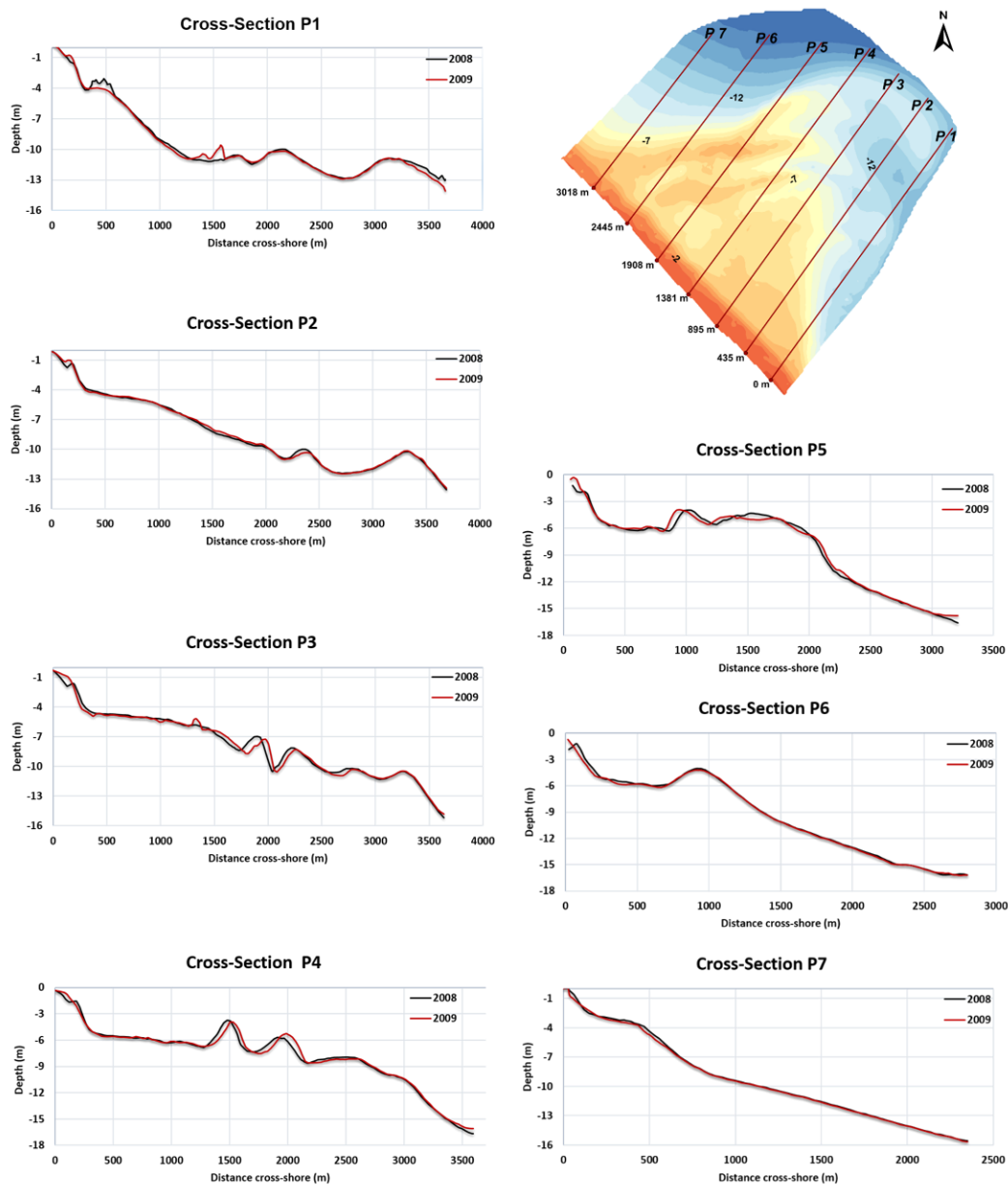


Figure 4-23. Comparison of cross-sectional profiles for 2008 and 2009. Overall, the profiles accreted between these surveys, and the seabed remained stable offshore of the terminal lobe.

The cross-section profiles show that during this period the ebb-tidal delta was generally stable with a few slight seaward bedform migrations close to the Entrance Channel, and some flattening of the western margin of the terminal lobe where it joins the shoreface (Figure 4-23).

Some bedform migrations are evident in group A cross-sectional profiles closest to the Entrance Channel. Along profile P1, the sediment that accumulated as swash bars on the narrow swash platform by 2008 appears to have moved down

to depth of around 10 m just landward of the first sandbar. Beyond this point, the seabed is stable until just offshore of the terminal lobe at 3200 m, where slight erosion lowered the seabed by up to 0.7 m from its' initial level. Along profile P2, there were no significant morphological changes. On the shoreface at a depth of about 1 m, minor accretion occurred that yielded a flatter slope, and a thin veneer of sediment (<0.3 m) was deposited on the swash platform.

Sandbar migrations are very clearly displayed by group B profiles, which represented the most dynamic part of the ebb-tidal delta during this period. Both profiles P3 and P4 show the bedforms migrating offshore, while bedforms along profile P5 migrated onshore. The sedimentation on the shoreface observed in group A profiles is also seen in group B profiles. However, for Profile P3 the shoreface accretion occurred at a shallower depth (0.4 m) than the other profiles. The swash platform extent remained much the same, a small sandbar developed at ~1300 m with height of 0.6 m. The sandbars flanking the swash platform migrated seaward by 105 m and 85 m (84 m.y^{-1} and 68 m.y^{-1}) for the first and second sandbars respectively. The last morphological change seen along this profile was at ~2700 m, where the third sandbar's crest migrated 50 m (40 m.y^{-1}) offshore. Beyond this location, the seabed was stable.

Along profile P4, accretion took place on the shoreface, while the lateral extent of the swash platform was relatively unchanged with no significant bedform variations. Seaward migrations are shown by the sandbars that located at distance between 1285 to 2630 m from the shoreline. The distance of these migrations varied between 50 m to 38 m (40 m.y^{-1} to 30 m.y^{-1}), where the largest distance is the migration of the first sandbar and the migration distances became shorter as the distance from shoreline increase. Subsequent to 2600 m, the seabed became stable without any changes by the end of observation period in 2009.

In contrast to the other group B profiles, profile P5 showed the dominant bedform migration was toward the shore. Sediment accretion on the shoreface was also seen in this profile, which elevated the seabed by up to 1.6 m. The first sandbar migrated 84 m (67 m.y^{-1}) onshore, which decreased the lateral extent of the swash platform. The second sandbar migrated faster shoreward, with the crest moving about 162 m, equal to a migration rate of 130 m.y^{-1} . The morphology of the second

sandbar was more undulating than in the earlier survey. Beyond 2330 m, the seabed was stable that confirming the second sandbar it as the outermost boundary of the ebb-tidal delta.

Group C profiles showed slight erosion during the observation period. Along profile P6, the lateral extent of the swash platform slightly decreased by ~38 m. However the position of the terminal lobe's crest remained the same after 15 months at around 900 m from the shoreline. Some slight erosion occurred on the swash platform and the shoreface resulting in the disappearance of the swash bar. Along profile P7, the boundary between swash platform and terminal lobe is not very clear as the swash platform transitions into an offshore sloping seabed. By 2009, the swash platform became narrower as the seaward margin of the swash platform migrated about 30 m landward. Slight erosion occurred at depths <6 m on the swash platform until 598 m offshore.

4.3.2.8 Bathymetry November 2009 to November 2010

During this observation period only 9,209 m³ was dredged from the Entrance Channel in July 2010 (Table 4-5). The SOI was neutral, dropping from slightly positive to slightly negative and back to slightly positive. The morphological indicate that erosion was the dominant process. Comparison of the 3D images in Figure 4-24 (upper panel), shows that the 5 main sandbars of the ebb-tidal delta retained their overall shapes and positions. However, by superimposing the contours for the two surveys, it is seen that the bedforms moved in a clockwise direction. In the area adjacent to the Entrance Channel the general direction of bedform migration is shorewards and bedforms along the western terminal lobe moved offshore (Figure 4-24, lower left panel).

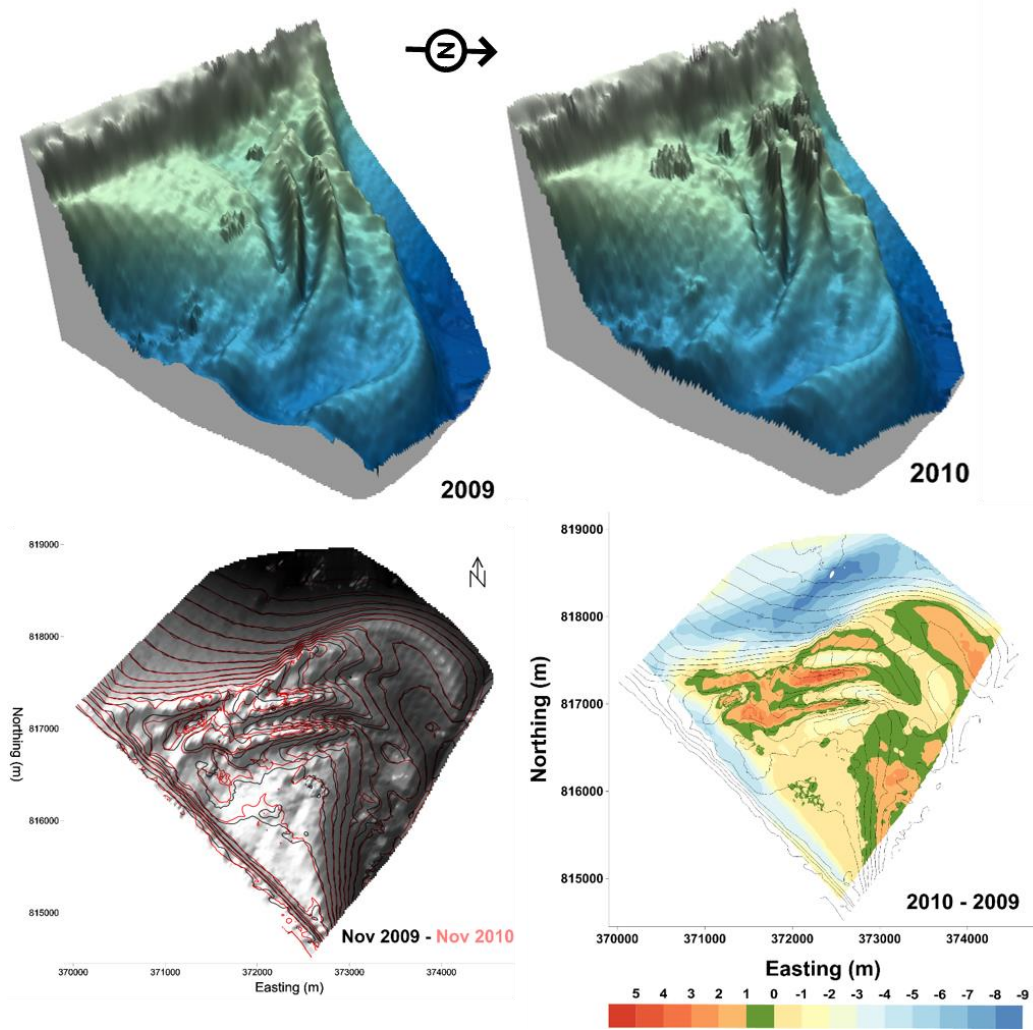


Figure 4-24. Morphology of the Matakana Banks ETD from SBES surveys in 2009 and 2010. The upper images are colour-shaded 3D surfaces interpolated from the SBES data. The lower left image is a shaded relief map of the 2009 bathymetry overlaid with the contours for the 2009 (black) and 2010 (red) surveys, and indicates clockwise movement of bedforms. The lower right image is a residual map that shows the locations where accretion (positive) and erosion (negative) occurred after 12 months of hydrodynamic forcing.

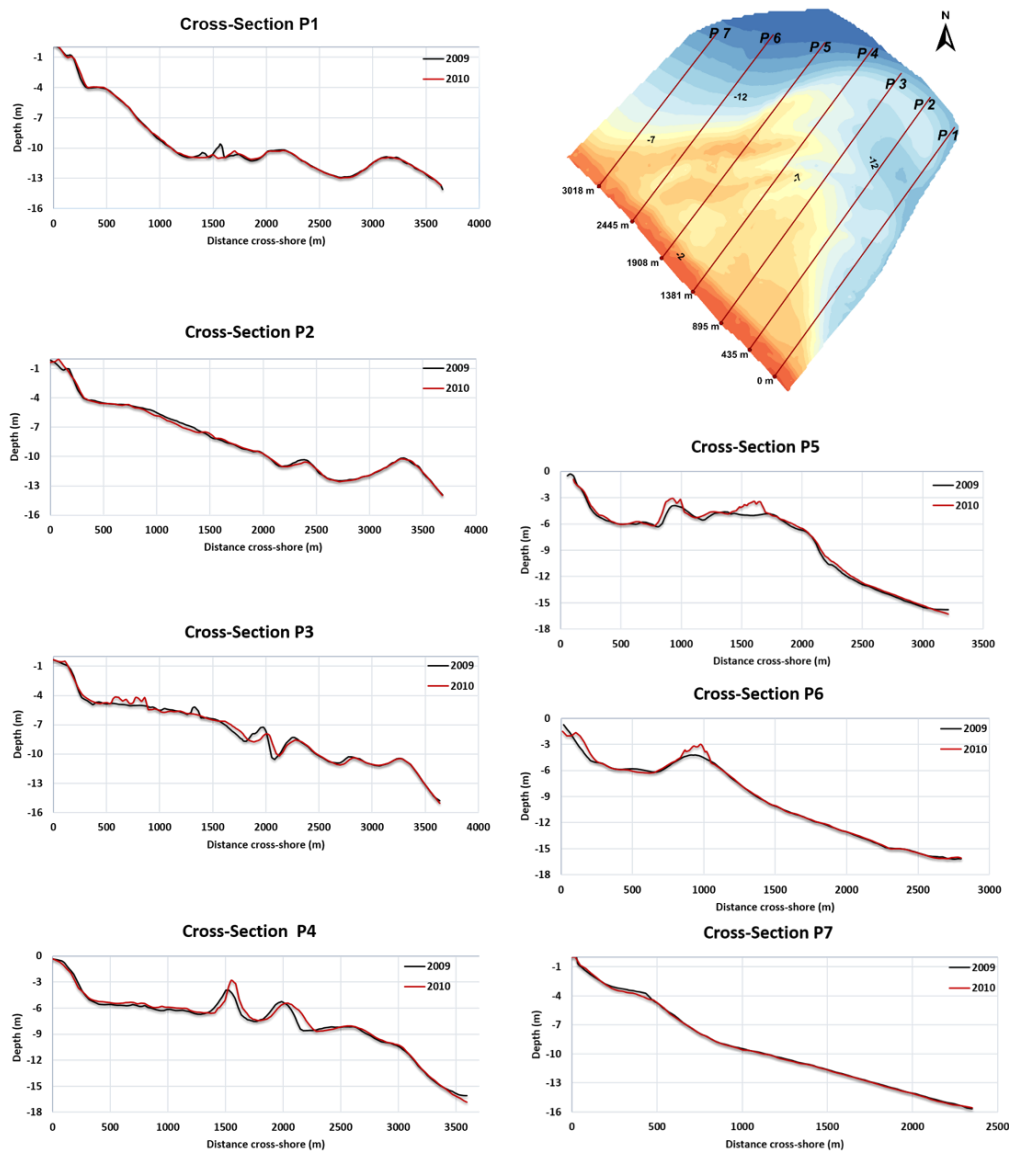


Figure 4-25. Comparison of cross-sectional profiles for 2009 and 2010. Overall, the profiles eroded between these surveys.

The dominance of erosion can be seen in the residual map (Figure 4-24, lower right panel), where erosion was prevalent on the swash platform, in troughs flanking the sandbars, along the shoreface, and on the outer part of the ebb-tidal delta in the north. Overall, erosion affected about 68% of the ebb-tidal delta area. However, accretion dominated on the inner sandbars of the ebb-tidal delta. Over the 1 year duration between surveys, around $14.3 \times 10^6 \text{ m}^3$ of sediment lost, which is equivalent to a sediment thickness decrease of 1.35 m over the ebb-tidal delta area (Table 4-5).

Comparisons of the cross-sectional profiles for 2009 and 2010 are shown in Figure 4-25. Similar to the group A profiles in the previous comparison, the morphology adjacent to the Entrance Channel shows very little variation. The only changes along profile P1 occurred at depths of ~10 m between 1300 m to 1760 m from the shoreline. Here, the sandbar crests were eroded and migrated offshore at rates of 93 m.y⁻¹ and 165 m.y⁻¹ for the first and second sandbar respectively. Beyond the second sandbar, variations in bathymetry were negligible and the crest of the terminal lobe was located at 3147 m.

Slight morphological changes evident in profile P2, with the main change being a slight seaward migration of the first sandbar. Minor accretion occurred on the shoreface, which elevated the seabed by <1 m. Slight erosion up to 0.7 m.y⁻¹ occurred on the swash platform between 886 to 1396 m. The trough landward of the first sandbar's trough remained in the same position, but the sandbar crest migrated seaward by up to 13 m.y⁻¹. Beyond the first sandbar, the seabed was stable and the terminal lobe crest was at 3350 m from the shoreline.

The sandbars in group B developed at shallower depths and closer to the shoreline than observed in group A. Bedforms along profiles P3 and P4 tended to migrate seaward and vice versa along profile P5.

A small amount of sediment was deposited on the shoreface area of profile P3, and this accretion extended offshore onto the swash platform at the depths < 5 m, with localized sediment accretion of 0.2 m to 0.8 m forming swash bars. Further seaward on the swash platform at ~1000 m, erosion occurred and three flanking sandbars migrated offshore. The landward trough and crest of the first sandbar migrated at rates of 67 m.y⁻¹ and 58 m.y⁻¹ respectively, while the corresponding components of the second sandbar migrated more slowly at 44 m.y⁻¹ and 18 m.y⁻¹ respectively. The third and final sandbar at ~2780 m and depths of around 10.5 m, migrated even slower, with the landward trough and crest migrating at rates of 33 m.y⁻¹ and 13 m.y⁻¹ respectively. Beyond the third sandbar, the seabed was stable and the terminal lobe crest was at about 3300 m from the shoreline.

A veneer of new sediment up to 0.4 m thick was accreted on the swash platform of profile P4. Offshore migration of the flanking sandbars migrated increased the lateral extent of the swash platform by ~70 m. The migration rates for

the 3 consecutive sandbars were 44 m.y⁻¹, 32 m.y⁻¹, and 15 m.y⁻¹ respectively, showing the same pattern of offshore reduction in rates as profile P3. Finally, the seabed became stable at 3075 m, which corresponded to the outer slope of the terminal lobe.

Shoreward migration of bedforms and accretion dominated profile P5. Slight accretion occurred at the shoreface and continued onto the swash platform. Pronounced shoreward migration, at a rate of 55 m.y⁻¹, was shown by the first sandbar, which narrowed the swash platform by about 34. The first sandbar also shoaled by 0.9 m. A reduced migration rate of about 20 m.y⁻¹ was shown by the subsequent sandbar. Seaward of 1392 m there was significant accretion of up to ~1.3 m, which reduced to slight accretion beyond 1723 m. However, there were no significant changes in the morphology until the profile end at 3000 m.

The swash platform narrowed and the terminal lobe migrated shoreward along profile P6 within group C. The upper shoreface eroded and a prominent swash bar developed, which moved the starting point of swash platform 13 m further offshore. The first sandbar (terminal lobe) moved slightly offshore (46 m.y⁻¹) and its' crest shoaled from a depth of 4.2 m to 3.2 m with the formation of multiple swash bars. Beyond 1050 m there was, no evident variation in morphology as the seabed stabilized and gently sloped seaward.

Along profile P7 slight erosion occurred at 215 m to 452 m with a maximum erosion rate of 0.5 m.y⁻¹. Otherwise, seabed level remained unchanged.

4.3.2.9 Bathymetry November 2010 to November 2011

Between these surveys La Niña conditions developed and 191,191 m³ of sediment was dredged from the Entrance Channel in July 2011. Comparisons of the surveys indicate erosion was the dominant process during this period. The 3D maps (Figure 4-26, upper panel) show that significant sediment loss occurred on the swash platform, including the disappearance of two groups of swash bars and the redistribution of a third group. Locations where erosion occurred are more clearly seen in the residual map (Figure 4-26, lower right panel), with about 88% of the ebb-tidal delta area affected by erosion. The most severe erosion (up to 7 m

difference in bed level) occurred along the SE margin of the ebb-tidal delta adjacent to the Entrance Channel.

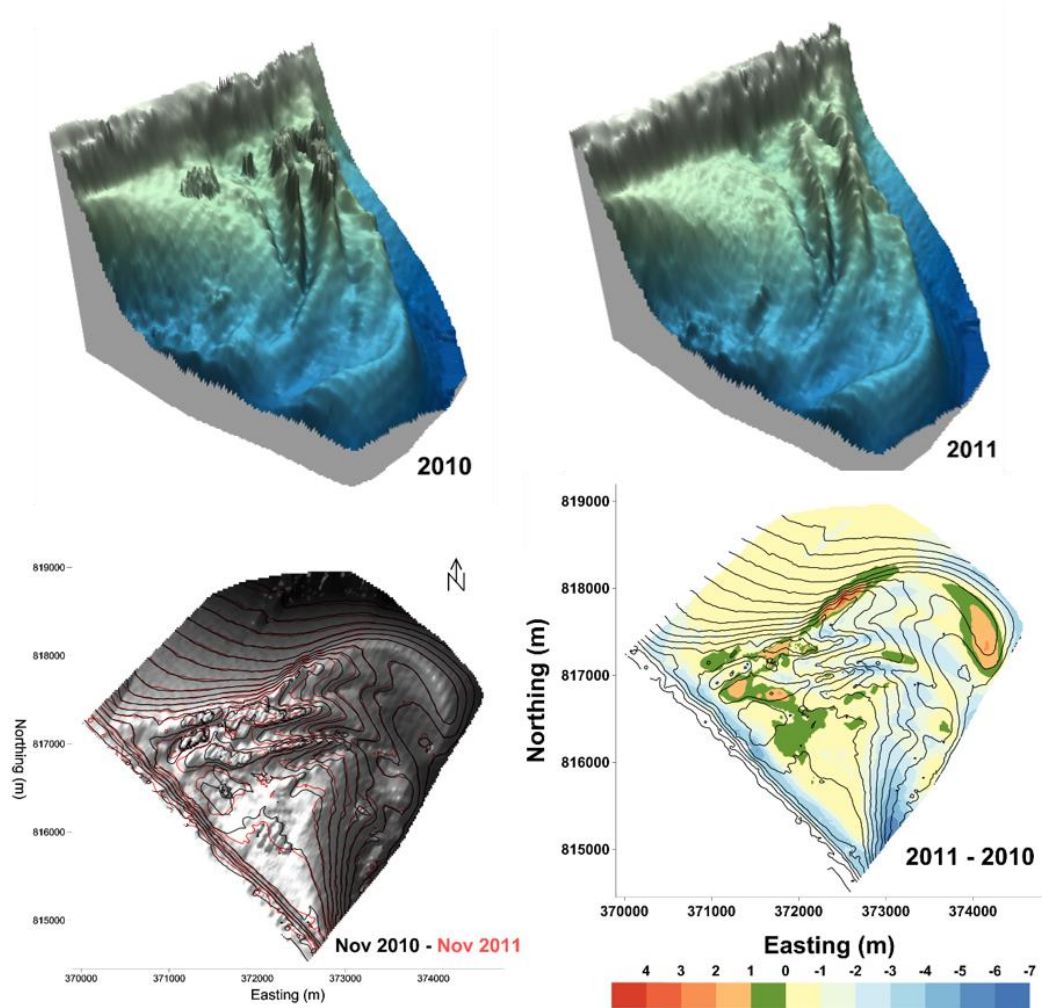


Figure 4-26. Morphology of the Matakana Banks ETD from SBES surveys in 2010 and 2011. The upper images are colour-shaded 3D surfaces interpolated from the SBES data. The lower left image is a shaded relief map of the 2009 bathymetry overlaid with the contours for the 2010 (black) and 2011 (red) surveys. The lower right image is a residual map that shows the locations where accretion (positive) and erosion (negative) occurred after 12 months of hydrodynamic forcing

Accretion only occurred over about 12% of the ebb-tidal delta area; at the tip of the spit-shaped terminal lobe, on the seaward slope and crest of the terminal lobe, and some parts of the swash platform (<3 m accretion). Hence, the net volumetric change between the surveys is erosion of $11.06 \times 10^6 \text{ m}^3$, equivalent to an average 1.02 m sediment thickness decrease.

Anti-clockwise bedform migration is identified from the superimposed contours map (Figure 4-26, lower left panel), with the bedforms close to the

Entrance Channel tending to migrate seaward (N-NW), and vice versa as the distance from the tidal inlet increased. However, on the swash platform, the direction of bedforms migration was more complex with no consistent pattern.

Comparison of the cross-sectional profiles (Figure 4-27) showed that within Group A, consistent with the previous survey period, bedform migration took place at greater depths and further offshore than for the other groups. As shown in profile P1, a steep shoreface links to a very narrow swash platform at ~4 m and extending to ~500 m from the shoreline. The profile then drops to a series of sandbars that occurred after ~1455 m at depths of ~10 m. These were associated with a variable bathymetry associated with sand waves, which ended at 1760 m, and the seabed stabilized subsequently.

Profile P2 recorded up to 0.5 m of erosion on the upper-shoreface. Further offshore, the seabed was stable until 1377 m, where a small swash bar or large sand wave at about 7.5 m depth progressively migrated offshore at a rate of 182 m.y^{-1} . Beyond this point, the seabed was stable and the terminal lobe's crest was located at 3345 m.

More variable morphology and a wider swash platform was characteristic of the central part of ebb-tidal delta as shown by profiles within group B (P3-P5). Along profile P3, localized erosion removed the swash bars that were present in 2010 on the middle of the swash platform. The eroded sediments seems to have been distributed along the profile as accretion further offshore along the profile infilled the troughs flanking both the first and second sandbars by up to 0.9 m.y^{-1} . The crest of first sandbar was located at ~2000 m appears to have been flattened leaving little relief. The second sandbar appears to have been stable, while the third sandbar, at 2822 m, migrated offshore migration at a rate of 24 m.y^{-1} . Beyond the third sandbar, starting at 2846 m, the seabed was stable and the last sandbar crest (terminal lobe) was located at about 3300 m.

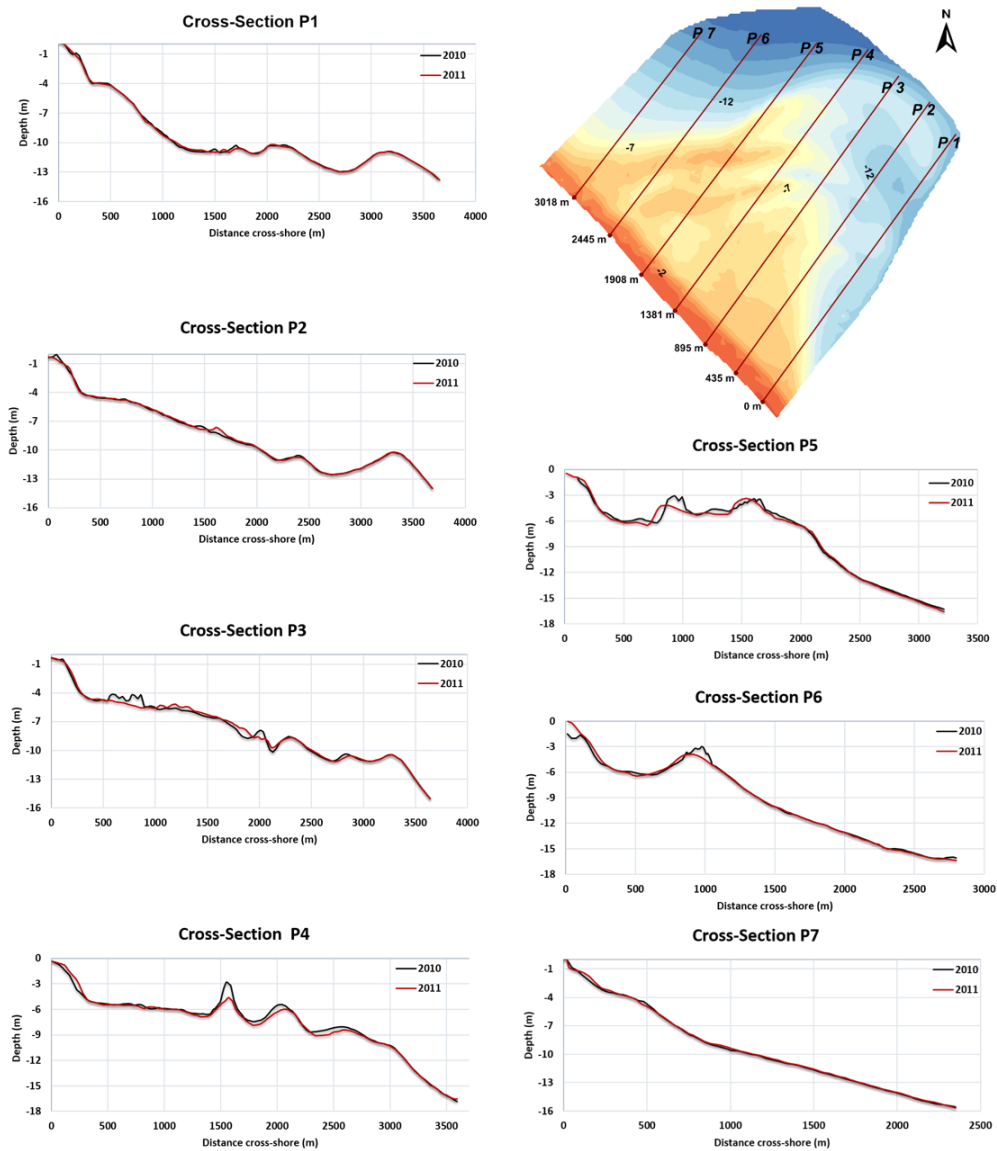


Figure 4-27. Comparison of cross-sectional profiles of surveys conducted in 2010 and 2011. Seaward migration of bedforms dominated for profiles adjacent to the Entrance Channel (P1-P4). However, in general, only small bathymetry variability occurred between these surveys.

Accretion on the slope, and sandbar migration associated with erosion are also displayed along profile P4. On the shoreface, sediment was redistributed from the upper to lower levels, resulting in accretion of the lower shoreface of up to 0.5 m. In contrast, the swash platform was relatively unchanged. The three sandbars on the seaward margin of the swash platform underwent significant changes. Heading offshore, the crests of each successive sandbar were lowered 2.1 m, 0.5 m and 0.3 m from their initial levels by erosion, and they migrated seaward at rates of 36 m.y^{-1} , 67 m.y^{-1} and 66 m.y^{-1} respectively. Beyond the outer sandbar at 2800 m and a depth of around 9 m, there were no significant changes.

Landward migration associated with erosion yielding a narrower swash platform and lower sandbar crests is a feature of profile P5. The lateral extent of the swash platform shortened from 465 m in 2010 to 317 m in 2011, with up to 0.5 m erosion of the platform. Seaward of the swash platform, the flanking sandbars migrated onshore with rates of 77 m.y⁻¹ and 65 m.y⁻¹ for the first and second sandbars respectively. The crest elevations of the first and second sandbars lowered by about 1.1 m and 0.4 m respectively. Offshore from the second sandbar, slight erosion occurred until ~2000 m, when the seabed became stable.

The least morphological was shown by group C profiles (P6 and P7). Significant sedimentation took place on the shoreface of profile P6, which thinned towards a narrow swash platform that formed a broad trough between the shoreface and the terminal lobe. Initially the terminal lobe was located at 975 m (2010), and by 2011 it had shifted onshore to 883 m from the shoreline, which was equivalent to a migration rate of 95 m.y⁻¹. The terminal lobe's crest was also lowered by about 1 m. Beyond the terminal lobe at 1038 m, morphological changes were no longer observed. Profile P7 was essentially stable, with only very slight accretion and erosion.

4.3.3 Short-Term (MBES) Ebb-Tidal Delta Bathymetry Changes

4.3.3.1 Bathymetry March – July 2013

Finer resolution 3D maps are displayed in Figure 4-28 (upper panel) based on 2 successive multi-beam echo sounder (MBES) surveys 5 months apart in March and July 2013. In between these surveys, no dredging occurred and ENSO conditions were neutral to developing El Niño. During this period, >45% of the significant wave heights were higher than 1 m and ~87% of wind speeds were higher than 5.5 m.s⁻¹. The main wind direction was north-east (Table 4-4). Both MBES surveys started at about 500 m from the shoreline, hence all the maps and cross-sectional profiles start seaward of the shoreface and omit the landward 500 m or so. The MBES surveys also extended further east than the SBES surveys so that they include the Entrance Channel and banks to the east of the channel.

The MBES survey data clearly show sand waves along the eastern margin, and smaller-scale bedforms over the surface of the ebb-tidal delta. It more clearly

shows the multiple bifurcations of three main systems of sandbars on the seaward margin, and also the sharp slope change between the terminal lobe (and Matakana Island shoreface beyond the ebb tidal delta) and the inner continental shelf.

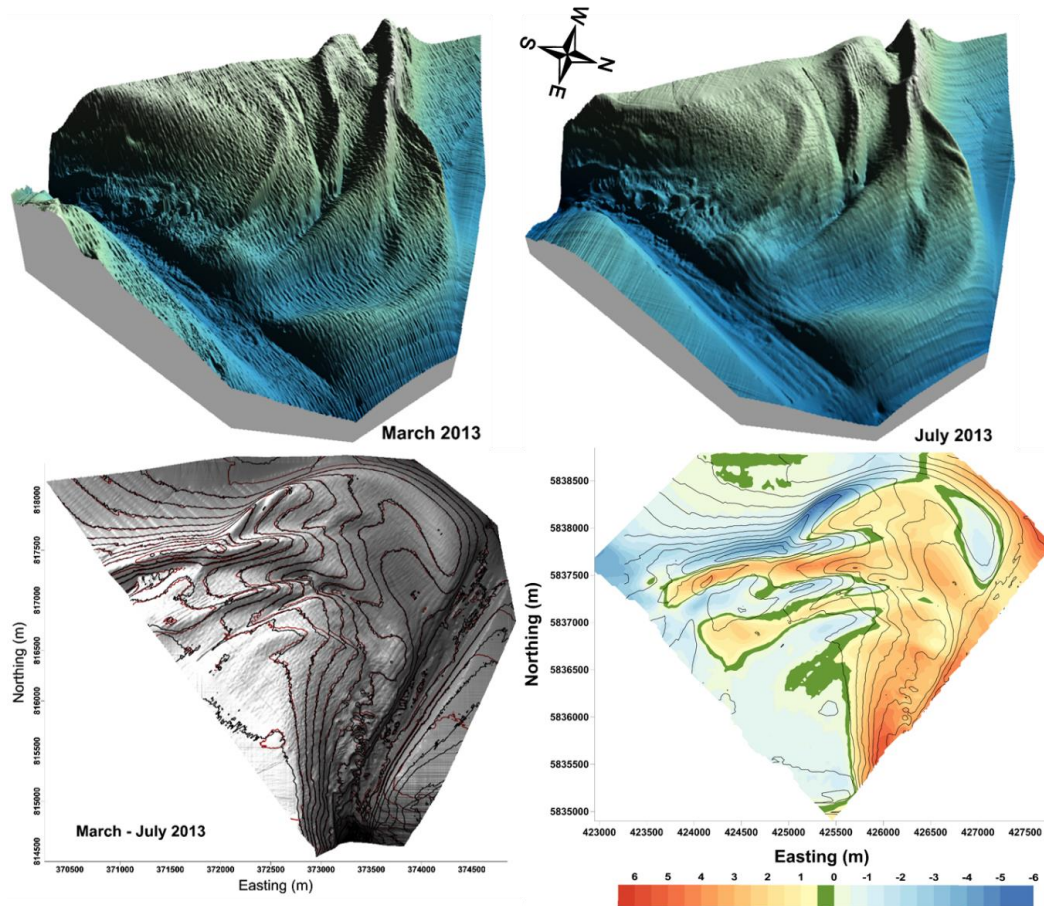


Figure 4-28. Morphology of the Matakana Banks ETD from MBES surveys in March and July 2013, which extended further east than the SBES surveys and included the Entrance Channel and banks to the east. The upper images are colour-shaded 3D surfaces interpolated from the MBES data, which was higher resolution than the earlier SBES surveys. The lower left image is a shaded relief map of the March bathymetry overlaid with the contours for the March (black) and July (red) surveys. The lower right image is a residual map that shows the locations where accretion (positive) and erosion (negative) occurred after 5 months of hydrodynamic forcing

The 3D images indicate that there were no significant changes to the ebb-tidal delta morphology over 5 months. However, a closer examination of the superimposed contour maps (Figure 4-28, lower left panel) reveals bedform movement; adjacent to the Entrance Channel bedforms migrated towards the shore in shallow water and offshore towards the NW in deeper water. The directions of bedform migrations became more complex on the shallow swash platform, while shoreward migration became dominant towards the terminal lobe.

The residual map (Figure 4-28, lower right panel) shows that strong accretion occurred along the areas adjacent to the Entrance Channel, particularly in deeper water. In contrast significant erosion occurred on the NW-N flanks of the terminal lobe; while mild erosion dominated the swash platform and the spit shaped terminal lobe in the east. Excluding the Entrance Channel and eastern banks that were not included in the SBES survey data (Figure 4-28), the net volumetric change indicated accretion of $\sim 4.165 \times 10^6 \text{ m}^3$, equivalent to 0.37 m average sediment accumulation.

Slight morphological changes are also displayed in the cross-sectional profiles (Figure 4-29). For the group A profiles, strong erosion occurred at the landward margin of the swash platform; the bed level in P1 dropped by ~ 1 m, while P2 only deepened by ~ 0.5 m. Comparing the MBES profiles with the November 2011 SBES profile suggests that the fluctuations at the ends of profile may be artefacts from the gridding of the MBES data, since the profiles were extracted from the gridded data. Therefore, the changes plotted in Figure 4.26 for the ends of each profile may not be real.

Mostly, the reliable observed morphological changes were seaward migrations of bedforms that occurred at depths from 10.2 m to 11 m in profile P1, and -7.7 m to -9.6 m in profile P2. These depths correspond to distances between 1100-1800 m and 1500-1900 m respectively. Along profile P1, the rate of offshore migration varied between 2.6 m.month^{-1} and 5.2 m.month^{-1} , while in P2 a higher migration rate of $\sim 7.2 \text{ m.month}^{-1}$ occurred. Offshore from these regions, no bathymetric variability was seen.

Considering group B profiles, which were the most dynamic in the MBES surveys, there were no significant changes in the bathymetry during the observation period. Along profile P3, slight offshore migration was seen on the swash platform at ~ 1500 m that shifted the sandbar at a rate of 9.4 m.month^{-1} . Seaward of this sandbar, thin accretion occurred until about 2060 m where localized erosion occurred. The erosion rate was very small, with a maximum erosion rate of about $0.06 \text{ m.month}^{-1}$. Beyond 2300 m the seabed was stable and the terminal lobe crest was located at a depth of 10.5 m, 3300 m from the shoreline.

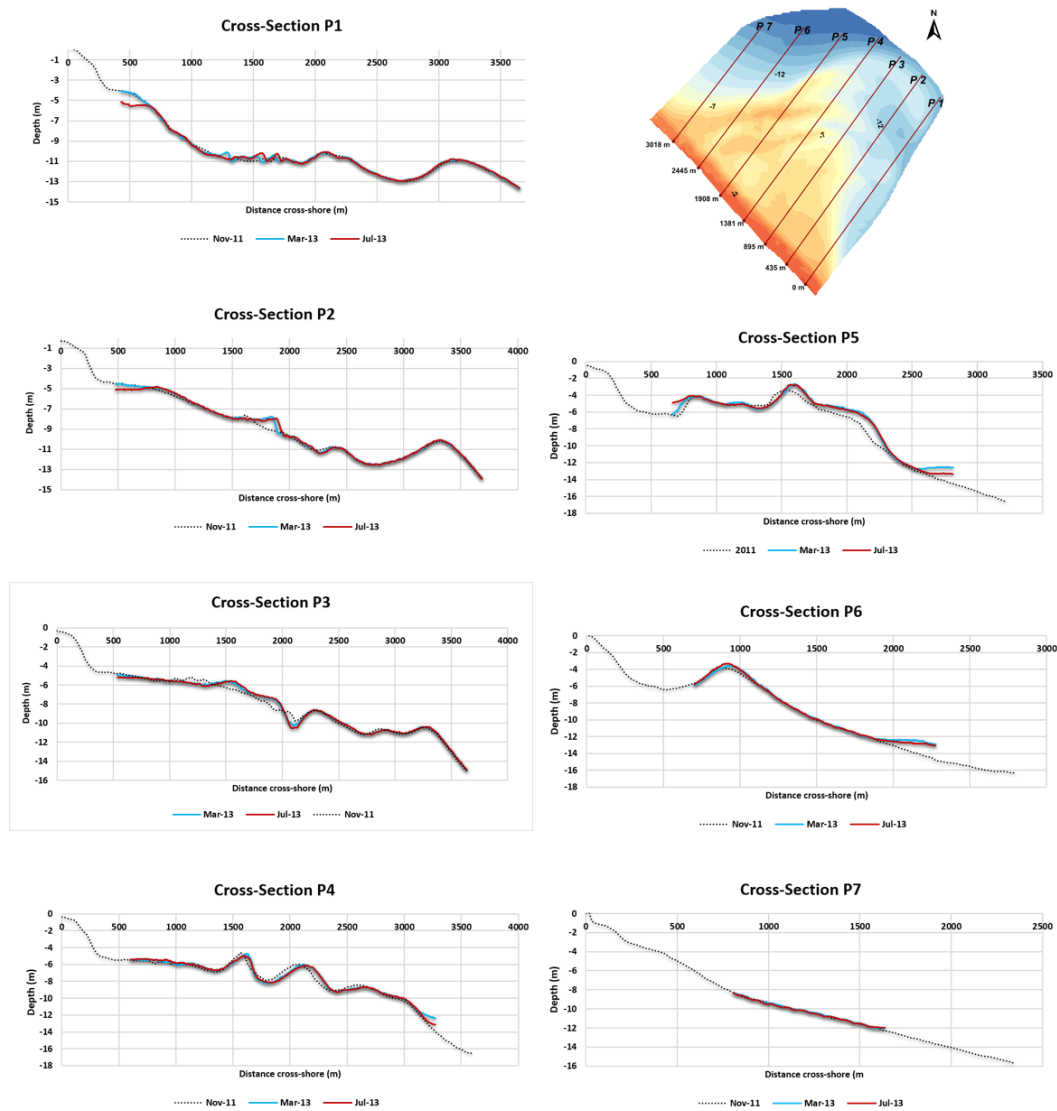


Figure 4-29. Comparisons of cross-sectional profiles from the November 2011 SBES survey and MBES surveys conducted in March and July 2013. Cross-shore distances for the MBES surveys were determined from the SBES reference shoreline (April 1998). Very little morphological change occurred within the 5 months between surveys. Some of the largest changes occurred at the margins of the MBES survey, which may be due to treatment of the boundaries by the gridding methodology used.

Profile P4 also displayed a thin veneer of accretion over the swash platform, and mild erosion associated with the shoreward migration of the first sandbar. The crest of the first sandbar eroded up to 0.3 m and shifted shoreward at $1.8 \text{ m}\cdot\text{month}^{-1}$. In contrast, the second sandbar migrated offshore at $8 \text{ m}\cdot\text{month}^{-1}$ and the crest lowered by 0.2 m. Beyond 2168 m, no morphological changes were observed. The terminal lobe was location at 2665 m, with the crest at a depth of 8.7 m. An absence

of bedform migration is evident in profile P5. Instead, very minor erosion occurred with maximum sediment thickness decrease of about 0.3 m.

Shoreward migration of the terminal lobe evident in the MBES survey data is still seen for profile P6. Along this profile, the terminal lobe crest was initially located at 940 m and migrated landward at a rate of 6.6 m.month⁻¹. Beyond the terminal lobe, the seabed was stable. No morphological changes were evident for profile P7.

4.4 Discussion

Observations over 13 years for the Matakana Banks ebb-tidal delta reveals that the delta appears to alternate between erosional and accretional phases, although some of the changes may be due to survey errors and not real, particular for SBES data. Sediment appears to be supplied to the ebb-tidal delta through the tidal inlet (Entrance Channel) and by the longshore transport along Matakana Island. From the bathymetric data it is not possible to identify any onshore transport from deeper waters offshore.

The movement of sand at a tidal inlet is complex due to reversing tidal currents, the effects of storms, and interactions with the longshore system (FitzGerald *et al.*, 2012). It is possible to sub-divide ebb-tidal deltas into regions with different dominant hydrodynamic forcings, and this is evident for Matakana Banks.

Comparing the locations of bedforms between two successive surveys of Matakana Banks indicated that the sandbars migrated in distinct patterns over the ebb-tidal delta platform. The tidal inlet and the tidal channels (Entrance Channel and former ebb channel) are the locations where the highest current velocities occurs and these are mostly dominated by coarse sands and shell gravel. Offshore migrating sand waves were also identified, predominantly within the former ebb channel. This is consistent with an ebb dominated estuary, where sand transport is offshore as indicated by the direction of sand waves migration along the tidal channel (FitzGerald *et al.*, 2012).

In general, the offshore transport wanes towards the terminal lobe and the ebb-jet weakens and wave action increasingly opposes the tidal flow. This results in the deposition of sediment on the terminal lobe. The bathymetric survey data

indicate this occurs at Matakana Banks for the former ebb channel, but it does not appear to be a significant contributor to sedimentation in the Entrance Channel as observed by Spiers *et al* (2009). The development of multiple sand bars on the terminal lobe on Matakana Banks, also suggests that wave driven longshore transport of sediment may be a significant source of sediment.

However, waves and flood-tidal flows generally redistribute sediment from the terminal lobe across the delta platform (Pickrill, 1985). The bathymetric survey results indicates that this occurs over Matakana Banks, and that most of the observed morphological variability was a consequence of the migration of bedforms associated with this sediment redistribution. This is consistent with many studies that report that landward flow dominates over the ebb-tidal delta swash platform due to the combined effects of wave energy and tidal current segregation (Hine, 1975); (Oertel, 1975); (FitzGerald, 1984).

Often it is assumed that the combination of these processes results in inlet bypassing with sediment entering the tidal inlet from the updrift side, and bedforms forming and migrating along the coast on the downdrift side. However, the bathymetric survey results indicate that the sediment primarily recirculates over the Matakana Banks ebb-tidal delta, with the main bedform migration occurring on what previous studies have identified as the updrift side (Spiers *et al*, 2009). This is consistent with the study of Bartholomä *et al.* (2010) who found that sediment recirculates in the Otzum ebb-tidal delta system between the German Bight barrier islands of Langeoog and Spiekeroog. Little sediment appears to bypass this ebb-tidal delta, based on sedimentological sequences collected over the ebb tidal shoal.

One interesting feature of the recirculation of sediment over Matakana Banks is that the direction of migration of bedforms appears to switch between clockwise and anticlockwise circulation. Since the surveys are mostly years apart, and the circulation changes occur on the swash platform, they are probably a consequence of interannual changes in wave conditions as indicated by the MetOCean wave hindcast data shown in Figure 4-3. Macky *et al.* (1995) analysed wave conditions for the Katikati Entrance ebb-tidal delta between 1991 and 1993. They reported significant variability in wave conditions, and the resulting sediment transport, with a small net longshore transport towards the northwest during their study. It was noted that the study coincided with predominantly El Niño conditions, and that this may have led to different wave conditions and sediment transport directions from

that normally experienced (previous studies indicated a net southwest longshore transport). Therefore, it would be informative to consider the observed changes in circulation and ebb-tidal morphology in relation to the antecedent El Niño-Southern Oscillation (ENSO) conditions.

The state of ENSO can be defined by the Southern Oscillation Index (SOI), which reflects the difference in atmospheric pressure between Darwin and Tahiti (Gordon, 1985). Gordon (1985) examined the effect of the SOI on New Zealand weather; he found that the negative values of SOI (i.e., El Niño conditions) are associated with anomalous southerly to westerly air flow (the direction varying with the season). The corollary is that La Niña conditions are associated with anomalous northerly to easterly flow. It follows from Gordon’s findings that La Niña conditions result in larger wave events and higher sea levels on the north and east coast (Macky et al., 1995); (Bell and Goring, 1998). The opposite occurs during El Niño. The influence of El Niño and La Niña (ENSO extremes) on the northeast coast of New Zealand is summarized in Table 4-6 (de Lange, 2000).

Table 4-6. Summary of the observed ENSO extreme effects on the northeast coast of New Zealand (taken from de Lange, 2000)

	<i>El Niño</i>	<i>La Niña</i>
<i>Air temperature</i>	Decreased	Increased
<i>Atmospheric pressure</i>	SE to NW pressure gradient	NW to SE pressure gradient
<i>Wind direction</i>	More southwesterly winds (offshore)	More northwest-northeasterly winds (onshore)
<i>Storm frequency</i>	Reduced extratropical cyclone activity	More extratropical cyclone activity.
<i>Sea surface</i>	Decreased	Increase
<i>Sea level</i>	Drops	Rises
<i>Wave climate</i>	Reduced sea component	Increased sea component
<i>Wave steepness</i>	Reduced	Increased
<i>Near bed flow</i>	More onshore	More offshore
<i>Coastal response</i>	Tendency to accrete	Tendency to erode

4.4.1 Group Areas of the Ebb-Tidal Delta

Observations of bathymetric changes over the entire period reveals that the ebb-tidal delta can be subdivided into 3 zones depending on the primary hydrodynamic forcings that determine the morphology, as also found by (FitzGerald *et al*, 2012). These zones were identified as Groups A, B and C in the

results, where the groups consisted of cross-shore profiles that displayed similar morphological changes.

Group A is the area adjacent to the tidal inlet (Entrance Channel), including the former ebb channel, where the bedform movements were bi-directional, and predominantly forced by ebb and flood tidal currents. Overall, there was a net seaward migration, suggesting that Tauranga Harbour is an ebb-current dominated. However, the magnitude of bedform migrations was not as high as those in the shallower part of the ebb-tidal delta (swash platform), and the furthest bedform migration observed was ~200 m toward offshore. The deeper areas along the tidal channel are armoured by gravelly shell fragments on the channel bed, or represent exposed resistant Pleistocene ridges that limit the availability of sediment to be transported by tidal currents. This suggests that the net sediment transport flux for Group A is lower than for the swash platform (Groups B and C). The Group A profiles show almost no variability further than about 3 km offshore, which indicates the outer limit of the ebb-tidal delta.

A shallow and broad swash platform is characteristic of group B cross-shore profiles. This is the region where the most dynamic bedform movement occurred resulting in the greatest morphological variability. Within this region, tidal currents are no longer the primary force determining the sediment distribution. Instead, the movement of sediment is determined by a combination of wave and tidal currents. Mostly the bed variations associated with offshore swash bar migrations occurred at relatively shallow depths of less than 11 m between 1,400 m – 3,000 m offshore.

Although the bedforms on the swash platform appear to migrate landwards, it is also evident that there has been an overall extension of sand bars on the margin of the swash platform and on the terminal lobe, toward the north of the ebb-tidal delta. This is well documented in the 3D surface maps from 1998 to 2011, resulting in additional lines of swash bars further offshore by the end of SBES observation period.

The source of the sediment in this accumulation is unclear, and require more detailed analyses of the sediment compositions together with measurements of bedforms and ebb versus flood currents in order to determine the sand-dispersal patterns (Komar, 1996), or numerical simulations, or a combination of both. Potential sources of sediment include the offshore transport of sediment by the ebb-jet (from the Group A region), longshore sediment transport (from the Group C

region), or landward transport from the continental shelf (Meade, 1969). Subsequent chapters in this study will assess sediment textural data, measured hydrodynamic conditions and numerical simulations.

As the ebb-tidal delta reaches its' NW boundary limit, the swash platform narrows and the terminal lobe welds onto the surf zone offshore bars of Matakana Island (Group C). This region was relatively stable during the period considered, apart from reduction in the extent of the swash platform and shoreward migration of the terminal lobe. This suggests some redistribution of sediment from the terminal lobe onto the swash platform, or into the extending swash bars in the Group B region.

4.4.2 Sediment Transport Patterns

Figure 4-30 summarizes the hydrodynamic conditions, wind rose, ENSO state, dredging volume, monthly volumetric changes, orientation of the bedform migration, and maximum migration rates for the survey periods considered.

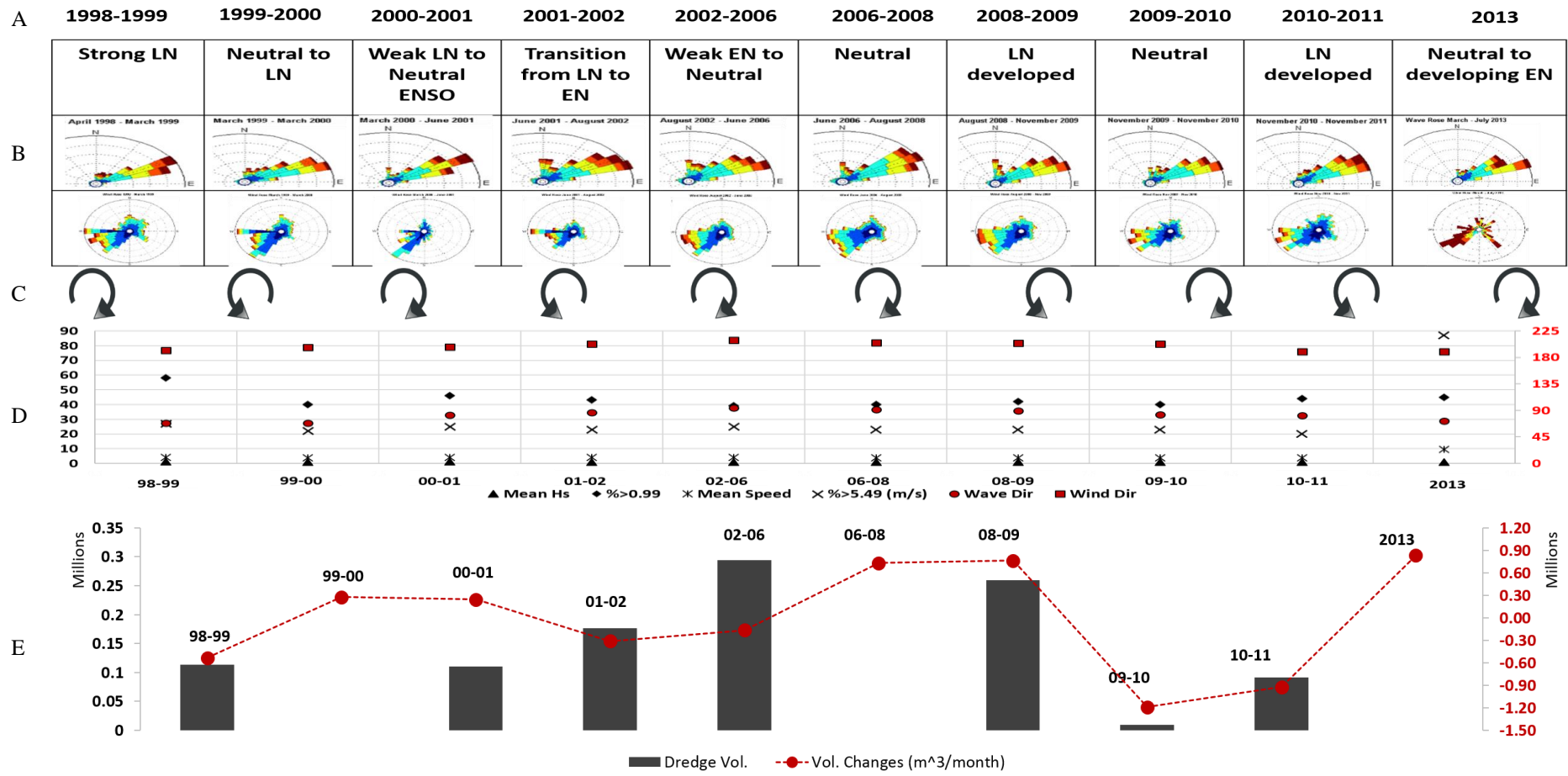


Figure 4-30 Plots of the relationship among the ENSO condition where LN is La Niña and EN is El Niño (A), wave and wind roses (B), clockwise and anticlockwise direction of bedform migration (C), statistics of hydrodynamic regimes (Table 4-4) (D), and dredging volume and monthly volumetric changes (Table 4-5) (E) for Matakana Banks ebb-tidal delta between surveys. Detailed wave and wind roses are given in Appendix 1.

Over the observation period, the dominant wave direction was from the northeast and the dominant wind was southeasterly. The highest mean significant wave height (H_s) seems to be related with a strong La Niña during 1998-1999. Weak El Niño and neutral ENSO conditions with a mean H_s of about 1 m or less. There does not appear to be an obvious correlation between ENSO state and the direction of sediment circulation on the swash platform, or the volume changes observed. However, there does appear to be some relationship between mean wave and wind directions, and volume changes

Oertel (1972) has described the complexity of sediment movements over inlet shoals in response to the interactions of waves and tidal currents. They identified that concentrated breaking of the waves in shoal areas (Figure 4-31) enhanced sediment suspension, and produced bores that tended to move sand shoreward. The net sediment movement, however, depends on the relative magnitudes of the superimposed tidal currents, with the direction of sediment movement governed by whether the current is associated with the flood or ebb tide.

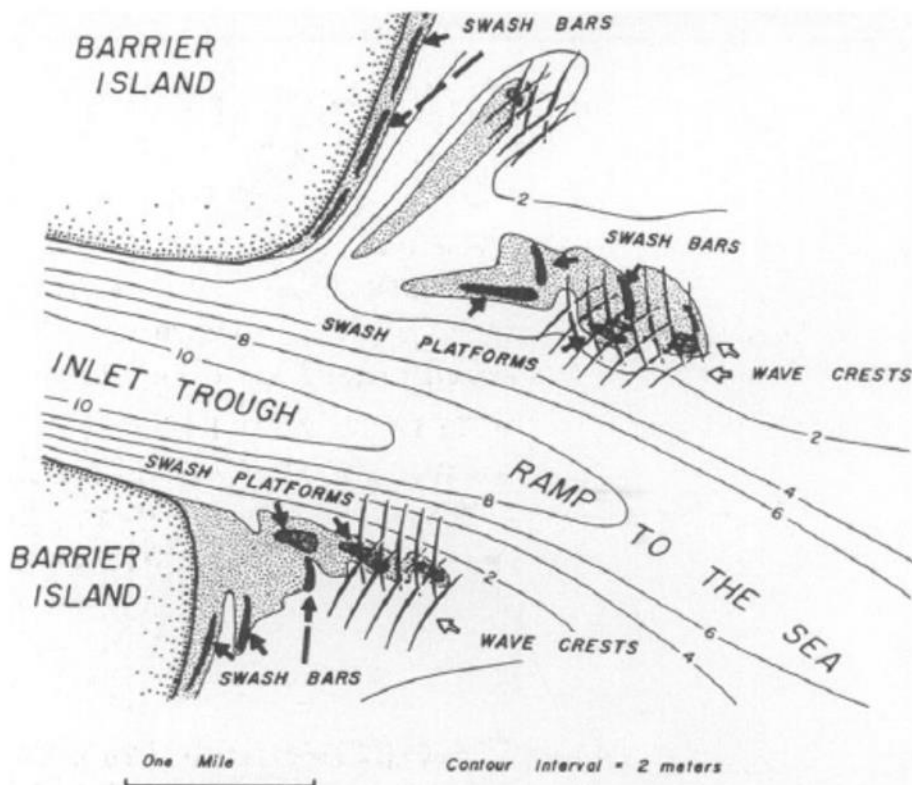


Figure 4-31. Generalized sketch map illustrating the topographic features at tidal inlets along the Georgia coast. Refracted wave crests generally interfere along the axis of seaward extending shoals (taken from Oertel, 1972).

The orientation of bedforms indicates the current direction and sediment transport pathways. During the ebb tide, the current that transports the sediment leaves the tidal inlet and distributes the sediment over the ebb-tidal delta until it wanes at the terminal lobe. The Matakana Banks ebb-tidal delta systems mostly located on the northern side of the tidal inlet as a constricted ebb-tidal delta in the classification of Hicks and Hume (1996). During ebb tide, the tidal currents form an anticlockwise pathway from the tidal inlet to N-NW, and the current reverses back towards the inlet during flood tide (Spiers *et al*, 2009).

North-easterly waves (which are perpendicular with the orientation of Matakana shoreline), generate near-bed currents that can move sediment shoreward from the deeper part of the ebb-tidal delta onto the swash platform. In addition wave refraction over the shallow shoals tend to produce a consistent pattern of longshore transport divergence along the shoreline, irrespective of the incident wave direction. The wave currents and tidal currents interact to produce the overall sediment transport, which suggests that bedforms should migrate anti-clockwise. Spiers *et al* (2009) demonstrated that sediment transport over the eastern remnant of the Tauranga Entrance ebb-tidal delta, located to the east of the Entrance Channel, is dominated by a persistent clockwise rotation driven in this manner.

However, the bathymetric survey data indicate that the directions of sediment movement reverse at multi-year time scales. Similar patterns of behaviour have been reported previously for the Katikati Inlet ebb-tidal delta at the northwestern end of Matakana Island (Hicks *et al.*, 1999). They attributed this the migrating bars and flood channels altering the interactions between tidal currents and waves. The more recent study of Eelkema *et al.* (2012) concluded that the reorientation is related to the changes in cross-shore and alongshore tidal currents. They suggested that redistribution of tidal currents is most likely an effect of the waves reworking the shoals, a weakening influence of the tidal currents, and associated balance between sediment supply from different sources.

Variations in the wave climate due to the El Niño-Southern Oscillation (ENSO) has been linked to adjustment in the morphology of tidal inlets through variations in longshore sediment transport (Hicks *et al.*, 1999). Anti-clockwise bedform migration on the Matakana Banks swash platform (Figure 4-30) seems to be related with a developing La Niña extreme. However, a clockwise bedform migration pathway is detected from the bathymetric comparison of 1998 to 1999,

when a strong La Niña extreme occurred (Figure 4-30). A drop in the sea level, and more onshore near bed flow are characteristic of El Niño conditions de Lange (2000), suggesting there may be an increased onshore flux from deeper areas around the terminal lobe. This may explain the apparent clockwise bedform migration (shoreward adjacent to main tidal channels and seaward on the swash platform – terminal lobe) during periods of neutral to the El Niño development (Figure 4-29). Specifically, the net sediment movement is still anticlockwise, but the increased onshore flux results in the accumulation of sediment within the terminal lobe source area for wave driven sediment transport onto the swash platform.

4.4.3 Dredging and ebb-tidal delta volumetric changes

Assessing the volumetric changes within the ebb-tidal delta system cannot be done by directly relating the dredged volume with the gain and loss of the ebb-tidal delta. Figure 4-30 shows the hydrodynamic conditions, dredging quantities and the volumetric fluctuations over the observation period. It is evident that the volumetric fluctuations of the ebb-tidal delta were not solely dependent on the volume of dredged sediment. Instead the occurrence of storm wave events may combine with dredging to determine the volume change

Over the entire observation period, ENSO conditions varied from strong La Nina to weak El Nino, and both seemed to negatively or positively affect the ebb-tidal delta volume. Significant sediment gain is indicated during the years of no dredging in between 1999-2000 and 2006-2008, or little volume of dredging with storm events in 2010-2011. Therefore, the relationship with potential drivers of morphological change are likely complex and interrelated.

During La Niña extremes, coastal erosion is more prevalent due to elevated sea levels, onshore winds and larger, steeper waves (Table 4-6). Figures 4-4 and 4-30 shows that the two highest mean significant wave heights occurred during a strong La Niña and weak La Nina to neutral ENSO respectively. The first event was during 1988-1999, when the mean H_s was around 1.2 m with almost 60% of mean $H_s > 0.99$ m. The second event was during 2000-2001, when the mean H_s was around 1.1 m, with about 46% of $H_s > 0.99$ m. For these periods, the percentage of wind speed higher than 5.49 m/s, or stronger than moderate breeze, (Beaufort, 2015) were 27% and 25% respectively (Figure 4-30).

The combination of intense storm events and a high volume of dredged sediment, seems to increase the erosion rate, as evident during 1998-1999. However, the ebb-tidal delta quickly recovered during the absence of dredging before the next biennial campaign. This coincided with relatively calm wave-wind conditions (Neutral to La Niña phase), which may allow the ebb-tidal delta to accrete instead of erode. Thus, even though 45% of significant wave heights were > 0.99 m during 2000-2001, the volumetric change of ebb-tidal delta was still positive (accretion).

Relatively calm hydrodynamic conditions during 2002-2006 (weak El Niño to Neutral phase), when the largest volume of sediment was dredged, were associated with no increase in erosion. Slight accretion was evident during the period of no dredging and neutral ENSO phase between 2006-2008. Between 2008-2009 dredging commenced and about 40% of mean H_s were > 0.99 m as the La Niña phase started developing. This does not appear to have caused significant erosions.

However, the large volume of dredging during 2008-2009 may have contributed to volumetric changes in the following period (2009-2010) where there was a significant volume loss from the ebb-tidal delta. This occurred during neutral ENSO conditions, with only about 9,000 m^3 sediment dredged from the Entrance Channel. Since the dredged volumes represent the portion of recirculating sediment captured by the Entrance Channel (Spiers et al, 2009) _it is not clear where the sediment eroded from the ebb-tidal delta went during this period.

Low dredged sediment volume before the period of 2010-2011 may have allowed the ebb-tidal delta volume to recover (erosion rate decreased) even though the percentage of mean H_s waves > 0.99 m was about 45% (La Niña developed). Alternatively, the sediment removed by during the erosion phase was located in an area where it could easily be transported back into the survey area, or the erosion represents an error between surveys.

In the absence of dredging, increased wave intensities and moderate winds did not negatively affect the volume of the ebb-tidal delta, between MBES surveys over 5 months in 2013. Overall, the volume of the ebb-tidal delta seems to depend on the volume of dredged sediment in the previous survey period, the frequency and duration of larger wave events and the dominant wind direction and speed. In particular, the occurrence of storms or larger wave events during La Niña conditions

may increase the tendency to erosion for period during or after dredging commenced. However, there are insufficient data to test this relationship statistically.

4.4.4 Single- vs Multibeam Echosounder Surveys

In order to assess the reliability of the bathymetry data from SBES survey, the monthly volumetric changes obtained by selected SBES surveys were compared with the monthly volumetric changes calculated from MBES data. The selected bathymetry were comparable, as the 2006-2008 SBES surveys and the March – July 2013 MBES were conducted with no dredging and Neutral and Neutral to El Nino ENSO conditions respectively. The result shows that monthly volumetric changes calculated from the MBES survey was about 104,000 m³ or about 14% higher than by SBES survey. The difference may due to the lower density of bathymetric data of SBES than MBES surveys. Limited coverage of SBES beam on the seafloor surface is prone to uncertainty of the morphology of features between the survey lines, and be affected by bedforms moving across transect lines. Hence, to provide a higher accuracy for bathymetric mapping that yields more accurate calculated volume, MBES surveys are recommended for monitoring the ebb-tidal delta.

4.4.5 Conceptual Model

The results of repetitive bathymetric surveys of the study area revealed that in general the Matakana Banks ebb-tidal delta can be fitted well with the standard model of ebb-tidal delta morphology described in (Hayes, General morphology and sediment patterns in tidal inlets, 1980). However, Matakana Banks ebb-tidal delta shows some variations as the results of the geological setting of Tauranga Harbour (Figure 4-32); stable main ebb/flood channel, the outer and inner blind channels, fixed position of the terminal lobes and offset headlands that constricts the delta growth.

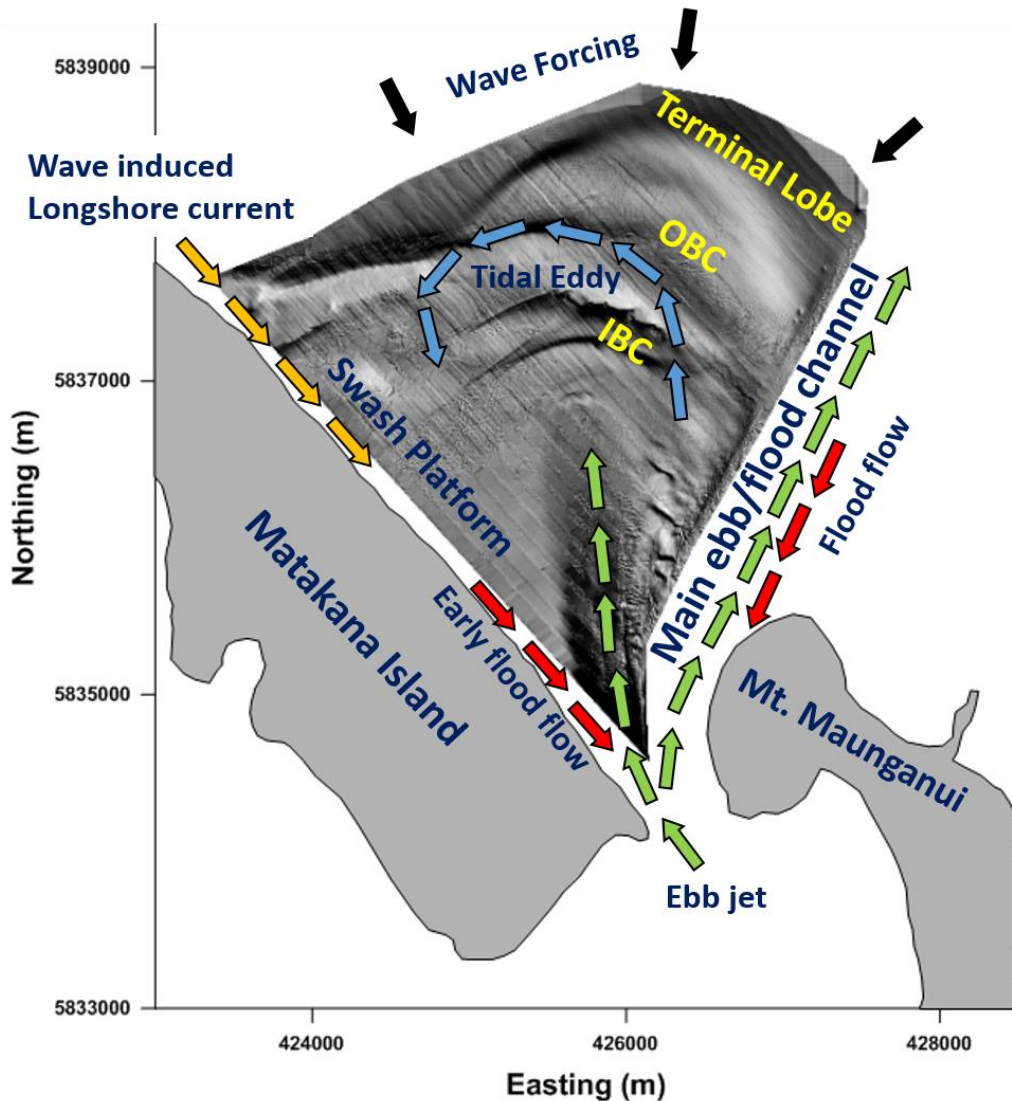


Figure 4- 32 The conceptual model of Matakana Banks ebb-tidal delta morphology. The OBC and IBC are abbreviation for outer blind channel and inner blind channel.

As indicated by de Lange *et al.* (2015) that it is likely that much of the ebb-tidal delta is anchored by the embedded Pleistocene sediments, hence the analysis of 13 years bathymetry surveys presented in this study reveal that the main shape of the ebb-tidal delta always remain the same, mostly the morphological variability occurred due to the migration of mobile sand on the swash platform and at the flanks of the Entrance Channel.

Dredging along the Entrance Channel creating a deep channel through the Pleistocene ridge (de Lange *et al.*, 2015), channel deepening that cuts through the consolidated sediment and routine maintenance dredging yielded a stable tidal inlet

(FitzGerald, 2012) that remain approximately in the same position. Further, the lateral distribution of the ebb-tidal delta is also constricted by the presence of offset headland (Mt. Maunganui) at the SE of the Entrance Channel that acts as the wave shelter. Hence the Matakana ebb-tidal delta can be defined as the constricted ebb-tidal delta (Hicks and Hume, 1996).

As a consequence, the pattern of currents that influence sediment transport is modified and is no longer as symmetrical as assumed in standard models. For the Tauranga Entrance ebb-tidal delta, the dominant tidal flows occur within the dredged channel, with a weaker remnant ebb jet and associated tidal recirculation occurring over the Matakana Banks to the west of the channel. The small platform west of the dredged channel has even more restricted tidal circulation (Spiers, 2013). The incoming flood from the offshore (East) is mainly confined to the main ebb/flow channel. However, during the early flood tide the flood flow also enters the harbour through the marginal flood channel.

Combination of wave action and flood tide may significantly increase the sediment transport as longshore transport from the NE and the sediment from the offshore (East) into the shallow shoal (swash platform). During the wave events (storms), the waves becomes more dominant than the ebb-jet which is evident in the clockwise sediment transport patterns (see Section 4.4.2).

4.5 Summary

Bathymetric data obtained by SBES and MBES surveys of the ebb-tidal delta were used to measure and analyse the ebb-tidal delta morphological changes at different time scales. The analyses yielded a series of well-defined 3D images that presented the evolution of ebb-tidal delta components, particularly: the migration and evolution of sandbars on the seaward margin of swash platform; the migration and evolution of the terminal lobe; and the appearance and disappearance of swash bars on the shoreface and swash platform.

Sandbars on the margins of the swash platform progressively elongated towards the shore, and by 2011 they became attached to the shoreline. Shoreline-

attached sandbars can be advantageous to the down-drift beaches since they can be the source of sediment for wave-driven transport to disperse the sediment alongshore as demonstrated by Kana *et al.* (1999) and Gaudio and Kana (2001). However, the Matakana Banks bars have developed on the assumed updrift side of the ebb-tidal delta, and the data indicate that there may be a high degree of sediment recirculation, so their contribution to alongshore transport is unclear. By the end of SBES observation period in 2011, even though the sandbars had moved significantly, the main shape of ebb-tidal delta remained unchanged.

The directions of bedform migration inferred by comparisons of successive contour maps for pairs of consecutive surveys suggest a general anticlockwise circulation consistent with the presence of an ebb-jet and associated eddies. This involves offshore transport by currents of the ebb jet from the deeper tidal inlet onto the terminal lobe, followed by onshore transport around the terminal lobe and across the swash platform by wave-induced currents. However, observations also showed periods when this circulation appeared to reverse (clockwise), which mostly occurred during the phases of Neutral to developing El Niño ENSO conditions. There was also evidence from the NE growth of the elongated spit-shape of the terminal lobe across the Entrance Channel to support the proposed net littoral drift direction from NW to SE past the entrance (Healy *et al.*, 1977).

There was no apparent variations in the wave climate or wind climate, or tidal characteristics measured for the entrance to Tauranga Harbour during the observation period that can be linked to the net gain and loss of the ebb tidal delta volume. But the occurrence of storms or wave events may encourage erosion of the ebb-tidal delta particularly after a dredging phase. However, this is not always the case, as it was evident that in the absence of dredging activity, the ebb-tidal delta volume was stable or increase rate even despite storm events.

The measured volumetric changes appear to be large. However, much of the observed changes from SBES surveys resulted from the movement of swash bars and sandbars, and therefore depended on their positions relative to the survey transects at the time of the survey. Hence, the volumetric changes probably represent a redistribution of the sediment within the delta, and not necessarily losses and gains from the ebb-tidal delta system (Ramli and De Lange, 2013a).

High-resolution multibeam echo sounder (MBES) surveys produced digital elevation models of the bathymetry with a finer resolution than the single beam echo sounder (SBES) surveys that were restricted to observations along sounding lines. Only two MBES surveys five months apart were available for analysis. These surveys revealed that the general patterns of bedform migration were the same as described by the longer-term SBES bathymetric surveys. However the calculated monthly volumetric changes resulting from SBES and MBES surveys over periods with similar forcing conditions were compared, and MBES survey showed about 140,000 m³ or 14% more volume change.

Based on the morphological changes over the observation period, including bedform migration rates and evolution, the offshore distance and depths at which morphological elements occur, and the extent of the swash platform, the ebb-tidal delta can be divided into 3 main areas;. These were represented by three sets of cross-shore profiles; group A consisting of profiles P1 and P2; group, B consisting of profiles P3, P4 and P5; and group C consisting of profiles P6 and P7. The characteristics of these three areas are:

- Group A is located adjacent to the tidal inlet, where sediment transport and bedform migration in the deeper regions was dictated by tidal current velocities associated with the ebb jet. At distances between 1300 m to 2500 m and depths from 9 m to 13 m bedforms consisted mostly of sand waves, which migrated seaward. On the shallow margins (1-5 m depth) of the tidal inlet close to shore (< 500 m offshore) bedforms migrated shoreward. These consisted mostly of swash bars and contributed to a shore parallel system of swash bars along the Matakana Island shoreface, Shoreward migration in the shallows adjacent to the inlet throat is due to a westward divergence of velocity vectors at the distal end of the jet consistent with the observations of Spiers *et al.* (2009) along the eastern flank of the Entrance Channel. Superimposed contour maps revealed that towards the offshore end of the Entrance Channel in the west, bedforms increasingly began to move perpendicular to the orientation of the channel. This resulted in sediment being transported onto the sandbars flanking the swash platform, particularly the terminal lobe. Bedform migration rates measured from cross-shore profiles varied between 10 m.y⁻¹ to 182 m.y⁻¹. In this part of the ebb tidal delta, the swash platform progressively developed and extended seaward

with increasing distance from the Entrance Channel. Close to the tidal inlet (profile p1) the swash platform was narrow with a width that varied from 75 m to 270 m over time, while at profile P2 it extended to 700 m. The swash platform was located at depths of <5 m.

- Group B profiles represent the region of the ebb tidal delta where wave influences start to significantly influence the morphology. Sediment transport by waves that are refracted by the sandbars and break on swash bars, particularly during storms, result in this area being the most dynamic part of the ebb-tidal delta morphology during the observation period. Group B profiles are characterized by a broad shallow swash platform, which narrows alongshore towards the west. The width of the swash platform between the shoreface and the first trough of complex of flanking sandbars offshore ranged from 1200 m to 2000 m. Complex patterns of bedform migration occurred on the swash platform. Swash bars migrated alternately shoreward and seaward rather than continuously in the same direction at depths between 2.8-10 m. Bedform migration rates for Group B profiles were very variable but did not exceed 162 m.y⁻¹.
- Group C profiles were located close to the western boundary of the ebb-tidal delta where the swash platform disappears and the terminal lobe welds onto the offshore bars of Matakana Island (Ramli and de Lange, 2013b). This region was the least dynamic area during the observation period. The main morphological change observed was the progressive flattening of the sandbar on the terminal lobe to leave a residual “small bump” by 2011.

4.6 References

- Balouin, Y., Howa, H., and Michel, D. (2001). Swash platform morphology in the ebb-tidal delta of Barra Nova inlet, South Portugal. *Journal of Coastal Research*, 784-791.
- Barnard, P.L., Erikson, L.H., Elias, E.P.L., and Dartnell, P. (2012). Sediment transport patterns in the San Francisco Bay Coastal System from cross-validation of bedform asymmetry and modelled residual flux. *Marine Geology*, 1-24.
- Bartholoma, A., Ernstsens, V.B., Flemming, B.W., and Bartholdy, J. (2004). Bedform dynamics and net sediment transport paths over a flood-ebb tidal cycle in the Gradyb channel (Denmark), determined by high-resolution multibeam echosounding. *Danish Journal of Geography 104 (1)*, 45-55.
- Beaufort, F. (2015). *Beaufort Wind Scale*. England: U.K. Royal Navy. Retrieved from Storm Prediction Center: NOAA/Natioal Weather Service: <http://www.spc.noaa.gov/faq/tornado/beaufort.html>
- Beck, T.M., and Kraus, N.C. (2011). New ebb-tidal delta at an old inlet, Shark River inlet, New Jersey. *Journal of Coastal Research Special Issue 59*, 98-110.
- Bell, R.G., and Goring, D.G. (1998). Seasonal variability of sea level and sea-surface temperature on the north-east coast of New Zealand. *Estuarine, Coastal and Shelf Science Vol. 46, Issue 2*, 307-318.
- Brannigan, A. (2009). *Change in Geomorphology, Hydrodynamics and Surficial Sediment of Tauranga Entrance Tidal Delta System (MSc Thesis)*. Hamilton, New Zealand: University of Waikato.
- Caress, D.W., Thomas, H., Kirkwood, W.J., McEwen, R., Henthorn, R., Clague, D.A., Paull, C.K., Paduan, J., and Maier, K.L. (2008). High-Resolution Multibeam, Sidescan, and Subbottom Surveys Using the MBARI AUV D. Allan B. In J. a. Reynolds, *Marine Habitat Mapping Technology for Alaska* (pp. 47-68). Alaska Fairbanks: Alaska Sea Grant Collage Program, University of Alaska Fairbanks.
- de Lange, W. (1991). *Wave climate for No.1 Reach, Port of Tauranga, Tauranga Harbour, Report to the Port of Tauranga Ltd*. New Zealand: University of Waikato.
- de Lange, W. (2000). Interdecadal Pacific Oscillation (IPO): a mechanism for forcing decadal scale coastal change on the northeast coast of New Zealand. *Journal of Coastal Research*, 657-664.

- de Lange, W.P., Moon, V., and Johnstone, R. (2015). Evolution of the Tauranga Harbour entrance: Influences of tsunami, geology and dredging. *Australasian Coasts & Ports Conference 2015*, (pp. 1-7). Auckland, New Zealand.
- DeWitt, N.T., Flocks, J.G., Hansen, M., Kulp, M., and Reynolds, B.J. (2007). *Bathymetric survey of the nearshore from Belle Pass to Caminada Pass, Louisiana: methods and data report*. Virginia: USGS.
- Eelkema, M., Wang, Z.B., and Hibma, A. (2012). Ebb-tidal delta morphology in response to a storm surge barrier. *Jubilee Conference Proceedings, NCK-Days*, (pp. 137-141).
- El-Hattab, A. (2014). Single beam bathymetric data modelling techniques for accurate maintenance dredging. *The Egyptian Journal of Remote Sensing and Space Sciences, Vol. 17.*, 189-195.
- FitzGerald, D. (1984). Interactions between the ebb-tidal delta and landward shoreline: Price Inlet, South Carolina. *Journal of Sedimentary Petrology, Vol. 54(4)*, 1303-1318.
- FitzGerald, D. (2005). Tidal Inlets. In M. (. Schwartz, *Encyclopedia of Coastal Science* (pp. 958-965). Dordrecht: Springer.
- FitzGerald, D. (2012). Morphodynamics and Facies Architecture of Tidal Inlets and Tidal Deltas. In R. Davies Jr., *Principles of Tidal Sedimentology* (pp. 301-333). New York: Springer Science+Business Media B.V.
- FitzGerald, D., Buynevich, I., and Hein, C. (2012). Morphodynamics and Facies Architecture of Tidal Inlets and Tidal Deltas. In R. a. Davis Jr, *Principles of Tidal Sedimentology* (pp. 301-333). New York: Springer Science+Business Media B.V.
- FitzGerald, D., Buynevich, I., and Hein, C. (2012). Morphodynamics and Facies Architecture of Tidal Inlets and Tidal Deltas. In R. a. Davis Jr., *Principles of Tidal Sedimentology* (pp. 301-333). New York: Springer Science & Business Media.
- Fontolan, G., Pillon, S., Quadri, F.D., and Bezzi, A. (2007). Sediment storage at tidal inlets in northern Adriatic lagoon: Ebb-tidal delta morphodynamics, conservation and sand use strategies. *Estuarine, Coastal and Shelf Science Vol. 75*, 261-277.
- Galparsoro, I., Borja, A., Legorburu, I., Hernandez, C., Chust, G., Liria, P., and Uriarte, A. . (2010). Morphological characteristics of the Basque continental shelf (Bay of Biscay, northern Spain); their implications for

Integrated Coastal Zone Management. *Geomorphology Vol. 118, Issue 3-4*, 314-329.

- Gaudio, D.J., and Kana, T.W. (2001). Shoal bypassing in mixed energy inlets: geomorphic variables and empirical predictions for nine south Carolina inlets. *Journal of Coastal Research*, 280-291.
- Gordon, N. (1985). The Southern Oscillation and New Zealand weather. *Monthly weather review*, 114., pp. 371-387.
- Hayes, M. (1980). General morphology and sediment patterns in tidal inlets. *Sedimentary Geology Vol. 26*, 139-156.
- Hayes, M. (1980). General Morphology and sediment patterns in tidal inlets. *Sedimentary Geology Vol. 26 Issue 1-3*, 139-156.
- Healy, T.R., Harray, K.G., and Richmond, B. (1977). *The Bay of Plenty Coastal Erosion Survey. Occasional Report 3*. Hamilton, New Zealand: Department of Earth Sciences, University of Waikato.
- Heath, R. (1975). Stability of some New Zealand coastal inlets. *New Zealand Journal of Marine and Freshwater Research Vol. 9 No. 4*, 449-457.
- Hicks, D.M. and Hume, T.M. (1997). Determining sand volumes and Bathymetric Change on an Ebb-Tidal Inlets and Tidal Delta. *Journal of Coastal Research*, 407-416.
- Hicks, D.M., and Hume, T.M. (1996). Morphology and size of ebb tidal deltas at natural inlets on open-sea and Pocket-bay coast, north island, New Zealand. *Journal of Coastal Research*, 12 (1), 47-63.
- Hicks, D.M., and Hume, T.M. (1996). Morphology and size of ebb tidal deltas at natural inlets on open-sea and pocket-bay coasts, North Island, New Zealand. *Journal of Coastal Research*, 47-63.
- Hicks, D.M., Hume, T.M., Swales, A., and Green, M.O. (1999). Magnitudes, spatial extent, time scales and causes of shoreline change adjacent to an ebb-tidal delta, Katikati Inlet, New Zealand. *Journal of Coastal Research*, 220-240.
- Hine, A. (1975). Bedform distribution and migration patterns on tidal deltas in the Chatham Harbor Estuary, Cape Cod, Massachusetts. In L. (. Cronin, *Estuarine Research, Vol. 2: Geology and Engineering*. (pp. 235-252). New York: Academic.
- Kana, T.W., Hayter, E.J., and Work, P.A. (1999). Mesoscale sediment transport at southeastern U.S. tidal inlets: conceptual model applicable to mixed energy settings. *Journal of Coastal Research*, 303-313.

- Kearns, T.A., and Breman, J. . (2010). Bathymetry: the art and science of seafloor modeling for modern applications. In J. (. Breman, *Ocean Globe ESRI Press* (p. 274). Redlands: ESRI Press, ISBN 978-1-58948-219-7.
- Komar, P. (1996). Tidal-inlet processes and morphology related to the transport of sediments. *Journal of Coastal Research, Special Issue No. 23*, 23-45.
- Kraus, N. (2000). Reservoir Model of Ebb-Tidal Shoal Evolution and Sand Bypassing. *Waterway, Port, Coastal, and Ocean Engineering Vol. 126 No. 3*, 305-313.
- Macky G.H., Latimer, G.J., and Smith, R.K. (1995). Wave climate of western Bay of Plenty, New Zealand, 1991-93. *New Zealand Journal of Marine and Freshwater Research Vol. 29, No. 3.*, 311-327.
- Malvern. (2005). *Mastersizer 2000. Advanced Technology Made Simple.* . Southboro: Malvern Inc. Limited.
- Marino, J.N., and Mehta, A.J. (1988). Sediment trapping at Florida's east coast inlets. Lecture notes on coastal and estuarine studies Vol. 29. In D. a. Aubrey, *Hydrodynamics and sediment dynamics of tidal inlets* (pp. 284-296). New York: Springer-Verlag.
- Meade, R. (1969). Landward transport of bottom sediments in estuaries of the Atlantic coastal plain. *Journal of Sedimentary Petrology, Vol. 39*, 222-234.
- Micallef, A., Le Bas, T.P., Huvenne, V.A.I., Blondel, P., Huhnerbach, V., and Deidun, A. (2012). A multi-method approach for benthic habitat mapping of shallow coastal areas with high-resolution multibeam data. *Continental Shelf Research 39-40*, 14-26.
- Nittrouer, J.A., Allison, M.A., and Campanella, R. (2008). Bedform transport rates for the lowermost Mississippi River. *Journal of Geophysical Research Vol. 1113*, 1-16.
- NIWA. (2013). *Tide Forcaster*. Retrieved from NIWA Taihoro Nukurangi: <http://www.niwa.co.nz/services/online-services/tide-forecaster>
- NIWA. (2014, March 30). *NIWA Taihoro Nukurangi*. Retrieved from The National Climate Database: http://cliflo.niwa.co.nz/pls/niwp/wgenf.genform1_proc
- Oertel, G. (1972). Sediment transport on estuary entrance shoals and the formation of swash platforms. *Journal of Sedimentary Petrology, Vol. 42.*, 858-868.

- Oertel, G. (1975). Ebb-tidal deltas in Georgia estuaries. In L. (. Cronin, *Estuarine Research, Volume 2: Geology and Engineering*. (pp. 267-276). New York: Academic.
- Pickrill, R. (1985). Sedimentation in an ebb-tidal delta, Rangauru Harbour, Northland, New Zealand. *New Zealand Journal of Geology and Geophysics, Vol. 28*, 531-542.
- Ramli, A.Y., and de Lange, W.P. (b). (2013b). Short-Term Ebb Tidal Delta Variability Using Video Imagery and MBES Surveys. *The 7th International Conference on Asian and Pacific Coasts (APAC 2013)*. Bali, Indonesia: APAC 2013.
- Ramli, A.Y., and de Lange, W.P. (2013a). Dredging Impacts on the Stability of an Ebb Tidal Delta System. *Coasts & Ports 2013 Conference*. Sydney: Coasts and Ports 2013.
- Ruggiero, P., Kaminsky, G., and Plant, N. (1998). Coastal morphologic variability of high energy dissipative beaches. *Proceeding of the 26th International Conference on Coastal Engineering* (pp. 3238-3251). Copenhagen, Denmark: ASCE.
- Software, G. (2011). *Surfer-Quick Start Guide*. Colorado, USA: Golden Software, Inc. Retrieved from www.goldensoftware.com.
- Spiers, K. (2013). *Investigation of access channel sedimentation processes and the impact of capital dredging on harbour circulation patterns (PhD thesis)*. Hamilton, New Zealand.: University of Waikato.
- Spiers, K.C., Healy, T.R., and Winter, C. (2009). Ebb-Jet Dynamics and Transient Eddy Formation at Tauranga Harbour: Implications for Entrance Channel Shoaling. *Journal of Coastal Research*, 234-247.
- Walton, T.L., Adams, W.D. (1976). Capacity of inlet outer bars to store sand. *Proceedings of the 15th Coastal Engineering Conference*. (pp. 1919-1937). New York: American Society of Civil Engineers.
- Yin, J., Zou, Z.L., Dong, P., Zhang, H.F., Wu, G.O., and Pan, Y.N. (2012). Experimental research on unstable movements of sandbars under wave actions. *Water Science and Engineering Vol. 5, Issue 2*, 175-190.

Chapter 5: Field Measurement Campaign



Figure 5 –1 Instruments and equipment used for hydrodynamic and turbidity measurements during this project: (A) InterOcean S4; (B) C3 Fluorimeter, (C) stainless steel frame for mounting instruments; (D) pinger; (E) Acoustic Doppler Velocimeter; and (F) Acoustic Doppler Current Profiler.

5.1 Introduction

The hydrodynamic processes of a coastal area are a result of interactions between short-term wind-induced waves and tidal currents, and longer-term factors such as changing water levels, seasonal changes in weather patterns, and anthropogenic activities. The mobility of sediment in the nearshore area is related to the capability of the wave and tidal currents to move and transport sediments, and the quantity of suitable sediment available.

Hence, field data should cover sufficient temporal and spatial scales. Temporal scales should represent all condition occurring during ebb-flood, spring-neap tide, storm-calm condition, and during different season of the year. Different

hydrodynamic conditions may generate different morphological features in the nearshore area. For example; high and steep storm waves move material offshore from the upper beach. This erodes the nearshore area and forms one or more bars near where the waves break. Vice versa, smaller and not so steep waves, occurring during calm periods move beach material back onshore (Kamphuis, 2000). For calibration and verification purposes of the numerical model, the hydrodynamic regimes are required (Van Rijn, 2007). Further, the sediment grain size distribution is required to define the spatial distribution of sediment grain size and bottom roughness parameters in Delft3D Flow model.

To identify the main factors that control the hydrodynamic processes in the study area a major field programme undertaken that deployed instruments to record the waves and tidal currents, obtained surficial sediment samples, and measurements of suspended sediments. In addition, wind data for the deployment period were extracted from the NIWA ClifFlo database (NIWA, 2013).

5.1.1 Acknowledgements

The field measurement was funded by the Port of Tauranga, Ltd. Several people assisted with the field programme, including programming and deploying the instruments, and moorings, and recovering the instruments and sediment traps. In particular, I would like to thank Dean Sandwell, Dirk Immenga, the Scuba Diver team (Dudley Bell and Warrick Powrie), Steve Hunt, Alex Port, Ehsan Jorat and David Culliford for their help. I would also like to thank Dr de Lange and Shawn Harrison for help in downloading and processing the raw data from the instruments.

5.1.2 Aim

The aim of the field programme was to identify and quantify the hydrodynamic processes that drive sediment transport over the ebb-tidal delta. This was required to assess the direction and magnitude of longshore transport along Matakana Island, and provide calibration and verification data sets for numerical modelling to assess the stability of ebb-tidal delta under various hydrodynamic regimes. The data collection was intended to extend over a lunar cycle (29 days) to include a perigee-apogee tidal cycle, and two spring-neap cycles.

5.2 Instruments and Methods

The field programme finally ran over 27 days from 11 April to 5 May 201, being terminated 2-3 days early due to concerns about storm damage and burial of instruments. The sampling period covered a wide range of hydrodynamic regimes including storm and fair weather conditions, and almost two whole neap-spring tidal cycle. Eleven observation sites were located at the harbour entrance and on the Matakana ebb-tidal delta (Figure 5-2). The locations and settings of the instruments are summarized in Table 5-1. All of the instruments were installed on frames and anchored on the seabed by SCUBA divers. Each of frames was equipped with a sediment trap to collect any sediments settling out of suspension (Ramli and de Lange, 2013). An acoustic pinger was attached to each frame to assist with finding the instruments for servicing during the deployment and recovery at the end of deployment period.

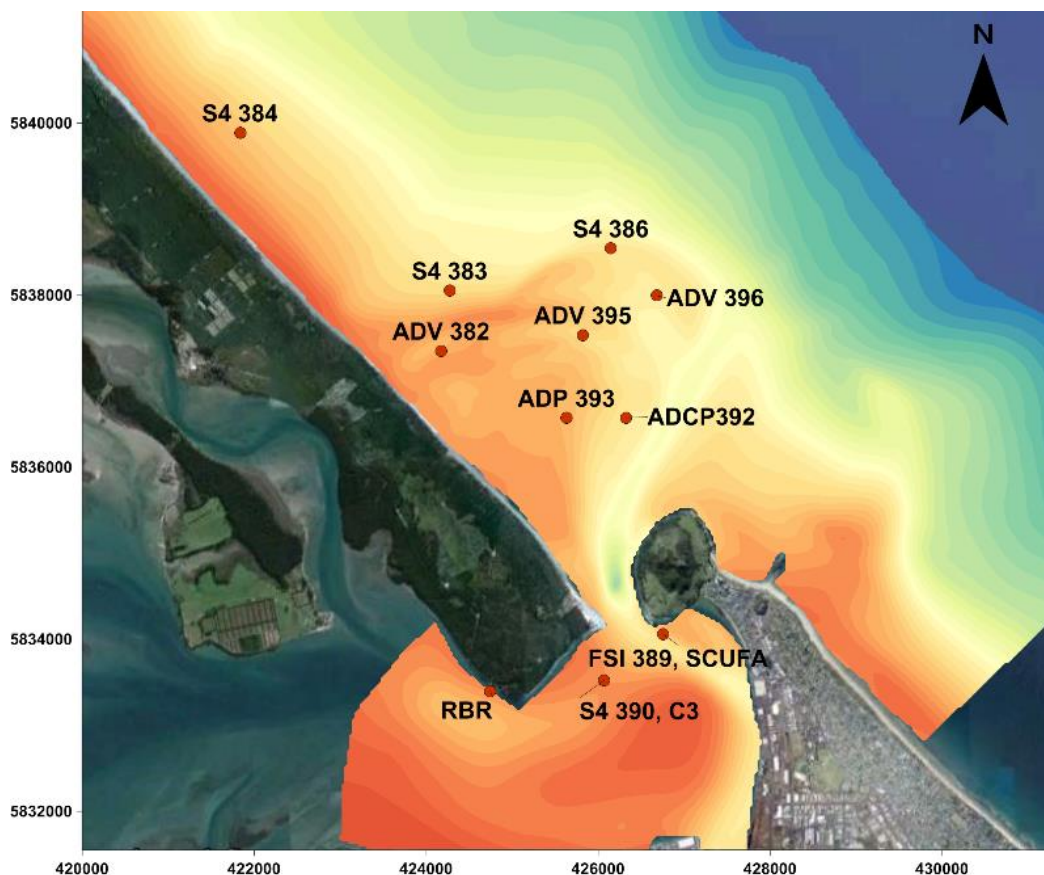


Figure 5-2. Instrumented seabed frame locations within the Entrance Channel and over Matakana Banks ebb-tidal delta during the field programme. Note that the location of S4 station 385 further

to the northwest along Matakana Island is not shown as this instrument did not record usable data.

Table 5-1. Summary of the deployed instruments, and their locations and settings during 11 April – 8 May 2013.

Station ID	Location (WGS84)		Instrument type	Water depth (m)	Height above the seabed (m)	Sampling intervals and averaging intervals
	Latitude	Longitude				
382	-37.6078	176.14091	ADV	6	0.25	300 sec, 60 sec
383	-37.6015	176.14211	S4	10	1	300 sec, 60 sec
384	-37.5848	176.1147	S4	9.2	1	300 sec, 60 sec
385	-37.5621	176.09173	S4	8.7	1	300 sec, 60 sec
386	-37.5972	176.16338	S4	14.5	1	300 sec, 60 sec
389	-37.6377	176.1698	FSI	19.6	0.5	60 sec, 20 minutes
390	-37.6425	176.1619	S4	5.3	1	300 sec, 60 sec
392	-37.615	176.1652	ADCP	12.2	0.5	2 sec, 120 sec
393	-37.6149	175.1573	ADP	8	0.5	300 sec, 60 sec
395	-37.6063	176.1596	ADV	10	0.5	300 sec, 60 sec
396	-37.6022	176.1694	ADV	12	0.5	300 sec, 60 sec
RBR	-37.6442	176.1619	RBR	4.4	2	10 minute

5.2.1 Observational Techniques and Analysis Methods

Several different types of instrument were deployed to collect different types of data. The following sections discuss each of the instruments used, their settings and the purpose for their deployment.

5.2.1.1 Acoustic Doppler Velocimeter

The SonTek/YSI Triton Acoustic Doppler Velocimeter (ADV) is a single-point, high-resolution, 3D Doppler current meter. The ADV measures the velocity of water using a physical principle called the Doppler Effect (SonTek/YSI Inc., 2001). In this study, the ADV current meters were moored at three shallow locations on the swash platform of Matakana Banks in order to measure waves and tidal currents. The instrument was programmed to record the currents every 300 s with an averaging interval of 60 s. Each ADV was installed on a stainless steel frame at a height of 25 cm above the seabed

5.2.1.2 S4

There were 5 InterOcean S4 ADWs deployed in the study area in order to measure the direction and magnitude of horizontal current motion. The hardware and firmware of the S4 current meter controls and measures the voltages resulting from the motion of a conductor (seawater) through a magnetic field, which is generated around the S4. The S4s were installed on the frame at the height of 1 m above the sea bed and each of them was configured to record data at 2 Hz in bursts of 300 s duration, with special record blocks every 60 s. Bursts were recorded every 30 minutes.

One S4 that was located the furthest northwestern along the Matakana Island shoreface, station 385, failed to record data. This instrument was intended to obtain data to assess the longshore current supplying sediment along Matakana Island to the ebb-tidal delta. However, the S4 at station 384 did work and provided the necessary data, although it is closer to the influence of the ebb-tidal delta.

5.2.1.3 FSI Acoustic Current Meter

Falmouth Scientific, Inc. (FSI) current meters use phase-shift acoustic transit-time technology to provide high-accuracy point velocities in 2 or 3 dimensions. The phase-shift measurement principle allows ACM current meters to measure accurately, even in slow moving water and in water with no reflectors present (e.g., deep water or very clear water). Internal compass and tilt sensors provide magnetic horizontal current vector direction, without the need for specific orientation of the current meter during deployment. Because the meters measure a finite volume to provide a point velocity, FSI current meters can also provide data in very shallow water or very near the ocean bottom (FSI, 2009).

A FSI current meter was installed on a frame and located to the east of Cutter Channel inside the harbour (Sta. 389) at about 50 cm above the seabed. This ACM current meter was configured to record the current in 60 s bursts every 20 minutes.

5.2.1.4 SCUFA Fluorometer

Normally the fluorescence channel of the SCUFA (Self-Contained Underwater Fluorescence Apparatus) Fluorimeter is configured to detect chlorophyll a, cyanobacteria, or rhodamine WT tracer dye. However, in addition to the fluorescence sensor, there is an optional turbidity sensor, which was installed

on the SCUFA used. The turbidity sensor measures the turbidity level through 90° light scatter. Turbidity data are recorded simultaneously with the fluorescence data, allowing for meaningful comparisons between fluorescence and turbidity data (TURNER DESIGNS, 2004).

In order to record the turbidity, SCUFA was configured to record turbidity data every 5 minutes during the deployment, and this instrument was installed on the same frame as the FSI current meter (Sta. 389) inside the harbour. The turbidity concentration data from SCUFA readings are recorded in Nephelometric Turbidity Units (NTUs).

In the conjunction with the SCUFA, a C3 submersible fluorometer equipped with a turbidity sensor was also installed at station 390 to record water turbidity during field measurement in *Relative Fluorecense Units* (RFUs). The C3 was deployed to obtain a turbidity reading every 30 minutes.

5.2.1.5 Acoustic Doppler Current Profiler (ADCP)

A RDI 1200 kHz WorkHorse Sentinel ADCP (TELEDYNE RD Instruments, 2001) instrument was configured as upward-looking and mounted on a stainless steel frame to record a time series of vertical velocity profiles within the former ebb channel beneath the expected location of the ebb-jet, adjacent to the Entrance Channel.

As a self-contained system, the instrument contains its own battery for power and internal recorder for the storage of all data. The WorkHorse Sentinel can be used for several-month autonomous current profile deployments from temporary or permanent mountings. Internal processing resolved the acoustic Doppler signal into 29 bins, each of which represented a layer of water defined by the acoustic travel time from the head of the transducer. The first bin was centred at 1.05 m from the ADCP and each bin was 0.50 m wide. These bins are interpreted as depth levels, and may include ghost levels above the sea surface that result from reflection of the beams at the surface. The ADCP was configured to internally average bursts of pings every 120 seconds and record a time series of these ensemble averages. Each of the resulting ensemble record is given an incremental record number as well as a time stamp. The time was recorded in Julian days.

5.2.1.6 RBR Submersible Tide Gauge

The RBR Submersible tide gauge is designed to record water levels for long term monitoring of tidal activity in remote locations (RBR Ltd., 2013). A RBR type TWR 2050 was fastened below water level onto a pile at Matakana Wharf inside the harbour (Fig. 3–2) and it was configured to record the water level every 10 min.

5.2.1.7 Acoustic Doppler Profiler

A 3 MHz Sontek/YSI Argonaut Acoustic Doppler Profiler (ADP) was installed on the swash platform of Matakana Banks (Figure 5-2) to measure profiles of current speed and direction by transmitting high-frequency bursts of sound through the water column. The instrument was set to collect data with averaging and sampling intervals of 60 s and 300 s respectively. However, during the initial post deployment recovery the Scuba divers were not able to locate the instrument as it had been buried by the migration of bedforms. The ADP was recovered later when the instrument was re-exposed, and the data downloaded. The data prior to the burial of the sensors were usable, but the subsequent data were affected and hence were rejected.

5.2.1.8 Sediment and Water Sampling

In order to obtain the sediment grain size distribution in the study area and to estimate sediment deposition/accumulation rates, cylindrical tube sediment traps were deployed (Thomas and Ridd ,2004; and Szmytkiewicz and Zalewska, 2014). Several studies have defined certain criteria that a sediment trap must meet in order to minimize bias in estimates of sedimentation rates. The sediment trap should have (1) a cylindrical collection vessel (tube) (Gardner (1977); Gardner (1980a); Gardner (1980b); and Hargrave and Burns (1979)) with (2) an inner tube diameter of ≥ 45 mm (Blomqvist and Hakanson, 1981) and (3) an aspect ratio (height:diameter, H:D) of 3 to 5 (Wahlgren and Nelson, 1977); (Blomqvist and Kofoed, 1981), and aspect ratio greater than 10 in turbulent environments, i.e., currents of approximately 0.5 ms^{-1} (Bloesch and Burns, 1980); (Lau, 1979); and (Hargrave and Burns, 1979). Further, for good collection efficiency under most ocean current velocities, a cylindrical trap aspect ratio >5 is required (Hargrave and Burns (1979); Blomqvist and Hakanson (1981); and Butman *et al.* (1986)).

According to Gardner (1980a) calculation of trap efficiency is determined by dividing the flux measured by the trap (mass/cm²/time) by the sedimentation rate within a test flume (mass/cm²/time). Flux measured by the trap is calculated by the weight (in milligram) divided by the total surface area of cylinder ($=2\pi r (r + h)$) and converted to a daily flux (mg/cm²/day). Then the ratio of flux measured by the trap to the actual sedimentation rate is multiplied by 100 and defined as the trapping efficiency. An efficiency of 100% means that the sediment trap collected particles at the same rate as the surrounding flume bed. However, the efficiency of the sediment traps used in this study cannot be presented as no laboratory evaluation for sedimentation rate on the flume was done in this study. The data do give the relative distribution of sedimentation rates between the sites sampled.

In this study, the sediment traps were made of PVC pipe with an internal diameter of 5.35 cm ($D = 2.r$) and depth of 36 cm (h), which gives an aspect ratio of 6.7. They were installed on each stainless steel frame with the bottom end of trap closed using an end cap in order to catch sediment. The top was closed with another end cap by a diver, before they were retrieved at the end of deployment period (Table 5-2).

Table 5-2. *Deployment period of sediment traps*

Station	Date		Number of days
	Start	Retrieved	
382	11 April 2013	8 May 2013	27
383		19 April 2013	8
384		8 May 2013	27
386		14 May 2013	33
390		8 May 2013	27
393			
395			
396			

Seawater was sampled at just below the sea surface during the high tide slack water at 10:20 am and during low tide slack water at 14:40 pm. Each of the samples was about 20 litres, and was used for total suspended solids analysis and turbidity censor calibration (SCUFA and C3). The sampling location was inside the harbour at the same station with the FSI and SCUFA (St. 389, Figure 5-2). The result from total suspended solids analysis was then used to determine the suspended-material concentration parameter in the numerical modelling.

5.3 Data analysis

5.3.1 Acoustic and Backscatter Data

Data recorded by the S4s were processed by InterOcean software (APPIBM and WAVE) (InterOcean Inc., 2013) in order to extract the water depth (m), current direction (°) current magnitude (cm.s⁻¹) and wave conditions. Wave data were calculated from the 300 s burst data, providing wave height and periods at intervals of 30 minutes. The data obtained from the S4s were then analysed using standard methods in Matlab to obtain the average depth, current velocity and direction. In order to analyse the relationship between wave energy, longshore sediment supply, shoreline erosion, and ebb-tidal delta morphology, the wave energy flux or wave power “P” (W.m⁻¹) was calculated by using the formulae of USACE (2008):

$$P = \frac{1}{2} E_0 C_0 \quad (\text{Equation 5.1})$$

$$E_0 = \frac{\rho g H^2}{8} \quad (\text{Equation 5.2})$$

$$C_0 = \frac{gT}{2\pi} \quad (\text{Equation 5.3})$$

hence,

$$P = \frac{\rho g^2 H^2 T}{32\pi} \quad (\text{Equation 5.4})$$

where

P = wave power (W.m⁻¹)

E_0 = energy density (kg.s²)

C_0 = wave celerity (m/s)

ρ = sea water density 1025 kg/m³

g = acceleration of gravity (m/s)

H = wave height

T = wave period

Data from the ADV were analysed by using View Triton Pro0150 that gives:

- Time,
- Velocities in E, N, U directions,

- Standard errors,
- Signal amplitudes,
- Heading, Pitch and Roll,
- Mean temperature,
- and Mean Pressure (dBar) and Standard Deviation Pressure (dBar).

The mean pressure (dBar) was converted to depths (m) using the formula in UNESCO Technical Papers in Marine Science No. 44 (Fotonoff and Millard Jr., 1983). Firstly the variation of gravitational acceleration with latitude and pressure was calculated as:

$$g \left(\frac{m}{sec^2} \right) = 9.780318 * [1.0 + (5.2788 * 10^{-3} + 2.3 * 10^{-5} * x) * x] + 1.092 * 10^{-6} * p \quad (\text{Eq. 5-5})$$

where

$$x = \left[\sin \left(\frac{\text{latitude}}{57.29578} \right) \right]^2$$

p = pressure (decibars)

Then, depth is calculated from the pressure as:

$$\text{depth (m)} = \left[\left(\left((-1.82 * 10^{-15} * p + 2.279 * 10^{-10}) * p - 2.2512 * 10^{-5} \right) * p + 9.72659 \right) * p \right] / g \quad (\text{Eq. 5-6})$$

where

p = pressure (decibars)

g = gravity (m/sec²)

The Argonaut ASCII data file from the ADP was downloaded in long format that includes:

- Time (year, month, day, hour, minute, and second),
- Water velocity in X, Y, Z directions (cm/s),
- Velocity standard deviation in X, Y, Z directions (cm/s),
- Heading, pitch and roll (deg) with the standard deviations respectively,
- Mean temperature (°C) and mean pressure (dBar),

- Standard deviation for the mean pressure (dBar),
- Power level (battery voltage) (Volts),
- Cell begin and end (m),
- Speed (cm/s), and
- Direction (°).

Raw data from the ADCP was downloaded from the instrument using WinADCP software (RDI, 2001) and processed in Matlab 2012a using a toolbox named `rdradcp.m` (Pawlowicz, 2010). The routine to calculate water depth was performed using the same procedure as the ADV data mentioned earlier.

5.3.2 Sediment Grain Size Analysis

The sediment samples were oven dried at 105°C, split to produce a 50 g subsample, and sieved on a 2 mm mesh (-1.0 phi) to determine the weight percentage of the coarser fraction, mainly shell fragments. The remaining sediment < 2 mm, was further split and 2–3 g and was soaked with 10% of hydrogen peroxide solution to eliminate any organic materials in the sediment sub-sample. Afterwards the dry weight of the treated sediment sub-sample was recorded, and the sub-sample was analysed using a laser diffractometer (Malvern Ltd., 2005).

The statistical parameters of sediment grain size distribution were determined by the software package Mastersizer 2000 that was linked to the diffractometer (Malvern Ltd., 2005). Statistical parameters of grain size distribution were then summarised into particle size categories and subcategories according to the scheme of Udden and Wentworth (1968)

5.3.3 Total Suspended Solid Analysis

Total suspended solid (TSS) analysis is normally performed on an aliquot of the original sample (Gray *et al*, 2000). In this study, this analysis was done by transferring the 20l seawater sample into a water tank, where it was agitated with a drill fitted with a stirring paddle in order to keep any particles in suspension. A sub-sample of the suspension was then collected in a 100 ml bottle. The analysis was continued by filtering the sub-sample using the following items (Fig. 5–3):

- Buchner Funnel – A ceramic funnel with a flat or fitted base that provides support to a disposable filter.
- Pre-weighed glass-fibre filter GC-50 size 70 mm with fine-porosity (<0.45 micron particle retention)
- Vacuum Filter Flask – Glass flask equipped with a side arm for vacuum pump connection and a rubber stopper to provide seal with funnel. The flask is used to collect the filtered seawater that passes through the filter.
- Vacuum pump



Figure 5-3. Equipment for TSS analysis used in this study. (A) Bucher funnel and (B) Glass flask to collect the filtered water.

After the filtering process was completed, the glass-fibre filters were oven-dried at 105°C for 4 hours. When drying was complete, the filters were reweighed. The drying and weighing procedure was repeated three times in order to achieve a consistent dry weight for the filter with the residue.

The TSS value was determined by using the formula:

$$TSS \left(\frac{mg}{L} \right) = \frac{(Residue+filter)(mg)-Filter(mg)}{Sample\ filtered\ (mL)} \times 1000 \left(\frac{mL}{L} \right) \quad (\text{Eq. 5-7})$$

5.4 Results

5.4.1 Sea Level and Wave Data

All the instruments deployed in the study area recorded the depth during the deployment period. The depth data were analysed using Matlab T-tide toolbox (Pawlowicz *et al.*, 2002) to obtain the tidal constituents for each location.

The tides in the vicinity of Tauranga Harbour are known to be semi-diurnal and vary between micro-tidal and meso-tidal in tidal range. The largest tidal constituents determined by previous studies were the *principal lunar semidiurnal constituent* M2 and the *principal solar semidiurnal constituent* S2. The tidal constituents obtained by this study are consistent with the previous studies, and the tidal amplitude and phase lag for the dominant constituents are summarized in Table 5–3. The field program lasted for about 27 days, which is not sufficient to extract the larger lunar elliptic semidiurnal constituent N2 (at least 27.55 days for tidal harmonic analysis (Hicks, 2006)). Hence, the N2 constituent cannot be determined from the field data.

During the deployment period from April, 11th to May, 8th 2013 the tides ranged between 1.2 – 1.3 m for *neap tides* and up to 1.9 m for *spring tides*. The maximum tidal range was recorded by the FSI at Sta. 389 in the Entrance Channel (Figure 5–2).

In Table 5–3, the phase data show that the M2 tide travelled from the northern-most part of the study (station 384) to station 390 and station 389 inside the harbour, and took approximately 9-11 minutes. From the eastern side of the ebb-tidal delta (station 386) the M2 took about 6 minutes to enter the harbour and reach station 390. Tidal current speeds were the highest in the tidal inlet and around the Entrance Channel, whilst the lowest current speeds were recorded at Sta. 384 located furthest from the tidal inlet (Figure 5–4 and Table 5-4). During both spring and neap tides, current speeds decreased with increasing distance from the tidal inlet. The slowest currents were found offshore from the ebb-tidal delta (Sta. 384) and along the terminal lobe (Sta. 383 and 386). Table 5–5 summarizes the maximum and minimum tidal current speeds for the spring and neap tides during the deployment.

Table 5-3. Amplitude (m) and phase lag (°) for the dominant tidal constituents measured during the deployment period.

Station	Amplitude (m)				Phase (°)			
	O1	K1	M2	S2	O1	K1	M2	S2
384	0.01	0.05	0.72	0.079	347.6	339.2	199.6	279.6
383	0.01	0.05	0.73	0.08	341.9	340.1	202.8	257.6
386	0.01	0.06	0.73	0.09	350.4	348.6	202.5	257.9
382	0.01	0.05	0.72	0.08	342.9	343.8	201.5	256.1
395	0.01	0.05	0.70	0.08	355.1	329	197.3	275
396	0.01	0.05	0.72	0.09	355.6	337.5	197.1	273
392	0.01	0.05	0.75	0.07	334.9	336.6	196.9	272.8
393	0.01	0.05	0.73	0.08	20	345.5	199	254.1
389	0.01	0.05	0.70	0.08	13.4	345.7	210.9	261.8
390	0.02	0.06	0.69	0.07	21.4	343.7	208.8	293.5
RBR	0.01	0.05	0.71	0.06	343.4	351.3	217.9	278.2

Table 5-4. Mean, maximum and minimum values of the tidal current speeds and directions during the field measurements.

Station	Current Speed (m/s)			Current Direction (°)		
	Mean	Maximum	Minimum	Mean	Maximum	Minimum
384	0.01	0.017	0.002	52.5	345.7	2.2
383	0.029	0.06	0.006	266.5	336.8	31
386	0.111	0.394	0.004	200	359	2.5
382	0.089	0.575	0.002	N/A	N/A	N/A
396	0.123	0.329	0.002	186.8	360	0
395	0.128	0.376	0.027	227	360	0
392	0.363	0.817	0.003	191.4	358	3
393	0.28	0.59	0.02	148	360	0
389	0.199	0.793	0.004	N/A	N/A	N/A
390	0.736	1.098	0.034	173.9	304.3	21

*N/A = not available

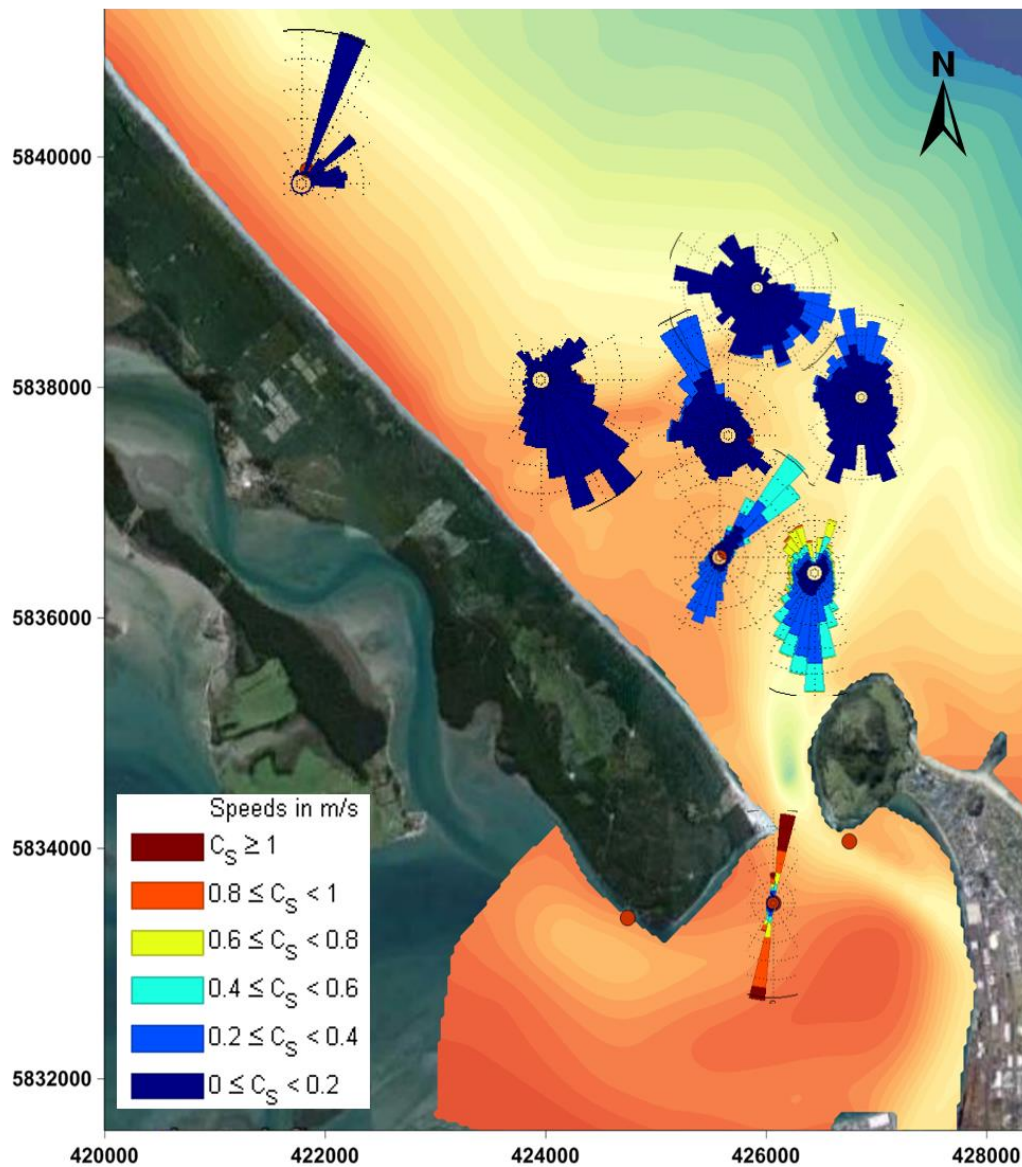


Figure 5-4. Tidal current roses for field measurements from 11 April to 8 May, 2013. Strong tidal currents occurred inside the harbour near the tidal inlet and adjacent to the Entrance Channel, whereas offshore the tidal current speeds rarely exceed 0.4 m/s.

There were three storm events during the deployment that were recorded in the wave data as shown by the wave statistic time series (Figures 5-5, 5-6 and 5-7), as well in the backscatter data recorded by the ADCP (Figure 5-8).

Table 5-5. Ranges of tidal current speeds (m/s) for spring and neap tides during field measurements. Spring tide I was on April, 14 2013, spring tide II on April 28 2013, neap tide I on April 20 2013, and neap tide II on May, 5 2013.

<i>Spring Tide I</i>										
<i>Sta.</i>	382	383	384	386	389	390	393	392	395	396
<i>Min</i>	0.006	0.01	0.002	0.01	0.006	0.06	0.03	0.03	0.03	0.004
<i>Max</i>	0.15	0.04	0.02	0.28	0.39	1.1	0.56	0.8	0.38	0.33
<i>Spring Tide II</i>										
<i>Min</i>	0.009	0.007	0.003	0.02	0.01	0.06	0.02	0.01	0.03	0.009
<i>Max</i>	0.14	0.06	0.02	0.37	0.63	1.09	0.56	0.81	0.38	0.32
<i>Neap Tide I</i>										
<i>Sta.</i>	382	383	384	386	389	390	393	392	395	396
<i>Min</i>	0.005	0.01	0.003	0.016	0.009	0.1	0.02	0.05	0.04	0.002
<i>Max</i>	0.31	0.04	0.02	0.13	0.54	1.08	0.58	0.78	0.18	0.15
<i>Neap Tide II</i>										
<i>Min</i>	0.008	0.01	0.003	0.005	0.01	0.05	0.02	No Data		
<i>Max</i>	0.44	0.05	0.02	0.37	0.48	1.08	0.59			

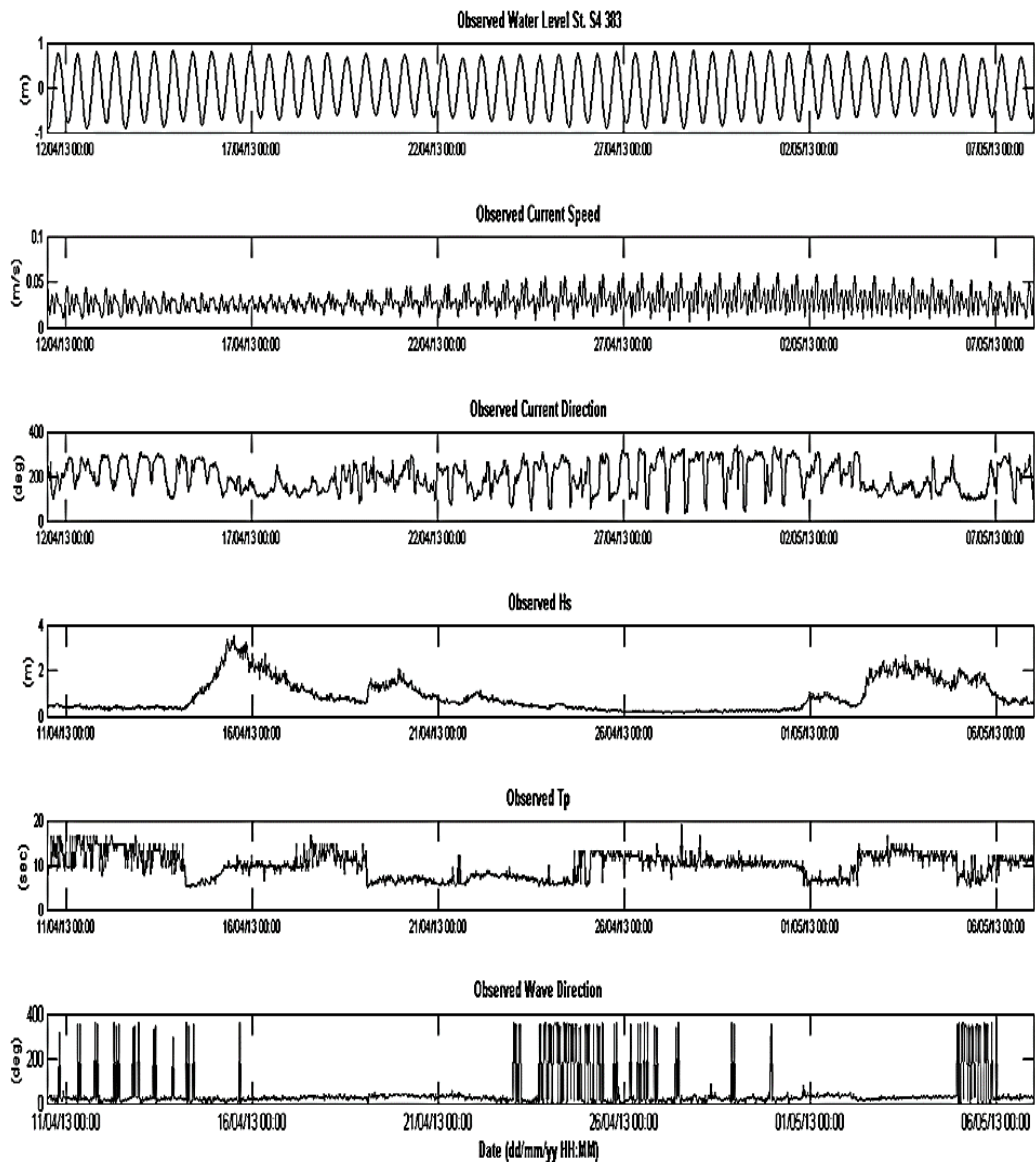


Figure 5–5. Time-series of hydrodynamic condition on the terminal lobe of the Matakana Banks (St. 383). Current speeds were less than 0.1 m/s during the deployment. Storm events are indicated by increased significant wave heights that almost reached 4 m.

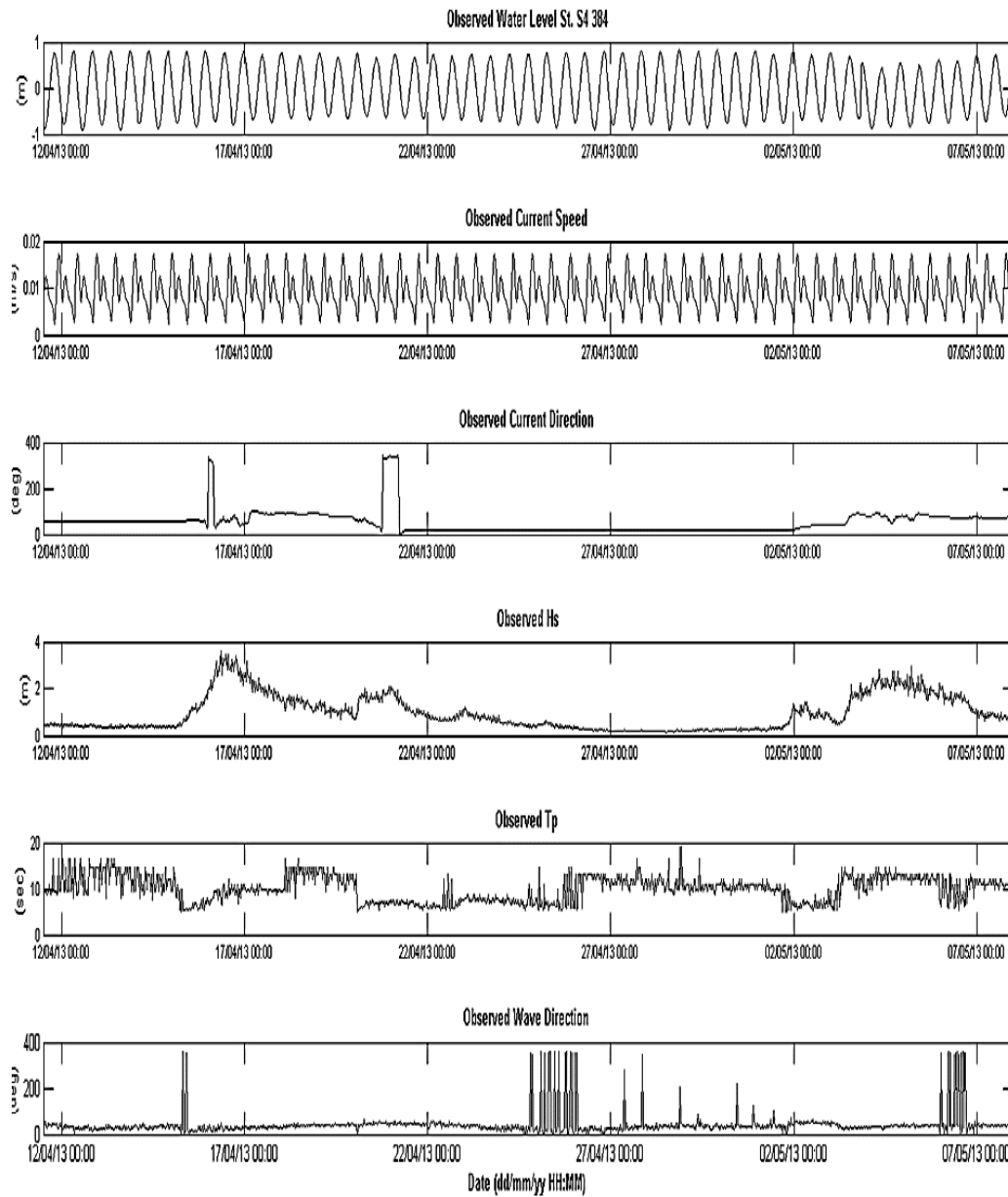


Figure 5-6. Time series of hydrodynamic conditions at the most northern part of Matakana Banks St. S4 384.

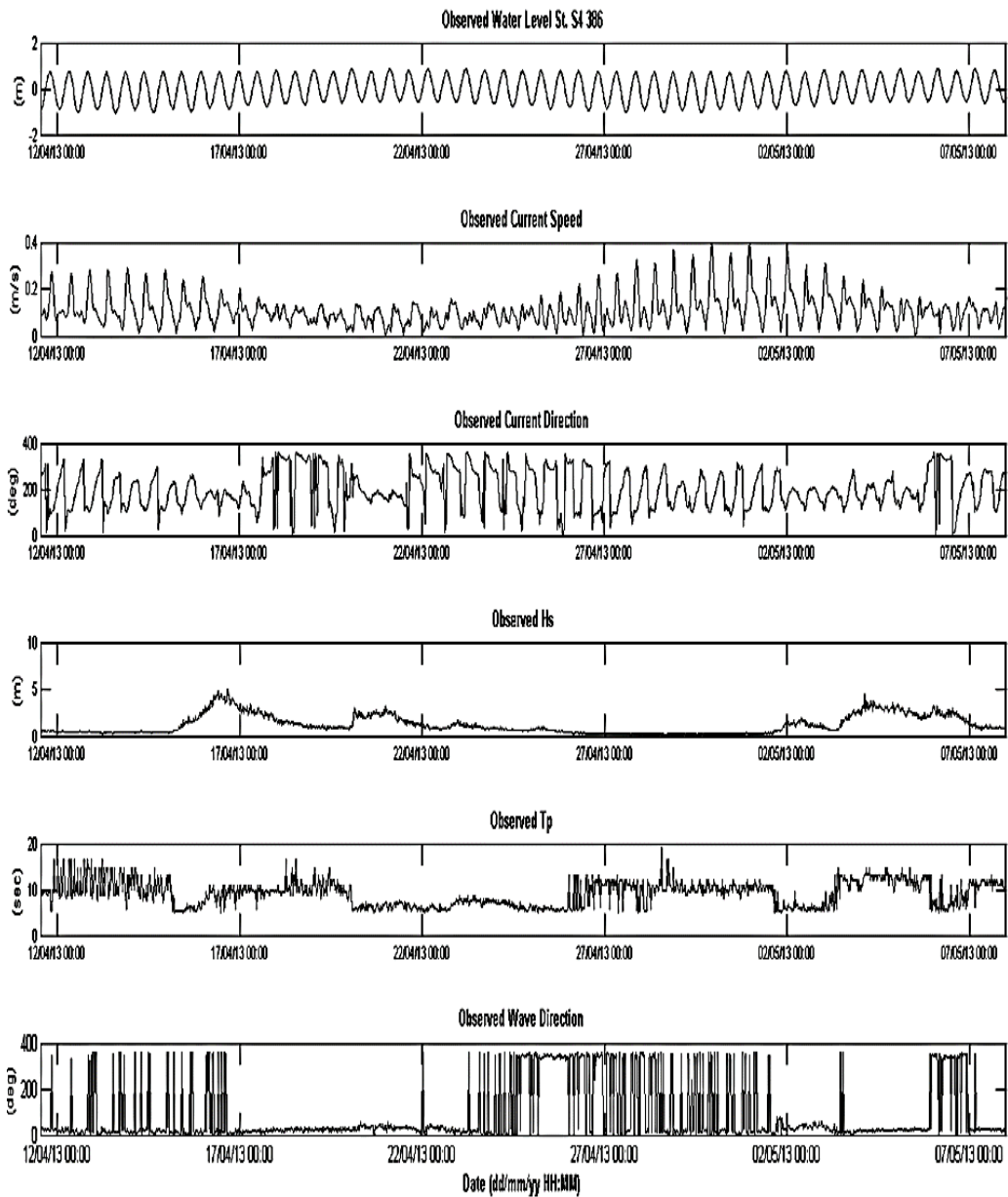


Figure 5-7. Time-series of hydrodynamic condition on the most eastern part of the Matakana Banks (St. 386).

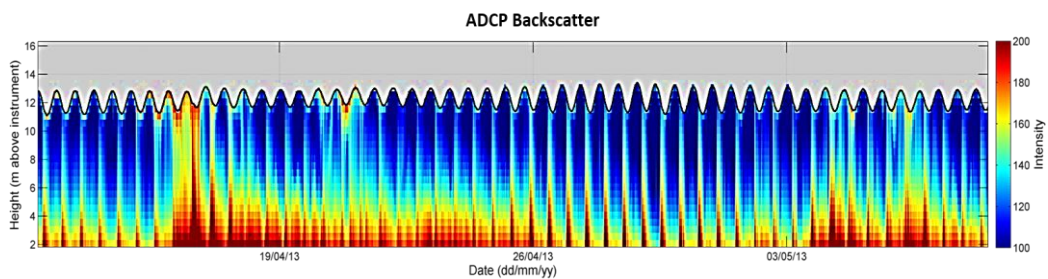


Figure 5-8. Backscatter time-series recorded by ADCP at St. 392 (Entrance Channel) representing depths above the instrument and high intensities indicate increased suspended sediment in the water column during storm events. A smaller peak in suspended sediment is also evident during the last half of each ebb tide.

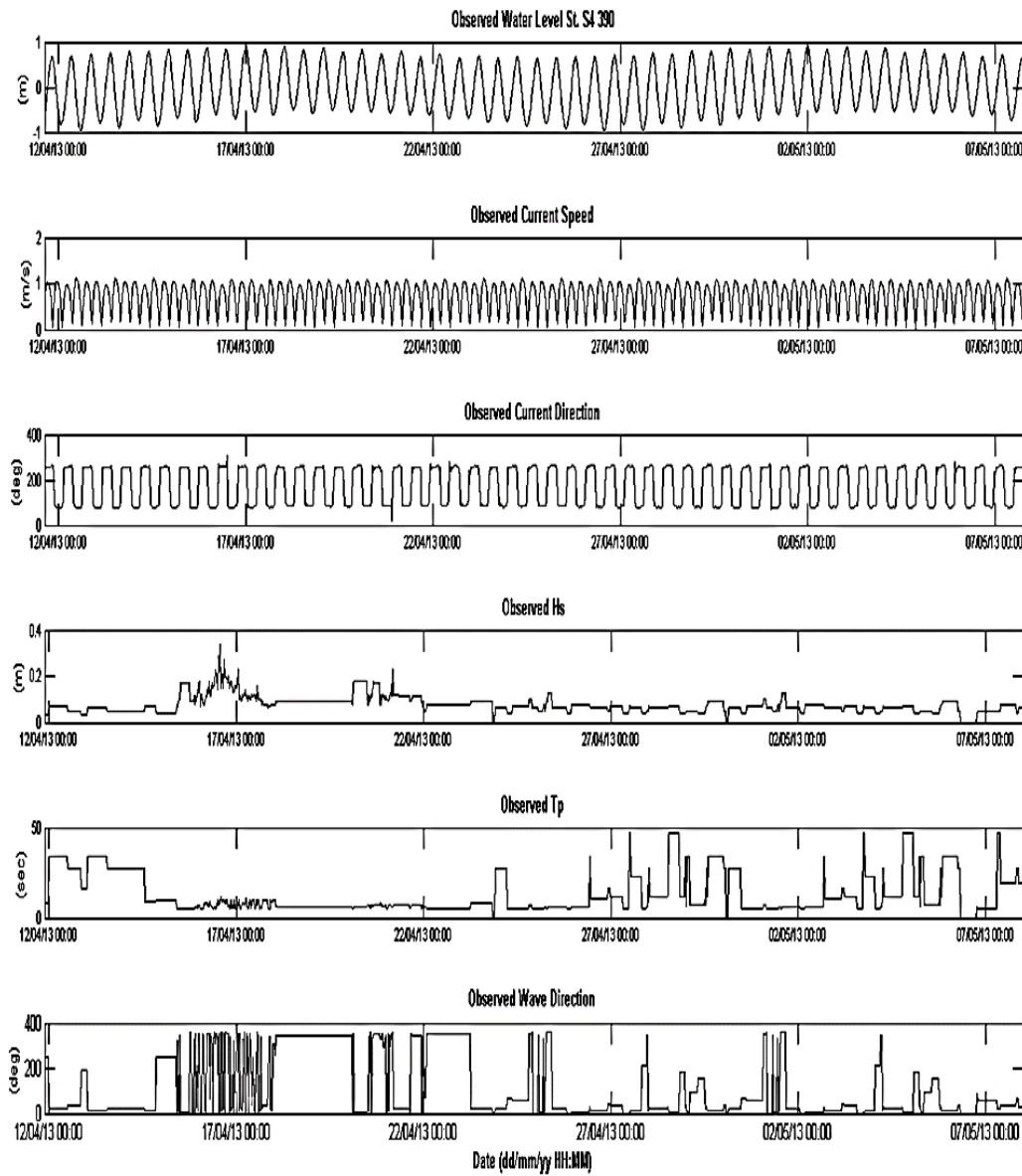


Figure 5-9. Time-series of hydrodynamic condition inside the Tauranga Harbour at the Entrance Channel recorded by the S4 (St. 390). Significant wave heights rarely exceed more than 0.4 m and longer wave periods detected.

Inside the harbour (St. 390) waves were much smaller than in the more exposed areas offshore (Figure 5-9 and 5-10).

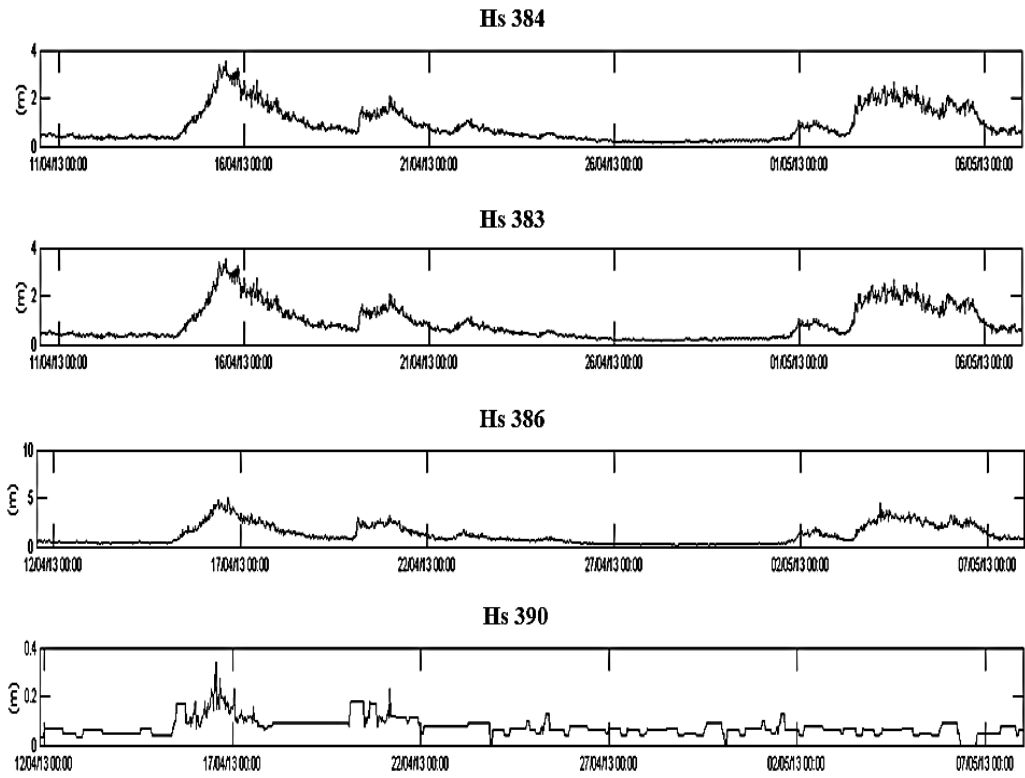


Figure 5–10. Time-series of the significant wave heights along the Matakana Banks from the north (St. 384) to inside the harbour (St. 390).

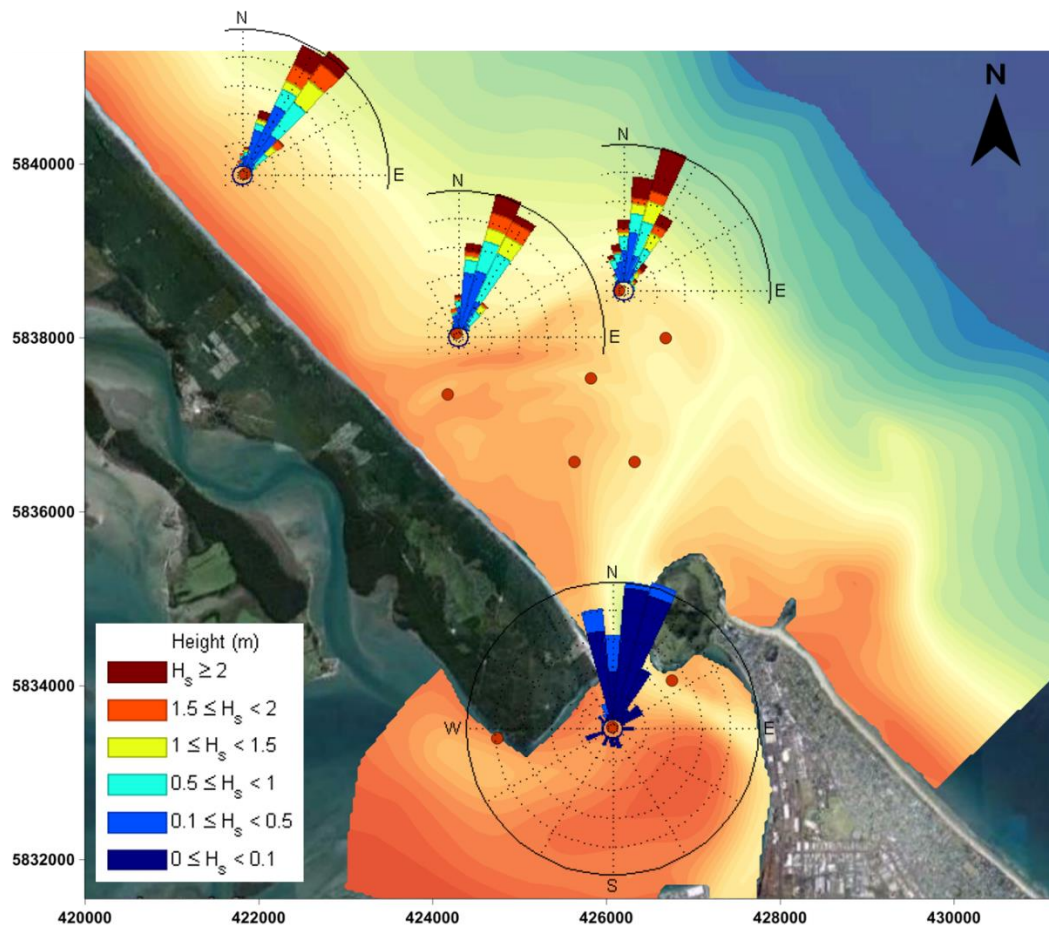


Figure 5-11. Wave roses indicating wave directions recorded by the S4s during the deployment period from 11 April – 8 May, 2013.

Overall, waves predominantly travelled from the northerly quadrant towards the southeast (Figure 5-11). The wave records show that the predominant approach angles range between NW and NE. The most frequent approach directions are NE for the offshore areas, and NW inside the harbour, which represent approximately >90% and 23% of the data respectively. The most frequent significant wave heights (H_s) are between 0.06 m and 0.23 m (Table 5-6). Wave heights in the offshore areas < 1 m occurred between 58% to 70% of the time, 1 to 1.99 m were around 20% to 26%, and > 2 m occurred between 9% to 22% of the time (Table 5-7).

Wave periods ranged mostly between 5 to 19 seconds, with the mean periods between 9.2 to 10.0 seconds offshore. Longer period waves occurred inside the harbour (St. 390), here the wave period ranged between 5 – 46.5 seconds (Table 5-6, Figure 5-12) and the mean period was 12.7 seconds. However, due to the small size of the longer period waves at this site, they probably represent instrument noise,

and not real features. Therefore, the modal period is probably a more useful statistic than the mean for station 390.

Table 5-6. *Statistics of the measured waves in the study area.*

<i>Station</i>	<i>H_s (m)</i>				<i>Peak Period (sec)</i>				<i>Direction (°)</i>	
	Max	Min	Mean	Mode	Max	Min	Mean	Mode	Mean	Mode
384	3.63	0.14	0.94	0.18	19	5	10	10.9	41.2	39
383	3.52	0.14	0.85	0.2	19	5	9.9	10.9	49.1	24.7
386	5.08	0.16	1.19	0.23	19	5	9.2	10.9	86.7	0
390	0.34	0.01	0.07	0.06	46.5	5	12.7	5.2	108.2	346.5

Table 5-7. *The percentage of occurrence for H_s less than 1m, between 1 to 1.99m and higher than 2m.*

<i>Station</i>	<i>% H_s</i>		
	< 0.99m	1 – 2	>2m
384	63	26	11
383	70	21	9
386	58	30	22
390	100	-	-

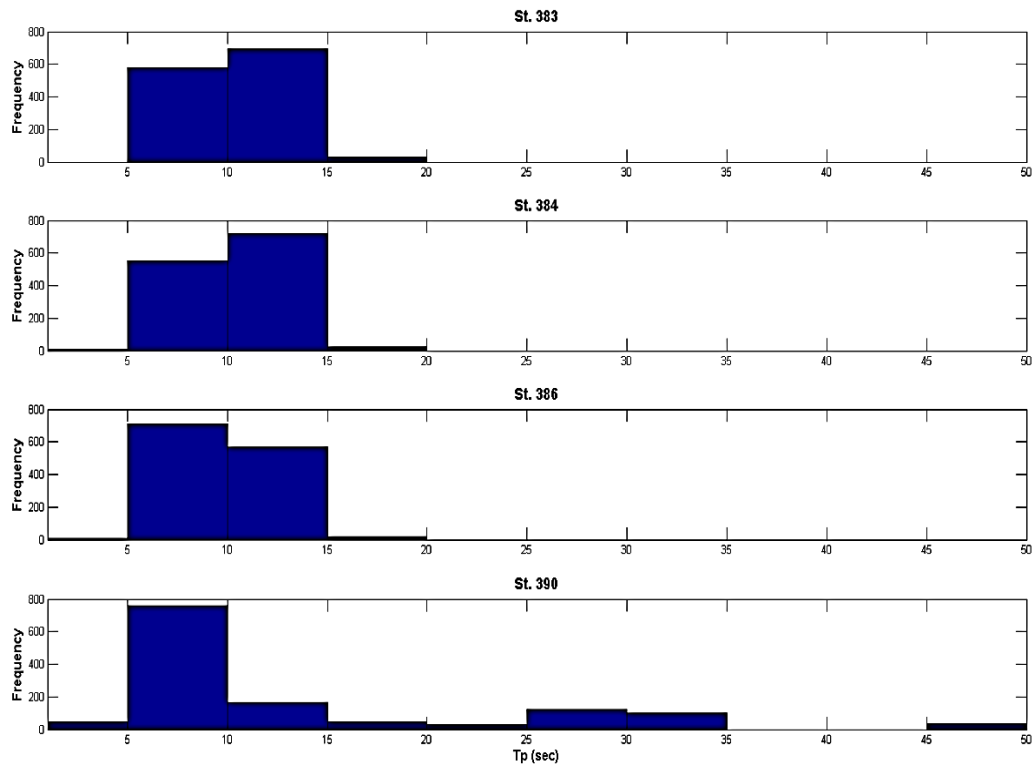


Figure 5–12. Histograms of the time series observed wave peak periods (T_p). Peak periods on the locations at the north of Matakana Banks (St. 383 and 384) were predominantly ranged between 10 to 15 sec. Shorter peak periods on the offshore part (east) ranged from 5 to 10 sec. Inside the harbour (St. 390) long period waves are detected, but the waves with periods >25 s probably represent instrument noise and not real waves.

5.4.2 Storm Events and Wave Power

The significant wave height H_s and period T_p were used to calculate the corresponding energy level or wave power (Table 5-8). At least three “storm” or severe wave events were identified in the time-series plots of H_s (Figures 5-5 to 5-10). The first storm was on the April 16th, and the second and third events respectively were on April 20th and May 4th 2013. The first storm produced the highest significant wave heights, while the highest wave power was reached during the third storm event due to longer peak periods. The third storm also had the longest duration of increased wave height.

Figure 5-13 shows that the offshore wave power for the Matakana Banks during field measurements was predominantly below $5 \times 10^4 \text{ W.m}^{-1}$, but increased up to $21.6 \times 10^4 \text{ W.m}^{-1}$ during storm events. Overall, for the whole period of field

campaign the average wave power ranged from 1.02×10^4 to 1.9×10^4 W.m^{-1} for the offshore measurement sites, and dropped to about 63.6 W.m^{-1} inside the harbour.

Table 5-8. The highest significant wave height H_s (m) and period T_p (s) during storm events corresponding to the wave power P (kgms^{-3}). The 3rd storm event was not detected inside the harbour, hence no data presented (St. 390). The Wave power is in 10^4 .

Wave Properties	Storm events											
	I				II				III			
	Location/Sta.				Location/Sta.				Location/Sta.			
	384	383	386	390	384	383	386	390	384	383	386	390
H_s (m)	3.63	3.52	5.08	0.34	2	1.98	3.11	0.18	2.82	2.62	4.38	-
T_p (s)	7.2	9.3	8.7	9.3	6.5	6.2	7.2	6.2	13.1	14.6	13.1	-
P (W.m^{-1})	8.2	9.9	1.9	0.09	2.2	2.1	5.9	0.02	8.9	8.6	21.6	-

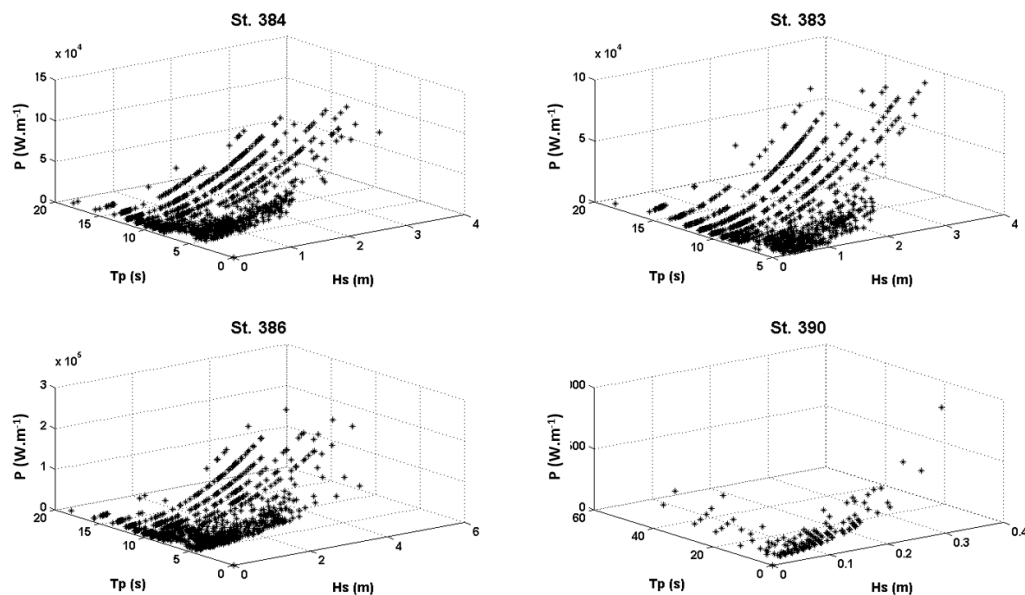


Figure 5-13. Variation of wave power P (W.m^{-1}) with significant wave height and peak period during field measurements.

5.4.3 Water Turbidity and Total Suspended Solids

Water turbidity was recorded by the turbidity sensor (SCUFA) inside the Tauranga Harbour, and ranged from 0.08 to 7.051 NTU (Figure 5-14). The average and mode of turbidity for 27 days field measurement were about 0.31 and 0.093 NTU respectively. The occurrence of high turbidity inside the harbour during the

last week of April 2013 (22 – 30 April 2013) does not correspond with the storm wave events outside the harbour, which occurred earlier in April.

This turbidity event may be related to a period of heavy rainfall that represented more than double normal April rainfall (284 mm, 236% of normal) recorded in Tauranga (NIWA, 2013); (WeatherWatch, 2013) ; (Bay of Plenty Times, 2013). Heavy rainfall combined with high discharge have been observed to increase turbidity level (Goransson *et al.*, 2013), and has previous been reported for Tauranga Harbour by (Davies-Colley, 1976). The Port of Tauranga has now installed a network of turbidity sensors within the Port area that can assess the sources of harbour turbidity

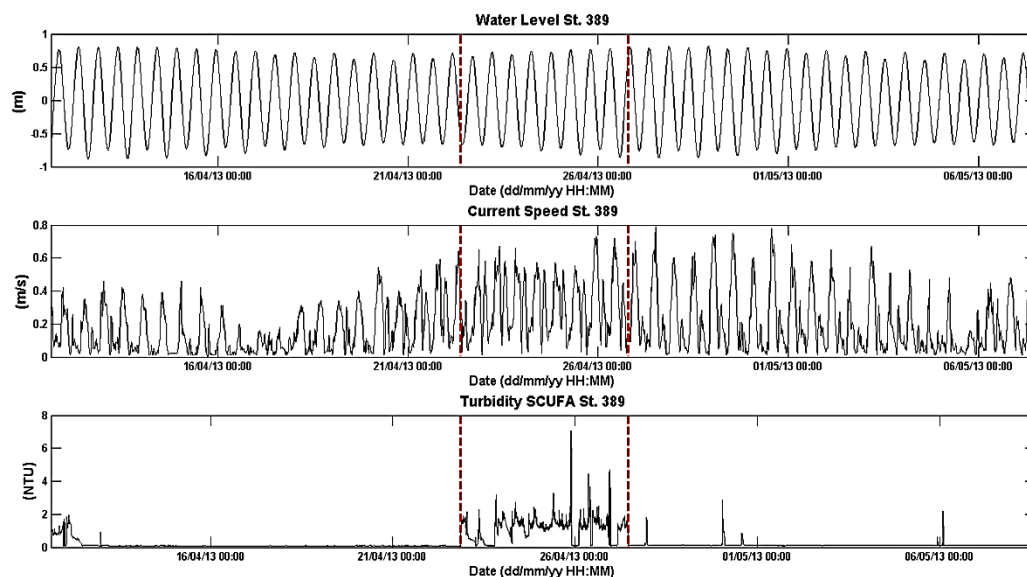


Figure 5-14 Time series of turbidity recorded by SCUFA (third panel) during field measurement, along with the corresponding water level (first panel) and tidal current speed (second panel). Red dashed lines indicate the period when persistent high turbidity was occurring.

The relationship between turbidity measured by C3 submersible fluorimeter (RFU) and total suspended solid was obtained by comparing the total suspended solids (TSS) and C3 readings in the laboratory. Results from the TSS analysis shows that the average sediment concentration is about 0.206 mg.l^{-1} inside the Tauranga Harbour. A good agreement of 0.7 is achieved by plotting both C3 readings and TSS measurement (Figure 5-15). During the deployment period the

C3 was buried in the sand, which affected the turbidity measurements. Hence, the C3 results are not presented in this study.

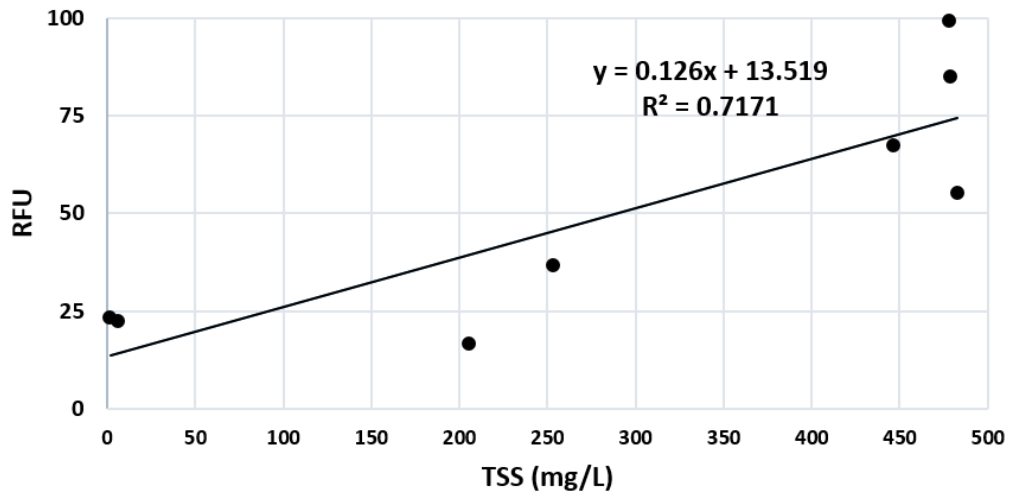


Figure 5-15. Plot of the C3 fluorometer reading (RFU) against the total suspended solid (TSS). Water was sampled from inside the Tauranga Harbour (St. 389) during half-ebb and half-flood.

5.4.4 Spatial Distribution of Sediment Grain Size and Sedimentation Rate

Grain size parameters have been used in many different sedimentary environments to derive sediment transport pathways (viz. McLaren and Bowles, 1985; Le Roux and Rojas, 2007). The spatial distribution of mean grain size, sorting and higher order statistics is closely related to sediment transport patterns (Sha, 1990).

The median grain sizes (D_{50}) and Udden – Wentworth classification of each sample are summarized in Table 5-9. The median (D_{50}) sediment grain size distribution for the study area was sub-divided into three areas (Figure 5-16):

- (1) The Entrance and Western Channels, which were primarily composed of coarse sand with $D_{50}=632 \mu\text{m}$;
- (2) The main body of the ebb-tidal delta (predominantly the swash platform), which was composed of medium sand ranging from 253 to 309 μm ; and
- (3) The northwestern area of the ebb tidal delta (terminal lobe and Matakana Island shoreface), where fine sand was found ranging from 171 to 205 μm .

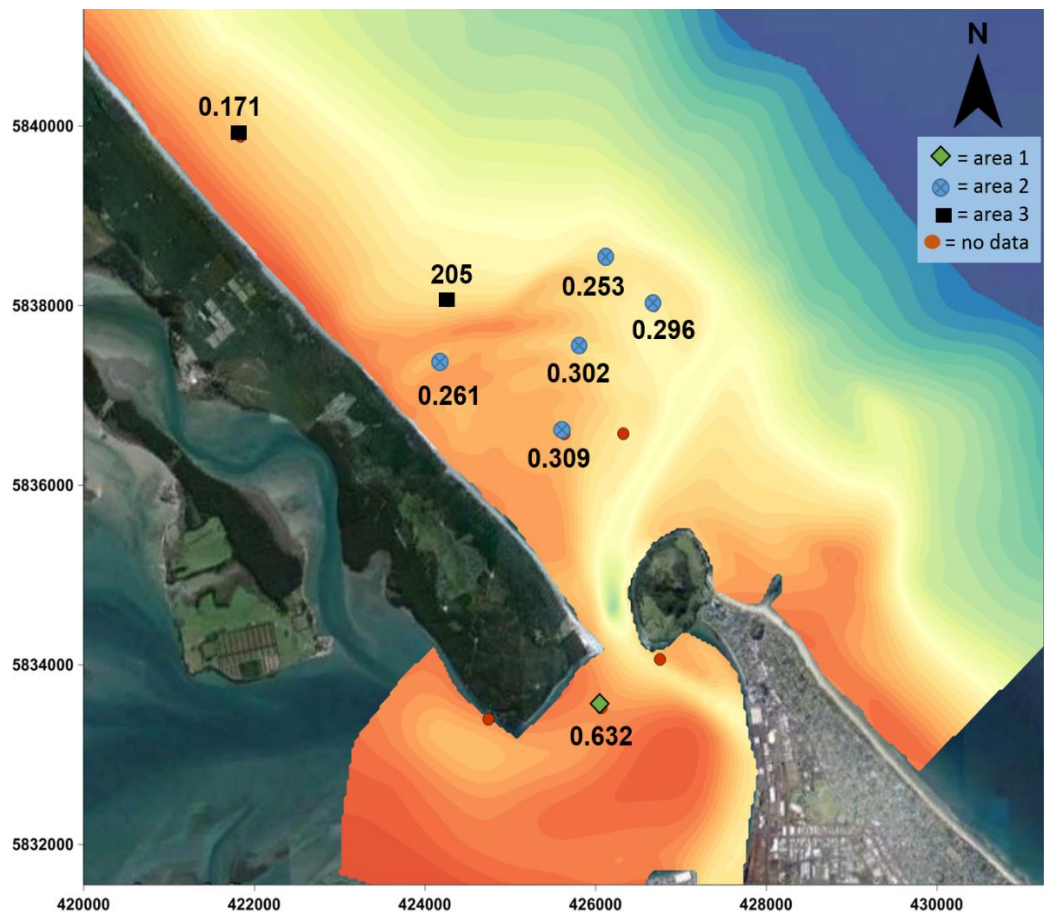


Figure 5-16. Median sediment grain size D_{50} (millimetres) sampled at the measurement stations (Table 5-9).

Table 5-9. Summary of sediment grain characteristics at each measurement station based on the Udden-Wentworth and Folk classifications (Folk, 1968).

Station sample	D ₅₀		D ₉₀ (µm)	Mean (µm)	Kurtosis		Mode (µm)	Skewness	
	Value (µm)	Equal to			Value	Equal to		Value	Equal to
382	261.327	med sand	445.271	284.548	1.066	Mesokurtic	258.096	1.03	Very fine skewed
383	205.261	fine sand	424.035	250.869	16.628	Extremely leptokurtic	195.424	3.282	Very fine skewed
384	171.162	fine sand	609.849	270.121	8.664	Extremely leptokurtic	153.813	2.879	Very fine skewed
385	136.282	fine sand	1395.034	492.244	-1.082	Very platykurtic	1255.653	0.767	Fine skewed
386	253.127	med sand	436.623	272.908	0.883	Platykurtic	255.292	0.781	Fine skewed
390	632.353	coarse	1023.135	680.623	1.534	Very leptokurtic	623.881	1.095	Fine skewed
393	309.361	med sand	518.847	334.498	0.751	Platykurtic	306.921	0.936	Fine skewed
395	302.081	med sand	686.924	373.983	5.746	Extremely leptokurtic	281.116	2.055	Very fine skewed
396	296.54	med sand	470.012	315.348	0.556	Very platykurtic	296.333	0.836	Fine skewed

The sediment traps were not all retrieved at the same time, as the instruments did not require servicing at the same times. The first instrument servicing, including retrieval of sediment traps was done on 19 April 2013, and recovered the sediment trap at St. 383. Due to stormy weather and difficulty relocating the instrument frame, the sediment trap at St. 390 was retrieved on 14 May 2013. Otherwise, the remaining sediment traps were retrieved on 8 May 2013 when the field measurement campaign ended. Overall, for the whole period of the field measurement campaign, the sediment traps captured from 274 to 1,874 grams of sediment (Table 5-10).

The least captured sediment mass was found in the trap at St. 390 (Entrance Channel-inside the harbour) where the highest tidal current velocities occurred. Either the presence of a shell lag limited the sediment availability, or the high velocities affected the trap efficiency by preventing sediment from settling into the trap, resulting in a low sedimentation rate. On the shallows of the ebb-tidal delta (swash platform) the sedimentation rates ranged from 51.59 to 106.83 mg/cm²/day. In the deeper part of the ebb-tidal delta (>12 m deep), at the north terminal lobe (St. 386) and at the distal end of the Entrance Channel (St. 396), the sediment influx decreased to between 33.2 to 92.4 mg/cm²/day. At the NW terminal lobe where the depth is around 10 m, the sediment influx was about 128 mg/cm²/day.

The highest sediment influx of about 305 mg/cm²/day was found at the furthest station from the tidal inlet (St. 385), on the Matakana Island shoreface to the northwest of the ebb-tidal delta. The InterOcean S4 ADW at this station failed to record useful data, so the cause of the high flux is uncertain, but possibly is due the effect of storm waves during the deployment.

Table 5-10. *Dry weight of sediment captured by the sediment traps and the sedimentation rate (influx) at each station.*

<i>Station</i>	<i>Deployment time (day)</i>	<i>Dry weight (gram)</i>	<i>Influx (mg/cm²/day)</i>
382	27	905.01	51.59
383	8	665.38	128.02
384	27	1723.64	98.26
385	8	1583.18	304.60
386	27	582.39	33.20
390	33	274.12	12.79
393	27	1823.03	103.92
395	27	1873.98	106.83
396	27	1621.63	92.44

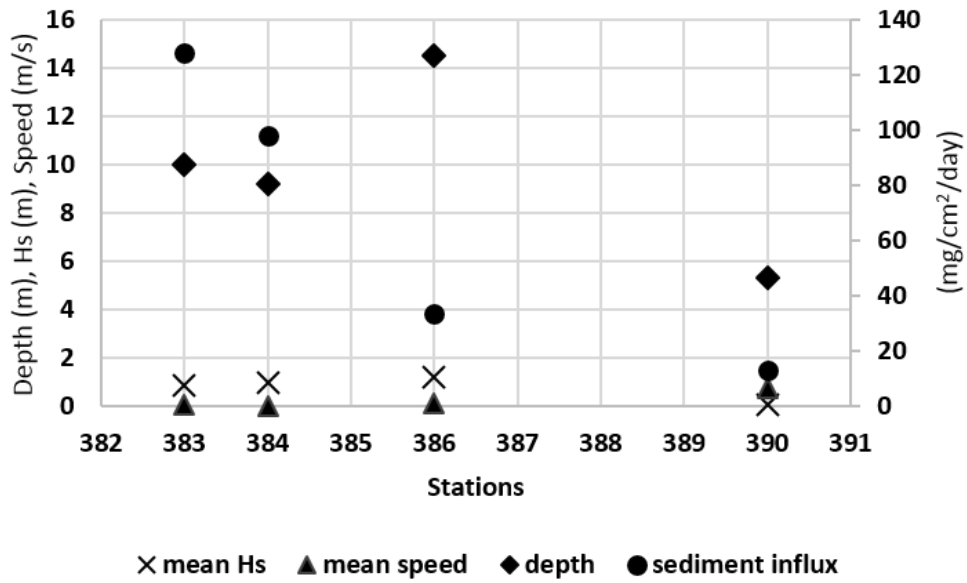


Figure 5-17. Plots of sediment influxes ($\text{mg}/\text{cm}^2/\text{day}$) obtained from the sediment traps against the current speed (m/s), wave heights (m), water depth (m) show that the sediment influx increased as the tidal influence decreased.

Figure 5-16 displays the plots of sediment influxes against the current speed, wave heights, depth, and the station locations. It is clearly seen that the least sediment influx corresponds with the location where the highest current velocity occurred. At St. 390 (inside the harbour, adjacent to tidal inlet), the mean current speed is about $0.736 \text{ m}/\text{s}$, whereas the two highest sediment influx is found at St. 383 and 384 (northern terminal lobe) with mean current speed are 0.03 and 0.01 respectively (Table 5-4). Site 390 also had the coarsest sediment, with a high proportions of shell fragments in the sediments. Low sediment transport rates were also reported by (Pickrill, 1985) for flows across a lag surface on the channel floor.

In the offshore areas, the mean wave height appears to vary inversely with the magnitude of sediment influx. Depth also appears to influence the magnitude of sediment influx, Pace *et al.* (1987) indicated that sediment fluxes determined by sediment traps declined with depth, and were greater in areas of greater biological productivity. For the ebb-tidal delta at Tauranga it is inferred that the sedimentation depends on the availability of sediment upstream from the site, and the amount of wave induced suspension of sediment, with high tidal velocities being associated with either bedload transport as migrating bedforms, or negligible sediment

entrainment due to bed armouring as reported by Black *et al.* (1989) for Whangarei Harbour.

5.5 Summary

The field measurement campaign was intended to identify and quantify the hydrodynamic regime for the study area, and was conducted for 27 days, from 11 April to 5 May, 2013. This deployment was shorter than planned due to the need to recover instruments before a predicted storm event. Tidal currents and waves were measured every 30 minutes at 4 locations on the Matakana Banks and along the Matakana Island shoreline by InterOcean S4s. The furthest northwest S4 (Sta. 385) failed to record; therefore, no data from this station was presented. An InterOcean S4 and a Falmouth Scientific FSI were also deployed inside the harbour, to measure tides and waves.

Significant wave heights, including storm events, ranged from 0.14 m to 5.08 m immediately offshore from the Matakana Banks. The predominant offshore wave approach directions were from the northwest to east (41° to 108°). Inside the harbour, wave heights are modified by the bathymetry and filtering by the tidal inlet, resulting in a decrease in recorded wave heights and longer periods. Offshore, the maximum wave heights varied between 3.52 to 5.08 m, whilst wave heights hardly exceeded 0.34 m inside the harbour. Mean peak periods ranged from around 9.2 to 10.0 s for the offshore areas and were around 12.7 s inside the harbour.

Wave energy within the study area ranged between 10×10^4 to 23×10^4 W.m^{-1} offshore, and was lower with a mean of about 64 W.m^{-1} inside the harbour. The first wave event produced the highest waves. However, a combination of high waves with long periods during the third storm event recorded, produced the maximum wave power ($21.6 \times 10^4 \text{ W.m}^{-1}$) observed. The third wave event was also the longest duration.

An upward looking RDI ADCP was used to measure tidal velocity profiles in 12 m depth adjacent to the Entrance Channel at the southern part of the ebb-tidal delta. This site was intended to capture the ebb jet behaviour. Backscatter intensities measured by ADCP shows that there was a significant increase in suspended sediment associated with three storm events during the field measurement

campaign, with the peak intensities occurring during the first storm. The duration of the increased sediment suspensions was similar for all three storms, despite their different durations. The backscatter data also indicated a peak in suspended sediment for the first half of each flood tide. To the east of the ADCP, a Sontek Argonaut ADP was deployed in the northern side of the tidal inlet to measure the ebb-jet vertical current profile. Tidal currents over the shallowest part of the ebb-tidal delta (swash platform) were measured by Sontek ADVs.

The highest tidal velocities occurred within the Western Channel inside the harbour. In order to measure turbidity in the water column, a C3 fluorimeter was deployed in the Western Channel, and a SCUFA was deployed inside the harbour closer to the entrance. However, during the deployment period the C3 was buried in the sand, hence its result is not presented in this study. Water sampled from inside the harbour indicates a total suspended solid concentration of about 0.206 mg.l^{-1} and a correlation factor of 0.7 between the C3 readings and TSS analysis result.

The study area is consistent with the typical spatial sediment grain size distribution for an ebb-tidal delta environment, as previously described by Sha (1990) where the deep inlet channel and the offshore area serve as source areas for the ebb-tidal delta and have coarse, relatively poorly sorted sediments. The spatial distribution of D_{50} reflects the tidal current conditions and the main source of the sediment. The coarsest sand with D_{50} $632 \mu\text{m}$, mixed with shell lags, was found in the Entrance Channel and the grain size decreased with increasing distance from the entrance.

Calculation of sedimentation rates at the instrument stations was based on the amount of sediment settled in sediment traps divided by the total surface area of the cylinder trap and converted to a daily rate. The results show that high sedimentation rates are found in shallow shoal area (swash platform), where wave action is high and tidal currents are low. Here, the sedimentation rates ranged between 51.59 to $106.83 \text{ mg/cm}^2/\text{day}$. In the deeper parts of the ebb-tidal delta ($>12 \text{ m}$ deep), at the north terminal lobe (St. 386) and at the distal end of the Entrance Channel (St. 396), sedimentation rates decreased to between 33.2 and $92.4 \text{ mg/cm}^2/\text{day}$. The lowest sedimentation rate of $12.79 \text{ mg/cm}^2/\text{day}$ was found inside the harbour adjacent to the inlet throat (St. 390).

5.6 References

- Bay of Plenty Times. (2013, May 4). *Tauranga sunniest centre as April goes to extreme*. Retrieved from Bay of Plenty Times:
http://www.nzherald.co.nz/bay-of-plenty-times/news/article.cfm?c_id=1503343&objectid=11098260
- Black, K.P., Healy, T.R., and Hunter, M.G. (1989). Sediment dynamics in the lower section of a mixed sand and shell-lag tidal estuary, New Zealand. *Journal of Coastal Research Vol. 5, Issue 3*, 503-521.
- Bloesch, J., and Burns, N.M. (1980). A critical review of sediment trap technique. *Hydrology, Vol. 42(1)*, 15-55.
- Blomqvist, S., and Hakanson, L. (1981). A review on sediment traps in aquatic environments. *Arch. Hydrobiogy, Vol. 91*, 101-132.
- Blomqvist, S., and Kofoed, C. (1981). Sediment trapping - a sub-aquatic in situ experiment. *Limnology Oceanography, Vol. 26.*, 585-590.
- Butman, C.A., Grant, W.D., and Stolzenback, K.D. (1986). Predictions of sediment trap biases in turbulent flows, a theoretical analysis based on observations from the literature. *Journal of Marine Research, Vol. 44*, 645-693.
- Davies-Colley, R. (1976). Some field techniques used in a study of Tauranga Harbour. *Proceedings of the New Zealand Ecological Society, Vol. 23* (pp. 33-37). New Zealand: New Zealand Ecological Society.
- Folk, R. L. (1968). *Petrology of Sedimentary Rocks*. Austin, Texas: Hemphill Publishing Company.
- Fotonoff, N.P., and Millard Jr, R.C. (1983). Unesco technical papers in marine science: Algorithms for computation of fundamental properties of seawater. *Unesco/SCOR/ICES/IAPSO Joint Panel on Oceanographic Tables and Standards and SCOR Working Group 51*, 25 - 28.
- Gardner, W. (1977). *Fluxes, dynamics, and chemistry of particulates in the ocean. PhD thesis*. Massachusetts: Massachusetts Institutes of Technology/Wood Hole Oceanography Institute of Massachusetts.
- Gardner, W. (1980a). Sediment trap dynamics and calibration: a laboratory evaluation. *Journal of Marine Research, Vol. 38.* , 17-39.
- Gardner, W. (1980b). Field assessment of sediment traps. *Journal of Marine Research, Vol. 38.*, 41-52.
- Goransson, G., Larson, M., and Bendz, D. (2013). Variation in turbidity with precipitation and flow in a regulated river system - river Gota Alv, SW Sweden. *Hydrology Earth System Science, 17.* , 2529-2542.

- Gray, J. G. (2000). *Comparability of Suspended-Sediment Concentration and Total Suspended Solids Data*. Reston, Virginia: U.S. Geological Survey. Water-Resources Investigations Report 00-4191.
- Hargrave, B.T., and Burns, N.M. (1979). Assessment of sediment trap collection efficiency. *Limnology Oceanography*, Vol. 24, 1124-1136.
- Hicks, S. (2006). *Understanding Tides*. USA: National Oceanic and Atmospheric Administration (NOAA).
- InterOcean. (2013, May). *S4 Application Software for Windows*. Retrieved from www.interoceansystems.com:
http://www.interoceansystems.com/sw_s4appwin.htm
- Lau, Y. (1979). Laboratory study of cylindrical sediment traps. *Journal of Fisheries Research Board of Canada*, Vol. 36., 1288-1291.
- Le Roux, J.P., and Rojas, E.M. (2007). Sediment transport patterns determined from grain size parameters: Overview and state of the art. *Sedimentary Geology* Vol. 202, 473-488.
- Malvern, I. L. (2005). *Mastersizer2000: Advanced Technology Made Simple*. Southboro: Malvern Inc. Limited.
- McLaren, P. and Bowles, D. (1985). The effects of sediment transport on grain-size distributions. *Journal of Sedimentary Petrology*, Vol. 55, No. 4, 457-470.
- Munk, W. (1950). Origin and Generation of Waves. *Proceedings of First Conference on Coastal Engineering* (pp. 1-4). Long Beach, California: Council on Wave Research.
- NIWA. (2013, May 3). *Climate Summary for April 2013*. Retrieved from NIWA: <https://www.niwa.co.nz/climate/summaries/monthly/climate-summary-for-april-2013>
- NIWA. (2013, July 1). *The National Climate Data Base*. Retrieved from NIWA Taihoro Nukurangi: <http://cliflo.niwa.co.nz/pls/niwp/wgenf.genform1>
- Pace, M.L., Knauer, G.A., Karl, D.M., and Martin, J.H. (1987). Primary production, new production and vertical flux in the eastern Pacific Ocean. *Nature*, Vol. 325. , 803-804.
- Pawlowicz, R. (2010, March 10). *Rich Pawlowicz's Matlab Stuff*. Retrieved from RDADCP: <http://www.eos.ubc.ca/~rich/#RDADCP>
- Pawlowicz, R., Beardsley, B., and Lentz, S. (2002). Classical tidal harmonic analysis including error estimates in MATLAB using T_TIDE. *Computer & Geosciences* Vol. 28, 929-937.
- Pickrill, R. (1985). Sedimentation in an ebb-tidal delta, Rangauru Harbour, Northland, New Zealand. *New Zealand Journal of Geology and Geophysics*, Vol. 28, 531-542.

- RDI. (2001). *RD Instruments: WinADCP User's Guide*. Acoustic Doppler Solutions.
- Sha, L. (1990). Surface sediments and sequence models in the ebb-tidal delta of Texel Inlet, Wadden Sea, The Netherlands. *Sedimentary Geology*, Vol. 68, 125-141.
- Sorensen, R. (1993). *Basic Wave Mechanics: For Coastal and Ocean Engineers*. New York: John Wiley & Sons, Inc. .
- Szmytkiewicz, A., and Zalewska, T. (2014). Sediment deposition and accumulation rates determined by sediment trap and ²¹⁰Pb isotope methods in the Outer Puck Bay (Baltic Sea). *Oceanologia* Vol. 56(1), 85-106.
- TELEDYNE RD Instruments. (2001). *WorkHorse Sentinel ADCP User's Guide*. San Diego, California: RD Instruments.
- Thomas, S., and Ridd, P.V. (2004). Review of methods to measure short time scale sediment accumulation. *Marine Geology* 207, 95-114.
- Turner Designs. (2013). *C3 Submersible Fluorometer*. Retrieved from Turner Designs: <http://www.turnerdesigns.com/products/submersible-fluorometer/c3-submersible-fluorometer>
- USACE. (2008). "Coastal Hydrodynamics", Coastal Engineering Manual, No. 1110-2-1100 (Part II). *United States Army Corps of Engineers*, 608.
- Van Rijn, L. (2007). *Manual Sediment Transport Measurements in Rivers, Estuaries and Coastal Seas*. The Netherlands: RIKZ, Aqua Publications.
- Wahlgren, M.A., and Nelson, D.M. (1977, Jan-Dec). Factors affecting the collection efficiency of sediment traps in Lake Michigan. *RER Div. Annual Report, ANL. 76-88, Part III*, pp. 107-110.
- WeatherWatch. (2013, May 3). *April-The month the rain returned*. Retrieved from WeatherWatch.co.nz: <http://www.weatherwatch.co.nz/content/april-month-rain-returned>

Chapter 6: Morphodynamic Modelling: Model Set-Up and Validation

6.1 Introduction

Coastal structures and any activities that maintain them can result in unavoidable impacts to the coastal environment. The most visible impact is the morphological changes at the shoreline and erosion or accretion of sand bodies adjacent to the shorelines, which can lead to negative perceptions of coastal development. Hence, the efforts to minimize negative impacts, including intensive monitoring and research to improve understanding of coastal processes, are substantial. Accurate predictions of short- and long-term impacts that could occur from anthropic activities simulating morphological changes are often necessary, and attempts to do so have been evaluated by many coastal engineers and scientists such as Elias *et al.*, (2006); Lesser, (2009); and Ruggiero *et al.*, (2009).

The morphology of an ebb-tidal delta strongly depends on the magnitudes of tidal currents (both the cross-shore and the along shore components) and on the characteristics of the incoming waves (Walton and Adams, 1976; Sha, 1989). The Matakana Banks ebb-tidal delta is characterised by a strong tidal influence close to the tidal inlet and the Entrance Channel, a mixture of tidal and wave forces on the swash platform, and predominantly wave forces around the outer limits (Ramli and de Lange, 2013). Therefore, to assess the impacts of dredging on the ebb-tidal delta it is necessary to first assess the behaviour of the tide and wave forcing, allowing for a variable interaction between these key processes.

A study of influences of channel dredging on flow and sedimentation patterns at micro-tidal inlets, using the Coastal Modelling System, was reported by Beck and Wang (2009). They found that frequent channel dredging intensified the ebb-jet and the ebb flows. However, the ebb flow tended to become more concentrated

through the dredged channel, which resulted in a reduction in the strength of ebb currents over the rest of the ebb-tidal delta. The flow changes also and affected the sediment transport pattern for the delta.

In this study, coupled numerical models, consisting of DELFT3D modules that simulated water flow, sediment transport, dredging and spoil disposal, and wave processes, were used to simulate the factors involved in the morphological evolution of the Matakana Banks ebb-tidal delta. The inclusion of the dredging and spoil disposal module was intended to assist with evaluating the effects of historic and planned dredging, and assessing possible mitigation using an offshore spoil mound.

In the Delft3D model, morphodynamic modelling is based on the numerical solution of the three-dimensional shallow water equations in combination with a surface wave propagation model (wind waves) to generate the hydrodynamic forcing for sediment transport, and the advection-diffusion equation (to include lag effects) to assess the movement of sediment particles, with online bed up-dating after each time step (Tonnon *et al.*, 2007). However, due to the large calibration effort and, especially, the large computational time required, fully three-dimensional (3D) simulations of morphological evolution are often not very practical in engineering applications (Giardano *et al.*, 2010). Therefore, in this study the morphological modelling was carried out using the depth-averaged (2DH) mode. The model includes bed-load and suspended-load transports and a bed roughness predictor depending on the hydrodynamic and sediment conditions (van Rijn *et al.*, 2004).

The “online Delft3D-Wave” option was activated in order to include the influence of a time-series of wave conditions into the calculation of morphological changes. The changes are predicted from both bedload and suspension transport, and the erosion and deposition of non-cohesive sediment. The modelling also incorporated wind shear. The impact of dredging and dumping was investigated by incorporating the Port of Tauranga Ltd 2013 dredging plan as a “Man-made” process in the Delft3D Flow model. Several scenarios for dredging and different disposal sites were simulated.

6.1.1 Acknowledgements

The initial numerical grid for Tauranga Harbour was provided by Eva Kwohl and Christian Winter from the University of Bremen, Germany. Wave hindcast data for the wave boundary conditions in the wave model were provided by Brett Beamsley, MetOcean, Ltd.

6.2 Model Overview

In this study, the Delft3D FLOW model was the main modelling framework used to perform the hydrodynamic computations, sediment transport and morphological modelling. The evolution of wind-generated waves was simulated using the Delft3D-WAVE module, which may be better known as SWAN (Deltares, Delft3D-FLOW Simulation of multi-dimensional hydrodynamic flows and transport phenomena, including sediments. User Manual, Hydro-Morphodynamics, 2013). Delft3D-WAVE is a third generation spectral wave model that uses an Eulerian approach. In Delft3D-WAVE, the evolution of wind-generated waves is based on a two-dimensional wave action-density spectrum and is calculated simultaneously for each point in space. Delft3D-WAVE is capable of simulating wave propagation, wave generation by wind, non-linear wave-wave interactions and wave energy dissipation for specified bathymetry, wind, current and water level conditions.

By coupling Delft3D-WAVE to Delft3D-FLOW, wave-induced processes, such as shear stresses, and additional turbulence, are accounted for in the flow computations. The wave parameters calculated by the Delft3D-WAVE module are used as input for the Delft3D-FLOW module, which then computes wave-driven currents, enhanced turbulence, bed-shear stress and sediment stirring by wave breaking. Delft3D-FLOW and Delft3D-WAVE can exchange information by means of either offline or online coupling. Offline coupling uses completed Delft3D-FLOW simulation results to assess the effects of currents on waves, while online coupling iteratively combines the FLOW and WAVE simulations to assess the effects of the waves on currents and vice-versa (Deltares, 2011).

This study used online coupling as wave-current interactions are important for the evolution of an ebb-tidal delta. This meant that every 12 model minutes

(coupling time step) a new flow field (water level h and depth averaged currents u and v) was supplied from the flow model to the wave model module (Figure 6.1). Delft3D-WAVE then solved the balance equation for wave action density in the modelled domain and returned the peak wave frequency (f_p) and mean wave direction (Θ) to the Delft3D-FLOW module.

This information was used in the roller model of Delft3D-FLOW to compute the wave energy dissipation, from which the significant wave height (H_s) can be derived (Figure 6.1). Delft3D-FLOW also solved the two and three dimensional shallow water equations, also includes routines to calculate the sediment transport and update the morphodynamics (Giardano *et al.*, 2010). The hydrodynamic, sediment transport and morphodynamic equations were solved at the computational time step (6 s). The complete set of these coupled modules used to simulate morphological evolution is known as Delft3D-MOR (Deltares, 2013).

Online coupling was also used between the hydrodynamic and sediment transport/morphodynamics modules (Figure 6.1), so that the flow, transport and morphological updating are merged into the Sediment-Online model. Hence, only the wave model is executed separately (with bi-directional data communication between online model and wave model). The Sediment-Online modules enable the simultaneous computation of flow sediment transport and the associated morphological changes at every flow time step. The bed evolution can be accelerated after each time step by means of a so-called morphological upscaling factor (MORFAC). The MORFAC has to be specified by the user and the value depends on the expected dynamic response of the area of interest; very dynamic areas require a low MORFAC value, whereas for more stable environments the MORFAC can be increased (Tonnon *et al.*, 2007).

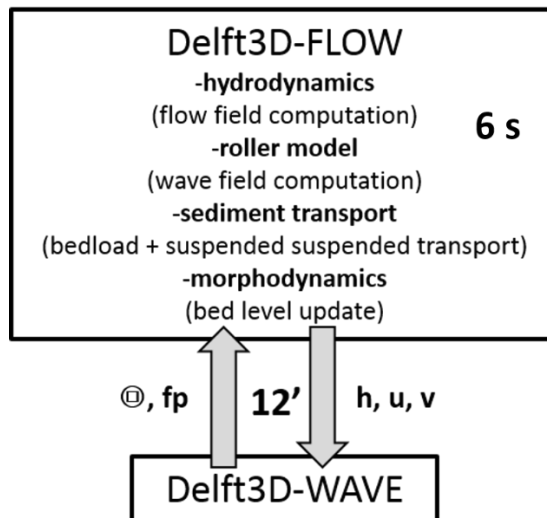


Figure 6-1. Schematic of the computations and exchange of key parameters for a morphodynamic simulation using Delft3D-MOR.

More specific details of the governing equations and numerical solution schemes for Delft3D models are described in Delft3D-FLOW User Manual (2013), Kwool (2010), and van Rijn and Walstra (2003).

6.3 Delft3D FLOW Model Setup

6.3.1 Computational Grid and Bathymetry

An initial computational grid with constant X and Y resolution of 200 m was developed by (Kwool, 2010). The grid mesh covered ~14 km offshore from the tidal inlet and the southeastern basin within Tauranga Harbour (Figure 6-3). To examine the morphological response of Matakana Banks within a reasonable computation time, a nested model with a finer grid was developed for the area of Matakana Banks ebb-tidal delta and the Centre Bank flood-tidal delta (Figure 6-2). This grid used variable sized square grids: the average spacing between grid lines for the nearshore area of interest is about 30 m, while for the offshore area it is about 150 m.

For the nested model, the initial bathymetry before the first capital dredging campaign in 1968 was digitized from the 1967 NZ 5412 hydrographic chart in UTM 60S coordinates (Figure 6-2, left). The current bathymetry was derived for 2013, particularly around Matakana Banks, using data obtained by a MBES survey in March 2013, supplemented where necessary with the 2012 NZ 5412 hydrographic chart (Figure 6-2, right). All the bathymetric data were gridded at 30 m resolution, interpolated by the triangular method, and saved as a depth file using DELFT

QUICKIN. The resulting file was in the correct format to be used in the computational grid.

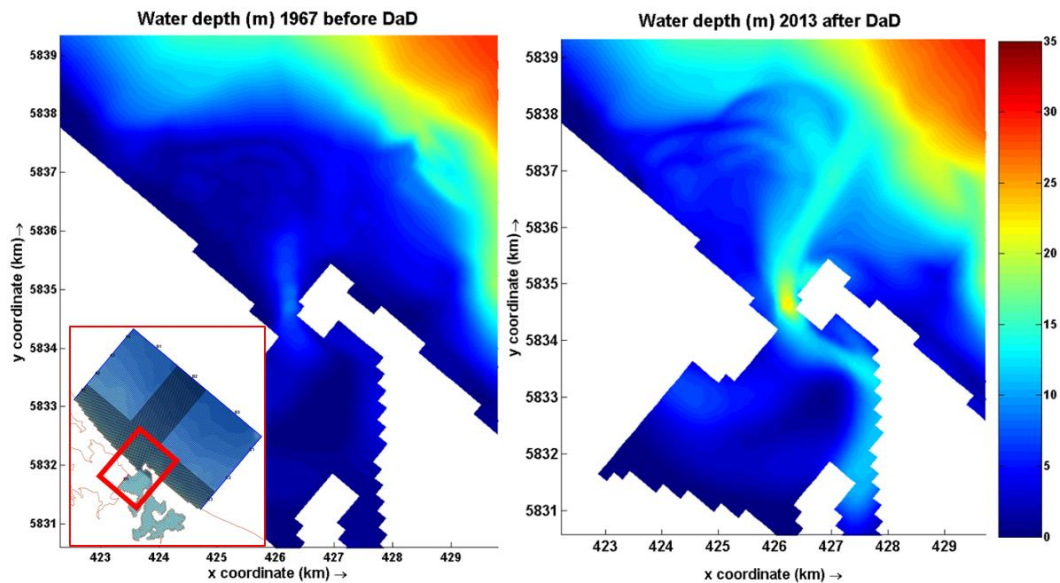


Figure 6-2. Delft3D computational grids for the 1967 bathymetry 1967 (left), before the first capital dredging was conducted, and for the 2013 bathymetry obtained by a MBES survey in March 2013 (right). Both figures were zoomed in for better visualization of the ebb-tidal delta and its surroundings. Index picture (lower left) shows the zoomed location.

6.3.2 Boundary Conditions

The initial estimates of water levels at the boundaries for the hydrodynamic models in this study were obtained from the NIWA online tide forecaster (NIWA, 2013). Then tidal harmonic analysis using the Matlab T_Tide toolbox (Pawlowicz *et al.*, 2002) was used to estimate the amplitude and phase of each of the 7 largest tidal constituents: O1, K1, M2, N2, S2, M4, and MS4 (Table 6-1). The locations where tidal forcing of water level boundaries was applied by Delft3D-FLOW to the main hydrodynamic model is displayed in Figure 6-3 and Appendix 2.

Table 6-1. Tidal amplitudes (amp) and phase for the 7 major constituents used to generate the tidal forcing on the boundaries of the initial model (Figure 6-3).

<i>Boundary</i>	<i>Tidal Constituent</i>	<i>Amp (m)</i>	<i>Phase (°)</i>						
NW	Station	A1		A2		A3		A4	
	<i>O1</i>	0.02	300	0.02	300	0.02	299	0.02	298
	<i>K1</i>	0.08	339	0.08	338	0.08	339	0.08	338
	<i>M2</i>	0.71	198	0.71	198	0.71	198	0.71	198
	<i>N2</i>	0.15	181	0.15	181	0.15	181	0.15	181
	<i>S2</i>	0.08	259	0.08	258	0.08	258	0.08	258
	<i>M4</i>	0.01	249	0.01	249	0.01	249	0.01	249
	<i>MS4</i>	0.01	207	0.01	207	0.01	207	0.01	207
NE	Station	B1		B2		B3			
	<i>O1</i>	0.02	298	0.02	297	0.02	294		
	<i>K1</i>	0.08	338	0.088	338	0.08	338		
	<i>M2</i>	0.71	198	0.71	198	0.71	198		
	<i>N2</i>	0.15	181	0.15	181	0.15	180		
	<i>S2</i>	0.08	258	0.08	258	0.08	258		
	<i>M4</i>	0.01	250	0.01	249	0.01	249		
	<i>MS4</i>	0.01	207	0.01	207	0.01	207		
SE	Station	C1		C2		C3			
	<i>O1</i>	0.02	297	0.02	297	0.02	297		
	<i>K1</i>	0.08	338	0.08	338	0.08	338		
	<i>M2</i>	0.71	198	0.71	198	0.71	198		
	<i>N2</i>	0.15	181	0.15	181	0.15	181		
	<i>S2</i>	0.08	258	0.08	258	0.08	258		
	<i>M4</i>	0.01	248	0.01	249	0.01	249		
	<i>MS4</i>	0.01	206	0.01	206	0.01	206		
Western Channel	Station	D1							
	<i>O1</i>	0.02	300						
	<i>K1</i>	0.08	343						
	<i>M2</i>	0.73	207						
	<i>N2</i>	0.15	190						
	<i>S2</i>	0.08	268						
	<i>M4</i>	0.01	267						
	<i>MS4</i>	0.01	226						

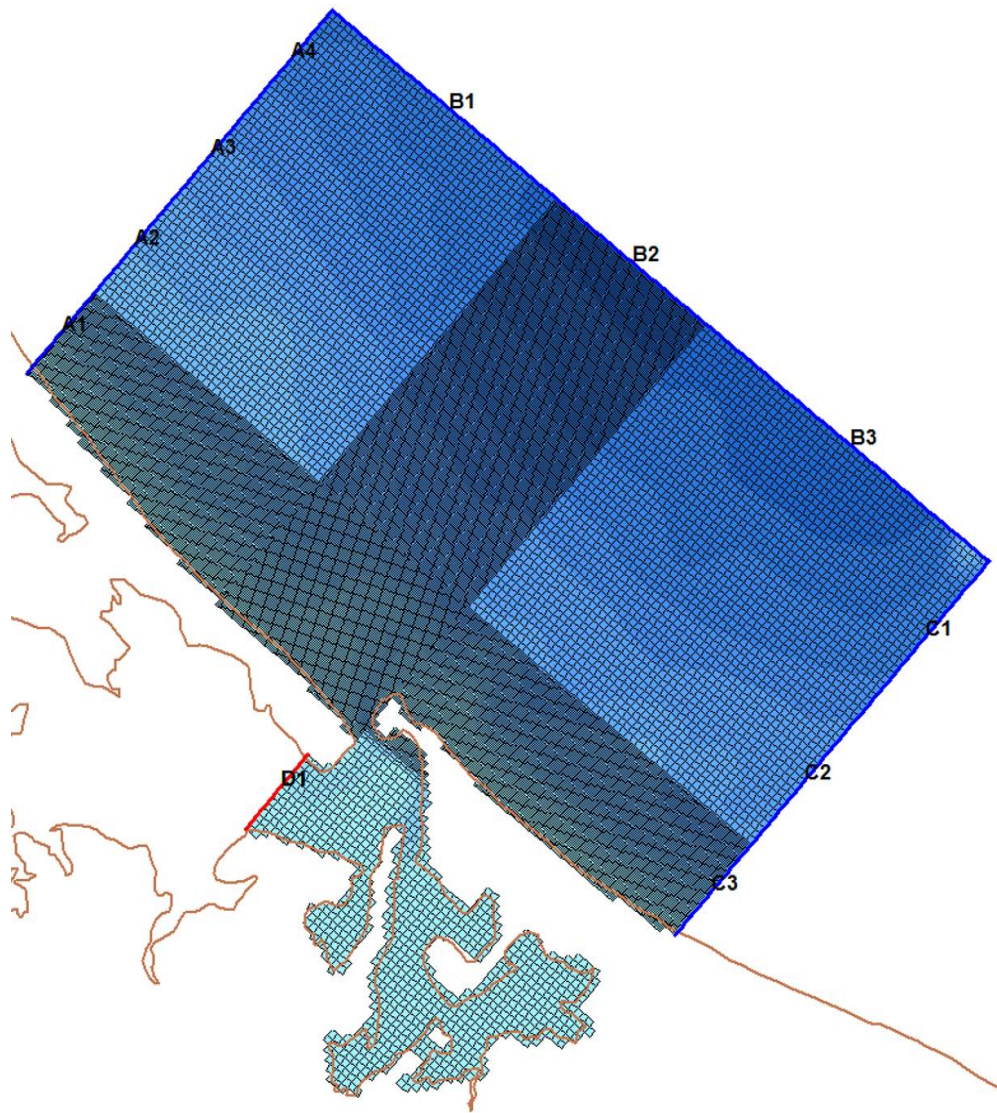


Figure 6-3. The locations where tidal forcing was applied to the 4 open boundaries in the initial hydrodynamic model.

The computational domain for the nested model was limited by closed boundaries corresponding to the mainland, Matakana Island, and an artificial closed boundary blocking off the upper Western Channel. While the Western Channel boundary was treated as an open boundary in the outer initial model (Figure 6-3), it created calibration problems within the nested model. These were solved by converting it to a closed boundary, which suggests that the flow in and out of the upper harbour via the upper Western Channel may not have a significant effect on the ebb-tidal delta. There are 4 open boundaries, where tidal forcing of water levels are imposed; a boundary inside the harbour (Stella Passage) and three offshore boundaries corresponding to the western, northern and eastern extents of the grid.

The morphological model evaluated the effect of the sediment transport conditions from the predicted sediment concentration associated with modelled flow and wave conditions. Hence, it was necessary to specify open boundary sediment concentrations. For the initial model the sediment concentrations at the boundary inside the harbour (D1) were defined by field measurement obtained from April – May 2013 (Ramli and de Lange, 2013) and a fixed value of $\sim 0.118 \text{ kg.m}^{-3}$ was used for the offshore suspended sediment concentration based on previous studies (Badesab *et al.*, 2012).

6.3.3 Model Parameter Settings

6.3.3.1 Time Step

The numerical stability of Delft3D-FLOW is largely dependent on the duration of the computational time step. The accuracy of parameters such as the reproduction of the important spatial length scales by the numerical grid, is also a function of the speed at which perturbations, such as waves, propagate through the grid. This dependence can be evaluated using the Courant-Friedrichs-Lewy number (CFL), defined by:

$$CFL = \frac{\Delta t \sqrt{gh}}{\{\Delta x, \Delta y\}} \quad (6-1)$$

where Δt is the time step (in seconds), g is the gravitational acceleration, h is the (total) water depth, and $\{\Delta x, \Delta y\}$ is a characteristic value (in many cases the minimum value) of the grid spacing in either direction.

Generally, the Courant number should not exceed a value of 10. But for problems with rather small variations in both space and time the Courant number can be taken substantially larger (Deltares, Delft3D-FLOW Simulation of multi-dimensional hydrodynamic flows and transport phenomena, including sediments. User Manual, Hydro-Morphodynamics, 2013). In this study, the minimum computational grid size was 30 m x 30 m, and the average depth was around 10.2 m, which with a 6 s time step yielded a Courant number of 2. This was considered acceptable.

6.3.3.2 Physical Parameters

The spatial distribution of median grain size around the Tauranga Harbour was used to define the bottom roughness parameter in the flow model. The distribution of Manning bottom roughness (M) was estimated from the Nikuradse roughness length, k_s using

$$M = \frac{25.4}{k_s^{\frac{1}{6}}} \quad (6-2)$$

After considering several relationships recommended in (Soulsby, 1997) to estimate k_s for flat beds. The Nikuradse roughness length was estimated from the median grain diameter (D_{50}) as approximately

$$k_s = 2.5 D_{50} \quad (6-3)$$

D_{50} data were obtained from 357 sites within the boundaries of the initial grid. These were used to estimate Manning bottom roughness values, which were then interpolated over the computational grid using DELFT3D-QUICKIN (Figure 6-4). Overall, the Manning values in the study area ranged from 0.020 close to the tidal inlet up to 0.030 for the northern margin of the ebb-tidal delta. For the offshore area where no sediment grain size data were available, the bottom roughness was assigned a constant value of 0.026, which is close to the middle of the range of values estimated from available data (Appendix 3).

The other physical parameters used for the Delft3D-FLOW and MOR simulations are defined in Table 6-2 and the schematized wind data set is given in Appendix 4.

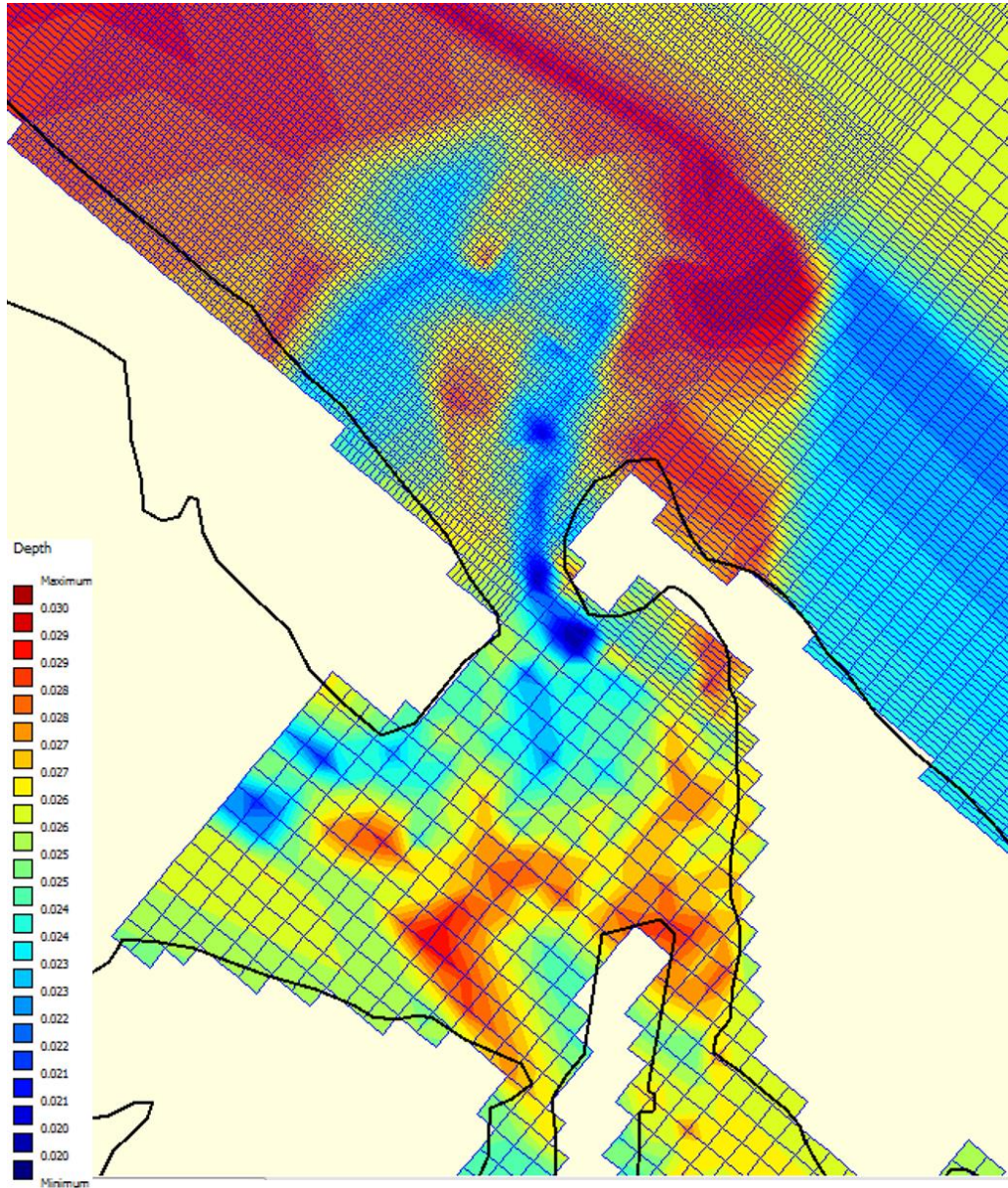


Figure 6-4. Map of the Manning bottom roughness estimated from the median grain size diameter (D_{50}) for the nested numerical model.

Table 6-2. *Physical parameters used for the Delft3D FLOW and MOR simulations.*

Data Groups	Parameters	Settings
Constants	Gravity	9.81 [m/s ²]
	Water density	1024 [kg/m ³]
	Air density	1 [kg/m ³]
Roughness	Roughness formula	Manning's n, see Appendix 6.2
	Stress formulation due to wave forces	Fredsoe
	Slip condition (wall roughness)	Free
Viscosity	Background horizontal viscosity/diffusivity	Uniform
	Horizontal eddy viscosity	1.2 [m ² /s]
	Horizontal eddy diffusivity	10 [m ² /s]
Sediment (FLOW-MOR model)	Sediment sand	
	Reference density for hindered settling	1600 [kg/m ³]
	Specific density	2650 [kg/m ³]
	Dry bed density	1600 [kg/m ³]
	Median sediment diameter [D ₅₀]	632 [μm]
	Initial sediment layer thickness at bed (uniform)	15 [m]
Morphology (FLOW-MOR model)	Update bathymetry during FLOW simulation	True
	Include effect of sediment on fluid density	False
	Equilibrium sand concentration profile at inflow boundaries	True
	Morphological scale factor	1 to 60
	Spin-up interval before morphological changes	720 [min]
	Minimum depth for sediment calculation	0.1
	van Rijn's reference height factor	1
	Threshold sediment thickness	0.05 [m]
	Estimated ripple height factor	2
	Factor for erosion of adjacent dry cells	0
	Current-related reference concentration factor	1
	Current-related transport vector magnitude factor	1
	Wave-related suspended transport factor	1
	Wave-related bed-load transport factor	1
Wind (FLOW-MOR model)	Uniform	
	Interpolation type	Block. See Appendix 6.2

The morphological model requires that the initial sediment thickness of the seabed be specified throughout the model domain. From the SBES and MBES survey data, it was determined that bathymetric variations associated with the Matakana Banks ebb-tidal delta occurred for depths <15 m (Chapter 4). Hence, this depth limit was assumed to be the initial sediment thickness of the ebb-tidal delta (Table 6-2).

The sediment within the Entrance Channel was coarser than other regions due to higher current velocities. A consequence of the removal of finer sediments and the availability of coarse sediment was that shells and shell fragments armoured the sediment, which limited the amount of entrainment and subsequent transport. The sediment distributions in these areas were bimodal, so the mean or median grain size was not a reliable indicator of the potential for sediment grains to be transported. Therefore, in order to predict the distribution of the sediment transported from the tidal inlet during flood and ebb tides, the model utilized the coarsest sediment fraction found in the study area (632 μm).

6.3.3.3 Numerical Parameters

The numerical method of Delft3D-FLOW is based on finite differences. To discretise the 3D shallow water equations in space, the model area is covered by a curvilinear grid, the variables of water level and velocity (u , v , w) are arranged in a special way on the grid. The pattern is called a staggered grid or Akarawa C grid arrangement, which has several advantages, such as boundary conditions can be implemented in a rather simple way and it may prevent spatial oscillations in the water levels (see Stelling (1984)). By this grid arrangement, the water level points (pressure points) are defined in the centre of a (continuity) cell and the velocity components are perpendicular to the grid cell faces where they are situated.

The process of drying and flooding is represented by removing grid points from the flow domain that become “dry” when the tide falls and by adding grid points that become “wet” when the tide rises. The flooding and drying grid cells are activated when water levels exceed a flooding threshold, while grid cells are deactivated when local water levels drop below half this threshold (Deltares, 2013).

In Delft3D, for the case of a steep bottom slope, the Mean option for depth at grid cell centres should be chosen, however in the study area where the bottom slope are relatively gentle, the “Max” option (default) is recommended. It is been found that “Max” procedure is more favourable and will produce a more smooth solution than the options described by Stelling *et al.* (1986) and Deltares (2013).

A smoothing time of 60 min (Delft3D-FLOW default) was selected in this study. The smoothing time determines the time interval in which the open boundary conditions are gradually applied, starting at the specified initial condition to the specified open boundary condition. This smoothing of the boundary conditions prevents the introduction of short wave disturbances into the model (Hosseini and Coonrod, 2011). The numerical parameters used in Delft3D-FLOW are presented in Table 6 – 3.

Table 6-3. Numerical parameter.

Drying and flooding check at	Grid cell centres and faces
Depth specified at	Grid cell corners
Depth at grid cell centres	Max
Depth at grid cell faces	Mor
Threshold depth	0.1 m
Marginal depth	-999
Smoothing time	60

6.3.3.4 Operations

The dredging and dumping module within Delft3D was activated, and an ASCII file (*.DAD) that defined the characteristics of all dredging, dumping and sediment nourishment activities in the simulation was provided. The dredging and dumping characteristics were based on the Port of Tauranga Ltd. 2013 dredging plan (Port of Tauranga Ltd, 2013). The locations for dredging and dumping were defined as polygons within a *.POL file. Both files are shown in Appendix 5.

The minimum remaining depth after dumping was specified to be 5 m and the distribution of the dumped sediment must fill the deepest part first. Any surplus of sediment is removed from the model (Deltares, 2013). Shallower minimum depths were tested, but were found to cause the model to become unstable and produce unrealistic sediment transport patterns.

6.3.4 Delft3D-WAVE (SWAN) Setup

The Delft3D-Wave model was set up to run in a coupled mode with the FLOW model with physical and numerical parameters set to the Delft3D-WAVE defaults.

6.3.4.1 Grid and Bathymetry

The wave grid used by Delft3D-Wave consisted of 93 offshore and 137 alongshore grid cells. The grid-cell resolution smoothly varied from ~160 x 140 m offshore (offshore and alongshore direction respectively) to 90 x 100 m near shore. The hydrodynamic conditions (water level, current and bathymetry) used for the wave computations resulted from the flow grid (online) coupling and was extended by the boundary values.

6.3.4.2 Wave Forcing

Time-varying and space uniform wave boundary conditions were implemented in the Delft3D-WAVE model. This type of wave boundary condition could not be set in GUI, so the keyword T-Series File was included in Data group General within the MDW-file (Deltares, 2013). The measured wave data set was used for the wave model calibration.

After a satisfactory calibration was achieved, for simulations using the *morphological factor* the measured wave heights for each boundary were averaged (see Appendix 6-1, D & E) to determine a characteristic wave height. The JONSWAP spectrum corresponding to the average wave heights was then used, with a peak enhancement factor of 3.3. The cosine power option was used for directional spreading.

6.4 Model Results

6.4.1 Comparison and Calibration

After calibration, the predictive capability of the flow model with regard to water levels and current velocities was verified by comparing measured and modelled values for a separate set of observations. The evaluation of predictive capability aims to express the goodness of fit between field data and model results

by simple and objective measures that assess different characteristics (Winter, 2007). Hence, a set of statistical parameters was used to assess the quality of the model results.

In this study the *Mean Error* (ME), the *Mean Absolute Error* (MAE), the *Relative Mean Absolute Error* (RMAE) and *linear correlation coefficient*, r , were used for assessment purposes. Definitions of these parameters are listed in Table 6-4. The simplest measure, r , assesses the degree of association between the observations and model predictions; do they trend in the same direction at the same time. The ME serves to indicate a general tendency of predictions towards overestimation or underestimation, a positive ME indicates that the model results on average overestimates the measured data (Winter, 2007); (Palacio et al., 2005). However, the ME can be affected by outliers and the neutralisation of positive and negative errors. Hence, the MAE and its' non-dimensional RMAE form are considered more robust measures of the scale of the difference between the observations and predictions (Winter, 2007)

Walstra *et al.* (2001) and van Rijn *et al.* (2002) proposed a set of standards for assessing model performance for different types of modelled parameters using the Relative Mean Absolute Error (RMAE) for time series data, and the Brier Skill Score (BSS) for morphological data (Murphy and Epstein, 1989); (Peet *et al.*, 2002) as listed in Table 6-5.

Table 6-4. *Statistical parameters used for model calibration and validation.*

Parameter	Equation
Mean Error	$ME = \frac{1}{N} \sum_{i=1}^N y_i - x_i \quad (6.2)$
Mean Absolute Error	$MAE = \frac{1}{N} \sum_{i=1}^N y_i - x_i \quad (6.3)$
Relative Mean Absolute Error	$RMAE = \frac{\frac{1}{N} \sum_{i=1}^N y_i - x_i }{\frac{1}{N} \sum_{i=1}^N x_i } \quad (6.4)$
Linear Correlation Coefficient, r	$r = \frac{\sigma_{xy}}{\sigma_x \sigma_y} \quad (6.5)$

Table 6-5. Statistical parameters used to assess the quality of the performance of modelled wave, velocity and morphology, where H = wave height, ΔH_m = error of measured wave height, V = velocity, ΔV_m = error of measured velocity, $z_{b,c}$ = bed level, $\Delta z_{b,m}$ = error of measured bed level, $z_{b,0}$ = initial bed level, index m = measured, index c = computed, (..) = averaging procedure over time series.

Value	Formula	Eq.
Wave height	$RMSE = \frac{ H_c - H_m - \Delta H_m}{H_m}$	(6.6)
Velocity	$RMSE = \frac{ V_c - V_m - \Delta V_m}{V_m}$	(6.7)
Morphology	$BSS = 1 - \frac{(z_{b,c} - z_{b,m} - \Delta z_{b,m})^2}{(z_{b,0} - z_{b,m})^2}$	(6.8)

The statistical parameters for wave height, current velocity and bed level are corrected for measurement errors (van Rijn et al., 2002), being $\Delta H_m=0.1$ m for wave height, $\Delta V_m=0.05$ m/s for current velocity and $\Delta z_{b,m}=0.1$ m for bed level in field conditions.

The performance of a morphological model relative to a baseline prediction can be judged by calculating the Brier Skill Score. This skill score compares the mean square difference between a baseline prediction and observation (Eq. 6.8, Table 6-5). Perfect agreement gives a Brier score of 1, whereas modelling the baseline condition gives a score of 0 (no skill). If the model prediction is further away from the final measured condition than baseline prediction, the skill score is negative.

The BSS is very suitable for the prediction of bed evolution. The baseline prediction for morphodynamic modelling will usually be that the initial bed remains unaltered. In other words, the initial bathymetry is used as the baseline prediction for the final bathymetry. A limitation of the BSS is that it cannot account for the migration direction of a bedform; it just evaluates whether the computed bed level (at time t) is closer to the measured bed level (at time t) than the initial bed level. If the computed bedform migration is in the wrong direction, but relatively small; this may result in a higher BSS score compared to the situation with bar migration in the right direction, but much too large. The BSS will even be negative, if the bed profile in the latter situation is further away from the measured profile than the initial profile (van Rijn et al., 2002).

The qualification of model performance by various authors is summaries in Table 6-6. The specified value ranges in Table 6-5 are recognised as a tough set of standards for models to achieve (van Rijn and Walstra, 2003; van Rijn *et al.*, 2002).

Table 6-6. Performance rating according to RMAE and BSS values.

Rating	Wave Height RMAE Van Rijn et al., (2002)	Velocity RMAE Van Rijn et al., (2002)	Velocity RMAE Walstra et al. (2001)	Morphology; BSS Van Rijn & Walstra, (2003)
Excellent	<0.05	< 0.1	<0.2	1.0 – 0.8
Good	0.05-0.1	0.1 – 0.3	0.2 - 0.4	0.8 – 0.6
Reasonable/Fair	0.1 – 0.2	0.3 – 0.5	0.4 – 0.7	0.6 – 0.3
Poor	0.2 – 0.3	0.5 – 0.7	0.7 – 1.0	0.3 - 0
Bad	>0.3	>0.7	>1.0	<0

As an alternative to these quantitative measures, de Jongste *et al.* (2013) show that a qualitative assessment of the similarity of sedimentation and erosion patterns of the model and observation can also be used to verify the morphodynamic behaviour predicted by the model.

6.4.2 Modelled Hydrodynamic Conditions

The 2DH Delft3D-FLOW model was run for 29 days coinciding approximately with the period when the field measurements were obtained (Chapter 5). The modelled water levels for all stations were reproduced well (Figure 6-5), however the fit for current velocities varies with the best fit achieved just inside the harbour entrance at Station 390 (Figures 6-6 and 6-7).

Over the swash platform and adjacent to the entrance channel on the ebb-tidal delta, the modelled current magnitude underestimated the measured velocities. Here, on average, the current speeds were 17% to 30% times lower during neap tide and 21% to 47% times during spring tide. The opposite occurred for the nearshore area beyond the ebb-tidal delta towards the north, where the model overestimated the measured current speed by factors of up to 115% and 200% during the neap and spring tide respectively. Inside the Harbour adjacent to the inlet throat, the model underestimated the current speed on average by about 20% to 23% during spring and about 11% to 28% during neap tide (Appendix 6).

The likely reason for the differences between predictions and observations is the influence of wave orbital currents on the measured currents recorded by the instruments. The pattern of over and underestimation is consistent with the distribution of wave heights and the increased asymmetry of the orbital velocities with decreasing water depth as the waves shoal over the ebb-tidal delta. The averaging process used to extract the mean tidal velocities from the observations for calibration and verification assumed that the wave orbital velocities were symmetrical (i.e. a zero residual wave-induced current). This assumption is only valid inside the Harbour (Station 390).

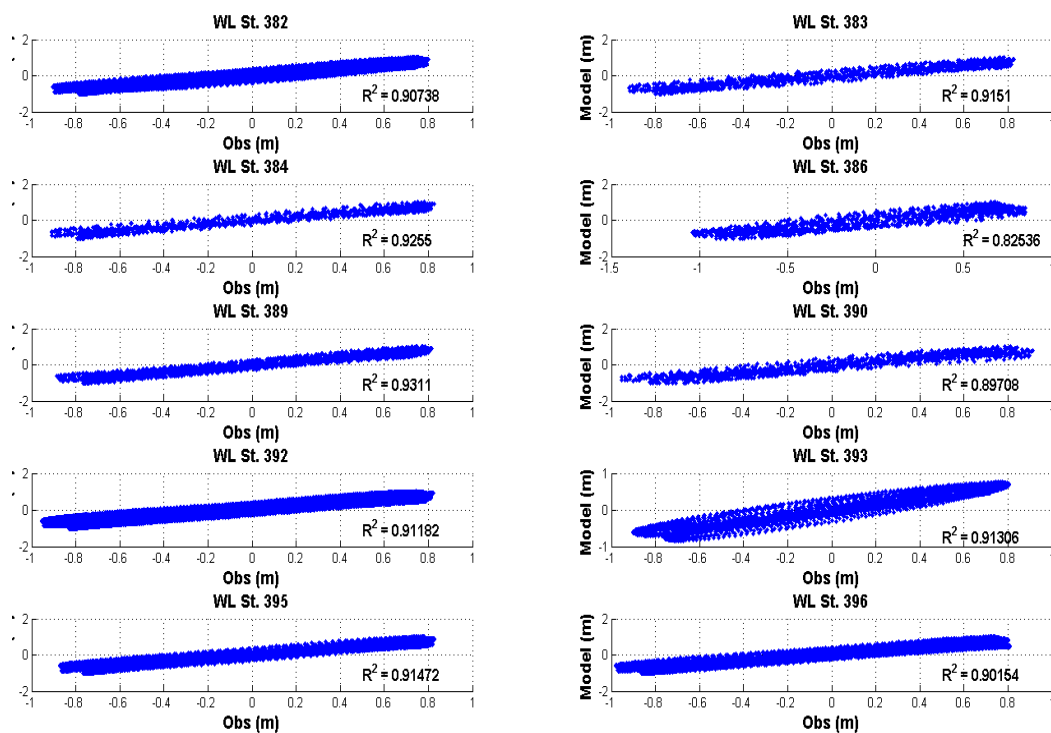


Figure 6-5. The correlation values (r^2) of the observed and modelled water level at each stations in the study area.

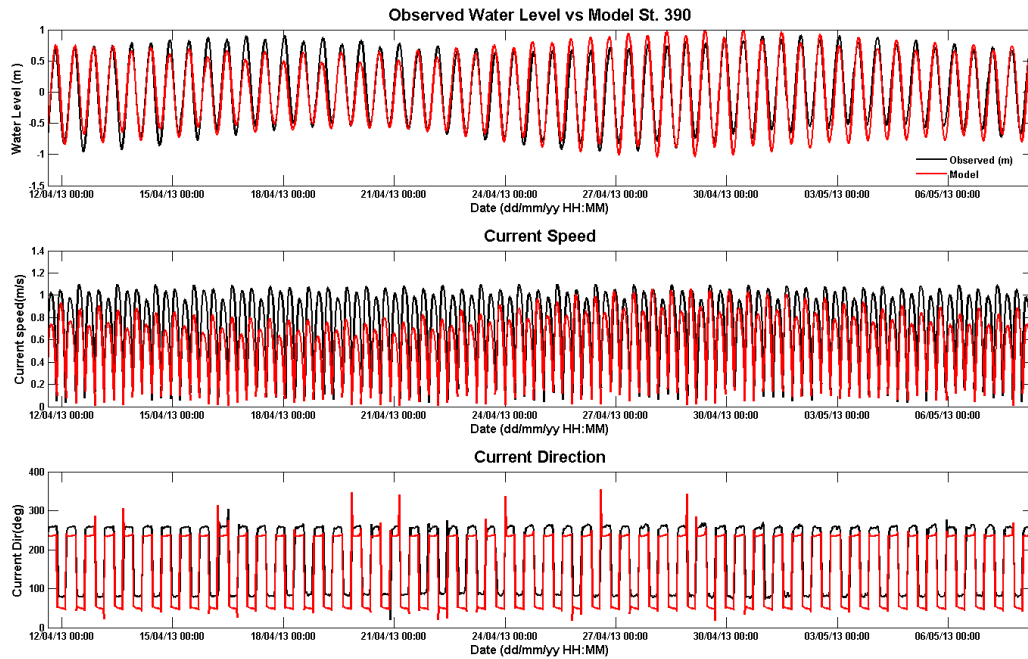


Figure 6-6. Time series of the observed and modelled water level, current magnitude and current direction at Station 390 inside the Harbour Entrance (Figure 6-7).

The model validation statistics for water levels for the ebb-tidal delta and adjacent areas are summarised in Table 6-7. Since the calibration for current speed and direction was obtained inside the harbour entrance, only the validation results for water level and current speed for Station 390 are summarized in Table 6-8.

The ME values for water levels indicate a tendency towards overestimation during spring tide and underestimation during neap tide. The corresponding MAE values are found to generally lie between 0.12 m to 0.20 m and 0.08 m to 0.23 m for spring and neap tide respectively. Field measurement at St. 390 (inside the Harbour) indicated that the mean tidal range for spring tide was around 1.62 m and 1.3 m during neap tide (see Chapter 5).

Inside the harbour, the modelled water level slightly overestimates the observation by 0.12 m during spring tide and underestimates the water level by about 0.13 m during neap tide. The MAE for depth averaged current speeds reveals that the model underestimates the observed speed by about 0.20 m/s during spring tide and by up to 0.29 m/s during neap tide. On the basis of average RMAE values, according to the standards proposed by Walstra *et al.* (2001) and van Rijn *et al.* (2002), the performance of the model for the current velocity inside the harbour is classified as being good to reasonable/fair. Along the Entrance Channel towards the offshore, the model seems to underestimate the current velocity, hence the model

performance classification for their RMAE values cannot be better than reasonable/fair (Walstra *et al.*, 2001 and van Rijn *et al.* 2002).

Table 4-7. Statistical parameters for measured and modelled water level for S4 stations on and near the ebb-tidal delta. Sp and Np denote for spring and neap tides respectively. The mean error (ME) and mean absolute error are defined in metres.

Statistical parameter	St. 384		St. 383		St. 386		St. 382		St. 396		St. 395		St. 393		St 392		St. 389	
	Sp	Np	Sp	Np	Sp	Np												
ME	0.01	-0.03	0.01	-0.04	0.13	-0.13	0.03	-0.03	0.07	-0.09	0.00	-0.02	0.02	-0.02	0.05	-0.05	0.001	-0.01
MAE	0.17	0.09	0.17	0.09	0.15	0.23	0.17	0.08	0.19	0.11	0.18	0.08	0.17	0.08	0.20	0.10	0.12	0.11
RMAE	0.32	0.21	0.31	0.21	0.27	0.53	0.32	0.20	0.35	0.25	0.34	0.20	0.33	0.19	0.35	0.22	0.24	0.26
r	0.95	0.98	0.95	0.98	0.98	0.86	0.95	0.98	0.94	0.98	0.94	0.98	0.94	0.98	0.94	0.98	0.97	0.96

Table 6-8. Statistical parameters for measured and modelled water level and current speed at Station 390 inside the harbour. RMAE and r are dimensionless.

Statistical parameter	Water level (m)		Current speed (m/s)	
	Spring	Neap	Spring	Neap
ME	0.01	-0.11	-0.19	-0.24
MAE	0.12	0.13	0.20	0.29
RMAE	0.24	0.31	0.27	0.39
r	0.97	0.96	0.94	0.69

6.4.3 Modelled Wave Conditions

To calibrate and verify the model’s ability to transform waves across the grid, 29-day records of half-hourly S4 wave measurements from nearshore areas and inside the harbour (Figure 6-7) were compared to the model results.

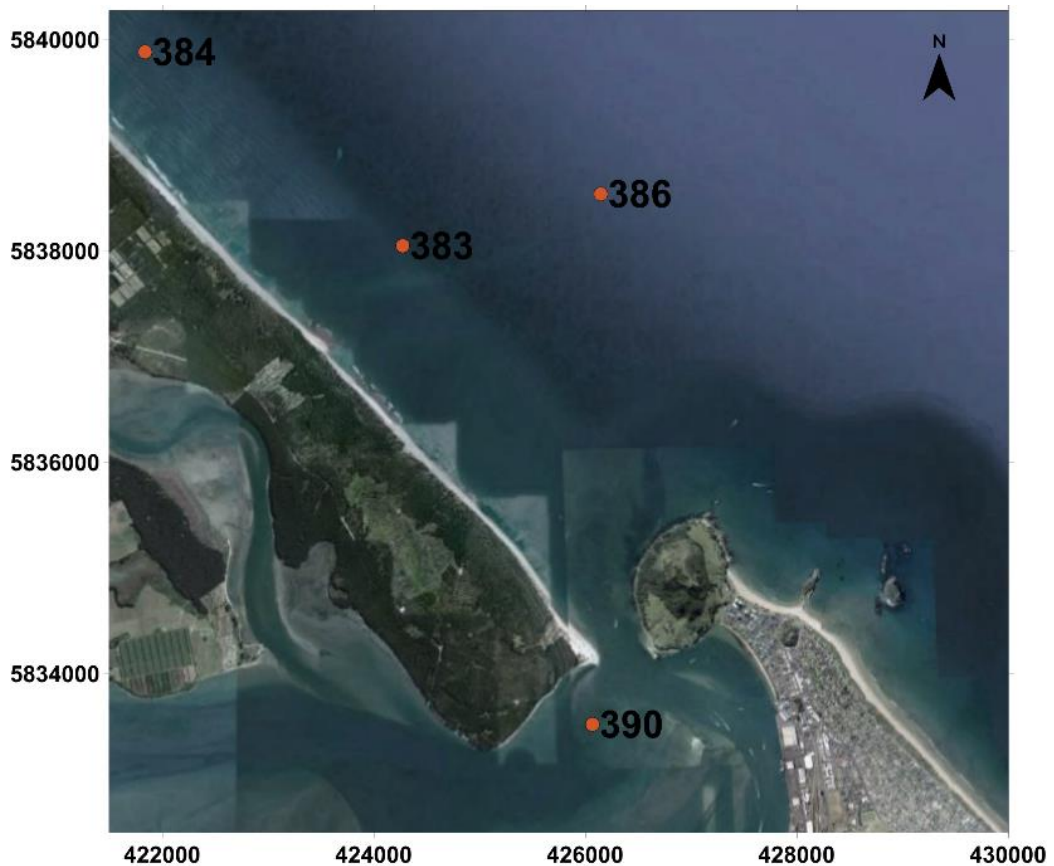


Figure 6-7. The locations of S4 deployments for measured wave data. These stations also recorded tidal elevations and current velocities.

The results of a comparison between predicted and measured wave heights, wave directions and periods, are shown in Figures 6-8, 6-9, 6-10 and 6-11.

As is evident from Figures 6-8 and 6-9, a fairly good correlation was obtained between the observed and modelled values for wave heights. The RMAE values for wave height within the nearshore area ranged between -0.06 to 0.18, which indicates that the model results may be rated as “Excellent to Good” according to the classification of van Rijn *et al.* (2002). The correlation is not as good at Station 390, with the model predicting more wave energy propagating into the Harbour than measured by the S4. Previous studies have found that the Harbour Entrance

significantly filters the incoming wind waves by frequency, predominantly removing longer period swell (de Lange and Healy, 1990). This can be seen in Figure 6-12, where there is a significant reduction in periods >8 s compared to the ebb-tidal delta. The model also predicts a high proportion of short period chop, which occur at periods too short to be measured by the S4 instruments used (< 3 s). This limitation of the instrumental data does not appear to be important outside the harbour (Figure 6-11).

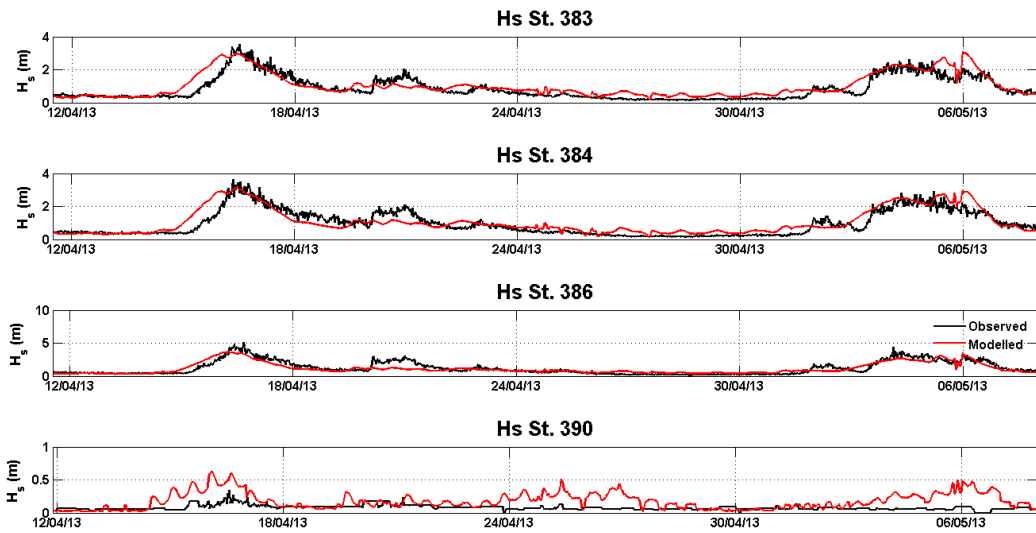


Figure 6-8. Predicted (modelled) wave height results and comparison with measured wave.

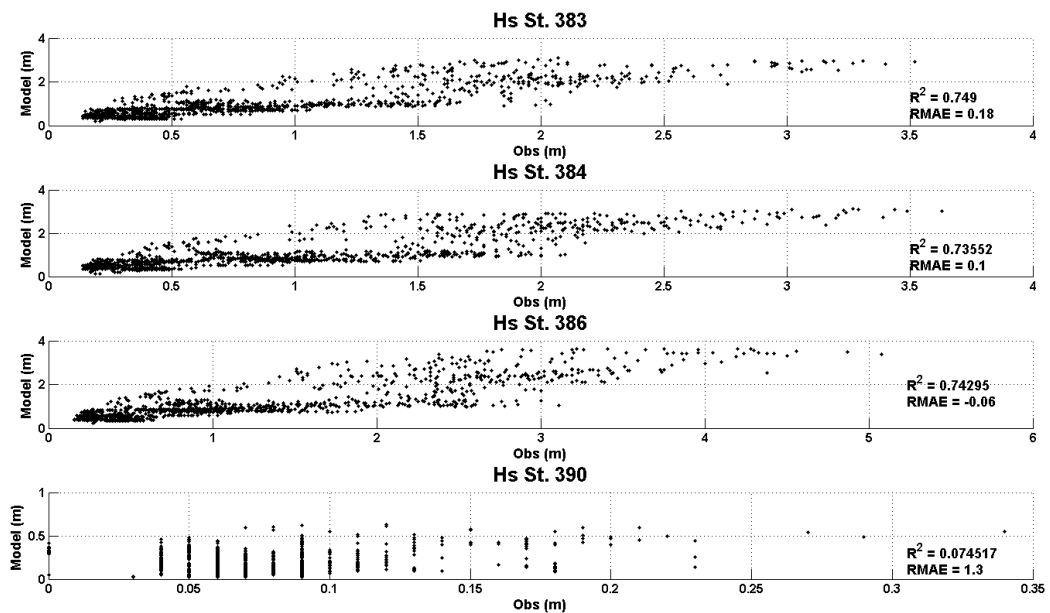
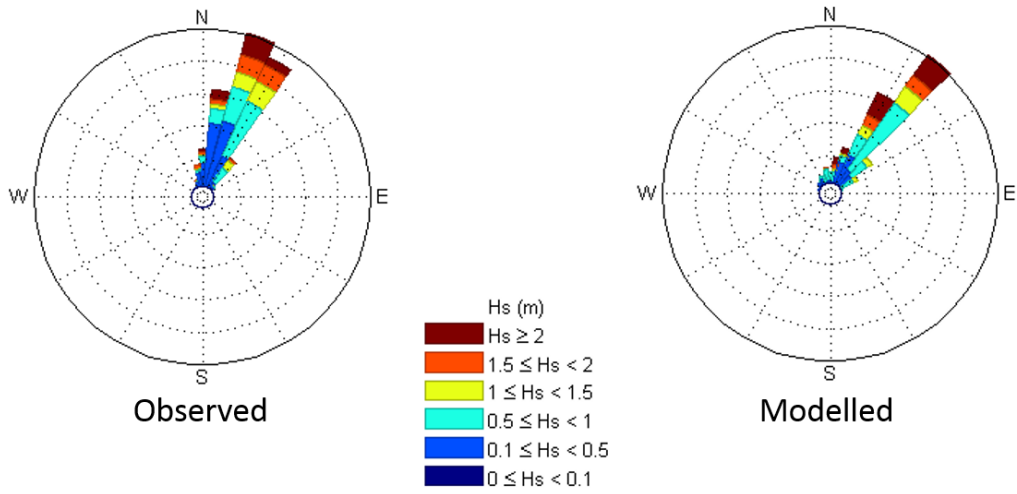


Figure 6-9. The R squared and RMAE values for predicted (modelled) and measured wave height.

Wave Rose St. 383



Wave Rose St. 384

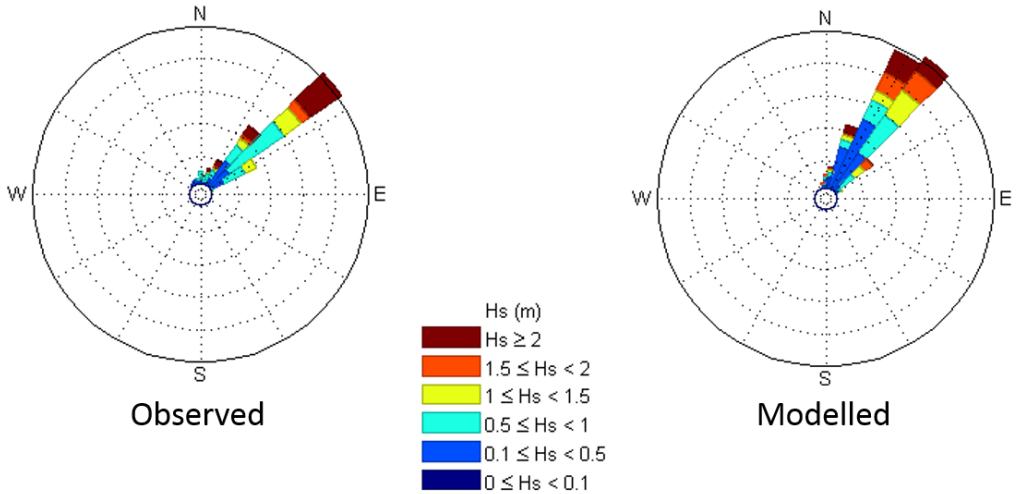
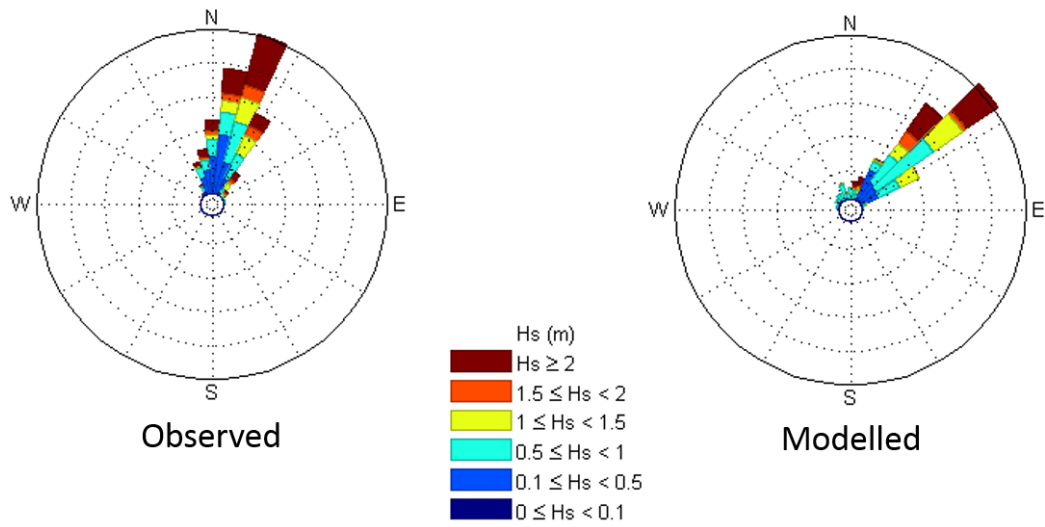


Figure 6-10. Wave roses of the observed and predicted wave directions and heights for the S4 stations in the nearshore area, northwest of the Entrance Channel.

Wave Rose St. 386



Wave Rose St. 390

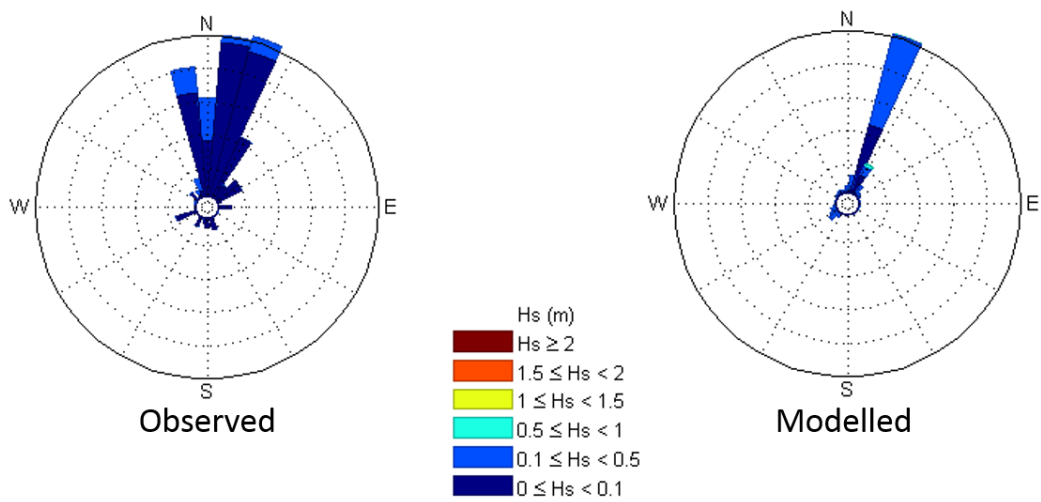


Figure 6-11. Wave roses of the observed and predicted wave directions and heights for the S4 stations in the offshore area (St. 386) and inside the harbour (St. 390)

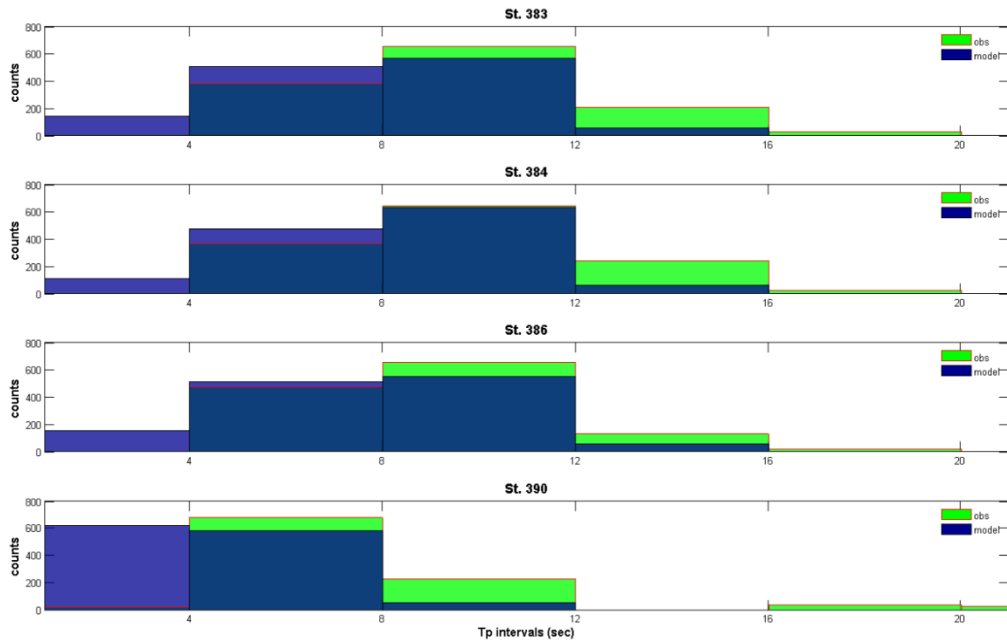


Figure 6-12. The observed and predicted wave periods. The dominant wave periods for near- and offshore areas lie between 8 s to 12 s.

The comparison of wave roses between measured and modelled wave directions and heights is presented in Figures 6-10 and 6-11. These indicate the modelled values fit well throughout the simulation period, and also indicates that the dominant wave approach direction is from NE and not more than 20% of wave incidents were from NW. Inside the harbour, the prominent wave directions were between 0° - 30° (NNE). The percentages were about 54% and 70% for measured and modelled respectively. The modelled waves shows narrower range of the main wave directions in between 0° – 60° . Summary for the frequency of significant wave heights (H_s) and wave directions in the study area is given in Appendix 7.

The dominant observed wave periods were between 8 s to 12 s for the ebb-tidal delta and offshore areas, which were replicated well by the model as shown in Figure 6-11. Inside the harbour long period waves > 16 s were observed. These long period waves occurred in about 25 % of the record, and they were attributed to seiching and these waves were not replicated by the model (Figure 6-12). Overall, both measurements and model predictions show the dominant wave periods in this area ranged from 4 s to 8 s.

6.4.4 Coupled Flow (Morph) – Wave Model

A comparison of sedimentation and erosion patterns between model results and observations was made, as well as volumetric analysis of the changes for several sub-domains, as an additional verification procedure (de Jongste et al., 2013; Nguyen *et al.*, 2010; Wilkens and Mayerle, 2005). Specifically, the morphodynamic predictions of the model were verified with a hindcast simulation for the period March to July 2013, which corresponded to the interval between two MBES surveys of the ebb-tidal delta (Chapter 4).

Overall, the observed and modelled sedimentation and erosion patterns around Matakana Banks ebb-tidal delta agree reasonably well (Figure 6-13). However, when comparing the magnitude of the predicted changes it is evident that the model underestimates sedimentation and erosion rates. Also, the model clearly demonstrated a tendency for flattening the sand bars on the swash platform and shifting the sediment shorewards. Hence, the model predicted accumulation of sediment along the shoreface (right panel, Figure 6-13), which are not evident in the measurements (left panel, Figure 6-13). The predicted accumulation predominantly occurred in shallow depths not included in the MBES surveys. Similar patterns of accretion of the shoreface and erosion of sand bars were evident in the longer-term morphological change analysis (Chapter 4). Therefore these differences can be neglected.

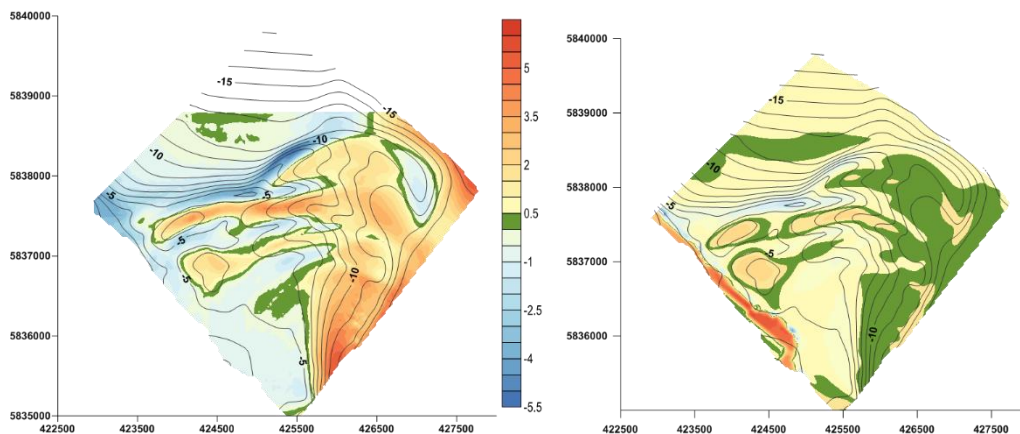


Figure 6-13. Observed (left) and modelled (right) sedimentation and erosion for Matakana Banks ebb-tidal delta over a 5 month period (March – July 2013).

The results of the volumetric calculations for the changes between the observed and modelled morphologies are displayed in Table 6-9. The volume

change for the Matakana Banks ebb-delta delta over the 5 months simulated indicates the model slightly overestimated the change by about 4%.

Table 6-9. Volumetric comparison between the observed and modelled of Matakana Banks ebb-tidal delta over a 5 month period.

<i>Methods</i>	<i>Observed (m³)</i>	<i>Modelled (m³)</i>
<i>Trapezoidal Rule</i>	70,952,557	73,887,688
<i>Simpson's Rule</i>	70,965,254	73,910,439
<i>Simpson's 3/8 Rule</i>	70,958,143	73,890,490
<i>Average volume</i>	70,958,651	73,896,206

Comparisons between the predicted and measured cross-shore profiles after 5 months (Figure 6-14), indicate that the predictions were better for deeper water and close to the Entrance Channel. The BSS between the observed and modelled morphology shows that the highest score of nearly 1 (excellent) is achieved adjacent to the Entrance Channel, and the BSS decreased to 0.3 (Reasonable/Fair) as the distance from the Entrance Channel increased (Table 6-10).

Table 6-10. Brier Skill Score.

	<i>BSS</i>					
<i>CS 1</i>	<i>CS 2</i>	<i>CS 3</i>	<i>CS 4</i>	<i>CS 5</i>	<i>CS 6</i>	<i>CS 7</i>
<i>0.99</i>	0.66	0.65	0.73	0.4	0.4	0.3
<i>Excellent</i>	Good	Good	Good	Reasonable/Fair	Reasonable/Fair	Reasonable/Fair

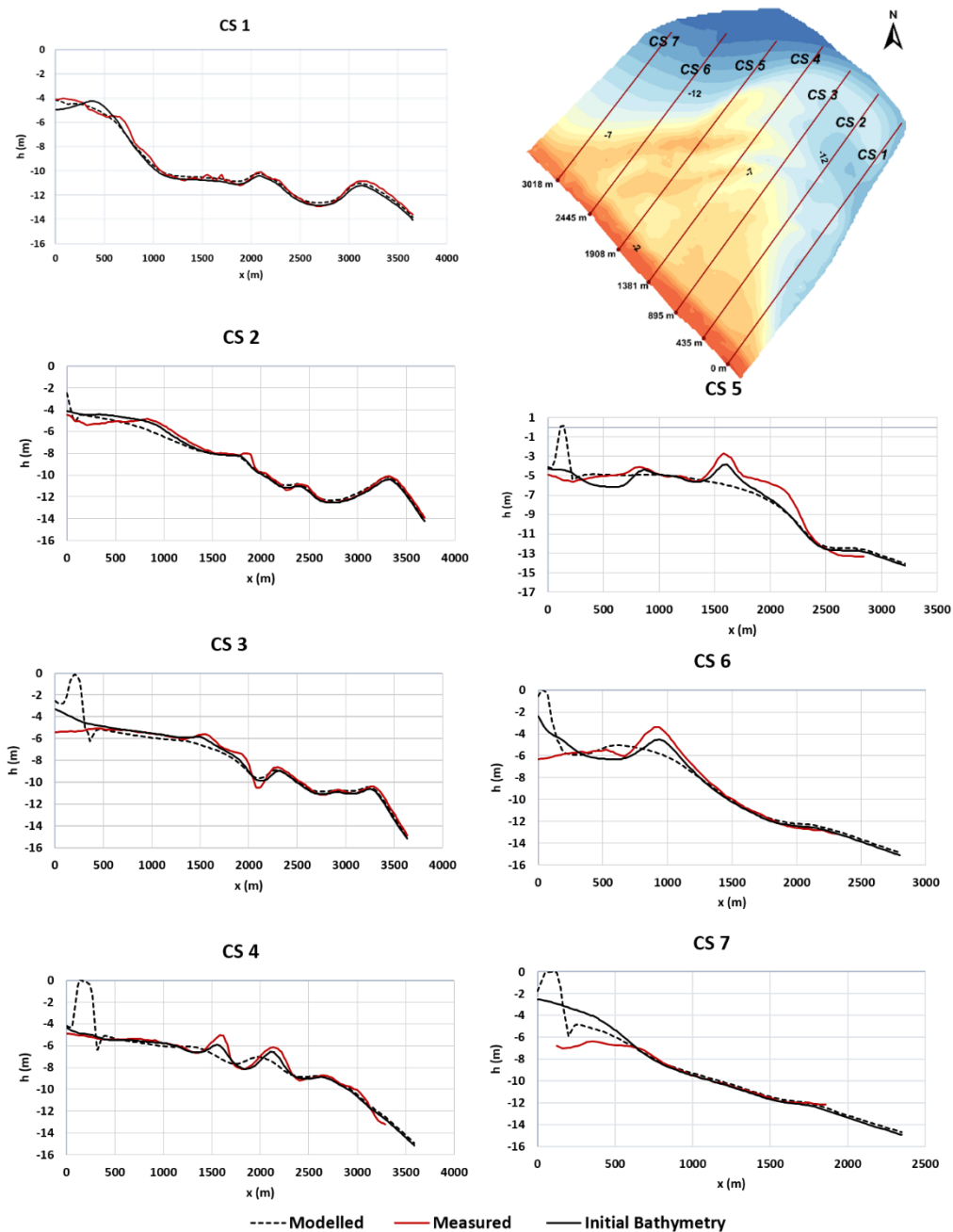


Figure 6-14. Comparison of the coupled Wave-Flow Morph model results with the measured bathymetry for 5 months morphological updating. The black line indicates the initial bathymetry (depth in metres), dashed line and red line indicate the modelled and measured bathymetry.

6.5 Summary/Discussion

The predictive capability of the two-dimensional depth-averaged Deflt3D-FLOW model was assessed by comparing model predictions with 29 days of hydrodynamic data obtained by field measurements in April – May 2013. Overall the predictions were in good agreement with the observations. The water levels were reproduced well by the model, yielding correlation coefficients, r , that ranged

from 0.94 to 0.98. It was found that the predictive capability of the model for current velocities was the best inside the harbour, where wave influences were minimal. The current velocity predictions were also reasonably good, with some underestimation of the current speeds, along the Entrance Channel where tidal flows are dominant.

Sensitivity tests of the Delft3D-WAVE model were done to assess the effect of different methods for specifying the wave conditions at the boundaries (not presented here). It was found that using time-series of wave data at the boundaries in conjunction with a time series of wind data produced a better agreement with the measured waves over the ebb-tidal delta than using single values of averaged wave and wind as the forcing. Wave measurements obtained over the delta and offshore were well reproduced by the model. The RMAE values for wave heights ranged between -0.06 to 0.18 indicating that the model results may be rated as “Excellent to Good” (van Rijn *et al.*, 2002). As the waves enter the tidal inlet, the wave heights significantly decreased to <0.5 m. However, the model still overestimated the wave heights at Station 390 inside the harbour. This probably occurs due to the model not replicating the wave filtering that occurs at the Harbour Entrance. The predicted wave direction is generally consistent with measured data outside the harbour. However, inside the harbour the hindcast wave directions were more focused than the measurement (a narrower range of directions).

Calibration and validation for the morphological model (coupled WAVE-FLOW Morph model) were undertaken for a 5 month simulation by comparing the cross-shore profiles along the ebb-tidal delta, erosion and sedimentation patterns, overall volumetric change, and by the model’s Brier Skill Score (BSS). The best agreement occurs adjacent to the tidal inlet with a BSS close to 1, corresponding to the region where the best calibration for hydrodynamic model was also achieved. This suggests the model is replicating tidal driven sediment transport well. Further from the Entrance Channel in areas dominated by shoaling and breaking waves, the agreement is not as good. However, the model did predict a shoreward movement of sediment from the sand bars to the shoreface, which was identified by the comparisons of long-term SBES survey data. This was not evident in the 5 month MBES survey comparison, probably because the MBES surveys did not fully measure the shallows close to the shore. Overall the model results indicates that

increasing sediment accumulation within the study area is inversely proportional to the magnitude of tidal influence (tidal current velocities).

In conclusion, after a comparison of the model predictions with the observations, it is evident that the Delft3D model is capable of simulating the hydrodynamic and morphological changes for the Matakana Banks ebb-tidal delta. However, the predictions are not uniformly reliable over the entire area. This is not surprising given that different hydrodynamic forcing processes appear to dominate in different areas as discussed previously in relation to the long-term morphological changes determined from SBES data.

6.6 References

- Badesab, F., von Dobeneck, T., Bryan, K.R., Müller, H., Briggs, R.M., Frederichs, T., and Kwohl, E. (2012). Formation of magnetite-enriched zones in and offshore of a mesotidal estuarine lagoon: An environmental magnetic study of Tauranga Harbour and Bay of Plenty, New Zealand. *Geochemistry, Geophysics and Geosystems*, 13(6).
- Beck, T.M., and Wang, P. (2009). Influences of channel dredging on flow and sedimentation patterns at microtidal inlets, West-Central Florida, USA. *Coastal Dynamics*, Paper No. 98, 1-15.
- de Jongste, L., Dusseljee, D., Smit, M., and Jansen, M. (2013). Morphological impact on ebb-tidal delta of reintroducing tide in a former estuary. *Coastal Dynamic*, 465-476.
- de Lange, W.P., and Healy, T. (1990). Wave spectra for a shallow meso-tidal estuarine lagoon: Bay of Plenty, New Zealand. *Journal of Coastal Research*, 189-199.
- Deltares. (2011). *Delft3D-WAVE Simulation of short-crested waves with SWAN. User Manual*. Delft, The Netherlands: Deltares.
- Deltares. (2013). *Delft3D-FLOW Manual: Simulation of multi-dimensional hydrodynamic flows and transport phenomena, including sediments. User Manual, Hydro-Morphodynamics*. Delft, The Netherlands: Deltares.
- Deltares. (2013). *Delft3D-FLOW Simulation of multi-dimensional hydrodynamic flows and transport phenomena, including sediments. User Manual, Hydro-Morphodynamics*. Delft, The Netherlands: Deltares.

- Elias, E.P.L., Cleveringa, J., Buijsman, M.C., Roelvink, J.A., and Stive, M.J.F. (2006). Field and model data analysis of sand transport patterns in Texel Tidal Inlet (the Netherlands). *Coastal Engineering* Vol. 53, 505-529.
- Forester, C. (1979). Higher order monotonic convective difference schemes. *Journal of Computational Physics*, Vol. 23, 1-22.
- Giardano, A., van der Werf, J., and van Ormondt, M. (2010). *Simulating Coastal Morphodynamics with Delft3D: case study Egmond aan Zee*. Delft, The Netherlands: Deltares Delft Hydraulics.
- Hosseini, S.M., and Coonrod, J. (2011). Coupling numerical and physical modeling for analysis of flow in a diversion structure with Coanda-effect screens. *Water*, Vol. 3, , 764-786.
- Kwoll, E. (2010). *Evaluation of the Tauranga Harbour numerical model*, Master Thesis MSc Programme Marine Geosciences. Bremen, Germany: University of Bremen.
- Lesser, G. (2009). *An Approach to Medium-term Coastal Morphological Modelling*. A PhD Dissertation. Delft, The Netherlands: CRC Press/Balkema.
- Murphy, A.H., Epstein, E.S. (1989). Skill scores and correlation coefficients in model verification. *Monthly Weather Review* 117., 572-581.
- Nguyen, D., Etri, T., Runte, K-H., and Mayerle, R. (2010). Morphodynamic modeling of the medium-term migration of a tidal channel using process-based model. *Coastal Engineering*, 1-13.
- NIWA. (2013). *Tide Forcaster*. Retrieved from NIWA Taihoro Nukurangi: <http://www.niwa.co.nz/services/online-services/tide-forecaster>
- Palacio, C., Mayerle, R., Toro, M., and Jimenez, N. (2005). Modelling of flow in a tidal flat area in the south-eastern German Bight. *Die Küste*, 69 PROMORPH, 141-174.
- Pawlowicz, R., Beardsley, B., and Lentz, S. (2002). Classical tidal harmonic analysis including error estimates in MATLAB using T_TIDE. *Computers & Geosciences* , 28(8), 929 - 937.
- Peet, A.H., Sutherland, J., Soulsby, R.L. (2002). *Skill assessment in coastal models*. HR Wallingford.
- Port of Tauranga Ltd. (2013). *Maintenance Dredging-Spoil Disposal Sites*. Tauranga, New Zealand: Port of Tauranga Ltd.
- Ruggiero, P., Walstra, D.J.R., Gelfenbaum, G., and van Ormondt, M. (2009). Seasonal-scale nearshore morphological evolution: Field Observations and numerical modeling. *Coastal Engineering*, Vol. 56, Issue 11-12, 1153-1172.

- Sha, L. (1989). Cyclic morphologic changes on the ebb-tidal delta, Texel inlet, the Netherlands. *Geology en Mijnbouw* 68, 35-48.
- Soulsby, R. (1997). *Dynamic of marine sands, a manual for practical applications*. Thomas Telford Publications, 294p.
- Stelling, G. (1984). On the construction of computational methods for shallow water flow problems. Technical Report. The Netherlands: Rijkswaterstaat.
- Stelling, G. (1984). On the construction of computational methods for shallow water flow problems. Technical Report. . The Netherlands: Rijkswaterstaat.
- Stelling, G.S., Wiersma, A.K., and Willemse, J.B.T. (1986). Practical aspects of accurate tidal computations. *Journal of Hydraulic Engineering*, Vol. 112 (9), 802-817.
- Tonnon, P.K., van Rijn, L.C., and Walstra, D.J.R. (2007). The morphodynamic modelling of tidal sand waves on the shoreface. *Coastal Engineering* Vol. 54, 279-296.
- van Rijn, L.C., and Walstra, D.J.R. (2003). *Modelling of Sand Transport in DELFT3D-ONLINE*. Netherlands: WL Delft Hydraulics.
- van Rijn, L.C., and Walstra, D.J.R. (2003). *Morphology of pits, channels and trenches; Part I: Literature Review and Study Approach*. Delft, The Netherlands: WL Delft Hydraulics report z3223.
- van Rijn, L.C., Walstra, D.J.R., Grasmeijer, B., Sutherland, J., Pan, S, and Sierra, J.P. (2002). *Simulation of Nearshore Hydrodynamics and Morphodynamics on the Time Scale of Storms and Seasons using Process-Based Profile Models*. In *The behaviour of a straight sandy coast on the time scale of storms and seasons: Process Knowledge and Guidelines for Coastal Management: End Document March 2002*. EC. MAST Project, MAS3-CT97-0086. COAST3D-EGMOND.
- van Rijn, L.C., Walstra, D.J.R., van Ormondt, M. (2004). *Description of TRANSPOR2004 and implementation in DELFT3D-ONLINE: final report*. WL | Delft Hydraulics report Z3748.10. Delft, The Netherlands.
- Walstra, D.J.R., van Rijn, L., Blogg, H., and van Ormondt, M. (2001). *Evaluation of a Hydrodynamic Area Model Based on the COAST3D Data at Teignmouth 1999*. Paper D4 of COAST3D Final Volume of Summary Papers. Report TR121. UK: HR Wallingford.
- Walton, T.L., and Adams, W.D. (1976). *Capacity of inlet outer bars to store sand*. Proceedings 15th Coastal Engineering Conference (pp. 1919-1937). Reston, Virginia: ASCE Press.
- Wilkens, J., and Mayerle, R. (2005). *Morphodynamic response to natural and anthropogenic influences in the Dithmarschen Bight*. *Die Küste* 69 PROMORPH, 311-337.

Winter, C. (2007). On the evaluation of sediment transport models in tidal environments. *Sedimentary Geology*, 202, 562-571.

Chapter 7. Simulation of Dredging and Spoil Disposal Impacts

7.1 Introduction

Within this chapter, the methodology that was used for predicting the impacts of channel dredging and dumping activities on the stability of an ebb-tidal delta is presented. Following the calibration and validation of the main numerical modelling components (tidal hydrodynamics, wave hydrodynamics, and morphological evolution), the impacts of dredging and proposed alternative spoil disposal sites were investigated via model simulations. The objectives of this chapter were:

1. To simulate the dominant physical processes responsible for the sediment transport and sediment deposition/erosion on the Matakana Banks ebb-tidal delta.
2. To identify and explain the effects of channel dredging and spoil disposal on sediment transport patterns and sediment deposition/erosion before and after the capital dredging in 1967 and 1992, and in response to the capital dredging programme that began in October 2015.
3. To investigate the short-term response of the ebb-tidal delta to maintenance dredging wave conditions.
4. To assess alternative sites for spoil disposal placement to minimise impacts on future maintenance dredging and mitigate any negative impacts from capital and maintenance dredging on Matakana Banks ebb-tidal delta.

7.2 Model Set-Up

7.2.1 Model Input

The calibrated hydrodynamic model (Delft3D-FLOW) coupled with the wave model (Delft3D-WAVE) were used to simulate sediment transport over the ebb-tidal delta before and after the Entrance Channel was formed during the 1967 Capital Dredging Programme. The four open boundaries were forced by tidal

elevations obtained from the NIWA online tide forecaster (NIWA, 2013) for 29 days from 10 April to 8 May 1967 (Appendix 8). The predominant wave direction over the area was assumed to be between NE and E as observed by this study in 2013. To evaluate the significance of storms on the morphodynamics of the ebb-tidal delta, a comparison between averaged wave heights and wave conditions with storm events over 2-year periods was also undertaken.

The initial bathymetry of the 1967 model was digitized from hydrographic chart NZ 5412 (published in 1966) in UTM 60S coordinates. The post capital dredging bathymetry was derived from the 2013 MBES surveys (Ramli and de Lange, 2013a) and the areas not covered by MBES were digitized from hydrographic charts NZ 5411 and NZ 5412 (published in 2004). This bathymetry was chosen because it included all of the cumulative changes caused by dredging and disposal (DaD) since 1967.

The sediment dredged since 1967 has consisted mainly of marine shelly and gravelly sands with only minor amounts (<5%) of silts and clays (Healy *et al.*, 1991a). For the purposes of this study, a single sediment grain size of 632 μm was used. This corresponds to coarse sand, and was found to account for the effects of sediment availability for the mixtures of grain sizes present during the model calibration (Chapter 6).

Table 7-1 summarizes the maintenance dredging volumes and textural types for each of dredging areas around Tauranga Harbour in 2013 (Johnstone, 2013, *personal communication*), and it indicates the typical pattern of sediment types dredged. Identification of sediment distribution on the dredged areas was done for the decision in choosing the adequate disposal site based on the dredged sediment characteristics. Material or sediment from the Entrance Channel is dumped to the site B and C, the inner harbour sand to the D site, and silty material from Stella Passage to site G. If some material from the Entrance Channel contains high shell fragments, then it is dumped in site D (Figure 7-2) (Johnstone, 2013, *personal communication*).

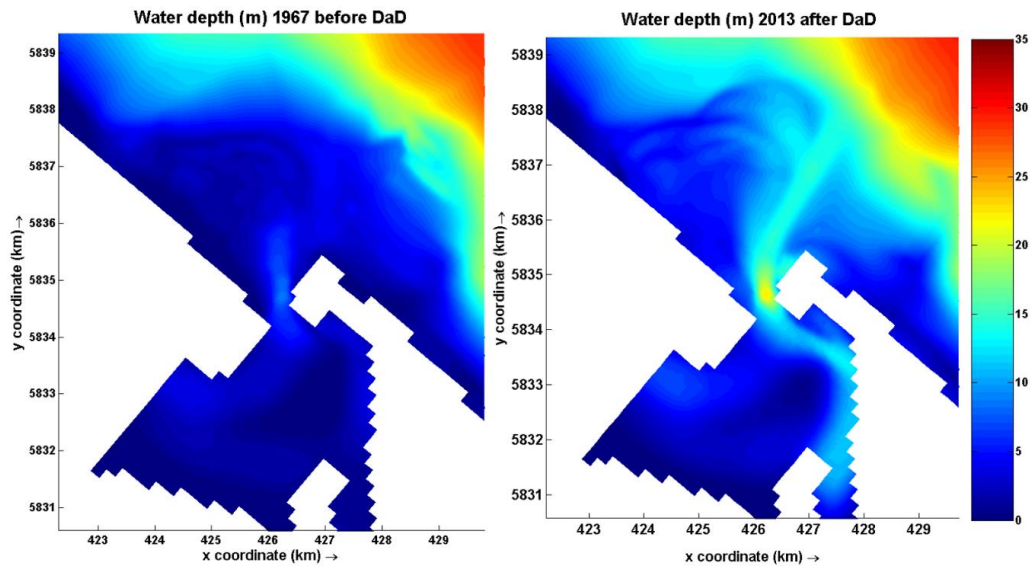


Figure 7-1. Matakana Banks ebb-tidal delta model bathymetries: before the first capital dredging in 1967 (left) and in 2013 after two capital dredging programmes (DaD = Dredging and Disposal).

Table 7-1. Summary of sediment types and volumes for different locations for the 2013 maintenance dredging by the Port of Tauranga (Johnstone, 2013, personal communication).

<i>Dredging areas</i>	<i>Material description</i>	<i>Volume (m³)</i>
<i>Entrance Channel</i>	Coarse sand and shell	120,211
<i>No 2 Reach</i>	Shell and sand	17,890
<i>Cutter Channel</i>	Sand and shell	N/A
<i>Maunganui Roads</i>	Sand and shell	27,978
<i>Stella Passage</i>	Silt and sand	27,678
<i>Total</i>		193,757

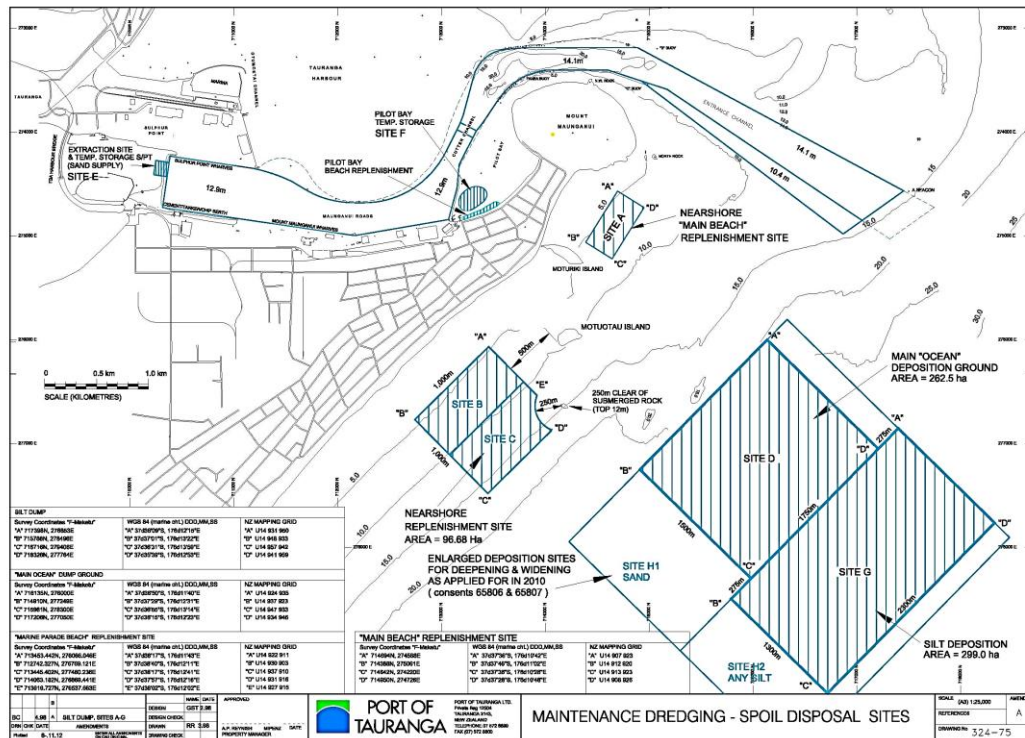


Figure 7-2. Spoil disposal sites for materials dredged from around the Tauranga Harbour. The map was provided by Tauranga Harbour, Ltd. (2013).

7.2.2 Morphological model setup

Ultimately, the main modelling objective of this study was to reproduce the observed morphological changes and predict future changes. Even though the real world morphological changes are determined by more complex processes than a numerical model can replicate, it is generally assumed that the simplifications required to produce a model do not significantly affect the results. A comparison between computed (modelled) and measured morphological changes helps to understand the accuracy of the model and therefore to what extent its' morphological predictions can be relied upon (Lesser, 2009).

A coupled model incorporating the morphological module (*morfac*) was calibrated and verified for the Matakana Banks region (Chapter 6). In order to predict morphological changes as a result of maintenance dredging, a *morfac* value of 60 was used to simulate 12-day periods, including a spring tide and a neap tide.

7.2.3 Alternative spoil disposal sites

Alternative spoil disposal sites were assessed in order to minimise the cumulative impact of the dredge and spoil disposal activities on the Matakana Banks ebb tidal delta. In particular, potential sites that could be used to mitigate any adverse impacts of the 2015-16 Capital Dredging Programme were evaluated.

The major aim of the New Zealand National Policy on the Sea Disposal of Waste, as outlined by the Marine Pollution Prevention document, is to encourage the establishment of ‘designated’ disposal sites especially in areas where the submission of multiple applications for disposal is likely (in Flaim, 2012). The primary advantage of having one designated site for disposal of dredged material is that the potential effects caused by disposal operations will be confined to specific areas. Further, disposal sites used by the Port of Tauranga have also functioned to supply sediments to renourish beaches. Concerns raised in the Environment Court about the potential collapse of the ebb tidal delta causing accelerated erosion of Matakana Island, led to a requirement to consider the use of designated disposal sites to renourish the ebb tidal delta. This study was established to identify sites that could supply sediment to the delta without significantly increasing maintenance dredging requirements.

Current spoil disposal sites used by the Port of Tauranga that supply sediment to the shore are located to the east of the Entrance Channel (Figure 7-2); the nearshore site B/C is at depth 5 m to 15 m SE Motuotau Island and site D is at depth 20 m to 30 m offshore. Most of the dredged material from inside the harbour is deposited at site D and site B/C is for the dredged material from the Entrance Channel (Johnstone, 2013, personal communication). In the model, all spoil disposal areas were set to maintain a minimum depth (water depth over the disposal mound) of 5 m. Further, once the spoil material was deposited at a disposal site, it was distributed to the deeper regions first.

There were 3 alternative spoil disposal sites for mitigating potential adverse effects of the 2015-2016 capital dredging considered in this study (Figure 7-3):

- a. Site TL is located at about 4,000 m from shoreline, offshore from the terminal lobe to the north-northeast of the Entrance Channel, at water depths > 20 m;

- b. Site New is located 1,700 m – 2,700 m from the shoreline, northeast of the ebb-tidal delta, at water depths between 10 m – 14 m; and
- c. Site NS is located the closest to Matakana Island, at about 500 m -1400 m from the shoreline, at depth 6 m – 8 m.

For all the simulations of alternative sites, it was assumed that the total volume of dredged material was dumped in the designated site at once, instead of in smaller increments. It was also assumed the locations dredged during maintenance dredging remained the same as during the last decade of port operations. The results are given later in this Chapter.

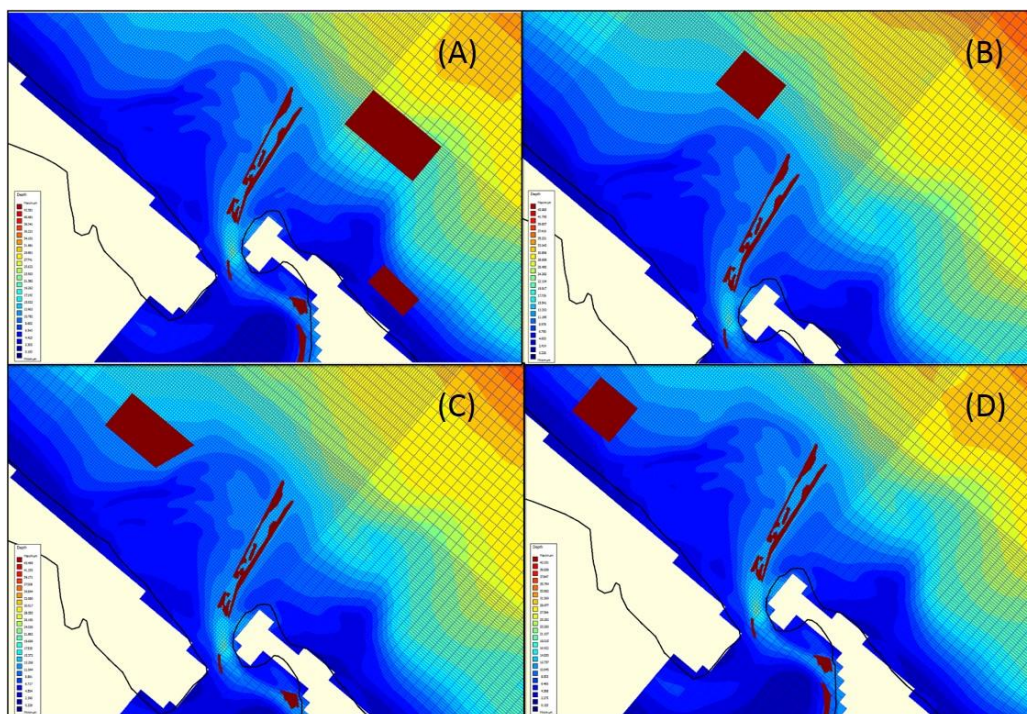


Figure 7-3. Existing and alternative spoil disposal sites modelled by this study. (A) Sites Act are the existing main spoil disposal sites B+C, and D+G+H1+H2 used by the Port of Tauranga (Figure 7-2), (B) Site TL is located near the outermost terminal lobe, (C) Site New is located at about 1,700 m from the shoreline to the west of the delta, and (D) Site NS is located closest to the shore to the west of the delta.

7.3 Results and Discussion

7.3.1 Hydrodynamic and sediment transport under interaction of tides and waves

The spatial extent of tidal current and wave influences over the ebb-tidal delta were simulated using coupled hydrodynamic and wave models. Spiers, *et al.*, (2009) previously observed that the maximum extent of the ebb-jet at the Tauranga Harbour Entrance is ~ 3.5 km seaward the inlet throat, which agrees with the MBES results (Chapter 4) and this was also evident in the hydrodynamic model used by this study.

Net sediment movement in tidal inlets depends on the relative magnitudes of the tidal currents, with the direction of the sediment movement governed by whether the current is associated with the flood or ebb tide (Komar, 1996). A measure of the relative current is the residual current derived by summing the tidal velocity vectors over a specified full or half tidal cycle (Cheng, 1990). Another way to consider the influence of currents on sediment transport is to assess the maximum sediment flux (transport rates) during ebb and flood tides.

Comparing the ebb and flood peak currents indicates that the ebb residual currents are stronger than flood residual currents, which indicates that the Tauranga Harbour Entrance is ebb dominant. Inside the harbour (station 390 – Lower Western Channel), modelled peak ebb currents are around 0.88 m/s and 0.76 m/s during spring and neap tide respectively. Whereas the flood currents are slightly weaker at around 0.75 m/s and 0.70 m/s (Figure 7-4).

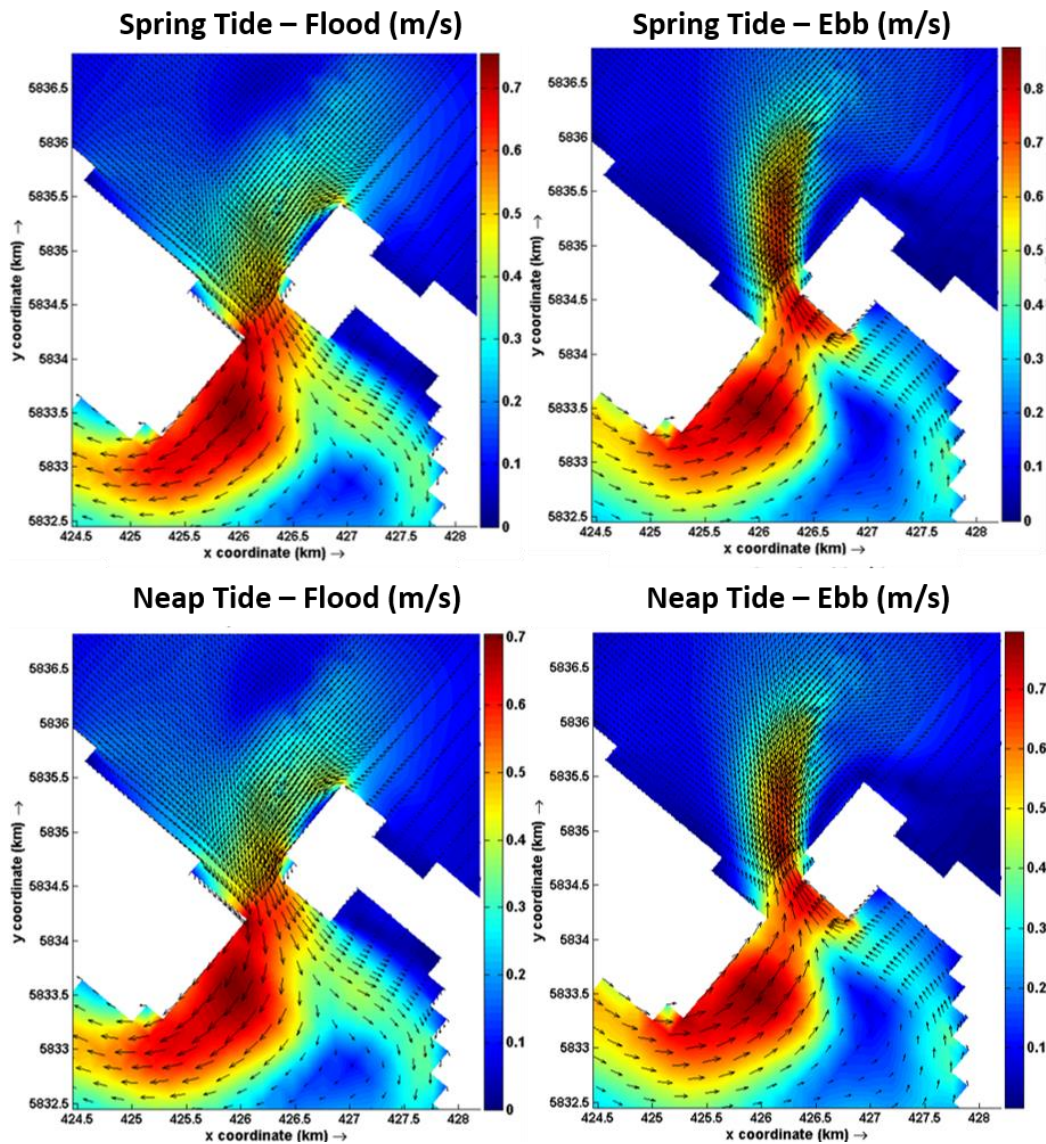


Figure 7-4. Peak current speed during the tidal cycle of spring (upper panels) and neap tides (lower panels). Stronger ebb currents indicates that the Tauranga Harbour is ebb-dominant. Both tide phases show stronger currents in Lower Western Channel than in Cutter Channel. Current speed was taken from Sta. 390 inside the Harbour. The colour shades indicate the current magnitude and the vectors (arrows) indicate the corresponding tidal current velocities.

Spiers (2013) indicated that an increase in residual currents on the eastern side of the ebb-jet results from the dredging, which reoriented the jet towards the east. Further, it was suggested that there was a reduction in the residual current speed over the northwestern part of the ebb-tidal delta due to the reduction in ebb-jet velocities induced by widening and deepening the Entrance Channel and the resultant realignment of the jet. However, the model used by Spiers was mainly validated using a 3-day long dataset combined with an 11 hour ADCP survey, and

the instruments were deployed predominantly on the eastern side of the ebb-tidal delta.

This study used a longer verification period covering a spring-neap cycle, and a larger spatial distribution of observations. The results of the modelled net current in this study didn't clearly show the reduction inferred by Spiers (2013). Instead they showed that the net current varies over the spring-neap tidal cycle. Figure 7-5 shows the net current (residual current) during the tidal cycle in spring (left panel) and neap (right panel) tides. It is seen that during neap tide, the ebb-currents were dominant inside the harbour, so that sediment is more likely to be exported from within the harbour onto the ebb-tidal delta. In contrast, during spring tide sediment from the ebb-tidal delta and shoreface were more likely to be transported into the harbour.

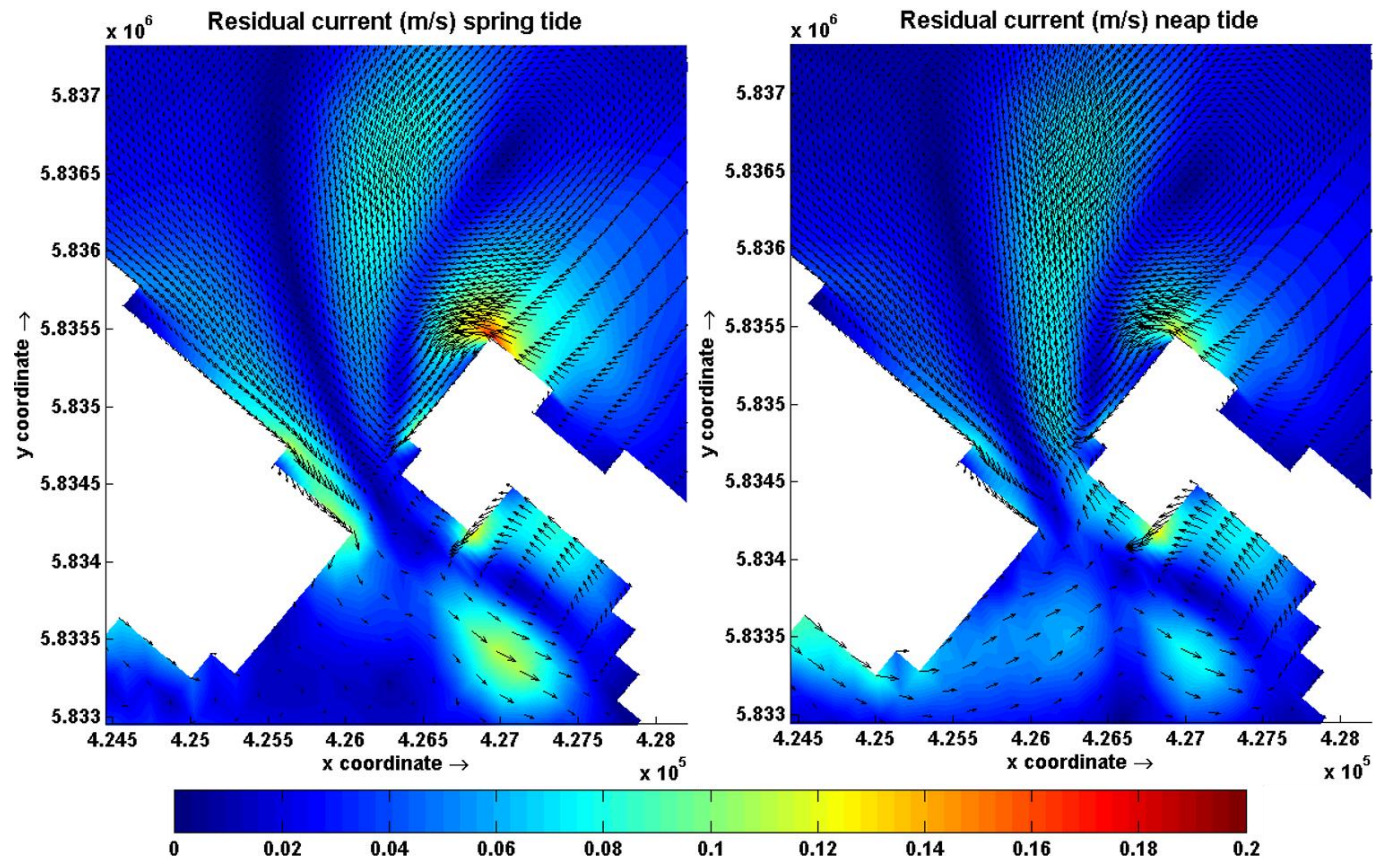


Figure 7-5. Computed residual current during spring and neap tides. It is shown that ebb currents were stronger than flood current and more sediment was transported offshore from the harbour during neap tide than in spring tide. Flood currents were deflected by the stronger ebb-jet back to offshore in the same path with ebb jets along the Entrance Channel. The model was simulated with tidal force only. The colour shades indicate the current magnitude and the vectors (arrows) indicate the corresponding residual tidal current velocities.

Figures 7-6 to 7-7 show the computed maximum sediment transport rates due to tidal forcing during two successive spring (Figure 7-6) and neap (Figure 7-7) ebb and flood half-tidal cycles. These indicate the maximum tidal residual currents that are responsible for the highest total sediment transport and associated patterns of sediment movement around the Entrance Channel and SE Matakana Banks. The predicted total tidal sediment transport was lower than $2.0 \times 10^{-16} \text{ m}^3/\text{s}/\text{m}$ during both spring and neap.

The maximum total sediment transport rates in Figures 7-6 and 7-7 do not include any wave influence. The Entrance Channel and adjacent deeper areas of the ebb-tidal delta are clearly influenced by the tidal currents, which is indicated by the bathymetric contour lines migrating landward during flood and vice versa during ebb tide on the NE terminal lobe, swash platform and to the SE of the Entrance Channel. The ebb current is the strongest along both sides of the Entrance Channel, as the ebb jet expands from the inlet throat towards the offshore margin of the delta. When the ebb jet reached the distal delta, close to the NE terminal lobe, its' velocity decreased, and a clockwise eddy was established, which is responsible for high sediment transport rates SE of Matakana Banks, as identified by Spiers (2013). High rates of sediment transport are also associated with strong tidal currents in the Lower Western Channel within the harbour during both ebb and flood.

When the tide is flooding, sediment is entrained from the swash platform, along the shoreface adjacent to the tidal inlet, both sides of the Entrance Channel and from the NE terminal lobe. However, less sediment is available to the east of the Entrance Channel, limiting sediment transport there. This sediment is transported into the harbour, and deposited on the flood tidal delta (Centre Bank) inside the harbour is indicated by low tidal current velocities and sediment transport rates (Figure 7-6). Around the margins of the Centre Bank, the tidal current velocities are sufficient to entrain sediments along the Cutter Channel, and parts of the Maunganui Roads and Otumoetai Channels.

Inside the harbour (Figure 7-6), high sediment transport rates were concentrated on the SE side of Matakana Island along the Lower Western Channel (LWC). Less sediment transport occurred in the Maunganui Roads and Cutter Channels, particularly during ebb tide when the currents were weaker. During neap

tide, the flood current is able to transport the sediment over the swash platform toward the harbour (Figure 7-7, lower left panel), while the ebb current transported the sediment only around the Entrance Channel.

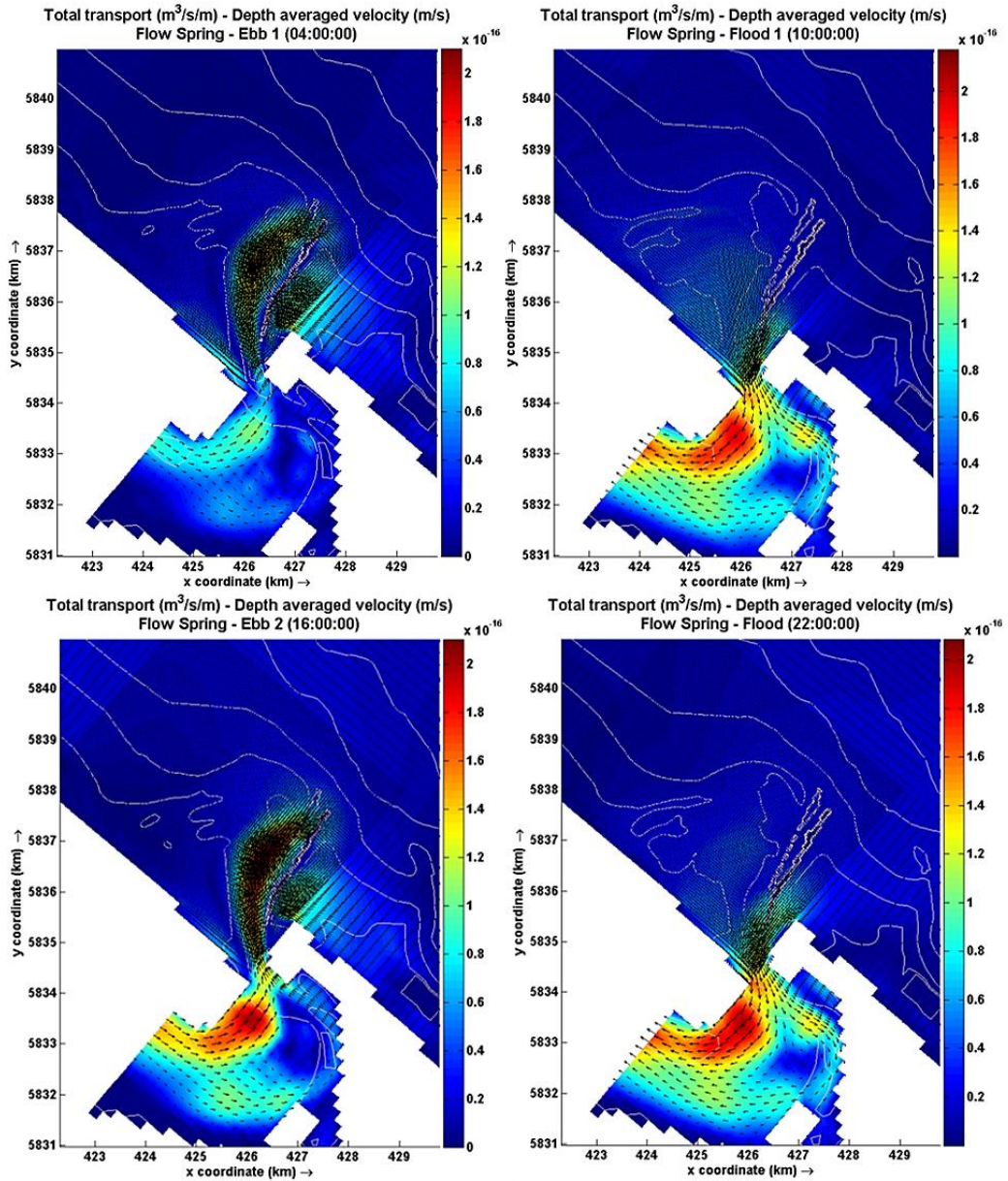


Figure 7-6. The maximum sediment transport rate ($m^3/s/m$) during consecutive ebb (left) and flood (right) half-tidal cycles for a spring tide modelled by tidal forcing only. The colour shades indicate sediment transport rate, the vectors (arrows) indicate the corresponding tidal current velocities and the contour lines show the bathymetry at the end of the tidal half cycle.

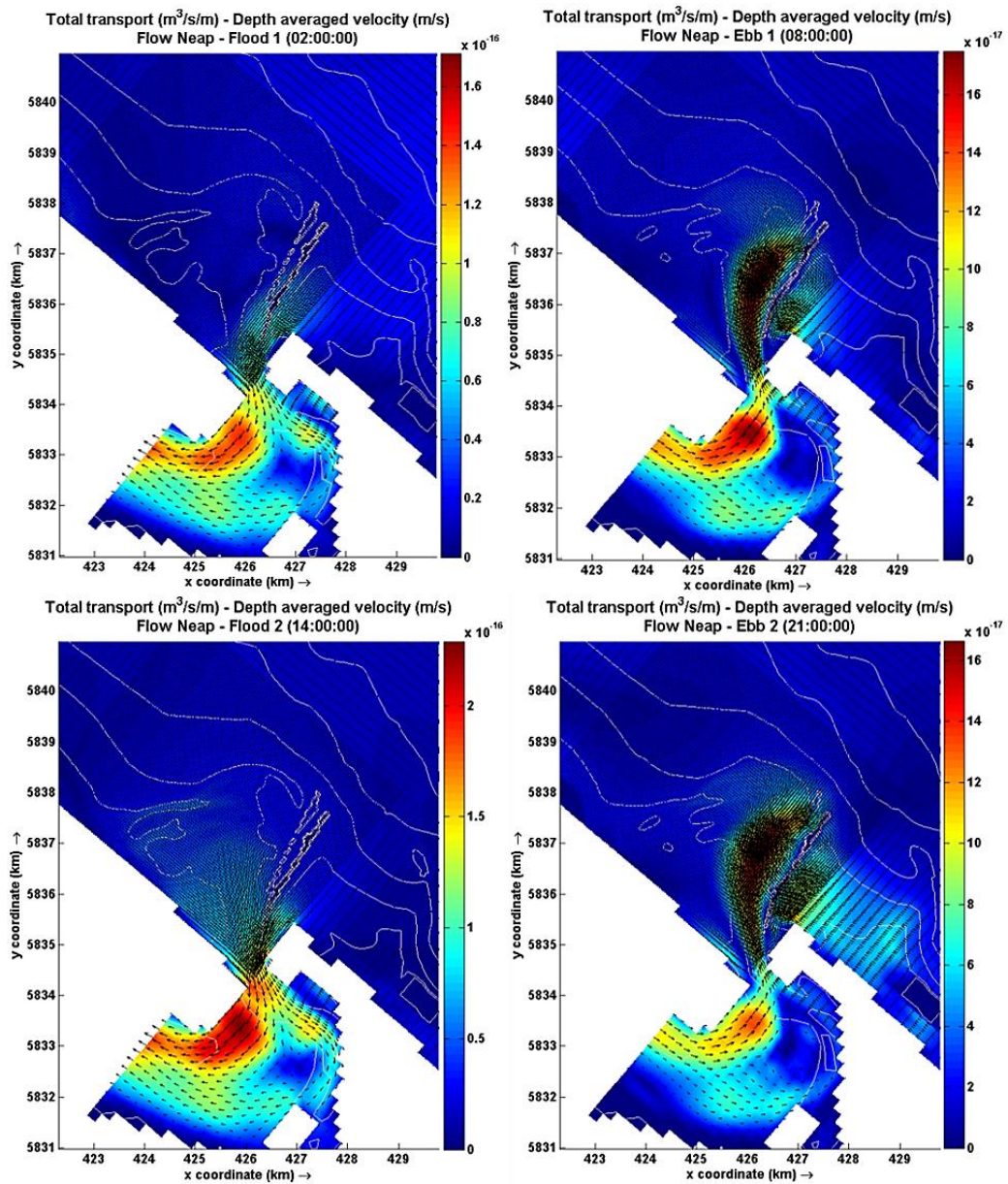


Figure 7-7. The maximum sediment transport rate ($m^3/s/m$) during consecutive ebb and flood half tidal cycles for a neap tide modelled by tidal forcing only. The colour shades indicate sediment transport rate, the vectors (arrows) indicate the corresponding tidal current velocities and the contour lines show the bathymetry at the end of the tidal half cycle.

The coupled FLOW-WAVE model results suggest that waves play a vital role in generating sediment transport over the ebb-tidal delta and along the shoreface. The WAVE model considered waves from the predominant wave direction between NNE and NE.

The wave component of sediment transport is illustrated by Figure 7-8 and 7-9, which show the distribution of significant wave height and sediment transport

rate superimposed on the bathymetry for spring and neap ebb and flood tidal cycles. The harbour entrance filters the wave energy passing through it, restricting most of the energy to a relatively narrow frequency band (de Lange, and Healy, 1990a). Hence, wave heights along the Entrance Channel were relatively low; less than 0.4 m and 0.6 m during first and second ebb tide respectively. On the shallow water over the northern terminal lobe, wave heights were higher than 0.5 m which able to rework the sediment and transport them toward the shore.

During spring – ebb tides (Figure 7-8, left panel), sediment transport are more intensive along the Entrance Channel, but its magnitudes were not as high as at along NW shoreface of Matakana Island and along the shore SE Mt. Maunganui.

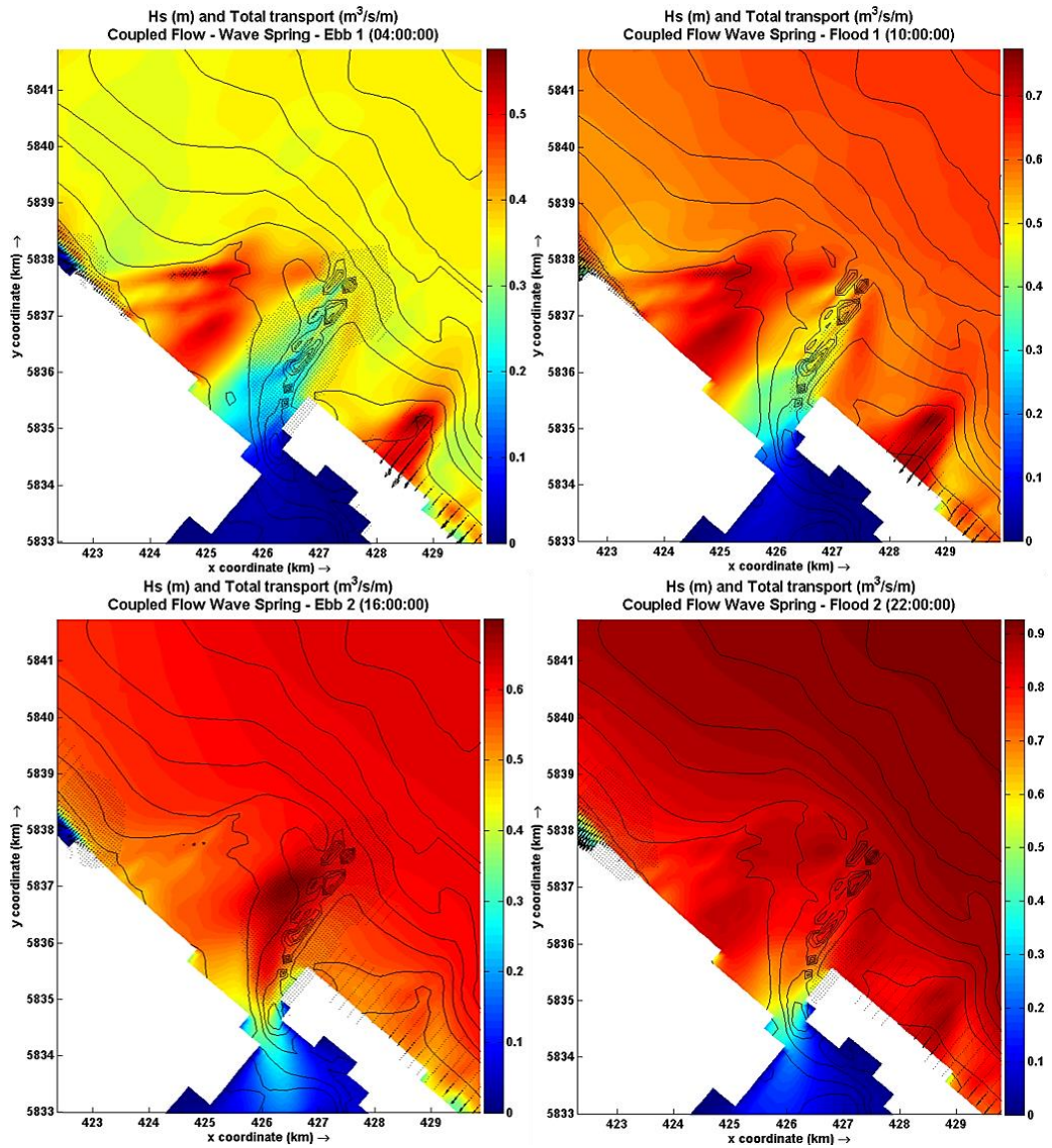


Figure 7-8. The computed significant wave height (H_s) during consecutive ebb (left) and flood (right) half tidal cycles for a spring tide predicted by the coupled FLOW-WAVE model (tidal currents and wave). The colour shades indicate wave height, the vectors (arrows) indicate the sediment transport rates and the contour lines show the bathymetry at the end of the tidal half cycle.

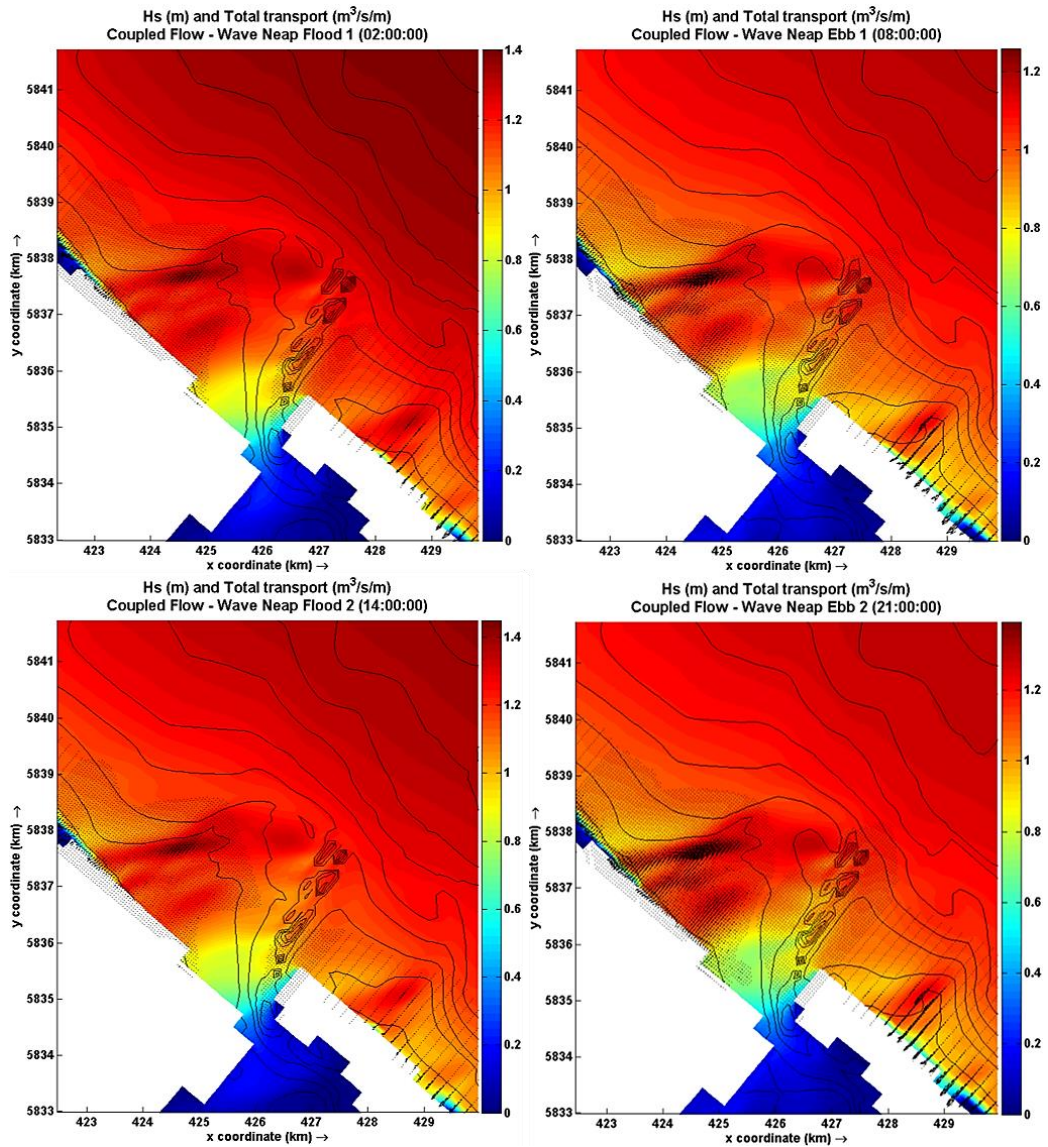


Figure 7-9. The computed significant wave height (H_s) during consecutive ebb (left) and flood (right) half tidal cycles for a neap tide predicted by the coupled FLOW-WAVE model. The colour shades indicate wave height, the vectors (arrows) indicate the sediment transport rates and the contour lines show the bathymetry at the end of the tidal half cycle.

During neap tide, waves are higher than during spring tide but those around the inlet throat and inside the harbour are relatively similar (Figures 7-8 and 7-9). On the offshore areas, the waves reached 1.4 m during the flood and 1.2 m during ebb tide. Both flood and ebb tides display similar sediment transport rates almost all over the ebb-tidal delta and along the NW and SE shoreface. However, the maximum sediment transport rate is higher during ebb tide. Around the Entrance Channel, although the magnitude is much smaller than other areas, a wider

distribution of sediment transport is seen when the tide is ebbing than when it is flooding.

Figures 7-10 and 7-11, show the patterns of sediment transport rate and depth averaged velocity when the wave forcing is included, in the same format as Figures 7-6 and 7-7, but with a different scale for the transport rates. The transport rate is determined by combining both bedload and suspended load transport, however, overall the predicted suspended load transport rates are small compared with the bedload transport.

It is seen that the wave-induced transport significantly alters the sediment transport pattern over the ebb-tidal delta (Ramli *et. al.*, 2015). Sediment transport is focussed along the NW shoreface of Matakana Island, SE Mt. Maunganui and over the swash platform. Sediment transport rates of up to $1.2 \times 10^{-4} \text{ m}^3/\text{s}/\text{m}$ of net occurred around the NW side of the swash platform and up to $1.8 \times 10^{-4} \text{ m}^3/\text{s}/\text{m}$ along NE margin by Mt. Maunganui. Because of the magnitudes of sediment transport induced by combined waves and currents are up to 4 times greater than due to tidal forcing alone, the sediment transport rates close to the tidal inlet and along the Entrance Channel are no longer dominant. The tide still influences the net sediment transport rates, but now the highest sediment transport rates consistently appear during the neap - ebb tide (Figure 7-11, right panel).

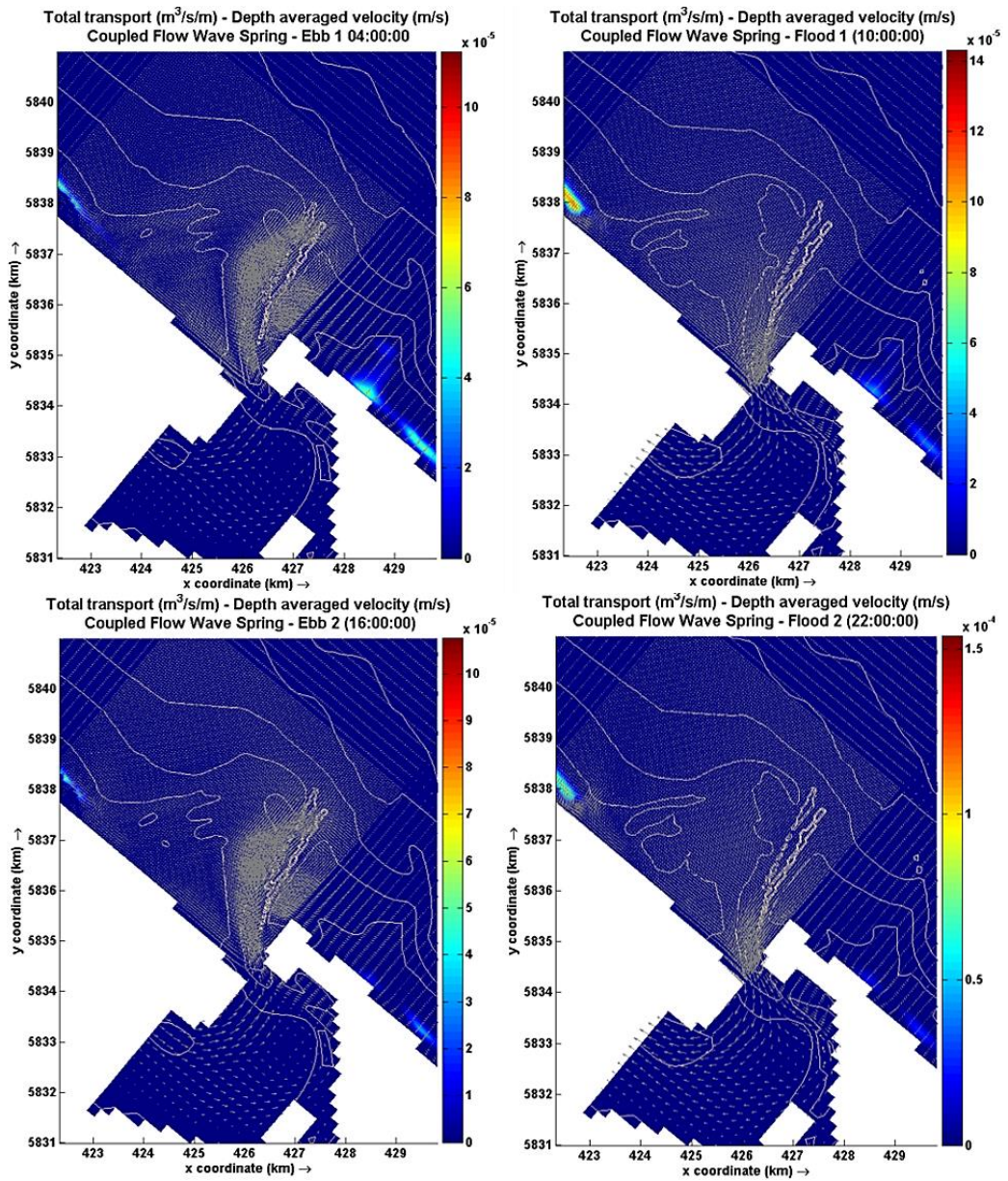


Figure 7-10. The maximum sediment transport rate ($m^3/s/m$) during consecutive ebb and flood half tidal cycles for a spring tide predicted by combined wave and tidal forcing. The colour shades indicate sediment transport rate, the vectors (arrows) indicate the corresponding tidal current velocities and the contour lines show the bathymetry at the end of the tidal half cycle.

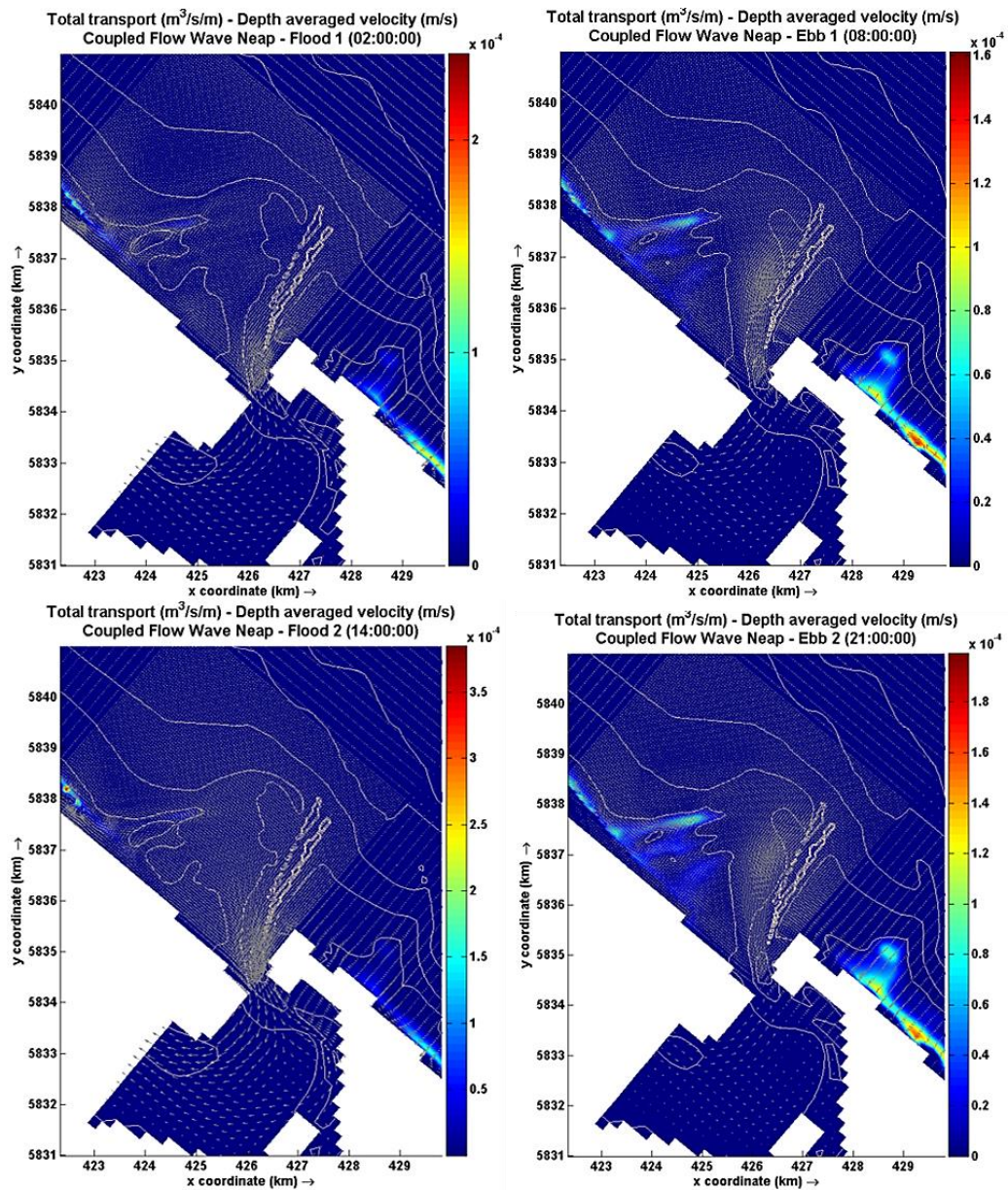


Figure 7-11. The maximum sediment transport rate ($\text{m}^3/\text{s}/\text{m}$) during consecutive ebb and flood half tidal cycles for a neap tide predicted by combined wave and tidal forcing. The colour shades indicate sediment transport rate, the vectors (arrows) indicate the corresponding tidal current velocities and the contour lines show the bathymetry at the end of the tidal half cycle.

7.3.2 Influence of tidal currents and waves on the sediment transport rate

Ebb-tidal deltas typically have segregated areas of landward versus seaward sediment transport that are controlled primarily by the way water enters and

discharges from the inlet, as well as the effects of wave-generated currents (Davis and Fitzgerald, 2004). From the model, it is clear that wave-induced currents significantly change the rate of sediment transport, which will affect ebb-tidal delta volume. Figure 7-12 (left panel) shows the computed mean net sediment transport rate due to tidal forcing only for a 12 day period. This indicates that the maximum rate is less than $1 \times 10^{-5} \text{ m}^3/\text{m}$, and this occurs inside the harbour (LWC) at the location where the maximum tidal currents occur in shallow water with high sediment availability.

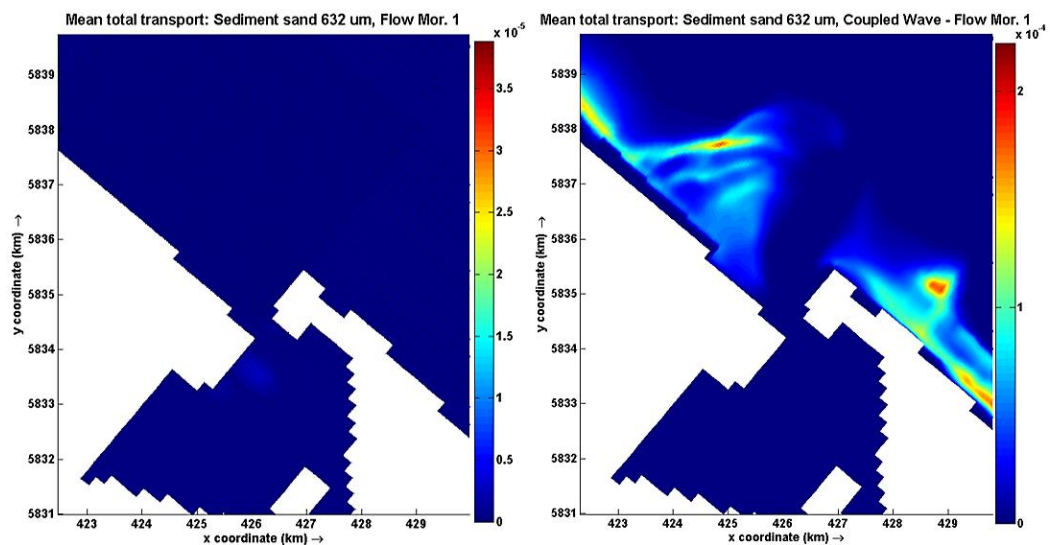


Figure 7-12. Mean total transport ($\text{m}^3/\text{s}/\text{m}$) for 12 days simulation time that covers spring and neap tidal cycle. It is clearly seen that the waves significantly increase the sediment transport on the shallow shoal of the ebb-tidal delta. Note the colour scale bars have an order of magnitude difference in range to allow the maximum area produced by tidal flows to be visible.

Considering the ebb-tidal delta region, both bedload and suspended load for each cross section examined in Chapters 4 and 6 can be quantified as the cumulative total transport over the 12 day period simulated (net sediment transport). When the model is forced solely by tidal flows (without waves), the maximum cumulative net sediment transport for 12 days simulation for the ebb-tidal delta cross-sections is about 549 m^3 . Waves significantly increase the quantity of cumulative net sediment transport (right hand panel, Figure 7-12), particularly at the cross-sections located between $\sim 400 \text{ m}$ to 2400 m from the tidal inlet. Including waves increases the maximum cumulative sediment transport on the ebb-tidal delta to around 9563 m^3 over 12 days (Figure 7-13).

The presence of waves resulted in more sediment being reworked and transported, hence involving the waves resulted in about $30.6 \times 10^3 \text{ m}^3$ difference in volume change between the models. The computed ebb-tidal delta volumes are around $490.2 \times 10^3 \text{ m}^3$ and $459.6 \times 10^3 \text{ m}^3$ for modelling solely with tidal forcing and by coupling the tides and waves respectively.

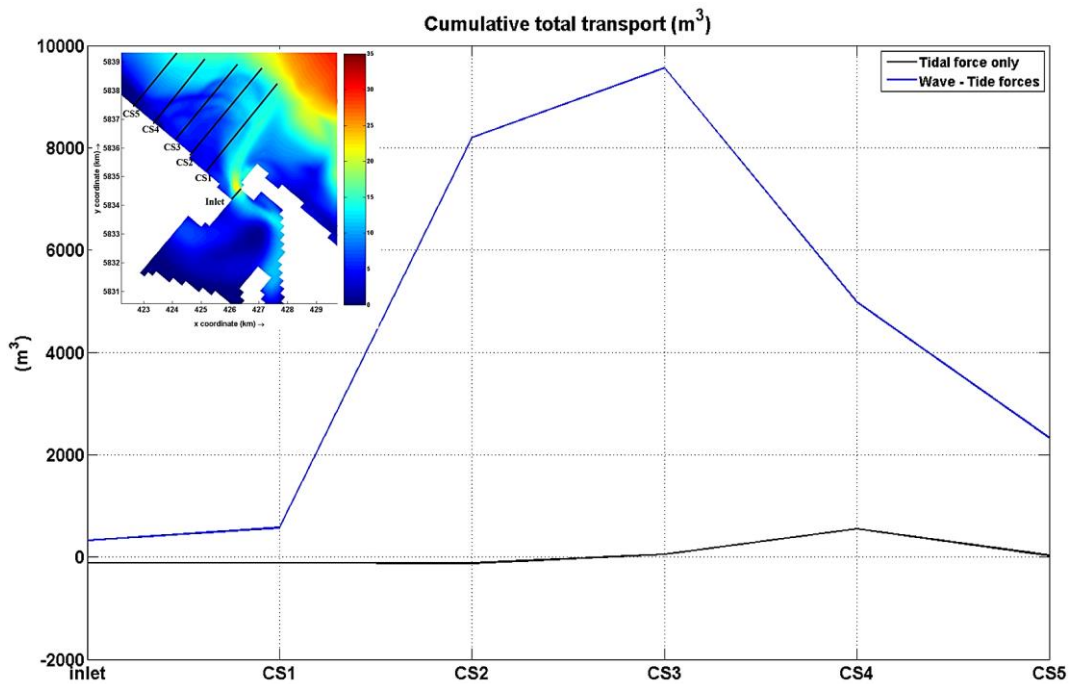


Figure 7-13. Comparison between the computed cumulative total (net) transport over 12 days (m^3) model with only tidal forcing and combined wave and tidal forcing, for the cross-shore transects across the ebb-tidal delta (see index map). Negative and positive values indicate seaward (sediment loss) and landward (sediment gain) transport of sediment respectively.

7.3.2 Influence of tides and waves on ebb-tidal delta daily volume changes

The volume changes of the ebb-tidal delta were calculated by setting the 10 April 2013 (start time of the model) volume as the initial ebb-tidal delta volume. The daily ebb-tidal delta volume change was calculated for 29 days using the coupled model showed volumetric fluctuations are related to the tidal conditions. Sediment volume increases over the ebb tide delta during the neap tide and vice versa for spring tide. The sediment gain and loss volume are around $8.9 \times 10^6 \text{ m}^3$

and $-8.9 \times 10^6 \text{ m}^3$ respectively, which indicates that sediment predominantly recirculates within the system.

Figure 7-14 shows the computed daily ebb-tidal delta volume changes for the period corresponding to the field programme in April-May 2013, and the observed tide water level, tidal current speed, and significant wave height for the same period. High current velocities during spring tides seem to contribute to volume loss from the delta, but the sediment is replaced during neap tides. The occurrence of high wave events (storm/swell) did not appear to directly relate to ebb-tidal delta volume fluctuations.

In the nearshore and swash platform areas, the waves entrain the sediment, and tend to move it onshore or offshore in the absence of other currents. This means the sediment remains within the surveyed area. However, tidal currents can transport sediment in and out of the surveyed area, such the sediment transport into and out of the harbour, which results in volume changes for the delta.

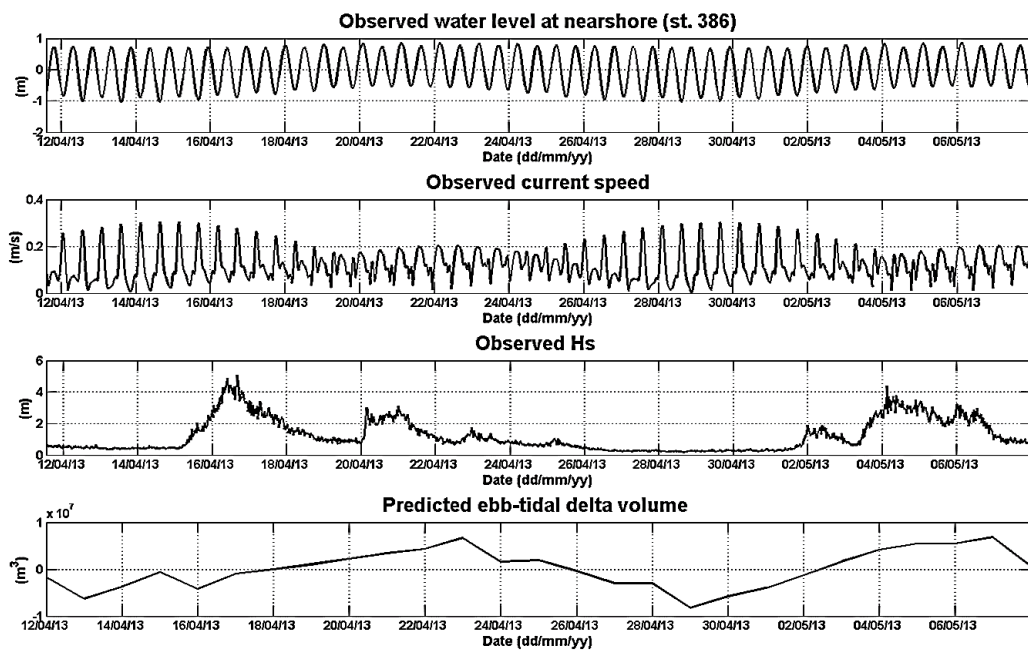


Figure 7-14. Flow-Wave coupled model predictions of daily volumetric changes for the Matakana Banks ebb-tidal delta, and the corresponding observations of tide, current speed, and significant wave height (H_s) (Ramli et al., 2015).

7.3.3 General sand dispersal trends: influence of dredging and storm events

Dabees and Kraus (2004) demonstrated that removal of sediment by dredging may interrupt the natural sediment bypassing of the integrated sediment-sharing tidal inlet system. They suggest that the predredging sediment bypassing rate will be only be re-established after the dredged feature returns to the volume at the time of dredging. At a tide dominated inlet, deepening of the tidal inlet by dredging changes the tidal circulation patterns.

The study of Brannigan (2009) revealed that historically the entrance to Tauranga Harbour underwent significant bathymetric changes prior to dredging (before 1968) owing to natural processes, with the main ebb tidal channel within the harbour moving from Maunganui Roads Channel to the Lower Western Channel between 1852 and 1954. At Tauranga it has been suggested that dredging resulted in the formation of opposing eddies on either side of the Entrance Channel, as evidenced by two-dimensional hydrodynamic modelling (Spiers *et al.*, 2009). However, flanking eddies are a common feature of ebb-jets (Nicolau del Roure *et al.*, 2009) and were probably present at Tauranga before dredging. The modelling of the pre-dredging 1954 bathymetry by Brannigan (2009) clearly shows a strong eddy to the east of the ebb-jet, and a weaker eddy on the west that is constrained by the very oblique orientation of the ebb-jet relative to the Matakana Island shoreline.

In this study, the influence of dredging on the tidal currents and sediment transport patterns over the Matakana Banks ebb-tidal delta and its surroundings were investigated by comparing the simulations for bathymetry conditions immediately before the commencement of capital dredging (1967), and after the completion of two capital dredging campaigns (2013). Figures 7-15 to 7-17 show comparisons of the tidal current speed and direction from three sites located inside the harbour to the offshore end of the Entrance Channel before the first capital dredging (1967), and after 45 years of capital and maintenance dredging and spoil disposal around the harbour. Deepening the channels increasingly confined the tidal flow to the channels, which increased the current speed at the inlet throat and along the Entrance Channel. The asymmetry between flood and ebb flows also changed.

In 1967, the modelled average current speed in the Lower Western Channel near the inlet throat (St. 390, Figure 5-2 in Chapter 5) during ebb tide is about 0.33 m/s and 0.38 m/s during flood (Figure 7-15). After dredging between 1968 and 2013, the average current speeds increased to 0.60 m/s and 0.50 m/s respectively. Near the middle of the Entrance Channel where the ADCP was deployed (Sta. 392, Figure 5-2 in Chapter 5), a significant change in tidal asymmetry is evident with the channel becoming more ebb dominated after dredging; the average flood current speed in 2013 was 2.5 times lower than in 1967 before the first dredging was conducted (Figure 7-16). A storm event, which was indicated in the measured wave data (Figure 5-9 and the observed Hs panel of Figure 7-14) and in the backscatter image (Figure 5-7), is clearly seen as a spike in the modelled current speed, especially at Stations 392 and 396 in the offshore area (Figures 7-16 and 7-17).

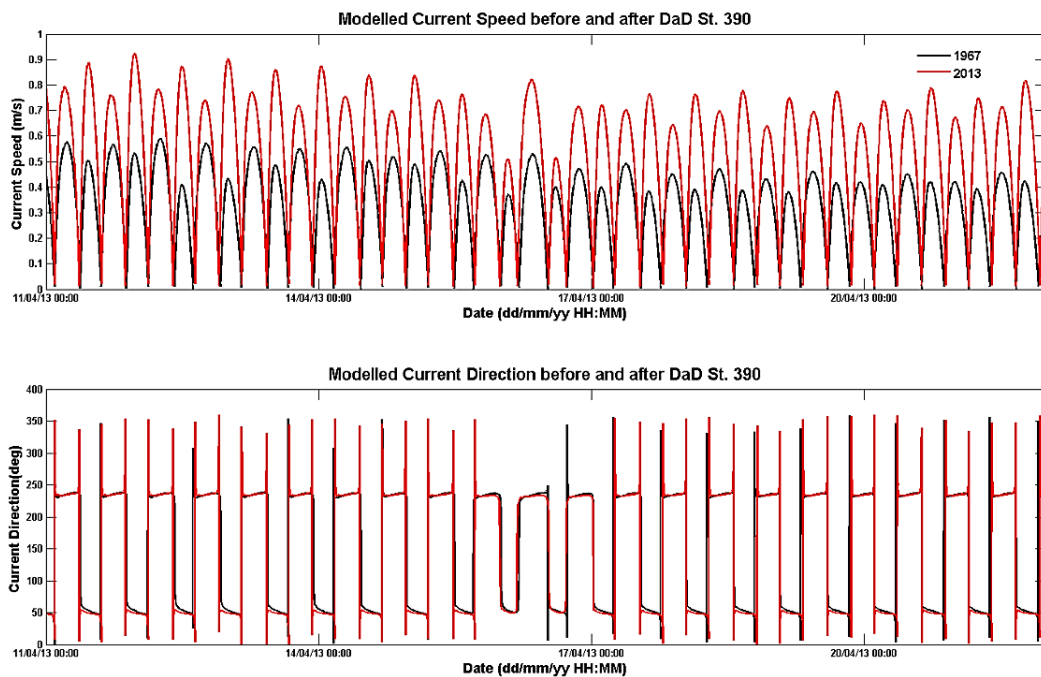


Figure 7-15. Comparison of the computed current speed and direction before and after DaD in the Lower Western Channel inside the harbour (St. 390).

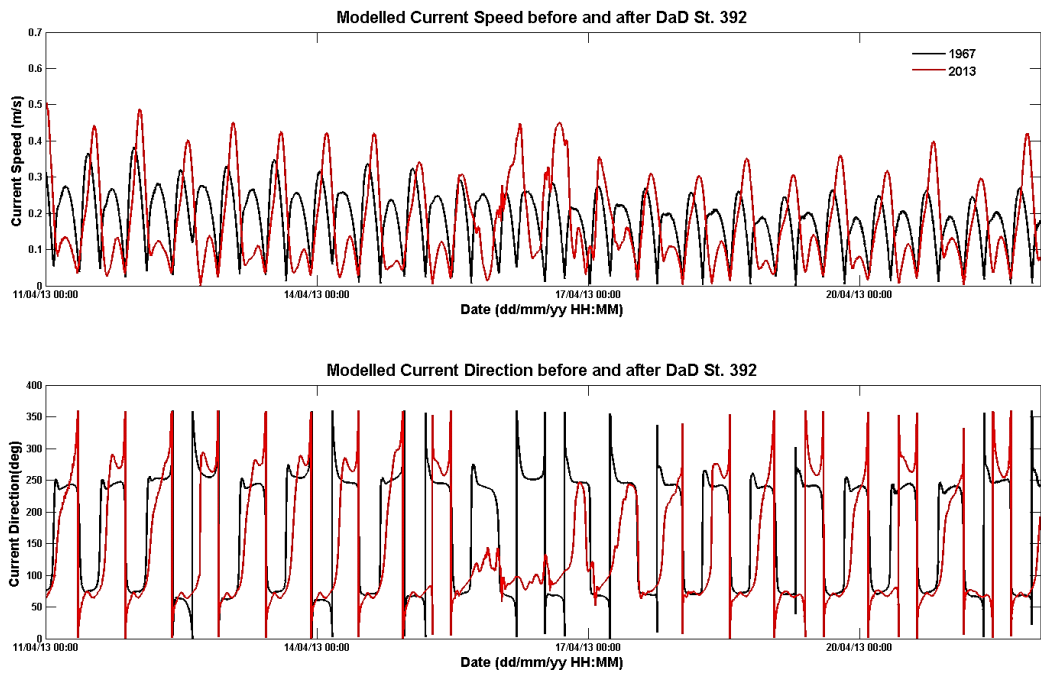


Figure 7-16. Comparison of the computed current speed and direction before and after DaD in the middle of the Entrance Channel (St. 392 - ADCP).

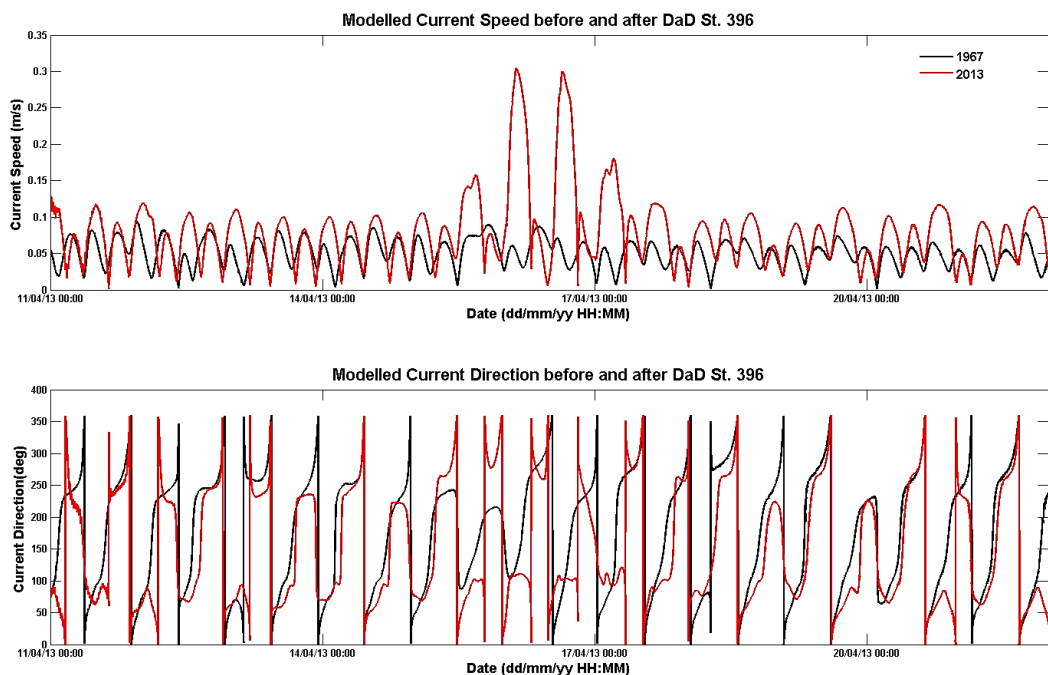


Figure 7-17. Comparison of the computed current speed and direction before and after DaD at the distal end of the Entrance Channel (St. 396).

Figure 7-18 shows the mean total transport over the ebb-tidal delta before the first capital dredging in 1968 based on 12-day and 2-year simulations, with and

without storm events (MORFAC 60). The 12-day simulation including one storm event shows the dominant areas of sediment transport are along the terminal lobe, the SE side of the ebb-tidal delta, and along the shoreface (Matakana Island beach and Mt. Maunganui beach). This pattern is consistent with sediment bar bypassing of the tidal inlet. At the distal end of what is now the Entrance Channel, the sediment transport patterns indicate that the historical pattern of shoaling was likely to continue in the absence of dredging. The simulation also indicates that the primary source of sediment was from the inner shelf (offshore) and that sediment accumulation resulted in up to 1.5 m and 2.5 m seaward shoreline movement along the NW and SE shoreface respectively (Figure 7-18, lower left panel).

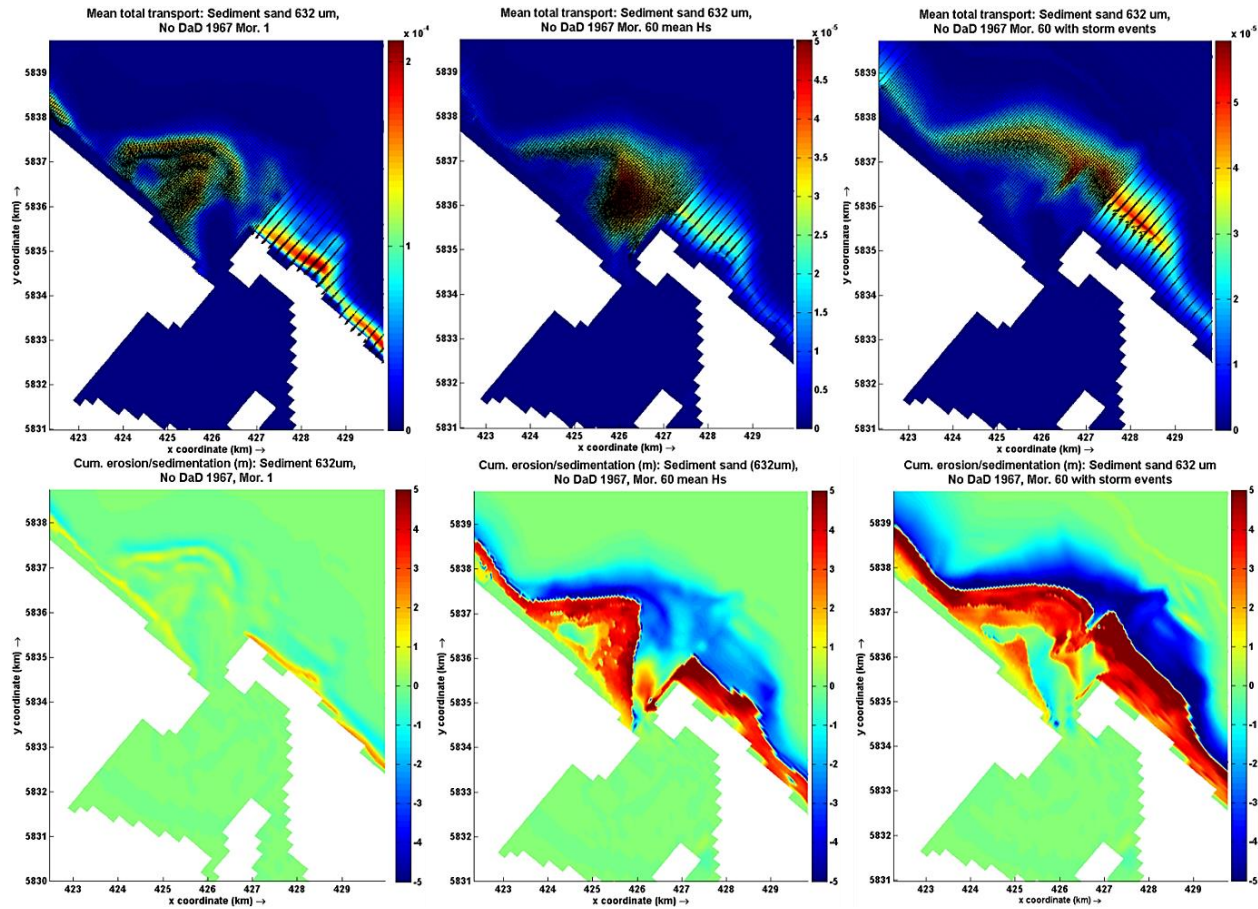


Figure 7-18. Computed mean total sediment transport before the first capital dredging in 1968 (upper panel) and spatial extension of cumulative erosion/sedimentation. Mor 60 denotes 2 years morphological modelling, while Mor 1 corresponds to a 12-day simulation. In the lower panels positive values correspond to accretion and negative values correspond to erosion.

Considering the longer-term (2-year) morphological simulations, the model with average wave forcing showed rapid shoaling in the area of the delta now occupied by the Entrance Channel (Figure 7-18, middle panels) and sediment transport towards both NW and SE on the flanks of the delta. The average wave conditions (0.8 m to 1.2 m) induced onshore sediment transport predominantly from the offshore periphery of the ebb-tidal delta. Vertical sediment accumulations of up to 5 m occurred around the terminal lobe and along the shoreface. The terminal lobe accretion, caused waves to break and refract further offshore, and induced sediment transport along both the NW and SE flanks of the ebb-tidal delta. Close to the shore, the wave heights were significantly reduced (< 0.2 m) limiting the sediment from being transported further onshore.

Including storm events in the model increased the magnitude of sediment being reworked and transported from the inner shelf, and hence accumulating on the terminal lobe (Figure 7-18, right panels). The influx of sediment from offshore may account for the apparent switching of the directions of bedform migration observed in the analysis of bathymetric survey data (Chapter 4). The deeper area of the terminal lobe (Entrance Channel) was entirely filled by sediment resulting in a significant decrease in wave influence and onshore sediment transport across the ebb-tidal delta. A zone of minor sediment accumulation of less than 1 m thick was still evident parallel with the ebb-jet direction from the tidal inlet toward NW, which indicates the tidal current influence around the inlet throat.

The patterns of sedimentation predicted by the 2-year morphological modelling are consistent with the long-term trends identified by Brannigan (2009), but appear to occur at a much faster rate than the historical changes. de Lange *et al.* (2015) suggested that major tsunami events in 1960 and 1964 resulted in bathymetric changes within the tidal inlet that would have affected the tidal flows, meaning that the 1967 simulation is not representative of the entire historical record. Overall, the 2-year model results are likely to indicate patterns, but are unlikely to provide a reliable prediction of the magnitude or rate of the changes that would occur in the absence of dredging and spoil disposal.

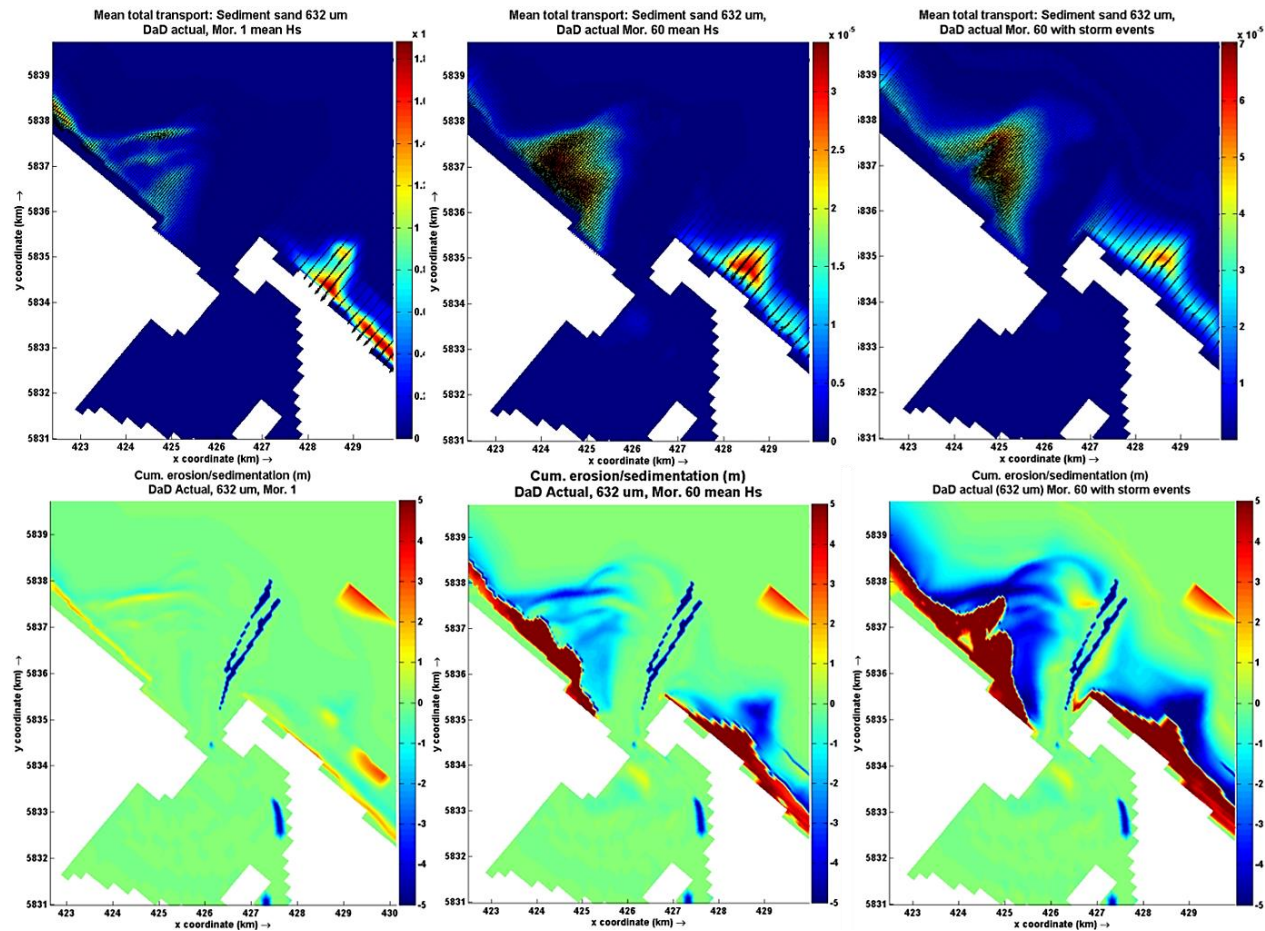


Figure 7-19. Mean total sediment transport and cumulative erosion/sedimentation after dredging and spoil disposal programme. Mor 60 denotes the 2 years morphological modelling, while Mor 1 corresponds to a 12-day simulation. In the lower panels positive values correspond to accretion and negative values correspond to erosion.

Figure 7-19 shows the mean total transport (upper panel) and the spatial patterns of cumulative erosion/accretion (lower panel) based on the post dredging (2013) bathymetry. The distal ebb-tidal delta was the region where the most severe erosion occurs following dredging, experiencing more erosion when storm events were included than indicated by average conditions. The short term (12-day) simulation indicated that a storm event decreases the ebb-tidal delta volume by $\sim 7.2 \times 10^3 \text{ m}^3$ for the post-dredging bathymetry. The longer period (2-year) simulations including storm events predict three times more erosion than for average conditions (Table 7-2).

Table 7-2. Calculated ebb tidal delta final volumes and volume changes for different simulation durations and wave conditions. *Mor 1* and *Mor 60* denote 12-day and 2-year predictions respectively. The ebb-tidal delta volume was calculated above a 15 m depth datum.

	Initial volume (x)	<i>Mor 1</i> mean $H_s(x_i)$	<i>Mor 1</i> with storm (x_{ii})	<i>Mor 60</i> mean $H_s(x_{iii})$	<i>Mor 60</i> with storm (x_{vi})
Volume (m^3)	72,064,827.61	72,517,131.28	72,524,400.75	70,069,399.83	66,103,836.06
$x_n - x$	-	452,303.67	459,573.14	-1,995,427.78	-5,960,991.55

The zones of accretion evident in the lower panels of Figure 7-18 along the sides of the Entrance Channel, and within the Harbour at the junction of the Cutter Channel and Maunganui Roads correspond to the main areas of biennial maintenance dredging since the 1992 capital dredging programme (Kruger, 1999; Braddock, 2006).

The offshore spoil disposal site at 20 m depth did not seem to be greatly affected by the inclusion of storm events in the simulations. Regardless of wave conditions or the length of the simulation period, only the SW side of the spoil mound was transported by waves. This occurred rapidly at the start of the simulations, and spoil mound stabilized afterwards with no further changes for the remainder of the simulation. This behaviour is consistent with that observed from monitoring of the disposal site (Harms, 1989; Warren, 1992), although the model does not account for consolidation of the spoil, which Warren et al. (1994) identify as an important control of sediment mobilisation from spoil mounds. In contrast, the nearshore disposal site in 5 m depth was strongly affected by the waves, with the degree of erosion being proportional with the simulation duration time and the

wave conditions used. Inclusion of storm events resulted in more material being dispersed. This behaviour is primarily a function of the minimum depth limit specified for the dredge spoil mound within the Delft3D model.

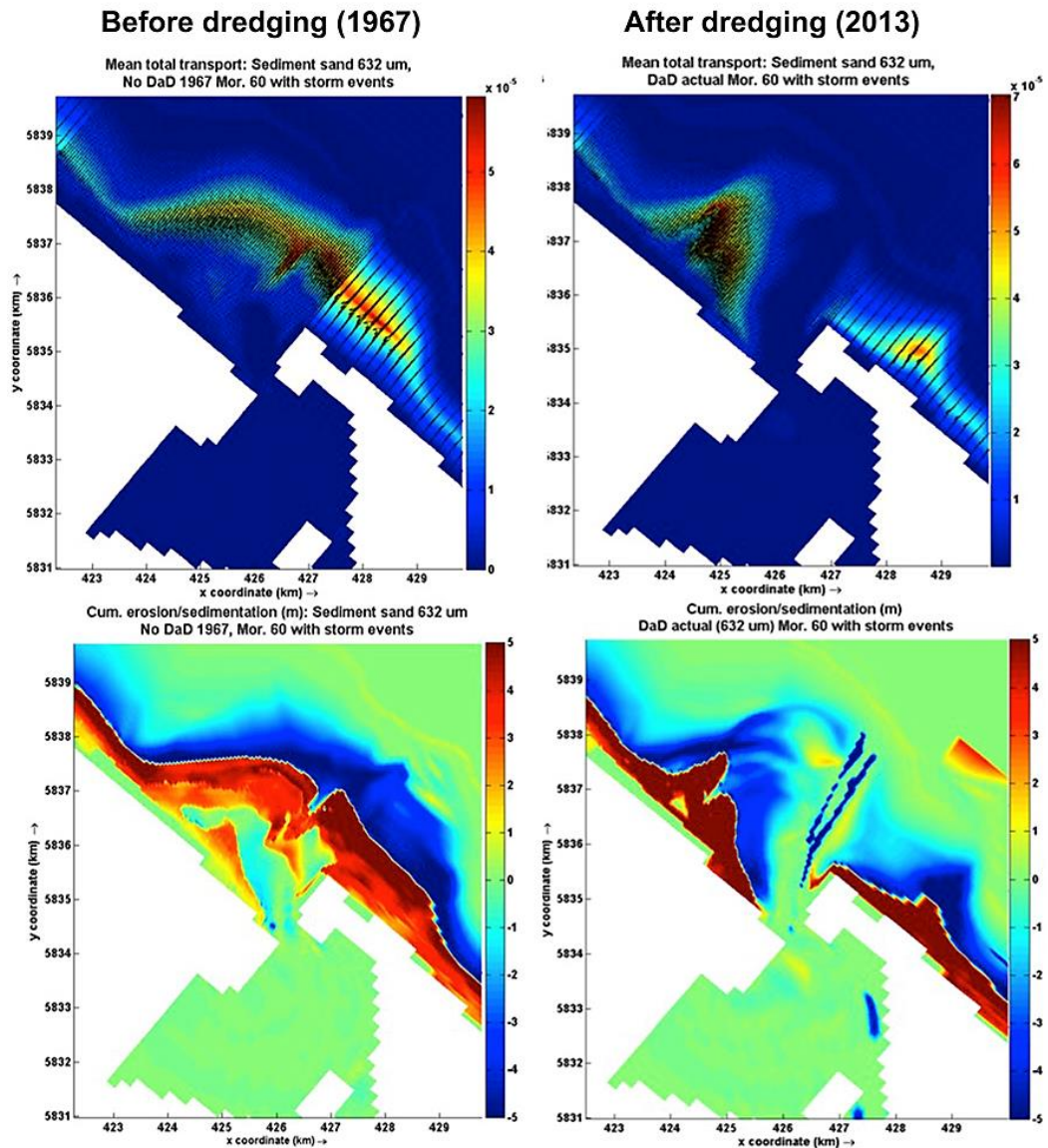


Figure 7-20. Comparison of the mean total transport of sediment sand (upper panels) and the spatial extent of erosion and accretion (lower panel) after 2 years simulation period with storm events.

The comparison of sediment distribution and the spatial extent of cumulative sediment erosion and accumulation in regards with storm events is presented in the Figure 7-20. Dredging across the ebb-tidal delta cut the sand bypassing from NW to SE at the ebb-tidal delta periphery by disrupting the shallow terminal lobe (Figure

7-20, upper right panel). Hence, the continuation of the ebb tidal delta from NW to SE is not apparent in the morphology of the “after dredging” ebb-tidal delta.

Including storm events into the model resulted in more sediment being eroded from the deeper part (offshore) and deposited in the shallow shoals along the margin of the ebb-tidal delta (Figure 7-20, lower left panel). Before dredging, the tidal inlet was shallower and broader, which resulted in more rapid sedimentation within the tidal inlet than predicted for the after dredging tidal inlet. Hence, the 2-year simulation with storm events predicted that the sediment would accumulate and eventually block the undredged tidal inlet (1967). In contrast, the “after dredging” ebb-tidal delta experienced mostly erosion over the body of the ebb-tidal delta, with deposition occurring along the shallower depth of Matakana Island shoreface (Figure 7-20, lower right panel). It is likely that more sediment was also transported into the harbour, and may have added to sedimentation of the flood tidal delta (Centre Bank). However, this area was not analysed by this study.

7.3.4 Alternative spoil disposal sites for mitigation

The alternative spoil disposal sites proposed to mitigate any adverse effects of the planned capital dredging were modelled. A 2-year period was simulated to correspond to the normal biennial maintenance dredging programme schedule. The 2013 bathymetry was used for the analysis, as the actual capital dredging depths and the staging of the channel deepening were not known when the modelling was undertaken.

Figure 7-21 shows the patterns of cumulative erosion/sedimentation and bed level comparisons after 2-year simulations (Mor. 60) for existing and each of the alternative sites with respect to a baseline condition without dredging and spoil disposal. Sediment accretion occurs along the shoreface of Matakana Island and SE Mt. Maunganui in each model simulation, although there are small localized differences suggesting minor regions of accretion and erosion along the shoreline. Overall, no major morphological differences are seen along the coastline between the various models.

Each simulation also indicated that the northern terminal lobe and the swash platform experienced slight accretion (< 4% compared with the initial bathymetry). This was expected as the previous simulations had indicated that sediment already moves onshore from the inner shelf, so the increased availability of sediment from spoil grounds should increase the onshore transport rate. In contrast, the northwest terminal lobe and areas immediately adjacent to the Entrance Channel experienced erosion of up to 16% and 5% respectively. However, this pattern of morphological change was indicated by the historical data obtained by repetitive SBES and MBES surveys, and does not appear to be a direct consequence of the addition of spoil grounds. Overall, the modelled shape of the ebb-tidal delta remained the same at the end of all the simulation periods.

The simulation with existing spoil grounds only (Figure 7-21, upper left panel) shows that sediment disposed within sites C and D is dispersed toward the shore, providing sediment to the SE shoreface (Mt. Maunganui Beach), which agrees well with the predictions of Healy *et al.* (1991) before the 1992 capital dredging, based on the findings of Harms (1989). During the 2-year simulation, more than 80% of dredged material at the offshore site D was dispersed. This implies a faster rate of dispersion than observed, and it is probably due to consolidation of the spoil reducing sediment availability from the real spoil mounds.

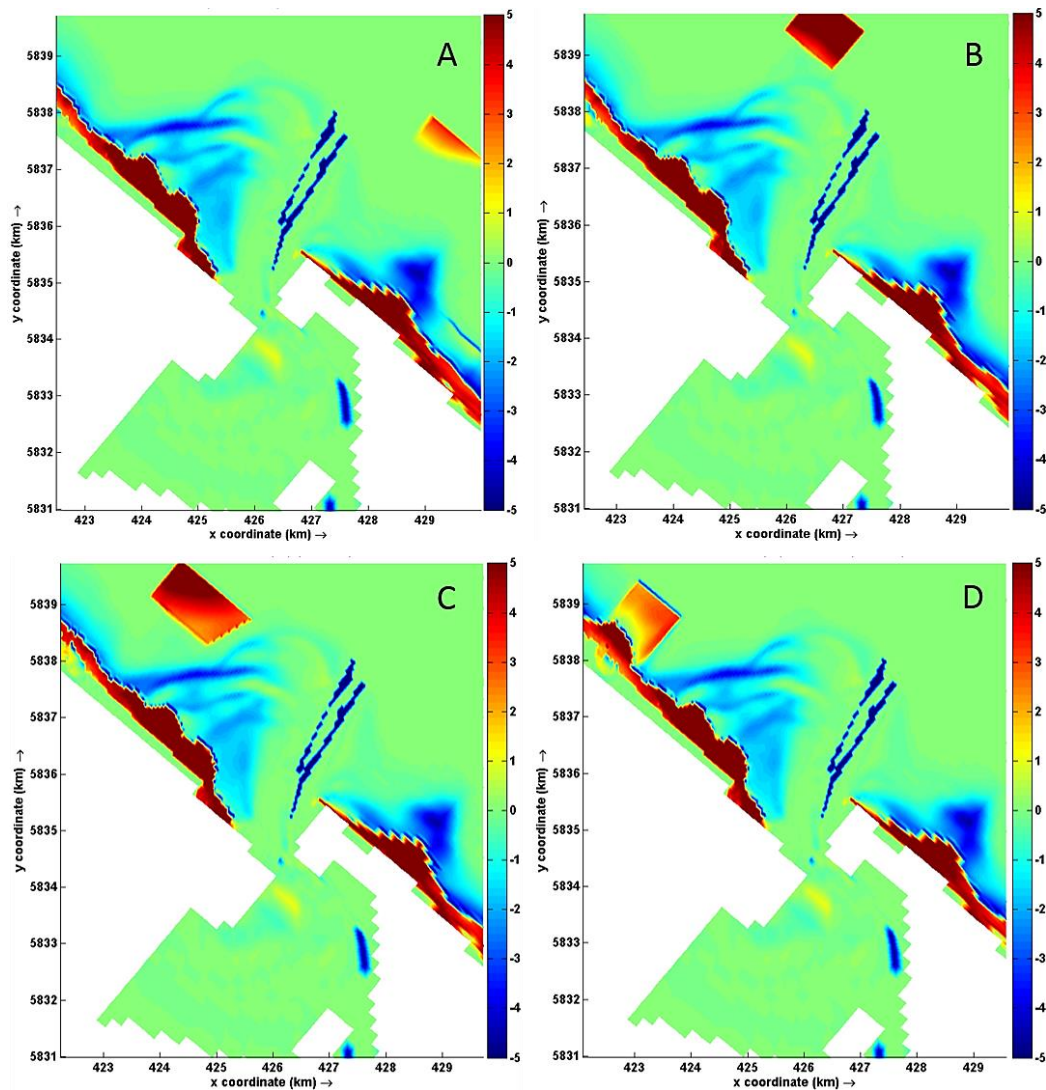


Figure 7-21. Computed patterns of cumulative erosion and sedimentation of the 2013 bathymetry, including different spoil disposal site options. (A) DaD Act corresponds to existing spoil disposal sites, (B) DaD TL corresponds to existing sites with the addition of a new site located north of the NE terminal lobe, (C) DaD New corresponds to existing sites with the addition of a new site located about 1,500 m from the shoreline, and (D) DaD NS corresponds to existing sites with the addition of a new site located near to the shore to the west of the ebb tidal delta.

The alternative disposal sites considered covered a range of depths and locations around the terminal lobe, starting from > 20 m at the outermost north of the ebb-tidal delta (DaD TL), to between 15 m to 10 m (DaD New) to the northwest, and < 8 m (DaD NS) towards the west (Figure 7-3). The different water depths were the dominant factor causing different degrees of sediment dispersion from the alternative disposal sites (Figure 7-21). The shallower the water depth (which also meant closer to the shoreline), the higher the proportion of the dredge spoil being dispersed. Hence, more accretion is seen at the NW shoreline due to site DaD NS

than predicted for the other alternatives. Overlaying the predicted bathymetric contour lines for each alternative spoil disposal site and the baseline bathymetric condition of no dredging, shows similar trends of morphological evolution to that shown by the analysis of historical bathymetric surveys (Chapter 4).

There are distinct differences between areas that are predominantly influenced by tides or waves (Figure 7-22). In particular, the contours adjacent to the Entrance Channel move offshore (tidal flow dominated) and vice versa on the shallow swash platform area further northwest (wave dominated).

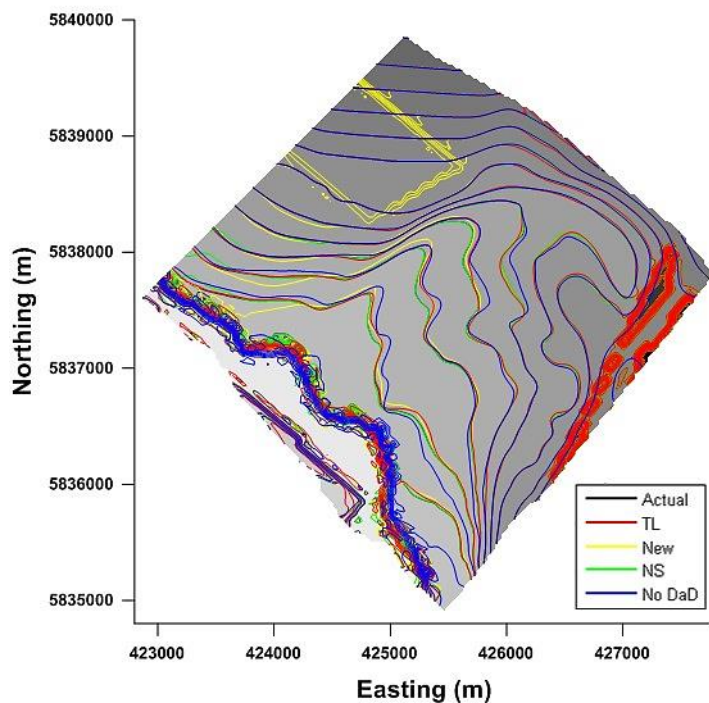


Figure 7-22. Comparison of 2-year (Mor. 60) ebb-tidal delta morphological changes resulting from different spoil disposal site alternatives, compared with the baseline morphology of no dredging (No DaD). Shaded grey colours denote the morphology of associated with the existing disposal sites (Actual).

The results indicate that the response of the ebb tidal delta to the inclusion of the nearshore site (DaD NS) almost perfectly imitates the response with existing sites. The largest differences are associated with a mitigation spoil disposal site near the NW terminal lobe (DaD New). This location results in a shift of the NW terminal lobe toward the south, resulting in a shrinkage of the NW ebb-tidal delta area.

Therefore, if the mitigation is required to supply sediment to the shoreface along Matakana Island, the nearshore site west of the ebb-tidal delta will be the most effective. This option also has the least impact on the ebb-tidal delta, and therefore the rate of sediment accumulation within the Entrance Channel. However, addition of sediment to the Matakana Island shoreface may increase the volume of sediment tidally bypassing the inlet, which could increase sedimentation within the harbour. This is not evident in Figure 7-21, but the model was not calibrated to assess this aspect.

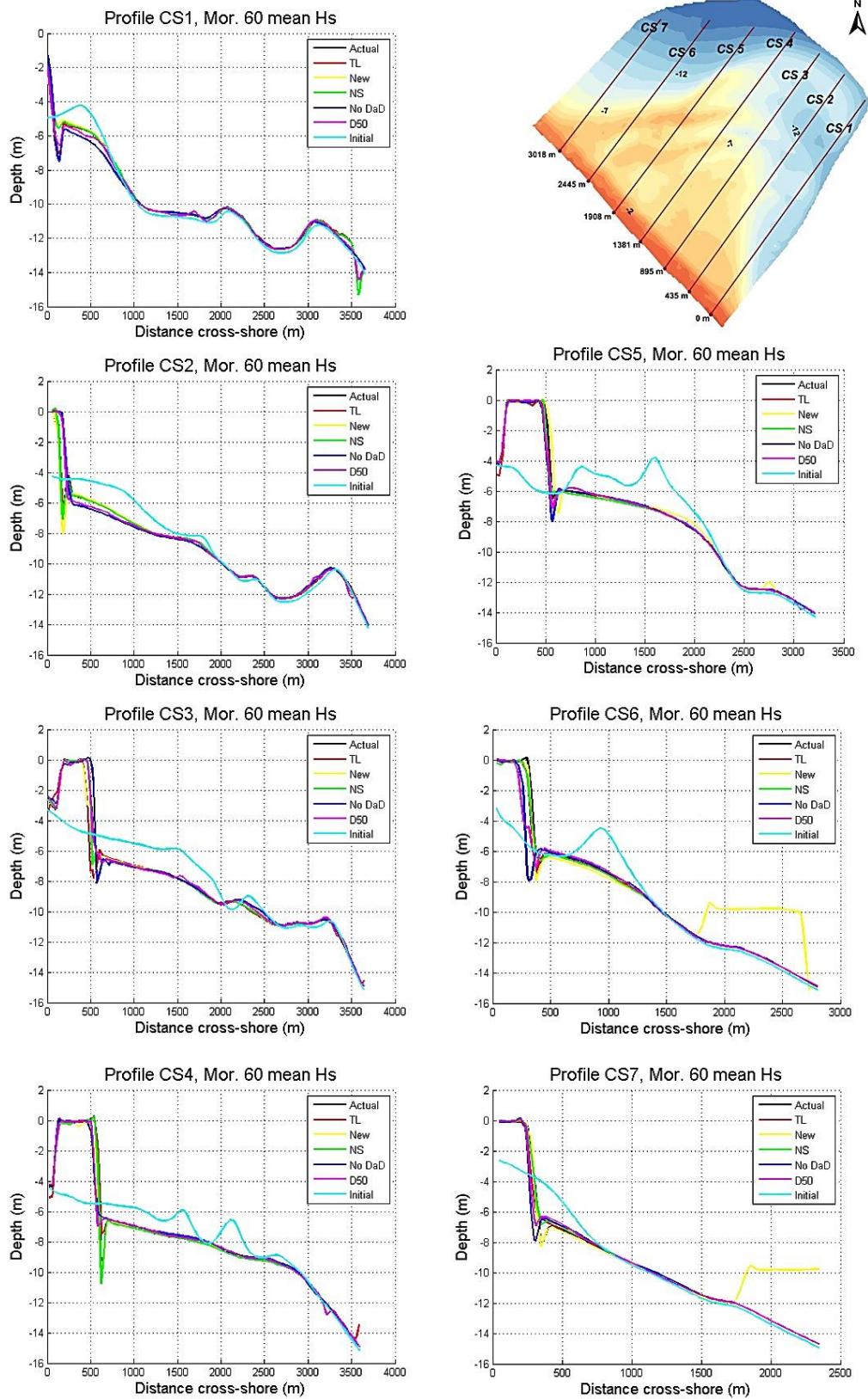


Figure 7-23. Comparison of bed level changes resulting from alternative spoil disposal sites with respect to no dredging after 2 years (Mor. 60). The initial bathymetry corresponds to the 2013 bathymetry.

Figure 7-23 displays a comparison of cross-shore profiles of the ebb-tidal delta for the different disposal site options compared to a no dredging baseline after a 2-year simulation. These profiles highlight the morphological changes occurring at different distances from the shoreline according to the predominant hydrodynamic regime. Adjacent to the Entrance Channel where tide influence is the greatest, the morphological changes predominantly occurred at distances of less than 1,000 m from the shoreline, consistent with the decreasing strength of the ebb jet with distance from the inlet. As the ebb-tidal delta morphology becomes shallower with gentle slopes (swash platform), waves increasingly influence sediment transport, and morphological changes extend further offshore to distances from 1,500 m to 2,700 m. Along the western margin to the ebb-tidal delta, the morphological changes predominantly occurred closer to the shore (< 800 m from the shoreline), as was also indicated by repetitive bathymetric surveys (Chapter 4).

The main differences between the alternative spoil disposal sites considered were evident at distances < 1,000 m from the shoreline in water depths < 10 m (Figure 7-18). Dredging and spoil disposal resulted in up to 0.6 m sediment accumulation at 180 m to 1000 m from the shoreline along cross-shore profile CS 1 adjacent to the Entrance Channel (water depths of 5-10 m). All the options modelled predicted accumulation of sediment along the shoreface by the end of simulation, however the area adjacent to the Entrance Channel experienced the least sediment accumulation relative to other areas along the shoreface of the ebb-tidal delta.

The computed cumulative sediment transport for the 2-year simulations shows that the sediment transport flux is the highest for the swash platform in the middle of the ebb-tidal delta where the lateral extent is also the widest, and the lowest cumulative sediment transport occurs adjacent to the Entrance Channel (Table 7-3).

Table 7-3. *The computed cumulative sediment transport along transects across the ebb-tidal delta between the tidal inlet and the northwestern margin of the ebb-tidal delta (Figure 7-13).*

<i>Cross-section</i>	<i>Inlet</i>	<i>CS1</i>	<i>CS2</i>	<i>CS3</i>	<i>CS4</i>	<i>CS5</i>
<i>Cumulative transport (m³)</i>	319.221	167.385	4655.37	6724.57	2947	816.577

Vectorising the sediment transport fluxes (Figure 7-24) allows the assessment of the longshore transport along the Matakana Island shoreface. The longshore transport direction alternates from NW to SE and vice versa. Higher waves during storm conditions ($H_s > 1.2$ m) produce larger sediment transport fluxes towards the shore (Figure 7-24, lower panels) than lower energy average conditions (Figure 7-24, upper panels). As the shoreface shallows close to the beach increasingly shore-parallel transport is evident. Overall, the magnitudes of the wave-induced sediment transport fluxes are low; rarely exceeding $2 \times 10^{-3} \text{ m}^3/\text{s}/\text{m}$.

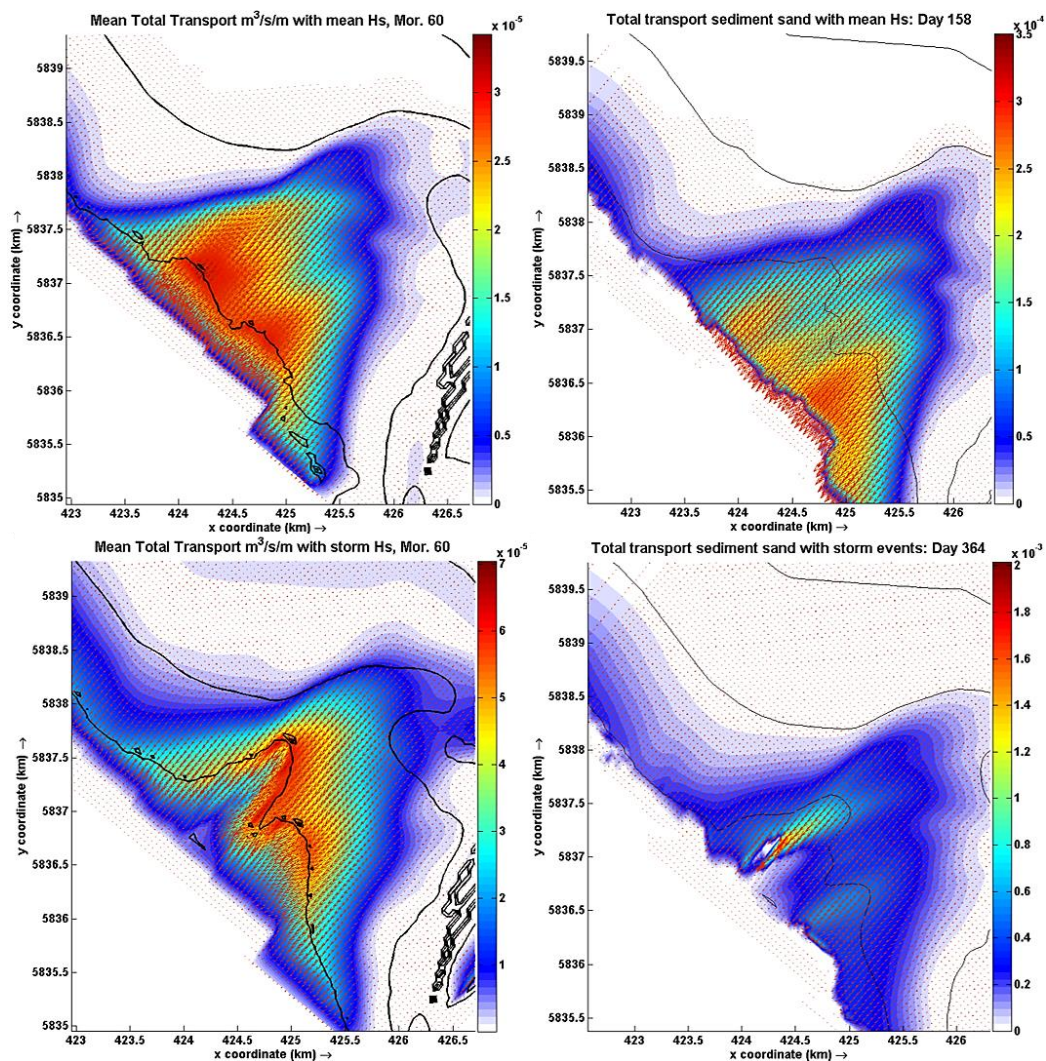


Figure 7-24. Mean and maximum total sediment transport flux magnitude and directions predicted by a 2-years (Mor. 60) simulation of actual maintenance dredging and disposal (DaD Act). The upper panels show the fluxes for average conditions, while lower panels show the sediment fluxes due to storm conditions with wave heights higher than 1.2 m. The predominantly onshore sediment flux directions become increasingly deflected towards the shallow surf zone, resulting in longshore sediment transport in both directions (from/to NW – SE) along the shoreface of Matakana Island. Shaded colours denote the mean total sediment transport magnitude ($\text{m}^3/\text{s}/\text{m}$).

7.3.7 Entrance channel infilling rate

Based on the historical dredging record, the average volume of dredged material removed from the Entrance Channel area over 18 years from 1996 to 2014 was about 93,0573 m³/year. The maximum volume dredged was 259,193 m³ in 2008, and the minimum dredged volume of about 9,209 m³ was in 2010 (Johnstone, 2016, personal communication).

The model results predicted that the amount of accretion was about 433,338 m³ after 2 years of No DaD (fixed grain size of 632 μm, averaged H_s), which represents an overestimation of the Entrance Channel infilling based on maintenance dredging volumes. However, inclusion of dredging and disposal in model simulations with a fixed grain size (Actual DaD, 632 μm, averaged H_s), predicts erosion of up to 1,800,000 m³ along the Entrance Channel. All the alternative site models also predicted erosion of about 1,800,000 m³, with the differences between the alternatives being less than 1,150 m³ (Table 7-4).

In contrast, the Actual DaD model simulations with a variable D₅₀ grain size varying from 136 – 632 μm, and average wave conditions H_s shows significant channel infilling (accretion/accumulation) of about 1.38 Million m³. This indicates that the sediment transport patterns are very sensitive to sediment grain size and wave conditions. Determining the grain size and wave height variations that actually occurred between the historic maintenance dredging events was beyond the scope of this study.

Table 7-4. Summary of sediment volume changes along the Entrance Channel predicted by 2-year modelling assuming no DaD, actual DaD, and DaD combined with alternative sites.

Model Setting	<i>D50 = 136 – 632 μm</i>	<i>D50 = 632 μm</i>				
	DaD Actual	No DaD	DaD Actual	DaD TL	DaD New	DaD NS
Volume (m ³)	1,377,043	433,338	-1,777,217	-1,777,829	-1,776,683	-1,777,285

7.3.5 Ebb-tidal delta volumetric comparisons for alternative disposal sites

In order to compare the volumetric changes resulting from each alternative spoil disposal site relative to the initial volume, the ebb-tidal delta was sub-divided into 4 sections; adjacent to the Entrance Channel, north terminal lobe, swash platform, and north-west terminal lobe (Figure 7-25).

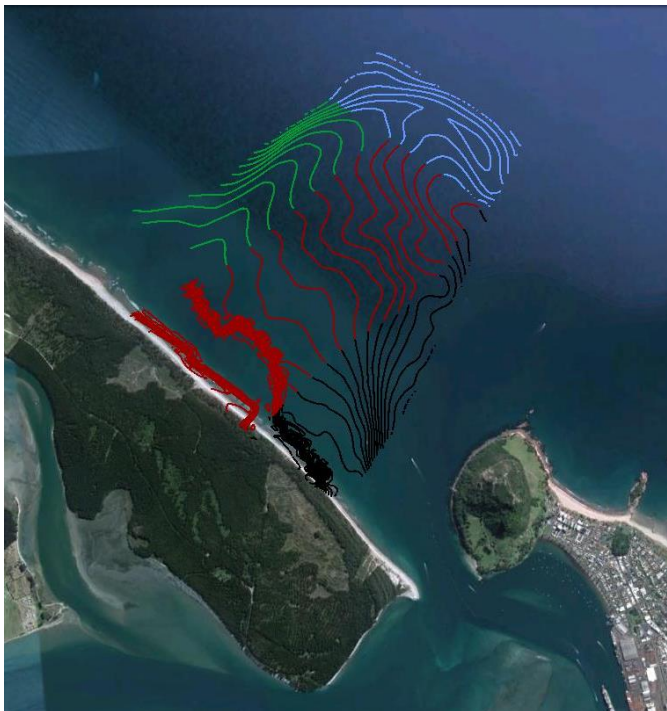


Figure 7-25. Sub-sections of Matakana Banks ebb-tidal delta which were used to obtain volumetric comparison for the alternative spoil disposal sites. The black coloured contours denote the area adjacent to the Entrance Channel, light-blue for the north terminal lobe, red for the swash platform, and green for the northwest terminal lobe.

Table 7-5 summarizes the volume changes for the sub-sections and entire ebb-tidal delta after 2-year simulations with and without any dredging operations, and incorporating different additional disposal sites to renourish the delta. It is evident that overall the models predict lower volumes than the initial condition. The reductions ranged from 1.2% (No DaD) to 3.7% (DaD TL) less than the initial volume of the entire ebb-tidal delta.

Table 7-5. Volume changes of ebb-tidal delta after 2 years simulation. Positive and negative values indicate accretion and erosion from the initial ebb-tidal delta volume respectively. EC denotes Entrance Channel, TL = terminal lobe, PF = platform and NWTL = northwest terminal lobe.

<i>Sections</i>	<i>Initial</i>	<i>No DaD</i>	<i>DaD Act</i>	<i>DaD TL</i>	<i>DaD New</i>	<i>DaD NS</i>
<i>Adjacent EC</i>	12,364,779	-34,566	-566,276	-553,626	-608,201	-534,457
<i>North TL</i>	4,080,443	150,327	106,788	106,788	119,145	118,406
<i>Swash PF</i>	29,281,428	859,809	100,797	100,797	253,070	223,487
<i>NWTL</i>	10,968,537	-1,670,213	-1,768,735	-1,768,735	-1,753,734	-1,834,321
<i>Total</i>	56,695,187	-694,643	-2,114,776	-2,114,776	-1,989,721	-2,026,886

However, the sediment losses did not occur uniformly across the whole ebb-tidal delta. Areas where erosion occurred were adjacent to the Entrance Channel and on the northwest terminal lobe, whilst accretion occurred on the north terminal lobe and on the swash platform. The No DaD simulation indicated the least erosion adjacent to the Entrance Channel with about 0.28% volume loss, whereas other simulations showed higher percentages of erosion at around 4.3% to 5% from the initial volume.

Overall the North West terminal lobe (NWTL) was the area that experienced the most erosion in all the models. This region also recorded the most erosion in the historical data obtained by repetitive bathymetry mapping from both single- and multi beam echo sounder surveys. The No DaD simulation predicted 15.2% volume reduction relative to the initial volume. All the simulations that included dredging and disposal, predicted more erosion than this; the Actual DaD volume decreased by 16.7%, DaD TL by 16.1%, DaD New by 16.0% and the highest erosion resulted from siting the mitigation spoil disposal site nearest to the shoreline – DaD NS by 16.72%.

Accretion occurred on the north terminal lobe (NTL) and on the swash platform (SPF). In these areas, the greatest accretion (volume increase) of 2.9% for SPF and 3.7% for NTL was achieved when there was no dredging activity. Including dredging and disposal, the NTL increased volume by 2.6% to 2.9% depending on the additional disposal sites included. With dredging, the swash platform continued to show some accretion. However the percentage increase was significantly lower than the 2.9% gain for the No DaD simulation. Within the SPF,

the Actual DaD model predicted a volume increase of 0.95%; 0.34% for the DaD TL model; 0.86% for the DaD New model; and 0.76% for the DaDNS model.

7.4 Summary

Coupled Flow-Wave modelling with morphology updating by Delft-Flow is capable of simulating many process that are relevant in coastal environment, both separately and in combination, such as tide, wind-wave and sediment transport processes. In this study, modelling of sediment transport has been achieved by adding bed-load and suspended-load sediment transport and morphological change to a 3D hydrodynamic flow model. The resulting coupled model was used for simulations of various alternatives for spoil disposal sites that could be used to mitigate adverse effects to Matakana Banks and Matakana Island resulting from capital dredging.

The sand body of Matakana Banks ebb-tidal delta prior to the first capital dredging in 1967 showed a continual arc of the terminal lobe from the north to southeast at the depth of about 5 m (Figure 7-20, upper left panel). The tidal inlet was shallow, with the deepest part of the inlet throat hardly exceeding 10 m depth. After the initial dredging programme that cut through the ebb-tidal delta, the shape of the ebb-tidal delta became bifurcated and more complex in its morphology. Focussing the tidal currents into a stronger ebb-jet increased the flow velocities, resulting in deepening of the inlet throat.

Changes in the current regime within the harbour due to dredging were also investigated by Mathew (1997) after the second capital dredging programme in 1991. He found that the Lower Western Channel near Panepane Point experienced a significant increase in the tidal current velocity after dredging, which agrees well with the comparison of modelled current prior and post dredging undertaken by this study.

As previously reported by Davies-Colley and Healy (1978), the bottom sediment of the Tauranga Entrance is mainly sand with a small gravel fraction of mollusc shells, shell fragments, and a very small proportion of pumice and rhyolite

fragments. Mud content is generally very low (< 1%). The field campaign in 2013 undertaken as part of this study revealed that the areas around the tidal inlet and Entrance Channel were mostly composed of coarse sand, with some shell fragments (Ramli and de Lange, 2013a). Hence, coarse sandy sediment 632 μm was used in the morphological model to replicate the transport of sediment dispersed from the spoil disposal site.

Capital dredging and associated dumping operations in Tauranga Harbour significantly altered the tidal currents around the tidal inlet. In particular the Entrance Channel has become more ebb-dominated with stronger ebb currents. This was observed by field measurements in April-May 2013 and simulated by the hydrodynamic model comparisons of before and after dredging. An ebb-dominated estuary was also indicated by the previous study of Kwoil and Winter (2011).

The Delft3D-Flow model results show that the tidal contribution to sediment transport is mostly concentrated in the area around the tidal inlet and SE portion of the ebb-tidal delta. The magnitude of the net tidal sediment transport during both spring and neap is low at about $1.6 \times 10^{-16} \text{ m}^3/\text{s}/\text{m}$ (Ramli *et al.*, 2015). In response to the ebb-jet, sand bars on both flanks of the Entrance Channel and on the NE terminal lobe move offshore during ebb flows, and vice versa during the flood tide. However, less sediment is transported back to the shore face, and more transport occurs along the eastern side of the inlet, resulting in a net movement towards the SE margin of the ebb tidal delta. Both spring and neap ebb-tides indicate that the sediment is deposited in the SE region of the ebb-tidal delta, but the sediment is distributed over a larger area during the neap ebb-tide. These results are consistent with the results of Spiers *et al.* (2009), who attributed the pattern to the formation of eddies flanking the ebb-jet.

Including wave and wind forcing into the model shows that the rate and extent of sediment transport increases, particularly in the breaker zone, such in the nearshore zone, over the shallow swash bars, and along the shallow terminal lobes of the ebb-tidal delta. This contrasts with the model based on tidal forcing only, which shows most transport occurred close to the tidal inlet. The tidal currents still produce the same underlying sediment transport pattern, but it is much smaller than the magnitude of wave-induced transport. Decreased water depth over the shallow shoal areas of the delta allows even small to moderate waves to cause an increase

in the bottom orbital velocity, and an increased potential for sediment resuspension (Bever and MacWilliams, 2013). The influence of waves appears to be stronger during ebb-tide.

Disposal of the spoil at the current dumping sites (inner shelf adjacent to the Tauranga) helps to stabilize Mt. Maunganui Beach as a result of shoreward migration of dredged material from the dumping site, as reported by Healy *et al.*, 1991. In this study, simulations of the dredged spoil dispersion for the alternative mitigation spoil sites reveals that most of dredged material was directly transported toward the shore rather than back into the Entrance Channel.

The presence of coarse sand with shell and shell fragments (Ramli and de Lange, 2013a) and very rapid consolidation of the dredged material (Moon *et al.*, 1994) stabilized the dumped material within the disposal site, particularly when it is dumped offshore deeper than 20 m. At least 1.07 m/s of tidal current and/or high wave (swell) incident induced currents are required to surpass the threshold velocity of the sediment motion (Miller *et al.*, 1977). During extreme storm conditions, suspended transport rates were still at least an order of magnitude smaller than bedload transport rates for the current disposal sites (Moon *et al.*, 1994).

The development (occurrence) of a large ebb-tidal delta on the ocean side of Tauranga Harbour indicates that the inlet is basically tidal, rather than wave dominated (de Lange and Healy, 1990a). Hence, the volume of Matakana Banks ebb-tidal delta varies with the tidal cycle, and the occurrence of high wave events (storm/swell) did not directly relate to ebb-tidal delta volume fluctuations. Overall there was accretion during neap tide and erosion during spring tide (Ramli *et al.*, 2015).

In general, the locations of erosion and accretion resulting from dredging and spoil disposal are consistent among the models and agrees well with the repetitive bathymetric surveys. The net volumetric difference among the models were less than 0.2%, however the smallest volumetric changes relative to the initial ebb-tidal volume are associated with spoil disposal located northwest of the ebb-tidal delta (DaD New). The shallowest disposal site (DaD NS) was the most effective at supplying sediment to the Matakana Island shoreface, and therefore would be suitable for mitigating shoreline erosion.

7.5 References

- Aagaard, T., Greenwood, B., and Larsen, S. M. . (2013). Total cross-shore sediment transport under shoaling waves on a steep beach. *Coastal Dynamics*, 39-50.
- Bever, A.J., and MacWilliams, M.L. (2013). Simulating sediment transport processes in San Pablo Bay using coupled hydrodynamic, wave, and sediment transport models. *Marine Geology vol. 345*, 235-253.
- Braddock, H. (2006). *Potential Suitability of Maintenance Dredged Sediments for Beach Renourishment at Pilot Bay (MSc Thesis)*. Hamilton, New Zealand: University of Waikato.
- Brannigan, A. (2009). *Change in Geomorphology, Hydrodynamics and Surficial Sediment of Tauranga Entrance Tidal Delta System (MSc Thesis)*. Hamilton, New Zealand: University of Waikato.
- Cheng, R. (. (1990). Residual currents and long-term transport. . In *Coastal and Estuarine Studies*, 38. (p. 544). New York: Springer-Verlag.
- Dabees, M.A., and Kraus, N.C. (2004). Evaluation of ebb-tidal shoals as a sand source for beach nourishment: general methodology with reservoir model analysis. *Proceedings 17th National Conference on Beach Preservation Technology* (pp. 1-21). Lake Buena Vista, Florida.: Humiston & Moore Engineers.
- Davies-Colley, R.J., and Healy, T.R. (1978). Sediment and hydrodynamics of Tauranga entrance to Tauranga harbour. *New Zealand Journal of Marine and Freshwater Research Vol. 12 No. 3*, 225-236.
- Davis JR, R.A., and Fitzgerald, D.M. (2004). *Beaches and Coasts*. UK: Blackwell Science Ltd.
- de Lange, W. (1988). *Wave Climate and Sediment Transport within Tauranga Harbour, in the Vicinity of Pilot Bay. D. Phil. thesis*. Hamilton New Zealand: University of Waikato, 225p.
- de Lange, W.P. and Healy, T.R. (1989). The wave climate of a shallow mesotidal estuarine lagoon. *Journal of Coastal Research Vol. 6, No. 1*.

- de Lange, W.P. and Healy, T.R. (1990). Renourishment of flood-tidal delta adjacent beach, Tauranga Harbour, New Zealand. *Journal of Coastal Research Vol. 6, No. 3*, 627-640.
- de Lange, W.P., and Healy, T. (1990a). Wave spectra for a shallow meso-tidal estuarine lagoon: Bay of Plenty, New Zealand. *Journal of Coastal Research*, 189-199.
- Flaim, B. (2012). *Sediment dispersion at the New Auckland marine disposal ground, Northeast New Zealand (PhD thesis)*. Hamilton, New Zealand: University of Waikato.
- Foster, G.A., Healy, T.R., and de Lange, W.P. (1996). Presaging beach nourishment from a nearshore dredge dump mound, Mt. Maunganui Beach, New Zealand. *Journal of Coastal Research*, 395-405.
- Harms, C. (1989). *Dredge spoil dispersion from an inner-shelf dump mound (MPhil thesis)*. Hamilton, New Zealand: University of Waikato.
- Healy, T.R., Harms, C., and de Lange, W.P. (1991a). Dredge spoil and inner shelf investigations off Tauranga Harbour, Bay of Plenty, New Zealand. *Proceedings Coastal Sediments Conference* (pp. 2037-2051). Seattle, Washington: American Society of Civil Engineers.
- Healy, T.R., McCabe, B., and Thompson, G. (1991). *Port of Tauranga channel deepening and widening programme, 1991 - 1992 Environmental Impact Assesment Report, 122p*.
- Komar, P. (1996). Tidal-inlet processes and morphology related to the transport of sediments. *Journal of Coastal Research, Special Issue No. 23*, 23-45.
- Kruger, J. (1999). *Sedimentation at the Entrance Channel of Tauranga Harbour, New Zealand (MSc Thesis)*. Hamilton, New Zealand: University of Waikato.
- Kwoil, E., and Winter, C. (2011). Determination of the initial grain size distribution in a tidal inlet by means of numerical modelling. *Journal of Coastal Research*, 1081-1085.
- Lesser, G. (2009). *An approach to medium-term coastal morphological modelling*. Leiden, The Netherlands: CRC Press/Balkema.

- Li, F., Dyt, C., and Griffiths, C. (2005). Multigrain coastal sedimentation model and its Terschelling beach application. In C. & (eds), *Hydrodynamics VI - Theory and Applications* (pp. 225-230). London: Taylor & Francis Group.
- Li, H., Lin, L., Burks-Copes, K.A. (2012). Numerical modeling of coastal inundation and sedimentation by storm surge, tides, and waves at Norfolk, Virginia, USA. *33rd Conference on Coastal Engineering*, (pp. 1-14). Santander, Spain.
- Mathew, J. (1997). *Morphologic changes of tidal deltas and an inner shelf dump ground from large scale dredging and dumping, Tauranga, New Zealand. PhD Thesis*. Hamilton, New Zealand: University of Waikato.
- Miller, M.C., McCave, I.N., and Komar, P.D. (1977). Threshold of sediment motion under unidirectional currents. *Sedimentology vol. 24*, 507-527.
- Miner, M.D., Kulp, M.A., FitzGerald, D.M., and Georgiou, I.Y. (2009). Hurricane-associated ebb-tidal delta sediment dynamics. *Geology Vol. 37*, 851-854.
- Moon, V., de Lange, W., Warren, S., and Healy, T. (1994). Post-disposal behaviour of sandy dredged material at an open-water, inner shelf disposal site. *Journal of Coastal Research*, 651-662.
- Nicolau del Roure, F., Socolofsky, S.A., and Chang, K.A. (2009). Structure and evolution of tidal starting jet vortices at idealized barotropic inlets. *Journal of Geophysical Research: Oceans*, 114(C5). doi:10.1029/2008JC004997, 17.
- NIWA. (2013). *Tide Forecaster*. Retrieved from NIWA Taihoro Nukurangi: <http://www.niwa.co.nz/services/online-services/tide-forecaster>
- Ramli, A. Y., and de Lange, W.P. (2013a). Dredging impacts on the stability of an ebb tidal delta system. *Coasts and Ports 2013*. Sydney, Australia.
- Ramli, A.Y., de Lange, W.P., Bryan, K., and Mullarney, J. (2015). Coupled flow-wave numerical model in assessing the impact of dredging on the morphology of Matakana Banks. *Australasian Coast and Port Conference 2015*, (pp. 1-6). Auckland, New Zealand.

- Spiers, K. (2013). *Investigation of access channel sedimentation processes and the impact of capital dredging on harbour circulation patterns (PhD thesis)*. Hamilton, New Zealand: University of Waikato.
- Spiers, K.C., Healy, T.R., and Winter, C. (2009). Ebb-Jet Dynamics and Transient Eddy Formation at Tauranga Harbour: Implications for Entrance Channel Shoaling. *Journal of Coastal Research*, 234-247.
- van Rijn, L. C. (2007). *Manual Sediment Transport Measurements in Rivers, Estuaries and Coastal Seas*. Netherlands: Rijkswaterstaat/RIKZ, Aqua Publications.
- Warren, S. (1992). *The geomechanics and dispersion of dredge spoil dumped in open water on the inner shelf, Tauranga, New Zealand (MSc thesis)*. Hamilton, New Zealand: University of Waikato.
- Warren, S., Moon, V., de Lange, W., and Healy, T.R. . (1994). Geomechanical properties of sandy dredge spoil and their implications for spoil mobilisation . *Proceedings of the International Coastal Symposium*, (pp. 522-527). Hilton Head Island, South Carolina USA.

Chapter 8: Conclusions and Recommendations

This study aimed to increase the understanding of the processes that control the stability of an ebb-tidal delta potentially affected by dredging activity. The study site of Matakana Banks ebb-tidal delta is located seaward of the eastern inlet of Tauranga Harbour. As the largest export port in New Zealand, the Port of Tauranga regularly undertakes maintenance dredging to maintain the navigational channel, and periodically undertakes capital dredging to allow larger ships to enter the Port. It was roughly 45 years between the first capital dredging in Tauranga Harbour and the last bathymetric survey taken for this study in 2013. This provides a useful period of time to assess the consequences of dredging.

Historical charts, field measurements and process-based numerical simulations with a depth-averaged hydrodynamic, wave, and sediment transport model were used to characterise the ebb-tidal delta and to evaluate the morphological changes of Matakana Banks over time in response to natural forcing and dredging. Calibration and validation of the model results with field measurement data showed satisfactory agreement that provided confidence in utilising the coupled models to predict dredging impacts and assess mitigation measures for any adverse impact from dredging activities.

8.1 Responses to Research Questions

8.1.1 What changes in ebb-tidal morphology were evident following capital dredging?

Before the first capital dredging of the Tauranga Harbour, and particularly the creation of the Entrance Channel, commenced in 1968 Matakana Banks was part of a fully developed arcuate ebb-tidal delta. From the inlet throat, the ebb-tidal delta extended about 4 km offshore, where the maximum depth at the delta's periphery (terminal lobe) was about 5 m. The maximum tidal inlet depth was less

than 10 m, and sediment bypassing occurred over the terminal lobe forming a continual zone of sediment transport from NW-N to SE (Chapter 7 and Figure 8-1).

After 2 periods of capital dredging (1968 and 1992), and predominantly biannual maintenance dredging over 45 years (1968 to 2013), the shape of ebb-tidal delta became bifurcated and more complex (Figure 8-1). The Entrance Channel was made by cutting through the swash platform and terminal lobe of the ebb-tidal delta (Figure 7-1), which affected sediment bypassing from NW-N to SE corresponding to the updrift and downdrift directions identified by previous studies (Figure 8-1).

Since capital dredging occurred, the offshore spatial extent of the delta slightly reduced to about 3,800 m from the inlet throat, and the tidal inlet became significantly deeper. The changes to the tidal inlet and creation of the Entrance Channel altered current velocities during both ebb and flood tides. In particular, the flood-current velocities in the middle of the Entrance Channel significantly decreased by an average of 2.5 times below the values predicted for the same area based on the bathymetry before 1968.

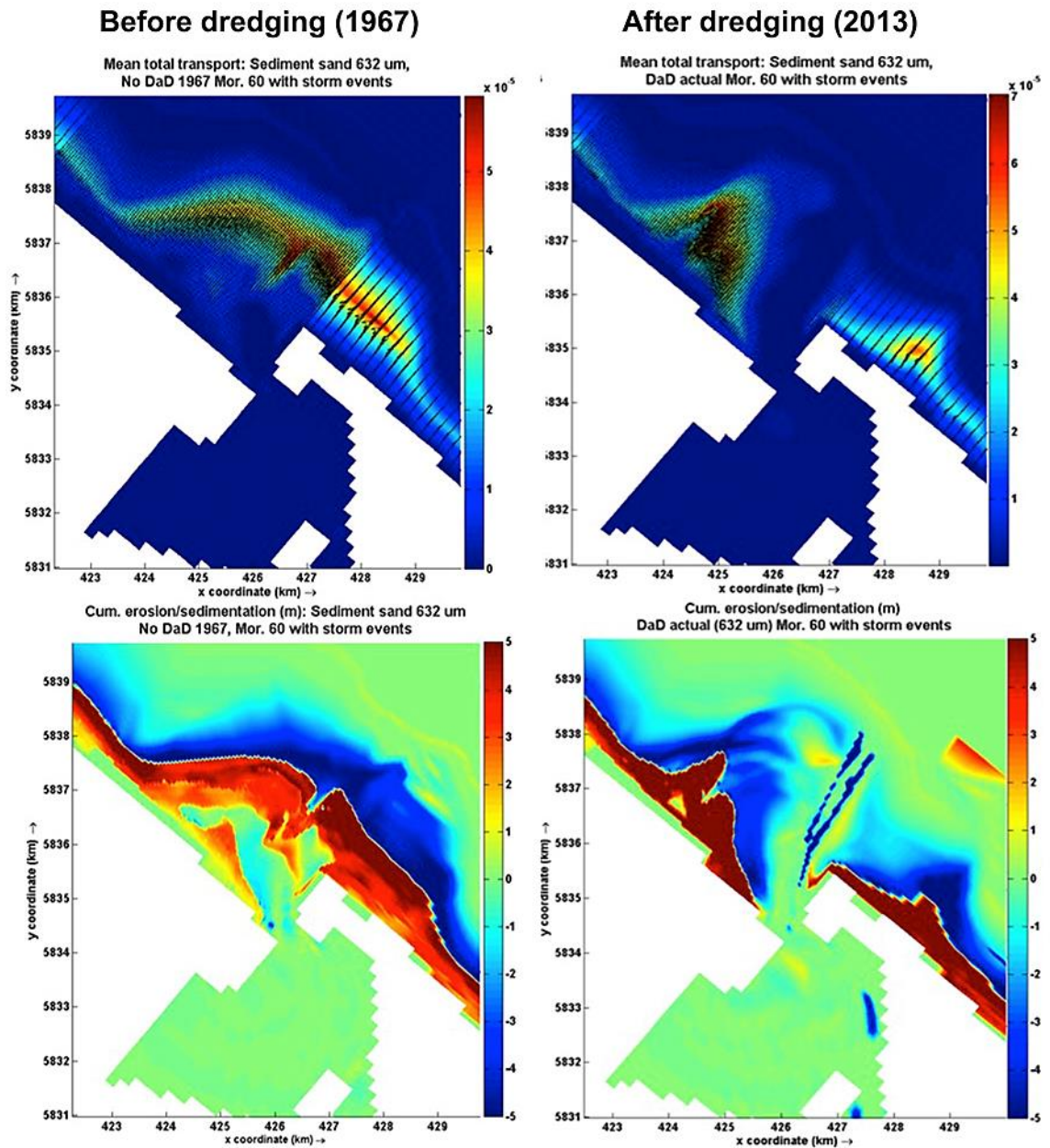


Figure 8-1. Comparisons of the patterns of sediment transport and erosion/accretion before and after capital dredging to create the Entrance Channel through the Matakana Banks ebb –tidal delta (See Chapter 7).

8.1.2 How did the ebb-tidal delta respond to biannual maintenance dredging? What changes in ebb-tidal delta size (volume and area) and shape were noticeable? Are there separate sub-regions based on morphology and hydrodynamic regime that respond differently to forcing?

Analysis of bathymetric maps was undertaken to identify any morphological changes of the ebb-tidal delta between 1998 and 2011. Generally, over this 13-year time span the main shape of the ebb-tidal delta remained the same, consistent with the historical analysis of Brannigan (2009). Mostly, morphological variability occurred due to the migration of mobile sand bars on the swash platform and the flanks of the Entrance Channel. Sand bars on the swash platform migrated towards the NW-N and welded onto the beach as they approached the NW terminal lobe (Figures 8-2 and 4-6). Adjacent to the Entrance Channel, the rate of sandbar movement is strongly related to tidal flows. Further away from the Entrance Channel, a combination of tides and waves drives sand bar migration over the middle part of the swash platform, and waves dominant at the ebb-tidal delta periphery (Chapters 4 and 7).

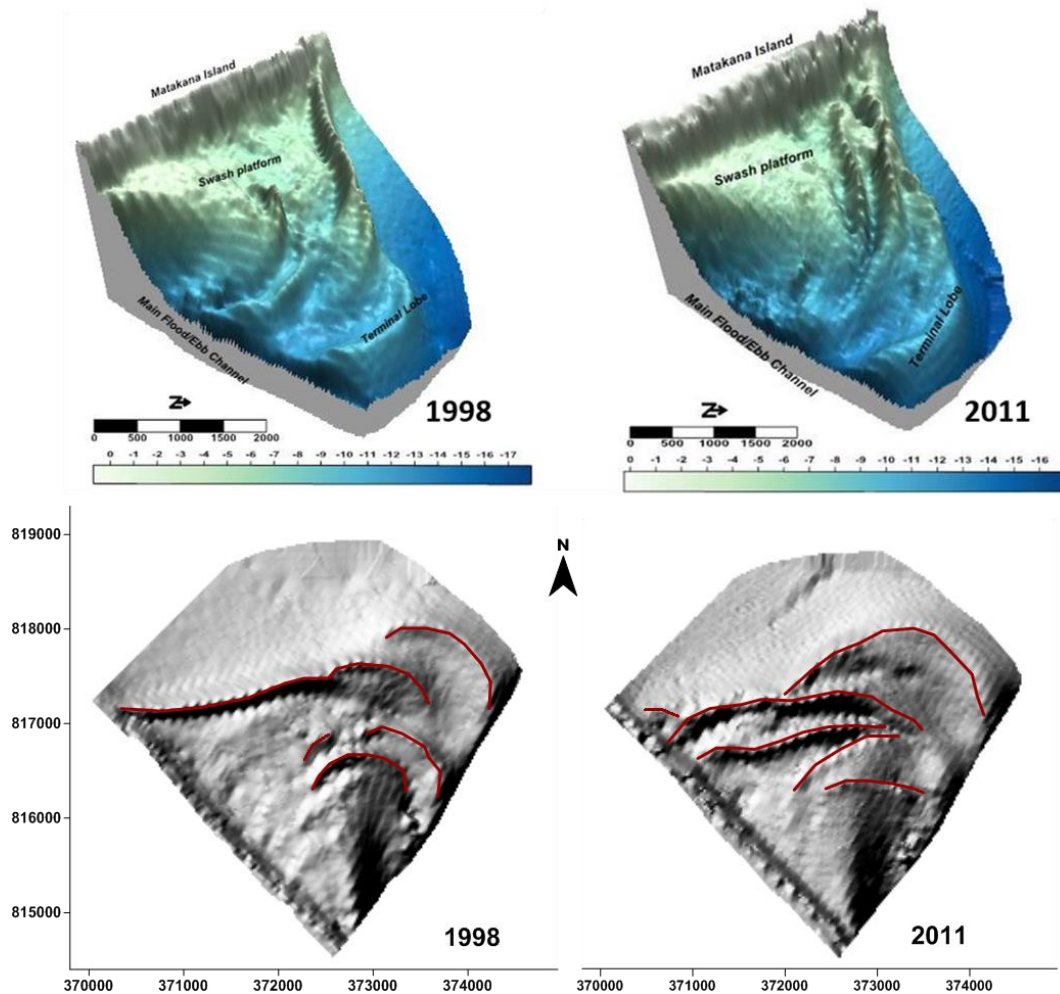


Figure 8-2. 3D (upper panels) and shaded relief surface (lower panels) maps of Matakana Banks ebb-tidal delta. It is clearly seen that from 1998 to 2011, the swash bars changed shape, became more complex, and migrated offshore (modified from Ramli & de Lange, 2013). Red lines (lower panels) denote the sand bars movement.

Hence, the ebb-tidal delta can be divided into 3 sub-regions according to the dominant hydrodynamic regime; (A) the area nearest (adjacent) to the tidal inlet where tidal currents dominate the hydrodynamic regime; (B) an area of shallow shoals (swash platform) where the influence of tidal currents is still present, but waves also play important role in forming the morphology; and (C) the peripheral area (terminal lobe) of the northwestern ebb-tidal delta where the influence of tide is minimal and waves are dominant (Figure 8-3).

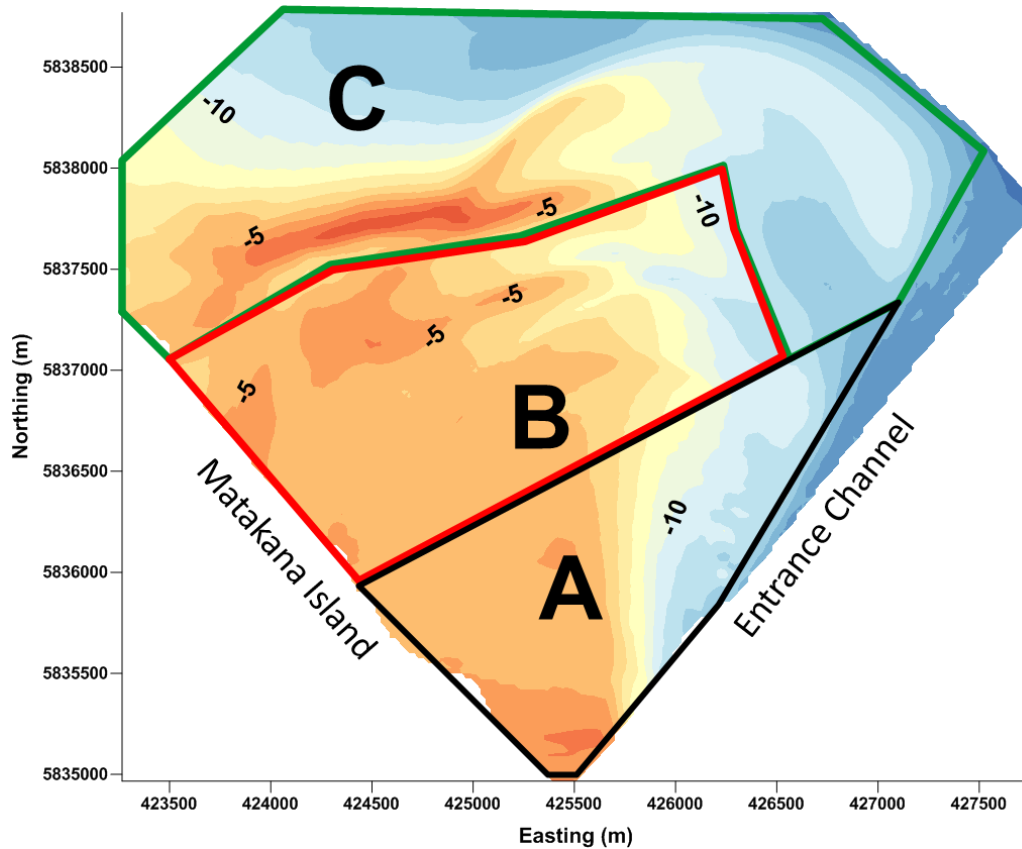


Figure 8-3. The sub-regions of Matakana Banks ebb-tidal delta based on the dominant hydrodynamic regime: tidal currents dominate (A); both waves and tide currents play important role (B); and the terminal lobe area where the influence of tide is minimal and waves are dominant (C).

Volumetric changes were calculated by subtracting the more recent volume from the previous one between 2 consecutive bathymetric surveys. The results show that between 1998 and 2011 the ebb-tidal delta intermittently gained and lost sediment. The largest sediment gain occurred from 2006 to 2008, with about 18.9 million m^3 of sediment added to the net ebb-tidal delta volume. During those years, the total area of ebb-tidal delta was about 7.98 million m^2 . Subsequently, between November 2009 and November 2010, the most severe sediment loss occurred, involving about 14.3 million m^3 volumetric difference. However, during same period the total area of the ebb-tidal delta expanded to about 10.5 million m^2 .

These changes suggested that the volume differences observed were largely a consequence of the redistribution of sediment moving material in and out of the single-beam echo sounder survey transects. Therefore, this study recommended the use of multi-beam echo sounder (MBES) surveys to provide a better spatial resolution and coverage. Only two such surveys were available for this study, so it

was not possible to definitively conclude if the MBES approach reduced the variation of ebb-tidal volumes between surveys.

No systematic pattern of ebb-tidal volume or area changes could be related to maintenance dredging activities during the period analysed. However, given the large inter-survey volume changes relative to maintenance dredging volumes, it is possible that small effects occurred that were swamped by the natural variability. When sufficient MBES survey and maintenance dredging data are available, this question should be re-evaluated.

There were no systematic variations in the wave climate or wind climate, or tidal characteristics measured for the entrance to Tauranga Harbour during the observation period that can be linked to the net gain and loss of the ebb tidal delta volume over the long term. The occurrence of storms or wave events may encourage erosion of the ebb-tidal delta, particularly after a dredging phase, and in the absence of dredging activity, the ebb-tidal delta volume may be stable or increase. However, this was not always the case.

8.1.3 How well did the process-based morphological model simulate the hydrodynamic processes in the tidal inlet and over the ebb-tidal delta? To what extent this approach can be utilized by this study to predict dredging impacts?

Numerical modelling started with simulations of hydrodynamic conditions using tidal forcing only. The computational grid boundaries were set up with 7 major tidal constituents and the model was run for 29 days to cover two neap and spring tidal cycles. One cycle was used for calibration, and the second for verification. These simulations produced very good agreement for the verification water levels, and “good to reasonably fair” agreement for the comparisons with the observed tidal current velocities and directions.

The next stage of modelling incorporated wave forcings and wave-current interactions. The modelled waves within the nearshore of Matakana Island and over the ebb-tidal delta were rated as “Excellent to Good” in comparison to observations. However, the model could not replicate the measured waves inside the harbour very well. This probably due to locally generated wind-waves inside the harbour (de

Lange, 1988; de Lange, and Healy, 1989), and wave height reduction near the tidal inlet because wave energy is spatially redistributed (Niemann, *et al.*, 2010).

The final stage of modelling added sediment transport and evaluated morphological changes. The morphological model simulated a 5-month period that corresponded to the interval between two successive MBES bathymetric surveys. In this study, a *morphological acceleration factor* tool option within the morphological model was used to reduce the calculation time for a long-term simulation. The comparison of the model predictions with the bathymetric survey data showed a good agreement with the patterns of sedimentation and erosion, and associated morphological changes. The quantitative skill score for the morphological changes depicted indicated that the best agreement between observation and model predictions occurred adjacent the tidal inlet and Entrance Channel (Skill score 0.99). However, the model slightly overestimated the volumetric changes by about 4% (Chapter 6).

Overall it was judged that the morphological model was suitable for hindcasting and predicting the impact of maintenance dredging and spoil disposal on the ebb-tidal delta. In particular the good quantitative skill score for morphological changes close to Entrance Channel gave confidence in the modelling of the dredging within the Entrance Channel.

8.1.4 What was the pattern of sand movement? What was the rate of change of the ebb-tidal delta, and what was the main hydrodynamic regime controlling the ebb-tidal delta sediment budget/volume?

The patterns of sand movement were identified by the simulation of sediment transport due to tidal currents only, and also by coupling the FLOW and WAVE models. Sediment transport generated by tidal flow is mostly concentrated in the area around the tidal inlet and the south-eastern portion of the ebb-tidal delta. During flood tide, the sediment along the shoreface adjacent to the tidal inlet and both flanks of the Entrance Channel are transported into the harbour. The pattern reverses during the ebb tide, but less sediment is transported back to the Matakana Island shoreface, and more transport occurs along the eastern side of the inlet, consistent with west to east inlet bypassing of the ebb tidal delta.

Waves significantly alter the sediment transport pattern over the ebb-tidal delta. The tidal currents still produce the same underlying sediment transport pattern around the tidal inlet, however wave-induced sediment transport fluxes were higher than those produced by tides only (Chapter 7). Incident waves from N-NE allow the sediment from the deeper areas seaward of the delta to be transported onshore, with more sediment being shifted onshore during larger wave events (storms). Within the shallow shoals on the swash platform, sediment transport becomes more intense during ebb-neap tide, possibly due to shallower water depths and weaker wave-current interactions. From the model simulations, sediment transport also occurs along the shallow terminal lobes (periphery) of the ebb-tidal delta, particularly in association with migrating sand bars.

The quantification of volumetric changes within the Matakana Banks ebb-tidal delta system was done by firstly defining the 15 m depth contour of the northern ebb-tidal delta as the outer limit, the Entrance Channel as the SE limit, and the NW boundary as the location where the terminal lobe welds onto the beach. From 1998 to 2011, the spatial extent (area) of the ebb-tidal delta fluctuated between $7.9 - 11.7 \times 10^6 \text{ m}^2$, with an average of $\sim 10.6 \times 10^6 \text{ m}^2$. From a point by point comparison of the elevation differences between two consecutive historic bathymetric surveys, the sediment thickness per unit area of the ebb tidal delta varied between -1.35 m during an erosion dominated period, to +1.20 m when accretion dominated (Chapter 4).

The results of one month numerical model simulation, including tides, wind and waves, and sediment transport reveal that the ebb-tidal delta volume fluctuates in response to the tidal cycle. High current velocities during spring tides contribute to a volume loss of delta, but the sediment is replaced during neap tides. Sediment gain and loss volumes are around $8.9 \times 10^6 \text{ m}^3$ and $-8.9 \times 10^6 \text{ m}^3$ respectively, which is a significant proportion of the maximum volume changes determined from the historical data ($18.9 \times 10^6 \text{ m}^3$ accretion and $14.3 \times 10^6 \text{ m}^3$ erosion respectively).

This suggests that the sediment is moved out of the area used for the volumetric comparisons during the spring tide, and returned during the neap, and does not really represent a net gain or loss from the system. It also implies that the determination of the stability of the ebb tidal delta by comparison of historical sediment volumes within the ebb tidal delta needs to account for different tidal conditions.

8.1.5 What are the impacts of maintenance dredging and spoil disposal on the ebb-tidal delta?

The impacts of dredging activity was determined by comparing sediment transport patterns, morphological changes and volumes of the ebb-tidal delta before and after dredging (Chapter 7, Figure 8-1). Further, the effects of alternative spoil disposal sites intended to renourish the ebb-tidal delta to mitigate any adverse erosion effects of dredging were assessed by morphological modelling.

All the alternative spoil disposal sites resulted in the supply of additional sediment to the ebb-tidal delta. Overall, the patterns of accretion and erosion over the ebb-tidal delta were very similar for all disposal sites considered. Slight accretion of <4% occurred on the northern terminal lobe and on the swash platform and some localized erosion occurred on the northwest (NW) terminal lobe and the flanks of the Entrance Channel, where sediment loss percentages up to 16% and 15% respectively. This suggests that the processes over the swash platform effectively redistribute any sediment introduced into the ebb-tidal system.

However, the model results indicate that it is likely that the spoil disposal site nearest to the shoreline in water depths between 6 to 8 m contributes significantly more sediment directly to the shoreface, resulting in more accretion along the Matakana Island shoreface. This is consistent with previous sand tracing experiments that indicated a shallow disposal site contributed directly to nourishment of Mt Maunganui Beach (Foster, *et al.*, 1996).

Volumetric changes determined as a consequence of capital dredging agree well with the morphological changes observed in the historical bathymetric surveys. The percentage of sediment changes predicted by actual dredging activity, and inclusion of alternative mitigation spoil disposal sites vary over a small range: between 4.5% to 5.0% sediment loss adjacent the Entrance Channel and 16.0% to 16.7% on the NW terminal lobe.

The NW terminal lobe was predicted to lose 16.7% of the initial sediment volume without mitigation. Locating the mitigation dredge spoil disposal close to the shoreline had no discernible impact (16.7% sediment loss), and the most effective spoil disposal site located near the NW terminal lobe only showed a

marginal improvement (16.0%). It is likely that the predicted volume losses are too high, as the model predicted a faster rate of morphological change than observed.

Accretion was observed on the northern terminal lobe and on the swash platform in response to dredging and the additional of mitigation disposal sites. This mostly resulted from wave-induced sediment transport from offshore, and over the shallow shoals of the swash platform. On the north terminal lobe, accretion resulted in gains of 2.6% to 2.9% in the comparison with the initial volume, and less than 1% accretion resulted over the swash platform. Overall, the differences in net volumetric changes predicted by the different simulations are very small (<2%), with the least volumetric change occurring for a spoil disposal site located to the northwest of the ebb-tidal delta.

The volume changes predicted by the simulation of actual dredging and disposal activity are larger than those determined from comparisons of historical surveys, which indicated an overall tendency for the ebb tidal to accrete and not erode as predicted by the modelling. Therefore, it is likely that the mitigation spoil mounds will cause more accretion than predicted by the models. However, the changes are still likely to be small compared to the annual variability observed. Given that the ebb-tidal delta appears to be quite stable overall, there does not appear to any useful function for mitigation spoil disposal sites, unless it is necessary to renourish the Matakana Island shoreface.

8.2 Recommendations for further research

8.2.1 Two dimensional versus three dimensional processes

Tauranga Harbour is a complex indented harbour with minor river flows (Bell and Stephens, 2012) that is assumed to be vertically well-mixed and well-flushed (Healy and Kirk, 1992; Tay, *et al.*, 2012). According to Tay *et al* (2013) a distinct horizontal salinity gradient was only found between the upper and lower harbour. The upper harbour area was not included in the computational grid area for this study. The 2DH model allows sediment transport to be computed with relatively simple approximation formulae for depth-averaged sediment transport, and the model run (simulation) time is about 250-800% shorter than a corresponding full 3D simulation (Luijendijk, *et al.* , 2010). Hence, the

hydrodynamic simulations in this study neglected stratification in current velocity, temperature and salinity.

Matakana Banks ebb-tidal delta is also bounded by the Matakana Island beach system on its western side. In the nearshore, where breaking waves cause (secondary) return flow currents, velocity fields are more complex than in deeper water or areas dominated by strong tidal flows. The cross-shore currents are usually rather weak compared to the maximum tidal and wave-driven longshore currents, but have significant residual effect on the cross-shore sediment transport and bed dynamics (Luijendijk, *et al.*, 2010). This is likely to be important if a mitigation spoil disposal site is required in response to erosion of the Matakana Island shoreline. Therefore, a further study concentrating on modelling the sediment transport in the surf zone/nearshore of Matakana Island taking into account this velocity stratification would better assess the impact of a shallow mitigation disposal site on the Matakana Island shoreline.

8.2.2 Morphological changes

The morphological simulations, including tides, wind-waves, and sediment transport, predicted sediment accretion (sand bar formation) along the shoreline, which may change the wave height and direction at the coast. Although the skill score for morphological changes produced by the model comparing to the bathymetric data are “excellent” around the tidal inlet to “reasonable/fair” at the furthest NW (where the ebb-tidal delta terminal lobe welds to the beach), it is considered that the morphological modelling of sand bar formation and migration along the shore face need further calibration. Due to study time limitations and difficulty obtaining permission to install a video camera overlooking the study site, it was necessary to drop the initial objective to conduct video imagery observations for defining shoreline variation and sand bar movement.

The model simulations and historical survey data indicate that the swash bars and longshore bars change in response to weather oscillations. This will change the surf characteristics, and affect erosion/accretion patterns along the Matakana Island. Both are of concern to the Public as expressed in appeals against the resource consents granted for the 2015/16 capital dredging. Therefore, the author suggests

further investigation into the shoreline variability in response to the wave regime and whether dredging program exacerbates or mitigates shoreline instability.

8.2.3 Changes in dredge spoil characteristics

For this study, biennial maintenance dredging activity was simulated with an uniform non-cohesive coarse sand (median grain size, D_{50} , of 632 μ m) representing the sediment grain size at the tidal inlet. A recent study by de Lange *et al.* (2014) identified a range of sediment textures from non-cohesive coarse sand to a stiff “mud” with 42% fines, which would be dredged during the 2015/16 capital dredging. It is unclear if the characteristics of sediment involved in future maintenance dredging will be substantially different. In particular, it is unclear how much sediment suitable for inclusion within mitigation dredge spoil disposal sites will be available. It would be useful to extend the modelling conducted by this study to include a wider range of sediment textures.

8.3 References

- Bell, R., and Stephens, S. . (2012). *Natural Hazards Research Platform: Storm-tide flooding hazard exposure for urbanised estuaries and harbours*. Hamilton, NZ: NIWA.
- de Lange, W. (1988). *Wave Climate and Sediment Transport within Tauranga Harbour, in the Vicinity of Pilot Bay*. D. Phil. thesis. Hamilton New Zealand: University of Waikato, 225p.
- de Lange, W.P. and Healy, T.R. (1989). The wave climate of a shallow mesotidal estuarine lagoon. *Journal of Coastal Research Vol. 6, No. 1*.
- de Lange, W.P., Moon, V., and Fox, B. (2014). *Distribution of silty sediments in the shallow subsurface of the shipping channels of Tauranga Harbour*. ERI report number 43 prepared for the Port of Tauranga Ltd. Hamilton, New Zealand: Environmental Research Institute, Waikato University.
- Foster, G.A., Healy, T.R., and de Lange, W.P. (1996). Presaging beach nourishment from a nearshore dredge dump mound, Mt. Maunganui Beach, New Zealand. *Journal of Coastal Research*, 395-405.
- Healy, T.R., and Kirk, R.M. (1992). Coasts. In J. a. Soon, *Landforms of New Zealand, 2nd edition*. (pp. 81-104). Auckland, New Zealand: Longman Paul Ltd.

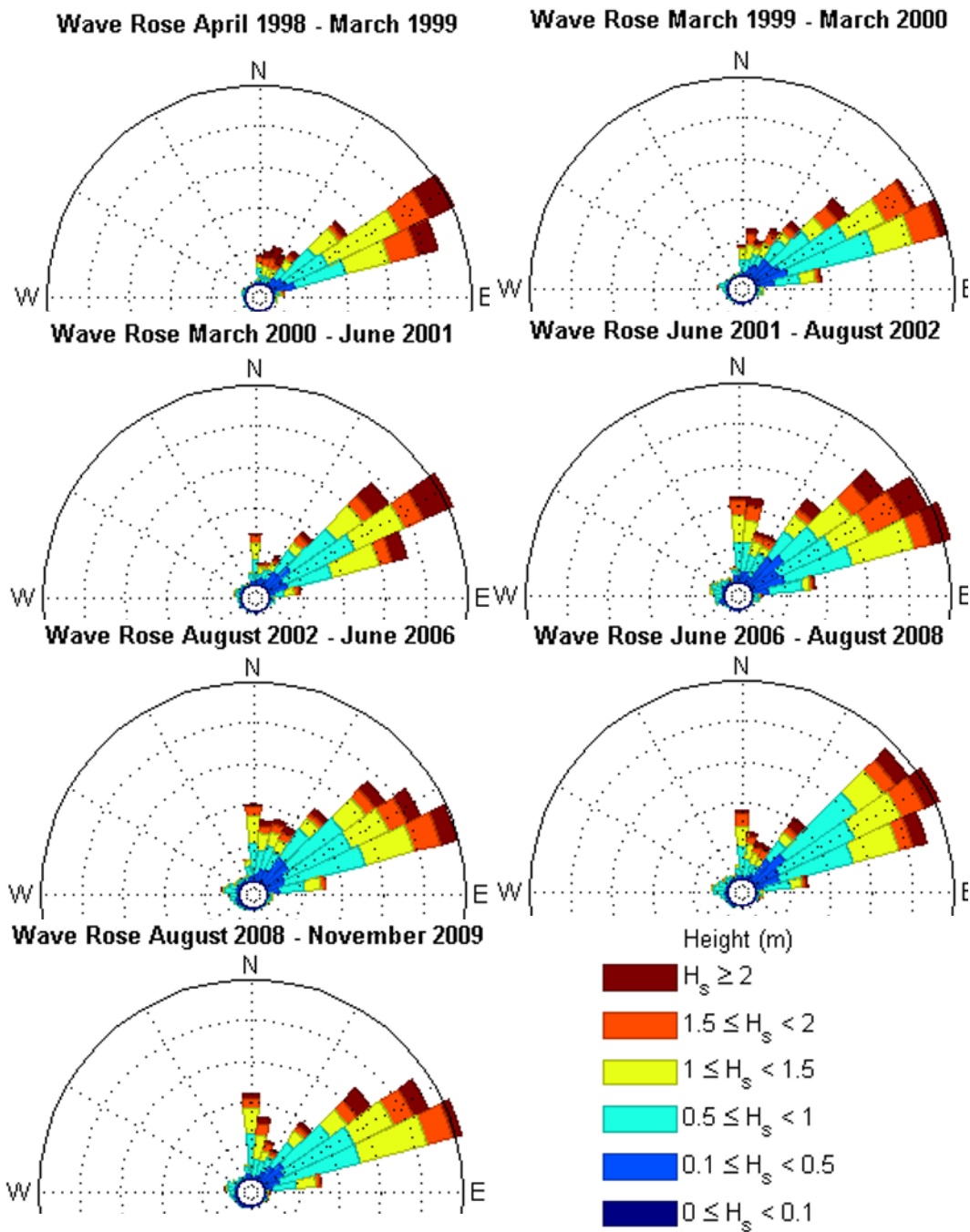
- Luijendijk, A.P., Henrotte, J., Walstra, D.J.R., and van Ormond, M. . (2010). Quasi-3D modelling of surf zone dynamics. *Coastal Engineering*, 1-12.
- Niemann, S.N., Sloth, P., Buhl, J., Deigaard, R., and Broker, I. (2010). Thyboron harbour - study of wave agitation and sedimentation. *Coastal Engineering*, 1-14.
- Tay, H.W., Bryan, K.R., de Lange, W.P., and Pilditch, C.A. (2013). The hydrodynamics of the southern basin of Tauranga Harbour. *New Zealand Journal of Marine and Freshwater Research* , 2-26.
- Tay, H.W., Bryan, K.R., Pilditch, C.A., Park, S., and Hamilton, D.P. . (2012). Variations in nutrient concentrations at different time scales in two shallow tidally dominated estuaries. . *Marine and Freshwater Research Vol. 63*, 95-109.

Appendices

Appendix 1

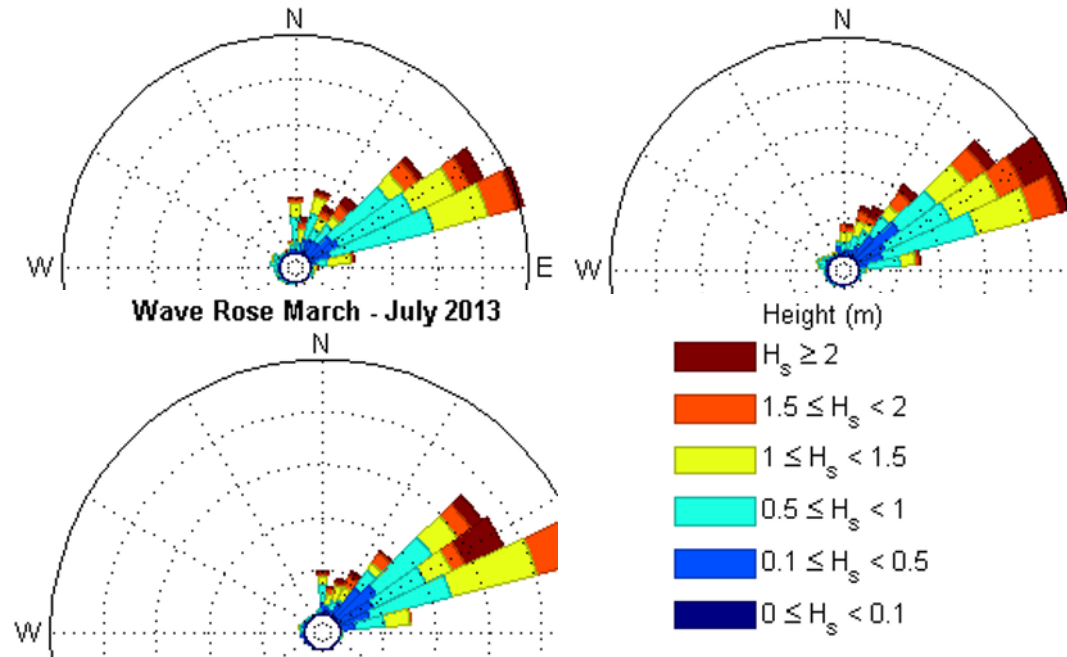
This appendix contains the wave and wind roses used for the analysis of the relationship between the climates and the morphodynamic regimes in Chapter 4.

A. Wave Roses from 1998 to 2013



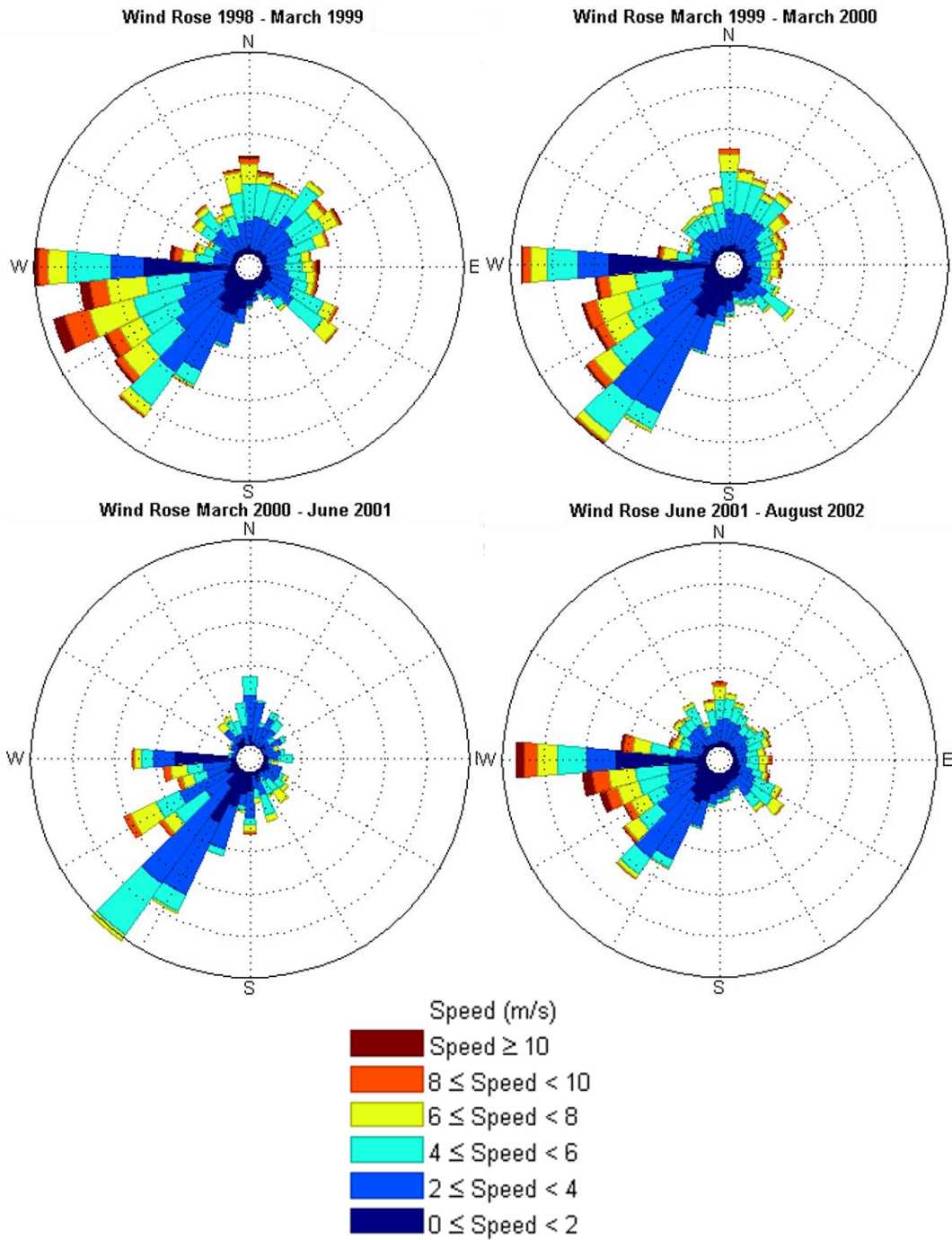
Source: *MetOcean Services International*

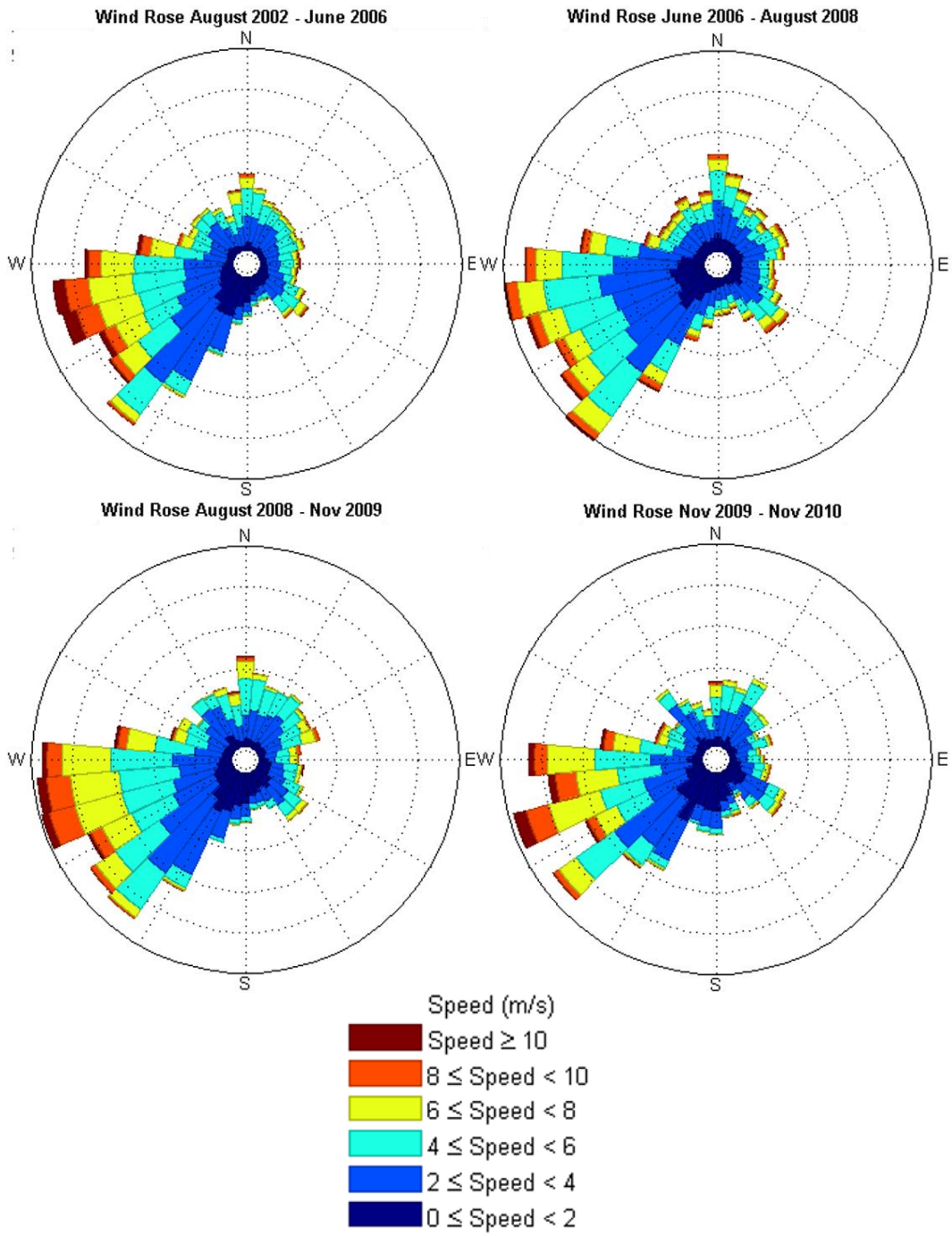
Wave Rose November 2009 - November 2011 Wave Rose November 2010 - November 2011

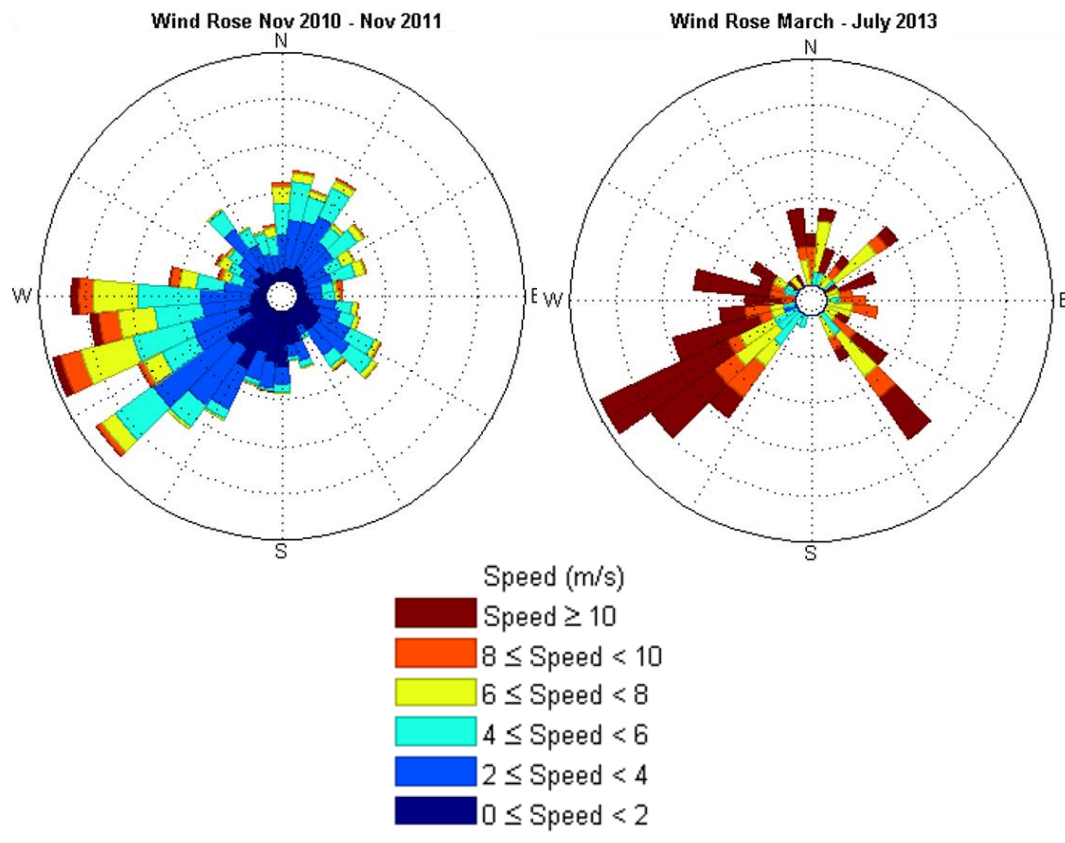


Source: *MetOcean Services International*

B. Wind Roses from 1998 to 2013







Appendix 2

A. Computational grid and monitoring stations

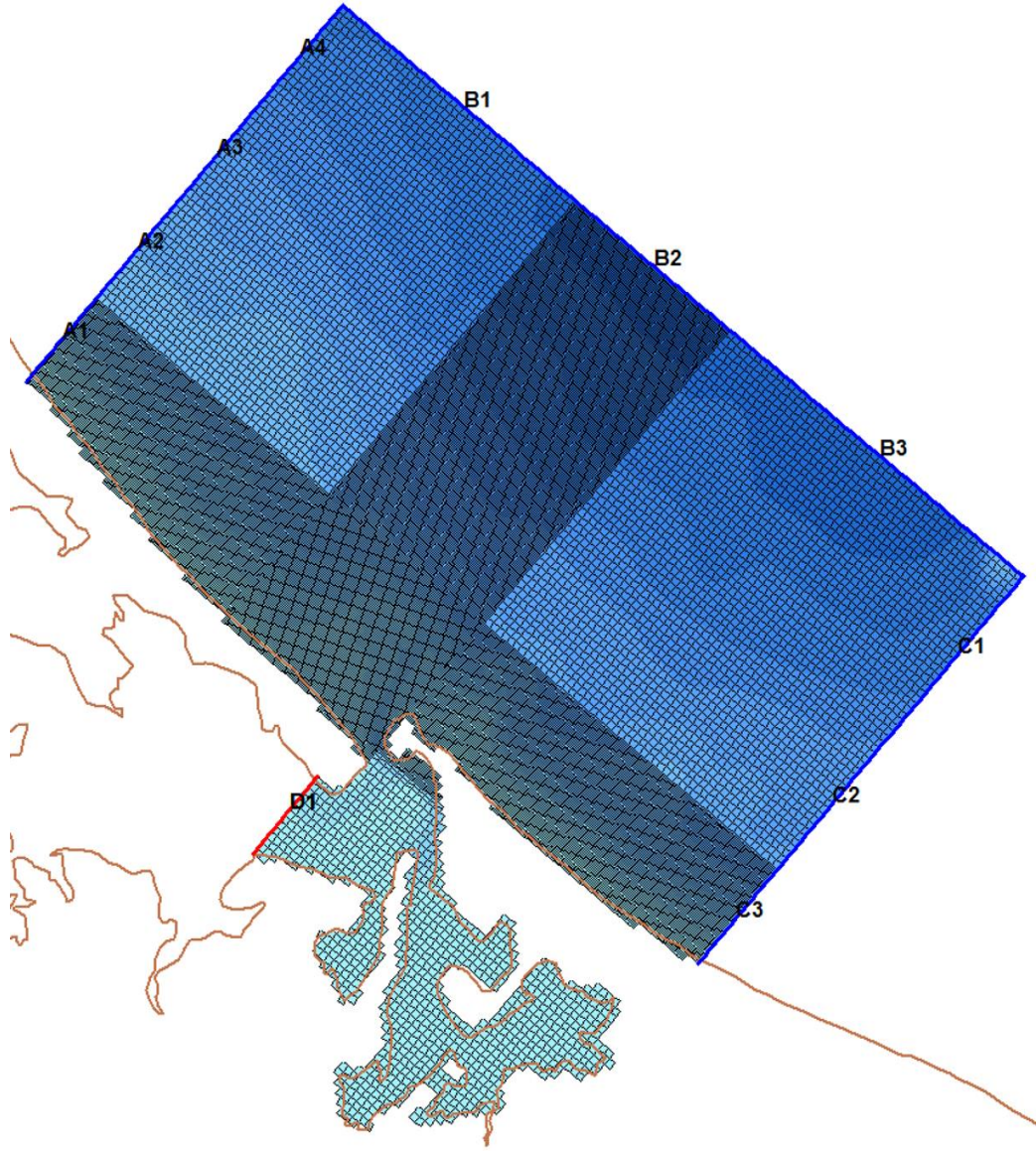


Figure Appendix 2A The computational grid for Flow model with the tidal boundaries and monitoring sets of observation stations and cross-sections.

B. Flow boundary conditions

A1		
O1	1.63E-02	3.00E+02
K1	8.39E-02	3.39E+02
M2	7.11E-01	1.98E+02
N2	1.48E-01	1.81E+02
S2	8.16E-02	2.59E+02
M4	5.80E-03	2.49E+02
MS4	6.60E-03	2.07E+02
C3		
O1	1.64E-02	2.97E+02
K1	8.38E-02	3.38E+02
M2	7.11E-01	1.98E+02
N2	1.48E-01	1.81E+02
S2	8.15E-02	2.58E+02
M4	5.80E-03	2.49E+02
MS4	6.50E-03	2.06E+02
D1		
O1	1.57E-02	3.00E+02
K1	8.41E-02	3.43E+02
M2	7.25E-01	2.07E+02
N2	1.47E-01	1.90E+02
S2	8.17E-02	2.68E+02
M4	5.70E-03	2.67E+02
MS4	6.50E-03	2.26E+02
C2		
O1	1.63E-02	2.97E+02
K1	8.39E-02	3.38E+02
M2	7.10E-01	1.98E+02
N2	1.48E-01	1.81E+02
S2	8.13E-02	2.58E+02
M4	5.80E-03	2.49E+02
MS4	6.50E-03	2.06E+02
C1		
O1	1.61E-02	2.97E+02
K1	8.39E-02	3.38E+02
M2	7.09E-01	1.98E+02
N2	1.48E-01	1.81E+02
S2	8.13E-02	2.58E+02
M4	5.80E-03	2.48E+02
MS4	6.50E-03	2.06E+02
B3		
O1	1.57E-02	2.94E+02
K1	8.41E-02	3.38E+02
M2	7.07E-01	1.98E+02
N2	1.47E-01	1.80E+02
S2	8.14E-02	2.58E+02
M4	5.80E-03	2.49E+02
MS4	6.50E-03	2.07E+02

B2		
O1	1.58E-02	2.97E+02
K1	8.38E-02	3.38E+02
M2	7.08E-01	1.98E+02
N2	1.47E-01	1.81E+02
S2	8.13E-02	2.58E+02
M4	5.80E-03	2.49E+02
MS4	6.50E-03	2.07E+02
A2		
O1	1.64E-02	3.00E+02
K1	8.38E-02	3.39E+02
M2	7.10E-01	1.98E+02
N2	1.48E-01	1.81E+02
S2	8.13E-02	2.58E+02
M4	5.80E-03	2.49E+02
MS4	6.60E-03	2.07E+02
A3		
O1	1.61E-02	2.99E+02
K1	8.41E-02	3.39E+02
M2	7.10E-01	1.98E+02
N2	1.48E-01	1.81E+02
S2	8.13E-02	2.58E+02
M4	5.80E-03	2.49E+02
MS4	6.60E-03	2.07E+02
A4		
O1	1.58E-02	2.98E+02
K1	8.43E-02	3.38E+02
M2	7.08E-01	1.98E+02
N2	1.47E-01	1.81E+02
S2	8.13E-02	2.58E+02
M4	5.80E-03	2.49E+02
MS4	6.50E-03	2.07E+02
B1		
O1	1.56E-02	2.98E+02
K1	8.42E-02	3.38E+02
M2	7.08E-01	1.98E+02
N2	1.47E-01	1.81E+02
S2	8.14E-02	2.58E+02
M4	5.80E-03	2.50E+02

C. Computational grid for Wave model

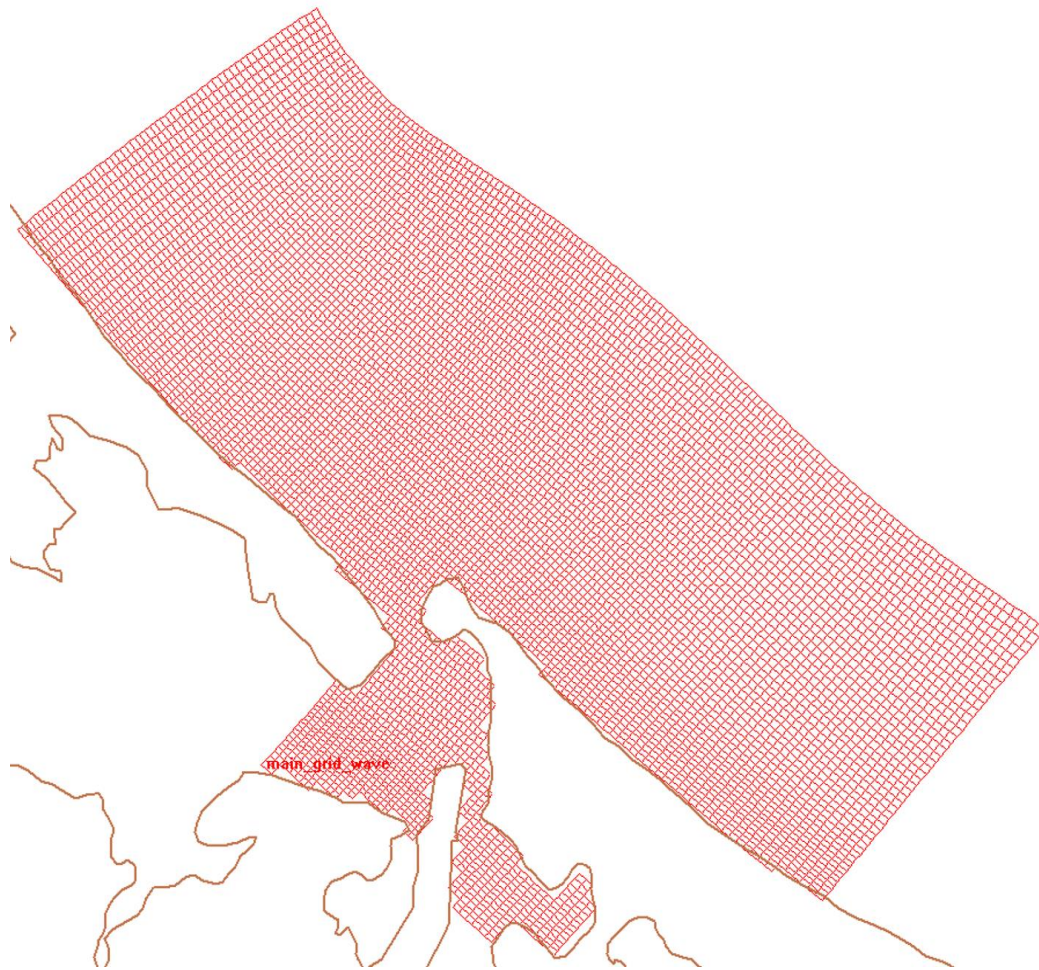


Figure Appendix 2C The computational grid for wave model

D. Wave boundary condition – non averaged wave height (for calibration purposes)

location	'North'				
time-function	'non-equidistant'				
reference-time	20130410				
time-unit	'minutes'				
interpolation	'linear'				
parameter 'time'	unit	'[min]'			
parameter 'WaveHeight'	unit	'[m]'			
parameter 'Period'	unit	'[s]'			
parameter 'Direction'	unit	'[N^o]'			
parameter 'DirSpreading'	unit	'[-]'			
	0	0.578375	9.30458	77.2311	4
	180	0.47088	9.28045	76.8711	4
	360	0.422415	9.27045	76.6833	4
	540	0.418303	9.25758	76.6833	4
	720	0.404952	9.23558	76.7233	4
	900	0.416602	9.20631	76.592	4

1080	0.413976	9.17831	76.272	4
1260	0.409217	9.15545	75.932	4
1440	0.401153	9.13009	75.6596	4
1620	0.393611	9.09345	75.3693	4
1800	0.4438	9.03831	75.0752	4
1980	0.556295	8.95253	74.6434	4
2160	0.514452	8.80298	76.7143	4
2340	0.440868	8.59486	76.4778	4
2520	0.430771	8.4725	76.3783	4
2700	0.441987	8.39463	76.2084	4
2880	0.403903	8.33536	75.807	4
3060	0.402702	8.28536	75.0665	4
3240	0.418085	8.23236	73.9414	4
3420	0.451378	8.17736	72.8774	4
3600	0.462359	8.13736	72.2906	4
3780	0.433342	8.109	72.2278	4
3960	0.400884	8.08436	72.1506	4
4140	0.38233	8.07141	71.996	4
4320	0.376721	8.076	71.9001	4
4500	0.37902	8.09223	71.8696	4
4680	0.427796	8.11123	71.8882	4
4860	0.452119	8.12631	71.9182	4
5040	0.424143	8.13318	71.8677	4
5220	0.402032	12.9317	30.1514	4
5400	0.396868	12.8617	28.5621	4
5580	0.398248	12.8099	26.9392	4
5760	0.398398	12.6808	41.6643	4
5940	0.39422	11.857	43.3819	4
6120	0.441461	11.5004	41.1377	4
6300	0.652171	11.1999	54.447	4
6480	0.71097	4.97671	42.7575	4
6660	0.63274	10.7004	52.156	4
6840	0.667974	10.3704	50.9563	4
7020	0.824922	5.02027	36.3683	4
7200	1.10533	5.55479	32.4878	4
7380	1.41915	5.76889	40.1343	4
7560	1.73211	6.22768	37.9724	4
7740	2.14128	6.47443	45.7153	4
7920	2.39543	7.02028	41.585	4
8100	2.66248	7.52915	51.2333	4
8280	2.90392	8.02137	43.5751	4
8460	3.45338	8.21019	53.0465	4
8640	3.57165	8.73397	56.1181	4
8820	3.6486	9.05115	43.8245	4
9000	3.69788	9.14525	46.5073	4
9180	3.61216	9.24064	47.8302	4

9360	3.33695	9.39631	49.6154	4
9540	3.31017	9.38819	52.0004	4
9720	3.0294	9.50578	53.2033	4
9900	2.65135	9.58356	53.6465	4
10080	2.4738	9.62974	53.9786	4
10260	2.42985	9.61152	54.3944	4
10440	2.20689	9.53352	54.3502	4
10620	1.99602	9.44416	54.152	4
10800	1.79897	9.38235	54.4955	4
10980	1.67306	9.37703	55.9065	4
11160	1.51115	9.42975	58.5849	4
11340	1.34751	9.49838	61.7433	4
11520	1.30395	9.55465	63.9949	4
11700	1.30477	9.57869	65.3686	4
11880	1.29853	9.52842	65.9799	4
12060	1.27145	9.43409	66.1791	4
12240	1.21945	9.34142	66.2572	4
12420	1.14367	9.27236	66.3194	4
12600	1.06975	9.24013	66.4017	4
12780	1.00575	9.23776	66.4262	4
12960	0.948109	9.24543	66.2266	4
13140	0.894361	9.24519	65.6929	4
13320	0.847506	9.23351	64.7542	4
13500	0.91284	9.21656	63.4568	4
13680	1.11964	9.19015	62.2062	4
13860	1.44009	5.09857	50.5693	4
14040	1.37737	5.61023	61.9105	4
14220	1.20389	5.70624	65.7731	4
14400	1.164	5.70692	69.1905	4
14580	1.35688	6.13144	80.314	4
14760	1.30322	6.36115	82.0418	4
14940	1.19526	6.23232	81.8426	4
15120	1.1919	5.89814	76.3408	4
15300	1.42423	6.39152	82.8845	4
15480	1.44068	6.54411	81.1948	4
15660	1.34763	6.46383	77.0905	4
15840	1.23448	6.32524	72.163	4
16020	1.15729	6.19542	68.9503	4
16200	1.19275	5.83871	49.1078	4
16380	1.17357	5.81521	48.2678	4
16560	1.08943	5.78295	48.6715	4
16740	0.956257	5.9796	53.5557	4
16920	0.893186	5.8823	56.2665	4
17100	0.873721	5.67929	54.8137	4
17280	0.906024	5.74393	50.3696	4

```

location      'SE'
time-function  'non-equidistant'
reference-time 20130410
time-unit     'minutes'
interpolation 'linear'
parameter 'time ' unit '[min]'
parameter 'WaveHeight' unit '[m]'
parameter 'Period' unit '[s]'
parameter 'Direction' unit '[N^o]'
parameter 'DirSpreading' unit '[-]'
    0      0.2876   17.49   27.32   4
    180    0.2572   17.28   27.4    4
    360    0.2458   17.2    27.45   4
    540    0.251    17.16   27.48   4
    720    0.249    17.1    27.51   4
    900    0.2548    17      27.53   4
   1080    0.2633   16.93   27.39   4
   1260    0.2738   16.91   27.39   4
   1440    0.2831   16.9    27.39   4
   1620    0.2934   16.91   27.4    4
   1800    0.3133   16.88   27.56   4
   1980    0.3099   16.84   27.57   4
   2160    0.3104   16.75   27.56   4
   2340    0.311    16.61   27.55   4
   2520    0.3155   16.37   27.53   4
   2700    0.32     15.94   26.61   4
   2880    0.3248   15.57   26.45   4
   3060    0.3378   15.42   26.45   4
   3240    0.3417   15.31   26.47   4
   3420    0.3413   15.23   26.52   4
   3600    0.3387   15.16   26.55   4
   3780    0.3288   15.08   26.76   4
   3960    0.3198   14.99   26.81   4
   4140    0.3139   14.89   26.84   4
   4320    0.31     14.75   26.94   4
   4500    0.3089   14.45   26.99   4
   4680    0.3148   13.88   26.36   4
   4860    0.3041   13.6    26.4    4
   5040    0.2999   13.43   26.39   4
   5220    0.297    13.32   26.33   4
   5400    0.2987   13.27   26.31   4
   5580    0.307    13.24   26.21   4
   5760    0.316    13.2    26.14   4
   5940    0.3213   13.11   26.19   4
   6120    0.3643   12.93   26.34   4
   6300    0.4979   11.98   27.59   4

```

6480	0.537	11.55	27.99	4
6660	0.5004	11.44	28.32	4
6840	0.526	10.93	31.46	4
7020	0.6395	5.031	28.96	4
7200	0.8749	5.607	27.8	4
7380	1.074	5.995	29.63	4
7560	1.29	6.424	28.76	4
7740	1.46	6.725	30.62	4
7920	1.612	7.434	28.98	4
8100	1.739	8.111	27.85	4
8280	1.83	8.665	29.69	4
8460	1.96	9.005	28.05	4
8640	2.013	9.317	29.19	4
8820	2.049	9.67	30.13	4
9000	2.073	9.984	27.25	4
9180	2.073	10.11	28.06	4
9360	2.044	10.13	29.1	4
9540	2.029	10.07	30.43	4
9720	1.963	10.07	31.76	4
9900	1.857	10.09	33.25	4
10080	1.788	10.08	34.16	4
10260	1.756	10.04	34.58	4
10440	1.689	9.92	34.69	4
10620	1.577	9.688	34.59	4
10800	1.432	9.538	34.57	4
10980	1.267	9.466	34.87	4
11160	1.13	9.413	35.49	4
11340	1.017	9.419	36.62	4
11520	0.9582	9.424	37.55	4
11700	0.9127	9.408	38.09	4
11880	0.8771	9.335	38.24	4
12060	0.8417	9.229	38.26	4
12240	0.8056	9.139	38.33	4
12420	0.768	9.086	38.4	4
12600	0.7299	9.081	38.38	4
12780	0.6926	9.125	38.19	4
12960	0.657	9.219	37.85	4
13140	0.6242	9.346	37.43	4
13320	0.5951	9.463	37.01	4
13500	0.6171	9.54	36.57	4
13680	0.6889	9.594	36.23	4
13860	0.9533	5.034	37.02	4
14040	1.053	5.538	39.01	4
14220	0.8826	5.65	40.65	4
14400	0.8349	5.636	41.66	4
14580	1.08	5.756	45.02	4

14760	0.962	6.251	47.77	4
14940	0.7837	6.053	46.62	4
15120	0.896	5.654	47.71	4
15300	1.157	6.225	49.58	4
15480	1.025	6.468	47.97	4
15660	0.8951	6.367	46.2	4
15840	0.832	6.158	43.62	4
16020	0.788	5.89	36.54	4
16200	0.7851	5.651	34.05	4
16380	0.7576	5.604	32.85	4
16560	0.7293	5.478	32.69	4
16740	0.6645	10.95	30.38	4
16920	0.6264	11.02	29.92	4
17100	0.6339	10.91	29.4	4
17280	0.6822	10.76	29.07	4

location 'East'
time-function 'non-equidistant'
reference-time 20130410
time-unit 'minutes'
interpolation 'linear'
parameter 'time ' unit '[min]'
parameter 'WaveHeight' unit '[m]'
parameter 'Period' unit '[s]'
parameter 'Direction' unit '[N^o]'
parameter 'DirSpreading' unit '[-]'

0	0.465547	9.26021	73.9603	4
180	0.371506	9.24323	73.5159	4
360	0.338203	9.23717	73.2913	4
540	0.337208	9.2211	73.2593	4
720	0.328475	9.19697	73.2041	4
900	0.353963	9.16821	72.9456	4
1080	0.34634	9.14219	72.4375	4
1260	0.343283	9.12219	71.8518	4
1440	0.34016	9.09921	71.3037	4
1620	0.33989	9.06628	70.7761	4
1800	0.408292	9.01769	70.1551	4
1980	0.542777	8.94285	69.3249	4
2160	0.497997	9.33001	69.8777	4
2340	0.405427	9.13012	69.3943	4
2520	0.380633	8.48963	71.9307	4
2700	0.391364	8.56378	70.6682	4
2880	0.37355	8.82744	67.9998	4
3060	0.392582	8.76387	67.1439	4
3240	0.410836	15.28	23.0729	4
3420	0.449015	15.2	23.3059	4

3600	0.451205	15.13	23.4748	4
3780	0.409188	15.04	23.7635	4
3960	0.375047	14.93	24.0956	4
4140	0.35399	14.8002	24.5475	4
4320	0.346887	14.6037	25.0992	4
4500	0.356484	8.10459	66.532	4
4680	0.423014	8.11883	66.7266	4
4860	0.445411	8.1277	66.8344	4
5040	0.398368	8.36423	64.8806	4
5220	0.363912	8.371	64.5376	4
5400	0.354037	11.6291	34.7235	4
5580	0.353483	12.9715	21.4765	4
5760	0.354296	12.915	21.2888	4
5940	0.352717	11.0025	43.9466	4
6120	0.412068	10.7425	44.3478	4
6300	0.62603	10.5797	42.667	4
6480	0.670985	3.68137	39.0475	4
6660	0.612686	3.899	41.11	4
6840	0.66046	4.24436	39.34	4
7020	0.815795	4.96341	35.2628	4
7200	1.10005	5.54535	31.9005	4
7380	1.39075	5.81348	37.6925	4
7560	1.71081	6.28749	35.4874	4
7740	2.0495	6.5273	41.5576	4
7920	2.32797	7.12607	37.4396	4
8100	2.69008	7.60062	47.531	4
8280	2.88789	8.14565	39.5852	4
8460	3.4289	8.31782	49.1077	4
8640	3.56375	8.96306	38.1959	4
8820	3.65177	9.27745	39.9679	4
9000	3.72384	9.3279	42.2243	4
9180	3.6945	9.40038	43.6658	4
9360	3.49426	9.48575	45.3582	4
9540	3.46915	9.46445	47.7815	4
9720	3.14292	9.59177	48.587	4
9900	2.72182	9.66678	49.0434	4
10080	2.52694	9.69811	49.3876	4
10260	2.51088	9.66867	49.6611	4
10440	2.28972	9.56719	49.4085	4
10620	2.06712	9.46166	48.992	4
10800	1.84986	9.38318	49.1505	4
10980	1.71525	9.347	50.3184	4
11160	1.51796	9.3425	52.8047	4
11340	1.30893	9.33958	56.0443	4
11520	1.21819	9.33408	58.3736	4
11700	1.17675	9.30375	59.5258	4

11880	1.15338	9.22662	59.8678	4
12060	1.13138	9.12549	59.976	4
12240	1.08751	9.02973	60.1456	4
12420	1.01863	8.95166	60.3356	4
12600	0.9513	8.89777	60.4271	4
12780	0.895663	8.85788	60.2635	4
12960	0.847459	8.82066	59.7393	4
13140	0.803983	8.80514	59.4726	4
13320	0.766001	8.85061	57.86	4
13500	0.816788	8.91848	56.344	4
13680	0.978743	8.98484	54.9535	4
13860	1.42218	5.0784	50.7065	4
14040	1.43792	5.60502	57.6245	4
14220	1.195	5.68528	60.4484	4
14400	1.21025	5.64194	63.3544	4
14580	1.4818	6.0053	67.9961	4
14760	1.31944	6.31543	74.6731	4
14940	1.13544	6.11848	74.4427	4
15120	1.21257	5.75265	69.4256	4
15300	1.50919	6.35662	75.5369	4
15480	1.42601	6.49765	74.1846	4
15660	1.29076	6.40802	70.5802	4
15840	1.18485	6.2636	65.8698	4
16020	1.10181	6.12605	63.1601	4
16200	1.14894	5.7533	43.7666	4
16380	1.12976	5.73475	42.8116	4
16560	1.06852	5.63517	43.1713	4
16740	0.93108	5.7604	47.9165	4
16920	0.857948	5.71215	50.8596	4
17100	0.845822	5.60166	49.9148	4
17280	0.890792	5.70632	46.0644	4

E. Wave boundary condition with averaged wave height (for long-term model with morfac)

location	'North'			
time-function	'non-equidistant'			
reference-time	20130410			
time-unit	'minutes'			
interpolation	'linear'			
parameter 'time'	unit '[min]'			
parameter 'WaveHeight'	unit '[m]'			
parameter 'Period'	unit '[s]'			
parameter 'Direction'	unit '[N^o]'			
parameter 'DirSpreading'	unit '[-]'			
0	1.204769	9.30458	77.2311	4
180	1.204769	9.28045	76.8711	4

360	1.204769	9.27045	76.6833	4
540	1.204769	9.25758	76.6833	4
720	1.204769	9.23558	76.7233	4
900	1.204769	9.20631	76.592	4
1080	1.204769	9.17831	76.272	4
1260	1.204769	9.15545	75.932	4
1440	1.204769	9.13009	75.6596	4
1620	1.204769	9.09345	75.3693	4
1800	1.204769	9.03831	75.0752	4
1980	1.204769	8.95253	74.6434	4
2160	1.204769	8.80298	76.7143	4
2340	1.204769	8.59486	76.4778	4
2520	1.204769	8.4725	76.3783	4
2700	1.204769	8.39463	76.2084	4
2880	1.204769	8.33536	75.807	4
3060	1.204769	8.28536	75.0665	4
3240	1.204769	8.23236	73.9414	4
3420	1.204769	8.17736	72.8774	4
3600	1.204769	8.13736	72.2906	4
3780	1.204769	8.109	72.2278	4
3960	1.204769	8.08436	72.1506	4
4140	1.204769	8.07141	71.996	4
4320	1.204769	8.076	71.9001	4
4500	1.204769	8.09223	71.8696	4
4680	1.204769	8.11123	71.8882	4
4860	1.204769	8.12631	71.9182	4
5040	1.204769	8.13318	71.8677	4
5220	1.204769	12.9317	30.1514	4
5400	1.204769	12.8617	28.5621	4
5580	1.204769	12.8099	26.9392	4
5760	1.204769	12.6808	41.6643	4
5940	1.204769	11.857	43.3819	4
6120	1.204769	11.5004	41.1377	4
6300	1.204769	11.1999	54.447	4
6480	1.204769	4.97671	42.7575	4
6660	1.204769	10.7004	52.156	4
6840	1.204769	10.3704	50.9563	4
7020	1.204769	5.02027	36.3683	4
7200	1.204769	5.55479	32.4878	4
7380	1.204769	5.76889	40.1343	4
7560	1.204769	6.22768	37.9724	4
7740	1.204769	6.47443	45.7153	4
7920	1.204769	7.02028	41.585	4
8100	1.204769	7.52915	51.2333	4
8280	1.204769	8.02137	43.5751	4
8460	1.204769	8.21019	53.0465	4

8640	1.204769	8.73397	56.1181	4
8820	1.204769	9.05115	43.8245	4
9000	1.204769	9.14525	46.5073	4
9180	1.204769	9.24064	47.8302	4
9360	1.204769	9.39631	49.6154	4
9540	1.204769	9.38819	52.0004	4
9720	1.204769	9.50578	53.2033	4
9900	1.204769	9.58356	53.6465	4
10080	1.204769	9.62974	53.9786	4
10260	1.204769	9.61152	54.3944	4
10440	1.204769	9.53352	54.3502	4
10620	1.204769	9.44416	54.152	4
10800	1.204769	9.38235	54.4955	4
10980	1.204769	9.37703	55.9065	4
11160	1.204769	9.42975	58.5849	4
11340	1.204769	9.49838	61.7433	4
11520	1.204769	9.55465	63.9949	4
11700	1.204769	9.57869	65.3686	4
11880	1.204769	9.52842	65.9799	4
12060	1.204769	9.43409	66.1791	4
12240	1.204769	9.34142	66.2572	4
12420	1.204769	9.27236	66.3194	4
12600	1.204769	9.24013	66.4017	4
12780	1.204769	9.23776	66.4262	4
12960	1.204769	9.24543	66.2266	4
13140	1.204769	9.24519	65.6929	4
13320	1.204769	9.23351	64.7542	4
13500	1.204769	9.21656	63.4568	4
13680	1.204769	9.19015	62.2062	4
13860	1.204769	5.09857	50.5693	4
14040	1.204769	5.61023	61.9105	4
14220	1.204769	5.70624	65.7731	4
14400	1.204769	5.70692	69.1905	4
14580	1.204769	6.13144	80.314	4
14760	1.204769	6.36115	82.0418	4
14940	1.204769	6.23232	81.8426	4
15120	1.204769	5.89814	76.3408	4
15300	1.204769	6.39152	82.8845	4
15480	1.204769	6.54411	81.1948	4
15660	1.204769	6.46383	77.0905	4
15840	1.204769	6.32524	72.163	4
16020	1.204769	6.19542	68.9503	4
16200	1.204769	5.83871	49.1078	4
16380	1.204769	5.81521	48.2678	4
16560	1.204769	5.78295	48.6715	4
16740	1.204769	5.9796	53.5557	4

	16920	1.204769	5.8823	56.2665	4
	17100	1.204769	5.67929	54.8137	4
	17280	1.204769	5.74393	50.3696	4
location		'SE'			
time-function		'non-equidistant'			
reference-time		20130410			
time-unit		'minutes'			
interpolation		'linear'			
parameter 'time ' unit '[min]'					
parameter 'WaveHeight' unit '[m]'					
parameter 'Period' unit '[s]'					
parameter 'Direction' unit '[N^o]'					
parameter 'DirSpreading' unit '[-]'					
	0	0.821807	17.49	27.32	4
	180	0.821807	17.28	27.4	4
	360	0.821807	17.2	27.45	4
	540	0.821807	17.16	27.48	4
	720	0.821807	17.1	27.51	4
	900	0.821807	17	27.53	4
	1080	0.821807	16.93	27.39	4
	1260	0.821807	16.91	27.39	4
	1440	0.821807	16.9	27.39	4
	1620	0.821807	16.91	27.4	4
	1800	0.821807	16.88	27.56	4
	1980	0.821807	16.84	27.57	4
	2160	0.821807	16.75	27.56	4
	2340	0.821807	16.61	27.55	4
	2520	0.821807	16.37	27.53	4
	2700	0.821807	15.94	26.61	4
	2880	0.821807	15.57	26.45	4
	3060	0.821807	15.42	26.45	4
	3240	0.821807	15.31	26.47	4
	3420	0.821807	15.23	26.52	4
	3600	0.821807	15.16	26.55	4
	3780	0.821807	15.08	26.76	4
	3960	0.821807	14.99	26.81	4
	4140	0.821807	14.89	26.84	4
	4320	0.821807	14.75	26.94	4
	4500	0.821807	14.45	26.99	4
	4680	0.821807	13.88	26.36	4
	4860	0.821807	13.6	26.4	4
	5040	0.821807	13.43	26.39	4
	5220	0.821807	13.32	26.33	4
	5400	0.821807	13.27	26.31	4
	5580	0.821807	13.24	26.21	4
	5760	0.821807	13.2	26.14	4

5940	0.821807	13.11	26.19	4
6120	0.821807	12.93	26.34	4
6300	0.821807	11.98	27.59	4
6480	0.821807	11.55	27.99	4
6660	0.821807	11.44	28.32	4
6840	0.821807	10.93	31.46	4
7020	0.821807	5.031	28.96	4
7200	0.821807	5.607	27.8	4
7380	0.821807	5.995	29.63	4
7560	0.821807	6.424	28.76	4
7740	0.821807	6.725	30.62	4
7920	0.821807	7.434	28.98	4
8100	0.821807	8.111	27.85	4
8280	0.821807	8.665	29.69	4
8460	0.821807	9.005	28.05	4
8640	0.821807	9.317	29.19	4
8820	0.821807	9.67	30.13	4
9000	0.821807	9.984	27.25	4
9180	0.821807	10.11	28.06	4
9360	0.821807	10.13	29.1	4
9540	0.821807	10.07	30.43	4
9720	0.821807	10.07	31.76	4
9900	0.821807	10.09	33.25	4
10080	0.821807	10.08	34.16	4
10260	0.821807	10.04	34.58	4
10440	0.821807	9.92	34.69	4
10620	0.821807	9.688	34.59	4
10800	0.821807	9.538	34.57	4
10980	0.821807	9.466	34.87	4
11160	0.821807	9.413	35.49	4
11340	0.821807	9.419	36.62	4
11520	0.821807	9.424	37.55	4
11700	0.821807	9.408	38.09	4
11880	0.821807	9.335	38.24	4
12060	0.821807	9.229	38.26	4
12240	0.821807	9.139	38.33	4
12420	0.821807	9.086	38.4	4
12600	0.821807	9.081	38.38	4
12780	0.821807	9.125	38.19	4
12960	0.821807	9.219	37.85	4
13140	0.821807	9.346	37.43	4
13320	0.821807	9.463	37.01	4
13500	0.821807	9.54	36.57	4
13680	0.821807	9.594	36.23	4
13860	0.821807	5.034	37.02	4
14040	0.821807	5.538	39.01	4

14220	0.821807	5.65	40.65	4
14400	0.821807	5.636	41.66	4
14580	0.821807	5.756	45.02	4
14760	0.821807	6.251	47.77	4
14940	0.821807	6.053	46.62	4
15120	0.821807	5.654	47.71	4
15300	0.821807	6.225	49.58	4
15480	0.821807	6.468	47.97	4
15660	0.821807	6.367	46.2	4
15840	0.821807	6.158	43.62	4
16020	0.821807	5.89	36.54	4
16200	0.821807	5.651	34.05	4
16380	0.821807	5.604	32.85	4
16560	0.821807	5.478	32.69	4
16740	0.821807	10.95	30.38	4
16920	0.821807	11.02	29.92	4
17100	0.821807	10.91	29.4	4
17280	0.821807	10.76	29.07	4
location	'East'			
time-function	'non-equidistant'			
reference-time	20130410			
time-unit	'minutes'			
interpolation	'linear'			
parameter 'time'	unit '[min]'			
parameter 'WaveHeight'	unit '[m]'			
parameter 'Period'	unit '[s]'			
parameter 'Direction'	unit '[N^o]'			
parameter 'DirSpreading'	unit '[-]'			
0	1.179728	9.26021	73.9603	4
180	1.179728	9.24323	73.5159	4
360	1.179728	9.23717	73.2913	4
540	1.179728	9.2211	73.2593	4
720	1.179728	9.19697	73.2041	4
900	1.179728	9.16821	72.9456	4
1080	1.179728	9.14219	72.4375	4
1260	1.179728	9.12219	71.8518	4
1440	1.179728	9.09921	71.3037	4
1620	1.179728	9.06628	70.7761	4
1800	1.179728	9.01769	70.1551	4
1980	1.179728	8.94285	69.3249	4
2160	1.179728	9.33001	69.8777	4
2340	1.179728	9.13012	69.3943	4
2520	1.179728	8.48963	71.9307	4
2700	1.179728	8.56378	70.6682	4
2880	1.179728	8.82744	67.9998	4
3060	1.179728	8.76387	67.1439	4

3240	1.179728	15.28	23.0729	4
3420	1.179728	15.2	23.3059	4
3600	1.179728	15.13	23.4748	4
3780	1.179728	15.04	23.7635	4
3960	1.179728	14.93	24.0956	4
4140	1.179728	14.8002	24.5475	4
4320	1.179728	14.6037	25.0992	4
4500	1.179728	8.10459	66.532	4
4680	1.179728	8.11883	66.7266	4
4860	1.179728	8.1277	66.8344	4
5040	1.179728	8.36423	64.8806	4
5220	1.179728	8.371	64.5376	4
5400	1.179728	11.6291	34.7235	4
5580	1.179728	12.9715	21.4765	4
5760	1.179728	12.915	21.2888	4
5940	1.179728	11.0025	43.9466	4
6120	1.179728	10.7425	44.3478	4
6300	1.179728	10.5797	42.667	4
6480	1.179728	3.68137	39.0475	4
6660	1.179728	3.899	41.11	4
6840	1.179728	4.24436	39.34	4
7020	1.179728	4.96341	35.2628	4
7200	1.179728	5.54535	31.9005	4
7380	1.179728	5.81348	37.6925	4
7560	1.179728	6.28749	35.4874	4
7740	1.179728	6.5273	41.5576	4
7920	1.179728	7.12607	37.4396	4
8100	1.179728	7.60062	47.531	4
8280	1.179728	8.14565	39.5852	4
8460	1.179728	8.31782	49.1077	4
8640	1.179728	8.96306	38.1959	4
8820	1.179728	9.27745	39.9679	4
9000	1.179728	9.3279	42.2243	4
9180	1.179728	9.40038	43.6658	4
9360	1.179728	9.48575	45.3582	4
9540	1.179728	9.46445	47.7815	4
9720	1.179728	9.59177	48.587	4
9900	1.179728	9.66678	49.0434	4
10080	1.179728	9.69811	49.3876	4
10260	1.179728	9.66867	49.6611	4
10440	1.179728	9.56719	49.4085	4
10620	1.179728	9.46166	48.992	4
10800	1.179728	9.38318	49.1505	4
10980	1.179728	9.347	50.3184	4
11160	1.179728	9.3425	52.8047	4
11340	1.179728	9.33958	56.0443	4

11520	1.179728	9.33408	58.3736	4
11700	1.179728	9.30375	59.5258	4
11880	1.179728	9.22662	59.8678	4
12060	1.179728	9.12549	59.976	4
12240	1.179728	9.02973	60.1456	4
12420	1.179728	8.95166	60.3356	4
12600	1.179728	8.89777	60.4271	4
12780	1.179728	8.85788	60.2635	4
12960	1.179728	8.82066	59.7393	4
13140	1.179728	8.80514	59.4726	4
13320	1.179728	8.85061	57.86	4
13500	1.179728	8.91848	56.344	4
13680	1.179728	8.98484	54.9535	4
13860	1.179728	5.0784	50.7065	4
14040	1.179728	5.60502	57.6245	4
14220	1.179728	5.68528	60.4484	4
14400	1.179728	5.64194	63.3544	4
14580	1.179728	6.0053	67.9961	4
14760	1.179728	6.31543	74.6731	4
14940	1.179728	6.11848	74.4427	4
15120	1.179728	5.75265	69.4256	4
15300	1.179728	6.35662	75.5369	4
15480	1.179728	6.49765	74.1846	4
15660	1.179728	6.40802	70.5802	4
15840	1.179728	6.2636	65.8698	4
16020	1.179728	6.12605	63.1601	4
16200	1.179728	5.7533	43.7666	4
16380	1.179728	5.73475	42.8116	4
16560	1.179728	5.63517	43.1713	4
16740	1.179728	5.7604	47.9165	4
16920	1.179728	5.71215	50.8596	4
17100	1.179728	5.60166	49.9148	4
17280	1.179728	5.70632	46.0644	4

Appendix 3

The following table summarises the median grain size (D50), calculated surface roughness length (ks), and calculated Manning ‘n’ values used for each grid cell to define the bed roughness.

Coordinate system UTM 60S		(D50)	ks	Manning
427255.3758	5837411.191	2.3	0.5076577	0.028438
427555.267	5837412.896	2.52	0.4358574	0.02917
428155.049	5837416.307	2.48	0.448111	0.029036
426953.7794	5837709.377	1.89	0.6745176	0.027123
427251.9658	5838010.974	2.28	0.5147444	0.028373
427551.857	5838012.679	2.55	0.4268876	0.029272
426665.8256	5835608.432	1.84	0.6983045	0.026967
426964.0113	5835910.029	1.87	0.6839336	0.02706
427263.9026	5835911.735	2.4	0.4736614	0.028769
427563.7938	5835913.441	1.86	0.6886907	0.027029
426957.1896	5837109.595	1.76	0.7381204	0.026719
426662.4143	5836208.215	1.37	0.9672281	0.025541
426960.6003	5836509.812	2.34	0.4937758	0.02857
427560.3828	5836513.223	2.5	0.4419417	0.029103
427558.6774	5836813.114	2.61	0.4094979	0.029475
428358.3867	5836817.662	2.7	0.3847326	0.029783
427257.0809	5837111.3	2.4	0.4736614	0.028769
426679.4749	5833209.301	1.19	1.0957572	0.025016
427279.2575	5833212.714	1.95	0.6470406	0.027311
426977.6597	5833510.899	1.08	1.1825721	0.0247
427277.551	5833512.605	1.68	0.7802066	0.026473
427577.4422	5833514.312	2.18	0.5516894	0.028047
426694.3839	5833927.149	2.36	0.4869779	0.028636
426986.1934	5832011.442	1.99	0.6293472	0.027438
427286.0846	5832013.149	2.25	0.5255603	0.028275
426984.4864	5832311.333	1.98	0.6337247	0.027406
427584.2689	5832314.747	1.59	0.8304286	0.026199
426682.8882	5832609.518	1.82	0.7080524	0.026904
427282.6709	5832612.931	2.07	0.5953987	0.027693
426981.0729	5832911.116	1.69	0.7748173	0.026503
427280.9642	5832912.823	2.5	0.4419417	0.029103
427580.8553	5832914.529	2.12	0.5751173	0.027853
425461.1422	5836501.285	1.66	0.7910979	0.026412
425761.034	5836502.99	1.69	0.7748173	0.026503

426360.8174	5836506.401	1.48	0.896222	0.025868
426059.2204	5836804.587	1.26	1.0438599	0.025219
425457.7316	5837101.069	0.48	1.7924441	0.023046
425757.6234	5837102.774	2.03	0.6121377	0.027565
426055.81	5837404.371	1.33	0.9944206	0.025424
426655.5931	5837407.781	1.46	0.9087328	0.025808
425454.3214	5837700.852	0.6	1.6493849	0.023368
425754.2132	5837702.557	1.13	1.1422893	0.024843
426353.9965	5837705.967	1.2	1.0881882	0.025045
426052.3999	5838004.154	1.56	0.8478777	0.026108
426652.1831	5838007.564	2.15	0.5632815	0.02795
426066.0425	5835605.021	1.29	1.0223776	0.025306
425464.5533	5835901.501	1.97	0.6381326	0.027375
425764.4451	5835903.207	2.02	0.6163954	0.027533
426062.6312	5836204.804	1.35	0.9807301	0.025483
425479.9083	5833202.474	2.22	0.5366034	0.028177
425778.0935	5833504.073	1.66	0.7910979	0.026412
426376.1704	5833807.377	1.18	1.1033787	0.024987
426381.29	5832907.703	1.2	1.0881882	0.025045
426086.5189	5832006.321	2.22	0.5366034	0.028177
426386.4105	5832008.028	2.48	0.448111	0.029036
425784.9203	5832304.506	2.09	0.5872017	0.027757
426384.7036	5832307.92	2	0.625	0.02747
426083.1051	5832606.104	1.31	1.0083022	0.025365
425781.5067	5832904.289	2.09	0.5872017	0.027757
426003.2756	5835567.676	1.57	0.842021	0.026138
426022.2528	5835394.841	1.13	1.1422893	0.024843
426043.9332	5835274.004	1.12	1.1502346	0.024814
426043.9332	5835274.004	1.17	1.1110534	0.024958
426112.8902	5835453.337	0.72	1.5177436	0.023694
426432.3481	5835530.13	0.68	1.5604132	0.023585
427025.934	5836623.146	2.25	0.5255603	0.028275
427526.4594	5837380.743	2.5	0.4419417	0.029103
427260.3619	5837589.161	2.3	0.5076577	0.028438
426901.4796	5833898.337	1.74	0.7484242	0.026657
427562.4348	5833692.167	2.34	0.4937758	0.02857
427513.3061	5833541.937	1.82	0.7080524	0.026904
427514.7851	5833282.032	1.13	1.1422893	0.024843
427570.7974	5832222.701	1.26	1.0438599	0.025219
420421.9249	5834191.363	1.49	0.8900314	0.025898
420330.0868	5833641.018	1.86	0.6886907	0.027029
420286.5533	5833385.852	1.24	1.0584316	0.025161
420267.4136	5833235.792	2	0.625	0.02747
420209.3407	5832900.569	1.48	0.896222	0.025868
420161.0936	5832595.393	1.16	1.1187813	0.024929

421144.8544	5833635.657	1.2	1.0881882	0.025045
421105.6081	5833505.476	1.83	0.7031616	0.026935
421066.4756	5833355.302	1.84	0.6983045	0.026967
420983.2692	5833044.928	0.73	1.5072598	0.023721
420909.7465	5832789.592	1.5	0.8838835	0.025928
422983.459	5833776.077	0.96	1.2851423	0.02436
422984.4828	5833596.141	1.11	1.1582351	0.024786
422985.6205	5833396.213	1.35	0.9807301	0.025483
422981.5609	5833231.243	1.35	0.9807301	0.025483
422982.2151	5833116.284	1.03	1.2242754	0.024558
423437.6989	5833883.627	1.22	1.0732068	0.025103
423424.3254	5833598.644	0.8	1.4358729	0.023914
423415.2391	5833438.644	0.9	1.3397168	0.024192
423401.0124	5833303.607	0.89	1.3490353	0.024164
423392.1821	5833098.624	1.39	0.953912	0.025601
424168.4042	5833717.84	1.86	0.6886907	0.027029
423999.3184	5833566.927	1.12	1.1502346	0.024814
423999.9725	5833451.968	0.71	1.5283003	0.023666
423889.5932	5832646.603	-0.84	4.4751254	0.019786
423742.3696	5833045.635	1.3	1.0153155	0.025336
424625.3453	5833350.561	1.39	0.953912	0.025601
424556.1385	5833215.212	0.91	1.3304627	0.02422
424506.7822	5833104.967	-0.82	4.413515	0.019832
424363.4556	5832819.244	1.29	1.0223776	0.025306
424230.0686	5832543.575	1.11	1.1582351	0.024786
424091.7119	5832262.879	1.24	1.0584316	0.025161
424032.4162	5832142.581	1.63	0.8077205	0.02632
424885.7069	5833272.069	0.93	1.3121459	0.024276
424841.3773	5833156.855	0.71	1.5283003	0.023666
424767.3998	5832981.491	1.04	1.2158187	0.024586
424703.3619	5832816.18	1.43	0.9278272	0.025719
424634.3542	5832645.843	1.68	0.7802066	0.026473
424570.3163	5832480.533	2.25	0.5255603	0.028275
424491.3976	5832295.144	1.71	0.7641502	0.026565
424442.0983	5832174.903	1.21	1.0806715	0.025074
424378.089	5832004.594	1.41	0.9407792	0.02566
424971.8425	5833067.626	0.22	2.1464136	0.022364
424928.6223	5832757.482	1.37	0.9672281	0.025541
424870.436	5832442.254	2.45	0.4575268	0.028936
424807.4223	5832097.008	1.33	0.9944206	0.025424
424763.7187	5831871.833	1.34	0.9875516	0.025453
425215.6735	5833258.952	0.69	1.5496346	0.023612
425216.1854	5833168.984	0.15	2.2531262	0.022184
425217.2094	5832989.049	1.05	1.2074204	0.024614
425218.1481	5832824.108	0.69	1.5496346	0.023612

425218.8592	5832699.154	1.23	1.0657936	0.025132
425220.566	5832399.262	0.84	1.3966089	0.024025
425226.7021	5832199.362	1.85	0.6934809	0.026998
425228.2384	5831929.459	1.41	0.9407792	0.02566
425229.4334	5831719.535	2.66	0.3955489	0.029646
425434.5703	5833440.138	0.85	1.3869618	0.024052
425480.1798	5833330.434	1.45	0.9150536	0.025779
425540.8977	5833200.822	1.38	0.960547	0.025571
425606.7844	5833041.25	0.8	1.4358729	0.023914
425687.7795	5832861.77	1.81	0.7129773	0.026873
425768.8032	5832677.292	1.82	0.7080524	0.026904
425870.0756	5832447.944	1.24	1.0584316	0.025161
426042.2617	5832054.053	2.34	0.4937758	0.02857
426092.9264	5831934.381	1.45	0.9150536	0.025779
426153.7298	5831789.775	1.65	0.7966004	0.026381
426254.9171	5831575.422	0.9	1.3397168	0.024192
426241.7183	5833894.583	1.11	1.1582351	0.024786
425603.5989	5833601.048	0.8	1.4358729	0.023914
425659.3185	5833471.407	1.17	1.1110534	0.024958
425731.3695	5833106.937	1.13	1.1422893	0.024843
425811.2554	5833122.387	0.72	1.5177436	0.023694
425882.1687	5832957.845	1.42	0.9342808	0.025689
425958.1372	5832783.335	0.82	1.4161049	0.023969
426059.4096	5832553.987	0.77	1.4660437	0.023831
426140.4617	5832364.51	1.92	0.6606363	0.027217
426216.4303	5832190	2.18	0.5516894	0.028047
426282.2603	5832040.424	1.98	0.6337247	0.027406
426393.6715	5831786.142	1.5	0.8838835	0.025928
425792.478	5833787.062	1.24	1.0584316	0.025161
425878.4712	5833607.61	1.03	1.2242754	0.024558
425974.4892	5833423.217	0.57	1.684042	0.023287
426050.3439	5833268.7	1.1	1.1662912	0.024757
426121.115	5833129.149	0.7	1.5389305	0.023639
426181.8044	5833004.535	0.38	1.921094	0.022781
426267.8261	5832820.086	1.27	1.0366494	0.025248
426368.8994	5832625.725	1.31	1.0083022	0.025365
426449.8661	5832451.243	0.86	1.3773814	0.02408
426545.8843	5832266.851	1.76	0.7381204	0.026719
426631.9062	5832082.401	1.11	1.1582351	0.024786
426753.2568	5831838.173	2.04	0.6079093	0.027597
426803.7793	5831743.492	2.22	0.5366034	0.028177
427021.3522	5828645.753	0.85	1.3869618	0.024052
427196.2888	5828646.749	0.36	1.9479114	0.022729
426991.2942	5829535.288	0.93	1.3121459	0.024276
427141.1829	5829546.138	1.11	1.1582351	0.024786

427286.1019	5829551.962	1.76	0.7381204	0.026719
427183.7473	5829971.241	1.56	0.8478777	0.026108
427533.6204	5829973.233	1.66	0.7910979	0.026412
427131.6024	5830350.818	1.88	0.6792093	0.027092
427341.5547	5830347.015	1.56	0.8478777	0.026108
865022.5655	5397983.533	2.01	0.6206828	0.027501
427566.5016	5830343.298	1.45	0.9150536	0.025779
427244.341	5830741.331	1.12	1.1502346	0.024814
427429.1031	5830772.373	0.97	1.2762652	0.024388
427574.079	5830768.2	1.33	0.9944206	0.025424
427326.8345	5831176.657	2.02	0.6163954	0.027533
427456.9581	5831147.408	2.15	0.5632815	0.02795
427602.0762	5831118.244	2.06	0.5995401	0.027661
427682.1325	5831103.705	2.22	0.5366034	0.028177
427367.6357	5831911.647	1.74	0.7484242	0.026657
427503.6109	5831732.48	2.36	0.4869779	0.028636
427579.2096	5831622.947	1.07	1.1907975	0.024671
427679.9416	5831488.565	2.44	0.4607091	0.028902
425917.2907	5833812.764	1.6	0.8246924	0.026229
426009.0579	5832618.679	0.97	1.2762652	0.024388
426099.4725	5833418.93	1.06	1.1990801	0.024643
426160.2188	5833284.32	0.43	1.8556545	0.022913
426210.8265	5833174.644	-0.06	2.6061644	0.021652
426271.5159	5833050.031	-0.01	2.5173889	0.021778
426347.4274	5832885.517	0.55	1.7075503	0.023233
426608.3574	5832707.061	1.42	0.9342808	0.025689
426759.0428	5832577.962	1.36	0.9739557	0.025512
426879.5967	5832473.683	1.17	1.1110534	0.024958
427015.2305	5832354.494	1.95	0.6470406	0.027311
427251.3118	5832150.906	1.77	0.7330218	0.026749
427341.7059	5832076.445	1.7	0.7694653	0.026534
427437.1551	5831992.016	1.95	0.6470406	0.027311
427562.7356	5831882.767	2.08	0.591286	0.027725
427668.2096	5831793.397	1.43	0.9278272	0.025719
427773.6552	5831709.026	2.2	0.5440941	0.028112
426189.2978	5833444.433	0.32	2.0026747	0.022624
426314.6793	5833370.171	0.52	1.7434296	0.023153
426374.9136	5833325.529	0.25	2.102241	0.022442
426420.3808	5833240.816	0.83	1.4063231	0.023997
426571.0661	5833111.716	0.97	1.2762652	0.024388
426706.6999	5832992.527	0.6	1.6493849	0.023368
426897.5698	5832828.668	1.05	1.2074204	0.024614
427063.3349	5832684.659	1.44	0.9214183	0.025749
427229.1001	5832540.65	2.15	0.5632815	0.02795
427369.7605	5832416.492	1.62	0.8133387	0.02629

427510.3925	5832297.332	1.4	0.9473229	0.02563
427651.0529	5832173.174	1.8	0.7179365	0.026842
427766.5801	5832073.865	0.97	1.2762652	0.024388
425946.9102	5833877.911	1.47	0.9024557	0.025838
426067.4072	5833783.628	0.36	1.9479114	0.022729
426132.6966	5833729.017	-0.45	3.4151006	0.020698
426238.1137	5833649.643	0.39	1.907824	0.022807
426333.506	5833575.211	0.74	1.4968484	0.023749
426403.8219	5833515.631	0.87	1.3678671	0.024108
426474.1095	5833461.049	0.66	1.5821957	0.02353
426569.5017	5833386.616	0.93	1.3121459	0.024276
426795.4727	5833202.963	1.08	1.1825721	0.0247
426941.1028	5833083.831	1.12	1.1502346	0.024814
427096.7578	5832959.759	1.38	0.960547	0.025571
427110.4439	5833189.761	1.33	0.9944206	0.025424
427357.204	5832866.272	1.83	0.7031616	0.026935
427553.6124	5832607.476	1.95	0.6470406	0.027311
427644.2625	5832488.031	1.57	0.842021	0.026138
427770.1274	5832328.801	1.57	0.842021	0.026138
426076.7211	5833903.641	0.7	1.5389305	0.023639
426171.9996	5833849.201	0.77	1.4660437	0.023831
426272.3047	5833789.792	1.12	1.1502346	0.024814
426397.6577	5833720.528	1.15	1.1265631	0.0249
426533.0923	5833636.327	0.53	1.7313868	0.023179
426658.4453	5833567.063	0.98	1.2674493	0.024416
426924.231	5833413.627	0.97	1.2762652	0.024388
427129.8394	5833294.836	1.79	0.7229301	0.026811
427285.2952	5833205.751	1.36	0.9739557	0.025512
427460.8006	5833106.782	1.57	0.842021	0.026138
427626.3096	5833007.757	1.43	0.9278272	0.025719
427771.7405	5832923.613	1.62	0.8133387	0.02629
427877.0437	5832864.232	1.67	0.7856334	0.026442
426266.8231	5833874.733	-0.19	2.8519093	0.021329
426392.0338	5833830.46	0.15	2.2531262	0.022184
426182.2235	5833809.273	-1.29	6.1132014	0.018784
426517.2446	5833786.187	0.24	2.1168633	0.022416
426667.5316	5833727.062	0.34	1.9751033	0.022676
426872.884	5833653.255	0.56	1.6957554	0.02326
427108.2824	5833569.623	0.69	1.5496346	0.023612
427378.7817	5833466.197	1.54	0.8597136	0.026048
427519.8971	5833262.067	2.07	0.5953987	0.027693
427649.793	5833272.803	0.98	1.2674493	0.024416
427774.7192	5833278.513	1.37	0.9672281	0.025541
427509.1043	5833401.96	1.1	1.1662912	0.024757
427493.3703	5833531.827	1.44	0.9214183	0.025749

427472.0977	5833756.632	0.98	1.2674493	0.024416
427456.2784	5833901.494	1.44	0.9214183	0.025749
426080.7808	5834068.61	1.12	1.1502346	0.024814
426190.997	5834024.252	1.17	1.1110534	0.024958
426341.2272	5833975.123	-0.27	3.0145196	0.021133
426451.4433	5833930.765	0.27	2.0732989	0.022493
426536.5832	5833901.259	0.51	1.7555561	0.023126
426671.9041	5833837.051	0.98	1.2674493	0.024416
426902.3328	5833748.392	0.8	1.4358729	0.023914
427152.9248	5833629.857	1.23	1.0657936	0.025132
427192.4552	5833710.056	1.45	0.9150536	0.025779
427246.8665	5833810.332	1.27	1.0366494	0.025248
427281.4841	5833875.508	1	1.25	0.024473
427360.6019	5834025.908	1.51	0.877778	0.025958
427405.0737	5834116.132	1.81	0.7129773	0.026873
427454.5437	5834206.383	1.87	0.6839336	0.02706
426946.8614	5833828.619	1.66	0.7910979	0.026412
426996.2461	5833933.865	0.94	1.3030822	0.024304
427030.8922	5833994.042	1.22	1.0732068	0.025103
427095.1861	5834114.368	1.26	1.0438599	0.025219
427174.304	5834264.769	1.35	0.9807301	0.025483
426726.2585	5833947.324	1.53	0.8656934	0.026018
426770.7588	5834032.549	1.52	0.8717148	0.025988
426835.5362	5834067.906	0.9	1.3397168	0.024192
426154.6731	5834258.968	0.59	1.6608573	0.023341
426310.1574	5834164.884	-0.49	3.5111122	0.020603
426466.4948	5833920.854	-1.04	5.1405691	0.019334
426575.4312	5834101.415	-1.55	7.3204285	0.018228
426139.5932	5834273.877	0.21	2.1613431	0.022338
426189.5182	5834284.158	-0.79	4.3226862	0.019901
426239.4717	5834289.441	0.21	2.1613431	0.022338
426339.3503	5834305.004	0.25	2.102241	0.022442
426389.2753	5834315.285	1.27	1.0366494	0.025248
426439.2288	5834320.567	0.94	1.3030822	0.024304
426489.1539	5834330.848	1.04	1.2158187	0.024586
425938.272	5834517.651	1.31	1.0083022	0.025365
426028.1542	5834533.158	1.28	1.0294888	0.025277
426103.0419	5834548.579	-0.04	2.5702846	0.021702
426172.9597	5834558.973	-0.9	4.665165	0.01965
426242.8775	5834569.368	-0.74	4.1754396	0.020016
426317.7651	5834584.789	-0.1	2.6794337	0.021552
426402.6491	5834600.267	2.15	0.5632815	0.02795
425932.3355	5834682.563	1.49	0.8900314	0.025898
426101.8192	5834763.501	0.11	2.3164702	0.022082
426196.4152	5834829.018	0.31	2.0166044	0.022598

426310.9187	5834909.643	0.84	1.3966089	0.024025
426375.6393	5834954.996	0.49	1.7800627	0.023072
425610.6312	5835000.628	1.7	0.7694653	0.026534
425860.541	5835002.05	1.65	0.7966004	0.026381
426050.5293	5834993.134	0.67	1.5712667	0.023557
426220.411	5835004.097	0.08	2.3651441	0.022005
426360.3604	5835004.893	1.28	1.0294888	0.025277
426198.9967	5835253.893	-0.09	2.6609255	0.021577
426033.1181	5835417.895	0.43	1.8556545	0.022913
425821.9998	5835626.625	1.44	0.9214183	0.025749
426046.9186	5835627.904	0.57	1.684042	0.023287
426246.8464	5835629.042	0.1	2.3325825	0.022056
426456.7704	5835630.236	0.89	1.3490353	0.024164
426711.6782	5835631.686	1.95	0.6470406	0.027311
426981.5804	5835633.221	2.3	0.5076577	0.028438
425480.1894	5835964.569	2.2	0.5440941	0.028112
425113.3026	5836317.366	0.79	1.4458602	0.023886
424726.423	5836670.05	0.48	1.7924441	0.023046
424354.538	5837022.819	2.22	0.5366034	0.028177
426054.9535	5835972.837	0.74	1.4968484	0.023749
425972.8788	5836342.248	1.65	0.7966004	0.026381
425834.4884	5836946.263	0.3	2.030631	0.022572
425711.4908	5837480.387	1.37	0.9672281	0.025541
426231.4253	5835703.929	-0.81	4.3830286	0.019855
426325.396	5835879.406	0.4	1.8946457	0.022834
426533.1029	5836270.459	0.6	1.6493849	0.023368
426730.9555	5836636.464	0.3	2.030631	0.022572
426968.3391	5837082.667	1.55	0.8537752	0.026078
427161.2223	5837443.645	1.85	0.6934809	0.026998
426804.4833	5836012.088	1.81	0.7129773	0.026873
426673.8197	5836136.304	0.82	1.4161049	0.023969
426166.2167	5836623.256	1.32	1.0013373	0.025394
425437.4425	5837328.878	0.74	1.4968484	0.023749
427219.0487	5836064.429	2.09	0.5872017	0.027757
427245.9964	5836599.406	2.3	0.5076577	0.028438
427272.6318	5837189.363	1.91	0.6652314	0.027186
427295.187	5835859.93	2.25	0.5255603	0.028275
427482.6735	5836290.854	2.19	0.5478786	0.028079
427723.3211	5837041.975	2.48	0.448111	0.029036
427985.9229	5837448.334	2.46	0.4543664	0.028969
428059.858	5834994.567	2.26	0.5219299	0.028307
428271.1975	5835625.561	1.29	1.0223776	0.025306
428267.2746	5836315.31	2.24	0.5292158	0.028242
428762.5735	5837112.863	0.24	2.1168633	0.022416
422850.7754	5834255.166	1.77	0.7330218	0.026749

427217.2547	5832865.476	1.29	1.0223776	0.025306
426352.1731	5836444.372	0.18	2.2067575	0.022261
427249.1222	5829901.636	1.32	1.0013373	0.025394
427324.0096	5829917.057	1.4	0.9473229	0.02563
427398.8686	5829937.477	2.46	0.4543664	0.028969
427478.7542	5829952.927	1.93	0.6560729	0.027248
427578.5186	5829988.484	1.68	0.7802066	0.026473
427217.2547	5832865.476	1.29	1.0223776	0.025306

Appendix 4

Wind data set for FLOW-MOR model

Time	Speed (m/s)	Direction (deg)
10 04 2013 00 00 00	2	203
11 04 2013 00 00 00	2.1	203
12 04 2013 00 00 00	1.5	203
13 04 2013 00 00 00	1.8	234
14 04 2013 00 00 00	0.9	31
15 04 2013 00 00 00	4	62
16 04 2013 00 00 00	10.5	68
17 04 2013 00 00 00	1.9	312
18 04 2013 00 00 00	1.8	253
19 04 2013 00 00 00	1.9	214
20 04 2013 00 00 00	3	135
21 04 2013 00 00 00	1.7	166
22 04 2013 00 00 00	1.4	259
23 04 2013 00 00 00	1.5	245
24 04 2013 00 00 00	3.9	276
25 04 2013 00 00 00	5.2	279
26 04 2013 00 00 00	8.7	259
27 04 2013 00 00 00	5.5	273
28 04 2013 00 00 00	3.3	254
29 04 2013 00 00 00	1.5	268
30 04 2013 00 00 00	1.1	169
01 05 2013 00 00 00	1.9	211
2 05 2013 00 00 00	2.8	130
3 05 2013 00 00 00	1.3	214
4 05 2013 00 00 00	4.3	113
5 05 2013 00 00 00	1.1	225
6 05 2013 00 00 00	7.2	335
7 05 2013 00 00 00	3.8	251
8 05 2013 00 00 00	2.3	222

Appendix 5

Dredging and dumping files.

A. Actual dredging and dumping specification.

[Dredge]		
Name	=	I1
DredgeDepth	=	13.78
Dump	=	DaD D
Percentage	=	100
[Dredge]		
Name	=	CT
DredgeDepth	=	4.72
Dump	=	DaD D
Percentage	=	100
[Dredge]		
Name	=	I2
DredgeDepth	=	1.26
Dump	=	DaD D
Percentage	=	100
[Dredge]		
Name	=	SP
DredgeDepth	=	13.78
Dump	=	DaD D
Percentage	=	100
[Dredge]		
Name	=	I4
DredgeDepth	=	1.96
Dump	=	DaD D
Percentage	=	100
[Dredge]		
Name	=	I3
DredgeDepth	=	0.54
Dump	=	DaD D
Percentage	=	100
[Dredge]		
Name	=	I7
DredgeDepth	=	2.35
Dump	=	DaD D
Percentage	=	100
[Dredge]		
Name	=	I5

DredgeDepth	=	17.29
Dump	=	DaD D
Percentage	=	100
[Dredge]		
Name	=	I6
DredgeDepth	=	8.43
Dump	=	DaD D
Percentage	=	100
[Dredge]		
Name	=	O1
DredgeDepth	=	18.47
Dump	=	DaD D
Percentage	=	100
[Dredge]		
Name	=	O2
DredgeDepth	=	5.86
Dump	=	DaD D
Percentage	=	100
[Dredge]		
Name	=	O3
DredgeDepth	=	0.34
Dump	=	DaD D
Percentage	=	100
[Dredge]		
Name	=	O4
DredgeDepth	=	0.58
Dump	=	DaD B
Percentage	=	100
[Dredge]		
Name	=	O5
DredgeDepth	=	1.28
Dump	=	DaD B
Percentage	=	100
[Dredge]		
Name	=	O6
DredgeDepth	=	24.24
Dump	=	DaD B
Percentage	=	100
[Dredge]		
Name	=	O7
DredgeDepth	=	65.13
Dump	=	DaD B
Percentage	=	100
[Dump]		
Name	=	DaD B

MinimumDumpDepth	=	5
DumpDistr	=	3
[Dump]		
Name	=	DaD D
MinimumDumpDepth	=	5
DumpDistr	=	3

B. Dredging and dumping locations (polygons in UTM 60S coordinates)

I1		
	12	2
	427218.7	5830996
	427540.1	5830944
	427566.1	5831004
	427592.8	5831001
	427616.5	5831020
	427594.3	5831116
	427566.1	5831129
	427536.4	5831122
	427457.7	5831141
	427341.2	5831135
	427309.3	5831042
	427218.7	5830996
CT		
	8	2
	427781.7	5831325
	427781.7	5831267
	427816.3	5831263
	427844.1	5831245
	427856.1	5831135
	427899.1	5831059
	427888.2	5831315
	427781.7	5831325
I2		
	11	2
	427418.7	5831209
	427475.1	5831162
	427529.2	5831186
	427480.9	5831265
	427507.3	5831478
	427537.3	5831542
	427513.1	5831585
	427516.6	5831646
	427470.5	5831660
	427407.2	5831289

	427418.7	5831209
SP		
	11	2
	427181	5831138
	427198.5	5831113
	427224	5831261
	427228.7	5831323
	427265.3	5831474
	427266.9	5831606
	427295.5	5831642
	427309.8	5831692
	427290.8	5831679
	427254.2	5831695
	427181	5831138
I4		
	11	2
	427298.8	5831647
	427303.4	5831624
	427324.5	5831621
	427379.3	5831713
	427396.4	5831825
	427376	5831874
	427357.5	5831880
	427327.8	5831841
	427305.4	5831748
	427312.6	5831695
	427298.8	5831647
I3		
	13	2
	427557.9	5831685
	427590.5	5831681
	427598.2	5831655
	427659.1	5831661
	427660	5831694
	427638.5	5831726
	427638.5	5831745
	427605.1	5831762
	427589.6	5831748
	427553.6	5831746
	427540.7	5831730
	427544.2	5831708
	427557.9	5831685
I7		
	5	2
	427279.3	5831840

	427311.7	5831832
	427371.1	5832004
	427350.4	5832013
	427279.3	5831840
I5		
	9	2
	427504.8	5832360
	427660.4	5832432
	427712.2	5832940
	427571.5	5833185
	427499.8	5833185
	427561.6	5833042
	427586.3	5832656
	427541.8	5832456
	427504.8	5832360
I6		
	15	2
	427576.7	5833399
	427620.6	5833393
	427695.1	5833445
	427713.2	5833408
	427745.3	5833428
	427695.1	5833677
	427458.3	5833744
	427367	5833751
	427366.3	5833721
	427406.7	5833696
	427443.7	5833649
	427437.4	5833609
	427454.8	5833563
	427502.2	5833541
	427576.7	5833399
O1		
	9	2
	426163.8	5834096
	426184.7	5834091
	426189.1	5834188
	426150.5	5834306
	426145	5834477
	426127.4	5834500
	426096.5	5834507
	426106.4	5834264
	426163.8	5834096
O2		
	20	2

	426087.2	5835480
	426089.6	5835443
	426163	5835445
	426178.1	5835461
	426173.5	5835481
	426182.8	5835502
	426200.3	5835483
	426193.3	5835387
	426256.2	5835264
	426300.5	5835284
	426315.6	5835474
	426356.4	5835592
	426313.3	5835609
	426258.5	5835476
	426221.2	5835511
	426230.6	5835542
	426258.5	5835725
	426253.9	5835777
	426227.1	5835767
	426087.2	5835480
O3		
	7	2
	426266.2	5835700
	426281	5835668
	426309.4	5835661
	426344.7	5835740
	426294.7	5835749
	426268.5	5835748
	426266.2	5835700
O4		
	6	2
	426527.3	5836122
	426562	5836105
	426625.5	5836226
	426602.4	5836261
	426559.1	5836235
	426527.3	5836122
O5		
	9	2
	426720.9	5836411
	426764.2	5836400
	426839.3	5836570
	426894.2	5836729
	426839.3	5836755
	426810.4	5836723

	426819.1	5836674
	426764.2	5836573
	426720.9	5836411
O6		
	22	2
	426406	5836087
	426438.6	5836054
	426482.7	5836032
	426520.4	5836041
	426532.6	5836181
	426498	5836206
	426548.5	5836299
	426610.6	5836353
	426668.7	5836350
	426687.1	5836420
	426645	5836465
	426654.1	5836474
	426979.6	5837143
	427095.7	5837285
	427129.6	5837371
	427300.9	5837519
	427407.1	5837731
	427400.8	5837834
	427448.7	5837996
	427424.8	5838040
	427400.8	5838033
	426406	5836087
O7		
	15	2
	426303	5835270
	426326.2	5835228
	426502.5	5835783
	426764.9	5836215
	427641.4	5837613
	427593.9	5837630
	427447.9	5837467
	427291.6	5837192
	427230.5	5837209
	427145.6	5837103
	427113.3	5836903
	426671.8	5836217
	426593.7	5836153
	426474.8	5835912
	426303	5835270
DaDB		

	5	2
	428967.6	5834065
	429686.9	5833362
	430019.6	5833699
	429302.5	5834406
	428967.6	5834065
DaDD		
	5	2
	428496.2	5837284
	429080	5837974
	430467.9	5836815
	429884.1	5836117
	428496.2	5837284

I = inside the harbour

O = outside the harbour

DaD = dumping/spoil site

Appendix 6

Comparisons between measured (observed) and predicted water levels, and current speed and direction for verification of the hydrodynamic model Delft3D-FLOW

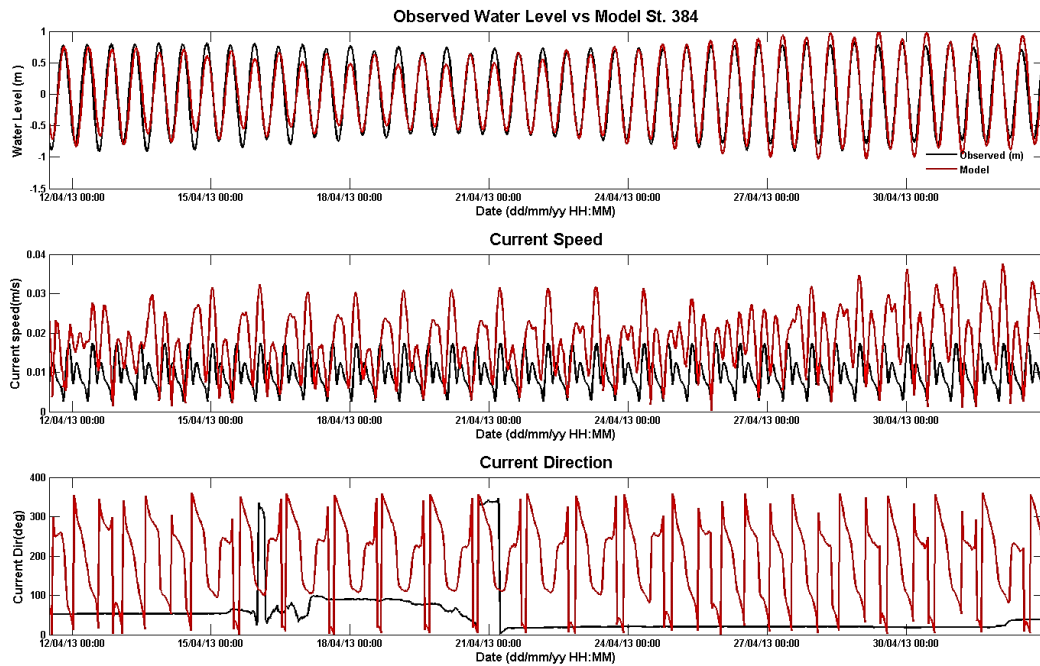


Figure 6.5a Observed and measured water level, current speed and direction of station 384.

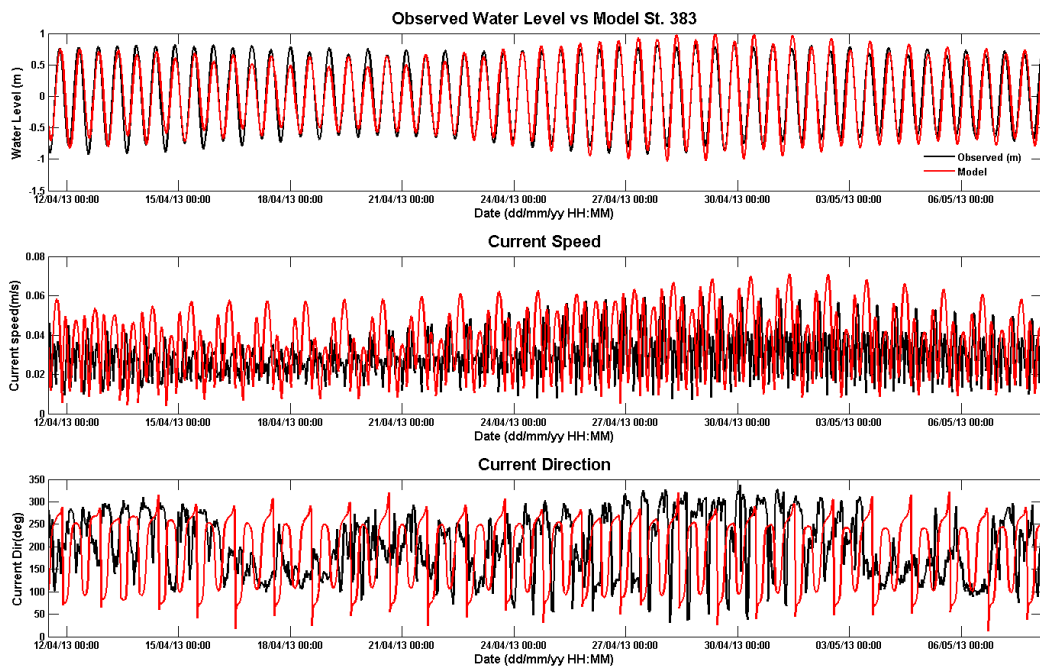


Figure 6.5b Observed and measured water level, current speed and direction of station 383.

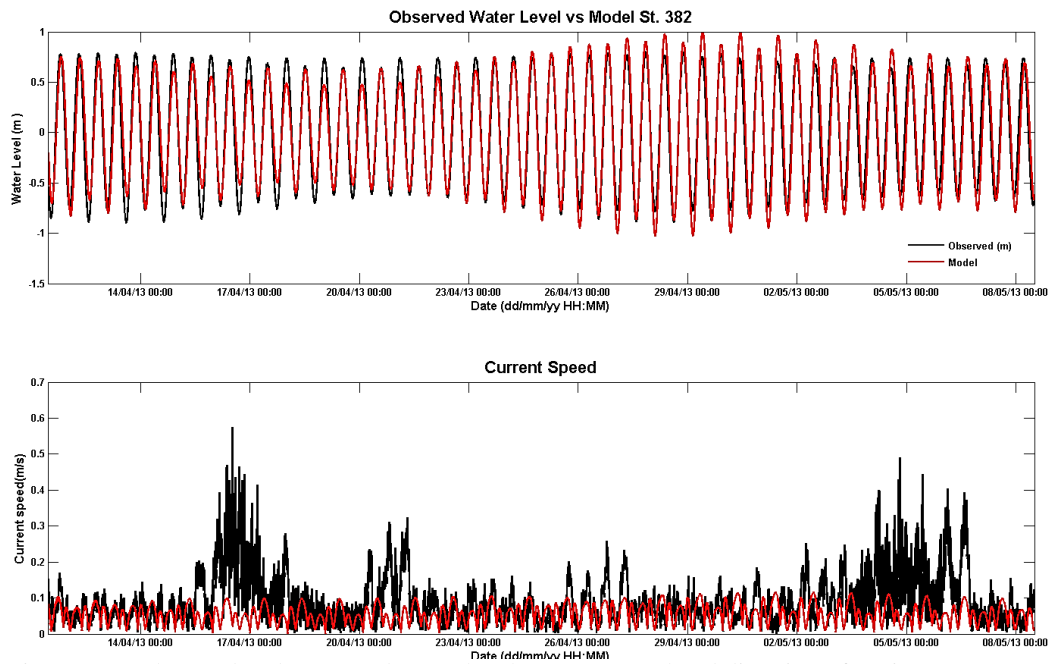


Figure 6.5c Observed and measured water level, current speed and direction of station 382.

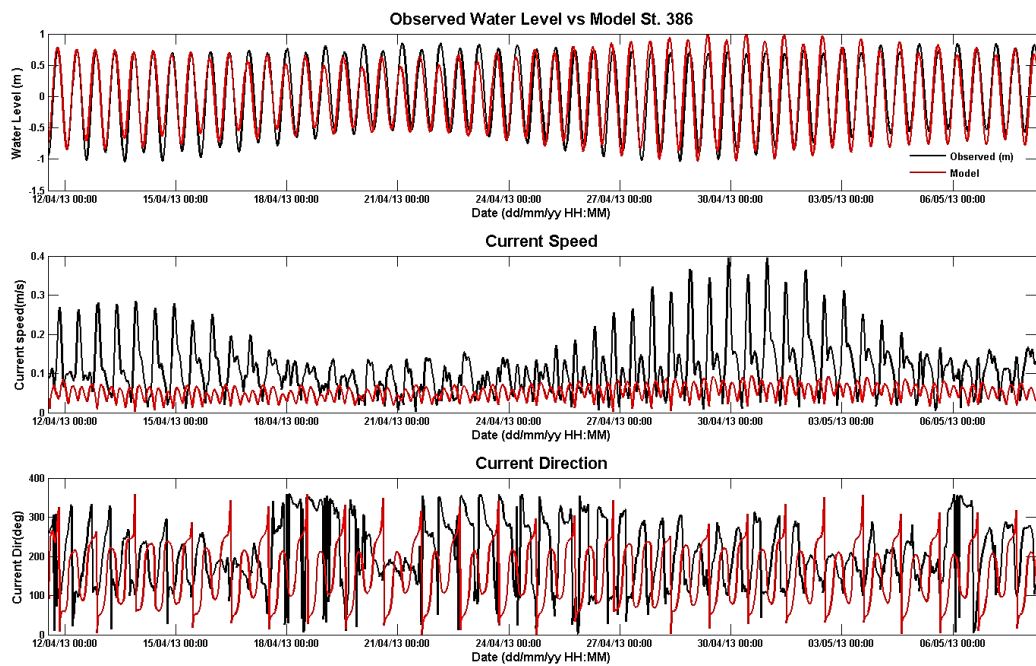


Figure 6.5d Observed and measured water level, current speed and direction of station 386.

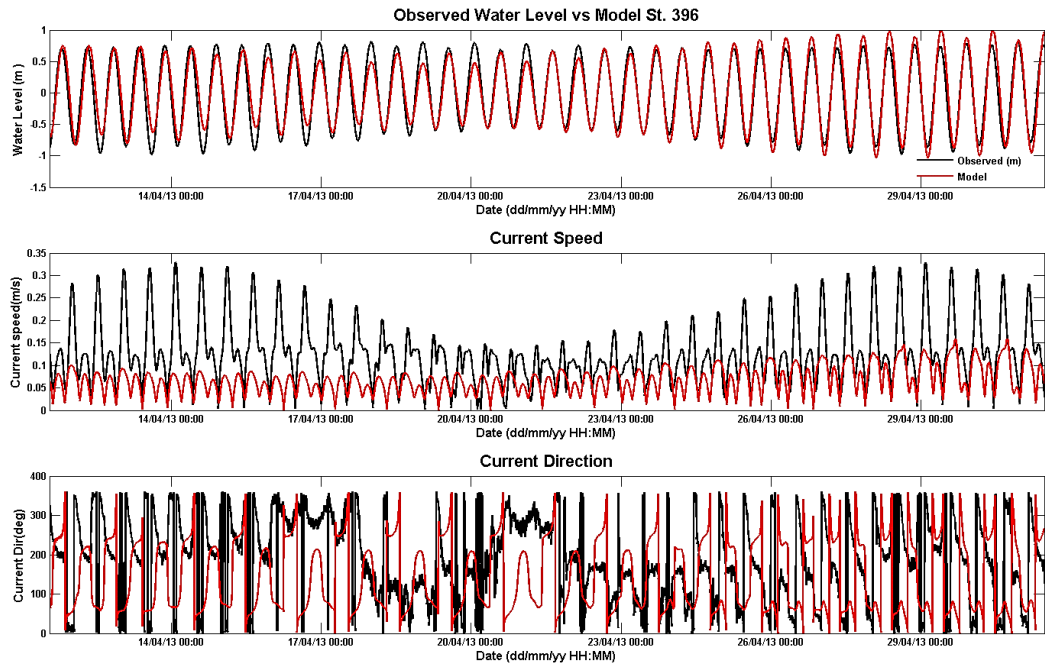


Figure 6.5e Observed and measured water level, current speed and direction of station 396.

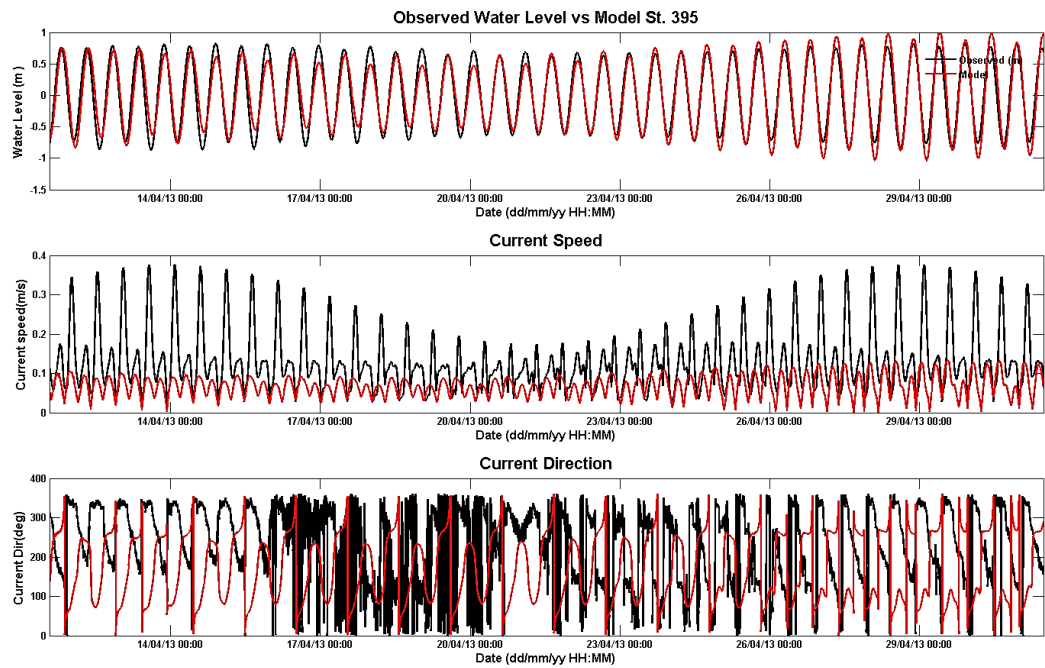


Figure 6.5f Observed and measured water level, current speed and direction of station 395.

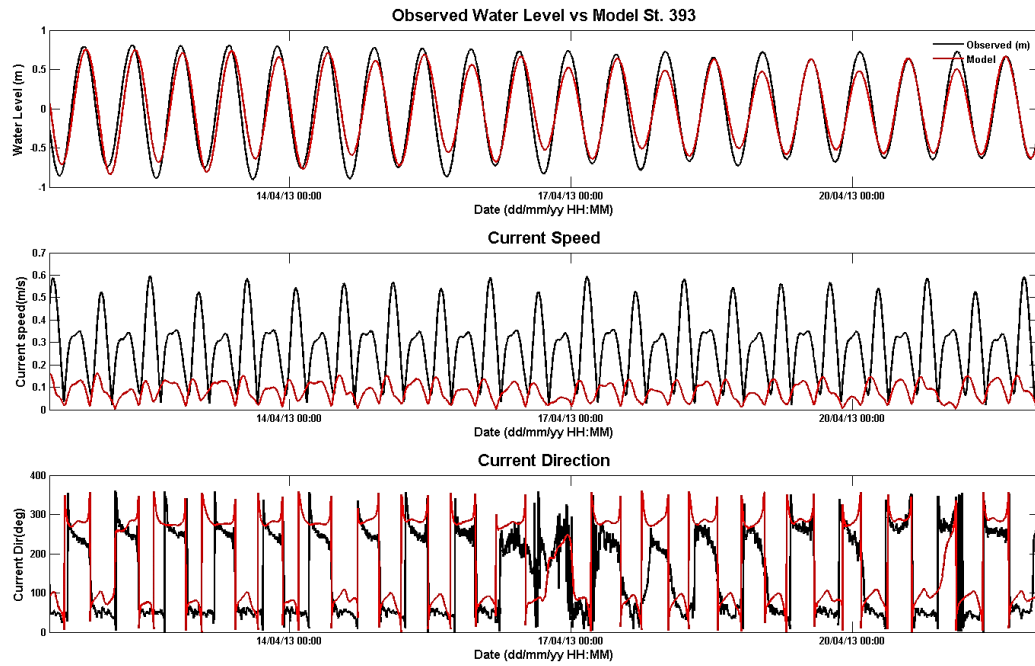


Figure 6.5g Observed and measured water level, current speed and direction of station 393

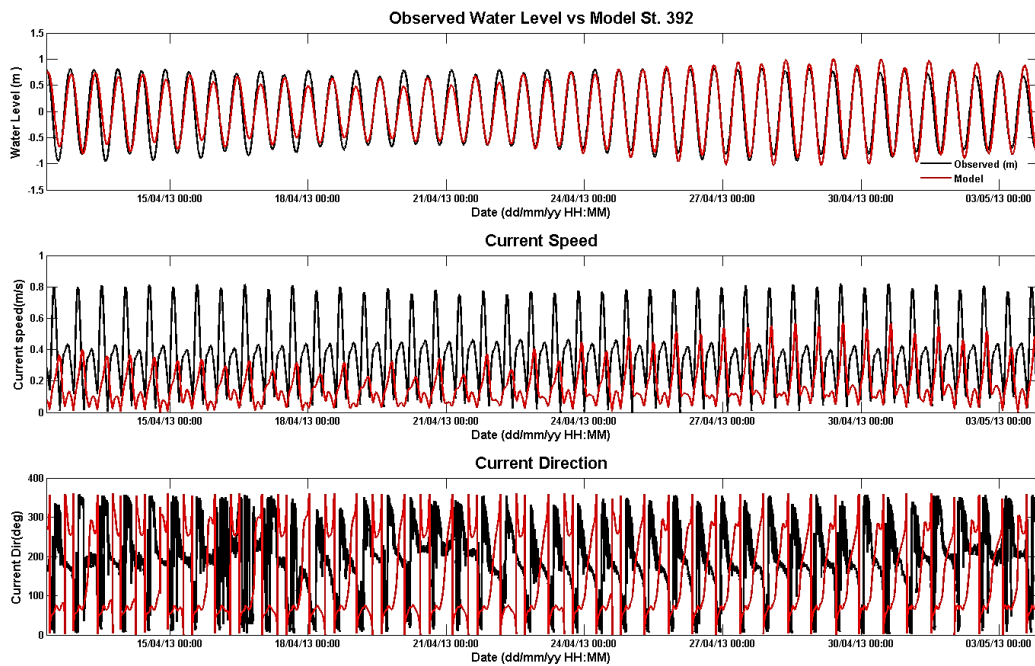


Figure 6.5h Observed and measured water level, current speed and direction of station 392

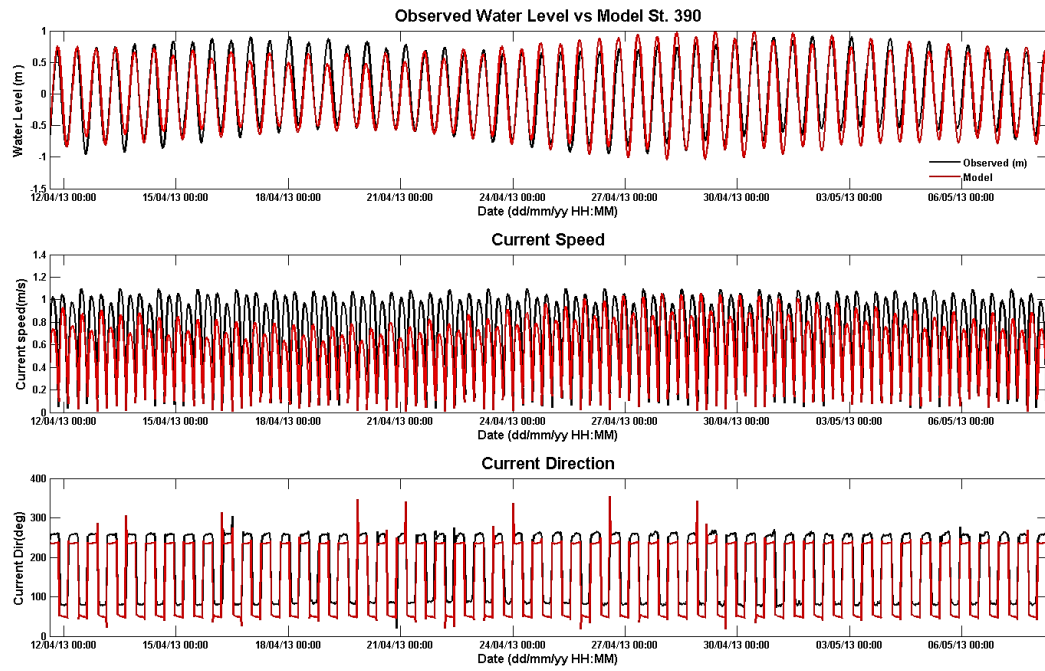


Figure 6.5i Observed and measured water level, current speed and direction of station 390

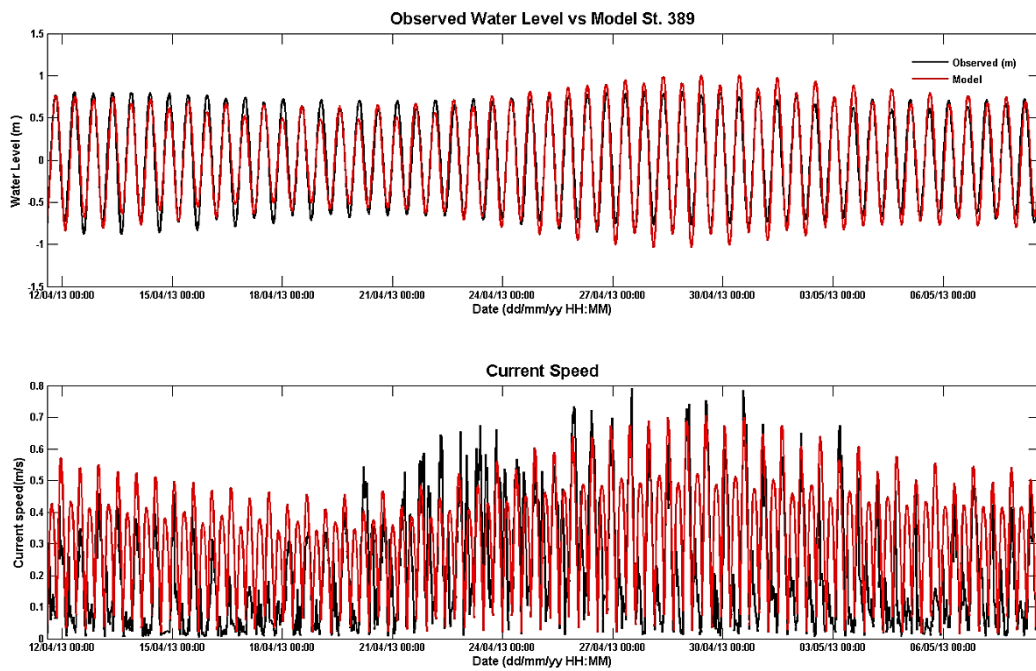


Figure 6.5j Observed and measured water level, current speed and direction of station 391

Appendix 7

Frequency distributions of measured and modelled significant wave height (H_s) and wave directions.

Sta. 383

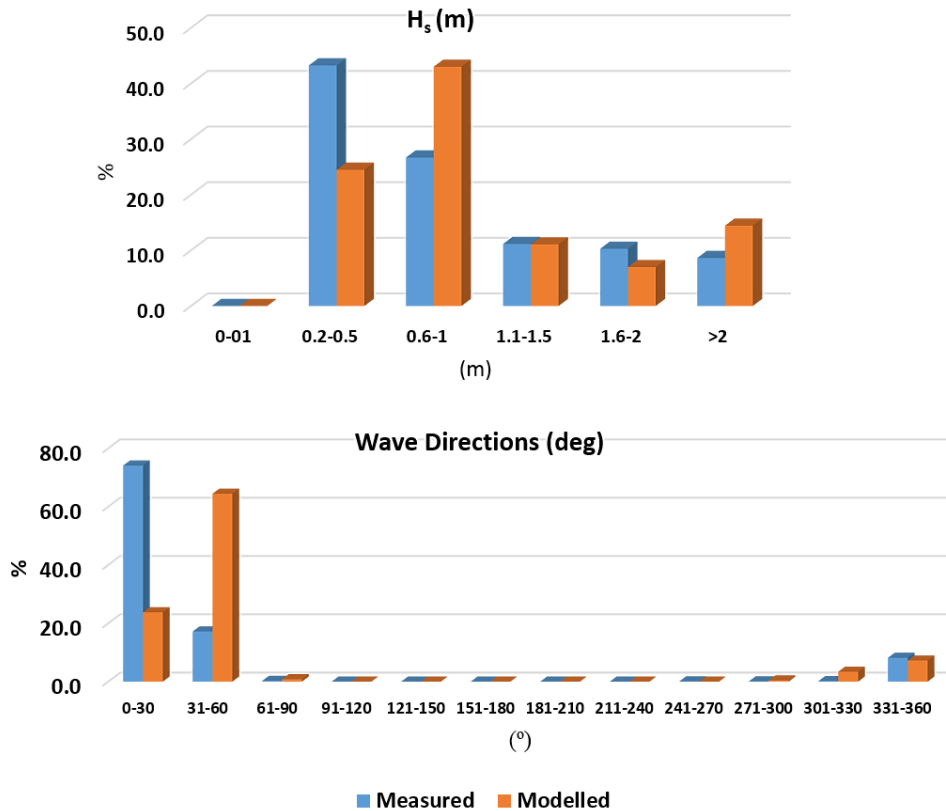


Table AP7-1 Summary of the frequency distribution (in %) of the incident significant wave heights and directions of measured and modelled waves at St. 383.

H _s			Wave direction		
Interval (m)	Measured	Modelled	Interval (°)	Measured	Modelled
< 0.1	0	0	0-30	74.1	23.8
0.2 – 0.5	43.2	24.5	31-60	17.2	64.4
0.6 - 1	26.7	43	61-90	0.2	0.8
1.1 1.5	11.1	11.1	91-120	0.0	0.0
1.6 - 2	10.3	7	121-150	0.0	0.0
>2	8.6	14.4	151-180	0.0	0.0
			181-210	0.1	0.0
			211-240	0.1	0.0
			241-270	0.2	0.4
			271-300	8.2	3.4
			301-330	0.1	7.2
			331-360	0.1	0.0

Sta. 384

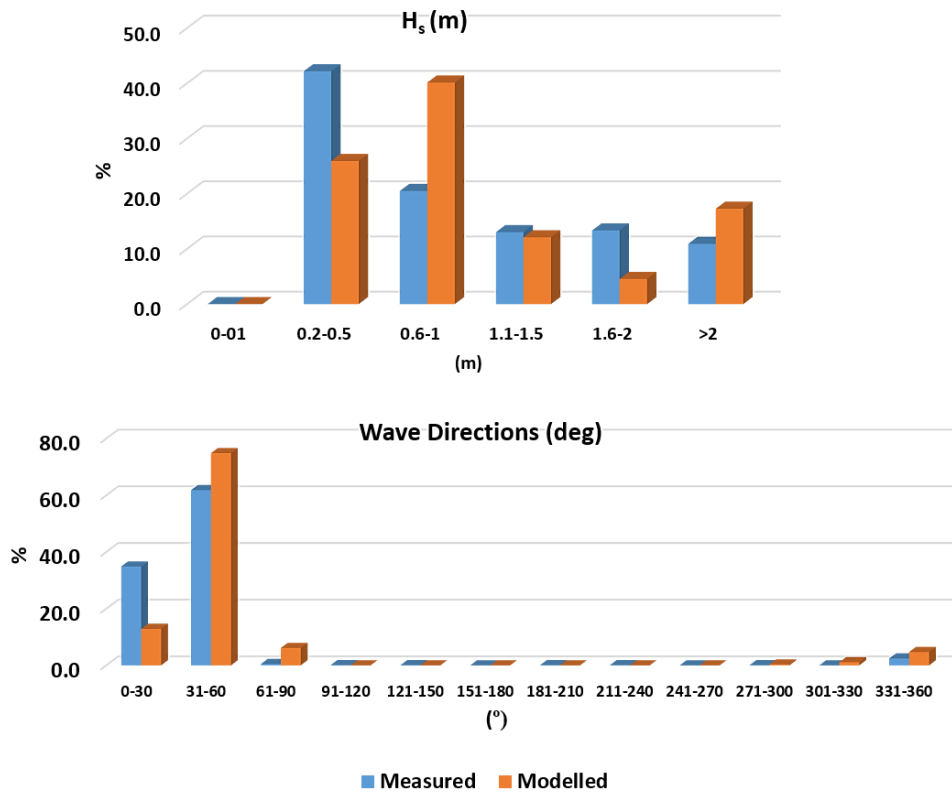


Table AP7-2 Summary of the frequency distribution (in %) of the incident significant wave heights and directions of measured and modelled waves at St. 384.

H_s			Wave direction		
Interval (m)	Measured	Modelled	Interval (°)	Measured	Modelled
< 0.1	0.0	0.0	0-30	34.9	12.9
0.2 – 0.5	42.2	25.9	31-60	61.8	74.9
0.6 - 1	20.5	40.1	61-90	0.5	6.1
1.2 1.5	13.0	12.1	91-120	0.1	0.0
1.6 - 2	13.4	4.6	121-150	0.1	0.0
>2	10.9	17.3	151-180	0.0	0.0
			181-210	0.1	0.0
			211-240	0.1	0.0
			241-270	0.0	0.0
			271-300	0.1	0.3
			301-330	0.0	1.1
			331-360	2.4	4.7

Sta. 386

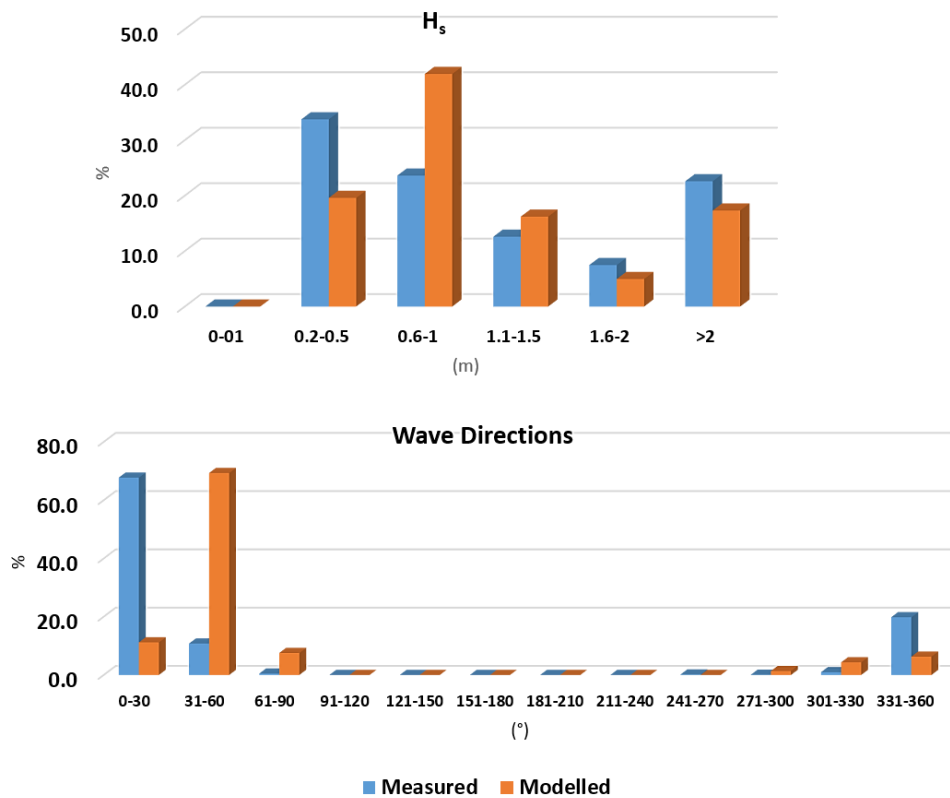


Table AP7-3 Summary of the frequency distribution (in %) of the incident significant wave heights and directions of measured and modelled waves at St. 386.

H _s			Wave direction		
Interval (m)	Measured	Modelled	Interval (°)	Measured	Modelled
< 0.1	0.0	0.0	0-30	67.7	11.2
0.2 – 0.5	33.8	19.6	31-60	10.8	69.3
0.6 - 1	23.6	41.9	61-90	0.5	7.6
1.3 1.5	12.6	16.2	91-120	0.0	0.0
1.6 - 2	7.5	5.0	121-150	0.0	0.0
>2	22.6	17.3	151-180	0.0	0.0
			181-210	0.0	0.0
			211-240	0.0	0.0
			241-270	0.2	0.0
			271-300	0.1	1.3
			301-330	0.9	4.3
			331-360	19.8	6.3

Sta. 390

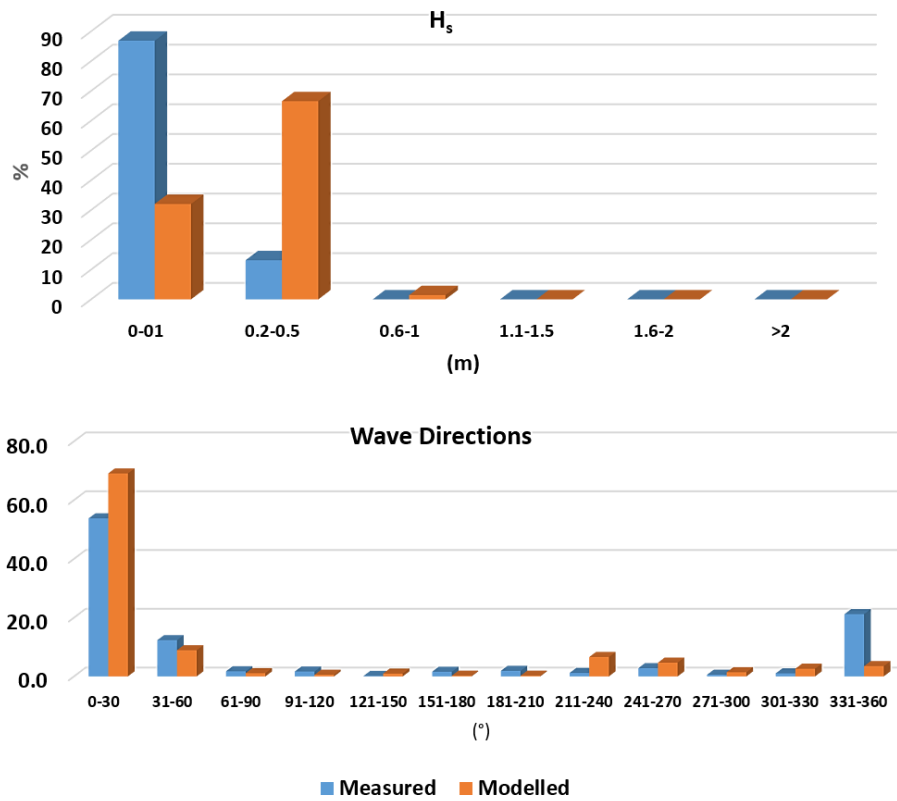


Table AP7-4 Summary of the frequency distribution (in %) of the incident significant wave heights and directions of measured and modelled waves at St. 390.

H _s			Wave direction		
Interval (m)	Measured	Modelled	Interval (°)	Measured	Modelled
< 0.1	86.9	32.0	0-30	53.8	69.1
0.2 – 0.5	13.1	66.5	31-60	12.4	8.9
0.6 - 1	0.0	1.4	61-90	1.8	1.1
1.4 1.5	0.0	0.0	91-120	1.7	0.6
1.6 - 2	0.0	0.0	121-150	0.2	1.0
>2	0.0	0.0	151-180	1.6	0.2
			181-210	1.9	0.2
			211-240	1.2	6.6
			241-270	2.8	4.7
			271-300	0.6	1.4
			301-330	1.0	2.6
			331-360	21.2	3.5

Appendix 8

Tidal boundaries for 1967 model

A1-67		
Tide	Amplitude	Phase
O1	0.0206	318.08
K1	0.0662	340.26
N2	0.1399	164.48
M2	0.5861	198.1
L2	0.0178	205
S2	0.0804	262.12
M4	0.0002	206.32
MS4	0.0001	248.42

A2-67		
Tide	Amplitude	Phase
O1	0.021	318.67
K1	0.0666	340.06
N2	0.1402	164.32
M2	0.5872	198.11
L2	0.0179	203.08
S2	0.0805	262.12
M4	0.0003	195.09
MS4	0.0001	248.33

A3-67		
Tide	Amplitude	Phase
O1	0.0212	318.51
K1	0.0665	340.09
N2	0.14	164.36
M2	0.5868	198.12
L2	0.0181	203.9
S2	0.0804	262.1
M4	0.0002	198.54
MS4	0.0001	243.92

A4-67		
Tide	Amplitude	Phase
O1	0.0206	318.08
K1	0.0662	340.26
N2	0.1399	164.48
M2	0.5861	198.1
L2	0.0178	205
S2	0.0804	262.12
M4	0.0002	206.32
MS4	0.0001	248.42

B1-67		
Tide	Amplitude	Phase
O1	0.021	318.66
K1	0.0661	339.59
N2	0.1396	164.27
M2	0.5857	197.91
L2	0.0178	204.37
S2	0.0802	261.92
M4	0.0003	171.24
MS4	0.0002	225.98

B2-67		
Tide	Amplitude	Phase
O1	0.0209	317.82
K1	0.0663	339.33
N2	0.1397	164.18
M2	0.5853	197.8
L2	0.0178	203.18
S2	0.0802	261.85
M4	0.0004	163.14
MS4	0.0001	225.18

B3-67		
Tide	Amplitude	Phase
O1	0.0205	317.77
K1	0.0662	339.32
N2	0.1396	163.78
M2	0.5842	197.55
L2	0.0176	203.61
S2	0.08	261.59
M4	0.0002	182.01
MS4	0.0002	252.52

C1-67		
Tide	Amplitude	Phase
O1	0.0207	317.16
K1	0.0661	339.66
N2	0.1399	163.87
M2	0.5862	197.53
L2	0.0179	203.76
S2	0.0801	261.47
M4	0.0002	176.7
MS4	0.0001	277.01

C2-67		
Tide	Amplitude	Phase
O1	0.0212	317.64
K1	0.0664	339.27
N2	0.14	163.68
M2	0.5871	197.45
L2	0.0179	203.76
S2	0.08	261.27
M4	0.0002	174.63
MS4	0.0001	216.05

C3-67		
Tide	Amplitude	Phase
O1	0.0217	318.37
K1	0.0666	339.19
N2	0.1402	163.77
M2	0.5877	197.41
L2	0.0178	204.31
S2	0.08	261.48
M4	0.0003	165.23
MS4	0.0001	252.79

D1-67		
Tide	Amplitude	Phase
O1	0.0205	321.15
K1	0.0644	345.69
N2	0.138	177.1
M2	0.5955	209.07
L2	0.0177	219.7
S2	0.0786	277.59
M4	0.0002	170.08
MS4	0.0002	337.02